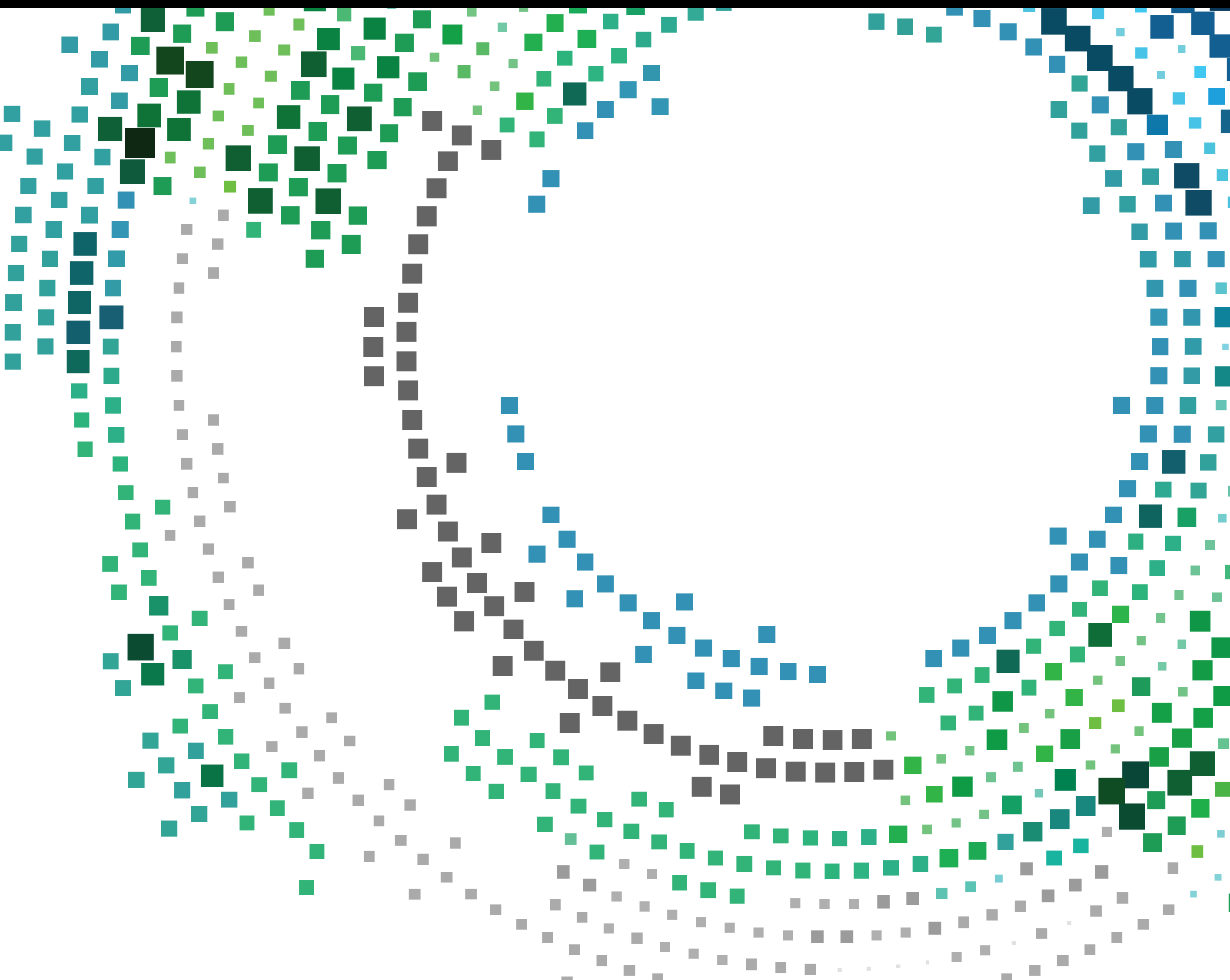


Architecture, Technologies, and Applications of Location-Based Services

Lead Guest Editor: Hsu-Yang Kung

Guest Editors: Xiao-Guang Yue, Chi-Hua Chen, and Feng-Jang Hwang





Architecture, Technologies, and Applications of Location-Based Services

Mobile Information Systems

Architecture, Technologies, and Applications of Location-Based Services

Lead Guest Editor: Hsu-Yang Kung


Guest Editors: Xiao-Guang Yue, Chi-Hua Chen,
and Feng-Jang Hwang



Copyright © 2023 Hindawi Limited. All rights reserved.

This is a special issue published in “Mobile Information Systems.” All articles are open access articles distributed under the Creative Commons Attribution License, which permits unrestricted use, distribution, and reproduction in any medium, provided the original work is properly cited.

Chief Editor

Alessandro Bazzi , Italy




Academic Editors

Mahdi Abbasi , Iran
Hammad Afzal , Pakistan
Ramon Aguero , Spain
Abdullah Alamoodi , Malaysia
Sikandar Ali, China
Markos Anastassopoulos, United Kingdom
Marco Anisetti , Italy
Claudio Agostino Ardagna , Italy
Ashish Bagwari , India
Jose M. Barcelo-Ordinas , Spain
Luca Bedogni , Italy
Dr. Robin Singh Bhadoria , India
Nicola Bicocchi , Italy
Peter Brida , Slovakia
Puttamadappa C. , India
Carlos Calafate , Spain
Juan C. Cano , Spain
Salvatore Carta, Italy
Pengyun Chen, China
Yuh-Shyan Chen , Taiwan
Wenchi Cheng, China
Gabriele Civitarese , Italy
Massimo Condoluci , Sweden
Rajesh Kumar Dhanaraj, India
Rajesh Kumar Dhanaraj , India
Almudena Diaz Zayas , Spain
Ahmed Farouk, Egypt
Filippo Gandino , Italy
Jorge Garcia Duque , Spain
L. J. García Villalba , Spain
Francesco Gringoli , Italy
Mian Ahmad Jan , Pakistan
Rutvij Jhaveri, India
Wei Jia, China
Adrian Kliks , Poland
Adarsh Kumar , India
Manoj Kumar, India
Quanzhong Li , China
Jian-Xun Liu , China
Juraj Machaj , Slovakia
Mirco Marchetti, Italy
Elio Masciari , Italy
Zahid Mehmood , Pakistan

Eduardo Mena , Spain
Massimo Merro , Italy
Aniello Minutolo , Italy
Senthilkumar Mohan, India
Jose F. Monserrat , Spain
Raul Montoliu , Spain
Mario Muñoz-Organero , Spain
Hamad Naeem, China
Giovanni Nardini , Italy
Mehrbakhsh Nilashi , Malaysia
Francesco Palmieri , Italy
Marco Picone , Italy
Alessandro Sebastian Podda , Italy
Maheswar Rajagopal, India
Amon Rapp , Italy
Michele Ruta , Italy
Neetesh Saxena, United Kingdom
Filippo Sciarrone, Italy
Floriano Scioscia , Italy
Mohammed Shuaib, Malaysia
Dr. Mueen Uddin, Brunei Darussalam
Michael Vassilakopoulos, Greece
Ding Xu , China
Laurence T. Yang , Canada
Kuo-Hui Yeh , Taiwan
Yugen Yi , China
Jianming Zhu, China

Contents




Architecture, Technologies, and Applications of Location-Based Services

Hsu-Yang Kung , Xiao-Guang Yue, Chi-Hua Chen , and Feng-Jang Hwang 
Editorial (4 pages), Article ID 9796535, Volume 2023 (2023)

Automatic Recharging Path Planning for Cleaning Robots

Bing Hao , He Du , Xuefeng Dai , and Hong Liang 
Research Article (19 pages), Article ID 5558096, Volume 2021 (2021)







Interactive Virtual Reality Touring System: A Case Study of Shulin Ji'an Temple in Taiwan

Jung-Hua Lo , Shih-Da Wu , and Min-Jie You 
Research Article (15 pages), Article ID 6651916, Volume 2021 (2021)

Rational Supplier Selection Based on Two-Phase Deep Analysis considering Fuzzy QFD and Game Theory

Feng Li , Senhao Luo , Yi Wang , and Chia-Huei Wu 
Research Article (12 pages), Article ID 9979017, Volume 2021 (2021)

Design of Smart Home Service Robot Based on ROS

Jiansheng Peng , Hemin Ye , Qiwen He , Yong Qin , Zhenwu Wan , and Junxu Lu 
Research Article (14 pages), Article ID 5511546, Volume 2021 (2021)


Three-Dimensional UWSN Positioning Algorithm Based on Modified RSSI Values

Qin Qin , Yi Tian, and Xin Wang
Research Article (8 pages), Article ID 5554791, Volume 2021 (2021)

Real-Time Collection Method of Athletes' Abnormal Training Data Based on Machine Learning

Yue Wang 
Research Article (11 pages), Article ID 9938605, Volume 2021 (2021)


Research on Artificial Intelligence Interaction in Computer-Aided Arts and Crafts

Juqing Deng  and Xiaofen Chen
Research Article (14 pages), Article ID 5519257, Volume 2021 (2021)


Research on Vertical Search Method of Multidimensional Resources in English Discipline Based on Edge Computing

Yi Xie 
Research Article (10 pages), Article ID 5518135, Volume 2021 (2021)


A Multipath Processing Technology Based on Multiparameter-Combined Observation in GNSS

T. Y. Zhou and B. W. Lian 
Research Article (11 pages), Article ID 5574443, Volume 2021 (2021)

Design of Enterprise Management System Based on Edge Computing Architecture


Yongzhong Yang, Zheng Mei, Benxia Zheng, and Shuoli Qiu 
Research Article (12 pages), Article ID 5512958, Volume 2021 (2021)

A Supply Chain Information Pushing Method for Logistics Park Based on Internet of Things Technology

Zhongqiang Zhang 

Research Article (11 pages), Article ID 5544607, Volume 2021 (2021)

Research on Biomechanical Simulation and Simulation of Badminton Splitting and Hanging Action Based on Edge Computing

Bo Zhang 


Research Article (8 pages), Article ID 5527879, Volume 2021 (2021)

The Bidirectional Information Fusion Using an Improved LSTM Model

Tianwei Zheng , Mei Wang , Yuan Guo, and Zheng Wang


Research Article (15 pages), Article ID 5595898, Volume 2021 (2021)

Cloud Classroom Design for English Education Based on Internet of Things and Data Mining

Xiaohua Luo 


Research Article (8 pages), Article ID 5555006, Volume 2021 (2021)

Gated Recurrent Unit with RSSIs from Heterogeneous Network for Mobile Positioning

Junxiang Wang, Canyang Guo, and Ling Wu 


Research Article (7 pages), Article ID 6679398, Volume 2021 (2021)

Research on the Application of Multimedia Elements in Visual Communication Art under the Internet Background

Wenli Liu 


Research Article (10 pages), Article ID 5525648, Volume 2021 (2021)

Research on Business English Translation Framework Based on Speech Recognition and Wireless Communication

Leida Wu and Lianguan Wu 


Research Article (11 pages), Article ID 5575541, Volume 2021 (2021)

Research on Sports Performance Prediction Based on BP Neural Network

Sitong Yang , Lina Luo, and Baohua Tan

Research Article (8 pages), Article ID 5578871, Volume 2021 (2021)

Web-Based Human-Machine Interfaces of Industrial Controllers in Single-Page Applications

Shyr-Long Jeng , Wei-Hua Chieng, and Yi Chen

Research Article (13 pages), Article ID 6668843, Volume 2021 (2021)


Research on Mining of Applied Mathematics Educational Resources Based on Edge Computing and Data Stream Classification

Liping Lu  and Jing Zhou

Research Article (8 pages), Article ID 5542718, Volume 2021 (2021)

Contents

Network Security Technology of Intelligent Information Terminal Based on Mobile Internet of Things

Ning Sun , Tao Li, Gongfei Song, and Haoran Xia


Research Article (9 pages), Article ID 6676946, Volume 2021 (2021)

Matching Sensor Ontologies with Simulated Annealing Particle Swarm Optimization

Hai Zhu , Xingsi Xue , Aifeng Geng, and He Ren 

Research Article (11 pages), Article ID 5510055, Volume 2021 (2021)

Tourism Destination Preference Prediction Based on Edge Computing

Bin Deng , Jun Xu, and Xin Wei



Research Article (11 pages), Article ID 5512008, Volume 2021 (2021)

Detecting Home and Work Locations from Mobile Phone Cellular Signaling Data

Yingkun Yang , Chen Xiong , Junfan Zhuo , and Ming Cai 


Research Article (13 pages), Article ID 5546329, Volume 2021 (2021)

Multiobjective Model and Improved Artificial Raindrop Algorithm for Virtual Network Mapping

Hejun Xuan , Xuelin Zhao, Lei You , Zhenghui Liu, and Yanling Li


Research Article (10 pages), Article ID 5542670, Volume 2021 (2021)

Research on the Balanced Relationship between Online Consumer Behavior and E-Commerce Service Quality Based on 5G Network

Yuna Si 



Research Article (12 pages), Article ID 5562996, Volume 2021 (2021)

Design of Minimizing Expected Energy of Multisource Wireless Cooperative Network Based on Multiobjective Optimization

Shusheng Wang 

Research Article (9 pages), Article ID 5517029, Volume 2021 (2021)

Online Learning Support Service System Architecture Based on Location Service Architecture

Yongyan Zhao  and Shaonan Shan 

Research Article (11 pages), Article ID 6663934, Volume 2021 (2021)

Community Public Safety Evaluation System Based on Location Information Service Architecture

Zili Zhao 



Research Article (10 pages), Article ID 6694757, Volume 2021 (2021)

Analysis and Prediction of Overloaded Extra-Heavy Vehicles for Highway Safety Using Machine Learning


Yi-Hsin Lin , Suyu Gu, Wei-Sheng Wu, Rujun Wang, and Fan Wu

Research Article (20 pages), Article ID 6667897, Volume 2020 (2020)


LEO Satellite Channel Allocation Scheme Based on Reinforcement Learning

Fei Zheng, Zhao Pi , Zou Zhou , and Kaixuan Wang

Research Article (10 pages), Article ID 8868888, Volume 2020 (2020)



An Improved Indoor Positioning Technique Based on Receiving Signal's Strength

Xingsi Xue , Xiaoquan Lin, Chaofan Yang, and Xiaojing Wu

Research Article (10 pages), Article ID 8822288, Volume 2020 (2020)

Editorial

Architecture, Technologies, and Applications of Location-Based Services

Hsu-Yang Kung ¹, **Xiao-Guang Yue**,² **Chi-Hua Chen** ³, and **Feng-Jang Hwang** ⁴

¹Department of Management Information Systems, National Pingtung University of Science and Technology, Taiwan

²School of Sciences, European University Cyprus, Cyprus

³College of Computer and Data Science, Fuzhou University, China

⁴School of Mathematical and Physical Sciences, University of Technology Sydney, Australia

Correspondence should be addressed to Chi-Hua Chen; chihua0826@gmail.com

Received 14 June 2022; Accepted 14 June 2022; Published 28 July 2023

Copyright © 2023 Hsu-Yang Kung et al. This is an open access article distributed under the Creative Commons Attribution License, which permits unrestricted use, distribution, and reproduction in any medium, provided the original work is properly cited.

Several location-based service (LBS) applications (e.g., navigation [1], location tracking [2], intelligent transportation systems (ITS) [3–6], location-based mobile commerce [7], location-based emergency services [8], and location-based event recommendation [9]) have been designed and implemented based on advanced positioning techniques and mobile/cellular communication techniques. For obtaining the LBS applications, mobile devices (MDs) and LBS servers are designed in the architecture of LBS. The LBS servers can receive and analyze the location information of MDs which can be estimated by advanced positioning techniques (e.g., satellite positioning, and mobile positioning) for providing LBS applications. For improving the accuracy of location information, the network signals including angle of arrival [10], time differences [11–14], and received signal strength indication (RSSI) [15] from satellites networks [16], mobile/cellular networks [17], and wireless networks [18] could be collected and analyzed to obtain more precise location information. Moreover, in recent years, artificial intelligence (AI) techniques including expert systems, rule-based systems, machine learning (ML) methods [19], and deep learning (DL) methods [20] have been adopted for the development of LBS applications. A variety of LBS applications in companies, organizations, and governments have been designed and implemented for obtaining location-based information and LBS to their MDs. This special issue covers

LBS architectures [21], satellite positioning techniques [22], mobile positioning techniques [23], positioning techniques based on ML methods [24], communication techniques [25], and ITS [26–28]. This special issue has collected papers on the principles of LBS and LBS technologies including the advanced satellites positioning techniques, advanced mobile/cellular positioning techniques, advanced indoor/outdoor positioning techniques, advanced ITS, advanced positioning techniques based on ML methods, advanced positioning techniques based on DL methods, advanced positioning techniques based on information security and network security techniques, advanced positioning techniques based on parallel computing and distributed computing techniques, and the implementation of LBS applications for smartphones [29–33]. The LBS applications in ITS, indoor/outdoor navigation systems, LBS for industry applications, LBS for education applications, LBS for art applications, and LBS for sport applications have also been mentioned. Topics covered in this special issue are categorized into the following eight themes: (1) mobile positioning methods, (2) navigation applications, (3) logistic applications, (4) core techniques, (5) LBS for industry, (6) LBS for education, (7) LBS for art, and (8) LBS for sports. A total of 32 accepted papers have been published; these papers are categorized into the aforementioned eight themes that are briefly introduced in this paper.

1. Mobile Positioning Methods

This special issue includes five papers on mobile positioning methods which are listed as follows. The RSSIs from mobile/cellular networks, wireless networks, wireless sensor networks, and heterogeneous network were collected and analyzed for indoor positioning [34–37]. Furthermore, the signals from satellites networks were collected and analyzed for outdoor positioning [38]. Detailed information of each article could be found in [34–38].

2. Navigation Applications

This special issue includes four papers on navigation applications which are listed as follows. The navigation applications based on LSB were developed for cleaning robots [39] and smart home service robots [40]. Moreover, the LSB and virtual reality techniques were implemented for tourism applications [41, 42]. Detailed information of each article could be found in [39–42].

3. Logistic Applications

This special issue includes three papers on logistic applications which are listed as follows. ML methods [43], game theory [44], and internet of things (IoT) [45] were developed for logistic applications based on LSB. Detailed information of each article regarding logistic applications could be found in [43–45].

4. Core Techniques

This special issue includes five papers on core techniques which are listed as follows. For improving optimization techniques, advanced particle swarm optimization (PSO) [46] and advanced Multiobjective Optimization (MO) [47, 48] were proposed to obtain LSB applications. For improving security and networking techniques, advanced network security technology [49] and advanced satellite channel allocation schemes were proposed to obtain LSB applications. Detailed information of each article on core techniques could be found in [46–50].

5. LBS for Industry

This special issue includes five papers on LBS for industry which are listed as follows. LSB techniques were applied on enterprise management systems [51], improved LSTM models for industry system [52], human-machine interfaces [53], e-commerce services [54], and public safety evaluation system [55] for providing industry applications. Detailed information of each article related to LBS for industry could be found in [51–55].

6. LBS for Education

This special issue includes five papers on LBS for education which are listed as follows. LSB techniques were applied on vertical search methods [56], cloud classrooms [57], speech recognition [58], data stream classification [59], and online

learning support service system based on LBS for providing education applications. Detailed information of each article on LBS for education could be found in [56–60].

7. LBS for Art

This special issue includes two papers on LBS for art which are listed as follows. The art applications based on LSB were developed for AI-based computer-aided arts [61] and visual communication art [62]. Detailed information of each article with respect to LBS for art could be found in [61, 62].

8. LBS for Sports

This special issue includes three papers on LBS for sport which are listed as follows. LSB techniques were applied on Athletes' abnormal training [63], sport performance prediction [64], and biomechanical simulation and simulation [65]. Detailed information of each article on LBS for sports could be found in [63–65].

Conflicts of Interest

The authors declare no conflicts of interest.

Hsu-Yang Kung
Xiao-Guang Yue
Chi-Hua Chen
Feng-Jang Hwang

References

- [1] G. Y. Chen, M. Gan, C. L. P. Chen, and L. Chen, "A two-stage estimation algorithm based on variable projection method for GPS positioning," *IEEE Transactions on Instrumentation and Measurement*, vol. 67, no. 11, pp. 2518–2525, 2018.
- [2] Z. Yu, L. Han, C. Chen, W. Guo, and Z. Yu, "Object tracking by the least spatiotemporal searches," *IEEE Internet of Things Journal*, vol. 8, no. 16, pp. 12934–12946, 2021.
- [3] M. He and F. Chen, "Extinction and stability of an impulsive system with pure delays," *Applied Mathematics Letters*, vol. 91, pp. 128–136, 2019.
- [4] C. H. Chen, F. J. Hwang, and H. Y. Kung, "Travel time prediction system based on data clustering for waste collection vehicles," *IEICE Transactions on Information and Systems*, vol. E102.D, no. 7, pp. 1374–1383, 2019.
- [5] M. Pan, Y. Liu, J. Cao, Y. Li, C. Li, and C. H. Chen, "Visual recognition based on deep learning for navigation mark classification," *IEEE Access*, vol. 8, pp. 32767–32775, 2020.
- [6] X. Ke and Y. Zhang, "Fine-grained vehicle type detection and recognition based on dense attention network," *Neurocomputing*, vol. 399, pp. 247–257, 2020.
- [7] P. Ramasamy, V. Ranganathan, V. Palanisamy, and S. Kadry, "Securing one-time password generation using elliptic-curve cryptography with self-portrait photograph for mobile commerce application," *Multimedia Tools and Applications*, vol. 79, no. 23–24, pp. 17081–17099, 2020.
- [8] C. L. Chen, T. T. Yang, Y. Y. Deng, and C. H. Chen, "A secure Internet of Things medical information sharing and emergency notification system based on nonrepudiation

- mechanism,” *Wireless Communications and Mobile Computing*, vol. 32, no. 5, 2021.
- [9] X. Liao, L. Zhang, J. Wei, D. Yang, and G. Chen, “Recommending mobile microblog users via a tensor factorization based on user cluster approach,” *Wireless Communications and Mobile Computing*, vol. 2018, Article ID 9434239, 11 pages, 2018.
 - [10] Y. Ma, L. Yang, and X. Zheng, “A geometry-based non-stationary MIMO channel model for vehicular communications,” *China Communications*, vol. 15, no. 7, pp. 30–38, 2018.
 - [11] B. V. Krishnaveni, K. S. Reddy, and P. R. Reddy, “Indoor positioning and tracking by coupling IMU and UWB with the extended Kalman filter,” *IETE Journal of Research*, pp. 1–10, 2022.
 - [12] M. Martalo, S. Perri, G. Verdano, F. De Mola, F. Monica, and G. Ferrari, “Improved UWB TDoA-based positioning using a single hotspot for industrial IoT applications,” *IEEE Transactions on Industrial Informatics*, vol. 18, no. 6, pp. 3915–3925, 2022.
 - [13] O. Bialer, D. Raphaeli, and A. J. Weiss, “Unsynchronized OFDM network positioning in multipath,” *Signal Processing*, vol. 168, p. 107344, 2020.
 - [14] Y. Wang, X. Shang, and K. Peng, “Relocating mining microseismic earthquakes in a 3-D velocity model using a windowed cross-correlation technique,” *IEEE Access*, vol. 8, pp. 37866–37878, 2020.
 - [15] C. Guo, L. Wu, C. Shi, and C. H. Chen, “Mobile positioning based on TAE-GRU,” in *Proceedings of the 2021 Web Conference*, Ljubljana, Slovenia, April 2021.
 - [16] Q. Guan, C. Fan, J. Zheng, G. Wang, and G. Chen, “Multistep weighted least squares estimation method for improving single-point positioning accuracy,” *Wireless Communications and Mobile Computing*, vol. 13, no. 3, 2019.
 - [17] H. Y. Kung, C. H. Chen, M. H. Lin, and T. Y. Wu, “Design of seamless handoff control based on vehicular streaming communications,” *Journal of Internet Technology*, vol. 20, no. 7, pp. 2083–2097, 2019.
 - [18] N. N. Xiong, W. Wu, C. Wu, and H. Cheng, “An improved node localization algorithm based on positioning accurately in WSN,” *Journal of Internet Technology*, vol. 20, no. 5, pp. 1323–1332, 2019.
 - [19] R. Cheng, Y. Song, D. Chen, and X. Ma, “Intelligent positioning approach for high speed trains based on ant colony optimization and machine learning algorithms,” *IEEE Transactions on Intelligent Transportation Systems*, vol. 20, no. 10, pp. 3737–3746, 2019.
 - [20] C. Shi, L. Fang, Z. Lv, and H. Shen, “Improved generative adversarial networks for VHR remote sensing image classification,” *IEEE Geoscience and Remote Sensing Letters*, vol. 19, pp. 1–5, 2022.
 - [21] Y. Peng, L. Wang, J. Cui, X. Liu, H. Li, and J. Ma, “LS-RQ: a lightweight and forward-secure range query on geographically encrypted data,” *IEEE Transactions on Dependable and Secure Computing*, vol. 19, no. 1, pp. 388–401, 2022.
 - [22] A. Kaczmarek, W. Rohm, L. Klingbeil, and J. Tchorzewski, “Experimental 2D extended Kalman filter sensor fusion for low-cost GNSS/IMU/Odometers precise positioning system,” *Measurement*, vol. 193, p. 110963, 2022.
 - [23] L. Altin, R. Ahas, S. Silm, and E. Saluveer, “Megastar concerts in tourism: a study using Mobile phone data,” *Scandinavian Journal of Hospitality and Tourism*, vol. 22, no. 2, pp. 161–180, 2022.
 - [24] C. Shi, Y. Dang, L. Fang, Z. Lv, and M. Zhao, “Hyperspectral image classification with adversarial attack,” *IEEE Geoscience and Remote Sensing Letters*, vol. 19, p. 5510305, 2022.
 - [25] W. Guo, J. Li, X. Liu, and Y. Yang, “Privacy-preserving compressive sensing for real-time traffic monitoring in urban city,” *IEEE Transactions on Vehicular Technology*, vol. 69, no. 12, pp. 14510–14522, 2020.
 - [26] A. A. Abdallah, C. S. Jao, Z. M. Kassas, and A. M. Shkel, “A pedestrian indoor navigation system using deep-learning-aided cellular signals and ZUPT-aided foot-mounted IMUs,” *IEEE Sensors Journal*, vol. 22, no. 6, pp. 5188–5198, 2022.
 - [27] I. Belhajem, Y. Ben Maissa, and A. Tamtaoui, “Improving low cost sensor based vehicle positioning with machine learning,” *Control Engineering Practice*, vol. 74, pp. 168–176, 2018.
 - [28] K. Dalton, M. Skrobe, H. Bell et al., “Marine-related learning networks: shifting the paradigm toward collaborative ocean governance,” *Frontiers in Marine Science*, vol. 7, p. 595054, 2020.
 - [29] H. Chen, H. Jin, and S. Wu, “Minimizing inter-server communications by exploiting self-similarity in online social networks,” *IEEE Transactions on Parallel and Distributed Systems*, vol. 27, no. 4, pp. 1116–1130, 2016.
 - [30] C. Shi, Y. Dang, L. Fang, Z. Lv, and H. Shen, “Attention-guided multispectral and panchromatic image classification,” *Remote Sensing*, vol. 13, p. 4823, 2022.
 - [31] W. Guo, Y. Shi, and S. Wang, “A unified scheme for distance metric learning and clustering via rank-reduced regression,” *IEEE Transactions on Systems, Man, and Cybernetics*, vol. 51, no. 8, pp. 5218–5229, 2021.
 - [32] C. Shi, Z. Lv, H. Shen, L. Fang, and Z. You, “Improved metric learning with the CNN for very-high-resolution remote sensing image classification,” *IEEE Journal of Selected Topics in Applied Earth Observations and Remote Sensing*, vol. 14, pp. 631–644, 2021.
 - [33] C. Wu, F. Wu, L. Lyu, Y. Huang, and X. Xie, “Communication-efficient federated learning via knowledge distillation,” *Nature Communications*, vol. 13, no. 1, p. 2032, 2022.
 - [34] X. Xue, X. Lin, C. Yang, and X. Wu, “An improved indoor positioning technique based on receiving signal’s strength,” *Mobile Information Systems*, vol. 2020, 8822210 pages, 2020.
 - [35] Q. Qin, Y. Tian, and X. Wang, “Three-dimensional UWSN positioning algorithm based on modified RSSI values,” *Mobile Information Systems*, vol. 2021, Article ID 5554791, 8 pages, 2021.
 - [36] J. Wang, C. Guo, and L. Wu, “Gated recurrent unit with RSSIs from heterogeneous network for mobile positioning,” *Mobile Information Systems*, vol. 2021, Article ID 6679398, 7 pages, 2021.
 - [37] Y. Yang, C. Xiong, J. Zhuo, and M. Cai, “Detecting home and work locations from mobile phone cellular signaling data,” *Mobile Information Systems*, vol. 2021, Article ID 5546329, 2021.
 - [38] T. Y. Zhou and B. W. Lian, “A multipath processing technology based on multiparameter-combined observation in GNSS,” *Mobile Information Systems*, vol. 2021, Article ID 5574443, 11 pages, 2021.
 - [39] B. Hao, H. Du, X. Dai, and H. Liang, “Automatic recharging path planning for cleaning robots,” *Mobile Information Systems*, vol. 2021, Article ID 5558096, 19 pages, 2021.

- [40] J. Peng, H. Ye, Q. He, Y. Qin, Z. Wan, and J. Lu, "Design of smart home service robot based on ROS," *Mobile Information Systems*, vol. 2021, Article ID 5511546, 14 pages, 2021.
- [41] J. H. Lo, S. D. Wu, and M. J. You, "Interactive virtual reality touring system: a case study of Shulin Ji'an Temple in Taiwan," *Mobile Information Systems*, vol. 2021, Article ID 6651916, 15 pages, 2021.
- [42] B. Deng, J. Xu, and X. Wei, "Tourism destination preference prediction based on edge computing," *Mobile Information Systems*, vol. 2021, Article ID 5512008, 11 pages, 2021.
- [43] Y. H. Lin, S. Gu, W. S. Wu, R. Wang, and F. Wu, "Analysis and prediction of overloaded extra-heavy vehicles for highway safety using machine learning," *Mobile Information Systems*, vol. 2020, Article ID 6667897, 20 pages, 2020.
- [44] F. Li, S. Luo, Y. Wang, and C. H. Wu, "Rational supplier selection based on two-phase deep analysis considering fuzzy QFD and game theory," *Mobile Information Systems*, vol. 2021, Article ID 9979017, 12 pages, 2021.
- [45] X. Xue, X. Lin, C. Yang, and X. Wu, "A supply chain information pushing method for logistics park based on internet of things technology," *Mobile Information Systems*, vol. 2021, Article ID 5544607, 11 pages, 2021.
- [46] H. Zhu, X. Xue, A. Geng, and H. Ren, "Matching sensor ontologies with simulated annealing particle swarm optimization," *Mobile Information Systems*, vol. 2021, Article ID 5510055, 11 pages, 2021.
- [47] S. Wang, "Design of minimizing expected energy of multi-source wireless cooperative network based on multiobjective optimization," *Mobile Information Systems*, vol. 2021, Article ID 5517029, 9 pages, 2021.
- [48] H. Xuan, X. Zhao, L. You, Z. Liu, and Y. Li, "Multiobjective model and improved artificial raindrop algorithm for virtual network mapping," *Mobile Information Systems*, vol. 2021, Article ID 5542670, 10 pages, 2021.
- [49] N. Sun, T. Li, G. Song, and H. Xia, "Network security technology of intelligent information terminal based on mobile internet of things," *Mobile Information Systems*, vol. 2021, Article ID 6676946, 9 pages, 2021.
- [50] F. Zheng, Z. Pi, Z. Zhou, and K. Wang, "LEO satellite channel allocation scheme based on reinforcement learning," *Mobile Information Systems*, vol. 2020, Article ID 8868888, 10 pages, 2020.
- [51] Y. Yang, Z. Mei, B. Zheng, and S. Qiu, "Design of enterprise management system based on edge computing architecture," *Mobile Information Systems*, vol. 2021, Article ID 5512958, 12 pages, 2021.
- [52] T. Zheng, M. Wang, Y. Guo, and Z. Wang, "The bidirectional information fusion using an improved LSTM model," *Mobile Information Systems*, vol. 2021, Article ID 5595898, 15 pages, 2021.
- [53] S. L. Jeng, W. H. Chieng, and Y. Chen, "Web-based human-machine interfaces of industrial controllers in single-page applications," *Mobile Information Systems*, vol. 2021, Article ID 6668843, 13 pages, 2021.
- [54] Y. Si, "Research on the balanced relationship between online consumer behavior and E-commerce service quality based on 5G network," *Mobile Information Systems*, vol. 2021, Article ID 5562996, 12 pages, 2021.
- [55] Z. Zhao, "Community public safety evaluation system based on location information service architecture," *Mobile Information Systems*, vol. 2021, Article ID 6694757, 10 pages, 2021.
- [56] Y. Xie, "Research on vertical search method of multidimensional resources in English discipline based on edge computing," *Mobile Information Systems*, vol. 2021, Article ID 5518135, 10 pages, 2021.
- [57] X. Luo, "Cloud classroom design for English education based on internet of things and data mining," *Mobile Information Systems*, vol. 2021, Article ID 5555006, 8 pages, 2021.
- [58] L. Wu and L. Wu, "Research on business English translation framework based on speech recognition and wireless communication," *Mobile Information Systems*, vol. 2021, Article ID 5575541, 11 pages, 2021.
- [59] L. Lu and J. Zhou, "Research on mining of applied mathematics educational resources based on edge computing and data stream classification," *Mobile Information Systems*, vol. article no. 5542718, 2021.
- [60] Y. Zhao and S. Shan, "Online learning support service system architecture based on location service architecture," *Mobile Information Systems*, vol. 2021, Article ID 6663934, 11 pages, 2021.
- [61] J. Deng and X. Chen, "Research on artificial intelligence interaction in computer-aided arts and crafts," *Mobile Information Systems*, vol. 2021, Article ID 5519257, 14 pages, 2021.
- [62] W. Liu, "Research on the application of multimedia elements in visual communication art under the internet background," *Mobile Information Systems*, vol. 2021, Article ID 5525648, 10 pages, 2021.
- [63] Y. Wang, "Real-time collection method of athletes' abnormal training data based on machine learning," *Mobile Information Systems*, vol. 2021, Article ID 9938605, 11 pages, 2021.
- [64] S. Yang, L. Luo, and B. Tan, "Research on sports performance prediction based on BP neural network," *Mobile Information Systems*, vol. 2021, Article ID 5578871, 8 pages, 2021.
- [65] B. Zhang, "Research on biomechanical simulation and simulation of badminton splitting and hanging action based on edge computing," *Mobile Information Systems*, vol. 2021, Article ID 5527879, 8 pages, 2021.

Research Article

Automatic Recharging Path Planning for Cleaning Robots

Bing Hao ¹, He Du ¹, Xuefeng Dai ¹, and Hong Liang ²

¹College of Computer and Control Engineering, Qiqihar University, Qiqihar, Heilongjiang Province, China

²College of Telecommunication and Electronic Engineering, Qiqihar University, Heilongjiang Province, China

Correspondence should be addressed to Bing Hao; haobing_learning@163.com

Received 10 February 2021; Revised 9 August 2021; Accepted 16 August 2021; Published 8 September 2021

Academic Editor: Hsu-Yang Kung

Copyright © 2021 Bing Hao et al. This is an open access article distributed under the Creative Commons Attribution License, which permits unrestricted use, distribution, and reproduction in any medium, provided the original work is properly cited.

To solve the problem of automatic recharging path planning for cleaning robots in complex industrial environments, this paper proposes two environmental path planning types based on designated charging location and multiple charging locations. First, we use the improved Maklink graph to plan the complex environment; then, we use the Dijkstra algorithm to plan the global path to reduce the complex two-dimensional path planning to one dimension; finally, we use the improved fruit fly optimization algorithm (IFOA) to adjust the path nodes for shorting the path length. Simulation experiments show that the effectiveness of using this path planning method in a complex industrial environment enables the cleaning robot to select a designated location or the nearest charging location to recharge when the power is limited. The proposed improved algorithm has the characteristics of a small amount of calculation, high precision, and fast convergence speed.

1. Introduction

Since the first autonomous mobile robot came out in the 1960s, mobile robot technology has developed rapidly. Mobile robot technology not only involves multiple disciplines such as artificial intelligence, pattern recognition, and automatic control but also involves many research topics such as navigation and positioning [1], sensor information fusion [2], path planning [3–5], and motion control [6]. In recent years, due to the advantages of saving labor cost, reusability, and intelligence, mobile robots have been applied to various fields: automatic assembly [7], sorting [8], and maintenance [9] of mobile robots in industrial field; mobile robots for surgery and rehabilitation in medical field [10]; and UAV [11] and AUV [12] in the military field. Among them, cleaning robot is the closest mobile robot to human life, which liberates people from tedious cleaning work coming out.

After decades of technological evolution, the development of cleaning robots is divided into three stages. The first phase started with the advent of the world's first cleaning robot. It was developed by the Swedish home appliance company Electrolux in 2001. The Trilobite sweeping robot produced in 2016 will automatically find the wall closest to

itself when it started to be used and scan along the wall to create a cleaning map. After the trilobite completes the scanning, the area of the map is used to calculate the cleaning time. When the battery is low, it will move to the charging stand for charging and then return to the original working position to continue cleaning. The second stage is to integrate positioning and navigation technology with SLAM to establish a map in real-time and design path planning to achieve. During the cleaning process, the Ecovacs series of cleaning robots combined with laser sensors can enable the robot to restore the room layout during the cleaning process, establish a real-time and accurate positioning system, and make the cleaning process more accurate and efficient. The third stage is to combine artificial intelligence with cleaning robots to realize the functions of human-computer interaction and recognition of complex obstacles and further realize the intelligence and efficiency of cleaning robots.

At any stage, the cleaning robot needs to automatically return to the charging location when the remaining power is limited, and, therefore, it is necessary to plan the return path. In [13], a new optimal path planning algorithm based on convolutional neural network (CNN) is proposed to quickly and efficiently explore the state space. However, it only applies to sampling based algorithms and needs to train the

parameters in advance. To solve the problem of convergence speed of ant colony algorithm, an improved ant colony optimization algorithm for mobile robot path planning based on grid method is proposed by Liu et al. [14]. The approach effectively generates good solutions quickly and lowers the risks of trapping in a local optimum. The disadvantage is that the convergence speed is too fast to get the optimal path. Ajeil et al. [15] propose a modification based on the standard ant colony optimization, which is implemented in association with grid-based modeling for the static and dynamic environments to solve the path planning problem. However, this algorithm has a large amount of computation and cannot quickly plan the path. Generally, the path planning algorithm is divided into two categories: heuristic algorithm [16] and artificial intelligence algorithm [3]. The traditional heuristic algorithm is determined according to the description situation of the established environment. It is usually based on the geometric mathematical model to complete the search of the robot path, and the solutions obtained are all definite values. This method increases exponentially with the complexity of the environment, resulting in very long computing time and inability to obtain a better solution, while the artificial intelligence algorithm applies the instinct of natural creatures to the robot path planning and uses the behavior of the group to find the global optimal solution in a complex space. The solution is not fixed. In complex industrial environments, robots often take a long time to calculate due to the complexity of the environment and cannot return to the charging place without collision and with a short path.

The traditional cleaning robot path planning algorithm is based on the two-dimensional path calculation of the environment map. The amount of calculation increases exponentially with the complexity of the environment, resulting in too long calculation time to reach the designated location. On the other hand, the cleaning robot has collided with the obstacle, causing the loss of the robot. Therefore, this paper combines the Dijkstra algorithm in the heuristic algorithm [17] and the improved fruit fly optimization algorithm (IFOA) in the artificial intelligence algorithm [18] to reduce the amount of calculation and avoid colliding with obstacles. First, the coordinate system of the cleaning robot is established, and the complex environment is modeled; secondly, to simplify the model and reduce the amount of calculation, the improved Maklink graph planning model is adopted; finally, the above-mentioned algorithm is used on this basis to realize the automatic recharging path planning of the cleaning robot.

The main contributions of this paper can be summarized as follows:

- (1) The improved Maklink graph further simplifies the complexity of industrial environment on the basis of Maklink graph. It prevents the cleaning robot from colliding with obstacles and speeds up the computation for later charging path planning.
- (2) It hybridizes the Dijkstra and IFOA to convert two-dimensional path planning into one-dimensional path planning and further reduces the computation.

The IFOA improves the searching precision and avoids too fast convergence rate on the basis of FOA.

- (3) Fixed and multiple charging locations are carried out by considering various complex environments to verify the effectiveness of IFOA. By comparing IFOA with FOA, ACA, and RRT in the same environments, it is proved that the proposed algorithm can make the cleaning robot return to the charging site without collision in a relatively short time.

2. Cleaning Robot Coordinate System

The cleaning robot studied in this paper adopts a moving structure of two standard wheels, each of which is equipped with an independent drive motor, and the purpose of changing the direction of movement of the robot is achieved by controlling the speed difference between the two wheels [19]. In the analysis process, the robot is modeled as a rigid body on wheels [20]. Take the ground as the global reference coordinate system: X and Y , robot local reference coordinate system: X_r and Y_r . The X_r is the longitudinal axis of the robot; Y_r is the lateral axis of the robot. The angle difference between the global reference system and the local reference system is determined by θ .

The global reference system and the local reference system are shown by

$$\dot{P} = (x, y, \theta)^T, \quad (1)$$

$$\dot{P}_r = (x_r, y_r, \theta)^T. \quad (2)$$

The mapping relationship between the two reference systems can be represented by orthogonal rotation transformation [21], as shown by

$$R(\theta) = \begin{bmatrix} \cos \theta & \sin \theta & 0 \\ -\sin \theta & \cos \theta & 0 \\ 0 & 0 & 1 \end{bmatrix}, \quad (3)$$

$$\dot{P} = R(\theta)\dot{P}_r, \quad (4)$$

$$\dot{P} = \begin{bmatrix} x_r \cos \theta + y_r \sin \theta \\ -x_r \sin \theta + y_r \cos \theta \\ \theta \end{bmatrix}. \quad (5)$$

Establishing the robot coordinate system is the primary condition for studying its specific position in the environmental area, judging the relative position of obstacles and the ending point, and laying the foundation for the next step of environmental modeling and path planning.

3. Environmental Modeling Method

Before the autonomous charging path of the cleaning robot is planned, it is necessary to know the specific locations of the cleaning robot, obstacles, starting point, and ending point in the environmental area. The robot is able to return to the charging place without collision with the obstacle [22]

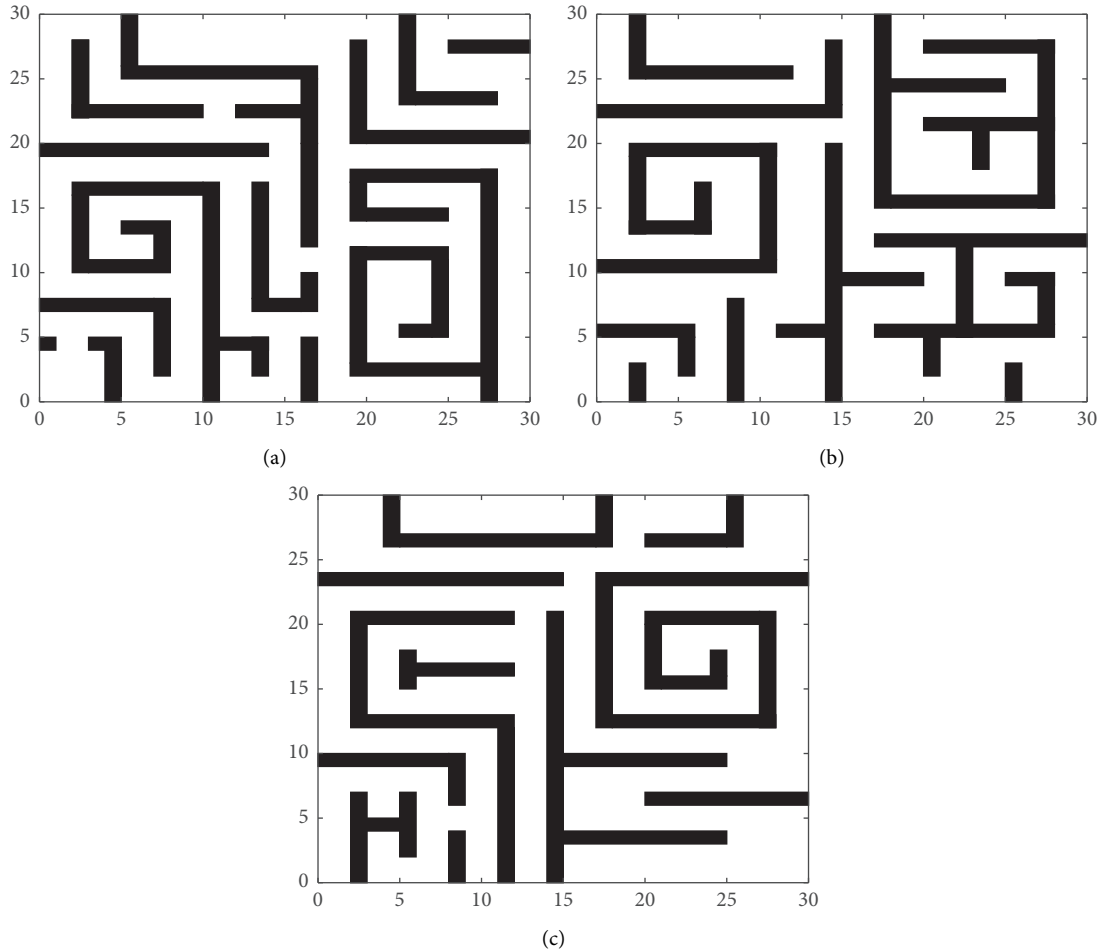


FIGURE 1: Return charging environment. (a) Map 1. (b) Map 2. (c) Map 3.

when the power is limited. Therefore, modeling the environment area has become the basic premise of the autonomy charging path planning of the cleaning robot. An appropriate environment model will help the robot to understand and recognize the environment and reduce the computational complexity of path planning.

3.1. Typical Environmental Modeling Methods.

Environmental modeling is to transform the external environment of the robot into a form that can be recognized by the computer. It is usually divided into three typical methods: Cell Decomposition Approach, Visibility Graph, and Topological Method [23]. Cell Decomposition Approach [24] is divided into precise unit decomposition and approximate unit decomposition. The main idea is to decrease the working environment of the robot into regular base areas, and each area is usually a grid. The description of the grid is used to realize the environment modeling. The advantage is that the model is constructed according to the actual environment, so it is easy to expand and maintain. The description of the environment depends on the fineness of the grid. The finer the grid is, the more the robot can recognize the information in the environment; the

disadvantage is the calculation of path planning based on this method. The quantity mainly depends on the unit decomposition and connected graph search operation. When the object density is high, and the environment is complex, the calculation quantity increases exponentially.

Visibility Graph [25] abstracts the obstacles in the working environment as polygons and connects the mutually visible nodes of the starting point and the target point with the vertices of the obstacle polygon. The unobstructed path between these vertices is the shortest distance between them. The main advantage is that it is simple to implement and is suitable for working areas with simple environments and sparse obstacles, so the path planning in the two-dimensional space of robots is more common. There are two problems in path planning using visual views: one is that the number of nodes and obstacle edges will increase with the number of obstacle polygons; the other is that when used in a complex environment, invalid path efficiency may be significantly reduced. It is not suitable for high-dimensional space above three dimensions.

The Topological Method [26] is a method of dimensionality reduction, in which path planning transforms high-dimensional geometric space into a connectivity problem. The topological graph is composed of nodes and arcs. The

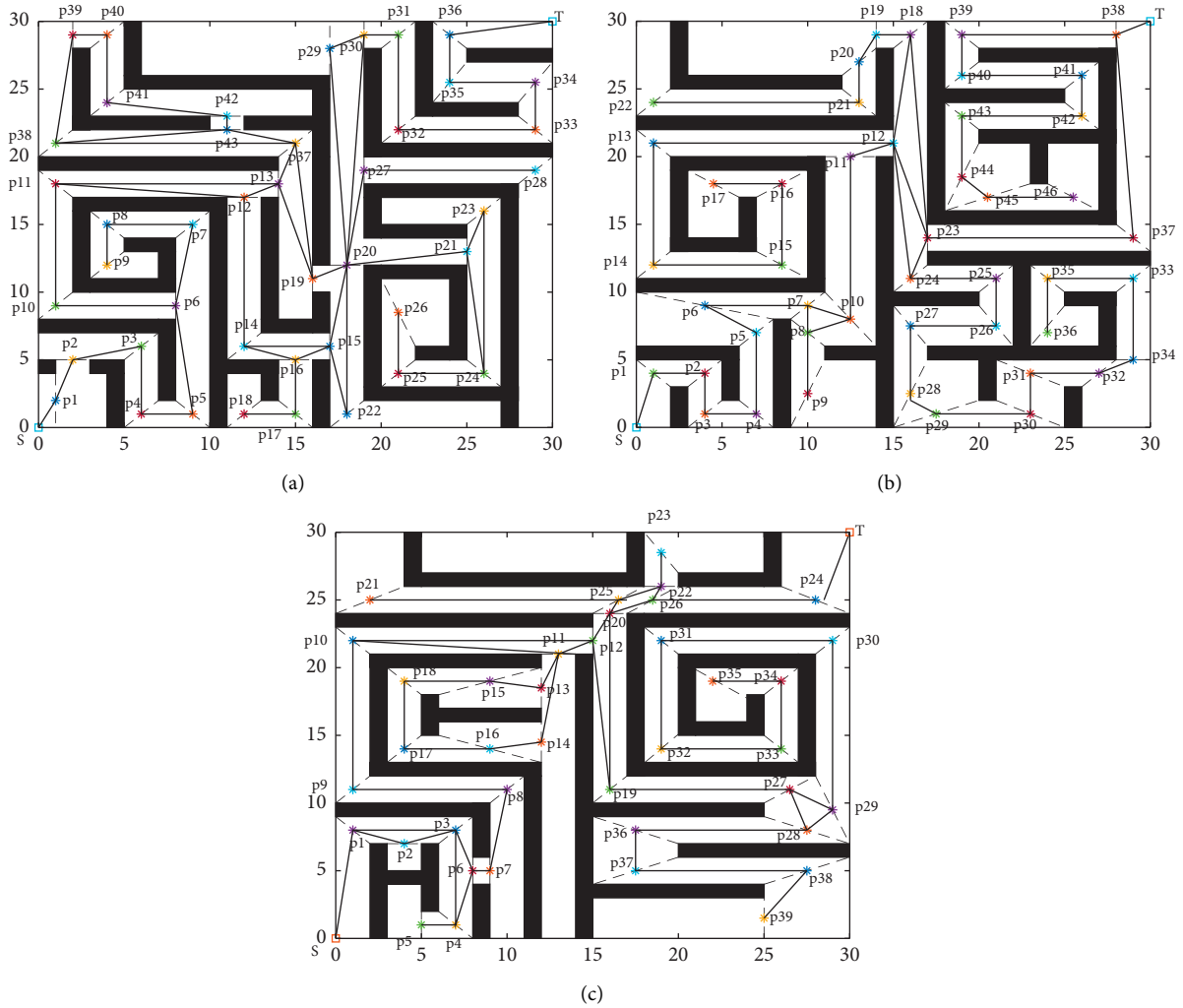


FIGURE 2: Environmental modeling of designated charging locations. (a) Map 1. (b) Map 2. (c) Map 3.

nodes represent a characteristic state or location in the environment. The arcs directly connected between the nodes are equivalent to the paths in the environment. The advantage of the topology method is that it simplifies the map's requirements for precise location, deletes the details of the map, and changes it to a more compact expression, so it reduces the modeling time and storage space and can quickly realize path planning. The disadvantages are also obvious. This method is only suitable for environments with space obstacles; otherwise, it is difficult to perform stable navigation control. On the other hand, when the number of obstacles increases, the environmental information in the topology map is difficult to modify, and the topology is complicated.

3.2. Environmental Modeling Based on Improved Maklink Graph. When the above three typical environment modeling methods are used in a complex environment with dense obstacles, they will cause a large amount of calculation and the robot to collide with obstacles. To solve this problem,

this paper proposes an improved Maklink graph modeling method, which transforms the complex environment into a simple graph theory algorithm to search path, effectively reduces the search, and provides a prerequisite for the next path planning.

The cleaning robot needs to return to the charging location as soon as the remaining power is limited. To solve this problem, this article studies two environments: one is how the robot chooses the shortest path to return to the charging place when a charging location is specified; the other is when there are multiple charging locations, how does the robot judge which is the closest place and return to the charging place with the shortest path?

Therefore, the establishment of a complex environment is shown in Figure 1, a square area with a side length of 30 meters, in which the black area is the wall or obstacle in the environment, and the white area is the area to be cleaned by the cleaning robot. To increase the complexity of the environment, a number of return-type "dead zones" are established in the figure to detect whether the robot can return to the charging place smoothly.

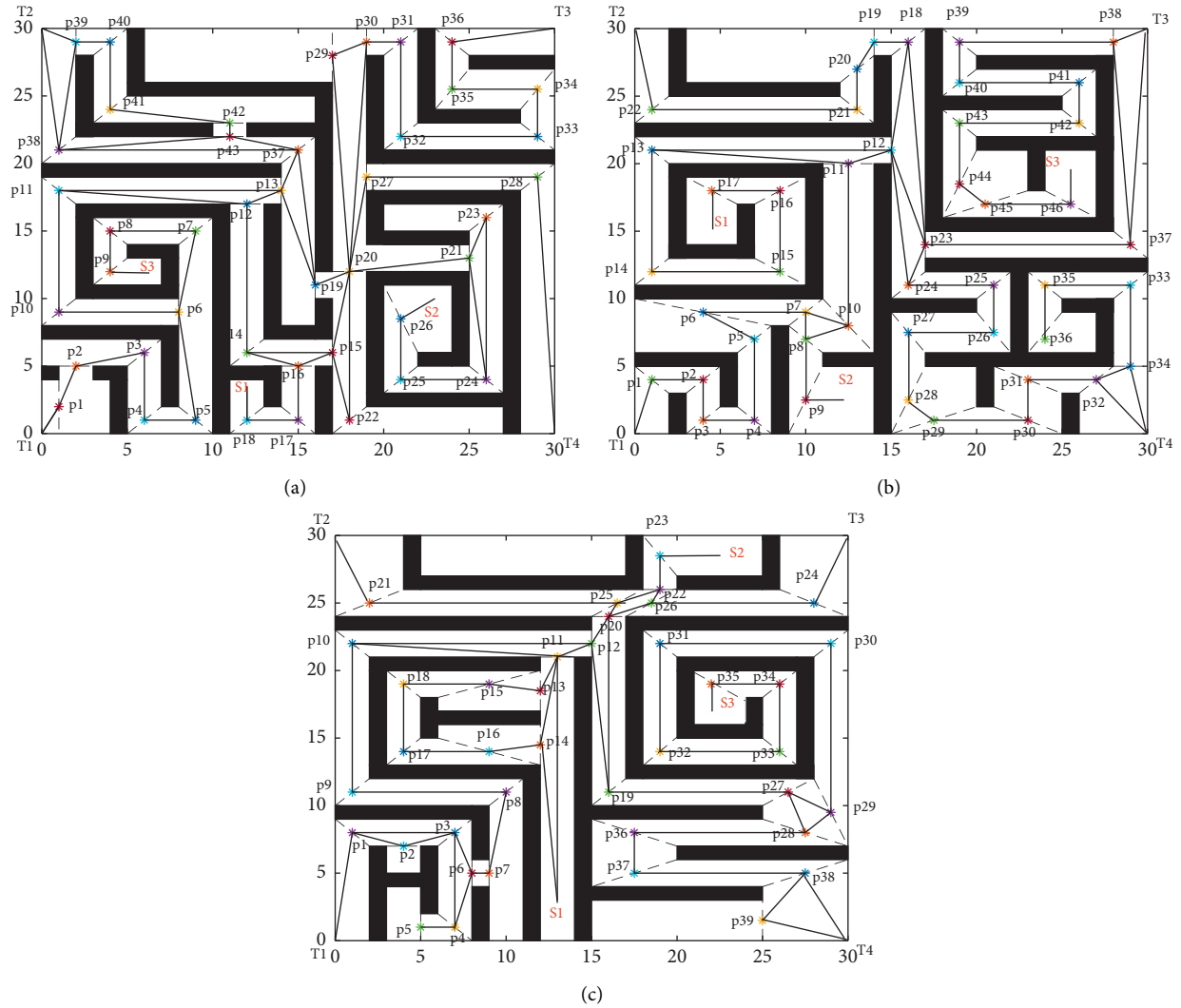


FIGURE 3: Environmental modeling of multiple charging locations. (a) Map 1. (b) Map 2. (c) Map 3.

3.2.1. *Improved Maklink Graph Environment Modeling Method.* The Maklink graph [27, 28] requires the following preconditions when modeling the working area of a cleaning robot:

- (1) The robot only performs motion planning in a two-dimensional plane environment, without considering the height of the robot and the environment;
- (2) Environmental boundaries and obstacles are approximated by convex polygons. The algorithm is based on accurate environment model and location.
- (3) The robot is approximated by “points,” which can appropriately expand the range of obstacles, so that the robot does not collide with obstacles when it moves.

The basic Maklink graph method divides the space to plan the free path that the robot does not collide with obstacles in the environment. It has the characteristics of simplicity and speed [29]. But there are two main disadvantages: one is that it is only suitable for convex polygonal

obstacles; the other is that when dealing with the environment model of complex obstacles, the planned link lines are cumbersome and nonintrusive [30].

Aiming at the above shortcomings, this paper proposes an improved Maklink graph modeling method, which is also suitable for concave polygons and complex obstacle environments, and reduces the number of link lines, thereby reducing the calculation and iteration of the path planning search space frequency. For concave polygons that can be split into two convex polygons that share vertices at the vertices, the purpose of taking the midpoint of the link line in the Maklink graph method is to plan a collision-free path with obstacles, so it is necessary to ensure that the adjacent midpoint is connected by a solid line. After connection, no matter how the robot moves at both ends of the dotted line at the midpoint, the connected solid line does not pass through the obstacle.

The specific steps of the improved Maklink graph method for environmental modeling are as follows:

- (1) Connect the vertices of the nearest obstacles in the environment with dotted lines one by one.

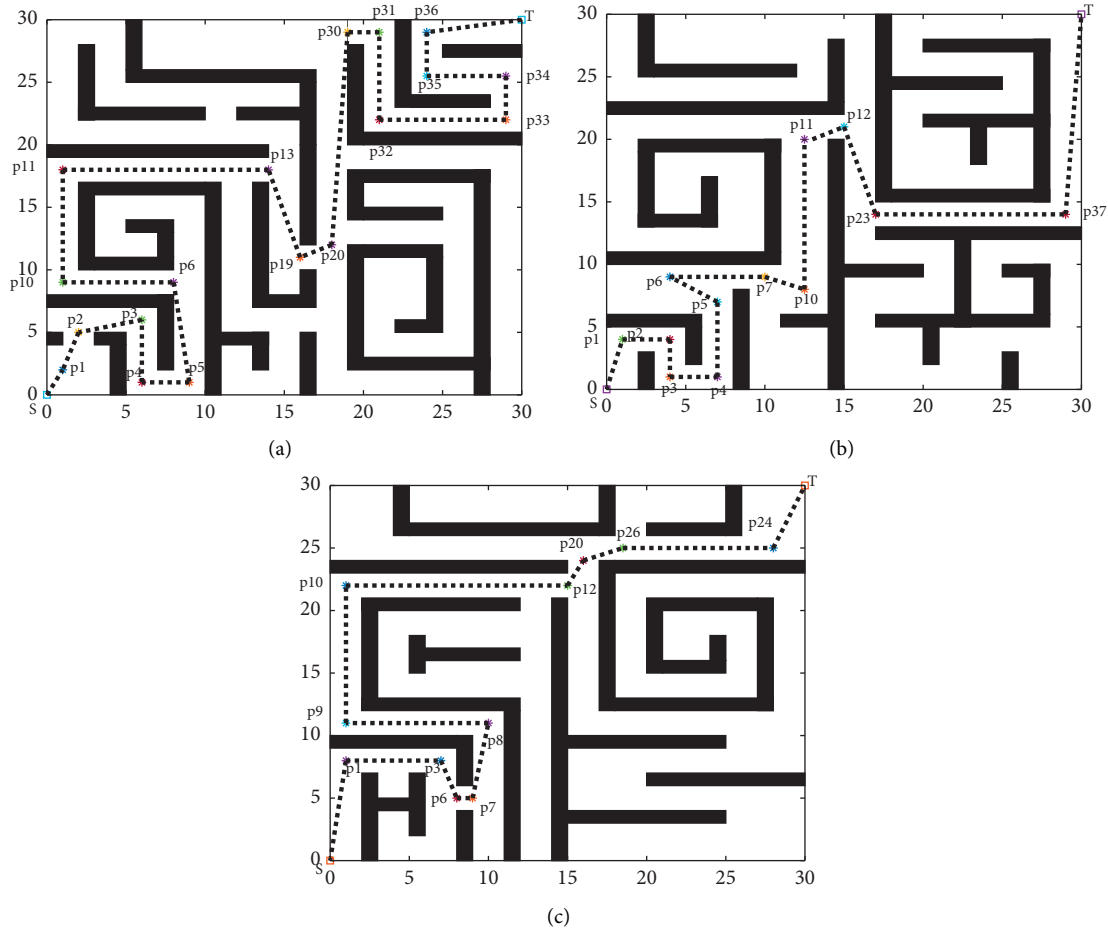


FIGURE 4: Preliminary path of charging location designated by Dijkstra algorithm. (a) Map 1. (b) Map 2. (c) Map 3.

- (2) Take the midpoint of the dotted line to connect with a solid line. When the two ends of the solid line move on the dotted line and cross the obstacle, increase the line from the obstacle to the vertical line of the boundary or the apex of the obstacle.
- (3) For a concave polygon, split into two convex polygons sharing the vertex at the vertex.

3.2.2. Environmental Modeling for One or More Charging Locations. When specifying a charging location, the improved Maklink map planning space is shown in Figure 2, and the midpoint sequence of the link line is identified as $p_0, p_1, p_2 \dots p_n, p(n+1)$. When the robot has low power when $p_0 = S$ (S coordinate is $(0,0)$), it needs to return to $p(n+1) = T$ (T coordinate is $(30,30)$) for charging, and connect S and T to the nearest midpoint to form the robot's free movement path.

When there are multiple charging locations, the improved Maklink map planning space is shown in Figure 3, and the midpoint sequence of the link line is identified as $p_0, p_1, p_2 \dots p_n \dots p(n+4)$. Suppose that the cleaning robot needs to be charged when it is located at points S_1, S_2, S_3 , and the available charging locations in the environment are located at the four corners of the map: $p(n+1) = T_1, p(n+2) = T_2,$

$p(n+3) = T_3, p(n+4) = T_4$. Connect S_1, S_2, S_3 and T_1, T_2, T_3, T_4 to the nearest midpoint to form a free movement path of the robot.

4. Cleaning Robot Charging Path Planning

After the improved Maklink graph environment modeling, the cleaning robot's charging path planning problem is transformed into the shortest path to solve the graph, and the path is two-dimensional path planning [31, 32]. To further reduce the solution space and calculation amount of the algorithm, this paper uses Dijkstra algorithm to simply plan the shortest path in the improved Maklink graph, which converts two-dimensional to one-dimensional path planning, but the resulting path is composed of points in the improved Maklink graph, not the shortest path. Therefore, this paper uses the improved fruit fly optimization algorithm to finely plan the path points, so that the cleaning robot returns to the charging point by the shortest path when the remaining power is limited.

4.1. Preliminary Planning Based on Dijkstra Algorithm. The Dijkstra algorithm was proposed by the Dutch mathematician E.W. Dijkstra in 1959. It is a typical shortest path algorithm for solving the shortest path of a directed graph

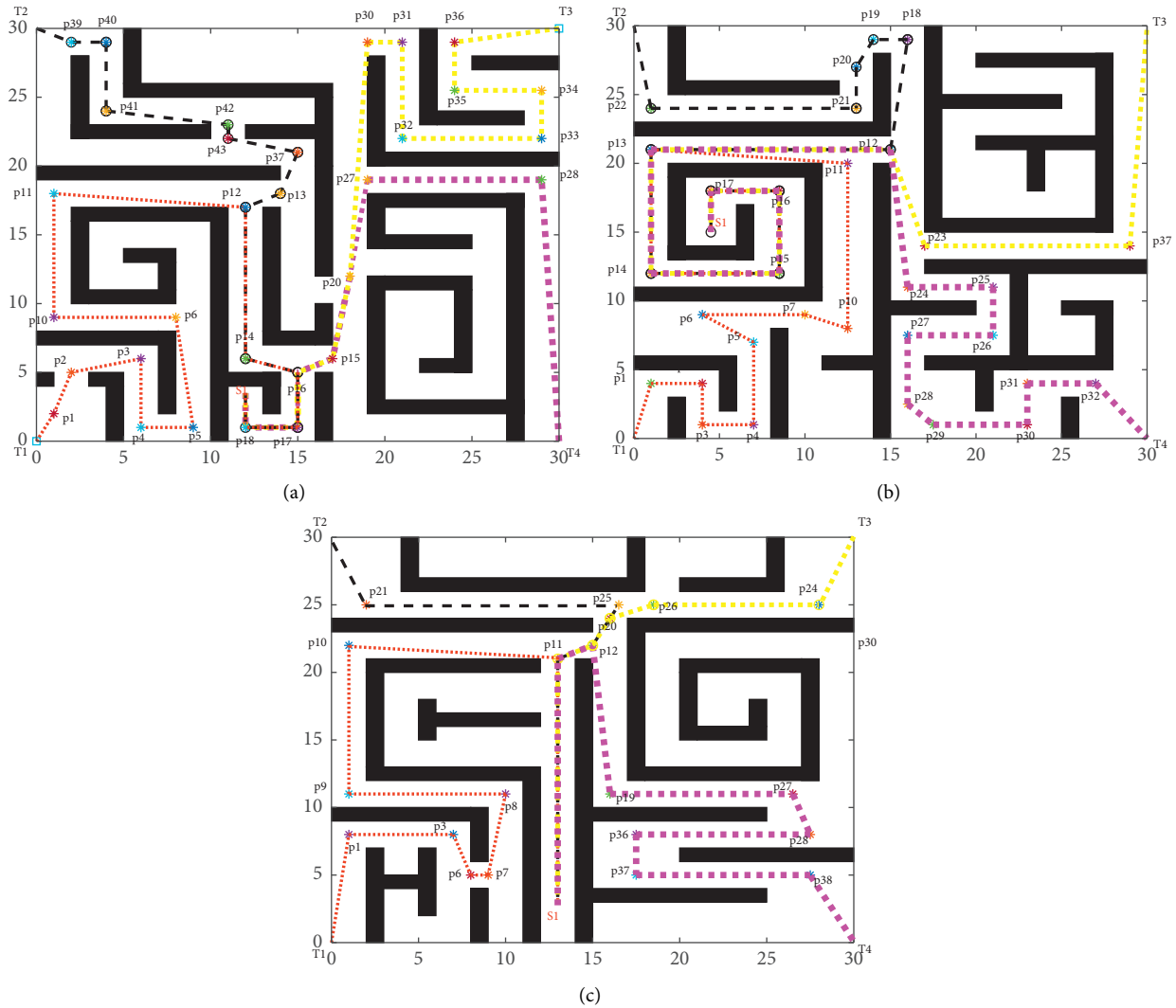


FIGURE 5: Dijkstra algorithm path when the starting point is in S1. (a) Map 1. (b) Map 2. (c) Map 3.

TABLE 1: Distance from S1, S2, and S3 to the four charging locations.

Map 1	T1 (0, 0)	T2 (0, 30)	T3 (30, 30)	T4 (30, 0)
S1 (12, 3.5)	76.2913 m	50.4909 m	69.9310 m	53.9134 m
S2 (23, 10)	92.2263 m	61.8426 m	80.2386 m	64.2238 m
S3 (6, 12)	41.6665 m	59.5753 m	96.7111 m	76.6636 m
Map 2	T1 (0, 0)	T2 (0, 30)	T3 (30, 30)	T4 (30, 0)
S1 (4.5, 15)	84.0328 m	74.8810 m	78.8113 m	87.6712 m
S2 (12.5, 2.5)	37.8648 m	55.7663 m	59.6965 m	68.5564 m
S3 (25.5, 20)	124.1846 m	109.0067 m	45.8574 m	107.9382 m
Map 3	T1 (0, 0)	T2 (0, 30)	T3 (30, 30)	T4 (30, 0)
S1 (13, 3)	73.3489 m	43.4753 m	40.0499 m	73.5339 m
S2 (23, 28.5)	72.6284 m	29.0777 m	21.3851 m	65.5631 m
S3 (22, 17)	132.6538 m	94.6245 m	130.8422 m	79.2115 m

[33]. Its main feature is the breadth-first preliminary traversal search algorithm, with the starting point at the center and being extended to the ending point. It can solve the shortest path of the node from the starting point to the ending point in the figure. The starting point S is specified

when calculating, and divides the points into two sets: H and U , H is to record the vertex of the calculated shortest path and the corresponding shortest path length. U is to record the vertex of the shortest path that is also solved and the distance from the vertex to the starting point S [34].

The specific steps of Dijkstra algorithm are as follows:

- (1) In initialization, specify the starting point S ; H only includes the starting point S , and U includes other vertices except for S
- (2) Select the vertex P with the shortest distance from U , add the vertex P to H , and remove the vertex P from U
- (3) At this time, update the distance of each vertex in U to the starting point S , and use P to update the distance of other vertices
- (4) Repeat steps (2) to (3) until all vertices are traversed

Dijkstra algorithm is used to generate a suboptimal path, which successively passes through the path nodes S, P_1, P_2, \dots, P_d and T . The Maklink lines corresponding to

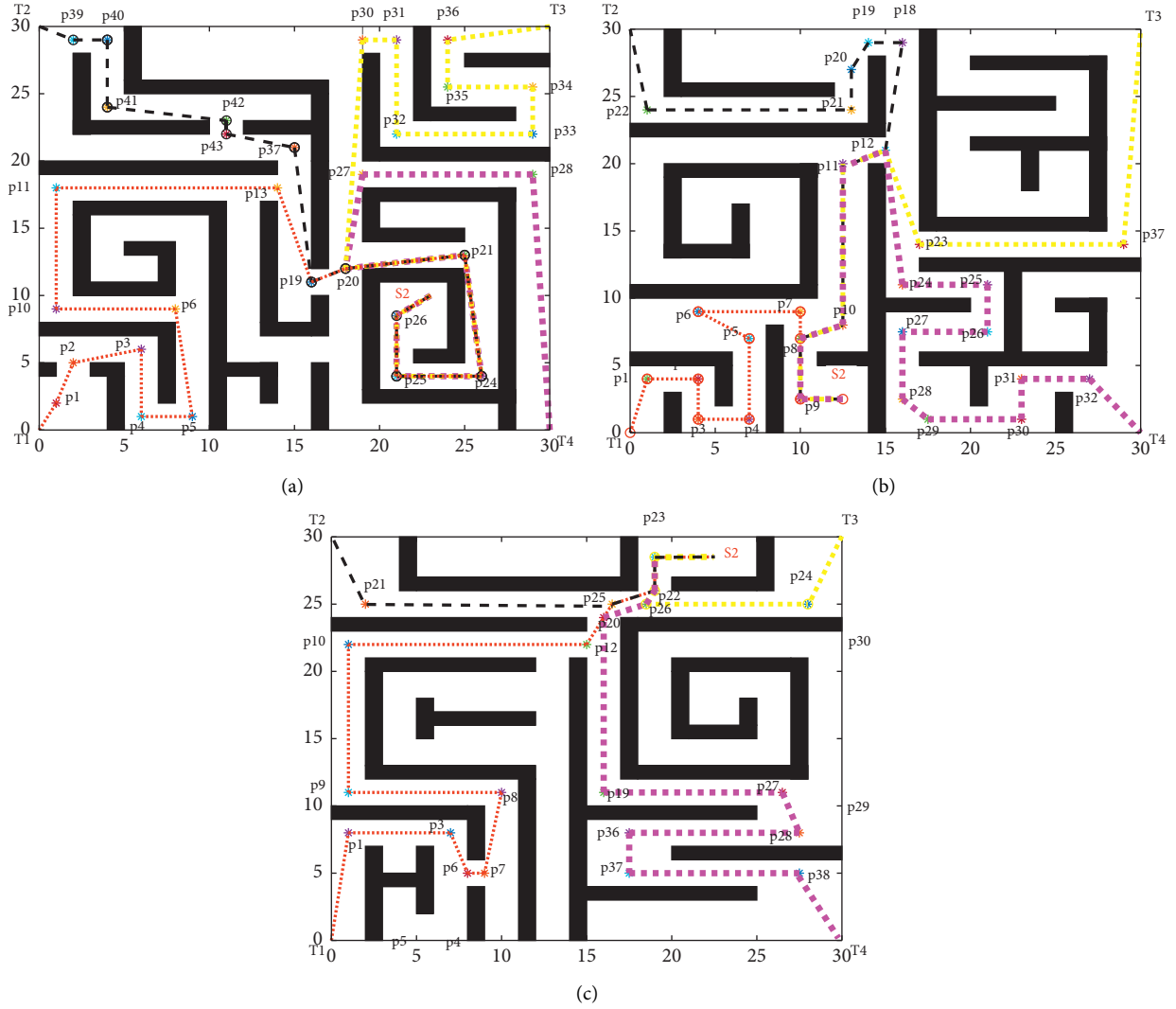


FIGURE 6: Dijkstra algorithm path when the starting point is in S2. (a) Map 1. (b) Map 2. (c) Map 3.

nodes are L_i ($i = 1, 2, \dots, d$). Let A and B be the two ends of C , and the mathematical model of other points on the chain route is

$$P_i(h_i) = P_i^{(0)} + (P_i^{(1)} - P_i^{(0)}) * h_i, \quad h_i \in [0, 1], i = 1, 2, \dots, d, \quad (6)$$

where h_i is the proportional parameter and d is the Maklink's path node.

It can be seen from equation (6) that when the path obtained by the Dijkstra algorithm passes through the Maklink lines, as long as a set of parameters (h_1, h_2, \dots, h_d) is given, a new path from the starting point to the end point can be obtained, and the solution of the fruit fly algorithm is expressed as (h_1, h_2, \dots, h_d) .

The preliminary path planning by Dijkstra algorithm of the designated charging location in Map 1 is $S \rightarrow p1 \rightarrow p2 \rightarrow p3 \rightarrow p4 \rightarrow p5 \rightarrow p6 \rightarrow p10 \rightarrow p11 \rightarrow p13 \rightarrow p19 \rightarrow p20 \rightarrow p30 \rightarrow p31 \rightarrow p32 \rightarrow p33 \rightarrow p34 \rightarrow$

$p35 \rightarrow p36 \rightarrow T$. In Map 2, it is $S \rightarrow p1 \rightarrow p2 \rightarrow p3 \rightarrow p4 \rightarrow p5 \rightarrow p6 \rightarrow p7 \rightarrow p10 \rightarrow p11 \rightarrow p12 \rightarrow p23 \rightarrow p37 \rightarrow T$. In Map 3 is: $S \rightarrow p1 \rightarrow p3 \rightarrow p6 \rightarrow p7 \rightarrow p8 \rightarrow p9 \rightarrow p10 \rightarrow p12 \rightarrow p26 \rightarrow p24 \rightarrow T$. As shown in Figure 4, the path experienced by the black dot is the preliminary path planned by the Dijkstra algorithm, with a total length of 116.2120 m in Map 1, 81.4383 m in Map 2, and 80.0383 m in Map 3.

The method of path planning for multiple charging locations is to use Dijkstra algorithm to first determine the distance from the starting point to the four charging locations and then select the shortest preliminary path based on the improved Maklink graph after sorting. The distance between the starting point and the four charging locations is shown in Table 1.

When the cleaning robot is in S1, the Dijkstra algorithm path of the four charging locations is shown in Figure 5. According to the relative distance, select the closest charging location T2 in Map 1: $S1 \rightarrow p18 \rightarrow p17 \rightarrow p16 \rightarrow p14 \rightarrow p12 \rightarrow p13 \rightarrow p37 \rightarrow p43 \rightarrow p42 \rightarrow p41 \rightarrow p40 \rightarrow p$

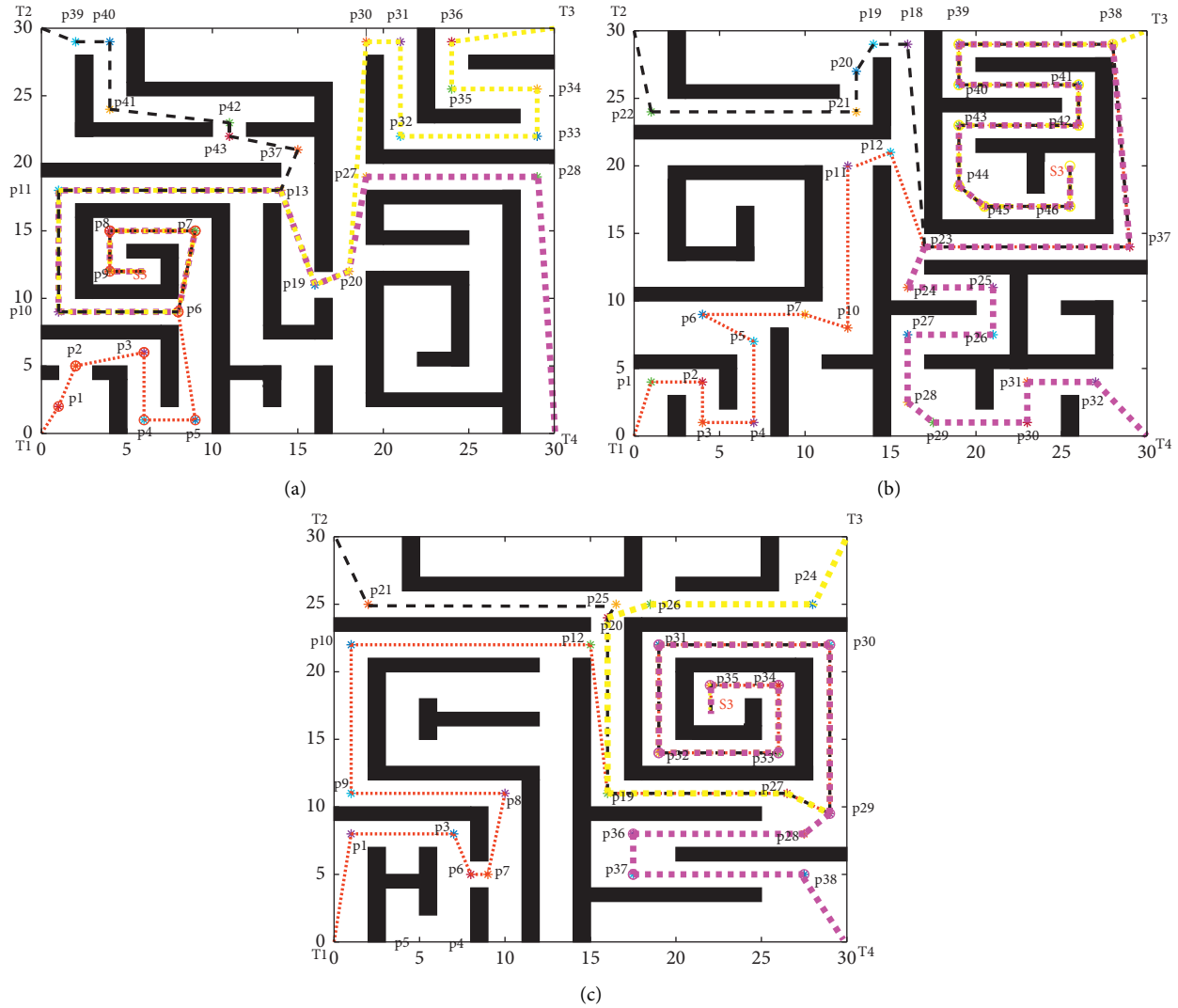


FIGURE 7: Dijkstra algorithm path when the starting point is in S3. (a) Map 1. (b) Map 2. (c) Map 3.

39→T2, the path length is 50.4909 m. Select the closest charging location T2 in Map 2: S1→p17→p16→p15→p14→p13→p12→p18→p19→p20→p21→p22→T2, the path length is 74.8810 m. Select the closest charging location T3 in Map 3: S1→p11→p12→p20→p26→p24→T3, the path length is 40.0499 m.

When the cleaning robot is in S2, the Dijkstra algorithm path of the four charging locations is shown in Figure 6. According to the relative distance, select the closest charging location T2 through the improved Maklink graph for preliminary path planning in Map 1: S2→p26→p25→p24→p21→p20→p19→p37→p43→p42→p41→p40→p39→T2, the path length is 61.8426 m. Select the closest charging location T1 in Map 2: S2→p9→p8→p7→p6→p5→p4→p3→p2→p1→T1, the path length is 37.8648 m. Select the closest charging location T3 in Map 3: S2→p22→p26→p24→T3, the path length is 21.3851 m.

When the cleaning robot is in S3, the Dijkstra algorithm path of the four charging locations is shown in Figure 7. According to the relative distance, select the closest charging location T1 through the improved Maklink graph for preliminary path planning in Map 1: S3→p9→p8→p7→p6→p5→p4→p3→p3→p2→p1→T1, the path length is 41.6665 m. Select the closest charging location T3 in Map 2: S3→p46→p45→p44→p43→p42→p41→p40→p39→p38→T3, the path length is 45.8574 m. Select the closest charging location T3 in Map 2: S3→p35→p34→p33→p32→p31→p30→p29→p28→p36→p37→p38→T4, the path length is 79.2115 m.

4.2. Fine Planning Based on IFOA. The path planned by the Dijkstra algorithm is only a preliminary plan based on the improved Maklink graph. The path can be further optimized by changing the position of the dotted line at the midpoint of the passing. In order to solve this problem, this paper

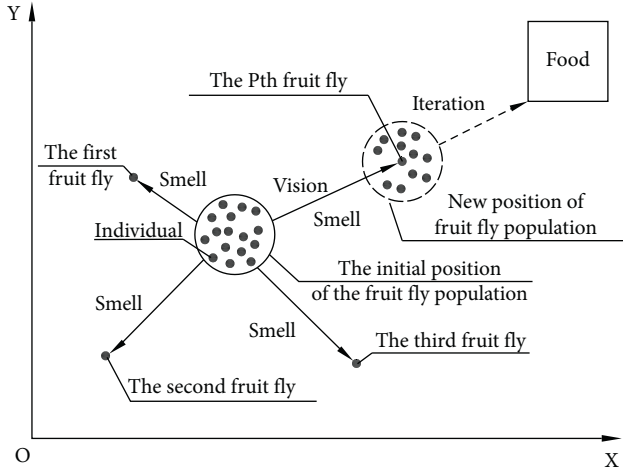


FIGURE 8: The iterative process of FOA.

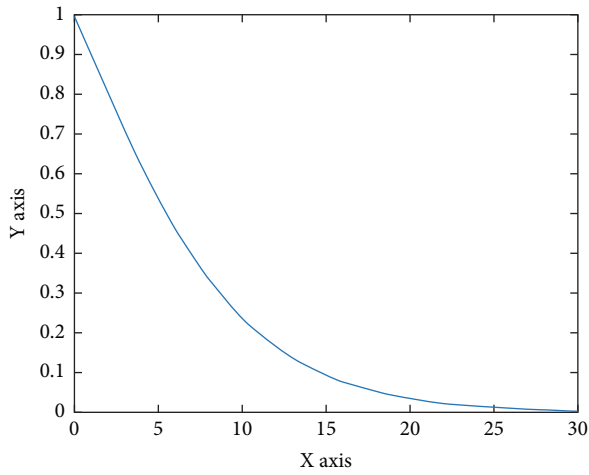


FIGURE 9: Variable distance function image.

proposes fine planning based on the fruit fly optimization algorithm (FOA). The reasons for using the FOA are as follows:

- (1) The calculation is simple and easy to implement
- (2) The global optimization ability is strong
- (3) It is suitable for two-dimensional search optimization problems [35]

The basic principle is based on the two stages of smell and vision during the foraging process of fruit fly. In the smell stage, the individuals in the fruit fly population choose the general direction and position to fly to the food according to the concentration of food pheromone in the air; the visual stage locates the specific position of the food according to the accurate visual position of the food and the position of the companion fruit fly and iterates the food continuously [36], as shown in Figure 8.

Basic FOA have many advantages and disadvantages:

- (1) The initial positions X -axis and Y -axis of the fruit fly population are randomly selected on the global

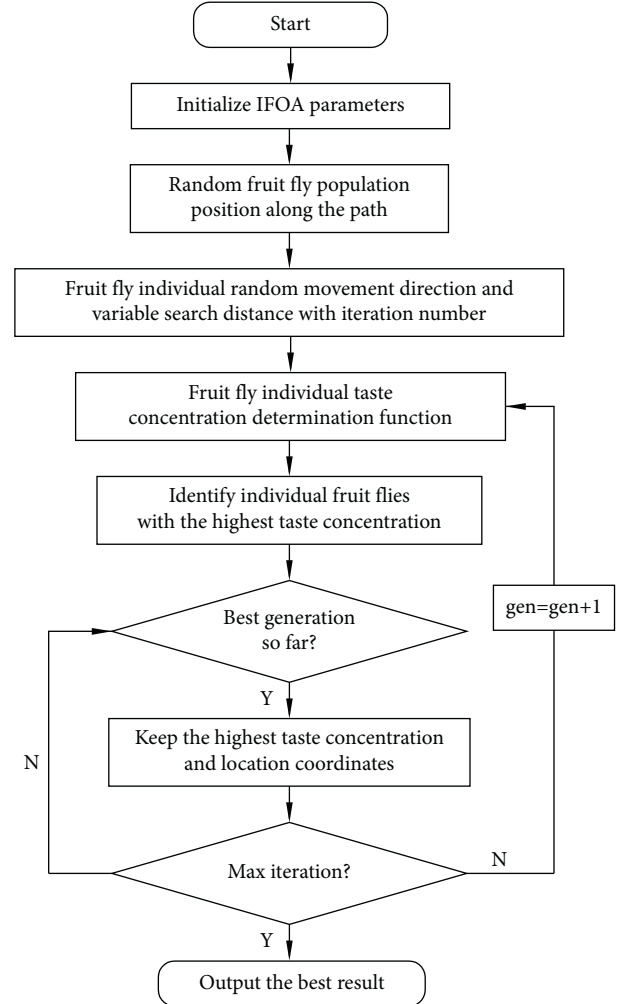


FIGURE 10: IFOA flowchart.

position, which may deviate greatly from the optimal solution, and the convergence speed is slow.

- (2) The flight distance of individual fruit fly searching for food by smell is a fixed value, and the value determines the searchability, and it cannot take into account the global and local searchability. To solve the above problems, this paper proposes an improved fruit fly optimization algorithm that limits the initial position and variable flight distance of the fruit fly population, which effectively accelerates the convergence speed and improves the ability of fine optimization in the later stage. The improvement method is as follows:

Position X -axis and Y -axis, limited to passing through the two ends of the dotted line at the midpoint $p(k)$ of the path; change the single flight distance. Dist of individual fruit fly to a variable function with the number of iterations:

$$\text{Dist} = \text{Len} \left(-\tan h \left(\frac{5 * \text{gen}}{\text{Maxgen}} \right) + 1 \right), \quad (7)$$

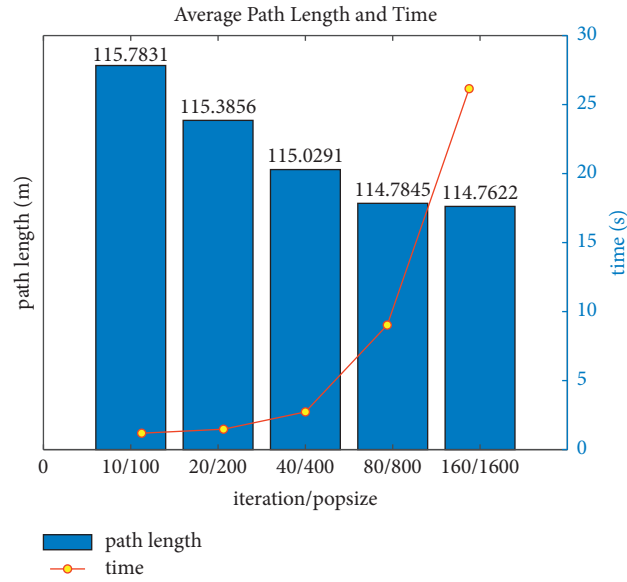


FIGURE 11: Selection of initialization parameters.

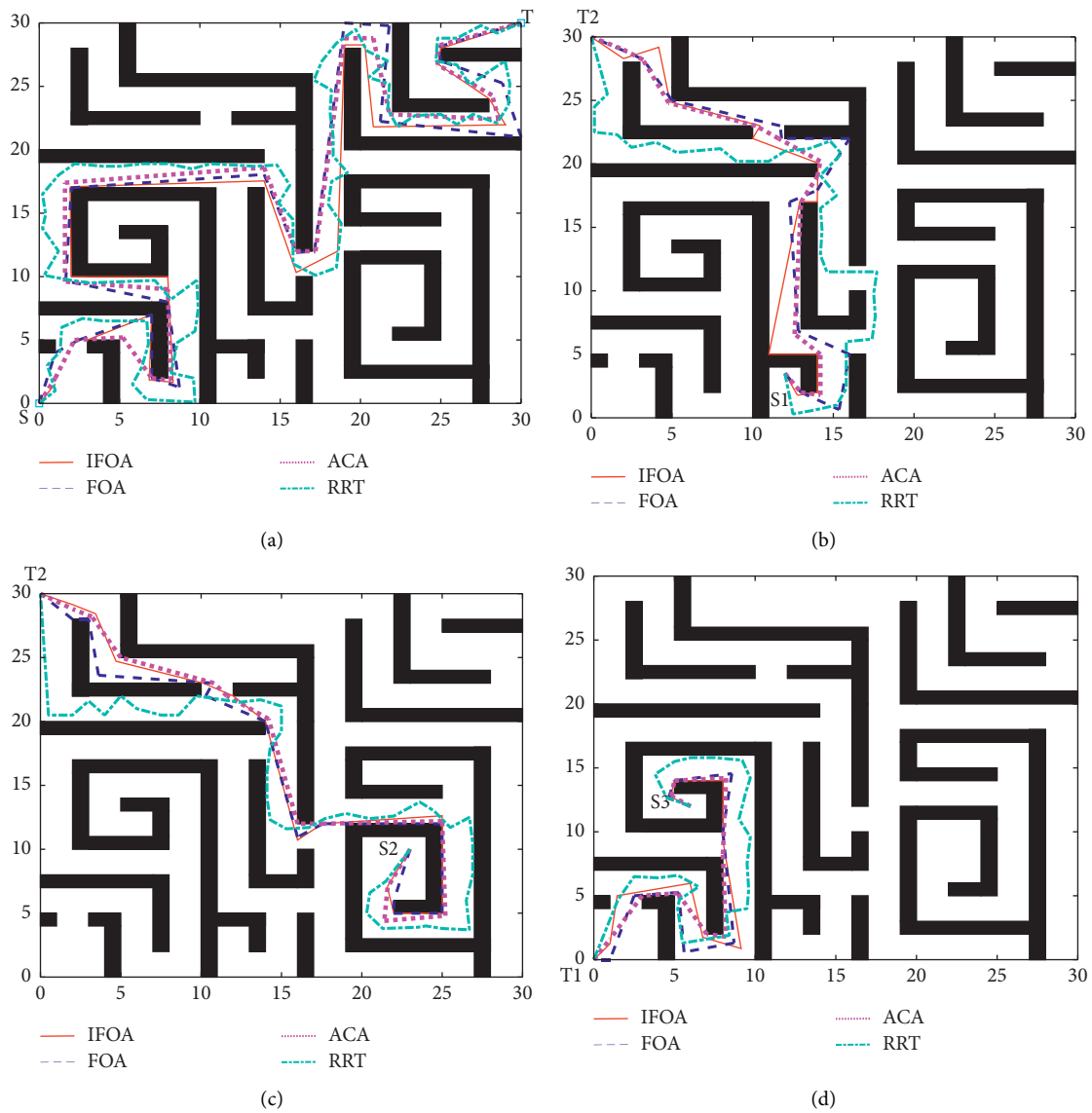


FIGURE 12: Comparison of optimal paths on Map 1. (a) S-T. (b) S1-T2. (c) S2-T2. (d) S3-T1.

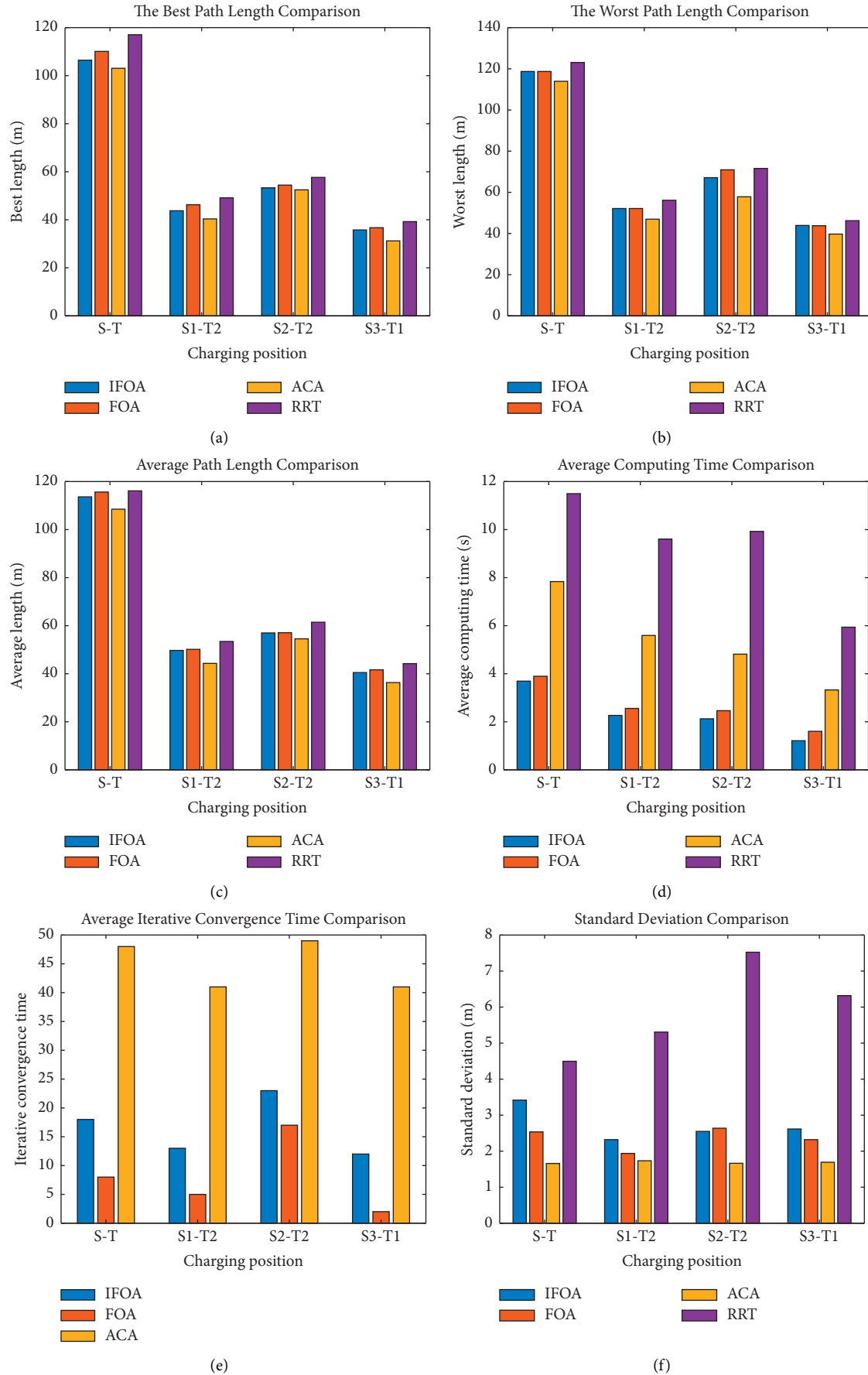


FIGURE 13: Comparison of evaluation indicators on Map 1. (a) The best path length comparison. (b) The worst path length comparison. (c) Average path length comparison. (d) Average computing time comparison. (e) Average iterative convergence time comparison. (f) Standard deviation comparison.

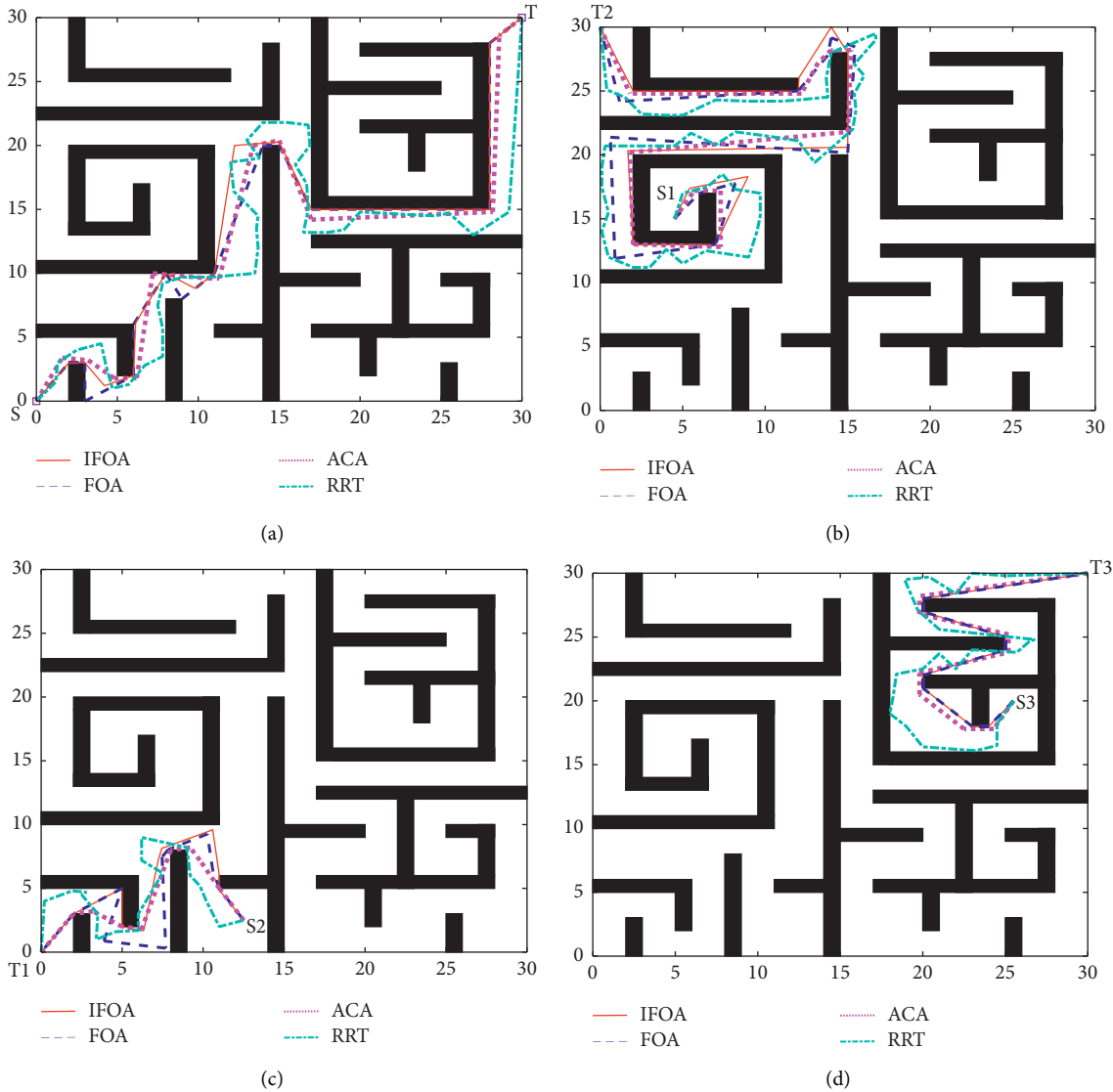


FIGURE 14: Comparison of optimal paths on Map 2. (a) S-T. (b) S1-T2. (c) S2-T1. (d) S3-T3.

where Len is a constant; gen is the current number of iterations; and $Maxgen$ is the maximum number of iterations. When $Len=1$ and $Maxgen=50$, the function image is shown in Figure 9.

It can be seen from the image that the larger search distance at the beginning of the iteration facilitates the movement of the optimal solution, and the smaller search distance in the later stage performs a fine search to improve the accuracy of the optimal solution.

The specific steps of the IFOA are as follows:

- (1) Initialize the parameters of the fruit fly optimization algorithm: population size: $popsiz$, the maximum number of iterations: $Maxgen$. Initialize the position of the fruit fly population on the path of Dijkstra algorithm: X_axis and Y_axis .

- (2) At the beginning of the fruit fly search, the individual fruit fly uses the sense of smell to find food:

$$\begin{aligned} X_p &= X_axis + Dist(2 * rand() - 1), \\ Y_p &= Y_axis + Dist(2 * rand() - 1), \end{aligned} \tag{8}$$

where $rand()$ is an arbitrary random number in the interval $[0,1]$, and $Dist$ indicates the distance of a single flight of the individual fruit fly as shown in equation (7).

- (3) Determine the taste concentration determination function of individual fruit fly. Since the fruit fly population needs to find the location of the food source, but the specific location of the food is unknown, first calculate the distance D from the origin

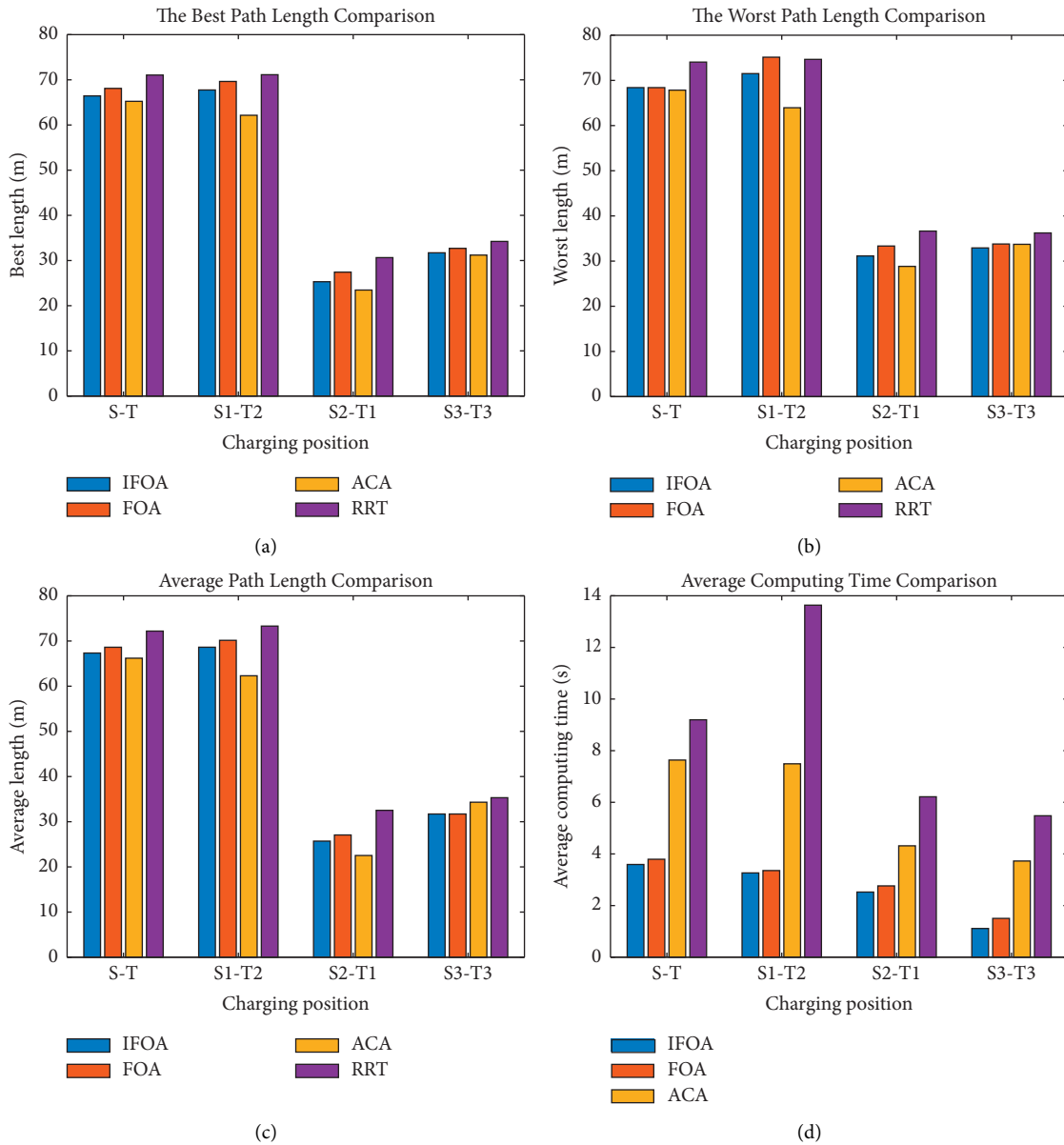


FIGURE 15: Continued.

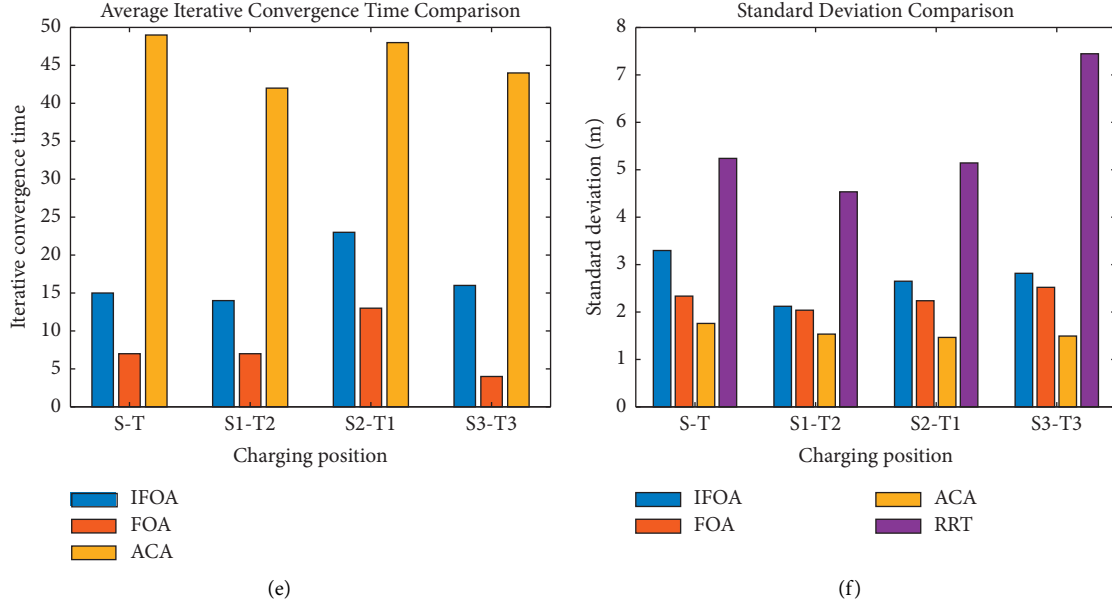


FIGURE 15: Comparison of evaluation indicators on Map 2. (a) The best path length comparison. (b) The worst path length comparison. (c) Average path length comparison. (d) Average computing time comparison. (e) Average iterative convergence time comparison. (f) Standard deviation comparison.

(0,0) and calculate the reciprocal of D as a judgment function of taste concentration:

$$D(i, j) = \text{sqrt}((X_p^2) + (Y_p^2)), \quad (9)$$

$$S(i, j) = \frac{1}{D(i, j)}.$$

- (4) Using the taste concentration judgment function to determine the taste concentration value of individual fruit fly,

$$\text{Smell}_p = \text{Function}(S(i, j)). \quad (10)$$

- (5) According to the taste concentration value of each individual fruit fly, keep the individual with the highest taste concentration value:

$$[\text{bestsmell}, \text{bestindex}] = \min(\text{Smell}), \quad (11)$$

where bestsmell is the optimal taste concentration value in this iteration and bestindex is the position coordinates corresponding to the optimal taste concentration value in the iteration.

- (6) According to the position of the fruit fly with a strong taste and the best taste in step (5), the fruit fly colony moves to the best position by vision.

$$\begin{aligned} &\text{if } \text{bestsmell} < \text{SmellBest}, \\ &\quad X_axis = X(\text{bestindex}, :), \\ &\quad Y_axis = Y(\text{bestindex}, :), \\ &\quad \text{SmellBest} = \text{bestsmell}. \end{aligned} \quad (12)$$

- (7) Iterative optimization to the maximum number of iterations Maxgen , repeat steps (2) to (5), according

to whether the taste concentration value of the current iteration is greater than the optimal taste concentration value that has been retained; if yes, proceed to step (6); otherwise, proceed to the next iteration until the maximum number of iterations is reached, and output the optimal result.

IFOA, compared with ant colony algorithm, genetic algorithm, and particle swarm algorithm, is simple and easy to implement, has fast convergence, and can get the optimal solution quickly, but the disadvantage of the algorithm is that it is only suitable for low dimensional solution and may fall into local minimum.

The flowchart of the IFOA is shown in Figure 10.

5. Simulation

To select the optimal FOA initialization parameters, this paper tests the connection between iteration, popsize, time, and path length. Figure 11 is obtained by repeating the test 30 times from S to T on map 1. Through Figure 11, it can be seen that the distance gradually decreases with the increase of iteration and population, but the time increases exponentially. Taking into account the time cost, the optimal FOA parameters are set as $\text{popsize} = 400$, $\text{Maxgen} = 40$.

To evaluate the performance of path planning based on the IFOA, this paper conducts a comparison test of the basic FOA, the IFOA, Rapidly Exploring Random Tree (RRT), and ant colony algorithm (ACA) under the environment of designated one or more charging locations. The FOA and IFOA parameters are set as $\text{popsize} = 400$, $\text{Maxgen} = 40$, $\text{Len} = 0.5$, the ACA parameters are set as $\text{popsize} = 400$, $\text{Maxgen} = 40$, Pheromone calculation parameters: 2, Pheromone selection threshold: 0.8, Pheromone update

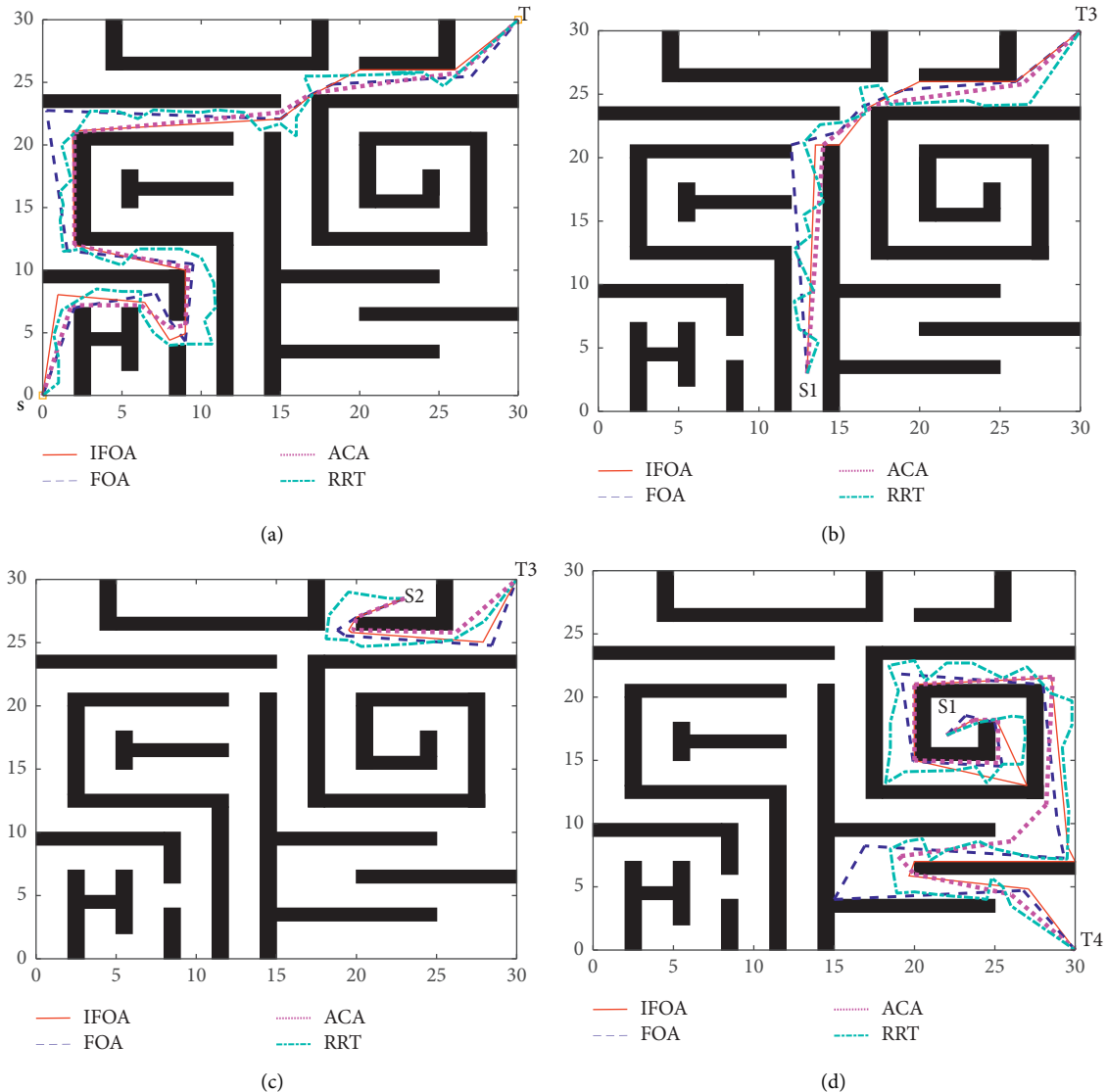


FIGURE 16: Comparison of optimal paths on Map 3. (a) S-T. (b) S1-T3. (c) S2-T3. (d) S3-T4.

parameters: 0.1, the RRT parameters are set as Step=2, MaxAttempts=1000, and the experiment is repeated 30 times on the same map with different starting and ending points.

The comparison of the optimal path and comparison of evaluation indicators on Map 1 is shown in Figures 12 and 13.

The comparison of the optimal path and comparison of evaluation indicators on Map 2 is shown in Figures 14 and 15.

The comparison of the optimal path and comparison of evaluation indicators on Map 3 is shown in Figures 16 and 17.

It can be observed from average path length, computing time and iterative convergence time in Figures 13 and 15 that IFOA is superior in the test environments. To check whether the algorithms are statistically different or not, the t -test is performed. The level 0.05 of significance is considered and shown in Table 2. The results indicate that IFOA

outperforms all other methods in all test environments, because the p values are smaller than the level 0.05 of significance.

The solid line is the IFOA, the dotted dashed line is the FOA, the dotted line is ACA, and the chain line is RRT.

From Figures 12 to 15, it can be seen that the path planned by IFOA is significantly better than FOA, and the smoothness of the path is also greatly improved. The path planned by IFOA is better than FOA planning. Although the path of ACA is short, the computing time is twice that of IFOA, and it converges after 40 times. Compared with RRT, IFOA has significant advantages in the path length and path smooth computing time. It can be seen from the eight sets of simulation experiments that, based on the improved fruit fly optimization algorithm (IFOA), the relative path has the fastest convergence speed, and the path obtained is better and smoother than FOA. In addition, it can be seen from the comparative test that the computing speed and convergence times of IFOA are better

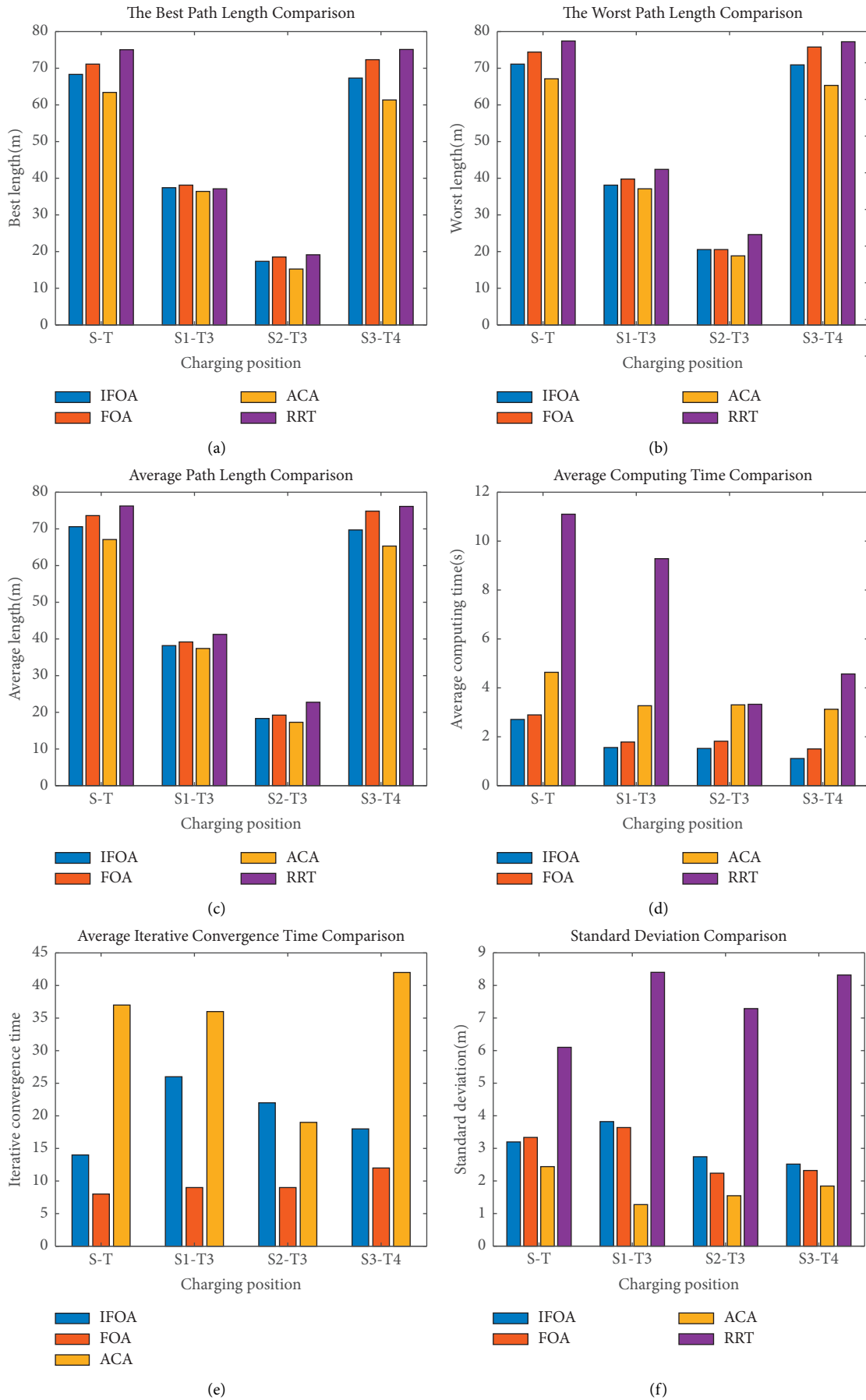


FIGURE 17: Comparison of evaluation indicators on Map 3. (a) The best path length comparison. (b) The worst path length comparison. (c) Average path length comparison. (d) Average computing time comparison. (e) Average iterative convergence time comparison. (f) Standard deviation comparison.

TABLE 2: Comparison of t -test between IFOA, FOA, and ACA (significant difference is represented by “+”).

Map 1	IFOA	FOA	ACA	RRT
S-T	—	$7.50e-05(+)$	$3.51e-07(+)$	$3.51e-09(+)$
S1-T2	—	$1.14e-03(+)$	$1.04e-06(+)$	$5.18e-11(+)$
S2-T2	—	$1.68e-05(+)$	$8.17e-07(+)$	$6.93e-06(+)$
S3-T1	—	$7.90e-04(+)$	$1.43e-05(+)$	$1.12e-13(+)$
Map 2	IFOA	FOA	ACA	RRT
S-T	—	$3.68e-04(+)$	$4.56e-06(+)$	$9.42e-11(+)$
S1-T2	—	$6.12e-05(+)$	$2.92e-06(+)$	$1.19e-06(+)$
S2-T1	—	$8.74e-05(+)$	$5.56e-07(+)$	$7.96e-09(+)$
S3-T3	—	$4.89e-04(+)$	$8.87e-07(+)$	$6.33e-12(+)$
Map 3	IFOA	FOA	ACA	RRT
S-T	—	$6.17e-05(+)$	$5.32e-03(+)$	$4.50e-09(+)$
S1-T3	—	$1.87e-03(+)$	$1.62e-04(+)$	$1.93e-12(+)$
S2-T3	—	$3.68e-07(+)$	$4.68e-05(+)$	$7.53e-08(+)$
S3-T4	—	$5.41e-05(+)$	$3.43e-03(+)$	$5.69e-05(+)$

than those of ACA. The algorithm converges to the best in the number of iterations before 25 times. Compared with an enhanced genetic algorithm [37], the improved Maklink graph is more suitable for complex environment. Compared with the improved particle swarm optimization [38], the convergence times of IFOA are the third of it; however, the convergence speed of IFOA is too fast to find the optimal solution. In [39], the authors proposed an improved version of fruit fly optimization (FOA) to solve the path planning problem. It solves the problem that the convergence speed of FOA is too fast; however, the amount of calculation is too high.

It proves the feasibility of using the IFOA to plan the return charging path of the cleaning robot, which can make the path without collision with obstacles and the shortest. It is guaranteed that the robot should choose the shortest path to the charging location under the condition of limited power.

6. Conclusions

Through eight sets of comparative experiments and analysis, the effectiveness and practicability of the proposed IFOA method are proved. The cleaning robot can return to the charging location as soon as possible without colliding with obstacles in a complex industrial environment. Through comparative experiments, it can be seen that the original algorithm has been greatly improved. The path obtained is not the shortest path, but the calculation time is shorter than other algorithms.

There are also many possible avenues for future work. First, we will study how to plan a path for dynamic obstacle avoidance when the environment is unknown [40]. Second, we will combine IFOA with other algorithms to shorten the path length. Furthermore, we will consider the path planning problem when multiple cleaning robots charge [41].

Data Availability

The data used to support the findings of this study are available from the corresponding author upon request.

Conflicts of Interest

The authors declare that there are no conflicts of interest regarding the publication of this paper.

Acknowledgments

This work was partially supported by the Basic Scientific Research Business Cost Scientific Research Project of Heilongjiang Provincial University (135509114) and the Joint Guiding Project of Natural Science Foundation of Heilongjiang Province under Grant LH2019F038.

References

- [1] Y. Yuan, W. Su, and Z. Li, “Brain-computer interface-based stochastic navigation and control of a semiautonomous mobile robot in indoor environments,” *IEEE Transactions on Cognitive and Developmental Systems*, vol. 11, no. 1, pp. 129–141, 2018.
- [2] R. Voges and B. Wagner, “Interval-based visual-LiDAR sensor fusion,” *IEEE Robotics and Automation Letters*, vol. 6, no. 2, pp. 1304–1311, 2021.
- [3] H.-y. Zhang, W.-m. Lin, and A.-x. Chen, “Path planning for the mobile robot: a review,” *Symmetry*, vol. 10, no. 10, p. 450, 2018.
- [4] U. Orozco-Rosas, K. Picos, and O. Montiel, “Hybrid path planning algorithm based on membrane pseudo-bacterial potential field for autonomous mobile robots,” *IEEE Access*, vol. 7, pp. 156787–156803, 2019.
- [5] U. Orozco-Rosas, O. Montiel, and R. Sepúlveda, “Mobile robot path planning using membrane evolutionary artificial potential field,” *Applied Soft Computing*, vol. 77, pp. 236–251, 2019.
- [6] J. Fu, F. Tian, and T. Chai, “Motion tracking control design for a class of nonholonomic mobile robot systems,” *IEEE transactions on systems, man, and cybernetics: Systems*, vol. 50, no. 6, pp. 2150–2156, 2018.
- [7] D. A. Duque, F. A. Prieto, and J. G. Hoyos, “Trajectory generation for robotic assembly operations using learning by demonstration,” *Robotics and Computer-Integrated Manufacturing*, vol. 57, pp. 292–302, 2019.
- [8] H. Yoshitake, R. Kamoshida, and Y. Nagashima, “New automated guided vehicle system using real-time holonic scheduling for warehouse picking,” *IEEE Robotics and Automation Letters*, vol. 4, no. 2, pp. 1045–1052, 2019.
- [9] K. Khateri, M. Pourgholi, M. Montazeri, and L. Sabattini, “A comparison between decentralized local and global methods for connectivity maintenance of multi-robot networks,” *IEEE Robotics and Automation Letters*, vol. 4, no. 2, pp. 633–640, 2019.
- [10] J. Trocraz, G. Dagnino, and G.-Z. Yang, “Frontiers of medical robotics: from concept to systems to clinical translation,” *Annual Review of Biomedical Engineering*, vol. 21, no. 1, pp. 193–218, 2019.
- [11] J. Tang, G. Chen, and J. P. Coon, “Secrecy performance analysis of wireless communications in the presence of UAV jammer and randomly located UAV eavesdroppers,” *IEEE Transactions on Information Forensics and Security*, vol. 14, no. 11, pp. 3026–3041, 2019.
- [12] A. Sahoo, S. K. Dwivedy, and P. S. Robi, “Advancements in the field of autonomous underwater vehicle,” *Ocean Engineering*, vol. 181, pp. 145–160, 2019.

- [13] J. Wang, W. Chi, C. Li, C. Wang, and M. Q.-H. Meng, "Neural RRT*: learning-based optimal path planning," *IEEE Transactions on Automation Science and Engineering*, vol. 17, no. 4, pp. 1748–1758, 2020.
- [14] J. Liu, J. Yang, H. Liu, X. Tian, and M. Gao, "An improved ant colony algorithm for robot path planning," *Soft Computing*, vol. 21, no. 19, pp. 5829–5839, 2017.
- [15] F. H. Ajeil, I. K. Ibraheem, A. T. Azar, and A. J. Humaidi, "Grid-based mobile robot path planning using aging-based ant colony optimization algorithm in static and dynamic environments," *Sensors*, vol. 20, no. 7, p. 1880, 2020.
- [16] T. T. Mac, C. Copot, D. T. Tran, and R. De Keyser, "Heuristic approaches in robot path planning: a survey," *Robotics and Autonomous Systems*, vol. 86, pp. 13–28, 2016.
- [17] B. K. Patle, G. Babu L, A. Pandey, D. R. K. Parhi, and A. Jagadeesh, "A review: on path planning strategies for navigation of mobile robot," *Defence Technology*, vol. 15, no. 4, pp. 582–606, 2019.
- [18] H. Gao, X. Song, L. Ding, K. Xia, N. Li, and Z. Deng, "Adaptive motion control of wheeled mobile robot with unknown slippage," *International Journal of Control*, vol. 87, no. 8, pp. 1513–1522, 2014.
- [19] T. Cabreira, L. Brisolara, and P. R. Ferreira Jr., "Survey on coverage path planning with unmanned aerial vehicles," *Drones*, vol. 3, no. 1, p. 4, 2019.
- [20] M. Radmanesh, M. Kumar, P. H. Guentert, and M. Sarim, "Overview of path-planning and obstacle avoidance algorithms for UAVs: a comparative study," *Unmanned Systems*, vol. 6, no. 2, pp. 95–118, 2018.
- [21] J. Delmerico, E. Mueggler, J. Nitsch, and D. Scaramuzza, "Active autonomous aerial exploration for ground robot path planning," *IEEE Robotics and Automation Letters*, vol. 2, no. 2, pp. 664–671, 2017.
- [22] H. Zhang, Y. Wang, J. Zheng, and J. Yu, "Path planning of industrial robot based on improved RRT algorithm in complex environments," *IEEE Access*, vol. 6, pp. 53296–53306, 2018.
- [23] L. C. Santos, F. N. Santos, and E. J. S. Pires, "Path planning for ground robots in agriculture: a short review," in *Proceedings of the 2020 IEEE International Conference on Autonomous Robot Systems and Competitions (ICARSC)*, pp. 61–66, IEEE, Ponta Delgada, Portugal, April 2020.
- [24] A. Khan, I. Noreen, and Z. Habib, "On complete coverage path planning algorithms for non-holonomic mobile robots: survey and challenges," *Journal of Information Science & Engineering*, vol. 33, no. 1, 2017.
- [25] Z. Li and W. A. Xu, "Path decision modelling for passengers in the urban rail transit hub under the guidance of traffic signs," *Journal of Ambient Intelligence and Humanized Computing*, vol. 10, no. 1, pp. 365–372, 2019.
- [26] Y. Yang, M. Jiang, and W. Li, "2D path planning by lion swarm optimization," in *Proceedings of the 2020 4th International Conference on Robotics and Automation Sciences (ICRAS)*, pp. 117–121, IEEE, Chengdu, China, June 2020.
- [27] T. Lei, C. Luo, and J. E. Ball, "A graph-based ant-like approach to optimal path planning," in *Proceedings of the 2020 IEEE Congress on Evolutionary Computation (CEC)*, pp. 1–6, IEEE, Rio de Janeiro, Brazil, July 2020.
- [28] J. Guo, X. Huo, and S. Guo, "Path planning of the spherical robot based on improved ant colony algorithm," in *Proceedings of the 2020 IEEE International Conference on Mechatronics and Automation (ICMA)*, pp. 273–278, IEEE, Beijing, China, August 2020.
- [29] G. Qing, Z. Zheng, and X. Yue, "Path-planning of automated guided vehicle based on improved Dijkstra algorithm," in *Proceedings of the 2017 29th Chinese Control and Decision Conference (CCDC)*, pp. 7138–7143, IEEE, Chongqing, China, May 2017.
- [30] M. Akram, A. Habib, and J. C. R. Alcantud, "An optimization study based on Dijkstra algorithm for a network with trapezoidal picture fuzzy numbers," *Neural Computing and Applications*, vol. 33, pp. 1–14, 2021.
- [31] A. Darvish and A. Ebrahimzadeh, "Improved fruit-fly optimization algorithm and its applications in antenna arrays synthesis," *IEEE Transactions on Antennas and Propagation*, vol. 66, no. 4, pp. 1756–1766, 2018.
- [32] R. Hu, S. Wen, Z. Zeng, and T. Huang, "A short-term power load forecasting model based on the generalized regression neural network with decreasing step fruit fly optimization algorithm," *Neurocomputing*, vol. 221, pp. 24–31, 2017.
- [33] S. Kanarachos, J. Griffin, and M. E. Fitzpatrick, "Efficient truss optimization using the contrast-based fruit fly optimization algorithm," *Computers & Structures*, vol. 182, pp. 137–148, 2017.
- [34] A. Babalik, H. İscan, and İ. Babaoğlu, "An improvement in fruit fly optimization algorithm by using sign parameters," *Soft Computing*, vol. 22, no. 22, pp. 7587–7603, 2018.
- [35] G. Wang, L. Ma, and J. Chen, "A bilevel improved fruit fly optimization algorithm for the nonlinear bilevel programming problem," *Knowledge-Based Systems*, vol. 138, pp. 113–123, 2017.
- [36] L. Wang, Y. Xiong, S. Li, and Y.-R. Zeng, "New fruit fly optimization algorithm with joint search strategies for function optimization problems," *Knowledge-Based Systems*, vol. 176, pp. 77–96, 2019.
- [37] M. Nazarahari, E. Khanmirza, and S. Doostie, "Multi-objective multi-robot path planning in continuous environment using an enhanced genetic algorithm," *Expert Systems with Applications*, vol. 115, pp. 106–120, 2019.
- [38] S. Shao, Y. Peng, C. He, and Y. Du, "Efficient path planning for UAV formation via comprehensively improved particle swarm optimization," *ISA Transactions*, vol. 97, pp. 415–430, 2020.
- [39] X. Zhang, X. Lu, S. Jia, and X. Li, "A novel phase angle-encoded fruit fly optimization algorithm with mutation adaptation mechanism applied to UAV path planning," *Applied Soft Computing*, vol. 70, pp. 371–388, 2018.
- [40] H. Lyu and Y. Yin, "COLREGS-constrained real-time path planning for autonomous ships using modified artificial potential fields," *Journal of Navigation*, vol. 72, no. 3, pp. 588–608, 2019.
- [41] X. Wang, H. Zhao, T. Han, H. Zhou, and C. Li, "A grey wolf optimizer using Gaussian estimation of distribution and its application in the multi-UAV multi-target urban tracking problem," *Applied Soft Computing*, vol. 78, pp. 240–260, 2019.

Research Article

Interactive Virtual Reality Touring System: A Case Study of Shulin Ji'an Temple in Taiwan

Jung-Hua Lo ¹, Shih-Da Wu ², and Min-Jie You ¹

¹Department of Applied Informatics, Fo-Guang University, Yilan 26247, Taiwan

²Management College, National Defense University, Taoyuan City 11258, Taiwan

Correspondence should be addressed to Jung-Hua Lo; jhlo@mail.fgu.edu.tw

Received 31 October 2020; Revised 7 August 2021; Accepted 17 August 2021; Published 25 August 2021

Academic Editor: Hsu-Yang Kung

Copyright © 2021 Jung-Hua Lo et al. This is an open access article distributed under the Creative Commons Attribution License, which permits unrestricted use, distribution, and reproduction in any medium, provided the original work is properly cited.

Most current tour guiding methods for Taiwanese temples employ graphic webpage frameworks combined with captioned pictures for introduction. This type of tour guiding lacks interactive presence. In addition, the audience may not be able to focus on browsing webpages or learn essential information from the introduction. This study adopted the Delphi method to evaluate the current developed system. This system was aimed at designing VR-based interaction that differs from conventional tour guiding methods to aid users in viewing the display space from their viewpoints. Users cannot only control camera view angles but also select the paths and guiding information as if they were walking in the temple. The analysis results revealed that, in general, the users perceived VR tour guiding as convenient and easy to use. The display and content of the tour guiding system presented clear information to the users, aiding them in gaining further understanding of the introduced item. Finally, the study results can serve as a reference for design research on VR applications in tour guiding.

1. Introduction

1.1. Research Background and Motivation. Religious activities in Taiwan are the most authentic cultural expression of the lives of the common people, combining the beliefs of Buddhist and Taoist deities and the rituals of heaven and ancestor worship, which are rich and diverse and reveal the deep cultural assets of Taiwan. A variety of temple fairs, temple parade techniques, and temple architecture and craftsmanship, based on religious beliefs, demonstrate the abundance of local culture. In recent years, many of the local activities promoted by the government have been aimed at attracting tourists by integrating the local tourism industry with the culture of religious beliefs as a regional feature. As a result, religious and cultural tourism is not only fostered in the region, but has also become a popular tourist activity. In the case of the Jian Temple in New Taipei City, this study, by examining the attractiveness of religious tourism in the process of promoting cultural tourism at regional temples, has developed a tour guiding system at the temple, making use of the temple's existing resources and textual and

pictorial descriptions to convey the unique local culture of Taiwan. Through daily contact, the temple naturally helps the worshippers and visitors to understand the history of the area and also imperceptibly enhances their cultural literacy so that the shrine is no longer just a center of faith, but also functions as a local exhibition hall, with the aim of boosting local cultural tourism. This kind of experience will help visitors to get a better sense of the culture of the Taiwanese people, and it is only through understanding the culture of Taiwan that they will be able to bond and identify with the land. Temples embody the living habits, customs, outlook on life, and values of the locals and exhibit a wide range of cultures. In addition, the loss of temple culture in Taiwan has prompted this study to delve into the cultural tourism of temples and to develop a tour guiding system for temples.

Tourist attractions usually present information through guided tours, documents, brochures, information plaques, and audio tours. These methods can fail to present visitors with accurate and precise information because of inadequate human resources or outdated text and audio materials. Such situations can leave visitors with poor impressions of the interactions or

services offered by attractions. With the rapid advancement of the Internet technology, the daily life of most people is becoming strongly entangled with the Internet and relevant technology applications. That is, the Internet has changed people's lifestyle and consumption habits. Technological advancement and the widespread use of personal intelligent mobile devices, such as smartphones and tablets, have enabled visitors to locate nearby tourist attractions directly using the camera and location-based services (LBS) of their mobile devices. The popularity of smartphones that offer a wide variety of application software (colloquially referred to as APP) in addition to basic telephone, Internet, and gaming functions has given rise to a new generation of APP that are armed with interactive features. Such interactive features, which may involve text, images, audio, and video, create an innovative user experience. Some have even incorporated another emerging technology that is growing in popularity: virtual reality (VR). VR's greatest selling point is that it enables users to experience a world in which the real and the virtual are seamlessly integrated [1, 2]; additionally, it allows users to interact with this world through certain ancillary devices (e.g., the display device) and experience the integration between the virtual and real worlds while controlling virtual items in the real-world environment. However, most mobile applications that offer tour services do not have a correct understanding of the places they are visiting due to lack of time, failure to read maps, or lack of tour guides. Or, the information of the tourist attraction is not up to date, which leads to incorrect information at the first place and in turn misunderstanding about the places they are visiting. Also, the mobile-guided tour APP available in the market are designed mostly with the general public in mind. There is still plenty of room for improvement. Based on the aforementioned reasons, we develop VR mobile guide system operated on smart phones through the corresponding scheme of integration with GPS function can be easily used without any geoinformation provided by Internet. This mobile guide system can be known as a personal-oriented LBS integrated with Google e-map, for users to use smart phones with GPS function as a guide tool, guiding users based on the routes chosen by users. The functions include query for nearby scenic areas, introduction to the content of scenic areas through different dimensions, presentation of photos on the history of scenic areas, spatial guide on e-map, and introduction of augmented reality direction of scenic areas. On the contrary, as digital technology advances and the smart mobile devices from launch to availability, mobile guide services have progressed to the interaction with reality information guide following the past static guide scheme. The study integrates jQuery Mobile, VR techniques, LBS, and other technologies to develop an VR mobile guide system so that users can find the information on the target destination in reality via the screen of smart phones to carry out the integration of reality guide and route guide functions, thereby providing reference and application for the establishment of the future mobile guide system [3–5].

1.2. Research Questions. This study focused on Ji'an Temple of Shulin District, New Taipei City, Taiwan. An interactive tour guiding of the temple was thus developed through VR

technologies. The Delphi method, which is an expert group decision-making technique, was employed on the basis of multiple rounds of questionnaire responses. Through cyclic feedback collection, various experts' comments were collected. Indicators that experts consistently agreed are critical in VR applications in interactive tour guiding were selected as the goal orientation for system development. Thus, this study was conducted to respond to the following three questions and also shown in Figure 1:

(Q1) What are the major dimensions and indicators established for the target touring mobile information system from the expert opinions?

(Q2) How to develop the target touring mobile information system that meets the indicators recommended by the expert opinions?

(Q3) The users' responses are important. What is the result of the Questionnaire for User Interaction Satisfaction (QUIS)?

The rest of this paper is organized as follows. In Section 2, the literature review of temple cultural tourism and VR technology is discussed. The expert assessment of the system was evaluated in Section 3. VR mobile touring system framework and development is proposed in Section 4. The questionnaire for user interaction satisfaction is discussed in Section 5. Finally, the conclusions and future studies are described in Sections 6 and 7, respectively.

2. Literature Review

In this section, we first introduce the Ji'an Temple and discuss the temple cultural tourism in Taiwan. Then, the VR applications installed on mobile devices for temple guidance are reviewed.

2.1. Temple Cultural Tourism and Ji'an Temple. Under the impact of urbanization, traditional folk culture and arts are facing a great dilemma in terms of preservation, and Taiwan's local culture is gradually in danger of disappearing, and temples are almost becoming the last reserves of these folk cultures and arts. The protection of temple culture is a way to preserve Taiwan's intangible cultural heritage so that these valuable folk arts can be passed on through folk beliefs and local temples can sustain operations through the boost of tourism. The continued conservation of folk art and culture creates a sense of identity and continuity and promotes the development of cultural diversity and pluralism. Intangible cultural heritages are a treasure shared by all people in Taiwan. They are the gems of wisdom from the ancestors' lives, an important asset in shaping Taiwan's unique style in a culturally homogenized world and an essential medium for bringing Taiwan's cultural content and characteristics to international attention [6, 7]. This study, by using the example of the Ji'an Temple in Shulin, aims to look into its background to learn about the past with literature review, and by collecting the characteristics of religious tourism and organizing and analyzing the factors driving tourists to engage in religious and cultural sightseeing tour,

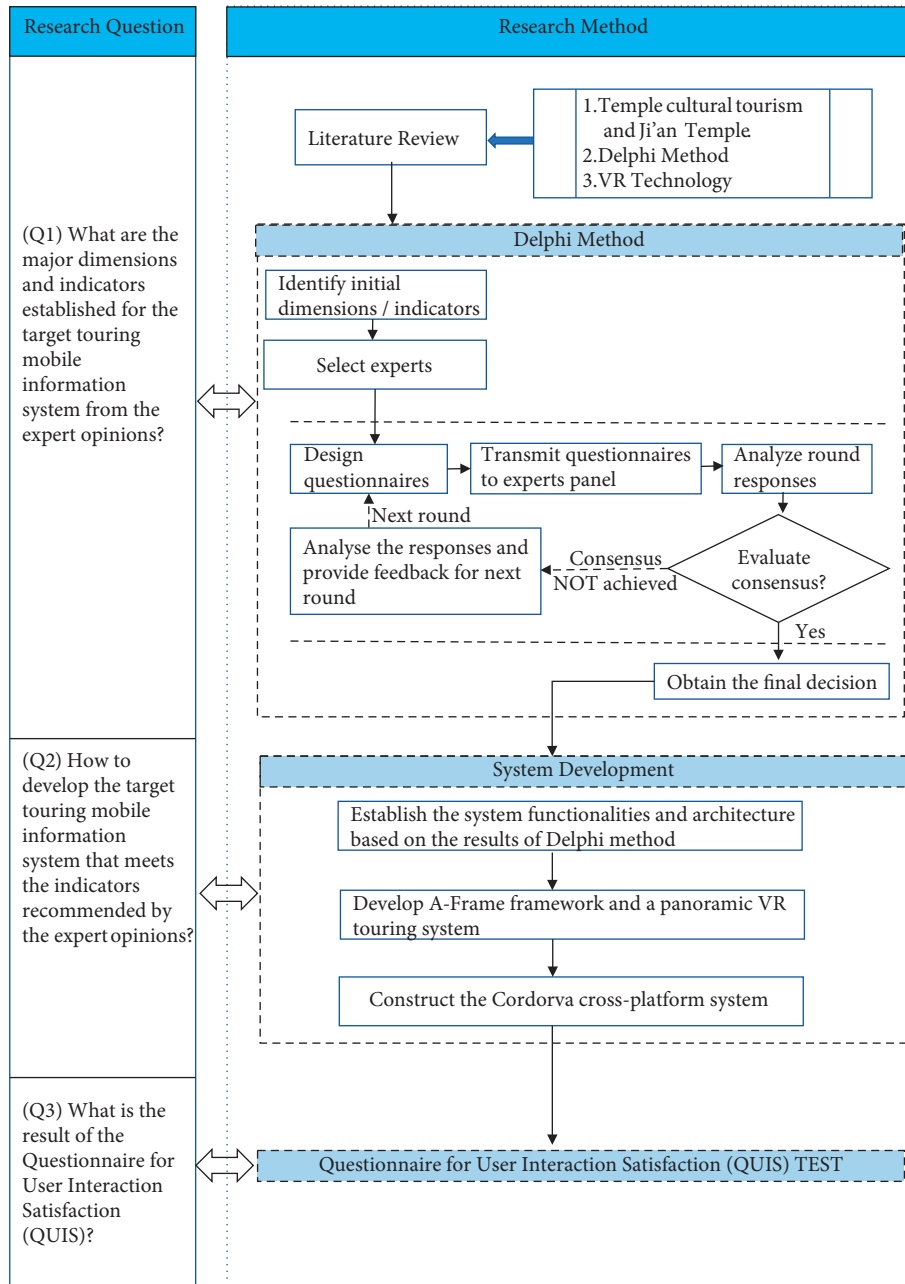


FIGURE 1: Research question statement.

it can, based on the analyzed data, identify the specific direction for development and serve as a basis for projecting the development of the functions of the tour guidance system. We have gathered information about the people, events, objects, and environment concerning the Jian Temple through historical and documentary materials, which have served as a reference for the planning and design of the guiding system, and then collected books, documents, cultural and historical materials, and data on websites related to the shrine, in order to gain a preliminary understanding of the historical background and local culture, as well as to find out the historical and cultural references of the shrine and to use these materials as a basis for research. Established over 230 years ago, the Jian Temple in Shulin,

New Taipei City, is the most representative shrine in the Shulin area. The Jian Temple is dedicated to Bao-SBheng Emperor [8–10], a deity in charge of medicine, who is well versed in astronomy and geography and is a skilled healer, specializing in the treatment of maladies and saving countless lives. It is said to be so effective that, in later times, he was revered as the “God of Medicine,” a deity to whom people pray for good health. One of the most special features of all temples worshipping Bao-Sheng Emperor is that there are divination prescription slips available in the temple. Therefore, for patients or their families, they can come to the temple to pray for the protection of the gods and also to seek prescriptions for medicine and then get medicines from the Chinese medicine shop and give to the patients. In general,

this type of prescription slips is no different from drawing a bamboo divination stick to ask for good fortune. However, before drawing the slip, apart from praying, one must also give a statement of one's condition to the deity and then draws a bamboo stick from the stick box and throws divination blocks to determine whether it is suitable for a prescription. Since the belief in healing is more or less helpful to the illness, the belief in Bao-Sheng Emperor has persisted for hundreds of years, making the temple building, sacrificial items, and festivals distinct from other shrines and becoming a unique temple in the region. This study aims at exploring the cultural tourism resources of temples from the perspective of religious tourism, and through the example of the Jian Temple, a guided tour system of the temple has been built to convey the unique local culture of Taiwan and to probe into its temple architecture, religious impressions, etc. By virtue of the impression and attractiveness of the destination, this study analyses the advantages of the development of religious and cultural tourism and uses a virtual model to integrate the tour system into the temple so that, through the explanation of specific displays and ritual activities in the temple, the visitors and worshippers can be impressed and moved, with the purpose of transmitting cultural messages and interpreting cultural language. In addition to preserving the cultural assets and linking them to the past, it also serves to pass on the wisdom of the ancestors and to explain the history and culture of the community so that the worshippers and visitors do not only hold incense sticks and worship on a religious sightseeing tour, but through the guided tour system, understand the reasons for worshipping, the origins of the faith, the history, and the importance of passing it on.

2.2. VR Technology. Gartner's Top 10 Strategic Technology Trends for 2020 [11] mentions VR and AR as one of the top 10 emerging technologies to watch in the coming years. VR is a simulated space and environment that can be made to feel like a real environment. VR can fully simulate human perception, allowing visitors to have an almost realistic experience [12–14]. In other words, a computer-generated virtual world in three dimensions enables the device to perform complex computations immediately when the user moves around, sending back an accurate 3D image of the world to create a sense of presence so that the user can see things in three dimensions in a timely and unrestricted way, as if they were there. These fictional worlds feature, to varying degrees, immersion, interaction, and imagination [15], created by a simulation system that integrates computer graphics technology, computer simulation technology, artificial intelligence, sensing technology, display technology, and parallel network processing. VR can be divided into the following three categories according to the way it is created: geometry-based VR, image-based VR, and hybrid VR, which are introduced below [16–23]:

- (1) **Geometry-based VR:** geometry-based VR scenes and objects are computed by computers, and the objects are created using computational geometric operations and mapping techniques to produce the so-called VR. Generally, 3D modelling tools (e.g., 3ds Max, Maya, and AutoCAD) are utilized to create the scenes, and then, different software is applied to build the required virtual environment depending on the needs on-site. Using various VR editing software (e.g., Unity), objects are imported and set with different attributes, and trigger events are added to the model objects as appropriate, as a way to communicate messages and show event-triggered interaction to achieve engagement with virtual scenes. This kind of VR production is time consuming and requires a lot of manpower to build the virtual environments, but the final result is very interactive and can be viewed from any angle and path.
- (2) **Image-based VR:** real images are used based on computer technology to create a virtual world that is comparable to our real environment. Since geometry-based VR is relatively expensive and takes longer to create, image-based VR, built on panoramic image technology, was created as a result. Image-based VR uses a camera, a tripod, and image-based VR editing software to present the viewer's surroundings in a cylindrical or spherical field of vision as a still image in VR. Today's digital cameras are evolving rapidly, making image-based VR production even easier. Developers can create the most realistic virtual scenes in a fraction of the time.
- (3) **Hybrid VR:** hybrid VR, by adding virtual objects to real images, is a technology that lies somewhere between geometry-based VR and image-based VR, with some of the advantages and disadvantages of the former two, but strikes a balance between them. The first step is to create a geometric virtual scene to simulate a real setting, but often due to the complexity of modelling the interior, a video virtual tour is adopted to complement the geometry and make the whole scene complete.

Geometry-based method can provide users with high interactivity and high immersion, but using this method to develop highly realistic artificial environment is time-consuming. In contrast, the image-based method can produce highly realistic artificial environment in a shorter time, making it a possible alternative to the geometry-based method. The virtual effect of the image-based method is to use the images of photos to be stitched together to develop a realistic panoramic virtual environment. Furthermore, it can use zoom in/out edges in artificial environments and perform hot-spot jumps and 360-degree panning between several artificial environments to achieve navigation.

Compared with the geometry-based method, the navigation function developed using the image-based method is limited. Especially, when the scale of the scene is large or the surface details of the objects in the scene are more complicated, the time consumed for modelling and rendering will increase sharply, and the requirements for hardware will also be relatively high. Moreover, VR provides virtual navigation of the environment and breaks the boundary between the virtual and the real, allowing users to combine highly interactive manipulation with the real environment, creating sensory stimulation and retaining an interactive, personalized experience. VR uses the technology of computers and displays to generate a 3D virtual world. Most of the current VR-related devices are designed with displays that completely envelop the space around the eyes, creating a seemingly realistic 3D virtual world in the user's field of vision. In addition, users can also combine sensors to control objects in the virtual world. The computer learns the user's body movements through the sensors and generates corresponding images to achieve an interactive situation with the user. Panoramic image navigation is one of the VR applications, and these technologies are becoming increasingly sophisticated, and the cost and technical barriers are not so high that users can quickly immerse themselves in the environment. Many of the country's tourist attractions now also adopt the panoramic image navigation system for guidance. For example, the Bureau of Cultural Heritage has developed a tangible cultural assets tour and management system that uses geo-information technology to incorporate spatial databases of tangible cultural assets in Taiwan, allowing users to collect information on scenic spots and make online enquiries, while integrating mobile devices to provide 360-degree panoramic tours so that the general public can interact with tangible cultural resources and enhance their understanding of and affinity with them. Panoramic VR [18–21] navigation is now widely used in many areas, especially after Facebook, YouTube, Twitter, and other social networking sites have launched 360-degree panoramic live streaming function; the application of scenic VR is more popular among users. The VR is designed based on the realistic environment, allowing users to use their own perspective to navigate independently and generate an immersive experience, hence, the highest level of realism and interactivity. By combining the new form of virtual tourism with real-world attractions through information systems development, network transmission, and panoramic VR technologies, travellers can utilize these integrated technologies over the Internet for pretrip preparation and itinerary planning of target destinations.

3. Methods

The Delphi method [24] is being increasingly used in investigation of variety of local, regional, and global issues among stakeholders in which a consensus is to be conducted [25–27]. Some of these areas included the development of information systems, and this method is also proven a popular tool to extract the unbiased information for a panel of experts [28–31]. Therefore, it would be

appropriate to adopt the Delphi method for obtaining a set of major dimensions and indicators established for the target touring mobile information system from the expert opinions. In the Delphi method, a series of condensed questionnaires is delivered to a group of experts, and their expert opinions are thus collected and examined to establish reliable technologies at a consensus. Here, several rounds of questionnaire responses were collected in an anonymous and non-face-to-face manner. After all questionnaire responses were investigated, the results along with new questionnaires were distributed to the experts as the reference for revising prior opinions. This process was repeated until disagreement among the experts was minimized and a concrete consensus was formed. The common advantages of the Delphi method are that the group composed of experts with various backgrounds can discuss a given topic from diverse perspectives and thereby extend the width of conclusions. Through the statistical data and opinions collected from the multiple rounds of questionnaire responses, a set of indicators was established for the expert's consensus initiatives.

3.1. Delphi Procedure. The Delphi method adopted in this research consisted of two rounds. In the first stage, 10 experts of relevant domains and objective perspectives were invited to provide their opinions through the Delphi questionnaire surveys. These experts could express their opinions freely. The aim of this stage was to enable brainstorming among the experts, rather than posing restriction on the experts' scope of thinking. When an expert found any dimension or indicator listed in the questionnaire insufficient or inappropriate, the expert was asked to provide their additional comments and suggestions. The questionnaire comprised three main dimensions and nine indicators. The experts were asked to rate the importance and feasibility of each indicator according to a 5-point Likert scale, with anchors of 1 (strongly disagree) and 5 (strongly agree) [32]. After the first round of questionnaire, we adopted content analysis to classify expert opinions, after which they developed the second-round questionnaire. Higher scores represented greater importance and practical feasibility of VR development for temple tour guiding.

3.2. Criterion Measure. In this research, we adopt some evaluation criteria [26, 33–36] to rank the importance of each of the component. This measurement includes the mean value (M), the standard deviation (SD), and the quartile deviation (QD). Furthermore, to assess agreement among experts, the stopping criteria are measured by using the coefficient of variation (CV) and Kendall's coefficient of concordance (W) [37]. Therefore, the comparison criteria are described as follows:

Suppose that indicator j is given the rating R_{ij} judged by the expert i , where there are in total n indicators and m experts' judges.

- (1) The mean value (M) of the total rating given to indicator j is defined as

$$\mathbf{M}_j = \frac{1}{m} \sum_{i=1}^m \mathbf{R}_{ij}. \quad (1)$$

- (2) The standard deviation (**SD**) of the total rating given to indicator j is defined as

$$\mathbf{SD}_j = \sqrt{\frac{1}{m} \sum_{i=1}^m (\mathbf{R}_{ij} - \mathbf{M}_j)^2}. \quad (2)$$

- (3) The quartile deviation (**QD**) of the total rating given to indicator j is defined as

$$\mathbf{QD}_j = \frac{(\mathbf{Q3}_j - \mathbf{Q1}_j)}{2}, \quad (3)$$

where $\mathbf{Q1}_j$ and $\mathbf{Q3}_j$ represent the 1st quartile and the 3rd quartile of the indicator j , respectively.

- (4) The coefficient of variation (**CV**) of the total rating given to indicator j is defined as

$$\mathbf{CV}_j = \frac{\mathbf{SD}_j}{\mathbf{M}_j}. \quad (4)$$

- (5) Kendall's coefficient of concordance (**W**) [14, 18] of the total rating is defined as

$$\mathbf{W} = \frac{12S}{(m^2(n^3 - n) - mT)}, \quad (5)$$

where the sum of squared deviations, S , is defined as

$$\begin{aligned} R_i &= \sum_{j=1}^m \mathbf{R}_{ij}, \\ \bar{R} &= \frac{1}{n} \sum_{i=1}^n R_i, \\ S &= \sum_{i=1}^n (R_i - \bar{R})^2. \end{aligned} \quad (6)$$

T is a correction factor for tied rating:

$$\begin{aligned} T &= \sum_{j=1}^m T_j, \\ T_j &= \sum_{i=1}^{g_j} (t_i^3 - t_i), \end{aligned} \quad (7)$$

in which t_i is the number of tied rating in the i th group having the same constant value of tied rating and g_j is the number of groups of ties in the set of rating for expert j .

3.3. Consensus Criteria. To obtain consensual and important opinions from a group of experts in this study, the major statistics used in the Delphi method are a measure of central tendency (**M**), level of dispersion (**SD** and **QD**), and level of

agreement and stability (**CV** and **W**). In general, the use of mean value to represent the central tendency is favoured [26–30]. Table 1 shows the level of importance based on the 5-point Likert scale. An indicator's mean score of more than 4.2 (“very high important”), or more than 3.5 and less than or equal 4.2 (“high important”) is recommended in the first round of Delphi procedure. A higher mean value indicates more importance of the critical factor. Furthermore, after justifying the mean value, standard deviations and quartile deviations are then identified to measure the amount of variation or dispersion of items. Table 2 shows the level of variation or dispersion according to **SD** and **QD**. In this study, the dispersion level is divided into three levels (high, moderate, and no consensus). The dispersion level is accepted as high if **SD** is less than or equal to 1 and **QD** is less than or equal to 0.5 [38, 39]. A low deviation indicates that the values tend to be close to the mean value (**M**), while a high deviation indicates that the values are spread out over a wider range. Moreover, we adopt the coefficient of variation (**CV**) and Kendall's coefficient of concordance (**W**) to determine whether a consensus has been met or not. It is an important issue to know when to stop the Delphi procedure. If the procedure is finished too early, the results may not be significant; and, if the process has too many rounds, the task may be too heavy to the experts and consequently contribute to withdrawals [38–40]. Table 3 shows the level of consensus determined by **CV** and **W**. For example, the level of consensus value ($0.8 < \mathbf{CV}$ and $0 \leq \mathbf{W} \leq 0.3$) shows a weak level of agreement of the experts' opinion, but still needs for additional round.

3.4. Analysis of Results. The questionnaire copies were distributed to 10 experts, who were willing to assist with the study. Before the experts filled in the questionnaire, they were asked to carefully read the instructions for responding to the questionnaire. The questionnaire responses were collected 2 weeks after distribution. The response rate was 100%. The questionnaire comprised three main dimensions and nine indicators, as shown in the first column of Table 4. Furthermore, consensus was reached on 2 out of 9 indicators, but there were two indicators did not achieve consensus. These include reminder function ($\mathbf{M} = 2.7 \leq 3.5$) and smart terminal management ($\mathbf{M} = 3.0 \leq 3.5$; $\mathbf{QD} > 0.5$); thus, these two indicators were removed in the next round. Moreover, **W** was computed to estimate the level of agreement and consensus among experts in the first round. The result ($\mathbf{W} = 0.3 \leq 0.3$) reveals a weak agreement and need for additional round.

The statistical analysis results of the first-round questionnaire responses revealed that the mean values of “reminder function” and “smart terminal management” were smaller than 3.5 and were thus deleted. Similarly, the second-round questionnaire copies were distributed to all experts who completed the first-round questionnaire. In total, 10 copies were distributed, and the response rate was 100%. Table 5 shows that all **SD** values are smaller than 1, **QD** and **CV** values are also equal or smaller than 0.5, and Kendall's **W** reaches a high level of consensus

TABLE 1: Level of importance.

Mean (M)	Level of importance
$4.2 < M \leq 5$	Very high important
$3.5 < M \leq 4.2$	High important
$2.7 < M \leq 3.5$	Moderate important
$M \leq 2.7$	Low important

TABLE 2: Level of dispersion.

Standard deviation (SD)	Quartile deviation (QD)	Level of dispersion
$0 \leq SD \leq 1$	$0 \leq QD \leq 0.5$	High
$1 < SD \leq 1.5$	$0.5 < QD \leq 1$	Moderate
$1.5 < SD$	$1 < QD$	Low and no consensus

TABLE 3: Level of agreement and consensus.

Coefficient of variation (CV)	Kendall's coefficient of concordance (W)	Level of agreement and stability
$0 \leq CV \leq 0.5$	$0.5 \leq W$	Good agreement, no additional round
$0.5 < CV \leq 0.8$	$0.3 < W \leq 0.5$	Moderate agreement, possible need for another round
$0.8 < CV$	$0 \leq W \leq 0.3$	Weak agreement, need for additional round

TABLE 4: Results for the Delphi first round.

Dimension/indicator	M	SD	QD	CV
<i>Functional perspective</i>				
Search function	4.5	0.67	0.50	0.15
Feedback function	4.5	0.67	0.50	0.15
Reminder function	2.7	0.78	0.5	0.29
<i>Technology integration</i>				
Smart terminal management	3.0	0.77	0.75	0.26
Social media integration	4.7	0.64	0.25	0.14
APP development	3.6	0.68	0.50	0.19
<i>Smart system</i>				
Tour guiding system	4.7	0.64	0.25	0.14
Navigation system	3.7	0.64	0.50	0.17
Archival system	3.9	0.70	0.50	0.18
Kendall's W = 0.30				

($W = 0.78 \geq 0.5$). These results reveal a better agreement and consensus on the responses in this round. At this stage, expert opinions had reached consensus; therefore, the third round of the questionnaire was considered unnecessary. The importance and feasibility of the indicators were evaluated according to a 5-point Likert scale. The importance and feasibility options were scored according to the expert opinions. The mean values of "navigation system" ($M = 3.9$) were between 3.4 and 4.2, and those of the remaining indicators were larger than 4.2. All these indicators were ranked as "very high important." Higher scores represent greater importance and practical feasibility of VR development for temple tour guiding.

4. VR Touring System Framework and Development

In this study, we use the Delphi method by the experience and intuition of experts to integrate the criteria for finding the functionalities of the interactive VR touring system

accurately. Moreover, according to Table 5, the system functionalities and system architecture are then established. This section provides an overview of the system functionalities and architecture. Finally, the A-Frame framework and panoramic VR construction process are also described.

4.1. System Functionalities. The local culture of Taiwan is conveyed through the system that allows the faithful and tourists to understand the history of the place. Therefore, after collecting in-depth information on the historical background and cultural references of the Jian Temple as well as visiting the site and interviewing the visitors, we found out that the general users would like to use the system to achieve the following purposes:

- (1) Planning and design of a site-specific guided tour to provide visitors with an understanding. As temples are interacting with people and are constantly being updated in the flow of time and space, the temples themselves are showcases that allow visitors to learn

and experience culture in a way that is not only spiritual but also subliminal. VR allows users to get to know the environment of the temple and the order and location of the rituals so that they can learn about it without being there.

- (2) By completing the planning of the guided tours, the temple grounds can become an exhibition space, which will not only attract visitors but also bring in crowds and give a different impression and experience to religious tourism. The VR application also allows users to learn about the history of the temple and the stories of the deities without ever visiting the site.

Therefore, we have initially summarized the three major dimensions and nine indicators for the actual construction of the virtual temple space in the form of an interactive tour and VR technology, and through the Delphi method, an expert group decision-making technique, we have implemented two rounds of questionnaires and conducted a round-robin feedback process to integrate the opinions of various experts, from which we have selected the important indicators for the application of VR in interactive tours, which have been agreed upon by the experts, as a reference for the introduction of the tour guiding system at the shrine. In addition, this study focuses on user interaction for system development, and under the framework of relevant software development methods, the user guide system is designed to be implemented on the temple site so that the system becomes an important medium for human interaction with the environment, allowing tourists to adopt a self-guided approach to stimulate their experience of traditional culture and add value to the guiding. After two less important and significant indicators were eliminated according to Table 5 of Delphi assessment processes, the requirement of the VR touring system was established. The VR system mainly demonstrated the temple space through interactive guiding and VR technologies. The goal of the system is to design VR-based interaction different from conventional tour guiding methods to help users view the display space from their points of view. The users cannot only control camera view angles but also select the paths and guiding information as if they were actually walking in the temple. Considering the results of the Delphi assessment, we propose the interactive VR touring system should be the next step in design modifications and a basis for future development. This VR touring system is divided into UI framework subsystem, VR guide subsystem, mobile APP subsystem, and archival subsystem, as depicted in Figure 2.

4.2. System Framework and Architecture. To be able to quickly prototype and evaluate VR touring experience, we focus on the web-based backend system as target application platform to meet the requirements specified in Section 4.1. Smart devices are usually equipped with a camera as well as mobile positioning and wireless Internet access; this study employed these features in a cross-platform VR mobile application with multimedia and LBS capabilities. The

system architecture comprises three major parts: the user, frontend, and backend views, as depicted in Figure 3. Moreover, these multimedia capabilities are supported a broad range of web-based application on many mobile device and not tied to specific wearable device/VR glasses or PC/Laptop. In this study, WebVR [41, 42] was built to present the virtual temple space with interactive guidance and VR technology so that users can browse the exhibition space from their own viewpoint and not only can they control the camera angle but also choose their own browsing path and navigation information, making them feel like they are actually in the scene. Finally, we used the Cordova framework to achieve cross-platform results and to reduce the problems caused by the difference in platforms among users.

4.2.1. Frontend of System Architecture. A-Frame [43] API is then used to construct WebVR effects. A-Frame is an open-source framework for the Three.js physical component system for VR experiences. Developers can create 3D and WebVR scenes using HTML, while incorporating popular game development patterns used by engines such as Unity. This technique offers a complete immersive and interactive experience including 360-degree content, interactive effects that support location tracking and control of the device, and cross-platform device usage such as VR glasses head-mounted displays, smartphones, and computer desktops. Furthermore, Primitives [43] in A-Frame Docs features basic geometric shapes (boxes, spheres, cylinders, planes, etc.), Collada models that can be created by importing 3D modelling tools or downloaded from the Internet, a sky that defines the background, and a camera that defines the angle from which the user views the scene, animation, light and shadow, panoramic video, etc. Through HTML tags, developers can easily create WebVR scenes. Thus, the VR tour guiding system built using A-Frame enabled the users to view the webpages on smart devices anytime and anywhere. With the immediate display on webpages, the applications of VR become increasingly convenient and improve users' visual experience. Moreover, the website system was presented in conventional text and graphics modes combined with fancy effects created using jQuery. Javascript was used to resolve problems between different browsers to present latest news and the most comfortable viewing experience to users. Social media were used to introduce the Ji'an Temple and create a brand on the social media platform to increase the popularity of the temple. The Facebook fan page of the temple attracts more than 2000 users. The manager can analyze and optimize relevant data through Google Analytics and FB data to evaluate whether posts achieve desired effects.

4.2.2. Backend of System Architecture. The main computer runs a Node.js server, and the server and its database are first established to provide VR mobile tour services. Relevant service elements are compiled to perform background services by rendering the VR scene with A-Frame. Through such interaction, the user can acquire information about an

TABLE 5: Results for the Delphi second round.

Dimension/indicator	M	SD	QD	CV
<i>Functional perspective</i>				
Search function	4.8	0.42	0.25	0.09
Feedback function	4.6	0.52	0.5	0.11
<i>Technology integration</i>				
Social media integration	4.7	0.48	0.5	0.10
APP development	4.5	0.71	0.5	0.16
<i>Smart system</i>				
Tour guiding system	4.8	0.42	0.25	0.09
Navigation system	3.9	0.57	0.25	0.15
Archival system	4.8	0.42	0.25	0.09

Kendall's $W = 0.78$

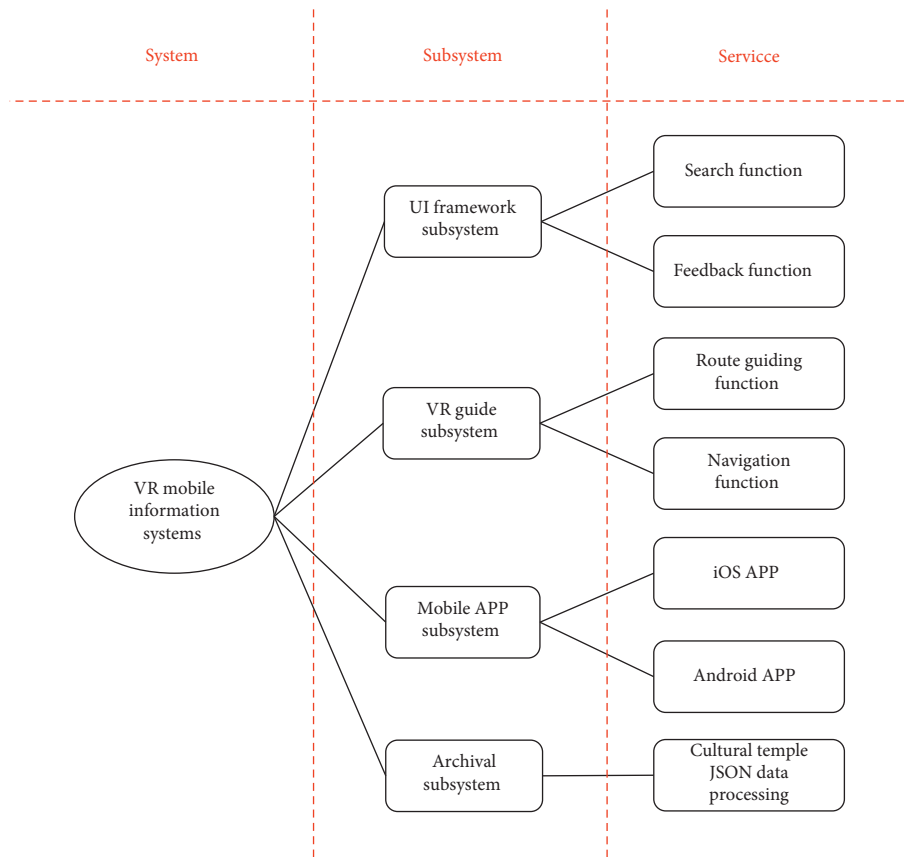


FIGURE 2: System functionalities.

attraction. In this manner, both modes integrate virtual images into a real-world setting, providing an interactive guided tour to users of the application. The Cordova plugin [44] is used to establish the cross-platform VR mobile tour system's backend data interface, which is connected and synchronized with the server and database. Cordova is an open-source mobile application development framework designed to enable programmers to develop cross-platform mobile applications with web-based application programming interfaces (APIs). It also grants JavaScript access to these interfaces to gain control of system hardware resources (e.g., camera or compass). Because smart devices run on numerous operating systems, Cordova can be used to help

programmers ensure that uniform results are achieved across various platforms, thus minimizing the problems users face when changing platforms. Cascading style sheets are used to organize the screen layout and control the background opacity. The final results are transmitted to a browser (HTML format).

4.2.3. *Some Discussion on the Panoramic VR Construction Process.* The use of virtual reality devices is becoming more and more popular, and with the increase in demand, developers are more actively betting on this. However, there is currently no standard specification for the service content of

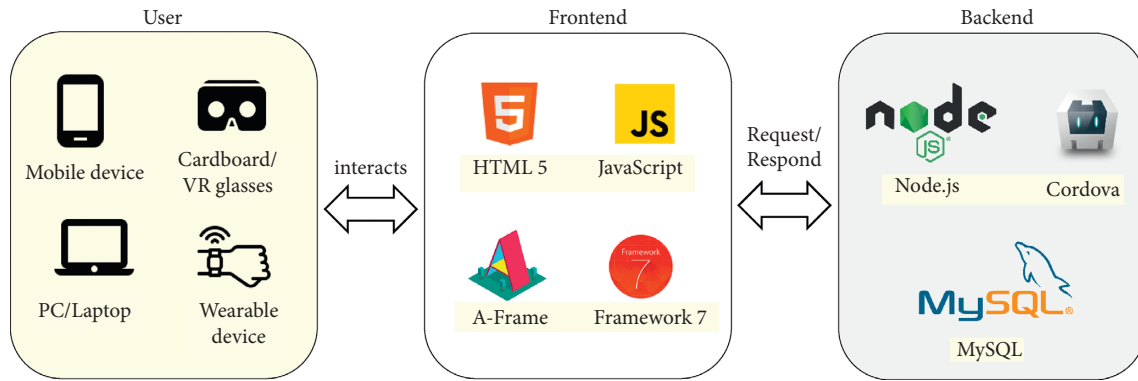


FIGURE 3: System architecture.

virtual reality; therefore, it is difficult for all users to achieve the best experience with the application of virtual reality. When the real-time update of a program is too slow, the screen resolution is too low, or the design does not consider the body feel and the environment, and it may cause discomfort to the user. This research has developed a VR system that can be applied to any device using only a web link. The previous VR devices are expensive, and each VR application usually has its own dedicated device, and the application programs of the devices are not in common with each other. Even if most people are interested in VR, they cannot afford the cost of enjoying VR. The development of WebVR is to solve the current bottleneck of VR promotion. To use WebVR technology, there is no need to learn new programming languages or new VR development software packages from previous VR developers. WebVR allows developers to quickly get started with the VR development model through web languages such as JavaScript and HTML. As in the past, you need to spend a lot of money to buy professional software. A simple web editor can immediately join the developer's team, which greatly reduces the entry barrier for VR development. Furthermore, through the open-source A-Frame framework, VR scenes can be used on mobile phones, PC, Oculus Rift, and HTC Vive. Using this construction method has the following advantages and characteristics: (1) A-Frame can reduce redundant codes. Redundant and complex code has become an obstacle for early adopters. A-Frame reduces the complex and redundant code to one line of HTML code. For example, only one `<scene>` tag is required to create a scene. (2) A-Frame is specially designed for web developers. It is based on DOM, so it can manipulate 3D/VR content like other web applications. Of course, it can also be used in conjunction with JavaScript frameworks such as React; (3) A-Frame makes the code structured. The code of Three.js is usually loose. A-Frame builds a declarative entity-component-system on top of Three.js. In addition, the components can be published and shared so that other developers can use them in the form of HTML.

Therefore, to provide users with a deeper understanding of the culture and sights of Ji'an Temple, VR display technology was employed in this project, with the aim of superimposing real-life images and data with computer-

generated virtual objects to create a complex visual sensory experience and increase users' knowledge of the area. However, to familiarize users with the local environment, we would design interactive and immersive VR tours with panoramic photos/videos of the area to enable users to learn about the culture and characteristics of the locality through the game and to increase their willingness to participate in the interaction, while the designers were able to add more tourist information to the existing tourist environment, thus increasing the feasibility of navigation. The following describes the steps and research methods required to build a panoramic VR navigation system, as shown in Figure 4. The first step is to use a panoramic camera to photograph the environment of the tour location shown in Figure 5 and dynamically load the JSON formatted scenery tour information to the server. The panoramic photographs/videos shot are imported into the A-Frame framework as a graphical scene builder, scripted for control and other related functions such as viewing angles, and developed for use in panoramic VR navigation via Cordova cross-platform.

4.3. System Demonstration. The VR tour guiding system built using A-Frame enabled the users to view WebVR on smart devices anytime and anywhere. With the immediate display on webpages, the applications of VR became increasingly convenient and improve users' visual experience. The website was presented in conventional text and graphics modes combined with fancy effects created using jQuery. JavaScript was used to resolve problems between different browsers to present latest news and the most comfortable viewing experience to users. A-Frame was used to create a VR system. In the VR system of Ji'an Temple tour guiding, a user can see a trigger spot in the center of the monitor (Figure 6). Users can swipe the screen of cell phone or move their cell phone to select a position they want to go. Clicking a position can trigger corresponding locations. Figure 7 demonstrates that films containing information of relevant cultural relics are available and audio guiding that can be played by clicking the play button below. In addition, social media are used to introduce Ji'an Temple and create a brand on the social media platform to increase the popularity of the temple. The manager of the fan page sometimes

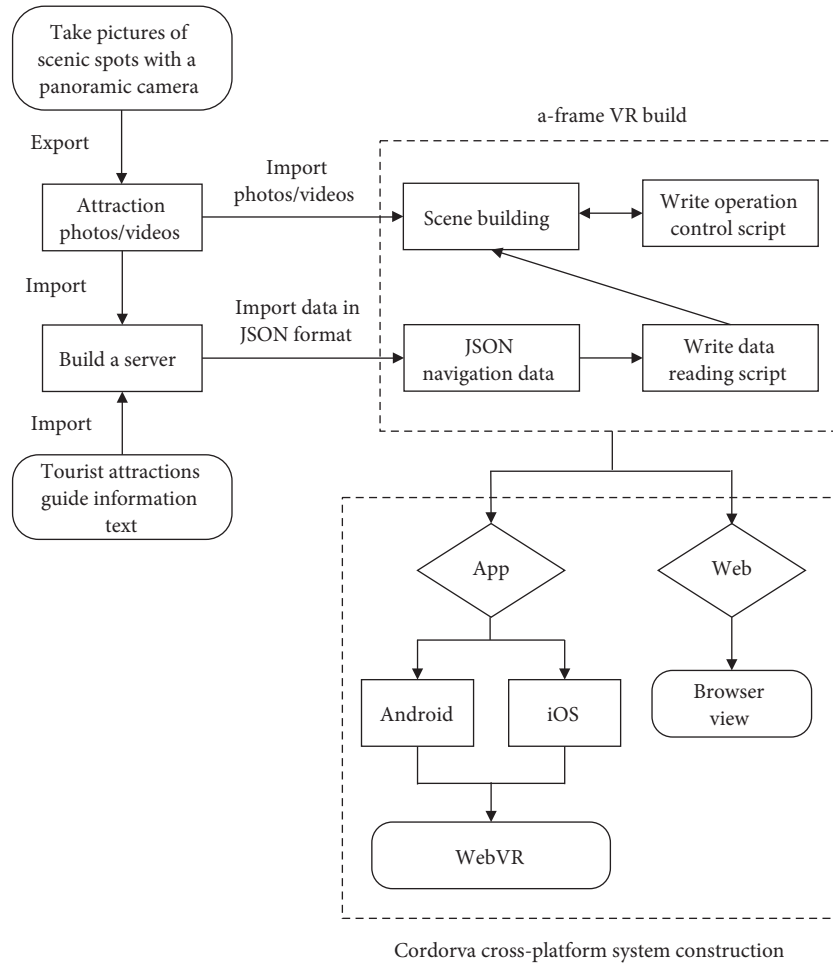


FIGURE 4: The workflow for building a panoramic VR touring system.



FIGURE 5: An example of the panoramic image in Ji'an Temple.

plan and design graphics and text contents of posts, and he can also analyze and optimize relevant data through Google Analytics and FB data to evaluate whether posts achieve desired effects. Finally, the display of operation of VR headset glasses is shown in Figure 8.

5. QUIS Results and Discussion

To understand the user's satisfaction with the usage of the VR touring system, we employed the Questionnaire for User Interaction Satisfaction (QUIS) [45] to conduct a quantitative

study. The survey respondents are mainly temple officials, pilgrims, and Internet citizens. Moreover, the main focus was on answering representative questions with adequate satisfaction and helpfulness. The questions were answered by users following their action learning using the VR touring system. The questionnaire had four dimensions: (1) overall reaction to the VR touring system; (2) display of the VR touring system; (3) contents of the VR touring system; and, (4) usage of the VR touring system. The questionnaire is divided into these four parts and contains 18 questions. Among them, the users were asked to rate the importance and feasibility of each



FIGURE 6: Independent control of tour routes.



FIGURE 7: Video story and audio guiding.

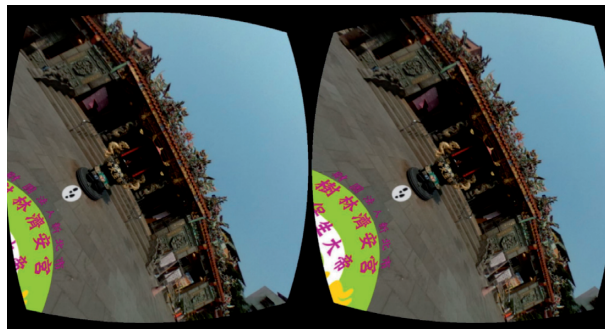


FIGURE 8: Display of operation of VR headset glasses.

indicator according to a 6-point Likert scale, with anchors of 1 (strongly disagree) and 6 (strongly agree) [32]. The aim was to obtain a general understanding of the satisfaction of each user, which could provide evidence and a foundation for data analyses. From Table 6, the mean values of the four dimensions revealed that the usage of the VR touring system as favorable (4.72); however, their overall satisfaction toward the tour guiding display was slightly lower (4.53). In a further analysis of various items, the median value of 3.5 was used for a 6-point Likert scale. The mean values of 18 items were higher than 3.5, the median value, suggesting that the users generally considered the VR touring system to be satisfactory.

The mean values of the first item “I think the VR touring system is (undesirable/excellent)” and the second item “I think the VR touring system is (difficult to use/easy to use)” were close to 5 points, indicating that the proposed system was easy to operate and excellent in quality. However, the mean values of the sixth item “I think the VR touring system is (dull/lively)” and the ninth item “The resolution clarity of the screen is (blurred/clear)” were 4.00 and 4.17, respectively, that is, the sixth item and the ninth item are the two poorer satisfactions. These results revealed that this system is generally satisfactory and easy to operate, but relatively uninteresting.

TABLE 6: QUIS result analysis.

Items	Rating	M	SD
	1 2 3 4 5 6		
<i>Overall reaction to the VR touring system</i>		4.53	
I think the VR touring system is:	Undesirable/excellent	5.00	0.739
I think the VR touring system is:	Difficult to use/easy to use	5.00	0.426
I think the VR touring system is:	Unsatisfactory/satisfactory	4.50	1.087
I think the performance of the VR touring System is:	Low/high	4.42	0.669
I think the VR touring system is:	Boring/exciting	4.25	0.622
I think the VR touring system is:	Dull/lively	4.00	1.044
<i>Display of the VR touring system</i>		4.61	
To read the information on the screen is:	Difficult/easy	4.83	0.835
The structure of system functionalities is:	Confusing/obvious	4.83	0.835
The resolution clarity of the screen is:	Blurred/clear	4.17	0.718
<i>Contents of the VR touring system</i>		4.67	
The word used for the functional button is:	Inconsistent/consistent	4.58	0.669
The relevance of touring contents and usage Requirements is	Never/always	4.67	0.778
The position of the message on the screen is:	Inconsistent/consistent	4.67	0.888
Does the touring help to further understand?	Never/always	4.75	0.622
<i>Usage of the VR touring system</i>		4.72	
To self-operate the VR touring system is:	Difficult/easy	4.83	0.937
To use the mobile tracking function is:	Difficult/easy	4.42	0.996
To use the audio and video touring Functions is:	Difficult/easy	4.92	0.996
Compared with the text navigation, is the VR touring system easier to understand?	Never/always	4.58	0.793
The prompt message displayed on the screen is:	Helpless/helpful	4.83	1.115

6. Conclusions

The system evaluation was divided into two stages: expert assessment and target user usability test. In the first stage, 10 experts of relevant domains and objective perspectives were invited to provide their opinions through the Delphi questionnaire surveys. Through literature review, we summarized three major dimensions and nine indicators for the experts to evaluate. Subsequently, based on the experts' opinions, two indicators (reminder function and smart terminal management) were removed. VR tour guiding was established thereafter. In the second stage, users, including students, Internet users, and pilgrims, were invited. VR tour guiding, based on the integrated outcomes of the Delphi expert questionnaires, was provided to these participants, and the usability of the system was tested. QUIS was employed to analyze the users' satisfaction to the tour guiding system; the satisfaction analysis comprised four main axes: the overall reaction, tour guiding display, tour guiding content, and tour guiding operation. The developed system was rated by the target users through the QUIS for its usability. This study analyzed the overall reaction to the tour-guiding system, display, content, and operation. The analysis results revealed that, in general, the users perceived VR tour guiding to be convenient and easy to use. The tour guiding system's display and content presented clear information to the users, aiding them in gaining further understanding of the introduced item. Statistical analysis results of the expert and user questionnaires revealed that interactive VR was

more efficient in communicating information to users than conventional text and graphics webpages. Because interactive VR tour guiding was incorporated into the proposed system, the interaction between the users and objects increased the users' concentration as well as information communication efficiency. Through this combination, a revolutionary method of tour guiding was developed. Conventional graphics and text interpretation can no longer satisfy the needs of the general public. Additional information technologies must be integrated with tour guiding to attract user attention by adding diverse options to interactive VR tour guiding systems. The easy-to-operate and convenient systems can provide unprecedented online browsing experience to users or customers of businesses and subsequently strengthen customers' attachment to businesses effectively.

7. Limitations and Future Studies

There is still room for improvement in this research in the future. First of all, our target sample is limited to the case of Ji'an Temple in Taiwan. It did not take into account the technological and cultural changes between different countries, so a limitation with our chosen method was that we were unable to make any detailed comparisons between application performance and user experience with other methods. Only QUIS research can be conducted. Furthermore, this research uses a panoramic image method to implement a VR navigation system. Although it has a three-

dimensional effect, the spherical virtual image will form an obvious intersection point stitching problem directly above and directly below the space. In the future, it is hoped that the problem of the intersection of the spheres can be improved without affecting the three-dimensional effect. In addition, at present, the concept of simulating the horizontal distance between the eyes is used to draw the scene horizontally. If you turn your head in other directions to watch, it will be visually distorted and the images will not be able to merge. In the future, further discussions can be made in this direction, which is expected to reduce the dizziness. Finally, the future application of VR combined with imagination can develop infinite possibilities; in addition to the existing visual and auditory senses, humans still have touch, smell, taste, and various other senses so that users can have a more immersive experience in the virtual world. Integrating these perceptions in the future will be one of the important directions. Therefore, including how to simulate various perceptions, how to combine, transmit, and synchronize various sensory signals, etc., are all important topics; in addition, new applications developed by VR, such as how to remotely control through VR and how to provide further 360° panoramic video services with lower latency will also drive the evolution and development of various new technologies.

Data Availability

The data used to support the findings of the study are included within the article.

Disclosure

Part of the results of this research is also published at the 3rd IEEE International Conference on Knowledge Innovation and Invention (<https://ieeexplore.ieee.org/document/9318862>).

Conflicts of Interest

The authors declare that they have no conflicts of interest regarding the publication of this paper.

Acknowledgments

This research was partially supported by the “Teaching Practice and Research Program” (PEE1080223), sponsored by the Ministry of Education and the Ministry of Science and Technology, Taiwan, R.O.C., under Grant MOST 108-2221-E-431-003.

References

- [1] Y. Xie, L. Ryder, and Y. Chen, “Using interactive virtual reality tools in an advanced Chinese language class: a case study,” *TechTrends*, vol. 63, no. 3, pp. 251–259, 2019.
- [2] H.-M. Chiao, Y.-L. Chen, and W.-H. Huang, “Examining the usability of an online virtual tour-guiding platform for cultural tourism education,” *Journal of Hospitality, Leisure, Sports and Tourism Education*, vol. 23, pp. 29–38, 2018.
- [3] B. O. Han, Y. H. Kim, K. Cho, and H. S. Yang, “Museum tour guide robot with augmented reality,” in *Proceedings of the 16th International Conference on Virtual Systems and Multimedia (VSMM)*, pp. 223–229, IEEE, Seoul, Korea, 2010.
- [4] D. M. Zhou, D. Shi, B. Wang et al., “Research on virtual tourist guide training system based on virtual reality technology,” in *Proceedings of the Third International Symposium on Knowledge Acquisition and Modeling*, pp. 155–158, IEEE, Wuhan, China, 2010.
- [5] J. H. Lo and G. Z. Gong, “Touring system using augmented reality-A case study of yilan cultural industries,” in *Proceedings of the 3rd IEEE International Conference on Knowledge Innovation and Invention (ICKII)*, pp. 204–207, IEEE, Kaohsiung, Taiwan, 2020.
- [6] Y. T. Hsu, “Recognition, designation, and local Practice of “folk custom and related cultural artifacts:” an example of “Yunlin Liu Fang Ma Guolu”” *Min Su Qu Yi*, vol. 193, pp. 221–265, 2016.
- [7] P. R. Katz, “Bridging the gaps: methodological challenges in the study of Taiwanese popular religion,” *International Journal of Taiwan Studies*, vol. 1, no. 1, pp. 36–63, 2018.
- [8] Shulin Ji'an Temple, 2021, <https://www.jian.org.tw>, In Chinese.
- [9] K. W. Hsieh, “A review and analysis of the studies of the Bao-sheng emperor belief,” *Journal of World Religions*, vol. 16, pp. 95–124, 2010, In Chinese.
- [10] J. H. Lo and M. J. You, “Design and implementation of the interactive virtual reality touring system-a case study of Shulin Ji'an temple in Taiwan,” in *Proceedings of the 3rd IEEE International Conference on Knowledge Innovation and Invention (ICKII)*, pp. 115–117, IEEE, Kaohsiung, Taiwan, 2020.
- [11] Gartner's Top 10 Strategic Technology Trends for 2020, 2021, <https://www.gartner.com/smarterwithgartner/gartner-top-10-strategic-technology-trends-for-2020/>.
- [12] A. Dix, A. J. Dix, J. Finlay, G. D. Abowd, and R. Beale, *Human-Computer Interaction*, Pearson Education, London, UK, 2004.
- [13] K. Choi, Y.-J. Yoon, O.-Y. Song, and S.-M. Choi, “Interactive and immersive learning using 360° virtual reality contents on mobile platforms,” *Mobile Information Systems*, vol. 2018, Article ID 2306031, 12 pages, 2018.
- [14] H. Huang and C.-F. Lee, “Factors affecting usability of 3D model learning in a virtual reality environment,” *Interactive Learning Environments*, pp. 1–14, 2019.
- [15] J. Steuer, “Defining virtual reality: dimensions determining telepresence,” *Journal of Communication*, vol. 42, no. 4, pp. 73–93, 1992.
- [16] Y. Chang and G.-P. Wang, “A review on image-based rendering,” *Virtual Reality & Intelligent Hardware*, vol. 1, no. 1, pp. 39–54, 2019.
- [17] J. H. Lee and C. E. Rhee, “Flexibly connectable light field system for free view exploration,” *IEEE Transactions on Multimedia*, vol. 22, no. 4, pp. 980–991, 2019.
- [18] D. Song, T. Li, W. Li, W. Nie, W. Liu, and A. Liu, “Universal cross-domain 3D model retrieval,” *IEEE Transactions on Multimedia*, 2020.
- [19] J. Park, I.-B. Jeon, S.-E. Yoon, and W. Woo, “Instant panoramic texture mapping with semantic object matching for large-scale urban scene reproduction,” *IEEE Transactions on Visualization and Computer Graphics*, vol. 27, no. 5, pp. 2746–2756, 2021.
- [20] O. Erat, M. Hoell, K. Haubenwallner, C. Pirchheim, and D. Schmalstieg, “Real-time view planning for unstructured lumigraph modeling,” *IEEE Transactions on Visualization and Computer Graphics*, vol. 25, no. 11, pp. 3063–3072, 2019.

- [21] J. Pirker and A. Dengel, "The potential of 360-degree virtual reality videos and real VR for education-A literature review," *IEEE Computer Graphics and Applications*, 2021.
- [22] T. Marrinan and M. E. Papka, "Real-time omnidirectional stereo rendering: generating 360° surround-view panoramic images for comfortable immersive viewing," *IEEE Transactions on Visualization and Computer Graphics*, vol. 27, no. 5, pp. 2587–2596, 2021.
- [23] H. Shum and S. B. Kang, "Review of image-based rendering techniques," in *Visual Communications and Image Processing*, vol. 4067, pp. 2–13, International Society for Optics and Photonics, Bellingham, WC, USA, 2000.
- [24] H. A. Linstone and M. Turoff, *The Delphi Method*, Addison-Wesley, Reading, MA, USA, 1975.
- [25] H. A. Linstone and M. Turoff, "Delphi: a brief look backward and forward," *Technological Forecasting and Social Change*, vol. 78, no. 9, pp. 1712–1719, 2011.
- [26] H. D. Musa, M. R. Yacob, A. M. Abdullah, and M. Y. Ishak, "Delphi method of developing environmental well-being indicators for the evaluation of urban sustainability in Malaysia," *Procedia Environmental Sciences*, vol. 30, pp. 244–249, 2015.
- [27] J. C. Brancheau, B. D. Janz, and J. C. Wetherbe, "Key issues in information systems management: 1994-95 SIM Delphi results," *MIS Quarterly*, vol. 20, no. 2, pp. 225–242, 1996.
- [28] A. P. C. Chan, E. H. K. Yung, P. T. I. Lam, C. M. Tam, and S. O. Cheung, "Application of Delphi method in selection of procurement systems for construction projects," *Construction Management and Economics*, vol. 19, no. 7, pp. 699–718, 2001.
- [29] C. W. Holsapple and K. D. Joshi, "Knowledge manipulation activities: results of a Delphi study," *Information & Management*, vol. 39, no. 6, pp. 477–490, 2002.
- [30] C. Okoli and S. D. Pawlowski, "The Delphi method as a research tool: an example, design considerations and applications," *Information & Management*, vol. 42, no. 1, pp. 15–29, 2004.
- [31] R. Schmidt, K. Lyytinen, M. Keil, and P. Cule, "Identifying software project risks: an international Delphi study," *Journal of Management Information Systems*, vol. 17, no. 4, pp. 5–36, 2001.
- [32] A. Joshi, S. Kale, S. Chandel, and D. Pal, "Likert scale: explored and explained," *British Journal of Applied Science & Technology*, vol. 7, no. 4, pp. 396–403, 2015.
- [33] K. Horner, M. Islam, L. Flygare, K. Tsiklakis, and E. Whaites, "Basic principles for use of dental cone beam computed tomography: consensus guidelines of the European academy of dental and maxillofacial radiology," *Dentomaxillofacial Radiology*, vol. 38, no. 4, pp. 187–195, 2009.
- [34] M. R. Geist, "Using the Delphi method to engage stakeholders: a comparison of two studies," *Evaluation and Program Planning*, vol. 33, no. 2, pp. 147–154, 2010.
- [35] P.-C. Chang, N.-T. Tsou, B. J. C. Yuan, and C.-C. Huang, "Development trends in Taiwan's opto-electronics industry," *Technovation*, vol. 22, no. 3, pp. 161–173, 2002.
- [36] S. Cafiso, A. Di Graziano, and G. Pappalardo, "Using the Delphi method to evaluate opinions of public transport managers on bus safety," *Safety Science*, vol. 57, pp. 254–263, 2013.
- [37] P. Legendre, "Coefficient of concordance," *Encyclopedia of Research Design*, vol. 1, pp. 164–169, 2010.
- [38] J. Henning and H. Jordaan, "Determinants of financial sustainability for farm credit applications-a Delphi study," *Sustainability*, vol. 8, no. 1, p. 77, 2016.
- [39] R. Ab Latif, A. Dahlan, Z. A. Mulud, and M. Z. M. Nor, "The Delphi technique as a method to obtain consensus in health care education research," *Education in Medicine Journal*, vol. 9, no. 3, 2017.
- [40] L. S. Rodrigues and L. Amaral, "Key enterprise architecture value drivers: results of a Delphi study," in *Proceedings of the Conference: 21st International Business Information Management Association Conference, IBIMA 2013*, Vienna, Austria, 2013.
- [41] S. G. Santos and J. C. Cardoso, "Web-based virtual reality with a-frame," in *Proceedings of the 14th Iberian Conference on Information Systems and Technologies (CISTI)*, pp. 1-2, IEEE, Coimbra, Portugal, 2019.
- [42] M. J. Prins, S. N. B. Gunkel, H. M. Stokking, and O. A. Niamut, "TogetherVR: a framework for photorealistic shared media experiences in 360-degree VR," *SMPTE Motion Imaging Journal*, vol. 127, no. 7, pp. 39–44, 2018.
- [43] S. Neelakantam and T. Pant, "Introduction to a-frame," *Learning Web-Based Virtual Reality*, Apress, Berkeley, CA, USA, 2017.
- [44] Cordova, 2021, <https://cordova.apache.org/>.
- [45] K. L. vNorman, B. Shneiderman, B. Harper, and L. Slaughter, *Questionnaire for User Interaction Satisfaction*, University of Maryland, College Park, MD, USA, 1989.

Research Article

Rational Supplier Selection Based on Two-Phase Deep Analysis considering Fuzzy QFD and Game Theory

Feng Li ¹, Senhao Luo ², Yi Wang ¹ and Chia-Huei Wu ³

¹Department of Management Science and Engineering, School of Information, Beijing Wuzi University, Beijing 101149, China

²Department of Management Engineering, School of Economics & Management, Xidian University, Xi'an 710071, China

³Department of Hotel Management and Culinary Creativity, Minghsin University of Science and Technology, Hsinchu 304, Taiwan

Correspondence should be addressed to Chia-Huei Wu; chiahuei530@gmail.com

Received 4 March 2021; Revised 23 June 2021; Accepted 15 July 2021; Published 26 July 2021

Academic Editor: Hsu-Yang Kung

Copyright © 2021 Feng Li et al. This is an open access article distributed under the Creative Commons Attribution License, which permits unrestricted use, distribution, and reproduction in any medium, provided the original work is properly cited.

Viewing from the perspective of a traditional manufacturing enterprise, the paper proposes a fuzzy comprehensive evaluation system model, which selects the most suitable supplier or suppliers to undertake the supply tasks and to achieve the purposes of reducing procurement costs and improving the supply quality and reliability, so as to fully meet customer demands. Based on decision-makers' preferences and suppliers' supply capabilities, subjective and objective weight of criteria are both developed for supplier selection with the corresponding weighting method, namely, quality function deployment (QFD) and entropy weight. Specially, the two-phase fuzzy QFD method combined with the trapezoidal fuzzy number (TFN) is creatively applied to realize the complicated conversion process. Furthermore, the game theory is employed to combine the advantages of the subjective and objective weighting method, by which the comprehensive weight can be determined. A numerical example is given to demonstrate the proposed modeling process. Through programming drawing images for comparative analysis and sensitivity analysis, study image trends, and draw conclusions, the proposed model effectively alleviates the weight deviation and has higher rationality and extensibility in supplier selection.

1. Introduction

Supplier selection is of great significance to the manufacturing. Selecting the optimal supplier can effectively reduce the procurement costs and improve the quality and reliability of the supply, thereby improving the enterprise's profit margin by minimizing the upstream costs of the supply chain [1]. At the same time, it can make contributions to improve the customers' satisfaction. Therefore, the subjective and objective factors that affect the working efficiency of the supplier should be considered adequately by manufacturers. Multicriteria decision making (MCDM) methods that can effectively determine subjective and objective weights of evaluation criteria have been applied to various fields, such as several frequently used methods of obtaining weights include analytic network process (ANP), quality function deployment (QFD), best worst method (BWM), grey relational analysis (GRA), and entropy weight.

However, both subjective and objective weights have their own limitations. In fact, the subjective weight only reflects the decision-makers' preferences and ignores the actual efficiency of suppliers, which is greatly affected by human factors. On the contrary, the objective weight focuses on the objective supply capabilities of suppliers and ignores factors such as the environment of the manufacturing enterprise and the interest relationship of the upstream of the supply chain, which are closely related to the experience of decision makers.

Game theory plays an important role in weighing the subjective and objective weight, which uses mathematical tools to study how the two sides with conflict of interest choose the optimal strategy, respectively [2]. In other words, game theory mainly studies the decision-making subjects interacting with each other, how to make decisions, and how to achieve equilibrium. Game theory was first used as a strategic bargain in economics [3], and then, it is widely used

in the management, engineering, and many other fields [4]. Compared with other tools, game theory better deals with the common disequilibrium in reality, and more effectively makes individual and collective rationality converge under the condition of incomplete information and imperfect competition. In addition, game theory provides a replicable template for solving complex interactions between contradictory subjects in the process of complex modeling, which is conducive to finding the optimal solution for all parties. It works well when two or more players have a conflict of interest. Similarly, because the subjective weighting method is affected by human factors, while the objective weighting method is absolutely objective, there is a big difference in the weight coefficient determined by the two methods for the same evaluation index. Game theory seeks the consistency or compromise of its correlation weight values in fully considering the foundation of the characteristics of the subjective and objective weight method, so as to minimize the deviation of the subjective and objective weight. In the process, they can be regarded as the two sides with conflict of interest, while the comprehensive weight is regarded as the benefit combination of the game. Therefore, the comprehensive weight based on Nash equilibrium is obtained and applied to rational supplier selection. In this paper, a rational weighting model combining with game theory is proposed to evaluate and select the most suitable suppliers. Considering both decision-makers' preferences and suppliers' capabilities, the subjective and objective weight of supplier evaluation criteria are developed for supplier selection with QFD and entropy weight. Among them, a two-phase fuzzy QFD method combined with TFN is creatively used to realize the complicated conversion process. The most critical step, game theory, is employed to combine the advantages of the subjective and objective weight, by which the comprehensive weight can be determined. The structure of the proposed model is shown in Figure 1.

The remainders of the paper are organized as follows. Section 2 is literature review. Section 3 introduces the preliminaries involved in the paper. The proposed fusion model based on two-phase fuzzy QFD, entropy weight, and game theory is introduced in Section 4. Section 5 demonstrates a numerical example to illustrate the effectiveness of the proposed model. Section 6 makes comparative analysis and sensitivity analysis. The final research conclusions are presented in Section 7.

2. Literature Review

Supplier selection is of great significance to the core competitiveness of manufacturing enterprises [5]. Choosing suitable suppliers is not only beneficial to reduce inventory costs and transaction costs but also improve the order fulfillment rate. At the same time, information technology and incentive mechanism are implemented to enable enterprises and suppliers to become a community of interests, and a rapid reaction system is established in order to shorten the procurement cycle and make an agile response to market demand. The common methods and related literature of supplier multicriteria evaluation are shown in Table 1.

There are many studies on supplier evaluation and selection for manufacturing enterprises. Dweiri et al. put forward the decision support model of supplier selection in AHP and further carried out sensitivity analysis to test the robustness of supplier selection decision [6]. Starting from the concept of elasticity, Ahmadi et al. used AHP to calculate the weight of sustainable development criteria and interferon gamma release assay to rank suppliers and proposed a structured and integrated evaluation decision model for sustainable suppliers in telecommunications industry [7]. Zavadskas et al. used fuzzy AHP to evaluate and select raw material suppliers for pipeline production [8]. Ayağ and Samanlıoğlu comprehensively considered the influence of quantitative and qualitative factors on supplier selection and proposed an intelligent solution method for the supplier selection problem based on fuzzy ANP [9]. Yazdani et al. solved the relationship between customer demands with decision-making trial and evaluation laboratory (DEMATEL) and then determined the degree of relationship between each pair of supplier criteria and customer demands by the QFD [10]. Lima-Junior et al. used fuzzy QFD to weight each indicator and then evaluated the degree of difficulty of supply to obtain information for each indicator evaluation [11]. Karsak and Dursun proposed a fuzzy multicriteria group decision-making method for supplier selection based on QFD, fuzzy information fusion, and binary language representation model [12]. Gupta and Barua used BWM to rank selection criteria and then used fuzzy TOPSIS to rank the weight of supplier selection criteria, aiming to select suppliers based on the green innovation ability of small- and medium-sized enterprises [13]. Rezaei et al. combined with screening and BWM and developed a three-phase supplier selection method [14]. Pitchipoo et al. adopted grey relational analysis (GRA) as performance indicators to determine the optimal suppliers, then used the principal component analysis and entropy weight method to evaluate the corresponding weight values of each performance indicators, and proposed an optional decision-making model to evaluate the relative performance of suppliers with multiple outputs and inputs [15]. Badi and Pamucar applied the mixed grey theory and Marcos method in a steel company's supplier selection decision to help it improve competitiveness [16]. Govindan and Sivakumar used the fuzzy technology of similarity ranking with fuzzy TOPSIS to evaluate and select potential suppliers and proposed a model to support the selection of the best green suppliers and the order allocation among potential suppliers [17]. Mousakhani et al. took into account the opinions of priority experts on the relative importance of criteria, calculated the weight of decision makers with the extended interval-2 fuzzy TOPSIS method, sorted the potential alternatives according to the interval-2 fuzzy hamming distance measure, and proposed a green supplier selection model based on the group decision method [18]. Blagojević et al. established a comprehensive entropy fuzzy pivot pairwise relative criteria importance assessment-data envelopment analysis (PIPRECIA-DEA) model to study how to determine the security state of B&H under particular uncertainty conditions [19]. Wei et al. obtained the optimal

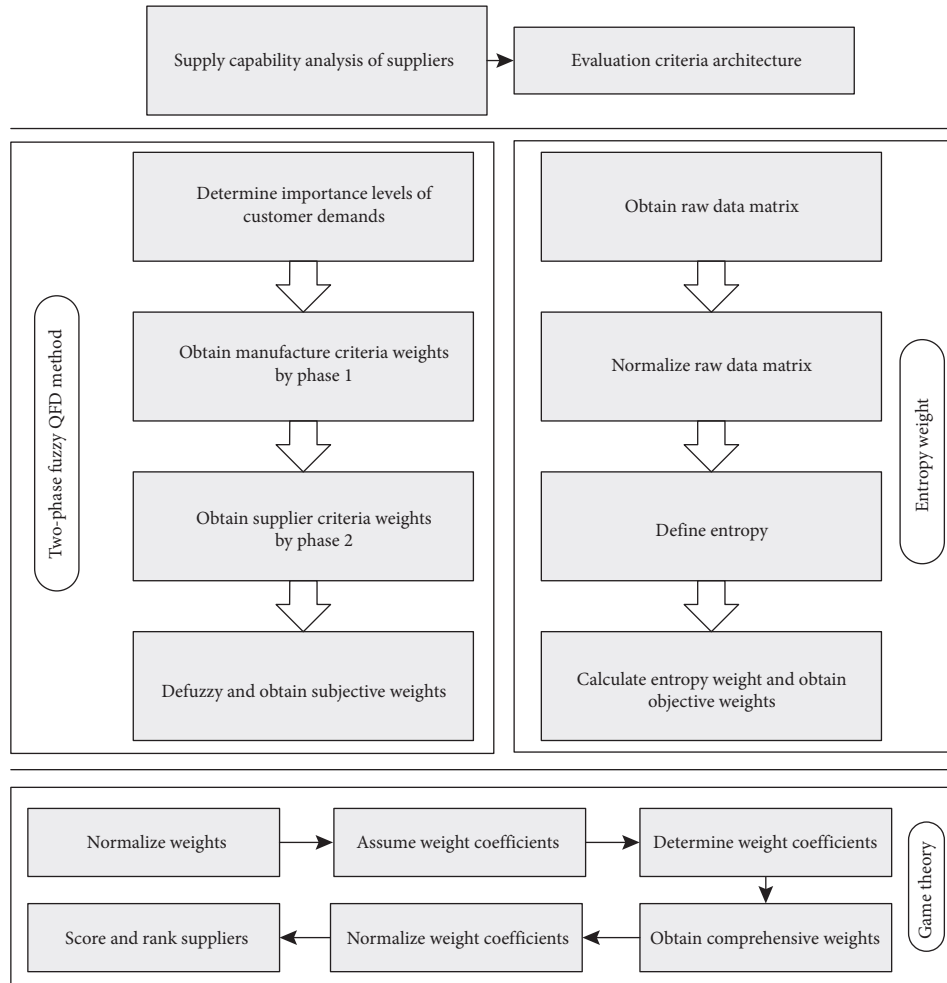


FIGURE 1: The structure of the proposed model.

TABLE 1: The common methods and related literature.

	AHP/ANP	QFD	BWM	GRA	TOPSIS	Entropy weight	Game theory
Zavadskas et al.	✓						
Dweiri et al.	✓						
Ahmadi et al.	✓						
Ayağ et al.	✓						
Yazdani et al.		✓					
Lima-Junior et al.		✓					
Karsak et al.		✓					
Gupta et al.			✓		✓		
Rezaei et al.			✓				
Pitchipoo et al.				✓		✓	
Badi and Pamucar				✓			
Govindan et al.					✓		
Mousakhani et al.					✓		
Blagojević et al.						✓	
Wei et al.						✓	
Wei et al.						✓	
Lai et al.	✓					✓	✓
Liu et al.	✓					✓	✓

choice with the largest Euclidean and Hamming distance from NIS and designed a probabilistic uncertain language coding method based on sine entropy weight, which is

applied in green supplier selection [20]. In order to obtain the optimal green supplier, Wei et al. provided an integrated model of entropy weight and multiattributive border

approximation area comparison (MABAC) under uncertain probabilistic linguistic sets (UPLTSs). Information entropy is used to calculate the weight of criteria, and UPLTSs are used to get the final ranking results of green suppliers [21]. At the same time, there are many innovative methods for supplier evaluation and selection. Hosseini and Khaled discussed the elasticity criteria of supplier selection, combined binomial logistic regression, classification regression tree, and neural network, used the integrated method to predict the elasticity of a single supplier, and used different supplier selection models to rank [22]. Chakraborty et al. applied D-number to solve the uncertainty problem in the process of supplier selection [23]. Durmić used the full consistency method (FUCOM) to determine the importance of the criteria [24]. Xiao et al. used criteria importance through the intercriteria correlation (CRITIC) method to determine the weight of criteria and proposed a new intuitionistic fuzzy multicriteria group decision-making method. Finally, an application example of green supplier selection in iron and steel industry is given, and an objective weighting method is used to improve the effectiveness of evaluation [25]. Lei et al. proposed probabilistic uncertain linguistic QUALIFLEX (PUL-QUALIFLEX) with the CRITIC method to obtain the optimal solution and applied the method to an application example of green supplier selection [26]. In the research on the flood risk assessment model based on fuzzy comprehensive evaluation, Lai et al. used AHP and entropy weight method to calculate the subjective and the objective weight, respectively, and combined the two with game theory to reflect the intention of decision makers and the information content provided by each indicator, effectively correcting the one side of the single weight method [27]. Then, in order to overcome the deficiency that AHP cannot deal with the dependence and interaction between elements at different levels quantitatively, Liu et al. proposed an ANP method based on game theory, which effectively solved the problem of supplier selection under uncertain environment, and adjusted the index weight with DEMATEL, making the evaluation result more reasonable [1].

However, the previous studies still have some drawbacks or challenges. QFD has the advantage of fully paying attention to customer demands, so many studies apply QFD to supplier selection. However, most of them that involve the QFD method only implement once or ignore the manufacturer criteria and directly implement the conversion from customer demands to supplier criteria, which makes the conversion process between criteria have gap, and the connection is not tight enough. Entropy weight has absolute objectivity. More importantly, both subjective and objective weights have limitations. In order to overcome these drawbacks, a fuzzy two-phase QFD method combined with TFN is creatively used to realize the complicated conversion process to select the most suitable supplier or suppliers to fully meet customer demands. On the basis of fully considering the characteristics of fuzzy QFD and entropy weight methods, the paper applies game theory to seek for the consistency or compromise of subjective and objective weight values from the perspective

of a traditional manufacturing enterprise, so as to minimize the deviation of subjective and objective weights.

3. Materials and Methods

3.1. Quality Function Deployment. QFD, also known as house of quality (HOQ), is a customer-driven product development method. Starting from the perspective of quality assurance, customer demands can be obtained through certain market survey methods, converting customer demands into technical demands in the product development stage by the matrix graphic method, and identifying which parameter is the most important to customer satisfaction. These key parameters form the measurement index of design content and are finally decomposed into various stages and functional departments of product development. In order to ensure the quality of final products, it is necessary to coordinate the work of various departments to make the products designed and manufactured truly meet the requirements of customers.

HOQ is the core tool for establishing the quality function deployment system. It realizes the quality function deployment process through a series of charts and matrices [28]. As shown in Figure 2(a), the HOQ looks like a house, with a row and column matrix filled with quantized values at the center of the house. The left wall represents the customer attributes, namely, customer demands (WHATs), while the ceiling is usually defined as product requirements (HOWs), i.e., how to design products to meet customer demands. The quantitative relationship between WHATs and HOWs is the core element of the QFD process. Other parts of the HOQ structure provide supporting information for the QFD. To be specific, the HOQ consists of the following parts: (A) represents the needs of customers; (B) represents engineering characteristics or methods; (C) represents the relationship matrix between WHATs and HOWs; (D) indicates the level of importance of expectations; (E) represents the customer benchmark; (F) represents the relationship among engineering characteristics.

QFD originated from the Japanese industry and gradually became a standard planning tool integrating collection, analysis, and optimization after the promotion by the Americans [29]. The main functions of QFD are reducing design changes, shorten development cycle, improve quality, improve customer satisfaction, and reduce design and manufacturing costs. QFD is applicable to both new product development and old product improvement, suitable for both general products and large complex products. It applies to both hardware and software products and service management, and it is an indispensable tool in the six sigma design process [30]. Toyota, General Motors, Volkswagen, Ford, and Chrysler all use QFD technology in the product planning process. For example, Toyota reduces the production cost of a commercial vehicle by 61% through QFD technology.

3.2. Entropy Weight. Information entropy theory was originally introduced by Shannon from thermodynamics to information theory [31] and has been widely applied in

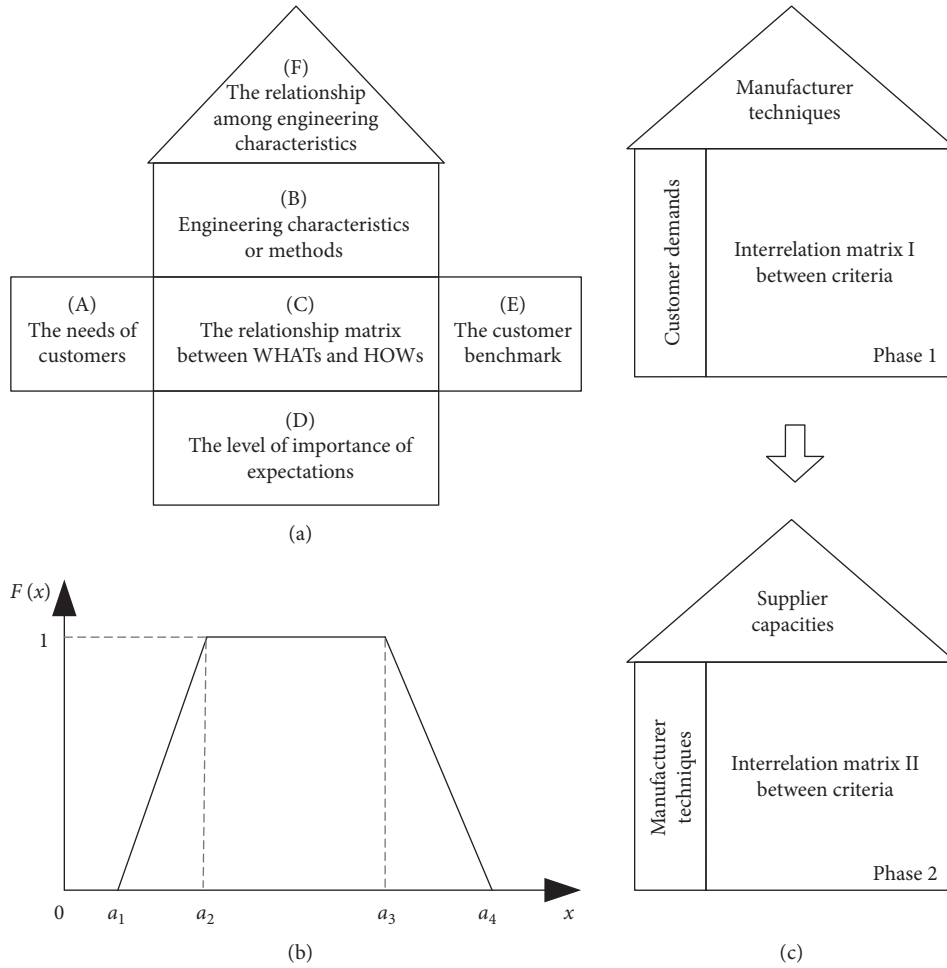


FIGURE 2: The graphics involved in preliminaries.

decision science, social economy, and other fields. Information entropy is an uncertain measure of a system in a disordered state [32], and for the entropy weight, it can reflect the useful quantitative information of the evaluation indexes. Supposing that there are m different states in a system and the probability of each state is P_i ($i = 1, 2, \dots, m$), then the entropy of the system is

$$E = -\frac{1}{\ln m} \sum_{i=1}^m p_i \ln p_i. \quad (1)$$

The basic idea of the entropy weight method is to determine the objective weight according to the index variability [33]. Generally speaking, the smaller the information entropy E of an index is, the greater the variation degree of the index value is, the more information it can provide, the greater the role it can play in the comprehensive evaluation, and the greater its weight will be [19]. On the contrary, the higher the information entropy E of an index is, the smaller the variation degree of the index is, the less the information it provides, the smaller the role it plays in the comprehensive evaluation, and the smaller its weight is [34]. Entropy weighting steps are shown in detail in Section 4.2.

3.3. *Game Theory.* The study of game theory originated in the 18th century and developed in the work of Zermelo, Borel, and Von Neumann [35]. In 1944, Von Neumann and Morgenstern published *The Theory of Games and Economic Behavior* [36], which laid a solid foundation for the theories and methods of cooperative games. In 1951, Nash proposed the concept of Nash equilibrium [37, 38], from which game theory began to flourish and was applied in economics, psychology, politics, and other fields.

Noncooperative static game with complete information, also known as a strategic game, is mainly composed of three elements: participants, strategy set, and utility function. In game theory, players are both rational and selfish. Each player has a set of all possible choices of strategies, and the specific combination of strategies of all players corresponds to a utility function. The utility function is an indicator to measure the benefit of participants from the game. It not only depends on the strategy choice of participants themselves but also is related to the strategies of other participants, reflecting the preferences of participants for the set of strategies. In the process of the game, when considering the opponent's strategy choice, no participant has the motivation to deviate from the strategy he chose, and the Nash equilibrium is reached. Nash equilibrium is the best

response of each participant to a given strategy from another participant.

3.4. *TFN*. Compared with traditional mathematics and real numbers, the fuzzy number is an important concept in fuzzy analysis. In 1976, Zadeh introduced the concept of fuzzy numbers. Since then, many scholars have carried out research on fuzzy numbers and proposed several fuzzy numbers of different backgrounds [39], such as *L-R* fuzzy number, triangular fuzzy number, and TFN. Now, the study of the fuzzy number has become more and more mature since TFN is an extension of the triangular fuzzy number and interval fuzzy number, which has a wider range of applications.

In previous literature, most scholars used TFN to deal with problems. However, since TFN is represented by four parameters, which provide more detailed description, it can provide more detailed solutions than triangular fuzzy numbers. As shown in Figure 2(b), TFN can be defined by four parameters (a_1 , a_2 , a_3 , and a_4), and the expression for the piecewise function [40] is as follows:

$$F(x) = \begin{cases} \frac{x - a_1}{a_2 - a_1}, & \text{if } x \in [a_1, a_2), \\ 1, & \text{if } x \in [a_2, a_3), \\ \frac{a_4 - x}{a_4 - a_3}, & \text{if } x \in [a_3, a_4], \\ 0, & \text{otherwise,} \end{cases} \quad \text{where } a_1 \leq a_2 \leq a_3 \leq a_4. \quad (2)$$

4. The Two-Phase Deep Analysis considering Fuzzy QFD and Game Theory

4.1. *Applying Two-Phase Fuzzy QFD to Calculate Subjective Weight*. By using the two-phase fuzzy QFD method, the complicated conversion process of customer demands to manufacturer techniques and to supplier capabilities is realized, and then, the subjective weight is calculated. The conversion process between criteria is shown in Figure 2. In addition, in order to make the evaluation more practical, the QFD relational matrix uses TFN to provide more detailed description.

According to the previous research, assuming that a group of TFN evaluation scale is represented by $\Omega = \{\text{EL}, \text{ML}, \text{M}, \text{MH}, \text{EH}\}$, the specific meaning is shown in Figure 3.

After completing the evaluation with TFN and calculating the subjective weight of supplier evaluation criteria based on the evaluation results, equations (3) and (4) are used to defuzzify and normalize the evaluation:

$$Q_i = \frac{1}{4} \sum_{a=1}^4 f_a, \quad i = 1, 2, \dots, m; \quad a = 1, 2, 3, \text{ and } 4, \quad (3)$$

$$N_{Q_i} = \frac{Q_i - \text{Min}_{i=1,2,\dots,m} Q_i}{\text{Max}_{i=1,2,\dots,m} Q_i - \text{Min}_{i=1,2,\dots,m} Q_i}, \quad (4)$$

where f_a is the fuzzy evaluation value of the trapezoid vertex, $a = 1, 2, 3$, and 4 , Q_i defines the defuzzified weight of the i th supplier evaluation criterion, N_{Q_i} is its normalized weight, $i = 1, 2, \dots, m$, and m is the number of supplier evaluation criteria.

4.2. Using Entropy Weight to Calculate Objective Weight

Step 1: normalizing the raw data matrix: there are m evaluation criteria and n evaluation objects, and the original data matrix B is as follows:

$$B = \begin{pmatrix} b_{11} & \dots & b_{1n} \\ \vdots & \ddots & \vdots \\ b_{m1} & \dots & b_{mn} \end{pmatrix}. \quad (5)$$

After normalizing, the matrix $C = (c_{ij})_{m \times n}$ is obtained, where the content of symbol c_{ij} is the normalized value of the j th evaluation object on the i th evaluation criterion, $j = 1, 2, \dots, n$. The normalization formulas of positive and negative indicators are, respectively, as follows:

$$c_{ij} = \frac{b_{ij} - \text{Min}_{j=1,2,\dots,n} b_{ij}}{\text{Max}_{j=1,2,\dots,n} b_{ij} - \text{Min}_{j=1,2,\dots,n} b_{ij}}, \quad (6)$$

$$c_{ij} = \frac{\text{Max}_{j=1,2,\dots,n} b_{ij} - b_{ij}}{\text{Max}_{j=1,2,\dots,n} b_{ij} - \text{Min}_{j=1,2,\dots,n} b_{ij}}. \quad (7)$$

Step 2: defining entropy: based on the original data matrix in Step 1, the entropy of the i th evaluation criterion is defined as the following equation:

$$E_i = -h \sum_{j=1}^n d_{ij} \ln d_{ij}, \quad i = 1, 2, \dots, m, \quad (8)$$

where

$$h = \frac{1}{\ln n}, \quad (9)$$

$$d_{ij} = \frac{c_{ij}}{\sum_{j=1}^n c_{ij}}.$$

Step 3: calculating entropy weight: based on the entropy obtained in Step 2, the entropy weight of the i th evaluation criterion is obtained through the following formulas:

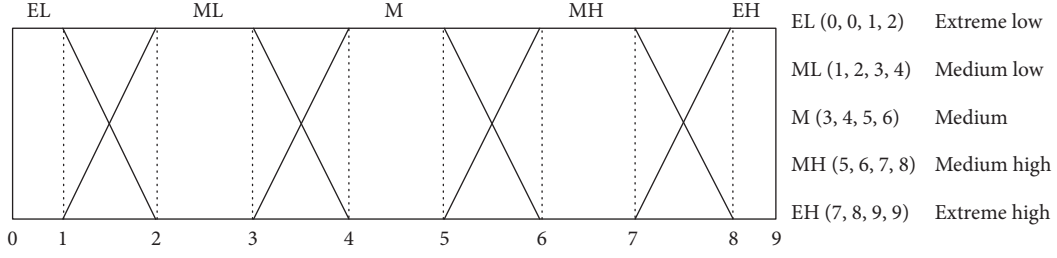


FIGURE 3: TFN evaluation scale.

$$W_{E_i} = \frac{1 - E_i}{m - \sum_{i=1}^m E_i}, \quad (10)$$

where

$$\sum_{i=1}^m W_{E_i} = 1, \quad 0 \leq W_{E_i} \leq 1. \quad (11)$$

4.3. Comprehensive Weight Based on Game Theory

Step 1: unifying vector definitions: use the following equation to unify the definition of each weight vector:

$$\begin{aligned} v_t &= u_t, \\ u_t &= (s_1, s_2, \dots, s_m), \\ \sum_{i=1}^m s_i &= 1, \end{aligned} \quad (12)$$

where u_t represents the weight vector obtained by Section 4.2, $t = 1, 2, \dots, r$, $r > 1$, and m is the number of supplier evaluation criteria.

Step 2: assuming weight coefficients: assume that the weight coefficient of each kind of weight is γ_t , and the comprehensive weight Z is expressed as follows:

$$Z = \sum_{t=1}^r \gamma_t v_t^T, \quad \gamma_t > 0. \quad (13)$$

Step 3: determining weight coefficients: the principle of determining γ_t is to minimize the deviation between the comprehensive weight and each weight:

$$\text{Min} \|Z - u_t\|^2 = \left\| \sum_{t=1}^r \gamma_t v_t^T - u_t^T \right\|^2. \quad (14)$$

According to the differential properties of the matrix [1], the condition for the optimal first derivative of equation (14) is as follows:

$$\sum_{t=1}^r \gamma_t \times u_t \times v_t^T = u_t \times u_t^T, \quad (15)$$

equivalent to

$$\begin{bmatrix} u_1 \cdot v_1^T & u_1 \cdot v_2^T & \dots \\ u_2 \cdot v_1^T & u_2 \cdot v_2^T & \dots \\ \vdots & \vdots & \vdots \\ \cdot & \cdot & \cdot \end{bmatrix} \begin{bmatrix} \gamma_1 \\ \gamma_2 \\ \vdots \\ \cdot \end{bmatrix} = \begin{bmatrix} u_1 \cdot u_1^T \\ u_2 \cdot u_2^T \\ \vdots \\ \cdot \end{bmatrix}. \quad (16)$$

By the above formula, the weight coefficients ($\gamma_1, \gamma_2, \dots$) can be solved.

Step 4: normalizing weight coefficients: weight coefficients are normalized by the following equation:

$$\gamma_t^* = \frac{\gamma_t}{\sum_{t=1}^r \gamma_t}. \quad (17)$$

So, the optimal weight coefficients γ_t^* are obtained. Meanwhile, the optimal comprehensive weight Z^* is obtained through the following equation:

$$Z^* = \sum_{t=1}^r \gamma_t^* v_t^T. \quad (18)$$

Step 5: scoring and ranking: according to the final scores and ranking, one or more suppliers participating in the evaluation with the highest score are selected.

5. Numerical Experiment

Considering the subjective preferences of decision makers and the objective supply capacities of suppliers, the proposed model has high extensibility, which is generally applicable to different criteria for manufacturers or suppliers. Therefore, assuming that there are suppliers A, B, C, D, E, F, and G, whose supply capacities are shown in Table 2, the supply capacities of suppliers are on time delivery rate (SC₁), defective rate of raw materials (SC₂), fast response time (SC₃), resistance to interruption risk rate (SC₄), and recycling rate (SC₅).

5.1. Evaluation Criteria Architecture. Different literature have different considerations and interpretations on the setting of customer and manufacturer evaluation criteria. After consulting and contrasting, we set the following evaluation criteria. Customer demand criteria are price (CD₁), quality (CD₂), service (CD₃), uniqueness (CD₄),

TABLE 2: The supply capacities of suppliers.

Supplier	SC ₁	SC ₂	SC ₃	SC ₄	SC ₅
A	95.3	1.20	1.50	69.3	55.0
B	94.5	1.40	1.85	61.0	61.2
C	87.2	1.00	1.30	78.2	65.7
D	84.6	1.30	1.80	75.9	60.4
E	93.5	1.30	1.75	62.0	62.2
F	86.2	1.00	1.20	79.2	66.7
G	82.0	1.50	2.20	73.5	55.0

and brand (CD₅). For the manufacturer technique criteria, process optimization (MT₁) is an operation method that is superior to existing processes in order to improve operational efficiency, reduce the production cost, strictly control the process procedures, and reorganize or improve the original process. The low defective rate (MT₂) is an important index to measure the technological level and the basic guarantee of product quality. Flexibility in production (MT₃) is a new requirement put forward by manufacturing enterprises in the face of rapidly changing market demand. Customer organization (MT₄) refers to the ability of manufacturing enterprises to attract customers and maintain customer loyalty. Buffer stock (MT₅) refers to the inventory quantity higher than the average demand, which can avoid the expected demand rise or imbalance between production stages. It can effectively reduce the risk of production interruption resulting in the failure of raw materials to be delivered on time in a short period of time due to extreme circumstances. Enterprise reputation (MT₆) can help enterprises establish a good public image and then improve the market competitiveness of enterprises.

5.2. The Application of Two-Phase Fuzzy QFD. Based on the evaluation scale in Figure 3, the decision makers evaluate customer demands and provide importance levels for them, as shown in Table 3. The weight values are expressed in aw_l , $l = 1, 2, \dots, L$.

In order to reflect the effect of manufacturer techniques on customer demands, the linguistic approach is used again to establish an interrelation matrix. The result of which the manufacturer technique is contributing more to customer demand is easily observed in Table 4.

The weight calculation of manufacturer techniques is processed, and TFN bw_m is used to express the result, as shown in Table 5:

$$cw_n = \frac{1}{M} \otimes [(bw_1 \otimes c_{1n}) \oplus (bw_2 \otimes c_{2n}) \oplus \dots \oplus (bw_M \otimes c_{Mn})], \quad (19)$$

where the array of row l and column m of the matrix is indicated by b_{lm} , $m = 1, 2, \dots, M$.

So far, the first phase of the proposed two-phase fuzzy QFD method is completed. Then, the matrix reflecting the effect of supplier capacities on manufacturer techniques is built at the beginning of the second phase and shown in Table 6.

TABLE 3: Importance levels of customer demands.

Demand	Importance level	aw_l
CD ₁	EH	(7,8,9,9)
CD ₂	EH	(7,8,9,9)
CD ₃	EH	(7,8,9,9)
CD ₄	MH	(5,6,7,8)
CD ₅	MH	(5,6,7,8)

TABLE 4: Interrelation between customer demands and manufacturer techniques.

CD/MT	MT ₁	MT ₂	MT ₃	MT ₄	MT ₅	MT ₆
CD ₁	EH	MH	EH	EH	EH	MH
CD ₂	EH	EH	EL	EH	EL	EH
CD ₃	EL	EL	EH	EH	EH	EH
CD ₄	ML	EL	ML	MH	EL	EH
CD ₅	ML	EH	ML	MH	MH	EH

The weight calculation of supplier capacities is processed, and the result is represented by TFN cw_n , as shown in Table 7:

$$cw_n = \frac{1}{M} \otimes [(bw_1 \otimes c_{1n}) \oplus (bw_2 \otimes c_{2n}) \oplus \dots \oplus (bw_M \otimes c_{Mn})], \quad (20)$$

where c_{mn} is the array of row m and column n of the matrix, $n = 1, 2, \dots, N$.

The fuzzy weight is defuzzified by equation (3), and the result is shown in Table 8.

5.3. The Application of Entropy Weight. On the basis of Table 2, the original data can be constructed with matrix B as follows:

$$B = \begin{bmatrix} 0.953 & 0.945 & 0.872 & 0.846 & 0.935 & 0.862 & 0.820 \\ 0.012 & 0.014 & 0.010 & 0.013 & 0.013 & 0.010 & 0.015 \\ 1.500 & 1.850 & 1.300 & 1.800 & 1.750 & 1.200 & 2.200 \\ 0.693 & 0.610 & 0.782 & 0.759 & 0.620 & 0.792 & 0.735 \\ 0.550 & 0.612 & 0.657 & 0.604 & 0.622 & 0.667 & 0.550 \end{bmatrix}. \quad (21)$$

The matrix A is normalized by equations (6) and (7) to get matrix C :

$$C = \begin{bmatrix} 1.000 & 0.940 & 0.391 & 0.195 & 0.865 & 0.316 & 0 \\ 0.600 & 0.200 & 1.000 & 0.400 & 0.400 & 1.000 & 0 \\ 0.700 & 0.350 & 0.900 & 0.400 & 0.450 & 1.000 & 0 \\ 0.456 & 0 & 0.945 & 0.819 & 0.055 & 1.000 & 0.687 \\ 0 & 0.530 & 0.915 & 0.462 & 0.615 & 1.000 & 0 \end{bmatrix}. \quad (22)$$

The matrix C is processed by equations (8) and (9) to get entropy E_1-E_5 .

$$E_1 = 0.844, \quad E_2 = 0.853, \quad E_3 = 0.880, \quad E_4 = 0.836, \quad \text{and} \quad E_5 = 0.804.$$

TABLE 5: The weight calculation of manufacturer techniques.

CD/ MT	MT ₁	MT ₂	MT ₃	MT ₄	MT ₅	MT ₆	<i>aw</i> ₁
CD ₁	(7,8,9,9)	(5,6,7,8)	(7,8,9,9)	(7,8,9,9)	(7,8,9,9)	(5,6,7,8)	(7,8,9,9)
CD ₂	(7,8,9,9)	(7,8,9,9)	(0,0,1,2)	(7,8,9,9)	(0,0,1,2)	(7,8,9,9)	(7,8,9,9)
CD ₃	(0,0,1,2)	(0,0,1,2)	(7,8,9,9)	(7,8,9,9)	(7,8,9,9)	(7,8,9,9)	(7,8,9,9)
CD ₄	(1,2,3,4)	(0,0,1,2)	(1,2,3,4)	(5,6,7,8)	(0,0,1,2)	(7,8,9,9)	(5,6,7,8)
CD ₅	(1,2,3,4)	(7,8,9,9)	(1,2,3,4)	(5,6,7,8)	(5,6,7,8)	(7,8,9,9)	(5,6,7,8)
<i>bw</i> _{<i>m</i>}	<i>bw</i> ₁ (21.600, 30.400, 42.600, 48.800)	<i>bw</i> ₂ (23.800, 32.000, 44.600, 51.800)	<i>bw</i> ₃ (21.600, 30.400, 42.600, 48.800)	<i>bw</i> ₄ (39.400, 52.800, 68.200, 74.200)	<i>bw</i> ₅ (24.600, 32.800, 45.400, 52.000)	<i>bw</i> ₆ (40.600, 54.400, 70.200, 75.600)	

TABLE 6: Interrelation between manufacturer techniques and supplier capacities.

MT/SC	SC ₁	SC ₂	SC ₃	SC ₄	SC ₅
MT ₁	EL	EH	ML	EL	EL
MT ₂	EL	EH	EL	ML	EL
MT ₃	EH	EL	MH	EH	EL
MT ₄	M	MH	M	MH	EH
MT ₅	EH	EL	MH	EH	EL
MT ₆	MH	MH	EH	MH	EH

TABLE 7: The weight calculation of supplier capacities.

MT/ SC	SC ₁	SC ₂	SC ₃	SC ₄	SC ₅	<i>bw</i> _{<i>m</i>}
MT ₁	(0,0,1,2)	(7,8,9,9)	(1,2,3,4)	(0,0,1,2)	(0,0,1,2)	(21.600, 30.400, 42.600, 48.800)
MT ₂	(0,0,1,2)	(7,8,9,9)	(0,0,1,2)	(1,2,3,4)	(0,0,1,2)	(23.800, 32.000, 44.600, 51.800)
MT ₃	(7,8,9,9)	(0,0,1,2)	(5,6,7,8)	(7,8,9,9)	(0,0,1,2)	(21.600, 30.400, 42.600, 48.800)
MT ₄	(3,4,5,6)	(5,6,7,8)	(3,4,5,6)	(5,6,7,8)	(7,8,9,9)	(39.400, 52.800, 68.200, 74.200)
MT ₅	(7,8,9,9)	(0,0,1,2)	(5,6,7,8)	(7,8,9,9)	(0,0,1,2)	(24.600, 32.800, 45.400, 52.000)
MT ₆	(5,6,7,8)	(5,6,7,8)	(7,8,9,9)	(5,6,7,8)	(7,8,9,9)	(40.600, 54.400, 70.200, 75.600)
<i>cw</i> _{<i>n</i>}	<i>cw</i> ₁ (107.433, 173.867, 285.267, 359.733)	<i>cw</i> ₂ (119.633, 190.400, 306.933, 384.233)	<i>cw</i> ₃ (109.167, 181.067, 293.533, 371.800)	<i>cw</i> ₄ (124.533, 202.133, 322.867, 401.733)	<i>cw</i> ₅ (93.333, 142.933, 236.800, 291.833)	

TABLE 8: Defuzzification and normalization.

Supplier criteria	Defuzzification weight	Normalization weight
SC ₁	231.575	0.197
SC ₂	250.300	0.213
SC ₃	238.892	0.203
SC ₄	262.817	0.224
SC ₅	191.225	0.163

Until now, the weight calculation of the proposed two-phase fuzzy QFD method is completed.

After the entropy, E_1-E_5 are obtained, and the entropy weight is calculated by equations (10) and (11) as follows:

$$W_{E1}=0.199, W_{E2}=0.188, W_{E3}=0.153, W_{E4}=0.209, \text{ and } W_{E5}=0.250.$$

Until now, the weight calculation of entropy weight is completed.

5.4. The Combination with Game Theory. Each weight vector processed by equation (12) and unification results are as follows:

$$v_1 = (0.197, 0.213, 0.203, 0.224, 0.163) \text{ and } v_2 = (0.199, 0.188, 0.153, 0.209, 0.250)$$

The matrix equation is calculated by equations (13)–(16) as follows:

With the MATLAB R2019a to assist the calculation, the weight coefficients' vector α can be obtained:

$$\gamma = [\gamma_1, \gamma_2] = [0.398, 0.615]. \quad (23)$$

Equation (17) is applied to normalize the weight coefficients vector α , and the optimal comprehensive weight W^* is obtained by equation (18) as follows:

$$\begin{aligned} \gamma^* &= [\gamma_1^*, \gamma_2^*] = [0.393, 0.607], \\ Z^* &= [0.198, 0.198, 0.173, 0.215, 0.216]. \end{aligned} \quad (24)$$

5.5. Suppliers Evaluation and Ranking. On the basis of the original data matrix B and the optimal comprehensive weight Z^* , the final scores and ranking of suppliers participating in the evaluation are calculated, as shown in Table 9.

Therefore, the comprehensive ranking of the suppliers is $G > D > B > E > A > C > F$.

6. Comparative Analysis and Sensitivity Analysis

In this chapter, through comparative analysis and sensitivity analysis, the rationality of the proposed method and the ranking result of the suppliers are, respectively, processed to prove the robustness.

6.1. Comparative Analysis. In this section, subjective and objective weights are calculated by fuzzy QFD and entropy weights, respectively. These two types of weights and the comprehensive weight calculated by the proposed method are drawn in the same coordinate system, and the broken line diagram is shown in Figure 4.

From the analysis of the figure, it can be seen that the weight value obtained by the single weight method is not convincing because there is no reference. Although subjective and objective methods have their own applicability, the weight values obtained by different methods vary greatly. The proposed method combined with game theory fully refers the existing weight values and solves each weight

TABLE 9: Score and rank.

Supplier	Score	Rank
A	0.718	5
B	0.773	3
C	0.709	6
D	0.775	2
E	0.758	4
F	0.694	7
G	0.822	1

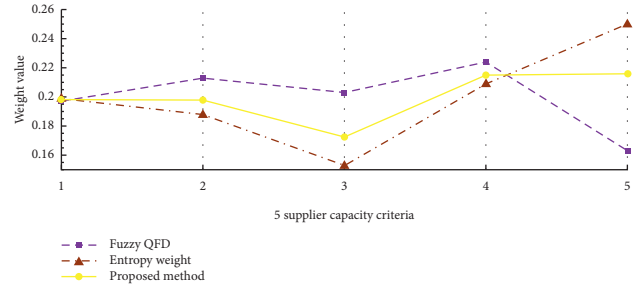


FIGURE 4: Supplier capacity criteria weights under three methods.

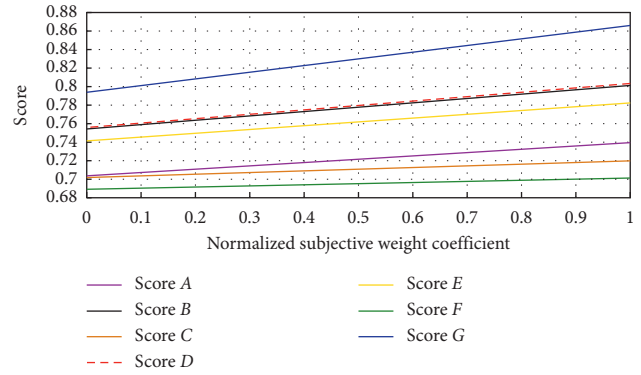


FIGURE 5: The supplier ranking with the variation of the subjective weight coefficient.

proportion problem through the combination of weight coefficients, which effectively alleviates the weight deviation. Under the same criterion, the comprehensive weight value is always in the range of subjective and objective weight values. Therefore, the comprehensive weight is the optimal equilibrium of subjective and objective weights, and the proposed method combined with game theory is more rational than the single method.

6.2. Sensitivity Analysis. This section studies the score and ranking of suppliers $A, B, C, D, E, F,$ and G when the normalized subjective weight coefficient γ_1^* varies continuously in the interval $(0, 1)$ and are drawn in Figure 5.

Analysis of the figure shows that, with the increase of the subjective weight coefficient, the scores of all suppliers are increasing. Suppliers A and G are more sensitive to the subjective weight coefficient, and their scores grow faster. When there are no decision makers participating in the evaluation, the suppliers' scores are completely determined

by their own supply capacities. When the decision makers participate in the evaluation moderately, the gap between suppliers A and C becomes significant. In other words, as the participation of decision makers increases, the gap among suppliers will become more obvious. The effective participation of decision makers can make it easier to select the most suitable suppliers.

7. Conclusions

Supplier selection is of great significance to the core competitiveness of manufacturing enterprises. The paper proposes a fuzzy comprehensive supplier evaluation system model to improve the supply quality and reliability, so as to fully meet customer demands. Based on decision makers' preferences and suppliers' supply capabilities, subjective and objective weights of criteria are both developed for supplier selection. Specially, the two-phase fuzzy QFD method is creatively applied to realize the complicated conversion process. Furthermore, the game theory is employed to combine the advantages of the subjective and objective weighting method, by which the comprehensive weight can be determined. Although the objective evaluation method can alleviate the excessive subjectivity of decision-making to a certain extent, the subjective decision-making ability of decision makers can still affect the decision-making process. Green supplier selection, computer aided evaluation, and artificial intelligence simulation decision are the future research direction [41–43]. Through comparative analysis and sensitivity analysis, some revelations are obtained:

- (1) The proposed method combined with game theory fully refers the existing weight values and solves each weight proportion problem through the combination of weight coefficients, which effectively alleviates the weight deviation. Therefore, the proposed method is more rational than the single method.
- (2) The proposed model has high extensibility, in which the subjective and objective weight can be replaced by other methods which are more suitable for solving the practical problem.
- (3) When the participation of decision makers increases, the gap among suppliers will become more obvious. The effective participation of decision makers can make it easier to select the most suitable suppliers.

In addition, the limitations of the proposed method are that the subjective evaluation and analysis process of suppliers requires decision makers to have sufficient experience and decision-making ability. Computer-aided decision-making can be used as a new combination direction.

Data Availability

No data were used to support the findings of this study.

Conflicts of Interest

The authors declare that there are no conflicts of interest regarding the publication of this paper.

Acknowledgments

This research was funded by Key Realm R&D Program of Guangdong Province (2019B020214002), Beijing Social Science Foundation (19ZDA12, 18GLB022, 17GLC066, and 19GLC051), Beijing Intelligent Logistics System Collaborative Innovation Center (BILSCIC-2019KF-12), Beijing Key Laboratory (no. BZ0211), Social Science Program of Beijing Municipal Education Commission (SM201810037001 and SM201910037004), Beijing Wuzi University Major Research Projects (2019XJZD12), "Central University Science Research Foundation of China" (JB170609), and China Postdoctoral Science Foundation (2016M590929).

References

- [1] T. Liu, Y. Deng, and F. Chan, "Evidential supplier selection based on DEMATEL and game theory," *International Journal of Fuzzy Systems*, vol. 20, no. 4, pp. 1321–1333, 2017.
- [2] L. Sun, Y. Liu, B. Zhang, Y. Shang, H. Yuan, and Z. Ma, "An integrated decision-making model for transformer condition assessment using game theory and modified evidence combination extended by D numbers," *Energies*, vol. 9, no. 9, p. 697, 2016.
- [3] A. G. Sanfey, "Social decision-making: insights from game theory and neuroscience," *Science*, vol. 318, no. 5850, pp. 598–602, 2007.
- [4] D. M. Frank and S. Sarkar, "Group decisions in biodiversity conservation: implications from game theory," *PLoS One*, vol. 5, no. 5, Article ID e10688, 2010.
- [5] G.-J. Cheng, L.-T. Liu, X.-J. Qiang, and Y. Liu, "Industry 4.0 development and application of intelligent manufacturing," in *Proceedings of the 2016 International Conference on Information System and Artificial Intelligence (ISAI)*, pp. 407–410, Hong Kong, China, June 2016.
- [6] F. Dweiri, S. Kumar, S. A. Khan, and V. Jain, "Designing an integrated AHP based decision support system for supplier selection in automotive industry," *Expert Systems with Applications*, vol. 62, pp. 273–283, 2016.
- [7] H. B. Ahmadi, S. H. Hashemi Petrucci, and X. Wang, "Integrating sustainability into supplier selection with analytical hierarchy process and improved grey relational analysis: a case of telecom industry," *The International Journal of Advanced Manufacturing Technology*, vol. 90, no. 9–12, pp. 2413–2427, 2017.
- [8] E. K. Zavadskas, Z. Turskis, Ž. Stević, and A. Mardani, "Modelling procedure for the selection of steel pipes supplier by applying fuzzy AHP method," *Operational Research in Engineering Sciences: Theory and Applications*, vol. 3, no. 2, pp. 39–53, 2020.
- [9] Z. Ayağ and F. Samanlıoğlu, "An intelligent approach to supplier evaluation in automotive sector," *Journal of Intelligent Manufacturing*, vol. 27, no. 4, pp. 889–903, 2014.
- [10] M. Yazdani, P. Chatterjee, E. K. Zavadskas, and S. Hashemkhani Zolfani, "Integrated QFD-MCDM framework for green supplier selection," *Journal of Cleaner Production*, vol. 142, pp. 3728–3740, 2017.
- [11] F. R. Lima-Junior and L. C. R. Carpinetti, "A multicriteria approach based on fuzzy QFD for choosing criteria for supplier selection," *Computers & Industrial Engineering*, vol. 101, pp. 269–285, 2016.

- [12] E. E. Karsak and M. Dursun, "An integrated fuzzy MCDM approach for supplier evaluation and selection," *Computers & Industrial Engineering*, vol. 82, pp. 82–93, 2015.
- [13] H. Gupta and M. K. Barua, "Supplier selection among SMEs on the basis of their green innovation ability using BWM and fuzzy TOPSIS," *Journal of Cleaner Production*, vol. 152, pp. 242–258, 2017.
- [14] J. Rezaei, T. Nispeling, J. Sarkis, and L. Tavasszy, "A supplier selection life cycle approach integrating traditional and environmental criteria using the best worst method," *Journal of Cleaner Production*, vol. 135, pp. 577–588, 2016.
- [15] P. Pitchipoo, P. Venkumar, and S. Rajakarunakaran, "Grey decision model for supplier evaluation and selection in process industry: a comparative perspective," *The International Journal of Advanced Manufacturing Technology*, vol. 76, no. 9–12, pp. 2059–2069, 2015.
- [16] I. Badi and D. Pamucar, "Supplier selection for steelmaking company by using combined Grey-MARCOS methods," *Decision Making: Applications in Management and Engineering*, vol. 3, no. 2, pp. 37–48, 2020.
- [17] K. Govindan and R. Sivakumar, "Green supplier selection and order allocation in a low-carbon paper industry: integrated multi-criteria heterogeneous decision-making and multi-objective linear programming approaches," *Annals of Operations Research*, vol. 238, no. 1–2, pp. 243–276, 2015.
- [18] S. Mousakhani, S. Nazari-Shirkouhi, and A. Bozorgi-Amiri, "A novel interval type-2 fuzzy evaluation model based group decision analysis for green supplier selection problems: a case study of battery industry," *Journal of Cleaner Production*, vol. 168, pp. 205–218, 2017.
- [19] A. Blagojević, Ž. Stević, D. Marinković, S. Kasalica, and S. Rajilić, "A novel entropy-fuzzy PIPRECIA-DEA model for safety evaluation of railway traffic," *Symmetry*, vol. 12, no. 9, p. 1479, 2020.
- [20] C. Wei, J. Wu, Y. Guo, and G. Wei, "Green supplier selection based on CODAS method in probabilistic uncertain linguistic environment," *Technological and Economic Development of Economy*, vol. 27, no. 3, pp. 530–549, 2021.
- [21] G. Wei, Y. He, F. Lei, J. Wu, C. Wei, and Y. Guo, "Green supplier selection with an uncertain probabilistic linguistic MABAC method," *Journal of Intelligent & Fuzzy Systems*, vol. 39, no. 3, pp. 3125–3136, 2020.
- [22] S. Hosseini and A. A. Khaled, "A hybrid ensemble and AHP approach for resilient supplier selection," *Journal of Intelligent Manufacturing*, vol. 30, no. 1, pp. 207–228, 2016.
- [23] S. Chakraborty, R. Chattopadhyay, and S. Chakraborty, "An integrated D-MARCOS method for supplier selection in an iron and steel industry," *Decision Making: Applications in Management and Engineering*, vol. 3, no. 2, pp. 49–69, 2020.
- [24] E. Durmić, "Evaluation of criteria for sustainable supplier selection using FUCOM method," *Operational Research in Engineering Sciences: Theory and Applications*, vol. 2, no. 1, pp. 91–107, 2019.
- [25] L. Xiao, S. Zhang, G. Wei et al., "Green supplier selection in steel industry with intuitionistic fuzzy Taxonomy method," *Journal of Intelligent & Fuzzy Systems*, vol. 39, no. 5, pp. 7247–7258, 2020.
- [26] F. Lei, G. Wei, J. Wu, C. Wei, and Y. Guo, "QUALIFLEX method for MAGDM with probabilistic uncertain linguistic information and its application to green supplier selection," *Journal of Intelligent & Fuzzy Systems*, vol. 39, no. 5, pp. 6819–6831, 2020.
- [27] C. Lai, X. Chen, X. Chen, Z. Wang, X. Wu, and S. Zhao, "A fuzzy comprehensive evaluation model for flood risk based on the combination weight of game theory," *Natural Hazards*, vol. 77, no. 2, pp. 1243–1259, 2015.
- [28] F. Franceschini, M. Galetto, D. Maisano, and L. Mastrogiacomo, "Prioritisation of engineering characteristics in QFD in the case of customer requirements orderings," *International Journal of Production Research*, vol. 53, no. 13, pp. 3975–3988, 2014.
- [29] M. Zairi and D. Ginn, "East meets West: a critical analysis on the evolution, growth and transfer of QFD from Japan to the West," *Asian Journal on Quality*, vol. 4, no. 1, pp. 1–19, 2003.
- [30] A. Kapur, L. Potters, and L. B. Mallalieu, "WE-C-214-02: six-sigma tools for a "No-Fly" patient safety oriented, quality-checklist driven, paperless multi-center radiation medicine department," *Medical Physics*, vol. 38, no. 6, p. 3807, 2011.
- [31] C. E. Shannon, "A mathematical theory of communication," *Bell System Technical Journal*, vol. 27, no. 3, pp. 379–423, 1948.
- [32] L.-h. Li and R. Mo, "Production task queue optimization based on multi-attribute evaluation for complex product assembly workshop," *PloS One*, vol. 10, no. 9, Article ID e0134343, 2015.
- [33] A. Liu, S. Luo, J. Mou, and H. Qiu, "The antagonism and cohesion of the upstream supply chain under information asymmetry," *Annals of Operations Research*, pp. 1–46, 2021.
- [34] Y. He, H. Guo, M. Jin, and P. Ren, "A linguistic entropy weight method and its application in linguistic multi-attribute group decision making," *Nonlinear Dynamics*, vol. 84, no. 1, pp. 399–404, 2016.
- [35] R. B. Myerson, *Game Theory*, Harvard University Press, Cambridge, MA, USA, 2013.
- [36] J. Von Neumann and O. Morgenstern, *Theory of Games and Economic Behavior (commemorative edition)*, Princeton University Press, Princeton, NJ, USA, 2007.
- [37] J. F. Nash, "Equilibrium points in n-person games," *Proceedings of the National Academy of Sciences*, vol. 36, no. 1, pp. 48–49, 1950.
- [38] J. Nash, "Non-cooperative games," *The Annals of Mathematics*, vol. 54, no. 2, pp. 286–295, 1951.
- [39] M. M. Gupta, "Fuzzy set theory and its applications," *Fuzzy Sets and Systems*, vol. 47, no. 3, pp. 396–397, 1992.
- [40] C. Babbar and S. H. Amin, "A multi-objective mathematical model integrating environmental concerns for supplier selection and order allocation based on fuzzy QFD in beverages industry," *Expert Systems with Applications*, vol. 92, pp. 27–38, 2018.
- [41] J. Lu, S. Zhang, J. Wu, and Y. Wei, "COPRAS method for multiple attribute group decision making under picture fuzzy environment and their application to green supplier selection," *Technological and Economic Development of Economy*, vol. 27, no. 2, pp. 369–385, 2021.
- [42] G. Wei, J. Wu, Y. Guo, J. Wang, and C. Wei, "An extended COPRAS model for multiple attribute group decision making based on single-valued neutrosophic 2-tuple linguistic environment," *Technological and Economic Development of Economy*, vol. 27, no. 2, pp. 353–368, 2021.
- [43] M. Zhao, G. Wei, C. Wei, and Y. Guo, "CPT-TODIM method for bipolar fuzzy multi-attribute group decision making and its application to network security service provider selection," *International Journal of Intelligent Systems*, vol. 36, no. 5, pp. 1943–1969, 2021.

Research Article

Design of Smart Home Service Robot Based on ROS

Jiansheng Peng ^{1,2}, Hemin Ye ¹, Qiwen He ¹, Yong Qin ¹, Zhenwu Wan ³,
and Junxu Lu ¹

¹Hechi University, 42 Longjiang Road, Yizhou 546300, China

²School of Electronic Engineering, Guangxi Normal University, Guilin, Guangxi 541004, China

³Hubei University of Education, Wuhan 430205, China

Correspondence should be addressed to Qiwen He; saymyself2006@163.com

Received 6 January 2021; Revised 2 March 2021; Accepted 16 June 2021; Published 28 June 2021

Academic Editor: Hsu-Yang Kung

Copyright © 2021 Jiansheng Peng et al. This is an open access article distributed under the Creative Commons Attribution License, which permits unrestricted use, distribution, and reproduction in any medium, provided the original work is properly cited.

At present, the functions of home service robots are not perfect, and home service robot systems that can independently complete autonomous inspections and home services are still lacking. In response to this problem, this paper designs a smart home service robot system based on ROS. The system uses Raspberry Pi 3B as the main control to manage the nodes of each sensor. CC2530 sets up a ZigBee network to collect home environmental information and control home electrical appliances. The image information of the home is collected by the USB camera. The human speech is recognized by Baidu Speech Recognition API. When encountering a dangerous situation, the GSM module is used to give users SMS and phone alarms. Arduino mega2560 is used as the bottom controller to control the movement of the service robot. The indoor environment map of the home is constructed by the lidar and the attitude sensor. The service robot finally designed and developed realizes the functions of wireless control of home appliances, voice remote control, autonomous positioning and navigation, liquefied gas leakage alarm, and human infrared detection alarm. Compared with the household service robots in the related literature, the household service robots developed by us have more complete functions. And the robot system has completed the task of combining independent patrol and home service well.

1. Introduction

In recent years, with the development of science and technology, various robots have appeared in people's lives, for example, handling robots in factories [1], medical robots in hospitals [2], service robots in hotels [3], food delivery robots in restaurants [4], and smart home service robots that reduce the burden on family members [5]. Among them, the smart home service robot is the closest to people's lives and the most used.

According to a recent survey by the World Health Organization, in 2015, the number of people over 60 years old in the world reached 900 million people, and by 2050, the number of people over 60 years old will reach 2 billion [6]. More and more elderly people are unable to complete some tasks smoothly due to their age. At this time, they need the assistance of smart home robots. And smart home service robots can be used as companion objects for the elderly so that they will not feel lonely at home. And with the aging of

the population becoming more and more serious, the demand for smart home service robots is also increasing.

Most young workers nowadays basically go out to work during the day and only spend a short time at home. If there is any dangerous situation at home, it is difficult to find out and take relevant measures at the first time. In recent years, home burglaries and gas leaks have occurred frequently. In order to ensure that the home is safe enough, there needs to be a "people" in the home at this time and can send alarm messages to the owner at any time when encountering danger so as to reduce the owner's economic loss. The "people" mentioned here are smart home service robots. In addition, this type of robot can help the owner do housework (such as sweeping the floor) to reduce the burden on the owner. In addition, when the owner who works outside wants to have hot water to drink as soon as he returns home, he can send corresponding instructions to the smart home service robot in advance to turn on the electric tea kettle

heating function, and the owner can drink hot water when he returns home.

In summary, smart home robots can share housework for people and reduce the burden on the owner and can bring a lot of convenience to people's lives. Especially for the elderly, smart home service robots bring convenience to their lives and add a lot of fun to their lives. In addition, the danger alarm function of the smart home service robot can make people's home life safer. Therefore, smart home service robots are becoming more and more important to people's daily lives. However, the functions of some smart home service robots are not yet perfect, so it is necessary to research and develop smart home service robots with more comprehensive functions.

The organizational structure of the rest of this article is as follows. Related work will be discussed in the second part. The third part introduces the overall design of the system in detail. In the fourth part, the hardware design of the motion system, power supply system, wireless communication system, alarm system, and autonomous navigation system is introduced. In the fifth part, the software design of the system is introduced, including motion system software design, wireless communication system software design, and autonomous navigation software design. The sixth part gives an introduction to system debugging. The seventh part compares the functions and experience of the smart home service robot. The eighth part is the summary of this article.

2. Related Work

With the development of electronic information technology and the improvement of people's living standards, people are increasingly yearning for the life of smart home [7]. The concept of smart home is to integrate different services in one home by using a common communication system [8]. Smart homes ensure economical, safe, and comfortable home operations, including highly intelligent functions and flexibility. In recent years, with the development of robotics technology, more and more robots are used in smart homes and become smart home service robots. These robots bring people an economic, safe, comfortable, and happy family life.

With the gradual aging of society, the number of elderly people has gradually increased. When there is only one elderly person at home, the mood and safety of the elderly are worthy of consideration. Wada K et al. invented a companion robot for the elderly named "Paro" [9]. "Paro" is a robot that can imitate animals. While bringing joy to the owner, there is no need to worry that it will bite you like a real animal. "Schpuffy" is also a companion robot [10]. It checks the owner's schedule every morning. If it finds that the owner has an appointment at 8:30, it will wake up the owner in advance at 8 o'clock. If the weather is very cold, it will remind the owner to wear more clothes to keep warm. It will say goodbye to the owner when the owner leaves, and it will lock the door when the owner leaves. Literature [11] is dedicated to the development of social robotic systems to provide companionship, care, and services to the elderly through information and communication technology (ICT),

thereby motivating them to stay active and independent and improve their well-being. The goal of this work is to enable these elderly people to live independently for as long as possible in their preferred environment by providing information and communication technology nursing services. As a service robot, the platform provides assistance to users and aims to solve the early preventive and health care problems of the aging process. The three robots mentioned above are mainly human-computer interaction functions, which are designed to bring convenience and joy to the owner, especially for the elderly, but they are not involved in other functions.

Saunders et al. deployed a commercial autonomous robot in an ordinary suburban house. This robot describes teaching, learning, and robot and smart home system design methods as an integral unit. Experimental results show that participants think this method of robot personalization is easy to use and can be used in real life [5]. Abdallah and others used open source solutions to build a completely independent intelligent assistant robot, specifically for the elderly to manage smart homes. The system is built around a voice communication module based on Mycroft AI for communicating with sensors and smart devices. It includes many software applications for recognizing faces, setting tasks, and answering specific questions and requests. The embedded system is used as the local server to manage the smart home and its applications. The results show that the robot can perform various forms of actions to answer user queries [12]. Berrezueta-Guzman et al. [13] introduced the design of smart home environment. In this project, the Internet of Things (IoT) paradigm is combined with the development of robotic aids to realize a smart home environment. In this environment, the included smart things can determine the behavior of the child in the process of doing homework in real time. There is also a robotic assistant in the project that interacts with the child and provides necessary companionship (supervision and guidance), just like the therapist would do. The purpose of this project is to create a smart place for treatment purposes in the family to help children who suffer from ADHD and find it difficult to complete their homework. The above three kinds of robots can all perform voice interaction, but they all lack the functions of hazard alarm and home appliance control.

Literature [14] explored the possibility of integrating wireless sensor networks and service robots into smart home applications. Service robots can be regarded as mobile nodes, providing additional sensor information, improving/fixing connectivity, and collecting information from wireless sensor nodes. The wireless sensor network can be regarded as an extension of the robot's perception ability, providing an intelligent environment for the service robot. The robot mainly realizes that the robot obtains effective information from the sensor network so as to control the related equipment. In 2018, Taiwanese researchers proposed a smart home control system. The system integrates the Internet of Things, wireless sensor networks, smart robots, and single board computers to realize smart home applications. They use wireless technology and automation equipment to avoid adding too many communication cables, making the house

more intelligent, keeping indoor activities smooth and tidy. This system brings intelligence and convenience to the family and makes the living environment more comfortable [15]. However, the above two types of robots do not have functions such as human-computer interaction and voice recognition.

The functions of the robots researched and developed in the above literature are not very comprehensive, and it is difficult to meet people's needs for a comfortable, convenient, safe, and fun home life. And they generally lack a home robot system that can independently complete the combination of autonomous inspections and home services. If the smart home service robot has incomplete functions and cannot complete the task of combining autonomous patrols and home services, this will bring a bad experience to users. In order to meet people's needs for a comfortable, convenient, safe, and fun home life, this paper has researched and developed a home robot system that has more complete functions and can independently complete independent inspections and home services. This system is a smart home service robot system based on ROS, which can help people manage and control household appliances, which brings convenience to people. Its voice recognition function makes the communication between the owner, and it simple and convenient. For the elderly, this function can make them no longer feel lonely when they are at home alone and at the same time increase the joy of life for the elderly. It can also detect the situation at home. When there is a dangerous situation, it will send out an alarm to the owner, thereby reducing the owner's economic loss and playing the effect of protecting the safety of the home.

3. Overall System Design

ROS (robot operating system) [16] is a metalevel operating system suitable for robot open source. Compared with other robot operating systems, ROS mainly has the following characteristics. (1) ROS provides a publish-subscribe communication framework for building distributed computing systems simply and quickly. (2) It provides a large number of simulation and data visualization tool combinations to configure, start, self-check, debug, visualize, login, test, and terminate system. (3) It also provides a large number of library files and realizes functions such as autonomous movement, operating objects, and perception of the environment. (4) The support and development of ROS constitute a powerful ecosystem.

ZigBee technology [17] is a low-rate and short-distance wireless transmission technology based on IEEE802.15.4. It is characterized by self-organizing network, supporting a large number of network nodes, low power consumption, low speed, low cost, safe, and reliable. ZigBee technology is widely used in the fields of home network, medical sensors, and servo execution.

Arduino is an open source electronic platform [18]. It has rich library resources and simple code structure, suitable for completing the driving of the robot and connecting with various electronic components to realize data collection and processing.

The system framework is shown in Figure 1. The ROS-based smart home service robot system uses Raspberry Pi 3 as the main control core board. It consists of lidar, attitude sensor, USB camera, CC2530 coordinator, CC2530 terminal node, relay module, MQ-5 module, SHT temperature and humidity module, Arduino mega2560, motor, motor drive module, human body infrared module, and GSM module. The ROS system is installed on the main control core board to exchange information with each module to control and run the entire system. The CC2530 coordinator and CC2530 terminal nodes construct a ZigBee network. The serial communication between the CC2530 coordinator and the main control core board realizes information exchange. The CC2530 terminal node drives the relay module, MQ-5 module, and SHT temperature and humidity module, respectively. These are used to collect environmental information at home and control household electrical appliances. Users can control the entire system by connecting the robot through the mobile phone.

4. System Hardware Design

4.1. Motion System Hardware Design

4.1.1. Mobile Chassis Structure Design. The movement method of robot movement adopts wheeled transmission method. The structure of the mobile chassis is shown in Figure 2. The a and the b are DC geared motors. A wheel and B wheel are used as driving wheels. The C wheel is a universal wheel as an auxiliary wheel. This constitutes a self-balancing robot mobile chassis.

4.1.2. Movement System Hardware Composition. The hardware of the robot motion system is composed of the L298P Moto Shield DC motor drive expansion board, the Arduino mega2560 development board, and the DC gear motor. The DC geared motor has a 13-wire AB two-phase Hall encoder. The phase A and phase B outputs of the encoder differ by 90°. The value read by the combination of two-phase is 4 times the term. The motor generates 780 pulses per revolution. Then, the speed n is as follows:

$$n = \frac{N}{4 \times 780 \times t}, \quad (1)$$

where N is the number of pulses in time t .

The system uses the external interrupt of the I/O port of the Arduino mega2560 development board to read the encoder pulse number. The speed of the geared motor is calculated by Equation (1). The controller outputs PWM through the driver to drive the reduction motor to rotate.

4.2. Power System Hardware Design. The power system structure is shown in Figure 3. The main power supply uses 11 V lithium battery. The secondary power supply uses 5V batteries. The main power supply supplies power to the gear motor through the L298P Moto Shield DC motor drive expansion board. Raspberry Pi power supply needs 5 V/2A to work properly. Therefore, the CKCY buck module (which

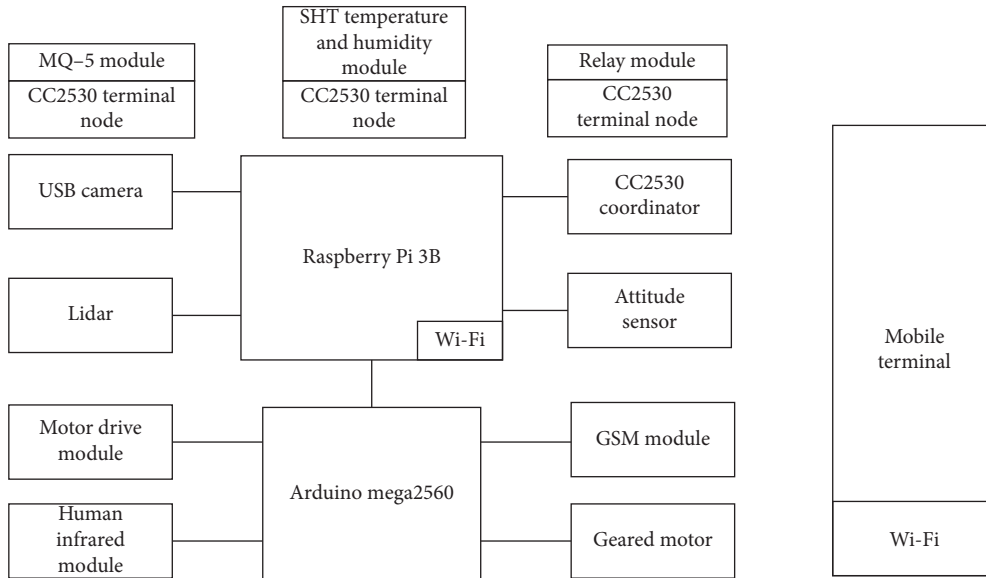


FIGURE 1: System framework diagram.

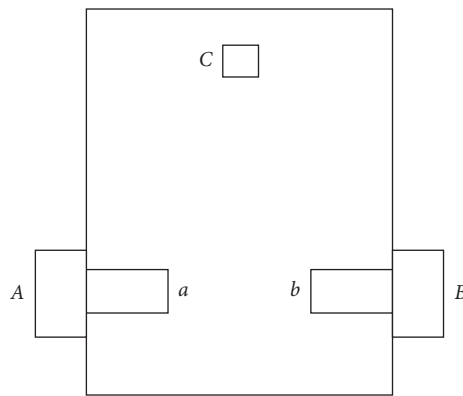


FIGURE 2: Structure diagram of mobile chassis.

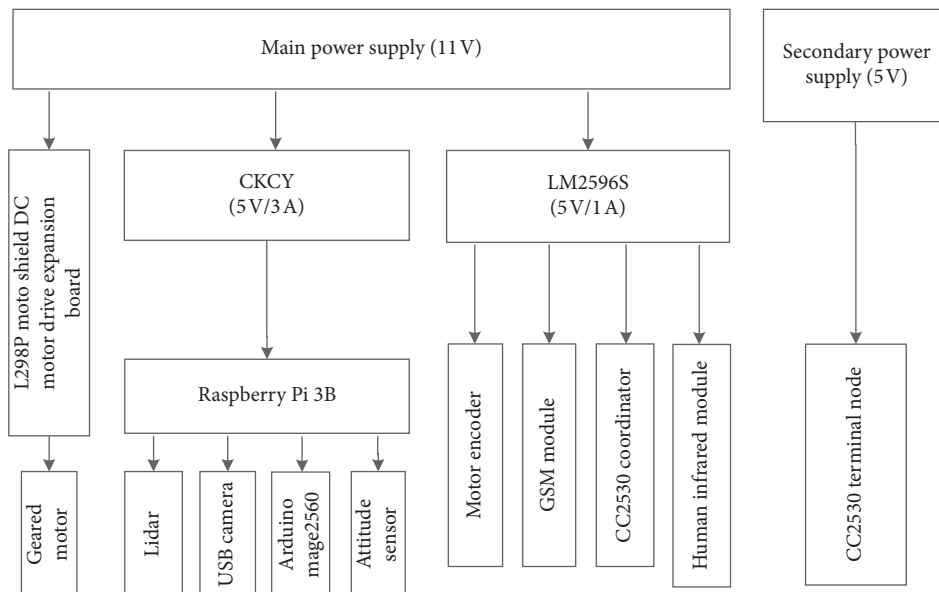


FIGURE 3: Ower system structure diagram.

can output 5 V/3A) is used to get 5 V power supply. The lidar, USB camera, Arduino mega2560, and attitude sensor are powered by the USB serial port of the Raspberry Pi. The main power supply is reduced to 5 V through the LM2596S buck module and supplies power to the motor encoder, GSM module, CC2530 coordinator, and human body infrared module. The CC2530 terminal node is directly powered by a 5 V secondary battery.

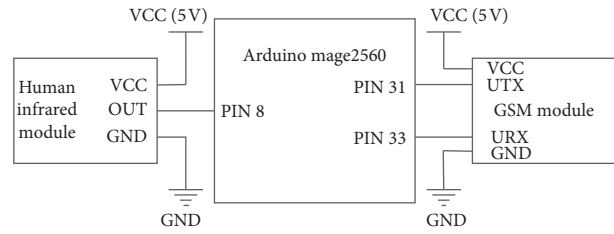


FIGURE 4: Human body module and GSM module wiring diagram.

4.3. Wireless Communication System Hardware Design. The coordinator and the terminal nodes constitute the hardware component of the wireless communication system. There can only be one coordinator in each network. The main functions of the coordinator are to establish a network, assign network addresses, and maintain a binding table. The terminal node is used for each device node of the network. The same network can have up to 256 end nodes. The MQ-5 module, SHT temperature and humidity module, and relay switch are connected to the terminal node for information collection and control of household electrical appliances.

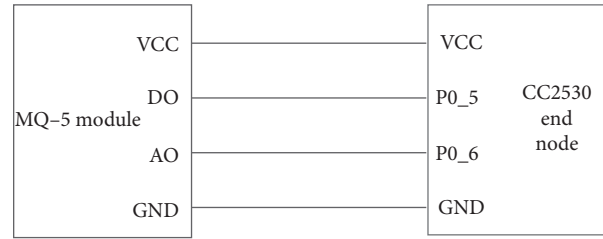


FIGURE 5: Wiring block diagram of MQ-5 module and CC2530 terminal node.

4.4. Alarm System Hardware Design. The human body infrared module, MQ-5 liquefied gas module, and GSM module constitute the hardware component of the robot alarm system. The human body infrared module is used to detect whether there are someone breaks into the house when living outdoors. MQ-5 liquefied gas module is used to detect whether there is a liquefied gas leak in the home. The GSM module is used to send text messages and dial phone calls to the residents. The wiring of human body infrared module, GSM module, and Arduino mega2560 is shown in Figure 4. The connection mode between the MQ-5 module and the CC2530 terminal node is shown in Figure 5.

operation of the Arduino mega2560. The CC2530 coordinator is mainly used to obtain data of CC2530 terminal nodes. Arduino mega2560 mainly obtains encoder data and human body infrared sensor data. Control motor drives and controls GSM module work. The service robot software framework is shown in Figure 7.

4.5. Autonomous Navigation System Hardware Design. The hardware components of the robot's autonomous navigation system are composed of lidar and attitude sensors. The system uses lidar to detect the surrounding environment through 360° scanning and ranging and then collects and processes the data. Finally, the system builds a digital map of the surrounding environment. The attitude sensor is used to obtain the data of acceleration, angular velocity, and magnetometer. In this way, the current real-time motion state of the robot can be solved. The wiring of Lidar, attitude sensor, and Raspberry Pi 3B is shown in Figure 6.

5.2. Motion System Software Design. The robot adopts the incremental PID method to adjust the movement speed. The specific steps for adjusting the movement speed are as follows:

5. System Software Design

5.1. Software Overall Design. The designed smart home service robot uses Raspberry Pi as the main control core. The system uses CC2530 coordinator to build the network and CC2530 terminal nodes to form a wireless control network. The system also uses Arduino mega2560 as the slave controller. The Raspberry Pi 3B mainly processes lidar data, attitude sensor data, USB camera data, voice recognition API, and CC2530 coordinator data and controls the

- (1) When the deviation value of the motor speed is obtained, the upper computer sets the moving speed of the service robot. The lower computer obtains the speed value sent by the upper computer. The encoder's own encoder is used to calculate the encoder's pulse to obtain the current actual speed of the service robot. Finally, the system subtracts the two to get the speed deviation value.
- (2) This system calculates the duty cycle through the PID incremental algorithm. The system obtains the latest 3 speed deviation values and then obtains the duty cycle through the PID incremental algorithm. It should be noted here that the minimum and maximum duty cycle values need to be set to avoid the motor rotating speed being too small or too large.
- (3) Let the drive motor rotate to achieve speed regulation. The obtained duty ratio is converted to the corresponding PWM output value. Let the output PWM drive the motor speed to achieve speed regulation. The change of the motor speed will in turn affect the speed deviation value. The duty cycle changes as the motor speed changes. The output PWM value also changes accordingly. This process is

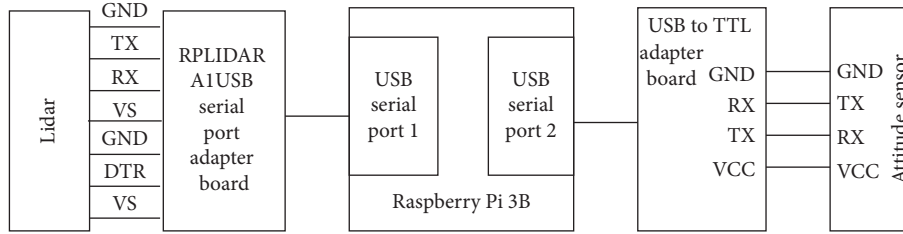


FIGURE 6: Wiring diagram of lidar and attitude sensor.

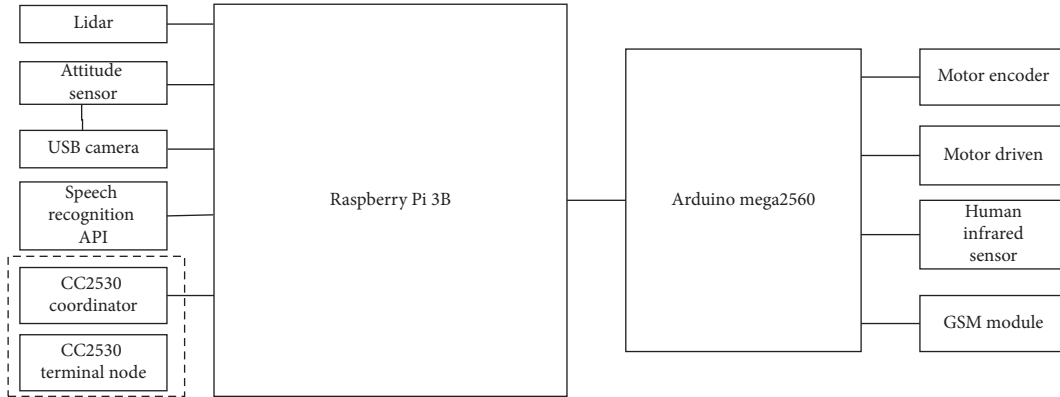


FIGURE 7: Software block diagram.

repeated, and the final motor speed tends to the set theoretical speed.

5.3. *Software Design of Wireless Communication System.* ZigBee technology is a low-rate and short-distance wireless transmission technology based on IEEE802.15.4. ZigBee technology has the characteristics of self-organizing network, supporting a large number of network nodes, low power consumption, low speed, low cost, safety, and reliability. ZigBee technology is widely used in the fields of home network, medical sensors, and servo execution. The robot wireless communication system uses ZigBee network for wireless communication. The ZigBee network is composed of a coordinator and terminal nodes and uses a star network topology as shown in Figure 8.

5.3.1. *CC2530 Coordinator Builds ZigBee Network.* In a wireless communication system, the coordinator is equivalent to the controller in the network. It dominates the entire network. From the establishment of the network to the processing and transmission of system data, including the realization of system functions, it is inseparable from the coordinator. The specific steps of the ZigBee network construction process are as follows. First, the system configures the type of coordinator and sets PAN_ID! = 0xFFFF coordinator. In this way, the coordinator will only generate one network. Then, the system configures the network channel and scan channel of the coordinator and configures the short address of the coordinator. Finally, the coordinator starts to wait for the terminal node to join. If the terminal node wants to join the network, it first needs to

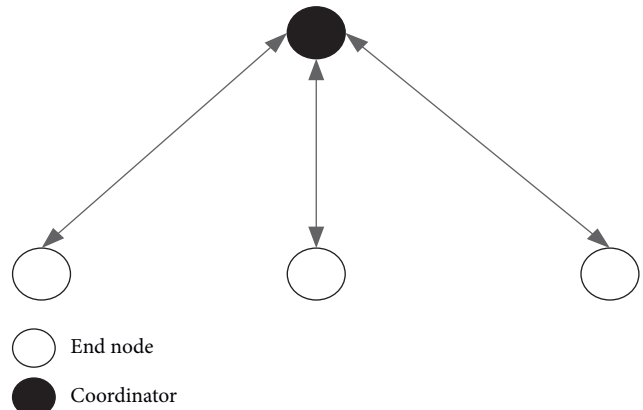


FIGURE 8: Star network topology.

configure the PIN_ID and network channel consistent with the coordinator. After receiving the request sent by the coordinator, the terminal node recognizes it. After the recognition results completely match, the network is built. The process for the coordinator to build a ZigBee network is shown in Figure 9.

5.3.2. *CC2530 Terminal Node Joins ZigBee Network.* There is a ZigBee network within the scope of the CC2530 terminal node. The terminal node matches the coordinator by scanning the channel. After a successful match, the terminal node applies for joining the network. If the coordinator agrees to the terminal node to access the network, the terminal node will receive the short address assigned by the coordinator and successfully access the network. The

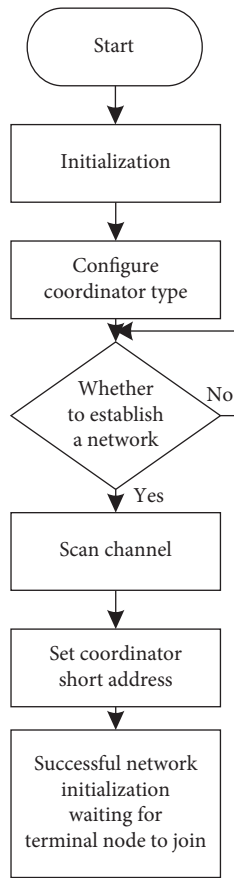


FIGURE 9: Coordinator network building flow chart.

process of the terminal node joining the ZigBee network is shown in Figure 10.

5.3.3. *CC2530 Coordinator Workflow.* The coordinator constructs the network and configures the network channel and initializes the address table. Then, the terminal node starts scanning. After the coordinator agrees, the terminal node joins the network to complete the ZigBee networking. After successful networking, the coordinator waits for the command sent by the host computer and executes the corresponding operation after parsing the command. For commands of the control-type terminal node, the coordinator sends commands to the terminal node. The terminal node performs the work, and there is no information feedback. For the instructions of the information collection terminal node, the coordinator sends a work command to the terminal node. The terminal node performs the work. The coordinator receives the information from the terminal node and sends it to the main control. The coordinator workflow is shown in Figure 11.

5.3.4. *Controlled Terminal Node Workflow.* The control terminal node is responsible for controlling household electrical appliances on the node. The workflow is as follows. First, it is initialized. Then, it starts to scan the network built by the coordinator and applies to join the network. If joining

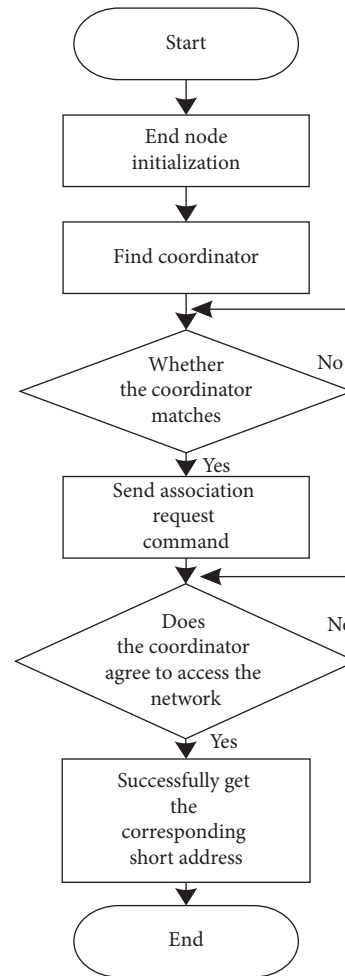


FIGURE 10: Flow chart of terminal node network connection.

the network is successful, the system setting indicator lights up. The control-type terminal node starts to obtain commands and analysis sent by the coordinator and judges whether to execute control. The control terminal node workflow is shown in Figure 12.

5.4. *Autonomous Positioning and Navigation Design.* At present, it is difficult to realize high-precision robot positioning and navigation with a single sensor. Therefore, multisensor fusion is carried out in the design of this paper, and the data collected by the attitude sensor and the lidar are fused to realize the high-precision pose estimation of the service robot in the environment map. SLAM (simultaneous localization and mapping) means simultaneous localization and map construction. It is a common method to solve robot localization and mapping, and it is a research hotspot in the field of robotics. The optimization of the SLAM process can be achieved through multisensor data fusion. Figure 13 is a basic structure diagram of multisensor data fusion. Firstly, relevant data are collected from the attitude sensor and lidar, and then the data are calculated and processed by the fusion model, and finally the robot pose is output.

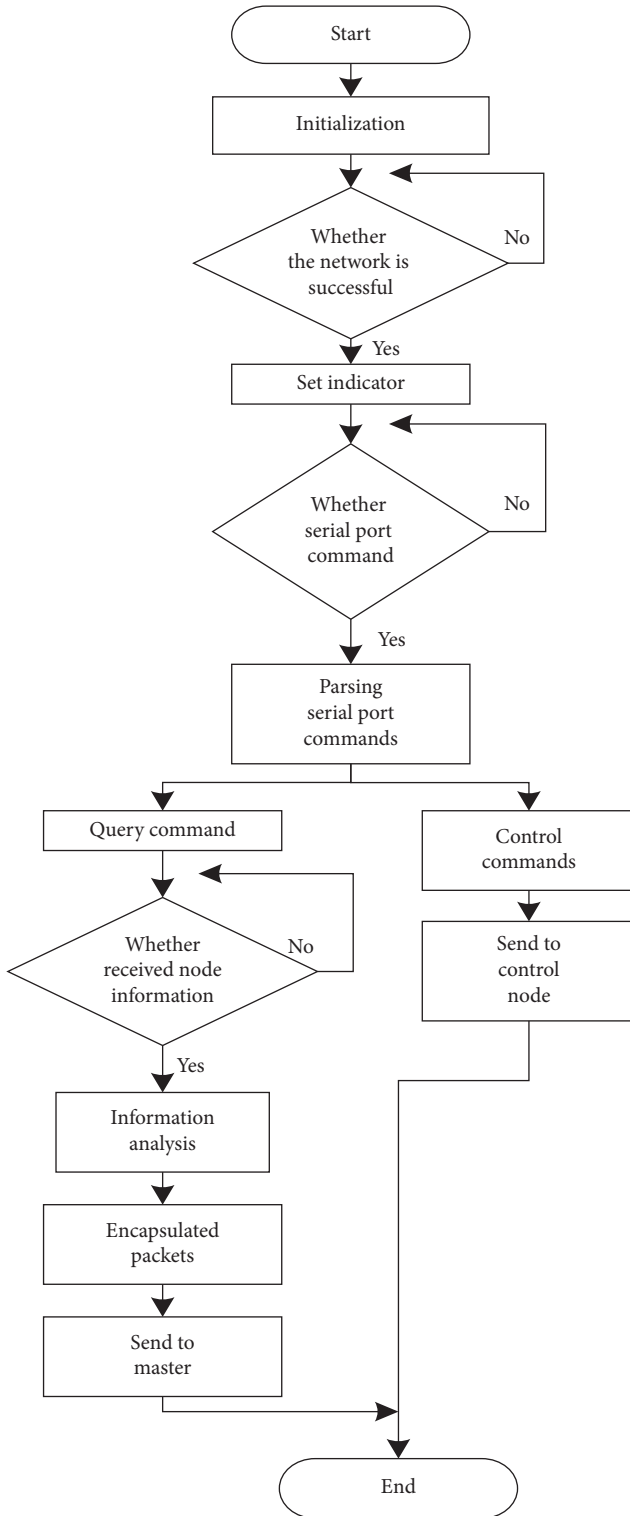


FIGURE 11: Coordinator work flow chart.

In the fusion model, a data fusion method based on BP neural network [19] is used to fuse the attitude sensor and lidar data, and finally the high-precision pose is output. BP neural network is one of the most widely used neural networks at present; it is trained according to the error back propagation algorithm. BP neural network uses the errors in

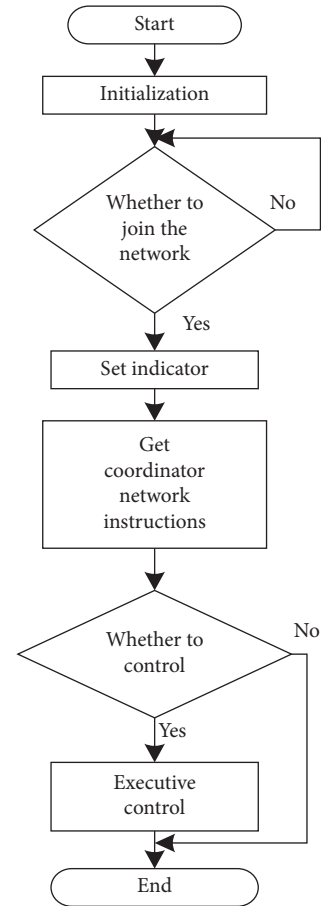


FIGURE 12: Controlled end node flow chart.

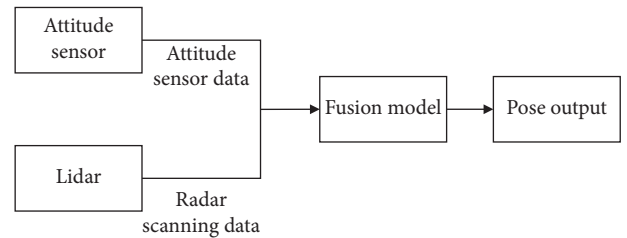


FIGURE 13: Basic structure diagram of multisensor data fusion.

each layer of the network to correct the partial derivatives of node weights and the corresponding weights. In the process of network learning, the error is propagated from the last output node to the entire BP neural network in each layer of the network in order to achieve the gradual convergence of the final output error. Figure 14 is the basic structure model of the BP neural network. The model has an input layer, a hidden layer, and an output layer. In the figure, I_i is the input data, W_{ij} is the connection weight between the nodes of each layer, and O_i is the output data. In order to make the target output closer to the true value, it is necessary to take the average of the three consecutive pose outputs to achieve data smoothing and denoising. The specific operations are as follows:

$$P_k = \frac{P_{k-1} + P_k + P_{k+1}}{3}. \quad (2)$$

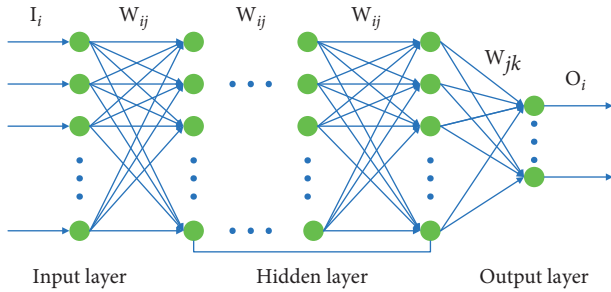


FIGURE 14: The basic structure model of BP neural network.

The designed BP neural network model takes the data of lidar and attitude sensor as input. Among them, the lidar has 440 data and the attitude sensor has 6 data, a total of 446 input data. There are three output data, which are x -axis coordinates, y -axis coordinates, and robot rotation angle. In the neural network training process, according to the error change and the analytical effect of the training model on the test data set, while ensuring the higher accuracy of the two parts, the number of nodes in the hidden layer is sequentially reduced in order to as much as possible use a smaller-scale neural network model. Finally, an ideal training result is obtained, as shown in Figure 15. As shown in Figure 15, in BP neural network, the training function used is `trainrp`, `logsig` is used as the transfer function between the first three layers, and the `purelin` linear function is used to adjust the output in the fourth layer.

In order to verify the effectiveness of using the designed BP neural network for data fusion to estimate the relative displacement of the robot, the situation of sensor data fusion is compared with the situation of using a single sensor for relative displacement estimation. Table 1 is the comparison of the relative displacement estimation error of the attitude sensor, the lidar, and the data fusion of the two sensors. Figure 16 is a comparison diagram of the relative displacement estimation error. It can be clearly seen from the figure that the accuracy of the relative displacement estimation of the two sensors using the BP neural network method designed in this paper is higher than that of using a single sensor.

5.5. Voice Control Software Design. This design uses the speech recognition API interface of Baidu AI platform for speech recognition. In addition, we use SnowBoy offline voice wake-up engine to achieve offline voice wake-up and voice interaction.

5.5.1. Baidu Speech Recognition API. We register an account on Baidu AI official website. Then, we create a speech recognition application and get the ID number and key as follows:

- (i) `APP_ID = '16188196'`
- (ii) `API_KEY = 'c8i1D8ncIKuUK8HOPYeESojR'`
- (iii) `SECRET_KEY = 'dhmLkQBjztATaDXrygYetKGQ0k46EiPn'`

We install the corresponding SDK on the Raspberry Pi 3B and build a speech recognition and speech synthesis platform. We write a node function in the SDK and let the function run as a node in the system.

5.5.2. Voice Wake Engine SnowBoy. The voice wake-up engine SnowBoy is used to wake up the robot. We use SnowBoy to train a model as the wake word of the robot. When the service robot awakened, it enters the working state of voice recognition so as to perform voice control on the service robot.

6. System Debugging

6.1. Robot Control Household Electrical Debugging. On the system, we send a command to the service robot to turn on the light. The service robot sends instructions to the terminal node that controls the lights through the CC2530 coordinator. The terminal node controls the on and off of the relay switch to control the light on and off. The control effect is shown in Figures 17 and 18. In the debugging process, we test the control distance of the service robot by continuously increasing the distance between the service robot and the terminal node. In the absence of walls or other obstacles, the control distance of the service robot is within 10 meters. If there are obstacles, the control effect will be greatly affected.

6.2. PID Parameter Debugging. The stability of the service robot movement requires tuning of PID parameters. This design uses empirical trial and error method to determine PID parameters through experiments. The service robot conducts experiments under the condition of only its own weight and determines the PID parameters. Considering that the service robot is in the actual practical teaching application scenario, the load will not change much in a short time. Therefore, the parameters determined after experiments are applicable in general. The specific operation method of PID parameter tuning is as follows. First, we determine a set of parameter values of k_p , k_i , and k_d and put the system into operation. Then, we set the desired motor speed. Observe the step response curve of the motor speed output through the `rqt_plot` tool, and continuously change the parameter values of k_p , k_i , and k_d to obtain a satisfactory step response curve.

6.3. Camera Information Collection and Debugging. The camera and the Raspberry Pi are directly connected through the USB serial port. Then, the PC is connected to the Raspberry Pi 3B remotely. The PC side runs the node (`usb_cam`) that starts the camera in the Raspberry Pi 3B, and then the PC side runs the `rqt_image_view` tool to obtain the image information of the camera as shown in Figure 19. By adjusting the focus of the camera, clear image information is obtained.

6.4. Human Infrared Detection Alarm Debugging. We issue commands to the service robot on the PC side. Let the

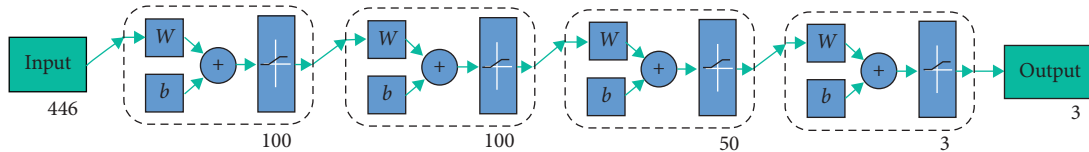


FIGURE 15: The final designed BP neural network model.

TABLE 1: Comparison of relative displacement estimation errors.

Time	Attitude sensor	Lidar	Attitude sensor and lidar data fusion
1	0.536	0.403	0.100
2	0.478	0.512	0.050
3	0.494	0.511	0.060
4	0.501	0.496	0.030
5	0.564	0.500	0.041
6	0.478	0.533	0.091
...
45	0.580	0.494	0.196
46	0.700	0.601	0.136
47	0.674	0.632	0.133
48	0.601	0.678	0.145
49	0.654	0.631	0.101
50	0.625	0.589	0.091

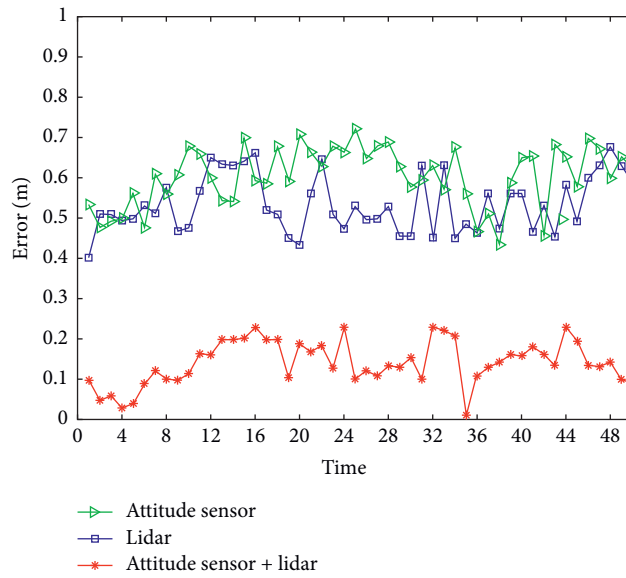


FIGURE 16: Comparison of relative displacement estimation errors.

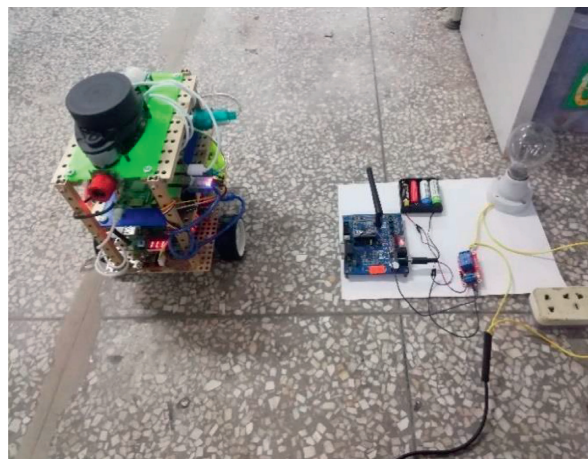


FIGURE 17: Effect picture before robot control.



FIGURE 18: Effect picture after robot control.

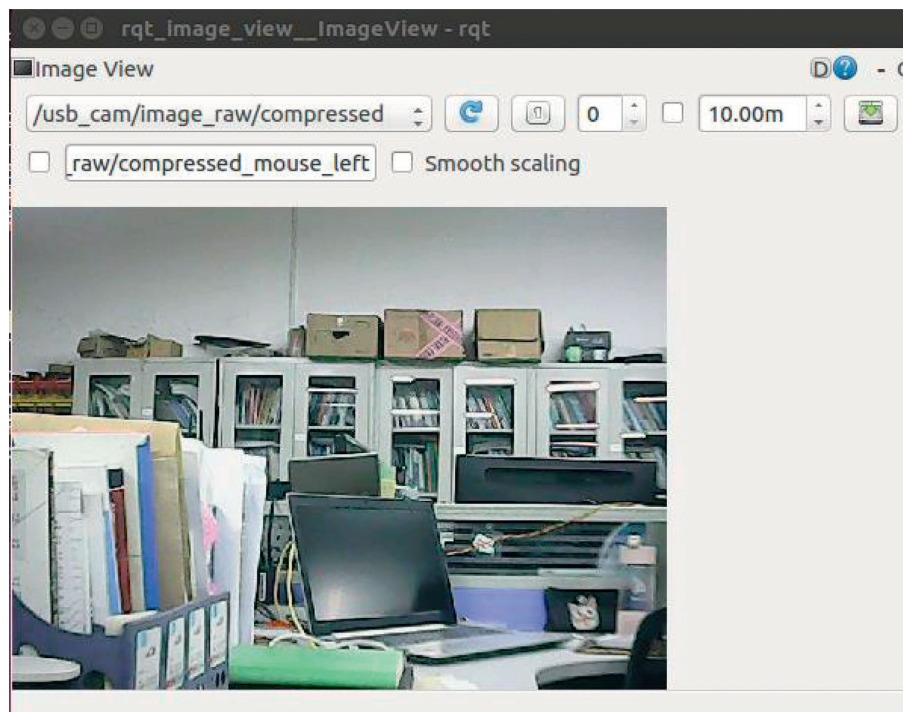


FIGURE 19: Information collected by the camera.

infrared module of the human body start to detect if there is a human being. The system uses Arduino mega2560 to control the GSM module to call and send text messages to users. This system can remind users in time by dialing. The user can know the specific information of the alarm by checking the short message. The test is shown in Figures 20 and 21.

7. Function and User Experience Comparison

In order to reflect the advantages of the home service robot designed in this article, we compared the robot function developed in this article with the robot function in the reference. We randomly selected 15 people, and each person experienced the robots in the following



FIGURE 20: Human infrared sensor detects someone.

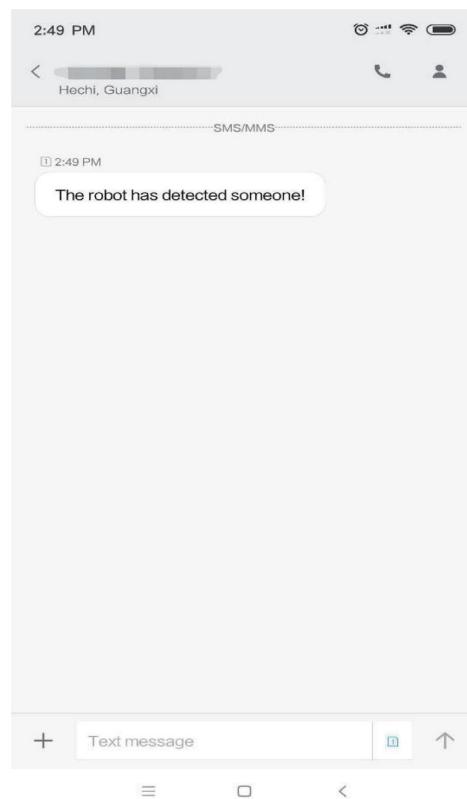


FIGURE 21: View SMS messages.

table for two days and then scored the experience of each robot. The results of the survey are shown in Table 2. It can be seen from the table that the home service

robot designed in this article has more complete functions than other robots, and the user experience is the best.

TABLE 2: Survey results.

Literature	Features	User experience
Reference [7]	Temperature and humidity measurement, camera, light control, flame/smoke alarm, human body infrared sensor	***
Reference [5]	Human-computer interaction	**
Reference [12]	Voice communication, face recognition, human-computer interaction	****
Reference [14]	Wireless sensor and robot communication	*
Reference [13]	Speech recognition, human-computer interaction	**
Reference [15]	Wireless control	*
Reference [16]	Robot walking (balanced walking motion)	**
The robot designed in this article	Robot walking, wireless communication, hazard alarm, autonomous navigation, indoor positioning, voice control, control of home appliances, human infrared detection warning, camera information collection	*****

8. Conclusion

Currently, smart home service robots have fewer functions, and it is difficult to meet people's needs for a comfortable, convenient, safe, and fun home life. And they still generally lack the ability to independently complete the task of combining autonomous patrols and home services. In response to this problem, this article has researched and developed a home robot system that has complete functions and can independently complete the task of combining autonomous patrols and home services. The system is based on ROS to design a smart home service robot system. It uses the framework and principles of the ROS system to build a distributed computing system through message publish-subscribe. The ZigBee networking structure between the CC2530 chip, the coordinator, and the terminal nodes is used to realize the ZigBee wireless networking. The voice control service robot is realized by Baidu AI voice recognition API. Using the combination of lidar and attitude sensor, the service robot realizes the establishment of maps and autonomous navigation of the indoor environment. Compared with related home service robots, the home service robots researched and designed in this paper have relatively sound functions and at the same time complete the task of combining independent inspections with home service. Compared with other home service systems, the system designed in this paper has a better user experience, making the user's life more comfortable, convenient, safe, and fun.

Data Availability

The data used to support the findings of this study are included within the article.

Conflicts of Interest

The authors declare that they have no conflicts of interest to report regarding the present study.

Authors' Contributions

Jiansheng Peng, Hemin Ye, Yong Qin, and Zhenwu Wan contributed equally to this work.

Acknowledgments

The authors are highly thankful to the Research Project for Young and Middle-Aged Teachers in Guangxi Universities (ID: 2019KY0621), to the Natural Science Foundation of Guangxi Province (No. 2018GXNSFAA281164), and to the support by National Natural Science Foundation of China (No. 62063006). This research was financially supported by the project of outstanding thousand young teachers' training in higher education institutions of Guangxi, Guangxi Colleges and Universities Key Laboratory Breeding Base of System Control and Information Processing.

References

- [1] S. Gürel, H. Gultekin, and V. E. Akhlaghi, "Energy conscious scheduling of a material handling robot in a manufacturing cell," *Robotics and Computer-Integrated Manufacturing*, vol. 58, pp. 97–108, 2019.
- [2] G. Niu, B. Pan, Y. Fu et al., "Development of a new medical robot system for minimally invasive surgery," *IEEE Access*, vol. 8, pp. 144136–144155, 2020.
- [3] J. W. Jia, N. Chung, and J. Hwang, "Assessing the hotel service robot interaction on tourists' behaviour: the role of anthropomorphism," *Industrial Management & Data Systems*, vol. 121, 2021.
- [4] Y. Sun, L. Guan, Z. Chang et al., "Design of a low-cost indoor navigation system for food delivery robot based on multi-sensor information fusion," *Sensors*, vol. 19, no. 22, 4980 pages, 2019.
- [5] J. Saunders, D. S. Syrdal, K. L. Koay et al., "“Teach me—show me”—end-user personalization of a smart home and companion robot," *IEEE Transactions on Human-Machine Systems*, vol. 46, no. 1, pp. 27–40, 2015.
- [6] World Health Organization, *10 Facts on Ageing and the Life Course*, World Health Organization, Geneva, Switzerland, 2014, <http://www.who.int/features/factfiles/ageing/en/>.
- [7] R. Turjamaa, A. Pehkonen, and M. Kangasniemi, "How smart homes are used to support older people: an integrative review," *International Journal of Older People Nursing*, vol. 14, no. 4, Article ID e12260, 2019.
- [8] M. R. Alam, M. B. I. Reaz, and M. A. M. Ali, "A review of smart homes—past, present, and future," *IEEE Transactions on Systems, Man, and Cybernetics, Part C (Applications and Reviews)*, vol. 42, no. 6, pp. 1190–1203, 2012.
- [9] K. Wada, T. Shibata, T. Asada et al., "Robot therapy for prevention of dementia at home," *Journal of Robotics and Mechatronics*, vol. 19, no. 6, 691 pages, 2007.

- [10] D. Lee, T. Yamazaki, and S. Helal, "Robotic companions for smart space interactions," *IEEE Pervasive Computing*, vol. 8, no. 2, pp. 78–84, 2009.
- [11] D. Portugal, P. Alvito, E. Christodoulou et al., "A study on the deployment of a service robot in an elderly care center," *International Journal of Social Robotics*, vol. 11, no. 2, pp. 317–341, 2019.
- [12] N. H. Abdallah, E. Affes, Y. Bouslimani, M. Ghribi, A. Kaddouri, and M. Ghariani, "Smart assistant robot for smart home management," in *Proceedings of the 020 1st International Conference on Communications, Control Systems and Signal Processing (CCSSP)*, pp. 317–321, El Oued, Algeria, March 2020.
- [13] J. Berrezueta-Guzman, I. Pau, M. L. Martín-Ruiz et al., "Smart-home environment to support homework activities for children," *IEEE Access*, vol. 8, pp. 160251–160267, 2020.
- [14] W. Wang Huiyong, W. Huang Min, and H. Min, "Building a smart home system with WSN and service robot," in *Proceedings of the 2013 Fifth International Conference on Measuring Technology and Mechatronics Automation*, pp. 353–356, Hong Kong, China, January 2013.
- [15] H. Hsu, K. Yu, W. Ouyang, and C. J. Xu, "Constructing a smart home control system with the Internet of things," in *Proceedings of the 2018 IEEE Asia-Pacific Conference on Antennas and Propagation (APCAP)*, pp. 1-2, Auckland, New Zealand, August 2018.
- [16] W. Guan, S. Chen, S. Wen et al., "High-accuracy robot indoor localization scheme based on robot operating system using visible light positioning," *IEEE Photonics Journal*, vol. 12, no. 2, pp. 1–16, 2020.
- [17] O. P. Bodunde, U. C. Adie, O. M. Ikumapayi et al., "Architectural design and performance evaluation of a ZigBee technology based adaptive sprinkler irrigation robot," *Computers and Electronics in Agriculture*, vol. 160, pp. 168–178, 2019.
- [18] I. González and A. J. Calderón, "Integration of open source hardware Arduino platform in automation systems applied to Smart Grids/Micro-Grids," *Sustainable Energy Technologies and Assessments*, vol. 36, Article ID 100557, 2019.
- [19] S. Song, X. Xiong, X. Wu et al., "Modeling the SOFC by BP neural network algorithm," *International Journal of Hydrogen Energy*, vol. 46, no. 38, pp. 20065–200077, 2021.

Research Article

Three-Dimensional UWSN Positioning Algorithm Based on Modified RSSI Values

Qin Qin , Yi Tian, and Xin Wang

Beihai Campus, Guilin University of Electronic Technology, Guilin 541004, China

Correspondence should be addressed to Qin Qin; qinqin@guet.edu.cn

Received 28 January 2021; Revised 28 March 2021; Accepted 16 June 2021; Published 23 June 2021

Academic Editor: Hsu-Yang Kung

Copyright © 2021 Qin Qin et al. This is an open access article distributed under the Creative Commons Attribution License, which permits unrestricted use, distribution, and reproduction in any medium, provided the original work is properly cited.

Sensor nodes in underwater wireless sensor networks (UWSNs) are in a three-dimensional space, and water fluidity continuously changes the positioning in water, the clock synchronization of underwater nodes is challenging, and ranging algorithms affected by water flow produce large errors. A three-dimensional UWSN positioning algorithm based on modified RSSI values is proposed to address the problem of UWSN positioning algorithms being susceptible to water influence and prone to unstable positioning and large positioning errors. An unlocated node screens the received anchor node signal strength and then makes a weighted correction to reduce the influence of the water environment and improve the ranging accuracy. A position estimation model is proposed and combined with a three-dimensional underwater model and least squares method to deduce the unlocated node's position on the basis of the distance between the unlocated node and the anchor node. The proposed algorithm effectively reduces the influence of the water environment on the ranging algorithm's accuracy and improves the performance of three-dimensional underwater positioning algorithms. Simulation results show that the proposed algorithm can effectively reduce the influence of the underwater environment on positioning algorithms.

1. Introduction

Sensor node positioning is a key technology in wireless sensor networks. With the development of terrestrial wireless sensor network applications, underwater wireless sensor network applications have attracted increasing attention. However, the complex underwater environment hinders the location of underwater wireless sensor networks (UWSNs) [1]. It also necessitates the consideration of all factors affecting positioning performance. Sensors in water are usually deployed in areas that cannot be easily accessed by humans or those with few infrastructure; meanwhile, common sensor nodes are randomly arranged [2]. The factors affecting underwater signal transmission must be considered when estimating the positions of sensor nodes relative to anchor nodes by using received signal strength. The result identifies the factors affecting transmission in a real environment. UWSNs comprise unevenly distributed sensor nodes, sparse nodes, and nodes that are easily affected by water fluidity. Anchor nodes that assist positioning can

improve the positioning accuracy of sensor networks [3–5]. Li et al. [6] proposed a weighted centroid ranging algorithm that is based on received signal strength indicators (RSSIs) and time difference of arrival (TDOA); this algorithm uses the distance parameter and signal strength between anchor nodes as a reference to correct the estimated distance between unlocated nodes and anchor nodes. It also reduces positioning errors relative to the traditional RSSI centroid. A positioning algorithm in [7] reduces positioning errors in an uneven node distribution by using RSSI values to optimize the single hop value in the DV-Hop algorithm. A three-sided RSSI centroid positioning algorithm was proposed in [8], and it is able to correct the path loss factor in an actual environment, reduce the ranging algorithm errors caused by the environment, and improve positioning algorithm accuracy. Zhang and Huang [9] aimed to correct RSSI values by dynamically acquiring path loss factors and reduce environment impact by combining three-sided centroid positioning algorithms. However, the positioning model needs to be adjusted regularly, and the error range of the acquired

path loss factors affects positioning algorithms. Although existing algorithms show improved positioning accuracy, the accuracy of ranging algorithms requires improvement [10]; an enhanced design for positioning algorithms is also needed as nodes cannot be synchronized accurately in an underwater environment, and they tend to influence positioning algorithms.

In sum, underwater positioning algorithms in UWSNs are prone to large errors, and they are susceptible to water fluidity. Moreover, the nodes comprising UWSNs are difficult to synchronize. A received signal strength ranging algorithm is low cost and requires simple technology and minimal hardware. However, underwater sensor nodes are difficult to replace, they are susceptible to the underwater environment, their energy is limited, and their cost is relatively high. Therefore, a three-dimensional UWSN positioning algorithm based on modified RSSI values is proposed in this work. Weighted and modified RSSI values reduce ranging errors. Combined with a three-dimensional underwater positioning model, the proposed algorithm can estimate the unlocated node position in a three-dimensional space by using the least squares method. The proposed algorithm shows improved robustness, reduces the impact of underwater fluidity on ranging, and enhances the accuracy of network node positioning.

2. Distance Conversion Model

2.1. Received Signal Strength Algorithm. A ranging algorithm based on received signal strength can convert the signal strength received by an unlocated node and sent by an anchor node in a certain distance. Specifically, a mobile anchor node sends the signal. During the transmission process, certain loss occurs because of the influence of the external environment. The longer the transmission distance is, the greater the signal loss will be and the smaller the RSSI value received by the unlocated node. The loss during transmission can be converted into an RSSI value through the path loss model. In an actual ranging process, the loss model uses a log-normal distribution model. The parameters in the model can be calculated by the actual distance between anchor nodes and by the algorithm measurement distance [11].

In the current work, the signal transmission attenuation model uses a log-normal distribution model:

$$\frac{p_r(d_0)}{p_r(d_{ij})} = \left(\frac{d_{ij}}{d_0}\right)^{N_p} \quad (1)$$

By simplifying formula (1) and taking the logarithm of each side, the following result is obtained:

$$p_r(d_{ij}) = p_r(d_0) - 10N_p \lg\left(\frac{d_{ij}}{d_0}\right) + X_\sigma \quad (2)$$

where $p_r(d_{ij})$ is the received power between d_{ij} nodes, $p_r(d_0)$ is the d_0 received strength path loss of unit distance, $p_r(d_0)$ can be obtained by measuring the actual distance between nodes, N_p is the channel attenuation index whose

value depends on the application environment, generally ranges from 2 to 5, and X_σ refers to the Gaussian distribution noise and is often expressed by a normal distribution.

The distance d_{ij} between nodes can be deduced from formula (2):

$$d_{ij} = 10^{A/10N_p}, \quad (3)$$

where d_{ij} is the communication distance between node i and node j . $A = p_r(d_0) - p_r(d_{ij}) + X_\sigma$. The signal strength sent by the nodes in the UWSN decreases with an increase in transmission distance. Moreover, the signals from sensor nodes suffer from losses to a certain extent. The unlocated nodes obtain N RSSI values with anchor nodes, and the distance value between unlocated nodes and multiple anchor nodes can be obtained by formula (3).

2.2. Weighted Correction of RSSI. The signal strength ranging algorithm is easily affected by the application environment, thereby resulting in ranging errors [12]. In practice, the temperature, salinity, obstacles, and density of the water environment cause signal losses and a decrease in signal strength. Water fluidity causes objects in water to move slightly [13]. Hence, the signal strength received by sensor nodes varies from time to time, eventually affecting distance estimation between nodes [14]. Thus, averaging and Gaussian filter methods are combined to weigh and modify RSSI values. A modified RSSI value improves ranging accuracy and positioning accuracy of UWSNs.

A mobile anchor node broadcasts signals regularly during its movement. Anchor nodes release signal N times at the same place to enhance the ranging accuracy. Each sensor node has a list of the ID numbers of mobile anchor nodes in different positions. After an unlocated node receives information from a mobile anchor node, the average Φ and variance α of the RSSI value of the same received ID can be calculated by the following formula:

$$\begin{cases} \Phi = \frac{1}{N} \sum_{i=1}^N P_i, & i = 1, 2, 3, \dots, N, \\ \alpha = \frac{1}{N-1} \sum_{i=1}^N (P_i - \mu), & i = 1, 2, 3, \dots, N. \end{cases} \quad (4)$$

According to formula (4), the same ID RSSI values received by the unlocated node are screened. The M RSSI values outside the $(\Phi - \alpha)$ and $(\Phi + \alpha)$ interval are cancelled, and the average value Φ^* within the interval is recalculated. The weighted formula of the RSSI value within the interval is as follows:

$$P = \frac{1}{N-M} \left(P_i \times \frac{1}{P_i - \Phi^*} \right). \quad (5)$$

According to formula (5), the weighted and modified RSSI values can be obtained. Then, the distance between the unlocated node and the anchor node can be calculated by substituting the obtained RSSI value into formula (3).

2.3. Position Estimation Model. As the anchor node moves through the network and broadcasts signals to the surroundings, the ordinary node receives information from the anchor node and uses the distance conversion model to calculate the distance between nodes. In this section, a position estimation model is proposed to obtain the location information of unlocated nodes on the basis of the distance between nodes.

2.4. Three-Dimensional Underwater Model. Wireless sensor networks on land generally require two-dimensional planar positioning, whereas UWSNs in special underwater environments require three-dimensional positioning [15–17]. Such requirements cannot be met by traditional positioning algorithms. Hence, research should consider how anchor and normal nodes send and receive signals in the three-dimensional underwater environment [18].

The positioning requirements of wireless sensor networks on land are generally two-dimensional planar positioning, while the special underwater environment requires UWSN to adopt a three-dimensional positioning. The traditional positioning algorithm cannot meet the requirement of underwater sensor nodes positioning. It is necessary to consider how the anchor node and normal node send and receive signals in the three-dimensional underwater environment.

As shown in Figure 1, signals in a UWSN diverge in a spherical shape when nodes communicate. Anchor nodes broadcast signals to unlocated nodes within the communication range. The signals are transmitted in a three-dimensional space, whose the coverage area is a sphere and the communication diameter is the radius.

In a three-dimensional underwater environment, unlocated nodes receive the information of n anchor nodes with the strongest signal. As shown in Figure 2, the sensor nodes in this model are equipped with pressure sensors to obtain their own depth information. Node depth can be directly converted into the Z -axis of node coordinates. The coordinates of unlocated nodes are (x, y, z) , and the coordinates of three anchor nodes are $A(z_1, y_1, z_1)$, $B(z_2, y_2, z_2)$, $C(x_3, y_3, z_3)$, $\dots, N(x_n, y_n, z_n)$. On the basis of the distance between unlocated nodes and n anchor nodes, the following equations can be obtained:

$$\begin{cases} (x - x_1)^2 + (y - y_1)^2 + (z - z_1)^2 = l_1, \\ (x - x_2)^2 + (y - y_2)^2 + (z - z_2)^2 = l_2, \\ \vdots \\ (x - x_n)^2 + (y - y_n)^2 + (z - z_n)^2 = l_n. \end{cases} \quad (6)$$

Three sensor nodes form a plane. An unlocated node in underwater node positioning requires three anchor nodes, and four nodes form a polyhedron. Four nodes need to be projected to a horizontal plane to achieve relative positioning. Three anchor nodes are mapped to the same plane as that of the unlocated node. The coordinate Z of the unlocated node can be obtained by its own pressure sensor. The mapped formula is as follows:

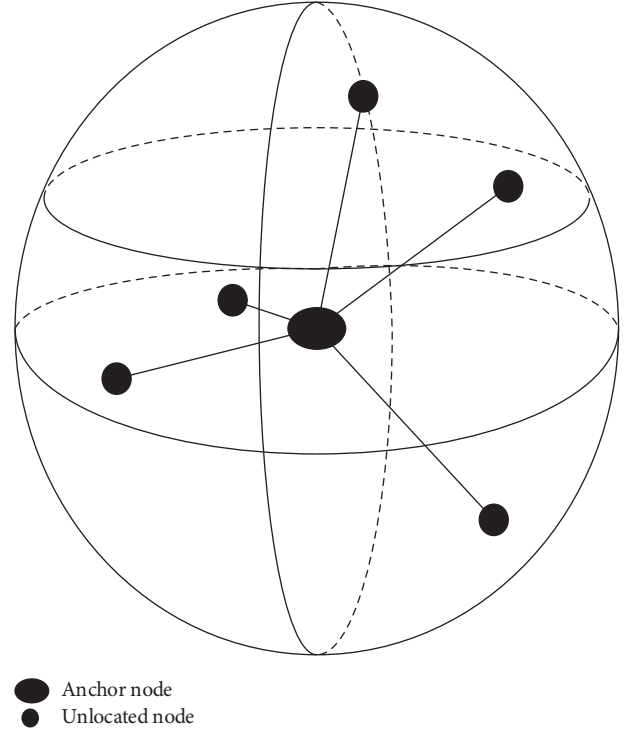


FIGURE 1: Sensor node sending and receiving signals.

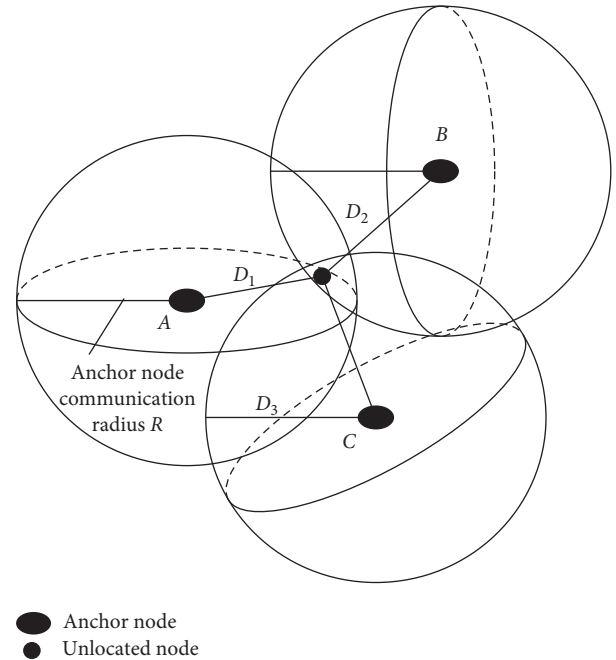


FIGURE 2: Sensor nodes sending and receiving signals.

$$\begin{cases} Y_1 = \sqrt{D_1^2 - (Z - Z_1)^2}, \\ Y_2 = \sqrt{D_2^2 - (Z - Z_2)^2}, \\ Y_3 = \sqrt{D_3^2 - (Z - Z_3)^2}. \end{cases} \quad (7)$$

From formulas (6) and (7), the coordinates of three anchor nodes on the same two-dimensional plane can be deduced as $A(X1, \sqrt{D_1^2 - (Z - Z_1)^2})$, $B(X2, \sqrt{D_2^2 - (Z - Z_2)^2})$, and $C(X3, \sqrt{D_3^2 - (Z - Z_3)^2})$.

2.5. Least Squares Position Estimation. The coordinates of N anchor nodes around the unlocated node D are $(x1, y1, z1)$, $(x2, y2, z2)$, $(x3, y3, z3)$, \dots , (xn, yn, zn) . The distance from these anchor nodes to node D can be calculated by the distance conversion model as $d1, d2, \dots, dn$. The unlocated node D can obtain its own depth through its pressure sensor. The three-dimensional underwater positioning model can convert the obtained coordinates into two-dimensional coordinates. The converted coordinates are $(x1, y1)$, $(x2, y2)$, \dots , (xn, yn) . Assuming that the two-dimensional coordinates of node D are (x, y) , the following formula can be obtained as

$$\begin{cases} (x_1 - x)^2 + (y_1 - y)^2 = d_1^2, \\ (x_2 - x)^2 + (y_2 - y)^2 = d_2^2, \\ \vdots \\ (x_n - x)^2 + (y_n - y)^2 = d_n^2. \end{cases} \quad (8)$$

Formula (9) is obtained by subtracting the last equation from the first equation of formula (8):

$$\begin{cases} x_1^2 - x_n^2 - 2(x_1 - x_n)x + y_1^2 - y_n^2 - 2(y_1 - y_n)y = d_1^2 - d_n^2, \\ x_2^2 - x_n^2 - 2(x_2 - x_n)x + y_2^2 - y_n^2 - 2(y_2 - y_n)y = d_2^2 - d_n^2, \\ \vdots \\ x_{n-1}^2 - x_n^2 - 2(x_{n-1} - x_n)x + y_{n-1}^2 - y_n^2 - 2(y_{n-1} - y_n)y = d_1^2 - d_n^2. \end{cases} \quad (9)$$

Formula (9) is converted into the linear equation $AX = b$, as shown in the following formula:

$$A = \begin{bmatrix} 2(x_1 - x_n) & 2(y_1 - y_n) \\ 2(x_2 - x_n) & 2(y_2 - y_n) \\ \vdots & \vdots \\ 2(x_{n-1} - x_n) & 2(y_{n-1} - y_n) \end{bmatrix}, \quad (10)$$

$$b = \begin{bmatrix} x_1^2 - x_n^2 + y_1^2 - y_n^2 + d_n^2 - d_1^2 \\ x_2^2 - x_n^2 + y_2^2 - y_n^2 + d_n^2 - d_2^2 \\ \vdots \\ x_{n-1}^2 - x_n^2 + y_{n-1}^2 - y_n^2 + d_n^2 - d_{n-1}^2 \end{bmatrix}. \quad (11)$$

Finally, the estimated position coordinate of the unlocated sensor node D is determined as $X = (A^T A)^{-1} A^T b$ by using the least squares method.

2.6. Three-Dimensional UWSN Positioning Algorithm Based on Modified RSSI Value. Differences exist between water and terrestrial environments [19]. Hence, in UWSN positioning, the algorithm adopted must consider underwater features [20], such as water fluidity, complex substances in water,

actual signal losses varying with anchor nodes' movement through different water areas, and signal strength changing with different obstacles in water [21]. Ranging algorithms based on signal strength produce large ranging error because of the instability of the underwater environment. An increase in ranging errors increases positioning errors accordingly. In this section, the weighted and corrected RSSI value is used to improve ranging algorithm accuracy. The value is combined with the three-dimensional underwater positioning method to improve the positioning accuracy of underwater nodes.

As shown in Figure 3, the three-dimensional positioning algorithm for the UWSN based on the revised RSSI value involves two stages: ranging (stage 1) and node positioning (stage 2). In stage 1, the mobile anchor node in the UWSN broadcasts information to the surrounding nodes through mobile communication. The unlocated node receives the RSSI value between itself and the anchor node. Moreover, the signal strength of each anchor node received by the unlocated node is converted into the distance between the unlocated node and each anchor node by the distance conversion model. In stage 2, the relative position of the unlocated node in the UWSN can be calculated with the distance between the sensor nodes in stage 1 by using the position estimation model. Then, the sensor node is located on the basis of the actual position of the anchor nodes.

The process of the proposed three-dimensional positioning algorithm is shown in Figure 4. The detailed steps are as follows:

Step 1: the mobile anchor node traverses the network according to the planned route, reaches the specified location, broadcasts signals for N times, and sends its own information list containing the ID number and three-dimensional coordinates (X_i, Y_i, Z_i) of the location.

Step 2: the unlocated node receives the information of the mobile anchor node and records the information list and signal strength on its own information list. The ID number of the same position corresponds to N signal strength.

Step 3: the node processes the data in the obtained information list. A unique RSSI value is obtained by correcting the signal strength at the same position through the weighted modified RSSI value model. The information list is updated. An unknown ID corresponds to a signal strength.

Step 4: according to the distance conversion model, only the input RSSI value gets the distance between nodes.

Step 5: the unlocated nodes repeat Steps 2, 3, and 4 to obtain the corresponding distance of three position IDs and convert the three-dimensional space ID into a two-dimensional space ID by using the three-dimensional positioning model.

Step 6: the maximum likelihood estimation method is used to calculate the two-dimensional coordinates of the positioning node. With the node's own depth

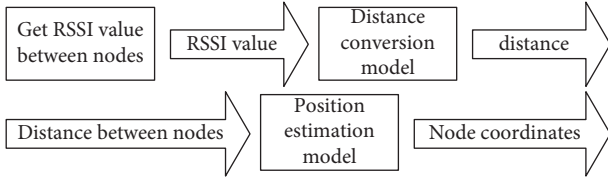


FIGURE 3: Algorithm model diagram.

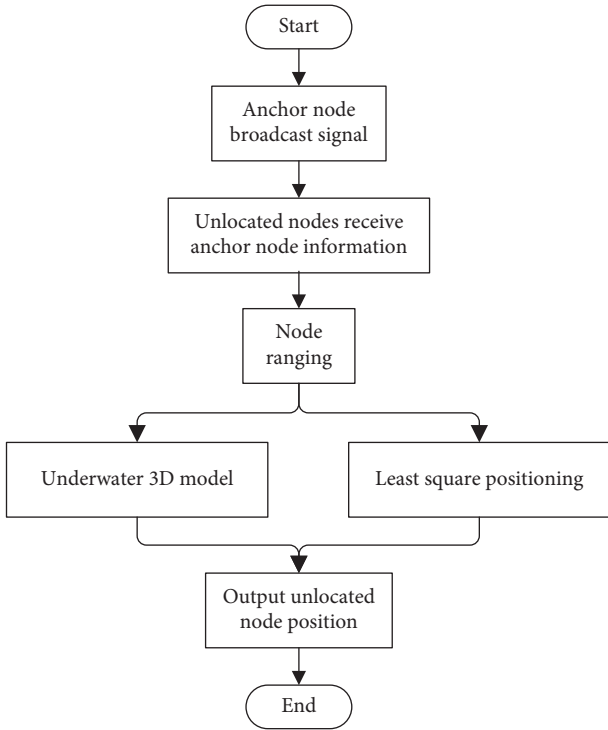


FIGURE 4: Algorithm flowchart.

information, the three-dimensional reverse conversion is carried out, and two-dimensional coordinates are converted into three-dimensional network coordinates. The estimated position of the unlocated node is obtained, thereby completing the network positioning.

3. Experimental Simulation

3.1. Experimental Environment Setting and Evaluation Index. MATLAB 2016a simulation software is applied to test the proposed positioning algorithm. A total of 50 ordinary sensor nodes are randomly arranged; the proportion of anchor nodes is 20%, and the communication radius of ordinary nodes is 20 m. Ordinary sensor nodes cannot be removed after being randomly deployed. Each anchor node is aware of its own position information. The logarithmic attenuation model is used in the signal propagation attenuation model in the experiment. The proposed algorithm is compared with the traditional RSSI location algorithm, the median RSSI location algorithm, and the DV-Hop location algorithm based on RSSI value optimization [22–24]. The simulation area is a cube region measuring

100 m × 100 m × 100 m. The distribution of underwater wireless sensor nodes in the simulation experiment is shown in Figures 5 and 6.

The evaluation indexes of the positioning algorithm in this work are as follows.

Average measuring distance: D_{ij}^* represents the average measuring distance between the i^{th} unlocated node and the j^{th} anchor node. D_{ij} represents the measuring distance between the i^{th} unlocated node and the j^{th} anchor node. m represents the number of anchor nodes, and n represents the unlocated nodes that can measure distance. The average measuring distance between an anchor node and a positioning node can be obtained by the following formula:

$$D_{ij}^* = \sum_{i=1}^n \left(\sum_{j=1}^m D_{ij} \right). \quad (12)$$

Node average positioning error: the difference between the estimated position and the actual position of unlocated sensor node i is the node positioning error marked as $error_i$. N represents the total number of unlocated sensor nodes. The sum of the positioning errors of all nodes divided by the number of positioning nodes is the average positioning error of nodes.

The smaller the node average positioning error is, the higher the positioning accuracy is and the better the performance of the positioning algorithm will be, as shown in the following formula:

$$P_{error} = \sum_{i=1}^N error_i. \quad (13)$$

Average maximum positioning error: in formula (14), $Merro_i$ represents the K^{th} maximum positioning error of the node and P_{Merro} represents the average maximum positioning error of the node:

$$P_{Merro} = \sum_{i=1}^K \frac{Merro_i}{K}. \quad (14)$$

The experimental parameter settings are shown in Table 1.

3.2. Experimental Results and Analysis. Given the 20 m communication radius of common nodes and the varying communication ranges of anchor nodes, the actual distance between nodes, traditional RSSI distance, median RSSI distance, and modified RSSI distance are compared in this work (Table 2). The actual distance is the real distance between the anchor node and the unlocated node. As the reference value for the ranging accuracy of the ranging algorithm, the absolute value of the difference between the measured distance based on the ranging algorithm and the real distance is the evaluation index for the accuracy of the ranging algorithm. The larger the difference is, the lower the accuracy of the ranging algorithm is, and vice versa. When the communication radius of the anchor node is the same, the absolute difference value between the distance obtained by the modified RSSI ranging algorithm and the actual

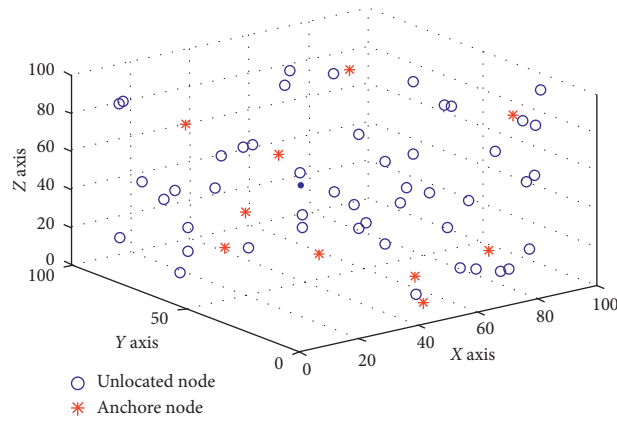


FIGURE 5: Three-dimensional distribution diagram of UWSN nodes.

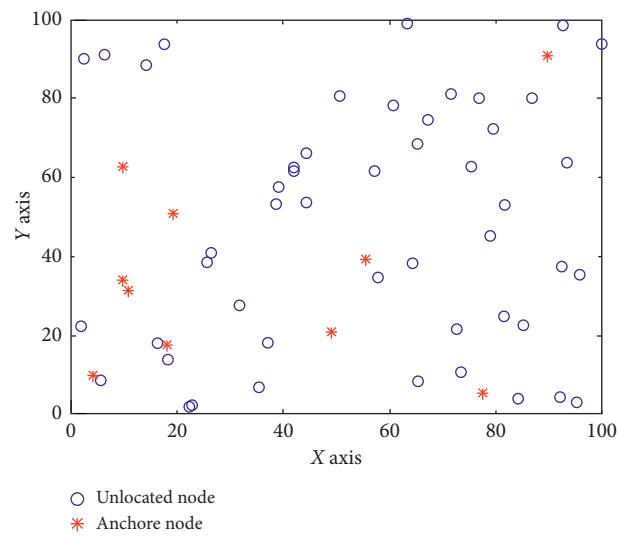


FIGURE 6: Top view of three-dimensional node distribution.

TABLE 1: Experimental parameter settings.

Parameter	Value
Simulation area side length (m)	100
Total number of sensor nodes (n)	50
Anchor node ratio (%)	20
Ordinary node communication radius (m)	20
Anchor node communication radius (m)	25, 30, 35, and 40
Signal transmission attenuation model	Logarithmic attenuation model
Path loss index	2

TABLE 2: Average measured distance between nodes.

Anchor node communication radius (m)	Actual distance (m)	Traditional RSSI ranging (m)	Median RSSI ranging (m)	Modified RSSI ranging (m)
25	12.9948	9.918	11.1843	11.9665
30	9.75967	7.7065	8.6203	9.0692
35	17.5656	15.7956	16.8796	17.1693
40	11.4812	12.2875	11.0354	11.6564

distance is the smallest. Moreover, the absolute difference value between the distance obtained by the traditional RSSI ranging algorithm and the actual distance is the largest. As the communication radius of the anchor node increases, the absolute difference values of the three ranging algorithms decrease again, but the absolute value of the modified RSSI ranging algorithm remains the smallest. Hence, the modified RSSI ranging algorithm is more accurate than other ranging algorithms.

Given the 20 m communication range of ordinary nodes and the varying communication ranges of anchor nodes, this work compares the average node positioning errors of the traditional RSSI positioning algorithm, DV-Hop-based positioning algorithm, and three-dimensional UWSN positioning algorithm based on revised RSSI values. The comparison is illustrated in Figure 7. Given different communication ranges of anchor nodes, the average positioning error of the modified RSSI positioning algorithm is lower than those of the traditional RSSI algorithm and DV-Hop algorithm. Moreover, the average positioning error decreases steadily with the increase of the anchor nodes' communication radius. Given a small radius, the DV-Hop algorithm produces a lower positioning error than the traditional RSSI algorithm; its error is close to that of the modified RSSI algorithm. The DV-Hop algorithm achieves positioning through multiple hops and thus achieves a higher positioning accuracy than the traditional RSSI algorithm in the network with sparse anchor nodes with a small communication radius. However, with an increase in the communication radius of anchor nodes, the information and calculation of nodes increase as well, thus leading to a continuous increase in errors. The revised RSSI algorithm does not need to carry out multiple data forwarding and data calculations and thus achieves reduced positioning errors. It also has high accuracy in the ranging phase and thus generates low positioning errors in the network.

Figure 8 presents a comparison diagram of the relationship between the average maximum positioning error and the anchor nodes' communication radius on the basis of the traditional RSSI positioning algorithm, DV-Hop positioning algorithm, and three-dimensional UWSN positioning algorithm based on modified RSSI values. The average maximum positioning error of the modified RSSI algorithm is lower than that of the traditional RSSI algorithm and DV-Hop algorithm (Figure 8). When the anchor nodes' communication radius is 25 m, the average positioning error of the DV-Hop algorithm is lower than that of the traditional RSSI algorithm and is close to that of the modified RSSI algorithm. However, its average maximum positioning error is higher than that of the traditional RSSI algorithm and modified RSSI algorithm. Moreover, its positioning stability is not high. With an increase in the anchor nodes' communication radius, the average maximum positioning error of the revised RSSI positioning algorithm decreases steadily and remains lower than that of the traditional RSSI algorithm. The newly proposed algorithm achieves a stable improvement in positioning accuracy. As underwater

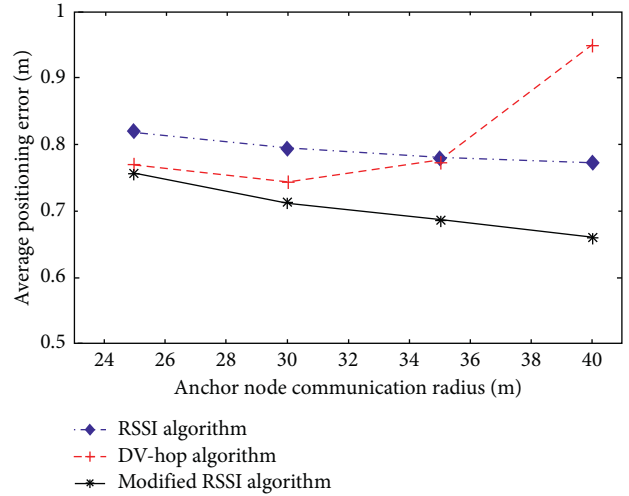


FIGURE 7: The average positioning error of nodes.

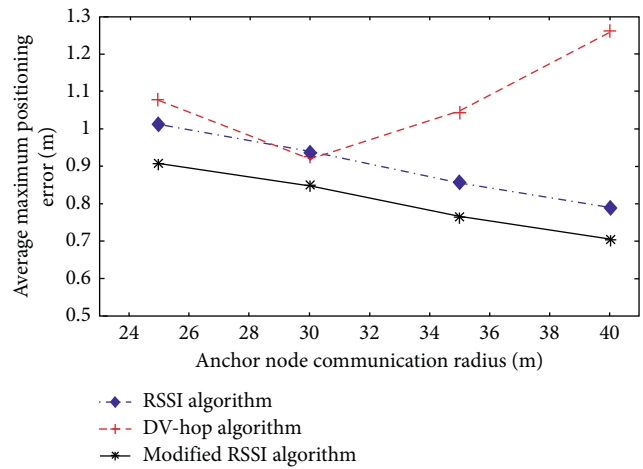


FIGURE 8: Average maximum positioning error.

network positioning is easily affected by water, a steady positioning algorithm is crucial.

4. Conclusions

A three-dimensional UWSN positioning algorithm based on modified RSSI values is proposed to address the problem of UWSN positioning algorithms being susceptible to water influence and prone to unstable positioning and large positioning errors. The unlocated node screens the received signal strength of the anchor node and then performs weighted correction to reduce the influence of the water environment and improve ranging accuracy. Combined with a three-dimensional underwater environment, the accuracy and stability of the positioning algorithm are improved, and the error of the underwater positioning algorithm is reduced. The algorithm is simulated with other related positioning algorithms through experiments. The results show that the proposed three-dimensional UWSN positioning algorithm based on modified RSSI values

remains stable, shows improved ranging accuracy, and reduces positioning error.

Data Availability

No data were used to support this study.

Conflicts of Interest

The authors declare that there are no conflicts of interest regarding the publication of this paper.

Acknowledgments

This work was supported by Natural Science Foundation of Guangxi (2019GXNSFAA245053), Guangxi Science and Technology Major Project (AA19254016/2019AA06002), Beihai Science and Technology Planning Project (202082023), and Beihai Science and Technology Planning Project (202082033).

References

- [1] Q. Meng, *Research on Distributed Positioning of Underwater Sensor Network Nodes*, Harbin Engineering University, Harbin, China, 2017.
- [2] T. Xu, J. Wang, W. Shi, J. Wang, and Z. Chen, "A localization algorithm using a mobile anchor node based on region determination in underwater wireless sensor networks," *Journal of Ocean University of China*, vol. 18, no. 2, pp. 394–402, 2019.
- [3] J. Yan, X. Li, X. Lu, and X. Guan, "Virtual-lattice based intrusion detection algorithm over actuator-assisted underwater wireless sensor networks," *Sensors (Basel, Switzerland)*, vol. 17, no. 5, p. 1168, 2017.
- [4] G. J. Han, C. Y. Zhang, T. Q. Liu et al., "A multi-anchor nodes collaborative localization algorithm for underwater acoustic sensor networks," *Wireless Communications and Mobile Computing*, vol. 16, no. 6, pp. 682–702, 2016.
- [5] S. Silmi, Z. Doukha, S. Moussaoui et al., "A self-localization range free protocol for wireless sensor networks," *Peer-to-Peer Networking and Applications*, pp. 1–11, 2011.
- [6] D. Li, J. Du, and L. Liu, "A data forwarding algorithm based on Markov thought in underwater wireless sensor networks," *International Journal of Distributed Sensor Networks*, vol. 13, no. 2, pp. 377–389, 2017.
- [7] H. D. source, Z. Xu, and P. Hu, "DV-Hop improved algorithm based on hop correction and LM optimization," *Computer Application Research*, vol. 1, pp. 206–219, 2019.
- [8] G. Wang, L. Wang, and H. Lu, "RSSI centroid localization algorithm based on mixed group intelligent algorithm optimization," *Computer Science*, vol. 46, no. 9, pp. 125–129, 2019.
- [9] H. Zhang and H. Huang, "Three-sided centroid positioning algorithm based on RSSI path loss factor dynamic correction," *Journal of Sensor Technology*, vol. 29, no. 11, pp. 1731–1734, 2016.
- [10] T. O. BuiP. Xu et al., "NBP-based localization algorithm for wireless sensor networks in NLOS environments," *Journal of Southeast University*, vol. 32, no. 4, pp. 395–401, 2016.
- [11] H. Xu, Y. Ding, R. Wang, W. Shen, and P. Li, "A novel Radio Frequency Identification three-dimensional indoor positioning system based on trilateral positioning algorithm," *Journal of Algorithms and Computational Technology*, vol. 10, no. 3, pp. 158–168, 2016.
- [12] K. Sabale and S. Mini, "Anchor node path planning for localization in wireless sensor networks," *Wireless Networks*, vol. 25, no. 1, pp. 49–61, 2019.
- [13] X. Ding and D. Shi, "Improving positioning algorithm based on RSSI," *Wireless Personal Communications*, vol. 110, no. 4, pp. 1947–1961, 2020.
- [14] L. Song, L. Zhao, and Y. Jin, "A DV-Hop positioning algorithm based on the glowworm swarmoptimisation of mixed chaotic strategy," *International Journal of Security and Networks*, vol. 14, no. 1, pp. 23–33, 2019.
- [15] X. Song, Y. Zhao, and L. Wang, "Gauss–Markov-based mobile anchor localization (GM-MAL) algorithm based on local linear embedding optimization in internet of sensor networks," *Cognitive Systems Research*, vol. 52, no. 0, pp. 138–143, 2018.
- [16] K. Hu, Z. Sun, H. Luo et al., "STVF: spatial-temporal variational filtering for localization in underwater acoustic sensor networks," *Sensors*, vol. 18, no. 7, pp. 2017–2104, 2018.
- [17] C. Liu, Z. Zhao, W. Qu et al., "A distributed node deployment algorithm for underwater wireless sensor networks based on virtual forces," *Journal of Systems Architecture*, vol. 97, no. 0, pp. 9–19, 2019.
- [18] Y. MAO, H. ZHAO, and D. YAN, "Weak node protection to maximize the lifetime of wireless," *Journal of Systems Engineering and Electronics*, vol. 29, no. 4, pp. 693–706, 2018.
- [19] R.-G. Tsai and P.-H. Tsai, "An obstacle-tolerant path planning algorithm for mobile-anchor-node-assisted localization," *Sensors (Basel, Switzerland)*, vol. 18, no. 3, p. E889, 2018.
- [20] Z. Lu, B. A. Bin, J. Wang et al., "A direct position determination method with combined TDOA and FDOA based on particle filter," *Chinese Journal of Aeronautics*, vol. 31, no. 1, pp. 161–168, 2018.
- [21] F. Ma, F. Liu, X. Zhang et al., "An ultrasonic positioning algorithm based on maximum correntropy criterion extended Kalman filter weighted centroid," *Signal, Image and Video Processing*, vol. 12, no. 6, pp. 1207–1215, 2018.
- [22] X. Wei, Y. Liu, S. Gao, X. Wang, and H. Yue, "An RNN-based delay-guaranteed monitoring framework in underwater wireless sensor networks," *IEEE Access*, vol. 7, Article ID 2899916, 2019.
- [23] M. Ali, A. Khan, H. Mahmood, and N. Bhatti, "Cooperative reliable and stability-aware routing for underwater wireless sensor networks," *International Journal of Distributed Sensor Networks*, vol. 15, no. 6, 2019.
- [24] S. Chang, Y. Li, Y. He, and H. Wang, "Target localization in underwater acoustic sensor networks using RSS measurements," *Applied Sciences*, vol. 8, p. 225, 2018.

Research Article

Real-Time Collection Method of Athletes' Abnormal Training Data Based on Machine Learning

Yue Wang 

Scientific Research Department, Gansu Police Vocational College, Lanzhou, Gansu 730046, China

Correspondence should be addressed to Yue Wang; wangyue2020@nwnu.edu.cn

Received 5 March 2021; Revised 23 May 2021; Accepted 25 May 2021; Published 3 June 2021

Academic Editor: Chi-Hua Chen

Copyright © 2021 Yue Wang. This is an open access article distributed under the Creative Commons Attribution License, which permits unrestricted use, distribution, and reproduction in any medium, provided the original work is properly cited.

Real-time collection of athletes' abnormal training data can improve the training effect of athletes. This paper studies the real-time collection method of athletes' abnormal training data based on machine learning. The main motivation of this paper is to collect the athletes' abnormal training data in time, which can help to evaluate and improve the training effect. Four sensor nodes are arranged in the upper and lower limbs of athletes to collect the angular velocity, acceleration, and magnetic field strength data of athletes in training state. The data are sent to the data transmission base station through wireless sensors, and the data transmission base station transmits the data to the data processing terminal. The data processing terminal calculates the difference between the sample values of each sensor to obtain the data dispersion of each sensor. The features of each dimension data in a time domain and frequency domain are obtained by using the dispersion degree to construct 32-dimensional feature vectors, and the extracted feature vectors are input into the hidden Markov model. The forward algorithm is used to obtain the probability of the final observation sequence, so as to realize the final collection of athletes' abnormal training data. The experimental results show that the accuracy and recall rate of the abnormal data collected by this method is higher than 98%, which requires less time.

1. Introduction

In competitive sports, the ultimate goal of sports training is to create excellent sports performance. The daily training of athletes is the most basic and controllable factor to improve competitive ability. Athletes' daily training is the basic way for coaches to understand athletes' sports conditions. Coaches need to analyze the athletes' sports situation [1], make clear the training situation of each athlete, evaluate the athletes' training status according to their own experience, and formulate corresponding training programs to further guide the training and improve the athletes' sports performance. With the accumulation of athletes' training data, it has become more and more difficult to manage and analyze these data by manual processing. Using the traditional data processing and database management function of a computer, it can solve the problem of athletes' training management, help coaches to manage athletes, convert sports performance, manage historical data, and improve the efficiency of data processing [2, 3]. The traditional data

analysis and processing methods only analyze the local or surface characteristics of the data and cannot get the description of the overall characteristics of the data which are hidden behind the data and the prediction of its development trend. The collection of athletes' abnormal training data focuses on the important information hidden behind the data. Data mining technology can extract valuable, unknown, hidden, and potentially useful knowledge from a large number of original data.

In the process of athletes' training and competition, coaches need to make corresponding training plans according to different athletes' individual conditions in order to improve athletes' sports levels. The traditional training method is that coaches make training plans according to their own training theory and experience, combined with the skill level of athletes. This training mode is highly subjective [4]. Coaches need to spend a lot of time analyzing athletes' posture, and it is difficult to objectively evaluate the training effect of athletes. The core of modern sports training is accuracy and efficiency. If the coach can

accurately control the abnormal data of training, it can greatly improve the effect of sports training. It is a new research direction to collect and analyze athletes' training data and determine athletes' abnormal training data, which is of great significance for improving the scientificity of coaches' training plans and improving athletes' training effects.

Artificial intelligence is a new comprehensive subject that is developed from computer science, cybernetics, information theory, and other disciplines; it is a science about understanding the internal mechanism of human intelligence and realizing it on the machine. Machine learning is the core content of artificial intelligence research [5–7]. It has been applied in all branches of artificial intelligence, such as natural language understanding, pattern recognition, computer vision, intelligent robot, and other fields [8]. As early as the 1950s, machine learning-related research began, mainly focusing on the connectionist learning of neural networks. From the 1950s to the 1970s, artificial intelligence research was in the "reasoning period," but with the development of research, it shows that machines with only logical reasoning ability cannot reach artificial intelligence [9]. In the 1980s, machine learning became an independent discipline and began to develop rapidly. Michalski et al. divided machine learning research into "learning in problem solving and planning" and "learning from instructions," and so on. Feigenbaum divided machine learning technology into four categories in his famous *Manual of Artificial Intelligence*, namely, "mechanical learning," "teaching-learning," "analogical learning," and "inductive learning". In the 21st century, machine learning has been applied in various fields. iFLYTEK's powerful real-time speech recognition technology and today's headline intelligent news recommendation system are all products of the rapid development of machine learning.

There are many literatures of the evaluation method for athletes based on benefit evaluation theory and regression analysis method which is proposed in reference [10]. The benefit evaluation theory and regression analysis method are used to evaluate the process of athletes' safety assessment, and the fusion analysis method is used to realize the monitoring and evaluation of physiological indicators. However, this method has poor adaptability to the safety assessment of athlete training and has a large time expenditure. In reference [11], an athlete training safety evaluation model based on big data fusion feature analysis is proposed. The model of integrated information statistics of athlete training safety is constructed and the method of fuzzy association rule scheduling is used to evaluate the safety of athlete training. However, the method carries out the evaluation of the safety of athlete training with a large amount of calculation and the anti-interference is not good. In reference [12], the evaluation method of athlete training safety based on rough set evaluation is proposed.

For the action recognition of human daily behavior, inertial sensors such as gyroscope and accelerometer are mainly used for algorithm classification and pattern recognition of daily behavior such as standing, walking, running, and lying [13]. Wang et al. identified daily activities

such as going up and down stairs, running, sitting down, and standing by acquiring data information of five inertial sensors worn in different positions of the body; Wu et al. used deep convolution neural network to classify and identify five kinds of human actions, including walking, sitting down, lying down, running, and standing, and achieved a recognition rate of 0.9126 on Actitraker open source database; Gu et al. used a variety of intelligent sensors in the room to identify the complex daily human behavior. The improved algorithm has a high recognition rate; Atalla used wearable sensors to identify the daily behaviors with different complexity and explored the accuracy of different sensor installation positions under different complexity actions through many experiments. Some researchers tried to use sensors for sports data monitoring and technical evaluation to achieve the effect of auxiliary training. The sensor of human body was used to detect the behavior characteristics of athletes, such as body posture, movement range, and speed, and based on the analysis and mining of athletes' behavior data, the technical loopholes were found out to help athletes to improve their technical level; Qaisar et al. used multiple acceleration sensors and gyroscopes to identify a variety of different bowling movements, analyze the technical level of action quality by qualitative and quantitative analysis, and make technical evaluation and feedback of bowling posture in bowling training teaching; King et al. designed golf clubs with embedded acceleration sensors. Through receiving data and calculating important parameters related to swing, such as golf club top position, speed, and direction, in the golf training of athletes or amateurs, the data can be analyzed to feed back the quality of users' swing, so as to achieve the effect of intelligent training.

The basic idea of inertial sensor recognition is that athletes wear simple and light data collection sensors and send the collected data to the processing terminal [14] in real time to identify the athletes' posture according to various posture data. This method can make up for the lack of image collection and recognition, has low requirements for the use environment and high recognition efficiency, and has become a hot research method of motion attitude recognition. Abnormal data's real-time collection is an important branch of pattern recognition, which has been widely concerned and developed in recent years. With the rapid development of microelectronics technology, the use of inertial sensors to identify human posture has become a research hotspot. Many researchers apply wearable devices to human auto disturbance recognition. Sensors are used to collect human acceleration, angular velocity, body temperature, heart rate, and much other information. Using the collected information to extract time domain space and frequency space characteristics of athletes' training actions is convenient to analyze athletes' abnormal training data [15]. The feature extraction can analyze the athlete's unit action and transfer the relevant attribute features as sample data to the machine classifier to realize the abnormal data division.

The contributions of this paper are summarized as follows:

This paper studies the real-time collection method of athletes' abnormal training data based on machine learning.

The sensor is used to collect athlete training data, and the features used for real-time collection of athletes' abnormal training data are extracted from time domain and frequency domain, respectively. The extracted features are used to accurately collect athletes' abnormal training data using the hidden Markov model in machine learning. The experimental results verify the effectiveness of this method in real-time collection of athletes' abnormal training data.

This paper is organized as follows. Section 2 presents the materials and methods. In Section 3, experimental results are presented and analyzed. Finally, Section 4 sums up some conclusions and gives some suggestions as the future research topics.

2. Materials and Methods

2.1. Collection of Sensor Signal. It is the basic condition to collect the abnormal data of athletes' training accurately to collect the data of human movement posture. In this system, there are four parts, which are sensors, transceiver, processor, and the power supply. The inertial sensor is used to collect human motion posture data. Through the magnetic sensor, angular velocity sensor, and acceleration sensor fixed on the athlete's body, the data related to human movement is collected [16], and the collected data are transmitted to the terminal processing device for posture recognition through a wireless sensor network. The power supply can provide power to the system. Data quality is the key to affect the accuracy of abnormal data collection in athletes' training.

The hardware structure of collecting athletes' abnormal training data is shown in Figure 1.

The hardware structure mainly contains data collection and data transmission, including four data collection nodes and one data transmission base station. The data collection node is composed of three-axis gyroscope MPU3050M, three-axis accelerometer, and magnetometer LSM303DLH, which collect the angular velocity and acceleration data of human body, respectively. The core component of the data sending base station is the wireless transceiver nRF24L01. The receiving node collects data and sends it to the data terminal through the wireless network. The core processing function of data collection module is completed by 32-bit ARM microcontroller STM32F103. The energy supply of the data collection module is provided by a 3.7V lithium-ion battery.

The data collection signal transmission includes two parts: one is that the sensor node sends the collected human posture data to the data transmission base station; the other is that the data transmission base station sends the data to the processing terminal. The signal transmission between the sensor node and data transmission base station is based on a wireless sensor network. The problem to be overcome is to reduce the data collision rate as far as possible [17], reduce the data loss, and improve the accuracy of data collection. The signal transmission between the data transmission base station and the processing terminal is based on the star topology network, using the time-division multiplexing protocol [18]. It is necessary to calibrate the clock deviation between different nodes to keep the time uniform.

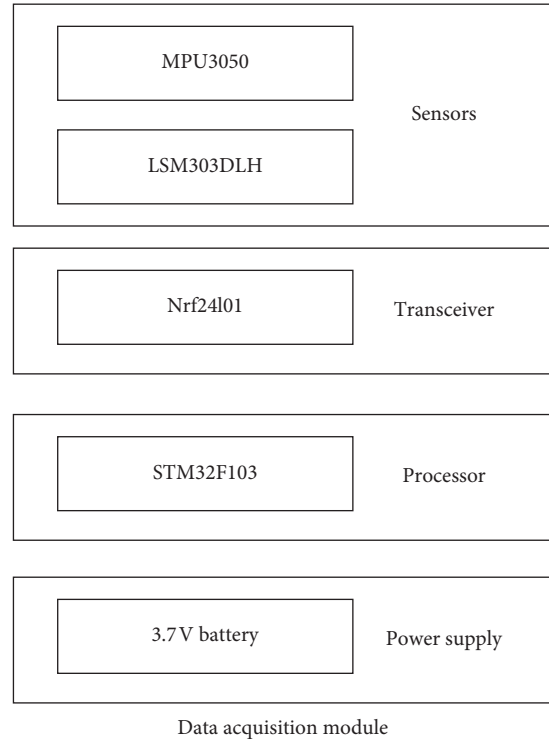


FIGURE 1: Diagram of data collection hardware structure.

In order to accurately collect the abnormal data of athletes' training, it is necessary to accurately grasp the movement posture data of athletes' upper and lower limbs. The sensor layout and data collection topology are shown in Figure 2.

Four sensor nodes are used to collect the angular velocity, acceleration, and magnetic field strength data of the upper and lower limbs of the athletes, and the data are sent to the data transmission base station through wireless sensors. The data transmission base station transmits the data to the data processing terminal.

2.2. Feature Extraction of Athletes' Training Data. After collecting the data of human motion posture, the training data of athletes are divided firstly, and the features of training data are extracted by using the divided data. The extracted features of training data of athletes are sent to the machine learning classifier to realize the collection of abnormal training data of athletes.

2.2.1. Division of Athletes' Training Data. The degree of dispersion is the difference between the values of the observed variables, and the difference between the sample values of the sensor signal is defined as the degree of dispersion. Taking the angular velocity as an example, ω_n^x represents the x -axis angular velocity data at the time n , ω_{n-1}^x represents the x -axis angular velocity data at the time $n-1$, and d_n^x represents the angular velocity difference between the x -axis angular velocity of the sensor at the time n and the previous time. The formula of dispersion d_n^x can be obtained as follows:

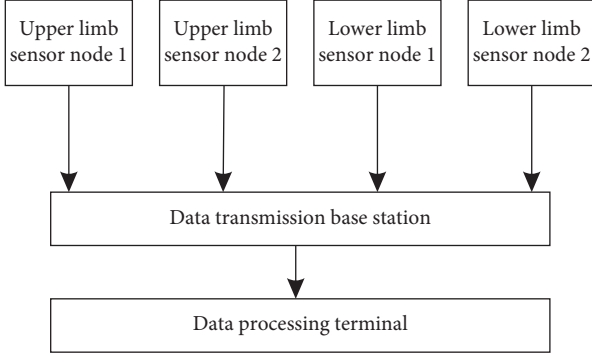


FIGURE 2: Topological structure diagram of athletes' training data collection.

$$d_n^x = |\omega_n^x - \omega_{n-1}^x|. \quad (1)$$

The movement data include angular velocity data and acceleration data [19]. In order to realize the accurate division of athletes' training data, it is necessary to comprehensively consider the characteristics of each sensor data [20].

D_n^x is used to represent the dispersion of acceleration sensor data at the time n , d_n^x is used to represent the dispersion of angular velocity sensor data at the time n , and $d_n^{a_x}$, $d_n^{a_y}$, $d_n^{a_z}$, $d_n^{g_x}$, $d_n^{g_y}$, and $d_n^{g_z}$ are used to represent the dispersion of acceleration and angular velocity of each axis, respectively. Then, D_n^a and D_n^g are obtained as follows:

$$\begin{aligned} D_n^a &= d_n^{a_x} + d_n^{a_y} + d_n^{a_z}, \\ D_n^g &= d_n^{g_x} + d_n^{g_y} + d_n^{g_z}. \end{aligned} \quad (2)$$

In the static state, the dispersion of acceleration and angular velocity are kept below the threshold λ_a and λ_g , respectively; in the moving state, the sensor data change rapidly with the athletes' actions [21], and the dispersion can reflect the difference degree of the sensor data, so according to the characteristics of the dispersion, the athletes' moving state can be divided.

γ_n is used to represent the state of the athlete's limbs at the n -th moment; when γ_n is 0, it means the static state, and when γ_n is 1, it means the moving state. The formula is as follows:

$$\gamma_n = \begin{cases} 0, & D_n^a < \lambda_a \text{ and } D_n^g < \lambda_g, \\ 1, & D_n^a \geq \lambda_a \text{ or } D_n^g \geq \lambda_g. \end{cases} \quad (3)$$

The data dispersion of each sensor is calculated, and the athletes' movement states can be divided by the threshold.

2.2.2. Extraction of Training Data. After data division, the unit action data composed of acceleration and angular velocity are obtained. Acceleration vector sum and angular velocity vector sum are represented by a_n and g_n , respectively. The formula is as follows:

$$\begin{aligned} a_n &= \sqrt{(a_n^x)^2 + (a_n^y)^2 + (a_n^z)^2}, \\ g_n &= \sqrt{(g_n^x)^2 + (g_n^y)^2 + (g_n^z)^2}. \end{aligned} \quad (4)$$

The three-axis acceleration, three-axis angular velocity, combined acceleration, and combined angular velocity form an 8-dimensional vector, and N is used to represent the number of sampling points in each unit action, so there are N sampling data in each dimension of the vector. If each unit action is taken as a sample, then each sample is an $N \times 8$ -dimensional matrix. The data features of each dimension of each sample are calculated [22], and the extracted signal features include time domain features and frequency domain features. Time domain features include mean value and variance. μ_a and δ^2 are used to represent the mean value and variance of some component of the increment speed of unit action, respectively, and the formula can be obtained as follows:

$$\mu_a = E(a) = \frac{1}{N} \sum_{i=1}^N a_i, \quad (5)$$

$$\delta^2 = \frac{1}{N} \sum_{i=1}^N (a_i - \mu_a)^2,$$

where a is a component of the acceleration.

The frequency domain features include the peak value of discrete Fourier transform and its corresponding frequency [23]. The discrete Fourier transform method is used to transform the signal from time domain to frequency domain. The Fourier transform result of the n -th sampling point is represented by $S_{\text{DFT}}(n)$, and the imaginary number unit is represented by j . The formula is as follows:

$$S_{\text{DFT}}(n) = \sum_{i=0}^{N-1} a_i e^{-j(2\pi/N)in}. \quad (6)$$

According to the results of Fourier transform, the peak value $S_{\text{DFT}}(K)$ is obtained. If the sampling point corresponding to the peak value of Fourier transform is K , the corresponding frequency f formula of Fourier transform is as follows:

$$f = K \times \frac{f_s}{N}, \quad (7)$$

where f_s is the sampling frequency of the sensor.

The features of each dimension data in time domain and frequency domain are obtained by feature calculation, and a 32-dimensional feature vector is constructed.

2.3. Collection of Athletes' Abnormal Training Data Based on HMM. Hidden Markov model is an efficient model in machine learning. The extracted 32-dimensional feature vectors are input into the hidden Markov model to realize the final collection of athletes' abnormal training data.

The hidden Markov model is a probability model about time series, which describes the process of generating unobservable state random sequence randomly from a hidden Markov chain and then generating an observation random sequence from each state [24]. The hidden Markov model is determined by the initial probability distribution π , the state probability distribution A , and the observation probability distribution B .

Let $Q = \{q_1, q_2, \dots, q_N\}$ be the set of all possible states and $V = \{v_1, v_2, \dots, v_M\}$ be the set of all possible observations, where N is the number of possible states and M is the number of possible observations; $I = \{i_1, i_2, \dots, i_T\}$ is the state sequence of length T and $O = \{o_1, o_2, \dots, o_T\}$ is the corresponding observation sequence.

The formula of state transition probability matrix A is as follows:

$$A = [a_{ij}]_{N \times N} \quad (8)$$

where $a_{ij} = P(i_{t+1} = q_j | i_t = q_i)$, $i = 1, 2, \dots, N$ and $j = 1, 2, \dots, N$, and a_{ij} is the probability of transition from state q_i at time t to state q_j at time $t + 1$.

The formula of the observed probability matrix B can be obtained as follows:

$$B = [b_j(k)]_{N \times M} \quad (9)$$

where $b_j(k) = P(o_t = v_k | i_t = q_j)$, $k = 1, 2, \dots, M$, $j = 1, 2, \dots, N$, and $b_j(k)$ is the probability of generating observation v_k when it is in state q_j at time t . π is the initial state probability vector; $\pi_i = P(i_1 = q_i)$ is the probability that $t = 1$ is in state q_i .

Hidden Markov model λ can be represented by the following symbols, namely,

$$\lambda = (A, B, \pi). \quad (10)$$

In formula (10), A , B , and π are called three elements of the hidden Markov model.

For a given hidden Markov model $\lambda = (A, B, \pi)$ and observation sequence $O = \{o_1, o_2, \dots, o_T\}$, the probability $P(O | \lambda)$ of the observation sequence in the model is calculated, and the final probability result is obtained by forward algorithm.

Firstly, forward probability is defined. In the model $\lambda = (A, B, \pi)$, the probability that part of the observation sequence at time t is o_1, o_2, \dots, o_t and the state is q_i is defined as the forward probability, which is denoted as

$$\alpha_t(i) = P(o_1, o_2, \dots, o_t, i_t = q_i | \lambda). \quad (11)$$

The process of obtaining the observation sequence probability $P(O | \lambda)$ is as follows:

(1) Initial value

$$\alpha_t(i) = \pi b_i(o_1). \quad (12)$$

(2) For $t = 1, 2, \dots, T - 1$, the formula is as follows:

$$\alpha_{t+1}(i) = \left[\sum_{j=1}^N \alpha_t(j) \alpha_{ji} \right] b_i(o_{t+1}). \quad (13)$$

(3) End

$$P(O | \lambda) = \sum_{i=1}^N \alpha_T(i). \quad (14)$$

The forward algorithm is to calculate the probability $P(O | \lambda)$ of observation sequence through the known hidden Markov model $\lambda = (A, B, \pi)$ and observation sequence $O = \{o_1, o_2, \dots, o_T\}$. $\alpha_t(j)$ is the forward probability when the observation is o_1, o_2, \dots, o_t and the state is q_j at the time t , and $\alpha_t(j) \alpha_{ji}$ is the joint probability when the observation is o_1, o_2, \dots, o_t and the state is q_j at the time t and q_i at the time $t + 1$. The sum of all possible N states q_j at the time t is the joint probability of o_1, o_2, \dots, o_t at the time t and q_i at the time $t + 1$. The product of this result and the observation probability $b_i(o_{t+1})$ is just the forward probability $\alpha_{t+1}(i)$ when the observation is o_1, o_2, \dots, o_t and the state is q_i at the time $t + 1$. For $t = T$, there are

$$\alpha_T(i) = P(o_1, o_2, \dots, o_T, i_T = q_i | \lambda). \quad (15)$$

So, the probability of the final observation sequence is $P(O | \lambda) = \sum_{i=1}^N \alpha_T(i)$.

The efficiency of the forward algorithm is to recursively deduce the forward probability to the global by using the path structure of the model to get the final probability $P(O | \lambda)$. Each recursion directly refers to the calculation result of the previous time [22], which avoids repeated calculation and reduces the time complexity of the algorithm from $O(TN^T)$ to $O(N^2T)$.

3. Results

In order to verify the effectiveness of the real-time collection method for abnormal data of athletes' training, 8 basketball players of sports major in a university are selected as the experimental objects, and 9 training movements including walking, running, jumping when there is no ball, standing dribbling, walking dribbling, running dribbling, shooting, passing, and catching when holding the ball are made. The sensors are placed on the upper and lower limbs of the athletes. A total of 12000 samples are collected, including 6000 upper limb movements and 6000 lower limb movements of standing dribble, walking dribble, shooting, passing, catching, and running dribble. During the sample collection process, the subjects completed the training according to the regulations.

The specific contents of the samples are shown in Table 1.

Considering that the real-time collection of athletes' abnormal training data is a binary classification problem, the collection accuracy, collection recall rate, $F1$ value, mean

TABLE 1: Athlete training actions and sample size.

Sports parts	Action	Number of samples (N)
Upper limb	Standing dribble	1000
	Walking dribble	1000
	Running dribble	1000
	Shot	1000
	Pass	1000
	Catch the ball	1000
Lower limbs	Walk	1000
	Run	1000
	Jump	1000
	Shot	1000
	Running dribble	1000
	Walking dribble	1000
Total		12000

square error, and AUC (area under the curve) value are used to measure the real-time collection performance of athletes' abnormal training data. The accuracy of collection indicates the proportion between the correct collection of abnormal data instances and all instances assigned to the class by the classifier. Recall rate represents the proportion of instances in a given category correctly classified by the machine learning classifier. The $F1$ value is a harmonic average of precision and recall. AUC is the probability that the positive instance selected randomly by the classifier is higher than the negative instance selected randomly (assuming that "positive" is higher than "negative"). When AUC is close to 1, it means that the collection accuracy is higher. When AUC is close to 0.5, it means that machine learning is a random classification condition, and the collection accuracy is poor. BP neural network and support vector machine are selected as comparison methods, and the above two methods are compared with the method in this paper.

Three methods are used to collect the peak signal-to-noise ratio of athletes' training data sample; the comparison results are shown in Table 2. The BP neural network method used in the experiment is proposed in reference [25]. The support vector machine method used in the experiment is proposed in reference [26].

The experimental results in Table 2 show that the peak signal-to-noise ratio of the sample signals collected by the proposed method is higher than 30 dB; the peak signal-to-noise ratio of the sample signals collected by BP neural network method is less than 30 dB; the peak signal-to-noise ratio of the sample signals collected by support vector machine method is less than 29 dB. The experimental results show that the quality of the action signal collected by the proposed method is significantly higher than that of the other two methods. The high quality of the signal collected by this method helps to accurately extract the training characteristics of athletes and provides a theoretical basis for the accurate collection of abnormal data of athletes' training.

The comparison results of the accuracy of collecting athletes' abnormal training data by three methods are shown in Figure 3.

The experimental results in Figure 3 show that the accuracy of the proposed method is significantly higher than that of the other two methods. The accuracy of the abnormal

data collected by the proposed method is higher than 98.5%; the accuracy of the abnormal data collected by BP neural network method and support vector machine method is lower than 96%. The performance of support vector machine method is the worst. According to Figure 3, the accuracy of abnormal data collection in athlete training of the method proposed in this paper is 4.3% higher than the BP neural network method on average and is 6.5% higher than the support vector machine method. So, we can see that the proposed method has high accuracy of abnormal data collection in athlete training and can be applied to the abnormal data collection in actual athlete training.

The comparison results of recall rate of athletes' abnormal training data collected by three methods are shown in Figure 4.

As can be seen from the experimental results in Figure 4, the recall rate of abnormal data collected by the proposed method is significantly higher than that of the other two methods. The recall rate of abnormal training data collected by the proposed method is higher than 98%; the recall rate of abnormal training data collected by BP neural network method and support vector machine method is lower than 97%. The performance of support vector machine method is the worst. According to Figure 4, the recall rate of abnormal data collection in athlete training of the method proposed in this paper is 4.7% higher than the BP neural network method on average and is 6.1% higher than the support vector machine method. So, we can see that the proposed method has high recall rate of abnormal data collection and superior collection performance.

The comparison results of $F1$ value of athletes' abnormal training data collected by three methods are shown in Table 3.

$F1$ value is an important index to measure the accuracy and recall rate of abnormal data collection. The closer the $F1$ value of abnormal data collection is to 1, the better the collection performance is. The experimental results in Table 3 show that the $F1$ value of athletes' abnormal training data collected by the proposed method is significantly higher than that collected by the other two methods. The $F1$ value of abnormal data collected by the proposed method is higher than 0.93, very close to 1; the $F1$ value of abnormal data collected by BP neural network method and support vector machine method is lower than 0.86. The results show that the proposed has high accuracy, high recall, and high reliability, which can provide a theoretical basis for coaches to make training plans.

The comparison results of mean square error (MSE) of athletes' abnormal training data collected by three methods are shown in Figure 5.

Experimental results in Figure 5 show that the mean square error of the abnormal data collected by the proposed method is significantly lower than that of the other two methods. The results show that the mean square error of abnormal data collected by the proposed method is lower than 0.04; the mean square error of abnormal data collected by BP neural network method and support vector machine method is higher than 0.05. The results show that the proposed method has low mean square error of abnormal data collection and high reliability.

TABLE 2: Comparison of peak signal-to-noise ratio.

Action	Method of this article (dB)	BP neural network method (dB)	Support vector machine method (dB)
Standing dribble	35.61	27.52	25.61
Walking dribble	34.25	26.48	26.34
Running dribble	36.52	25.61	27.85
Shot	34.15	26.85	24.05
Pass	35.62	27.52	25.64
Catch the ball	34.85	28.61	23.61
Walk	36.25	25.64	27.85
Run	33.45	26.34	26.58
Jump	31.52	29.52	28.64
Shot	34.52	24.81	26.34
Running dribble	33.65	23.52	21.52
Walking dribble	34.85	26.48	23.96

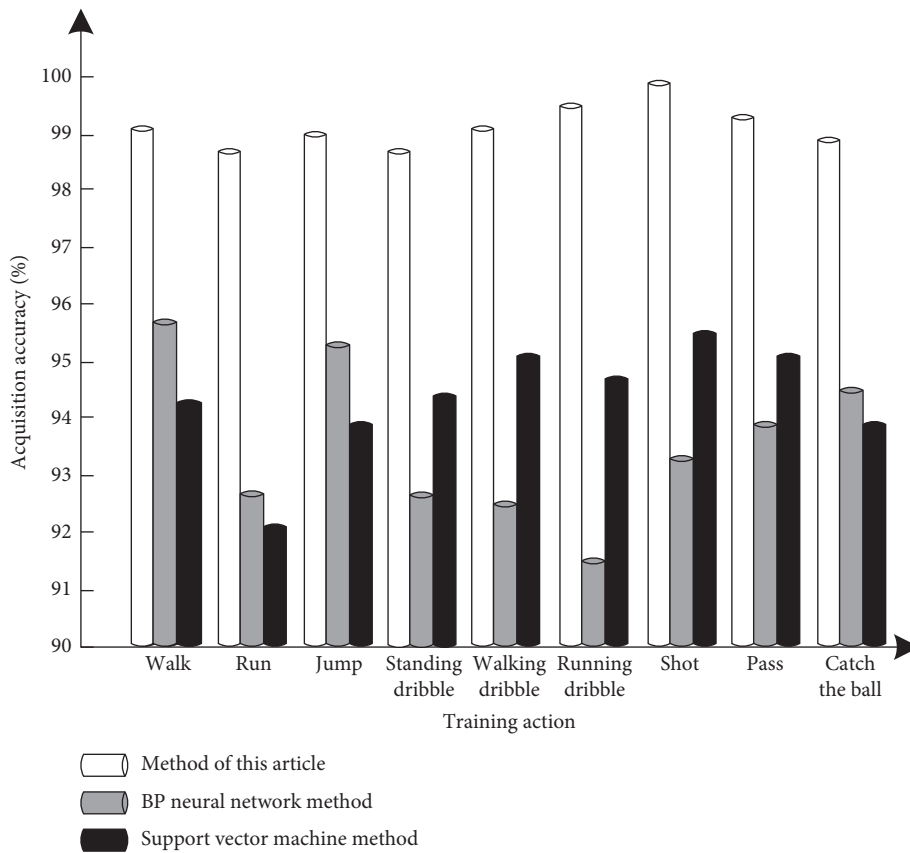


FIGURE 3: Comparison of collection accuracy.

AUC comparison results of athletes' abnormal training data collected by three methods are shown in Figure 6.

As can be seen from the experimental results in Figure 6, the AUC value of abnormal data collected by the proposed method is very close to 1, while the AUC value of abnormal data collected by BP neural network method and support vector machine method is very close to 0.5. The results show that the accuracy of the proposed method to collect abnormal data of athletes training is high, and the method of BP neural network and support vector machine to collect abnormal data of athletes training is mostly random

classification. The method of this paper to collect abnormal data of athletes training has high accuracy and high reliability.

The abovementioned experimental results effectively verify that the method in this paper has high accuracy in collecting abnormal data of athletes' training and has high performance in collecting abnormal data of athletes' training, which can be applied to the practical application of athletes' training. In order to further verify the real-time ability of collecting abnormal training data of athletes by this method, the proposed method is used to collect athletes'

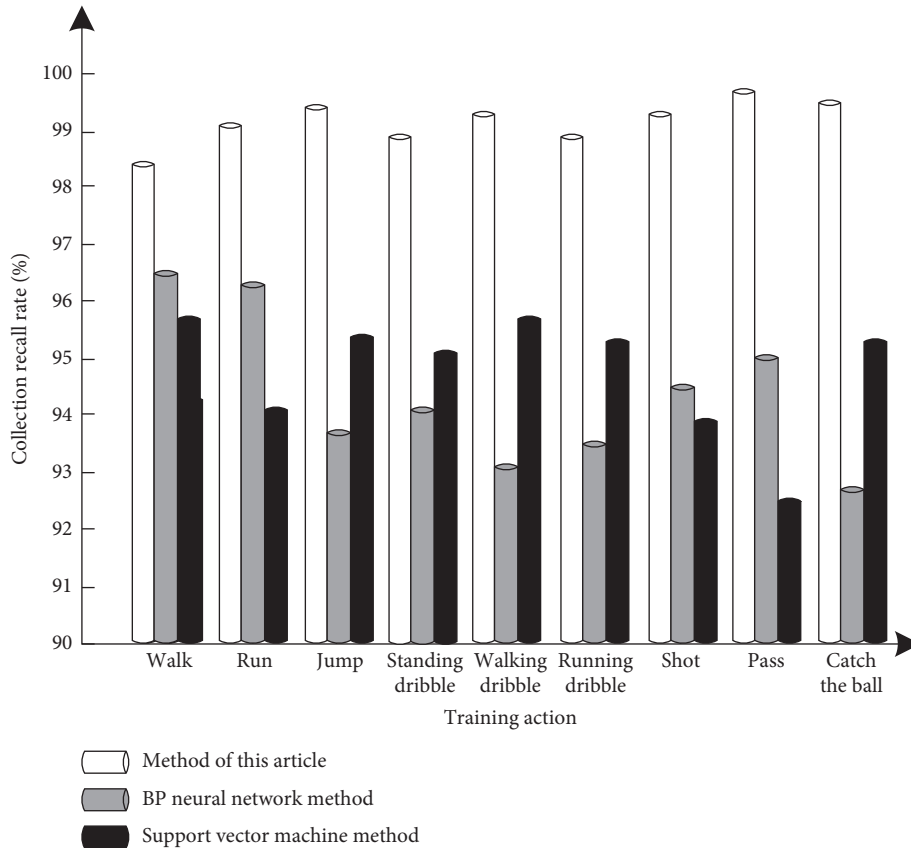


FIGURE 4: Comparison of collection recall rates.

TABLE 3: F1 value comparison.

Training action	Method of this article	BP neural network method	Support vector machine method
Walk	0.978	0.758	0.658
Run	0.986	0.851	0.711
Jump	0.984	0.762	0.658
Standing dribble	0.986	0.714	0.725
Walking dribble	0.934	0.824	0.714
Running dribble	0.946	0.762	0.725
Shot	0.945	0.824	0.685
Pass	0.952	0.841	0.765
Catch the ball	0.967	0.765	0.715

abnormal training data. The comparison results of collection time under different data samples are shown in Table 4.

Table 4 shows that the time cost of using the proposed method to collect athletes' abnormal training data is the lowest under different sample numbers. The comparison results show that the proposed method can quickly collect athletes' abnormal training data in a short time. This method not only has high accuracy but also needs less time to collect abnormal data. It can quickly obtain accurate abnormal data and has high practicability.

In this paper, we propose a real-time collection method of athletes' abnormal training data based on machine learning. According to [27], this paper proposed a HMM-based asynchronous H^∞ filtering for fuzzy singular Markovian switching systems with retarded time-varying delays. The computational complexity of the method proposed by our paper mainly depends on the characteristics of the training network, while the computational complexity of the method proposed in [27] is mainly dependent on the HMM method. So, we can draw that the performance of the method proposed by us is much better.

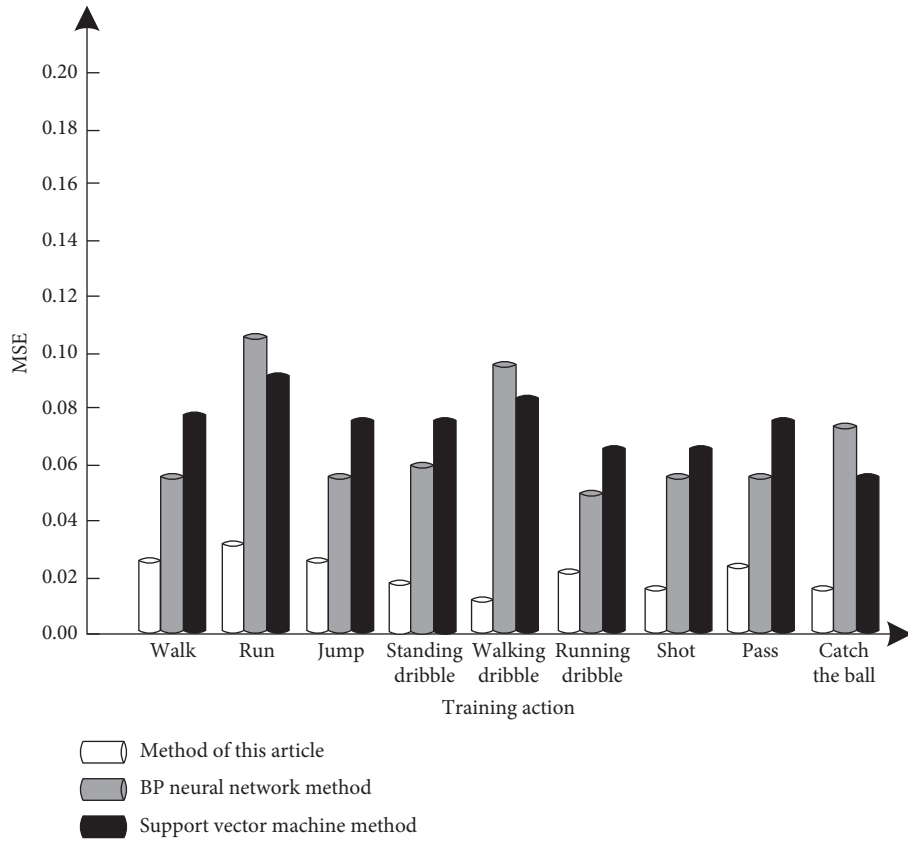


FIGURE 5: Comparison of mean square error.

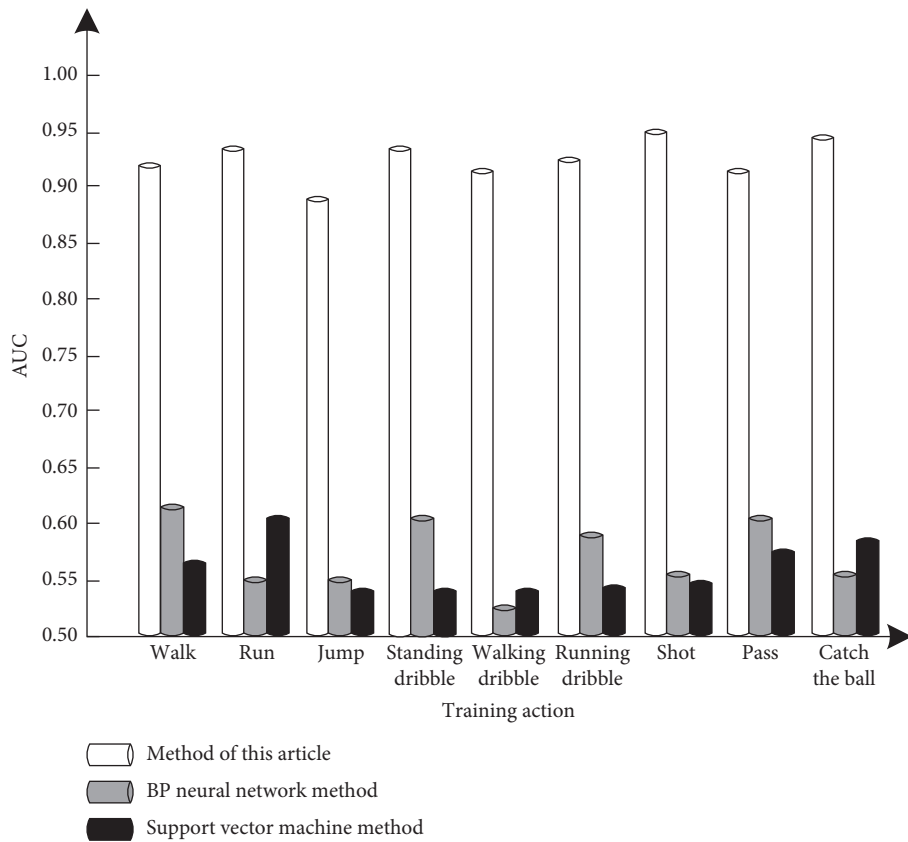


FIGURE 6: AUC comparison.

TABLE 4: Comparison of time cost of different methods.

Number of samples (N)	Method of this paper (ms)	BP neural network method (ms)	Support vector machine method (ms)
1000	32	105	135
2000	56	124	182
3000	72	135	234
4000	82	164	294
5000	91	185	335
6000	105	205	394
7000	111	234	435
8000	135	268	497
9000	159	342	581
10000	175	394	645
11000	235	428	785
12000	268	594	856

4. Conclusions

With the development of wireless sensor network and microelectronic equipment technology, athletes' abnormal training data collection has been widely concerned in various fields. The sensor equipment is used to collect the athletes' upper and lower limb movement state signals to extract the athletes' training characteristics, and the hidden Markov model is used in machine learning to complete the effective collection of athletes' abnormal training data. Selecting basketball players as the experimental object, the abnormal data collection of athletes' training is realized in the field of basketball. The experimental results effectively verify that the method is highly effective in collecting abnormal data of athletes' training. The research results provide a new collection scheme for abnormal data of sports training. The collected dataset will be made publicly available by the other researchers. For this new system, when we use it, it has a big structure size, which is not very easy to carry, so in order to facilitate large-scale use, its size must be reduced. In addition, we can speed up data processing.

Data Availability

The data used to support the findings of this study are available from the corresponding author upon request.

Conflicts of Interest

The author declares no conflicts of interest.

References

- [1] Q. L. Liu and X. P. Wang, "Real time monitoring simulation of abnormal state of large data in smart grid," *Computer Simulation*, vol. 36, no. 3, pp. 364–367, 2019.
- [2] H. Yao, P. Gao, P. Zhang, J. Wang, C. Jiang, and L. Lu, "Hybrid intrusion detection system for edge-based IIoT relying on machine-learning-aided detection," *IEEE Network*, vol. 33, no. 5, pp. 75–81, 2019.
- [3] Z. Wu, D. Rincon, and P. D. Christofides, "Real-time adaptive machine-learning-based predictive control of nonlinear processes," *Industrial & Engineering Chemistry Research*, vol. 59, no. 6, pp. 2275–2290, 2020.
- [4] H. A. Yavasoglu, Y. E. Tetik, and K. Gokce, "Implementation of machine learning based real time range estimation method without destination knowledge for bevs," *Energy*, vol. 172, pp. 1179–1186, 2019.
- [5] M. Yang, B. Ai, R. He, C. Huang, and J. Li, "Machine-learning-based fast angle-of-arrival recognition for vehicular communications," *IEEE Transactions on Vehicular Technology*, vol. 70, no. 2, pp. 1592–1605, 2021.
- [6] Y. Xu, D. Li, Z. Wang, Q. Guo, and W. Xiang, "A deep learning method based on convolutional neural network for automatic modulation classification of wireless signals," *Wireless Networks*, vol. 25, no. 7, pp. 3735–3746, 2017.
- [7] D. Liu, G. Zhu, Q. Zeng, J. Zhang, and K. Huang, "Wireless data collection for edge learning: data-importance aware retransmission," in *Proceedings of the 2019 IEEE 20th International Workshop on Signal Processing Advances in Wireless Communications (SPAWC)*, pp. 1–6, Cannes, France, July 2019.
- [8] X.-Q. Wang and J. Yin, "Application of machine learning in safety evaluation of athletes training based on physiological index monitoring," *Safety Science*, vol. 120, pp. 833–837, 2019.
- [9] G. Verrall, A. Hains, B. Ayres, and R. Hillock, "Influence of type and duration of training on the presence of an abnormal ECG in high-performance athletes," *Heart Asia*, vol. 11, no. 1, Article ID e011120, 2019.
- [10] M. Fakhar, M. R. Mahyarinia, and J. Zafarani, "On non-smooth robust multiobjective optimization under generalized convexity with applications to portfolio optimization," *European Journal of Operational Research*, vol. 265, no. 1, pp. 39–48, 2018.
- [11] G. Farnadi, S. H. Bach, M.-F. Moens, L. Getoor, and M. De Cock, "Soft quantification in statistical relational learning," *Machine Learning*, vol. 106, no. 12, pp. 1971–1991, 2017.
- [12] A. Rames, M. Rodriguez, and L. Getoor, "Multi-relational influence models for online professional networks," in *Proceedings of the 2017 International Conference on Web Intelligence, ACM*, pp. 291–298, Leipzig, Germany, August 2017.
- [13] J. F. L. de Oliveira, E. G. Silva, and P. S. G. de Mattos Neto, "A hybrid system based on dynamic selection for time series forecasting," *IEEE Transactions on Neural Networks and Learning Systems*, vol. 99, pp. 1–13, 2021.
- [14] C. Rea, K. J. Montes, K. G. Erickson, R. S. Granetz, and R. A. Tinguely, "A real-time machine learning-based disruption predictor in DIII-D," *Nuclear Fusion*, vol. 59, no. 9, Article ID 096016, 2019.
- [15] G. Daniel, F. Ceraudo, O. Limousin, D. Maier, and A. Meuris, "Automatic and real-time identification of radionuclides in gamma-ray spectra: a new method based on convolutional neural network trained with synthetic data set," *IEEE*

- Transactions on Nuclear Science*, vol. 67, no. 4, pp. 644–653, 2020.
- [16] M. Al-Saud, A. M. Eltamaly, M. A. Mohamed, and A. Kavousi-Fard, “An intelligent data-driven model to secure intravehicle communications based on machine learning,” *IEEE Transactions on Industrial Electronics*, vol. 67, no. 6, pp. 5112–5119, 2020.
- [17] C.-H. Chen, F. Song, F.-J. Hwang, and L. Wu, “A probability density function generator based on neural networks,” *Physica A: Statistical Mechanics and Its Applications*, vol. 541, Article ID 123344, 2020.
- [18] S. Sadiqbatcha, J. Zhang, H. Zhao, H. Amrouch, and X. D. Tan, “Post-silicon heat-source identification and machine-learning-based thermal modeling using infrared thermal imaging,” *IEEE Transactions on Computer-Aided Design of Integrated Circuits and Systems*, vol. 40, no. 4, pp. 694–707, 2020.
- [19] D. Xiao, F. Fang, J. Zheng, C. C. Pain, and I. M. Navon, “Machine learning-based rapid response tools for regional air pollution modelling,” *Atmospheric Environment*, vol. 199, no. 15, pp. 463–473, 2019.
- [20] Y. Yang, J. Lu, C. Yang, and Y. Zhang, “Exploring fragment-based target-specific ranking protocol with machine learning on cathepsin S,” *Journal of Computer-Aided Molecular Design*, vol. 33, no. 12, pp. 1095–1105, 2019.
- [21] G. Burlak, “Evaluation of the spectrum of a quantum system using machine learning based on incomplete information about the wavefunctions,” *Applied Physics Letters*, vol. 116, no. 2, Article ID 024101, 2020.
- [22] W. Yuan, G. Han, and D. Guan, “Learning from mislabeled training data through ambiguous learning for in-home health monitoring,” *IEEE Journal on Selected Areas in Communications*, vol. 39, no. 2, pp. 549–569, 2020.
- [23] B. B. Thomas, Y. Mou, L. Keeler, C. Magnan, and S. Agersborg, “A highly sensitive and specific gene fusion algorithm based on multiple fusion callers and an ensemble machine learning approach,” *Blood*, vol. 136, no. 1, pp. 12–13, 2020.
- [24] M. J. Bianco and P. Gerstoft, “Unsupervised machine learning for acoustic tomography and event detection,” *The Journal of the Acoustical Society of America*, vol. 146, no. 4, Article ID 2845, 2019.
- [25] T. Li, J. Sun, and L. Wang, “An intelligent optimization method of motion management system based on BP neural network,” *Neural Computing and Applications*, vol. 33, no. 4, pp. 707–722, 2020.
- [26] X. Liang, T. Qi, T. Qi, Z. Jin, and W. Qian, “Hybrid support vector machine optimization model for inversion of tunnel transient electromagnetic method,” *Mathematical Biosciences and Engineering*, vol. 17, no. 4, pp. 3998–4017, 2020.
- [27] G. Zhuang, W. Sun, S.-F. Su, and J. Xia, “Asynchronous feedback control for delayed fuzzy degenerate jump systems under observer-based event-driven characteristic,” *IEEE Transactions on Fuzzy Systems*, vol. 1, no. 99, pp. 1–15, 2020.

Research Article

Research on Artificial Intelligence Interaction in Computer-Aided Arts and Crafts

Juqing Deng  and Xiaofen Chen

School of Communication & Art Design, Wuxi Institute of Arts and Technology, Yixing 214206, China

Correspondence should be addressed to Juqing Deng; dengjuqing@wxgyxy.edu.cn

Received 29 January 2021; Revised 19 March 2021; Accepted 17 May 2021; Published 27 May 2021

Academic Editor: Hsu-Yang Kung

Copyright © 2021 Juqing Deng and Xiaofen Chen. This is an open access article distributed under the Creative Commons Attribution License, which permits unrestricted use, distribution, and reproduction in any medium, provided the original work is properly cited.

Background. With the continuous maturity of computer software and hardware technology, the theory and method of computer-aided art design have developed rapidly. *Objective.* Applying artificial intelligence theory to computer-aided process art design is one of the newly developed research hotspots, and it is also the development trend of industrial design modernization. *Methods.* On the one hand, it can transplant the research results in the field of artificial intelligence into computer-aided art design, and on the other hand, it expands the application field of artificial intelligence, so that the two can be perfectly combined to promote common development. *Results.* With the development of artificial intelligence technology, computer art has gradually become a very active field, and a large number of computer art works are available every year. *Conclusions.* This paper briefly describes the basic concepts of computer-aided art design and artificial intelligence and discusses the application of artificial intelligence in computer-aided art design.

1. Introduction

Computer-aided arts and crafts art design are a new type of technology that applies computer technology to art and art design, freeing staff from tedious and complicated work. Let the traditional arts and crafts art design improve the quality of arts and crafts art products while improving work efficiency. With the continuous advancement of computer technology, the emergence of artificial intelligence has added new vitality to computer-aided arts and crafts, and the level and efficiency of art and art design have been improved as never before [1].

A supply chain is a network of retailers, distributors, transporters, storage facilities, and suppliers that participate in the production, delivery, and sale of a product to the consumer. It is typically made up of multiple companies who coordinate activities to set themselves apart from the competition. There are three key parts to a supply chain: supply focuses on the raw materials supplied to manufacturing, including how, when, and from what location. Manufacturing focuses on converting these raw

materials into finished products. Distribution focuses on ensuring these products reach the consumers through an organized network of distributors, warehouses, and retailers.

In the application of electronic computers, hard devices and software related to image processing are increasing at a rate of 40% per year, that is, doubling every two years. The use of interactive computer-aided design system as an auxiliary tool for art creators to design arts and crafts has a very significant effect on reducing duplication of work, speeding up the design progress, enlightening creative ideas, and enriching the content of the work. With the development of artificial intelligence technology, computer art has gradually become a very active field, and a large number of computer art works are available every year [2, 3]. Many arts and crafts have the characteristics of repeating on a flat surface, which has often appeared in ancient art treasures. Using some simple graphic basic units, combined with the general principle of composition and the automatic generation technology of interlocking graphics, you can produce certain practical arts and crafts on computer colour monitors or ordinary colour (or black and white) TV screens

(graphic, for silk stretch, flower cloth, straw, batik, carpet, and other design use). The use of the joint money graphic automatic generation technology can automatically interlock and copy the mosaic graphics without any drying and overlapping and can be used for metal cutting, wood, leather, etc. without cutting, stamping, and cutting and processing and can also be used for the design of floor tiles, art floors, wallpapers, etc. [3].

Mobile information system is based on mobile equipment, through the high-performance wired and wireless communications networks for information and data transmission, to provide distributed GIS of the location-based information services anytime and anywhere. It integrates GIS, GPS, mobile communication and computer networks, and so on, and the advantages of these technologies will be integrated to information transfer through the high-performance communication networks, so that we can achieve mobile information of the industry and public information service. It also provides a convenient and economical way of technology for users on the exchange, access, and share and publish of information based on location, forming a GIS application way for portable terminals such as mobile phones. Mobile information system is especially applicable to commercial trade, government, tele-com, municipal construction, and other industries whose data have highly mobility and changes frequently.

Applying artificial intelligence theory to computer-aided process art design is one of the newly developed research hotspots, and it is also the development trend of industrial design modernization. On the one hand, it can transplant the research results in the field of artificial intelligence into computer-aided art design, and on the other hand, it expands the application field of artificial intelligence, so that the two can be perfectly combined to promote common development. With the development of artificial intelligence technology, computer art has gradually become a very active field, and a large number of computer art works are available every year. This paper briefly describes the basic concepts of computer-aided art design and artificial intelligence and discusses the application of artificial intelligence in computer-aided art design.

The specific contributions of this paper include the following:

- (1) Transplant research results in the field of artificial intelligence into computer-aided art design
- (2) Introduce the basic concepts of computer-aided art design and artificial intelligence
- (3) Discuss the application of artificial intelligence in computer-aided art design

The rest of this paper is organized as follows. Section 2 discusses artificial intelligence, followed by application of artificial intelligence in the design of computer-aided arts and crafts in Section 3. Theoretical model of artificial intelligence in the design of computer-aided arts and crafts is discussed in Section 4. Section 5 shows result analysis and discussion, and Section 6 concludes the paper with summary and future research directions.

2. Artificial Intelligence

Artificial intelligence, referred to as AI, is a new technical science that studies and develops theories, methods, techniques, and applications that simulate, extend, and expand human intelligence. The areas of the artificial intelligence are shown in Figure 1 [4]. The use of artificial intelligence can make various computer devices more humanized, extend and expand human intelligence, and realize the highest-level application of computers. The application of computer technology in people's lives has been expanding, and people have put forward new requirements for the ability of computers. The emergence of artificial intelligence technology has brought computer technology to a new level.

At present, there are mainly three research directions of artificial intelligence, namely intelligent interface, data mining, subject and multiagent system. Intelligent interface is mainly to study how people can communicate with computers more conveniently and intuitively; data mining mainly studies how to dig out people from complex, diverse, incomplete, large, fuzzy, and random application data. The process of knowing is having important or potentially meaningful information; the subject refers to the subject of artificial intelligence, which has certain independence, and mainly studies the ability of artificial intelligence to face the entity in the selection layer of belief, desire, intention, and ability. At present, the research of artificial intelligence has made some achievements in the reasoning ability and is developing towards the fuzzy processing function and the parallel processing function. The future development direction of artificial intelligence is artificial neural network. The advancement of artificial neural network will greatly promote the progress of society [5].

3. Application of Artificial Intelligence in the Design of Computer-Aided Arts and Crafts

The concept of computer-aided arts and crafts was put forward in the 1970s, and it has been widely concerned in the development process. It has experienced multiple stages of interaction, derivation, and generative, comprehensive, and intelligent progress [3]. For the time being, intelligence is the focus of computer-aided process development and the direction of future development. The biggest role of computer-aided arts and crafts in work is to replace some manual and repetitive operations, freeing up a large number of manual labor, so that people can put more energy into the research and development of new technologies and new arts and crafts. Under the help of computer-aided arts and crafts, people can realize the optimal allocation of limited resources, while reducing production costs and improving production efficiency. Computer-aided arts and crafts not only provide important support in production, but also solve a lot of designer's troubles in design. Some young designers who lack design experience can use computer-aided arts and crafts technology to improve the design level, improve the design grade, and alleviate the large demand for designers with rich design experience.

3.1. Intelligence. The most outstanding advantage that artificial intelligence brings to computer-aided arts and crafts design is intelligence. Computer-aided arts and crafts technology still has some links in the arts and crafts. It is difficult to get rid of the scope of auxiliary tools, but the addition of artificial intelligence has changed this. The current status makes computer-aided process design have certain intelligent analysis capabilities. Artificial intelligence is still in the state of research, and the application of artificial intelligence in computer-aided process design is mainly manifested in intelligent reasoning. In practical applications, the application forms of artificial intelligence are not unique, but various applications penetrate each other to form a comprehensive application form. In the field of computer-aided design, computer-aided mechanical product design is the most studied, while computer-aided art design and mechanical product design have certain convergence, so it can be inferred that the architecture of intelligent computer-aided art design includes science (layer, information technology layer, and intelligent design layer).

Applying artificial intelligence technology to the development of computer-aided art design (CAPP) system, CAPP system simulates people's thinking mode in knowledge acquisition, knowledge reasoning, etc., solves complex art and art design problems, and makes it "human intelligence". The feature is intelligent CAPP, which is an application of AI in CAPP. In the development of intelligent CAPP system, there are also intelligent methods such as fuzzy reasoning and chaos theory [6]. In practical applications, a variety of intelligent technologies are often combined to exert their own specialties, such as the characteristics of artificial neural networks with perceptual image thinking. Methods of fuzzy inference and other characteristics of logical thinking interpenetrate and combine, can play a complementary role, and improve the level of intelligence. There are few researches on CAPP design theory, and there are many researches on mechanical product design theory. The design theory and method consists of three parts: design theory foundation layer, design tool, and support technology platform layer. CAPP design theory and mechanical product design theory have commonality and particularity, especially in the intelligent design method. Therefore, it is considered that the intelligent CAPP design theory and method architecture consists of three layers, namely the foundation science layer, information technology layer, and intelligent design method layer.

3.2. Artificial Neural Network Technology. Art and craft design is a relatively large and cumbersome category. There are many uncertain factors in the design and production process. These uncertain factors are likely to cause problems in computer-aided art design and affect the efficiency of the entire design and production. The emergence of artificial neural network technology has improved the skills of computer-aided arts and crafts (CAPP) design, and these problems have been effectively controlled. In the process of dealing with the problem of the network world, the artificial

neural network simulates the principle of the biological nervous system. It is composed of a large number of nonlinear processing units. The units are highly paralleled by modern information technology. The artificial neural network has several characteristics when dealing with problems: fabric storage, parallel processing, self-organization and self-learning, and associative memory. The biggest advantage of applying artificial neural network technology to computer-aided art design is that this technology can adapt and adjust the system. When checking the initial basic values and the actual conditions inside the system, the neural network will monitor its own adaptability. The specific method of monitoring is to deduct and adjust from the beginning of the neural network to each node in the back and then push and adjust from the end of the neural network to better adapt to the network application.

In the design of product art and craft, there are many uncertain factors, which need to be solved by experience. The early establishment of CAPP system based on purely relying on group technology cannot solve the problem of obtaining this discrete knowledge well, design a search or derivative system. In recent years, the application of artificial intelligence technology in the development of CAPP system has made CAPP technology a great development [7]. Artificial neural network technology is one of the major applications of AI in CAPP system. Artificial neural network is an objective object that deals with the real world according to the principle of biological nervous system. It is composed of a large number of simple nonlinear processing units connected in parallel, with distributed storage of information, parallel processing, self-organization and self-learning, associative memory, etc. Characteristics are multilayer feed forward network error back propagation algorithm [8], as shown in Figure 2. The back-propagation algorithm is an algorithm for supervising the training of multilayer neural networks. Each training paradigm is calculated by two passes in the network: the first pass is calculated forward, from the input layer, and the layers are transmitted and processed and then generated. This picture shows the execution process of the neural network completely. Giving a picture, through the network supervision operation, the gradient is obtained and the gradient is updated, and finally the accurate result is obtained (an output, and an error vector of the difference between the actual output and the desired output; the second pass backwards, from the output layer to the input layer, using the error vector to modify the weight layer by layer).

3.3. Rough Set Technology. The rough set technology is an application form of artificial intelligence fuzzy control technology, which can effectively solve the ambiguity problem in computer-aided art design and achieve the purpose of solving the problem through comparative analysis. Artificial intelligence first lists the ambiguity problem as a table in the form of parameters, arranges the influencing factors corresponding to these problems according to the degree of influence, then horizontally lists some possible problems to set the weights, and finally eliminates them by certain algorithms. The redundant

parameters in the problem can finally find the correct answer to the fuzzy problem [9].

Rough set technology is another application of artificial intelligence in computer-aided art design. Rough set theory is a mathematical tool that is good at dealing with ambiguous and uncertain problems. In theory, “knowledge” is considered as a kind of classification ability for objects. Usually, a two-dimensional decision table is used to describe the domain information, and the column represents an attribute, a line represents an object, and each line represents a piece of information about the object. Attributes are divided into conditional attributes and decision attributes. Objects in the domain are divided into decision classes with different decision attributes according to different condition attributes. In the CAPP system, the expert system can be constructed by rough set theory, and the knowledge is acquired and optimized. The basic idea is to express the processing characteristics of various parts and the known processing methods into the form of conditional attributes and decision attributes. A part, a plurality of parts, forms a two-dimensional table, quantifies the attributes, organizes the decision table, and then uses a certain reduction algorithm to reduce the attribute set and attribute values, removing the redundant condition attributes and decision rules, and obtaining minimization of the set of decision rules, and when you input the machining features of the parts to be processed, you can get optimized processing techniques.

3.4. Genetic Algorithm. The genetic algorithm is influenced by Darwin’s theory of evolution. In the computer field, the scientific principle of genetics is used to simulate the process of biological evolution, and the screening of arts and crafts is completed. The genetic algorithm classifies each target art. All possible target arts and crafts are called domain, and the art and craft solutions are divided into different populations according to different types. The artisan solution contained in the domain will give a unique gene coding. In the case of genetic algorithm, each process art of different populations is compared and analyzed in the way of survival of the fittest, and the first generation of populations is crossed and evolved by genetic operators to produce the next generation of populations, and so on, to the last generation of the population which is the optimal solution.

Genetic algorithm is another application of artificial intelligence in computer-aided art design system [10]. Genetic algorithm is a computational model that simulates the evolutionary process of Darwin’s genetic selection and natural elimination. It is a method to search for optimal solutions by simulating natural evolutionary processes. The genetic algorithm begins with a population that represents a potential set of problems, while a population consists of a number of individuals genetically encoded, each of which is actually an entity with chromosomal features. Therefore, at the outset, it is necessary to implement mapping from phenotype to genotype, that is, encoding work, such as binary encoding. After the birth of the first generation, according to the principle of survival of the fittest and the principle of survival of the fittest, evolutionary generation

produces better and better approximate solutions. In each generation, individuals are selected according to the fitness of individuals in the problem domain and with the help of natural genetics. Genetic operators perform combination of crossovers and mutations to produce populations that represent new solution sets. This process will lead to a population of natural evolution like the descendant population that is more adapted to the environment than the previous generation, and the best individual in the last generation population is decoded, which can be used as a problem approximate optimal solution.

In the last three years, many methods are proposed to handle the computer aids arts and crafts; here we introduced three outstanding methods such as GNNA [11], RNNA [12], and CNNA [13], which can be used to solve the related works taking different kinds of network structures. GNNA is a graph-based network that build connections between different risk nodes that utilize the existing crafts pictures to design new arts and crafts. And RNNA uses a specific loss structure to keep the similarity of real and predicted crafts design that can make sure that the computer designed crafts are as similar as the real ones. CNNA is the basic model that needs more computation consuming to obtain the desiring performances, which can only obtain the crafts as simple as possible. However, these methods have their disadvantages respectively. GNNA is too slow, RNNA is so complicated, and CNNA also needs more spaces. They have their own corresponding advantages and shortcomings, and our proposal can handle these problems as much as possible, so we compared them with our proposal.

In this paper we utilize the entropy loss function to build the model for our research problems. It can be defined as follows:

$$\text{loss}(x, y) = \sum_{i=1}^n -p_i \log(1 - p_i), \quad (1)$$

where x and y are represented as the real arts and crafts’ score and difficulty and y means the predicted score and difficulty of our proposal. P_i means the probability of them when they are similar. The bigger the value of the loss is, the worse our proposal performed. And our proposal is used to train a model that fits the real and predicted arts and crafts, so that the machine can assist the arts and crafts designed.

And compared with the three methods, our proposal can deal with the problems easily and we also need a smaller computation space to build our model. However, our model may obtain a relative lower accuracy than others sometimes which may lead the prediction to be unstable.

4. Theoretical Model of Artificial Intelligence in the Design of Computer-Aided Arts and Crafts

4.1. Graphical Representation and Data Structure. The goal of the system is to generate a complete picture on the display called “picture”. The picture is superimposed by one or several basic patterns (BG) copied by interlocking transformation (I):

$$\text{PICTURE} = F(I_1(BG), I_2(BG), I_3(BG), \dots). \quad (2)$$

F represents the superposition relationship and I_i is one of the nine basic interlocking transformations, $I_i \in \{I_1, I_2, I_3, I_4, \dots\}$.

Since the postgenerated graphics may partially cover the original graphics when the overlay is performed, the overlay is ordered. The basic graphics (BG) is a superposition of a series of line segments (L_i). In the graphics library, the storage structure is

$$BG = (N\$, X, U, V, N, H, Z_0 - Z_5, L_0, L_1, L_2, \dots, L_N). \quad (3)$$

$N\%$ is the name of the basic graphic composed of strings, which is necessary for the graphics inventory to retrieve and print graphic data, $x \in \{0, 1\}$.

When $X = 0$, the pattern is high-resolution, with only two levels of brightness and darkness. When $X = 1$, the pattern is low-resolution, with 15 colors or 16 gray levels. $N + 1$ is equal to the number of line groups the basic figure has. H, U , and V are graphical interlocking parameters. $Z_0 - Z_5$ are optional parameters of the basic graphics, which may represent the number of times the graphics are copied in the horizontal and vertical directions or may represent the background or background brightness of the graphics.

Each line group (L_i) is sequentially connected by a series of ordered vertices (V_i) using straight line segments generated by the complement method. When $X = l$ (colour or multigradation), the line group should have a colour or brightness attribute (B_{ib}), and when the number of vertices of the line group L_i is large or equal to four and closed (i.e., the first and last vertices coincide), the line group constitutes the boundary of one (or more) enclosed area and thus also has the colour or brightness properties of the inner area (B_{ir}).

$$L_i \in [N_i \times B_{ib} \times \{V_0\} \times \{V_1\} \times \{V_2\} \times \dots \times \{V_{Ni}\} \times B_{ir}]. \quad (4)$$

x is the Cartesian product operator of the set, and items in square brackets may or may not appear.

$$N_i = \{-1, 0, 1, 2, \dots\}. \quad (5)$$

$N_i + 1$ is the number of vertices in the line group. When $N = -1$, it means an empty line group whose number of vertices is 0, and L_i has no other parameters.

$$\begin{aligned} B_{ib} &= \{1, 2, 3, 4, \dots, 16\}, \\ B_{ir} &= \{0, 1, 2, 3, \dots, 16\}. \end{aligned} \quad (6)$$

When $B_{ir} = 0$, the inside of the enclosed area is not filled.

The vertex V is determined by its pair of coordinate values in a Cartesian coordinate system:

$$V_i = (X_i, Y_i), \quad (7)$$

where X_i and Y_i are integers.

4.2. Graphics Transformation and Automatic Generation Technology of Interlocking Graphics. The process of

spreading the entire plane with congruent graphics without gaps and overlapping portions is called tessellation, and the inlaid graphics are called interlocking graphics. The vertices of the polygons (the number of sides must be greater than two, less than seven) can be embedded into the interlocking graph. The symmetry principle and the congruent linear transformation of the graph can form the interlocking transformation mode of the nine graphics. Nine ways can be derived from 29 interlocking graphics. The basic principle of graphical linear transformation and the algorithm for generating interlocking graphics are briefly introduced below [14].

For linear transformation,

$$\begin{cases} x' = ax + by + c, \\ y' = dx + ey + e. \end{cases} \quad (8)$$

It can be expressed as a standard method of 3×3 matrix :

$$[x', y', 1] = [x, y, 1] \cdot \begin{bmatrix} a & d & 0 \\ b & e & 0 \\ 0 & f & 1 \end{bmatrix}. \quad (9)$$

The most basic three linear transformations are as follows.

(1) Translation transformation:

$$[x', y', 1] = [x, y, 1] \cdot \begin{bmatrix} 1 & 0 & 0 \\ 0 & 1 & 0 \\ x'_k - x_k & y'_k - y_k & 1 \end{bmatrix}. \quad (10)$$

(x_k, y_k) and (x'_k, y'_k) indicate the coordinates of any known point in the before and after translation, respectively. The translation transformed by (10) is transformed into a T transform.

(2) Proportional transformation:

$$[x', y', 1] = [x, y, 1] \cdot \begin{bmatrix} P_x & 0 & 0 \\ 0 & P_y & 0 \\ 0 & 0 & 1 \end{bmatrix}. \quad (11)$$

(3) Rotation transformation centered on the origin of the coordinates:

$$[x', y', 1] = [x, y, 1] \cdot \begin{bmatrix} \cos \theta & -\sin \theta & 0 \\ \sin \theta & \cos \theta & 0 \\ 0 & 0 & 1 \end{bmatrix}. \quad (12)$$

When $\theta > 0$, it means clockwise rotation. The linear transformation used in the system can be successively performed by the above three basic transformations, and the transformed cascade matrix can be represented by the product of the basic transformation matrix. The linear transformations used in this system are as follows.

- (4) A rotation transformation centered on (x_c, y_c) , which is made up of $(-x_c, -y_c)$ translation, θ rotation ($\theta > 0$ is clockwise), and (x_c, y_c) translation cascade:

$$[x', y', 1] = [x, y, 1] \cdot \begin{bmatrix} \cos \theta & -\sin \theta & 0 \\ \sin \theta & \cos \theta & 0 \\ -x_c \cos \theta - y_c \sin \theta + x_c & x_c \sin \theta - y_c \cos \theta + y_c & 1 \end{bmatrix}. \quad (13)$$

When θ is equal to 180° , $\pm 120^\circ$, $\pm 90^\circ$, and $\pm 60^\circ$, the transformation determined by (13) is called C, C_3 , C_4 , and C_5 transformation. Table 1 shows the typical combination of C series and T, and their variations.

- (5) A reflection transformation with the line $y = x$ as the axis, which is 45° rotation, (1, -1) ratio and -45° rotation three basic transformation cascades.
- (6) Make reflective translation transformation, after mirror reflection of the horizontal or vertical axis of the point (x_c, y_c) , then translate the point to point $(-x_k, -y_k)$, which is made up of $(-x_k, -y_k)$ translation, (P_x, P_y) scale and (x_k, y_k) translation cascade. For horizontal axis reflection, $P_x = 1$, $P_y = -1$, and for vertical axis reflection, $P_x = -1$, $P_y = 1$. At this time, the reflection translation transformation can be expressed as

$$[x', y', 1] = [x, y, 1] \cdot \begin{bmatrix} 1 & 0 & 0 \\ 0 & -1 & 0 \\ x'_k - x_k & y'_k + y_k & 1 \end{bmatrix}, \quad (14)$$

$$[x', y', 1] = [x, y, 1] \cdot \begin{bmatrix} -1 & 0 & 0 \\ 0 & 1 & 0 \\ x'_k + x_k & y'_k - y_k & 1 \end{bmatrix}. \quad (15)$$

The transforms determined by (14) and (15) are referred to as G_h transform and G_v transform, respectively. Among the seven transformations T, C, C_3 , C_4 , C_6 , G_h , and G_v used in the construction of the interlocking pattern, except for the C transformation, the other transformations appear in pairs. Only half of the line group formed by the C transform is independent, so it forms a curve pair itself. In the TT, C_3C_3 , C_4C_4 , C_6C_6 , G_hG_h , and G_vG_v pair, only one curve is independent and can be determined by the user. The other subordinate line is separated by the above all. It is obtained by linear transformation, so that in each basic unit of the interlocking graphics, only half of the edges are independent, and the other half of the edges are generated by the independent edges by the congruent linear transformation. The T transform and the G transform cannot be combined with the C_3 , C_4 , C_6 transforms.

For the case of converting each basic graphic unit into an interlocking mosaic pattern, it is necessary to find the group that can be displayed on the translated and complex quadrilateral set, and determine a parallelogram grid, which

consists of two displacement vectors, the level in one level is determined, the length is H, and the other has a horizontal component and a vertical component. Volume V.H, U and V are the interlocking parameters mentioned above. When the line cluster moves enough times along the corresponding parallelogram grid, several congruent interlocking graphs are copied on the entire display screen.

$$H(\theta, x, y | u, v) = h(\theta | u) \prod_{n=1}^N h(x_n | u) p(y_n | x_n, v),$$

$$H(y | u, v) = \int h(\theta | u) \left(\prod_{n=1}^N \sum_{z_n} h(x_n | \theta) h(y_n | x_n, v) \right) d\theta. \quad (16)$$

Table 2 shows the typical combination of C series, T, G, and their variations.

4.3. Structure and Main Functions of the Graphic Design System. The equipment used in this system is CROMEMCO-52 microcomputer system, including DAZZLER graphic output interface board and an external colour monitor (can also use ordinary TV sets). To improve the interaction between graphic designers and systems, fully to play the function of the original graphics software resources of the system, the extended BASIC language (including several basic graphic command statements) and the corresponding GRAPHX•COM command file software interface are selected. It takes about one to two minutes to output an interlocking graphic picture composed of four to sixteen basic units on the monitor using the graphic design software package, and each basic unit can have up to 21 line groups [15]. In the case of low resolution, these line groups can have 15 different colors, and each line group can be connected by up to 21 vertices. In view of the fact that the system update memory capacity in the main memory is ZK byte RAM, the resolution is low, so it is not practical to increase the number of lines and vertices of the basic unit of the graphic, and one picture can be interlocked by multiple frames [16]. The graphics are superimposed, each interlocking graphic is interlocked by multiple graphic basic units, and the system has a large area automatic colour filling function, so the number of vertices and the number of line groups can satisfy the minimum actual needs. For more advanced graphics output devices, the system can be used with a little modification.

Since the DAZZLER graphical interface allows the program to easily and flexibly select two different

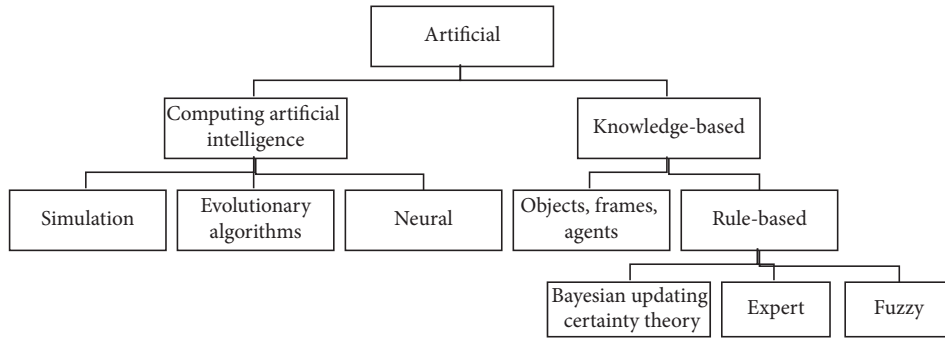


FIGURE 1: The areas of artificial intelligence.

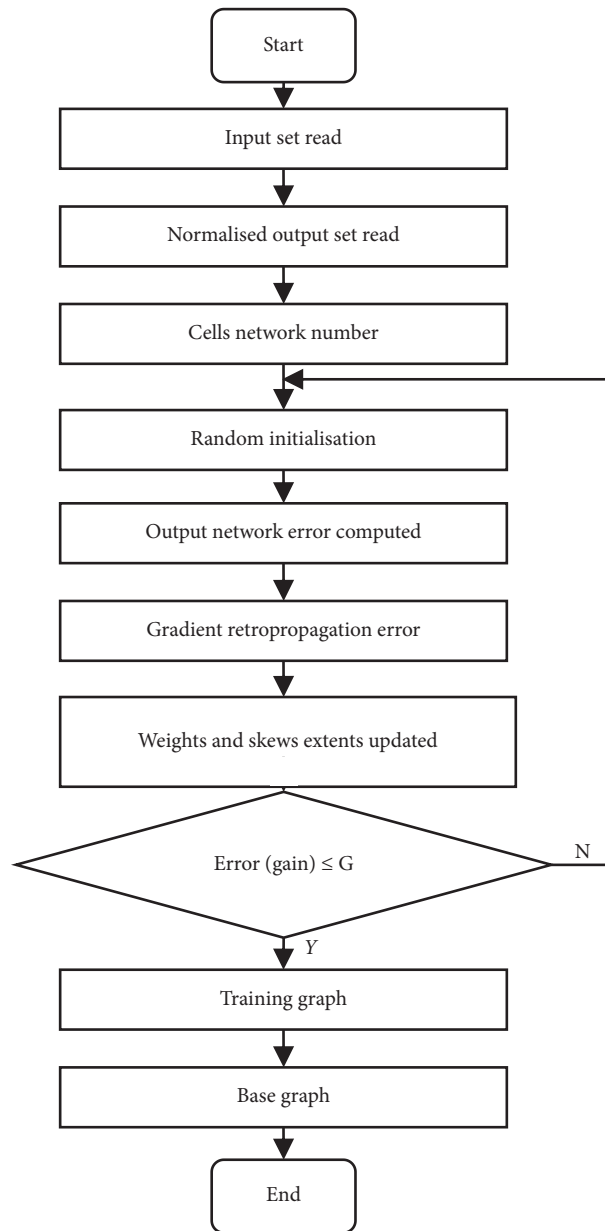


FIGURE 2: The backpropagation algorithm.

resolutions, the graphic designer can design two different types of graphics as needed.

4.3.1. Colour or Multigradation (Low Resolution). When the graphic has colour or multigradation (low resolution), the internal lines of the basic unit of the graphic are mainly used, and various arts and crafts graphics are designed by interlocking and copying the interior of the closed area. Since the interlocking graphics have the reciprocity of periodic repetition, it is easy to ensure that two consecutive or quadrilateral continuous images are obtained. This is very convenient for the design of many arts and crafts [17]. Since the pattern designer can arbitrarily choose the interlocking mode and the interlocking translation parameters, it is convenient to modify the ratio of the graphics in the x direction and the y direction and the number of copies of the basic unit and flexibly shift the entire screen up and down or left and right during copying [18]. Reflecting with the $y=x$ line as the axis, you can also flexibly modify the colour or brightness of any line group or all line groups, specify the background colour of the screen or modify the colour inside a certain closed area, and classify according to certain graphics. The sequence is superimposed to form a new picture, so even if you input a very simple graphic basic unit, you can change thousands of different patterns to make it easier for designers to compare the effects of various structures and tones. The system also has a loop-shaped database automatic design function, which can provide graphic designers with some optional art graphics to inspire the creative ideas of the art designers. Therefore, these graphics are suitable for silk, flower cloth, parquet floor, carpet, and wallpaper (design of arts and crafts such as straw and straw) [19, 20].

4.3.2. Black and White (High Resolution). When the graphic is designated as black and white (high resolution), the interlocking graphic is the main working mode by the boundary line of the graphic and the internal line. Since such graphics often form a gap-free, nonoverlapping interlocking pattern by the basic graphic unit translation, the system is applied in the processing of sheet metal processing (such as cutting and punching of various metal sheets, wood, leather, and paper) [21]. This can help designers save raw materials and reduce product costs. For most graphics, even if there is no gap at all, the closest basic unit can be found in 29 interlocking modes, so that the machining allowance is reduced as much as possible [22, 23].

In the nine main interlocking transformation modes, several different shapes of graphics can be skillfully combined to form a basic unit of interlocking graphics. In turn, the basic unit of the interlocking graphics can also flexibly use internal lines as needed. Divided into several different shapes of graphics. This kind of interlocking graphic design method based on boundary line has certain uses in building block design and modular upper floor planning and packaging design of irregular products [24]. It can also be used for building materials such as floor tiles and wallpaper (designed for use in batik, lace, and other crafts). Because only half of the boundaries of this type of graphics are

independent, the designer only needs to input half of the basic graphics plus the internal lines, so the system can copy multiples at any scale (only limited by display size and resolution). Such resulting graphics, thus greatly improving the design efficiency, and because the other half of the boundary line of the basic unit is generated by different interlocking methods, often have the effect that the designer did not expect [25]. Any graphic designer with elementary mathematics and a little English can use this graphic design program system to design various graphics after several hours of learning. Nine kinds of interlocking transformation graph generation programs exist in the floppy disk memory respectively. The graphic designer uses the host console keyboard and the character display terminal to perform man-machine dialogue. After selecting the interlock mode, three different methods can be used for graphic design [26].

(1) The Interaction Method Using Keyboard Input. After the designer specifies the resolution and background colour of the graphic (for colour or multigrav graphics) through the keyboard, the system draws the background colour on the colour monitor and displays the coordinate origin and the rough scale of the x and y axes [27]. You can enter the coordinates of known vertices and independent line group keys. For colour graphics, you also specify the colour of each line group. For the closed area, you also specify whether to fill and fill the code. Each time a key is entered, the system immediately displays it on the monitor and automatically joins the line group. After the independent line group is finished, the system immediately copies the corresponding subordinate line group to form a complete boundary line. The designer can then enter the internal line set. After the input process is finished, the system automatically copies and copies any number of graphic basic units in the x and y directions according to the designer's request to form an interlocking graphic picture [28]. During the entire input process, if the designer wants to change a certain line group that has just been input, the keyboard group can be easily erased from the screen by the keyboard, or the line group can be temporarily reserved for modification as a comparison, and when the interlock is copied, the invalid line group does not appear. If the designer believes that the graphics copied by the chain is necessary, all the graphic data can be printed for future copying or analysis. The system can automatically organize all the data and related parameters into data files according to the specified format and data structure. Into the disk, recopy on the monitor when needed [29, 30].

(2) Graphics Library Method. All data and partial interlocking parameters of the graphic basic unit are predetermined by the designer and organized into data files according to the specified data structure and stored in the disk to form a graphic library, which is called out from the disk during design and is spliced or superimposed on the monitor. Synthesize new pictures [31].

(3) Intelligent Graphic Database Automatic Design Method. According to certain composition rules and their own preferences, the art graphic designer combines the basic unit

TABLE 1: The typical combination of C series and T.

Transformations	Known points	Lonely points	Belonging points	Lonely line	Belonging line	Variation	Conditions
TTTTT	$x(0) = 0$	$x(1)$	$x(2) = x(1) + 20$	01	42	TTTT	$x(8) = y(8) = 0$
	$y(0) = 1$	$y(1)$	$y(2) = y(1) + 3$	13	54		$x(3) = 0.25x(1)$
	$x(3) = 50$	$x(4)$	$x(5) = x(2) - x(3) + 2$	23	04		$y(3) = 0.25y(1)$
	$y(3) = 10$	$y(4)$	$y(5) = Y(2) - y(3)$				
TCCTCC	$x(0) = 0$	$x(1)$	$x(2) = 0.125x(1) + 0.125x(3)$	01	23	TCTCC TCTC CCC	$x(8) = y(8) = 0$ $x(3) = 0.25x(1)$ $y(3) = 0.25y(1)$
	$y(0) = 0$	$y(1)$	$y(2) = 0.125y(1) + 0.125y(3)$	12	65		
	$x(6) = 25$	$x(8)$	$x(5) = 0.25x(1) + 25$	34	45		
	$y(6) = 0$	$y(8)$	$y(5) = 0.25y(1)$	67	78		
		$x(3)$	$x(4) = 0.125x(3) + 0.125x(1) + 15$				
$C_3C_3C_3C_2C_2$	$x(0) = 0$					$C_3C_3C_2$	$x(2) = x(1)$ $y(2) = y(1)$
	$y(0) = 0$						
	$x(2) = 10$	$x(1)$	$x(3) = 0.1x(1) - 0.322x(3) + 47$	12	05		
	$y(2) = 27$	$y(1)$	$y(3) = 0.35x(1) - 0.18y(3)$	01	54		
	$x(4) = 25$		$x(5) = -0.2x(1) + 0.23y(1)$	34	34		
	$y(4) = -27$		$y(5) = -0.23x(1) - 0.1y(1)$				

TABLE 2: The typical combination of C series, T and G.

Transformations	Known points	Lonely points	Belonging points	Lonely line	Belonging line	Variation	Conditions
$TG_{h1}Ch_1TG_{h2}G_{h2}$	$x(0) = 0$	$x(1)$	$x(3) = 0.2x(1) + 20$	01	05	$G_{h1}G_{k1}G_{h2}G_{k2}$	$x(1) = y(1) = 0$
	$y(0) = 0$	$y(1)$	$y(3) = 0.3y(1)$	23	43		
	$x(6) = 35$	$y(2)$	$x(5) = 0.2x(2) - 0.2x(1)$	12	34		
	$y(6) = 0$	$y(5)$	$y(5) = 0.2y(1) - 0.1y(2)$				
	$y(7) = 8.4$						
TCCTG _h G _h	$x(0) = 0$	$x(1)$	$x(2) = 0.1x(1) - 0.2x(3)$	12	32	TCTG _h G _h	$x(3) = x(1)$ $y(3) = y(1)$
	$y(0) = 0$	$y(1)$	$y(2) = 0.5y(1) + 0.1y(3)$	01	54		
	$x(6) = 35$	$y(7)$	$x(5) = x(1) + 35$	67	07		
	$y(6) = 0$	$x(3)$	$y(5) = y(1)$	34	64		
	$y(7) = 8.4$	$y(3)$	$y(4) = y(2)$				
$CG_hG_vG_hCG_v$	$x(0) = 0$	$x(1)$	$x(2) = 0.15x(1) + 0.5x(3)$	02	34	CG_vCG_v	$x(2) = x(1)$ $y(2) = y(1)$
	$y(0) = 0$	$y(1)$	$y(2) = 0.1y(1) + y(3)$	23	86		
	$x(5) = 35$	$y(2)$	$x(4) = x(3) + 0.5x(1) + 15$	45	07		
	$y(5) = 0$	$x(2)$	$y(4) = 0.2y(2)$	13	76		
		$x(6)$	$x(5) = x(1) + 80$				
		$y(6)$	$y(5) = 0.2y(1)$				

classification of various styles into a graphic data inventory and puts it on the disk. After the designer specifies the interlocking method and the background colour, the system is based on the graphical elements such as line, shape, structure, rhythm, and colour, according to the technical principle of artificial intelligence such as continuous reasoning and campaign judgment strategy. In the graphic combination, a basic unit (pattern) of a graphic is taken out, and according to the data in the basic unit and the interlocking mode and the background colour, the colours of the line group and the interlocking copy parameter are automatically selected within a certain range. Make a copy. After that, the system automatically selects another graphic basic unit to generate a new pattern superimposed on the original screen until the designer artificially terminates the process.

The system can automatically print out all the parameters of the entire graphics generation process.

No matter where the program is running, the system can use the ESC key to interrupt the operation and return to the center point. From the center point you can arbitrarily turn to one of the following ten exits (see Figure 3):

- (1) End the program run
- (2) Select a new interlock method
- (3) Modify, select, or specify the following data, parameters, or working methods
 - (a) Whether to clear the original content of the screen before the interlock copy, and if not clear, the new graphic is superimposed on the original screen

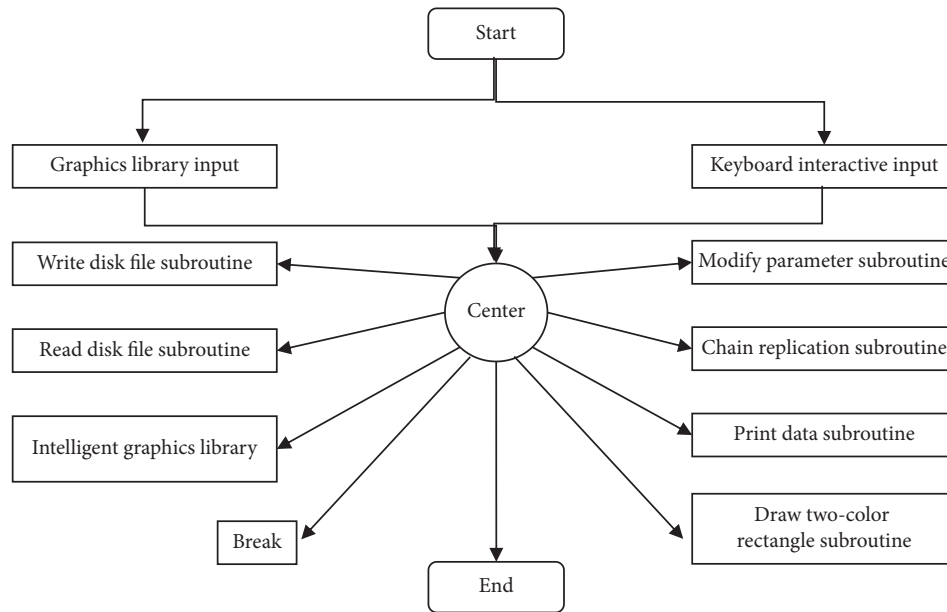


FIGURE 3: The construction and functions of the system.

- (b) Modify the number of interlocking translations E, F, thereby changing the scaling factor in the x and y directions
 - (c) Modify the amount of translation of the screen in a certain direction; the initial value is 0
 - (d) Determine if the graphic is rotated 90° (i.e., reflecting with a straight line $y=x$ as the axis of symmetry)
 - (e) Modify the interlock parameters H, U, V
 - (f) Determine whether to add a border on the screen
 - (g) For high-resolution black and white graphics, you can specify to exchange bright and dark pixels to get a black and white picture
 - (h) Modify the background colour or background brightness of the low-resolution graphics, or disable the background colour so that the original picture is not destroyed
 - (i) Modify the colour of any line group
 - (j) Adjust the colour of all line group
 - (k) Modify the colour in any enclosed area, and also prohibit colour filling
- (4) Print all data of the graphic basic unit and related interlocking copy parameters
 - (5) Directly transfer to the graphics library working mode, take out new patterns from the graphics library
 - (6) Use a two-colour rectangular pattern to form a graphic background
 - (7) Transfer to the AI database to automatically design work methods
 - (8) All the data of the basic unit of the graphic designed by the interactive method and the necessary

interlocking parameters are automatically organized into disk files and stored in the floppy disk according to the specified data structure

- (9) Take out the automatically saved graphic file and display it
- (10) Suspend the program and transfer to the BASCI standby state to perform the cross-over operation

5. Result Analysis and Discussion

This article is from the point of view of the convenience of application, the preparation of a simple program interface testing the algorithm. In program, when we click the menu "Preferences \rightarrow Draw Graphics [P]", it will pop up "Willow artwork main parameter settings" dialog box. When the parameters are set, clicking on the "OK" button, there will be "parameter confirmation" Prompt message, waiting for choice. When the "Y" button is selected, the drawing graph is displayed. When the "N" button is selected, the parameter needs to be reset. The "Willow Art Main Parameter Setting" dialog box will appear again. If the "Cancel" button is selected, the operating will be given up. When the graph is drawn successfully, if you want to adjust the parameters and obtain the new graph, we can click the menu "Reset Parameters" to reset the parameters. Drawing with current parameters is shown in Figure 4. Willow model is shown in Figure 5.

In order to analyze the script editing method and script stitching algorithm which is better researched in this paper, this dissertation also made an experimental platform for experiment data analysis, which can make accurate statistics and analysis of the data volume and the operation efficiency of the algorithm. For example, Figure 6 shows the experimental analysis platform.

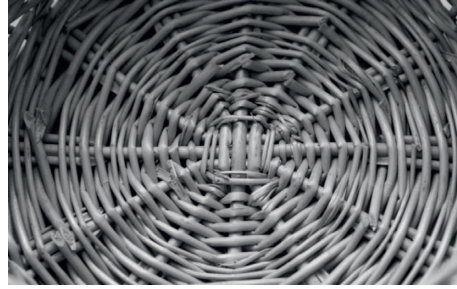


FIGURE 4: Drawing with current parameters.

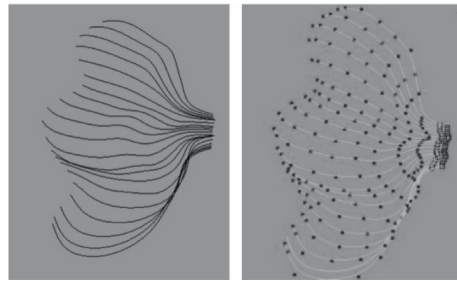


FIGURE 5: Willow model.

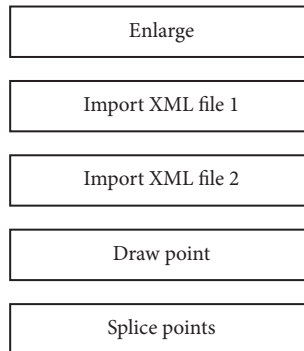


FIGURE 6: The experimental analysis platform.

This platform includes drawing points, zoom in, and calculate run time and other auxiliary functions. In the lab, on the computer of Intel Core22.66 GHz CPU, 3.SOGB memory, NVIDIA GeForce 8600GT graphics card, the traditional brute-force algorithm and the research method of this article are tested. Both methods can find the most suitable splicing point accurately. In Figure 7 and Table 3, we can see that the traditional brute force algorithm is not suitable for the scenario studied in this paper. When the amount of calculation data is large, it exceeds 2S. However, the method studied in this paper consumes an exponential increasing trend under the same conditions, but none of them exceeds 2S, and the percentage of efficiency improvement is significant, which verifies the effectiveness and efficiency of the proposed algorithm. In order to investigate the effectiveness of our proposal and other methods. Here,

we take F1-score into account to assess the experiment results, which can be defined as follows:

$$f1 - score = \frac{2 * precise * recall}{precise + recall},$$

$$precise = \frac{TP}{TP + FP},$$

$$recall = \frac{TP}{TP + FN}.$$
(17)

And we also compared the three methods proposed in the lasted three years, GNNA, RNNA, and CNNA, with our proposal to investigate the effectiveness of our methods. The results can be shown as in Figure 8. As we can see from Figure 8, the black curve represents the results of our

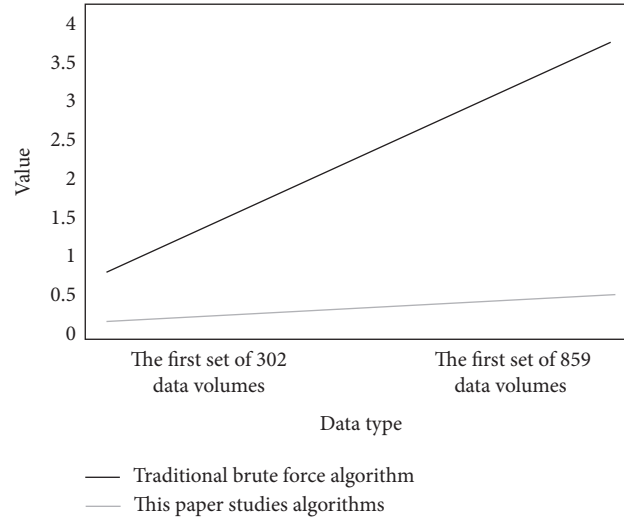


FIGURE 7: The advantages of the algorithm in this paper.

TABLE 3: The advantages of the algorithm.

	#node data	Xml file size (kB)	Traditional brute force algorithm time consuming (S)	This paper studies the time consuming of algorithms (S)	Improvement (%)
MyXml 1	101	15	0.757	0.165	76.99
MyXml 2	201	30	1.552		
MyXml 1	226	24	1.721	0.595	82.85
MyXml 2	633	68	3.470		

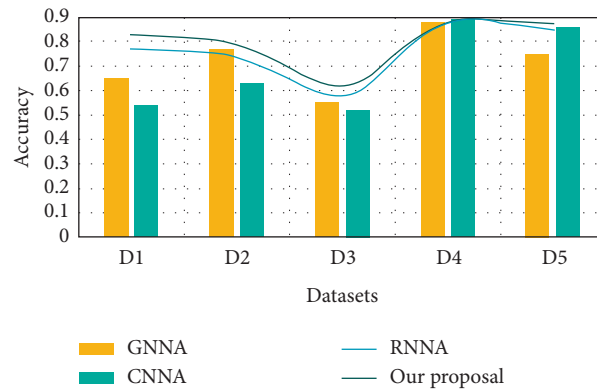


FIGURE 8: The results of our proposal and other methods.

proposal and others represent the other three methods results. As we can see on all datasets the results of our proposal are better than others except D4, which proves that all

methods obtain the same results. GNNA always obtain the worse results which may be caused by the lower generalization, but it can provide more diversities. CNNA, as the

basic one, can have worst accuracy and lower diversity. RNNa is located at the middle of them. Our proposal can provide high scores and also provide more diversity giving more new products. It indicated that our proposal can perform better than the other three methods.

In summary, the paper introduces the development of postprocessing algorithm of willow technology and starts with the software structure of postprocessing model generation. The realization process of the algorithm is introduced in detail. Then it introduces how to apply the postprocessing platform of animation and splicing the digital shadow script files to form a complete willow craft file. Finally, the effectiveness and efficiency of this algorithm are analyzed, and the usability of the algorithm is further verified and analyzed.

6. Conclusion

All in all, the emergence of artificial intelligence has revolutionized the design of computer-aided arts and crafts, not only replacing a lot of tedious and repetitive manual labour, but also improving the quality of production. The continuous improvement of artificial intelligence technology and the generation of various technologies and algorithms make computer-aided arts and crafts design more convenient and efficient, while the efficiency and quality are simultaneously improved, and also pointing out the direction for the development of artificial intelligence technology. The application of artificial intelligence algorithms puts forward great demands on the computing power of computers and our experimental equipment. Therefore, how to further improve the complexity and accuracy of the model is an important topic for our future research.

Intelligence is the main trend of CAPP system development in the future, but from the current level of artificial intelligence technology, it is impossible to make a substantial breakthrough in the intelligent level of CAPP system. To solve the problems of artificial intelligence technology, new breakthroughs must be made in some basic theories and basic sciences, such as in life sciences and mathematics. There must be new breakthroughs in other areas. It can be seen that in the foreseeable future, the development of intelligent CAPP system will still be based on the full use of human intelligence advantages, comprehensive application of various artificial intelligence technologies to achieve intelligent CAPP system. Through the above discussion, we believe that everyone has a certain understanding of the application of computer-aided art design and artificial intelligence and artificial intelligence in computer-aided art design. With the continuous development of artificial intelligence technology, the intelligent CAPP system will further develop the flexibility and effectiveness of knowledge acquisition, expression, and processing; improve the intelligent level of CAPP system; and thus improve the level of modern manufacturing technology. Although our method has achieved good accuracy at present, it is still unable to achieve considerable accuracy in the face of complex environment, and the training time of the model is long. In the

future, we will further optimize our model to improve the training speed of the model while ensuring the accuracy.

Data Availability

The data used to support the findings of this study are included within the article.

Conflicts of Interest

The authors declare that there are no conflicts of interest regarding the publication of this paper.

Acknowledgments

This work was supported by the Youth Fund of Humanities and Social Sciences and Art of the Ministry of Education in 2020 (No. 20YJC760014).

References

- [1] R. Rootberstein, "Arts and crafts as adjuncts to STEM education to foster creativity in gifted and talented students," *Asia Pacific Education Review*, vol. 16, no. 2, pp. 1–10, 2015.
- [2] I. Gatt and S. Karppinen, "An enquiry into primary student teachers' confidence, feelings and attitudes towards teaching arts and crafts in Finland and Malta during initial teacher training," *International Journal of Art & Design Education*, vol. 33, no. 1, pp. 75–87, 2014.
- [3] T. Petersen, "Computer-aided indexing in the arts: the case for a thesaurus of art terms," *Art Libraries Journal*, vol. 6, no. 3, pp. 6–11, 2016.
- [4] L. Seidenari, G. Serra, A. D. Bagdanov, and A. Del Bimbo, "Local pyramidal descriptors for image recognition," *IEEE Transactions on Pattern Analysis and Machine Intelligence*, vol. 36, no. 5, pp. 1033–1040, 2014.
- [5] P. Vogt, L. Kasper, and J.-P. Burde, "The sound of church bells: tracking down the secret of a traditional arts and crafts trade," *The Physics Teacher*, vol. 53, no. 7, pp. 438–439, 2015.
- [6] Y. Su, X. Chu, D. Chen, and X. Sun, "A genetic algorithm for operation sequencing in CAPP using edge selection based encoding strategy," *Journal of Intelligent Manufacturing*, vol. 29, no. 9–10, pp. 1–20, 2015.
- [7] D. C. Parkes and M. P. Wellman, "Economic reasoning and artificial intelligence," *Science*, vol. 349, no. 6245, pp. 267–272, 2015.
- [8] Z. Ghahramani, "Probabilistic machine learning and artificial intelligence," *Nature*, vol. 521, no. 7553, pp. 452–459, 2015.
- [9] E. S. Rigas, S. D. Ramchurn, and N. Bassiliades, "Managing electric vehicles in the smart grid using artificial intelligence: a survey," *IEEE Transactions on Intelligent Transportation Systems*, vol. 16, no. 4, pp. 1619–1635, 2015.
- [10] M. X. Xia, G. L. Shi, C. Chen et al., "Application and research of reverse engineering and laser manufacturing technology in the arts and crafts," *Journal of Guangxi University of Science & Technology*, vol. 8, 2016.
- [11] A. Burduk, "Artificial neural networks as tools for controlling production systems and ensuring their stability," *Lecture Notes in Computer Science*, vol. 8104, pp. 487–498, 2017.
- [12] Y. Gao, A. Xu, P. J.-H. Hu, and T.-H. Cheng, "Incorporating association rule networks in feature category-weighted naive Bayes model to support weaning decision making," *Decision Support Systems*, vol. 96, pp. 27–38, 2017.

- [13] S. Hoochang, H. R. Roth, M. Gao et al., “Deep convolutional neural networks for computer-aided detection: CNN architectures, dataset characteristics and transfer learning,” *IEEE Transactions on Medical Imaging*, vol. 35, no. 5, p. 1285, 2016.
- [14] S. Yang, Z. Gong, K. Ye, Y. Wei, Z. Huang, and Z. Huang, “EdgeRNN: a compact speech recognition network with spatio-temporal features for edge computing,” *IEEE Access*, vol. 8, pp. 81468–81478, 2020.
- [15] J. Zhang and D. Tao, “Empowering things with intelligence: a survey of the progress, challenges, and opportunities in artificial intelligence of things,” *IEEE Internet of Things Journal*, vol. 8, no. 10, pp. 7789–7817, 2021.
- [16] M. S. Hossain and G. Muhammad, “An audio-visual emotion recognition system using deep learning fusion for a cognitive wireless framework,” *IEEE Wireless Communications*, vol. 26, no. 3, pp. 62–68, 2019.
- [17] S. P. L. Kumar, J. Jerald, and S. Kumanan, “Feature-based modelling and process parameters selection in a CAPP system for prismatic micro parts,” *International Journal of Computer Integrated Manufacturing*, vol. 28, no. 10, pp. 1046–1062, 2014.
- [18] A. B. Yasrebi, A. Hezarkhani, P. Afzal et al., “Application of an ordinary kriging-artificial neural network for elemental distribution in kahang porphyry deposit, Central Iran,” *Arabian Journal of Geosciences*, vol. 13, no. 15, 2020.
- [19] R. Ayachi, M. Afif, Y. Said, and M. Atri, “Traffic signs detection for real-world application of an advanced driving assisting system using deep learning,” *Neural Processing Letters*, vol. 51, no. 1, pp. 837–851, 2020.
- [20] A. Dey, J. Lahiri, and B. Mukhopadhyaya, “LHC signals of triplet scalars as dark matter portal: cut-based approach and improvement with gradient boosting and neural networks,” *Journal of High Energy Physics*, vol. 2020, no. 6, 2020.
- [21] E. Davis and G. Marcus, “Commonsense reasoning and commonsense knowledge in artificial intelligence,” *Communications of the Acm*, vol. 58, no. 9, pp. 92–103, 2015.
- [22] M. Stoffel, F. Bamer, and B. Markert, “Neural network based constitutive modeling of nonlinear viscoplastic structural response,” *Mechanics Research Communications*, vol. 95, pp. 85–88, 2019.
- [23] F. Khelifi, A. Bradai, A. Benslimane, P. Rawat, and M. Atri, “A survey of localization systems in internet of things,” *Mobile Networks and Applications*, vol. 24, no. 3, pp. 761–785, 2019.
- [24] R. J. Duro, J. A. Becerra, J. Monroy, and F. Bellas, “Perceptual generalization and context in a network memory inspired long-term memory for artificial cognition,” *International Journal of Neural Systems*, vol. 29, no. 6, 2019.
- [25] B. Soulef, R. Khemiri, F. E. Sayadi, and M. Atri, “Fast CU partition-based machine learning approach for reducing HEVC complexity,” *Journal of Real-Time Image Processing*, vol. 17, 2019.
- [26] M. Amini, J. Rezaeenour, and E. Hadavandi, “A neural network ensemble classifier for effective intrusion detection using fuzzy clustering and radial basis function networks,” *International Journal on Artificial Intelligence Tools*, vol. 25, no. 2, 2016.
- [27] W. Kristjanpoller and M. C. Minutolo, “Forecasting volatility of oil price using an artificial neural network-GARCH model,” *Expert Systems with Applications*, vol. 65, pp. 233–241, 2016.
- [28] V. Vassiliades and C. Christodoulou, “Behavioral plasticity through the modulation of switch neurons,” *Neural Networks*, vol. 74, pp. 35–51, 2016.
- [29] B. Javier and J. M. Corchado Rodríguez, “Neural networks in distributed computing and artificial intelligence,” *Neuro-computing*, vol. 272, 2018.
- [30] H. C. C. Carneiro, C. E. Pedreira, F. M. G. França, and P. M. V. Lima, “A universal multilingual weightless neural network tagger via quantitative linguistics,” *Neural Networks*, vol. 91, pp. 85–101, 2017.
- [31] J. Cussens, M. Järvisalo, J.-H. Korhonen, and M. Bartlett, “Bayesian network structure learning with integer programming: polytopes, facets and complexity,” in *Proceedings of the Twenty-Sixth International Joint Conference on Artificial Intelligence*, Melbourne, Australia, August 2017.

Research Article

Research on Vertical Search Method of Multidimensional Resources in English Discipline Based on Edge Computing

Yi Xie 

Chongqing College of Humanities Science & Technology, Chongqing 401524, China

Correspondence should be addressed to Yi Xie; tyxy@cqrk.edu.cn

Received 4 February 2021; Revised 21 April 2021; Accepted 7 May 2021; Published 18 May 2021

Academic Editor: Hsu-Yang Kung

Copyright © 2021 Yi Xie. This is an open access article distributed under the Creative Commons Attribution License, which permits unrestricted use, distribution, and reproduction in any medium, provided the original work is properly cited.

The traditional vertical search method only considers the content of the webpage, and the global master node is not enough, which will lead to premature convergence and fall into the local optimum, resulting in insufficient multi-dimensional search of resources. Therefore, this paper proposes a multidimensional resource vertical edge based on the calculation of English subject search method. This paper analyzes the architecture of search engine firstly and then introduces the multiaccess edge computing architecture. At last, it constructs the vertical search task computing model of multidimensional resources in English discipline. By associating and traversing the attributes of multidimensional resources of English discipline, the vertical search of attribute information is realized offline, and the vertical search method of multidimensional resources of English discipline based on edge calculation is designed. In order to verify the effectiveness of the proposed method, a comparative experiment is designed. Experimental results show that the method can improve the resource search ratio and recall ratio, and it can also effectively improve the search efficiency. For an English subject resource data of 50 MB, the calculation methods of edge multidimensional resource data search recall rate can reach 97% and multidimensional resource data search time consumption is only 39 ms. The experimental results show that the performance of English subject multidimensional resources vertical search is much better.

1. Introduction

Current search engine on the overall development direction is divided into two categories. The first is to maintain the comprehensive characteristics of general search engines. Most search engines are “horizontal.” They have a wide range of searches, but they are not suitable for topic information searches in specific fields. Second, it develops towards the direction of thematic search engines, namely, the so-called “vertical” search engines [1, 2]. Although the general search engine has a comprehensive search ability, it often fails to search for professional knowledge. With the continuous expansion of Internet information, this search engine is more and more difficult to meet users’ requirements for information accuracy. While the vertical search engine is oriented to the vertical theme of a specific professional field, it can provide more advanced retrieval services, which can ensure that the collection of information in this field is more complete and the update speed

is faster [3]. In terms of providing professional information, the comprehensive engine has incomparable advantages [4]. Topic-oriented vertical search engine and general search engine have the following differences: first, general search engine for any user to provide any information query, while vertical search engine for professional users to provide them with information retrieval of their specialty; second, the general search engine crawls the network page by page, trying to traverse the entire Web [5]. The vertical search engine uses certain strategies to predict the position of relevant pages, dynamically adjusts the crawling direction of pages, and makes the system crawl as far as possible in the place where the web pages related to the topic are concentrated, which will save a lot of network resources. Finally, general purpose search engines require too much hardware, while vertical search engines save a lot of network resources by not traversing the entire Web and do not have their own large index database, so the hardware requirements are relatively low [6].

In order to improve the resource search ratio and recall ratio, relevant scholars have carried on the research. Xiao et al. proposed a Nutch based vertical resource search method [7] and implemented Chinese word segmentation with forward iterative and finite-granularity segmentation algorithm based on local and dynamically loaded word banks. The spatial vector model based on feature words and metadata labels was used to determine the topic relevance in the employment field [8]. Based on graphs to introduce web inbound links weighting factor and time attenuation factor improvement LinkRank sorting algorithms such as secondary development of Nutch and information on the web page to grab and filtering, employment information search and key recommendation is introduced into the employment domain ontology information, using Java framework technology to user query interface for secondary development, provides the key words such as smart reminder, customize the crawler, secondary search, set the date of the query results, subscribe to the query expansion query interface, such as was designed and implemented based on Nutch employment vertical search engine. This method can meet the needs of professional retrieval, but the search effect is low. Based on Lucene's big data subject oriented method [9], the vertical search engine on the basis of comprehensive study of the search method, this paper proposes a design for a particular topic of vertical search engine based on Lucene solution, using modular thought to the overall design, and the vertical search engine is divided into a collection subsystem, the index system, and query subsystem, with the subsystems not relying on each other, and the subject language information search engine is used as an example. The search object of this method is relatively single, and the scope of use is limited. Zheng et al. put forward based on the theme of Heritrix with Solr search engine optimization method [10], with the tools of Heritrix crawler and Solr full-text search engine for secondary development, and the tools to the default Heritrix crawler crawled the queue strategy and optimized allocation strategy; at the same time, with the introduction of IK Analyzer to improve Solr accuracy of Chinese word segmentation, this method has better efficiency of fetching, but resource data search takes too long. Liu et al. proposed a multidimensional intelligent scheme [11], which can be used to achieve stringent yet diverse QoS with limited resources in wireless communication system. It can improve the search efficiency effectively. In addition, Xie et al. proposed a distributed multidimensional pricing scheme for efficient application offloading in mobile cloud computing [12]. The main motivation of this is to propose a new pricing scheme based on multidimensional searching and mobile cloud computing. Although these methods improve the performance of resources searching in English discipline to a certain extent, they still cannot meet our demands.

Aiming at the problems of the above methods, this paper proposes a vertical search method for multidimensional resources of English subject based on edge calculation. We establish the multidimensional resource search model based on boundary computing, and then

the model is combined with English discipline to improve performance. This new method takes the advantages of multidimensional resource search and edge computing to improve the performance of English discipline. Mobile edge computing reduces the latency at which mobile terminals acquire popular content and the traffic pressure caused by devices frequently retrieving popular content from cloud data centers by bringing lightweight cache units and diverse services down to the edge of the network [13]. Therefore, edge calculation method can effectively improve the vertical search efficiency of multidimensional resources in English subject and improve the rate of resource acquisition.

The contributions of this paper are summarized as follows:

- (1) We consider a new vertical search method of multidimensional resources in English discipline. In recent years, many researchers gradually realized the importance of vertical search method to English subject but never found a good search algorithm to achieve efficient search. Therefore, the current research results in this field are not enough and are immature.
- (2) We propose a vertical search method of multidimensional resources in English discipline based on edge computing. This new strategy takes advantage of the edge computing, which can effectively improve the search efficiency.

This remainder of this paper is organized as follows: Section 2 presents architecture design and model building. Section 3 proposes the vertical search strategy of multidimensional resources in English discipline in detail. Test instances and performance metrics will be given in Section 4. In Section 4, experimental results are also presented and analyzed. Finally, Section 5 sums up some conclusions and gives some suggestions as the future research topics.

2. Architecture Design and Model Building

2.1. Search Engine Architecture. As a web application, you can sketch out the search engine architecture. Figure 1 shows the architecture of the search engine.

The collection of web pages, if only to do some simple experiments, but tens of thousands of web pages, many contradictions will not appear. However, in order to provide stable web data to large-scale search engines, it usually needs to collect millions of web pages every day, and it is ongoing [14–16]. The situation is much more complicated, and the core is to solve the problem of efficiency and quality comprehensively. Efficiency, in this case, is how to use as few resources as possible (computer equipment, network bandwidth, and time) to complete a predetermined amount of web page collection [17, 18]. In the occasion of bulk collection, usually considering about half a month to collect the web page is naturally the more the better. The so-called quality problem is to collect a limited number of pages in a

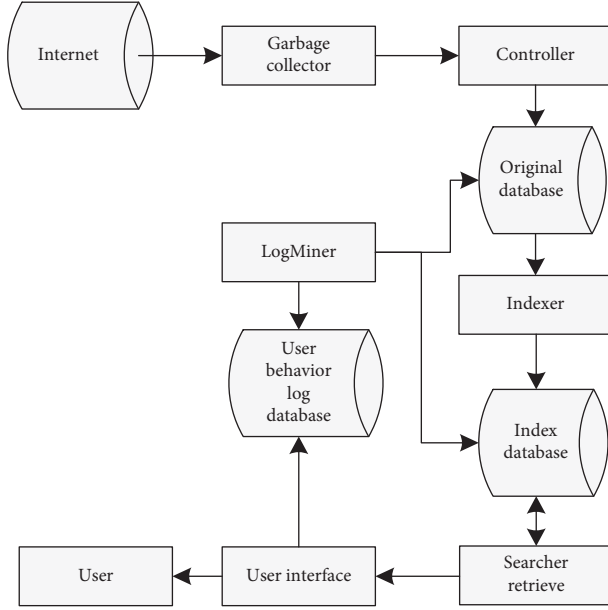


FIGURE 1: The search engine architecture.

limited amount of time, hoping that they will be as important as possible or not to miss those important pages [19].

2.2. Multiaccess Edge Computing Architecture. Edge computing refers to the network edge side, close to the content or data source integration, the core competence of the network, computing, storage, application of distributed open platform, came to the edge of intelligence services and meet the digital industry in agile, real-time business connection, data optimization, application of intelligent, security, and privacy protection of critical requirements [1]. It can serve as a bridge between the physical and digital world, enabling intelligent assets, intelligent gateways, intelligent systems, and intelligent services to be realized. Figure 2 shows the basic architecture of MEC (multiple access edge computing).

It is estimated that deploying the application server at the edge of the wireless network can save up to 35% of the bandwidth on the return line between the wireless access network and the existing application server [20]. Using edge computing cloud architecture, we can reduce 50% network latency in English subject multidimensional resource retrieval. When the processing time of the server is increased by 50~100 ms, the recognition accuracy can be improved by 10%~20% [21–24]. This means that, without improving the existing recognition algorithm, by introducing mobile edge computing technology, the recognition effect can be improved by reducing the transmission delay between the server and the mobile terminal [25, 26]. Therefore, this paper introduces its framework to effectively enhance the energy consumption in the network edge computing of multidimensional resources of English discipline, to maximize the energy efficiency ratio, to save energy, to achieve the optimal distribution of energy, and to maximize the profits of operators.

2.3. Task Computing Model. In order to improve the retrieval efficiency of English multidimensional resources, the components generated by the application partition model can be calculated locally on the terminal device or unloaded to the MEC server [23, 27, 28]. Two calculation models are established as follows:

- (1) Terminal equipment calculation model:

If component j is allocated to the terminal device for calculation, the time and corresponding energy consumption at the terminal are expressed as follows:

$$T_j^l = \frac{l_j}{f_l}, \quad (1)$$

$$E_j^l = P_c T_j^l. \quad (2)$$

l_j represents the calculation requirement of component j , that is, the total number of CPU cycles required. f_l represents the computing power of the mobile device, that is, the number of cycles that can be processed per unit time. P_c is the operating power of the mobile device, in W .

- (2) MEC server computing model:

If component j is allocated to the edge server for calculation, the time calculated at the MEC server and the corresponding terminal equipment energy consumption are expressed as follows:

$$T_j^o = \frac{l_j}{f_o}, \quad (3)$$

$$E_j^o = P_i T_j^o. \quad (4)$$

f_o represents the computing power of MEC server, which is far greater than that of terminal equipment. P_i is the power of the terminal device in the idle state, which is far less than the power calculated by the terminal device.

According to the partition model of application, the value of $e(i, j)$ represents the amount of data transferred from component i to component j . Each component can be calculated at the terminal or MEC server [29–31]. Considering that MEC server can cache the calculation results of front-end components, the time and energy consumed by data transmission between components can be ignored when the components with predependencies and postdependencies are calculated on the terminal device or MEC server at the same time [32, 33]. For existing component j , $\text{pre}(j)$ is used to represent the front-end component of component j . According to the application model, $\text{pre}(j)$ is a set of components. To set the front-end component i , consider the two following situations:

- (1) When $a_i = 0, a_j = 1$, the search time and the corresponding terminal energy consumption of English

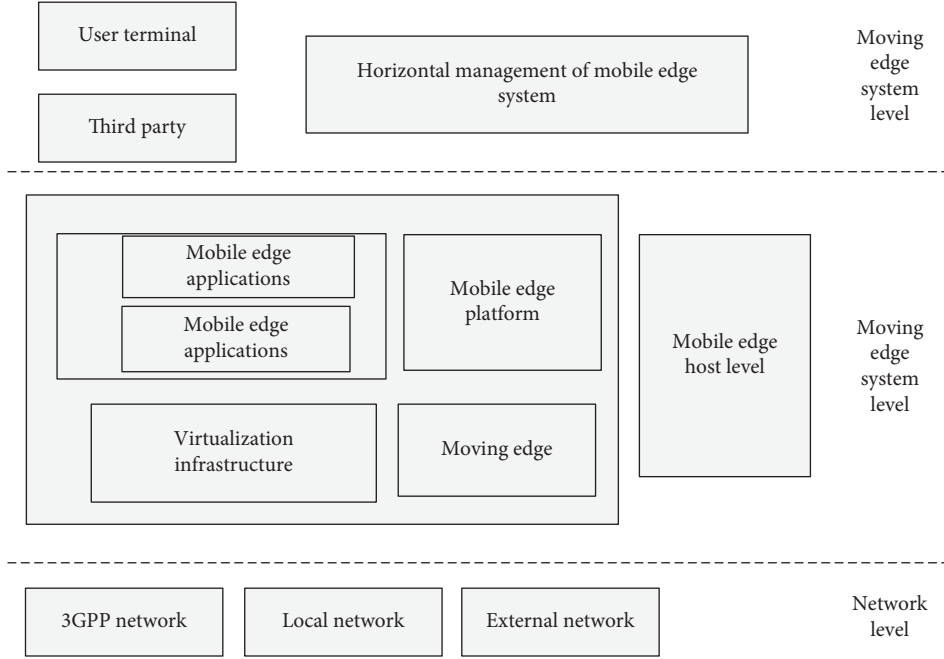


FIGURE 2: Basic structure of MEC.

subject multidimensional resource data are, respectively, as follows:

$$T_{i,j} = \frac{e(i,j)}{r_u}, \quad (5)$$

$$E_{i,j} = P_u T_{i,j}. \quad (6)$$

r_u is the uplink rate of the wireless channel. P_u is the power of the terminal device when searching for data.

- (2) When $a_i = 1, a_j = 0$, the search time and corresponding terminal energy consumption of English subject multidimensional resource data are as follows:

$$T_{i,j} = \frac{e(i,j)}{r_d}, \quad (7)$$

$$E_{i,j} = P_d T_{i,j}. \quad (8)$$

r_d is the downlink rate of the wireless channel. P_d is the power of the terminal equipment when extracting the corresponding data of English subject [34]. The application topology is shown in Figure 3.

The cost of computing English subject multidimensional data search should be based on the energy consumption and latency of all components. Considering the end-user experience, the completion time of the application is taken as the constraint condition, and the energy loss generated by the terminal device is taken as the optimization objective [35]. According to the application partition model, the application may be divided into a large number of components, and the parallel relationship between many

components is not excluded [36]. For example, in the application topology of Figure 3, if the calculation completion time of the component chain “1-3-4” is greater than that of the component chain “1-2-4,” then the calculation delay of the application will be equal to the calculation time of the component chain “1-3-4.” After the calculation of a component is completed, all the data required for the component can be obtained. Therefore, for the current component, the maximum value of the sum of the calculation completion time and data transmission time of all the front-end components is taken as the start time of the calculation. Based on the above analysis, let $\text{pre}(j)$ of component j be $i \in \text{pre}(j)$ and, combined with formulae (1), (3), (5), and (7), the calculation completion time of component j can be expressed as follows:

$$S_j = \max\{S_i + |a_i - a_j|T_{i,j}\} + (1 - a_j)T_j^l + a_jT_j^o. \quad (9)$$

In the above formula, the first term represents the time point when component j starts to calculate, and the second term represents the time consumed by component j in calculation, which is a recursive process. When all components are executed at the terminal, the calculation completion time of component j can be expressed as follows:

$$S_j^l = \max\{S_i\} + T_j^l. \quad (10)$$

If the delay of computing English subject multidimensional resource search time-consuming scheme is greater than that of all local computing, the computational search time is meaningless. Therefore, the delay constraint can be determined as follows:

$$S_m \leq S_m^l. \quad (11)$$

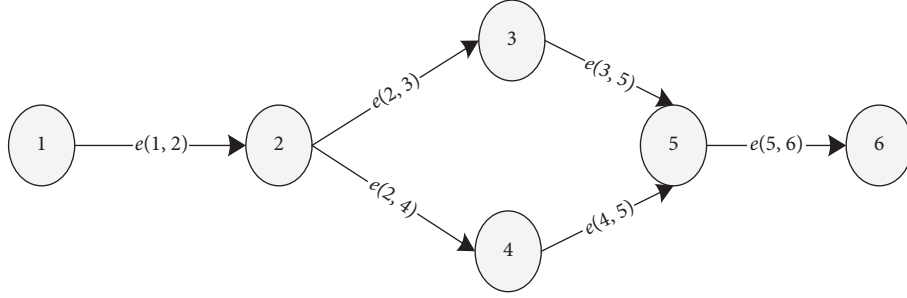


FIGURE 3: Application topology.

Through the above analysis, combined with formulae (1)–(4) and (7), the energy consumption optimization expression of terminal equipment under delay constraint is obtained:

$$\begin{aligned} \min E(A) &= \min \sum \left((1 - a_j) E_j^l + a_j E_j^o \right) + \sum_{j=1}^m \sum_{i \in \text{pre}(j)} |a_i - a_j| E_{i,j}, \\ \text{s.t.} \quad a: S_m &\leq S_m^l, \\ b: a_j &\in \{0, 1\}. \end{aligned} \quad (12)$$

The first term of the above formula represents the energy consumption generated by the terminal equipment when calculating the components of the application. The second term represents the energy consumption generated by terminals when searching for multidimensional resource data of English disciplines among related components. Constraint a means that the latency obtained by the application computing unloading scheme is less than that of the application computing at the terminal. Constraint b means that the component can be calculated on the terminal device or MEC server. Vector $A = [a_1, a_2, \dots, a_m]$ represents the delay optimization of English subject multidimensional resources for each application component.

3. Vertical Search of Multidimensional Resources in English Discipline

3.1. Data Attribute Association Traversal. The vertical search website of English subject multidimensional resources allows users to browse the entities they are interested in. The browsing process is completed by following the links to the result page or list page, where the list page contains a series of links to the entity specific information page (entity page). Let e be a collection of entities, each of which is provided with specific information by vertical search sites. Assuming that each entity can be described by some attributes $A = \{a_1, a_2, \dots, a_m\}$, a vertical search site conceptually queries the entity collection E by using some of the attributes in A . More precisely, the vertical query process returns those entities that satisfy the attribute expression. In order to understand the vertical query process in the form of relational tuples, it is assumed that each entity of set E has a

unique identifier, and T is a data table in the form of $\langle \text{id}, a_1, \dots, a_m \rangle$. In this way, a vertical query process can be expressed as follows:

$$q: \text{SELECT id FROM } T \text{ WHERE } a_1 = v_1, \dots, a_k = v_k. \quad (13)$$

In the above equation, a_1, \dots, a_k is an attribute in the multidimensional resource set A of English discipline, while v_1, \dots, v_k is a constant (i.e., attribute value). Without losing generality, we transform all predicates containing unequal number relations into equality predicates by introducing new attributes. For example, convert the predicate $a_i > 100$ to $a_i > 100 = \text{true}$, where $a_i > 100$ is a new attribute. After processing this way, we only need to focus on the predicate containing only the following form: $a_i = v_i$. We will only focus on the WHERE clause part of the query; that is, $q = \{a_1 = v_1, \dots, a_k = v_k\}$ and mark the entity ID set returned by q as E_q . We use the standard database theory label to identify the inclusion relation of a query; that is, if $E_q \subseteq E_{q'}$, then $q \subseteq q'$. Given a query q , we define its drill down query q' as a query with more attribute constraints than q ; that is, $q' = q \cup \{a_{k+1} = v_{k+1}\}$. Our method will rely on the “drill down” relationship to traverse the query from the vertical search site.

Like other websites, a vertical search site includes a page P and a link l to the page. However, a vertical search site also describes entity collection E and supports vertical query set Q . In particular, each entity has an entity page description. Search and browsing are accomplished by query links that return to list pages, where each query link represents a query in the collection Q , and each list page contains entity pages that point to the query requirements.

Definition 1. (query centered model). A vertical search website is a quad (P, l, e, Q, f) that satisfies the following conditions:

- (1) P is a collection of pages, including entity pages and list pages
- (2) L is a set of links, including query links and other links
- (3) E is a collection of entities described by vertical search sites

- (4) Q is the query set supported by vertical search website
 (5) $f: Q \rightarrow 2^P$

It is a mapping function from a list to the entities it lists. The goal of vertical information extraction is to associate entities with the attributes used in the queries that form them. The difficulty, however, is that queries do not appear explicitly in vertical search sites: the multidimensional resource search method for English disciplines sees only individual pages and the links that these pages contain. Therefore, the vertical information extraction problem required traversing all query q that the site could use and then, for each $q \in Q$, finding $E_q \subseteq E$ satisfying q . Given q and E_q , we can associate the entity set E_q with the attributes defined by Q as long as the qualifying problem is solved.

3.2. Attribute Information Is Searched Vertically Offline. This paper proposes an algorithm that can traverse all multidimensional resource data and find out its related entities. This method first searches the site vertically and then mines the query from the crawling data. According to the assumption that a list page belongs to a query at most, we group known list pages according to the query, and each group belongs to a query. To do this, we need to look at the similarity of the list pages. Formula (2) indicates that the list page contains not only its links to entities but also L_q and Q_q . The set of pages for P_q is often generated using the same mechanism based on a single template. Therefore, although each $p \in P_q$ contains different entity links, links in L_q and Q_q are basically the same because they use the same template and the input q is the same. Given a list page x , we collect all links to x and then strip out all links to physical pages (including some links to physical pages in E_q and L_q) and record the remaining set of links as l_x . Obviously, l_x contains some links between Q_q and L_q . Then, for the two list pages x and y , we compare their similarity using the Jaccard similarity coefficient $|l_x \cap l_y|/|l_x \cup l_y|$. According to the similarity, we can cluster the list pages according to the query. The next question is how to find the queries they represent from the clustered results. Suppose that P_q and P'_q represent the two clusters associated with q and q' . Although the two queries do not know, that is, we do not know the attribute/value pairs they represent, we can determine whether they have the relationship of $q' = q \cup \{a_i = v_i\}$. To do this, we discover the relationship by following these steps. We get E_q and E'_q from P_q and P'_q . This process is not always trivial, as not all links to entities in P_q are in E_q ; however, we can take advantage of additional clues, such as links to entities in Q_q often embedded in the same DOM structure in the list page. Verify whether $E'_q \subseteq E_q$ and $q' \in Q_q$ are true using assumptions. Moreover, for the same reason previously, we determined its $E'_q \subseteq E_q$ by determining whether the Jaccard similarity was close to 1.

$$\text{Jaccard}(q, q') = \frac{|E'_q \cap E_q|}{|E'_q|} \quad (14)$$

If the assumption is true, we determine the attribute/value pair of the query $\{a_i = v_i\}$. Assume that the following page fragment contains a link to q' :

```
<h2>Brand</h2>
...
<a href = http://link-to-query-q'>BVLGARI</a>
...
```

Through the anchor text (“Bvlgari”) in page links, we know that q' is more accurate than q because it contains an extra descriptor “Bvlgari.” Therefore, if we know that “Bvlgari” is a phrase or we find the attribute name “brand” in the DOM structure of the upper link, we can get $q' = q \cup \{\text{Brand} = \text{Bvlgari}\}$. This anchor-based approach is very general. Our survey found that more than 90% of vertical search sites can be processed by analyzing anchor text. Other websites use images instead of anchor text, and our method cannot deal with these websites. When all the query relationships are established, we can get a directed graph, in which each node represents a query, and each edge represents the relationship between queries. In particular, an edge $q_{i-1} \rightarrow q_i$ means that q_i is more refined than q_{i-1} , because the former has an additional condition: $a_i = v_i$. If $q_0 \rightarrow \dots \rightarrow q_k$ is the longest edge in the graph, we get $q_i = \{a_j = v_j | j = 1, \dots, i\}$. Therefore, we can traverse all queries and then complete the vertical search of multidimensional resources of English subject.

4. The Experiment

4.1. Experimental Parameters. According to the computational model, this simulation experiment scenario was set up: there was a small base station with MEC server deployed within a small cell scope, and multiple terminal devices were connected to the base station through wireless channels without considering the interference between channels. MEC server can sense the state of the task to be calculated for each terminal and make multidimensional resources vertical for the terminal. The specific simulation parameters are shown in Table 1.

On the basis of the above parameters, the vertical retrieval experiment is carried out.

4.2. The Acquisition Ratio of Different Methods. In the search engine domain, usually use two indexes to judge the performance of the system. One is the Harvest Rate, also known as precision, which reflects the subject-related accuracy of a web page retrieved. The other is the Target Recall, also known as Recall, which represents the percentage of pages that are recalled for a topic. The calculation method of these two indexes is as follows:

TABLE 1: Simulation parameters.

Parameters to describe	The parameter value
Terminals	25
Base station total bandwidth	8 MHz
Total computing power of MEC server	80 kHz
Signal-to-noise ratio S/N	30 dB
Terminal task data volume	$\sim U(2, 10)$ M
Terminal computing capacity	500 MHz

$$H = \frac{w_c}{s_a} \times 100\%. \quad (15)$$

In the above formula, H represents the harvest ratio of English subject resources, w_c represents the number of subject-related pages retrieved from English subject resources, and s_a represents the total number of pages retrieved from English subject resources.

$$T\% = \frac{w_c}{q_a} \times 100\%. \quad (16)$$

In the above equation, T represents the call rate of English subject resources, w_c represents the number of subject-related web pages retrieved from English subject resources, and q_a represents the number of all subject-related web pages retrieved from English subject resources.

In the experiment, the method in literature [8], the method in literature [9], the method in literature [10], and edge calculation vertical index method were used for collection. Search English resource pages for education and art topics, respectively, and the crawling time was 2 hours each time. The statistical data are shown in Tables 2–5.

From Tables 2–5, we can see the acquisition ratio of English resource web pages under different methods. When the resource type was English for education, the total number of pages of English resources was 123242, the access ratio of edge calculation method was 88.96%, that of the method in literature [8] was 63.74%, that of the method in literature [9] was 55.06%, and that of the method in literature [10] was 61.46%. When the resource type is art English resource, the total number of pages of English resource is 103524, the access ratio of edge calculation method is 95.31%, that of the method in literature [8] is 55.69%, that of the method in literature [9] is 52.78%, and that of the method in literature [10] is 63.41%. In conclusion, the method in this paper can obtain considerable acquisition ratios for resources of different topics. For vertical search, the accuracy of vertical search of multidimensional resources in English subject is generally judged by the harvest ratio, that is, the number of relevant topics to search divided by the total number of pages to search. The call rate is not suitable for vertical search, because the vertical search acquisition is a process of dynamic search page, in the actual cases, because the Internet structure is complex and rapidly changing, to statistics in the web as a whole, or the number of all topics related web pages in a web subset is difficult; for the experiment in this paper, significance is not big but will be the theme of the vertical search in a certain stage search page number as evaluation

index, to reflect the discovery rate of resources. Since the discovery rate of topic resources is in direct proportion to the number of relevant pages searched, the large number of topic pages searched means that the resource discovery rate is high. The resource discovery rate also reflects the resource coverage rate to some extent.

4.3. Recall Rate of Multidimensional Resource Data Search in English Discipline. In order to further verify the data search performance of the search method in this paper, the recall rate of multidimensional resource data in English discipline was obtained by using the method in literature [8], the method in literature [9], the method in literature [10], and the vertical index method of edge calculation. The results are shown in Table 6.

According to Table 6, for the English subject resources data of 20 MB, the search recall rate of English subject multidimensional resource data by the method in literature [8] is 82%, the search recall rate of English subject multidimensional resource data by the method in literature [9] is 81%, the search recall rate of English subject multidimensional resource data by the method in literature [10] is 82%, and the search recall rate of English course multidimensional resource data by the edge calculation method is 95%. For English subject resource data of 50 MB, the search recall rate of English subject multidimensional resource data by the method in literature [8] is 64%, the search recall rate of English subject multidimensional resource data by the method in literature [9] is 67%, the search recall rate of English subject multidimensional resource data by the method in literature [10] is 75%, and the search recall rate of English course multidimensional resource data by the edge calculation method is 97%. The average data search recall rates of the method in literature [8], the method in literature [9], the method in literature [10], and edge calculation vertical index method were 71.7%, 76.8%, 76.5%, and 95.5%, respectively. Analysis of the overall situation shows that the search recall rate of this method is significantly higher than that of the other three traditional methods. This is because this paper uses the multiaccess edge computing architecture to classify the resource information attributes of English disciplines and filter out some non-subject-related information. As a result, the search recall rate of resource data rises.

4.4. Multidimensional Resource Data Search of English Subject Takes Time. In order to verify the search efficiency of resource data, the time of multidimensional resource data search in English subjects was tested by the methods of literature [8], literature [9], literature [10], and the vertical index method of edge calculation, and the results are shown in Figure 4.

Figure 4 shows that when the amount of resource data is 15 MB, English subject multidimensional resource data search by the method in literature [8] took 58 ms, English subject multidimensional resource data search by the method in literature [9] took 52 ms, English subject multidimensional resource data search by the method in

TABLE 2: Vertical indexing methods for edge calculations.

Resource type	A vertical indexing method for edge calculations		
	The total number of pages	Related web pages	Proportion (%)
English resources for education	123242	109631	88.96
Art English resources	103524	98668	95.31

TABLE 3: Vertical indexing methods of literature [8].

Resource type	Method in literature [8]		
	The total number of pages	Related web pages	Proportion (%)
English resources for education	123242	78558	63.74
Art English resources	103524	57648	55.69

TABLE 4: Vertical indexing methods of literature [9].

Resource type	Method in literature [9]		
	The total number of pages	Related web pages	Proportion (%)
English resources for education	123242	67854	55.06
Art English resources	103524	54645	52.78

TABLE 5: Vertical indexing methods of literature [10].

Resource type	Method in literature [10]		
	The total number of pages	Related web pages	Proportion (%)
English resources for education	123242	75743	61.46
Art English resources	103524	65643	63.41

TABLE 6: Recall rates of resource data search under different methods.

English subject resource data volume (MB)	Recall rate of multidimensional resource data search in English discipline (%)			
	Edge calculation method	Method in literature [8]	Method in literature [9]	Method in literature [10]
5	98	67	73	78
10	99	69	78	79
15	97	78	82	69
20	95	82	81	82
25	96	75	85	79
30	97	79	72	73
35	92	81	78	83
40	95	63	76	85
45	93	68	71	71
50	97	64	67	75
55	92	63	82	68
Mean value	95.5	71.7	76.8	76.5

literature [10] took 52 ms, and English subject multidimensional resource data search by the edge vertical index calculation method took 16 ms. When the amount of resource data is 30 MB, English subject multidimensional resource data search by the method in literature [8] took 96 ms, English subject multidimensional resource data search by the method in literature [9] took 69 ms, English subject multidimensional resource data search by the

method in literature [10] took 88 ms, and English subject multidimensional resource data search by the edge vertical index calculation method took 23 ms. When the amount of resource data is 55 MB, English subject multidimensional resource data search by the method in literature [8] took 201 ms, English subject multidimensional resource data search by the method in literature [9] took 154 ms, English subject multidimensional resource data search by the

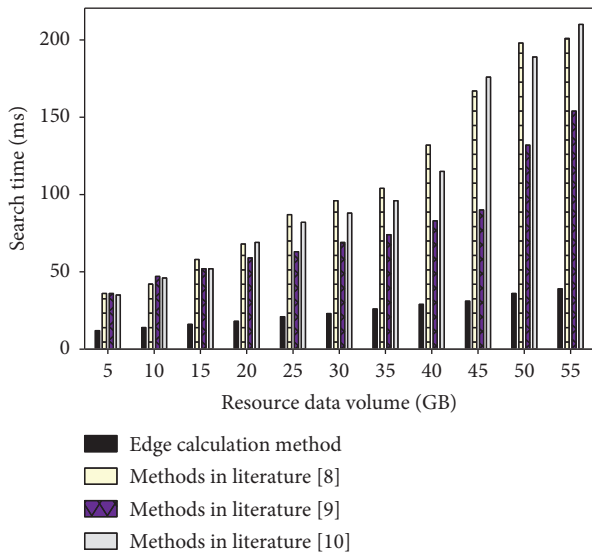


FIGURE 4: Multidimensional resource data search of English subject takes time.

method in literature [10] took 210 ms, and English subject multidimensional resource data search by the edge vertical index calculation method took only 39 ms. The time of multidimensional resource data search of English subject in this paper is much lower than that of other methods and has better search efficiency. This is because the edge algorithm is used to calculate the relevance of web page topics. This method can more accurately determine whether the web page is relevant, so as to obtain better search efficiency.

5. Conclusion

In order to solve the problem that the traditional vertical resource search method is not enough to grasp the whole world and that it is easy to converge too early and fall into the local-optimum trap, a vertical multidimensional resource search method in English subject based on edge calculation is proposed. By introducing the multiaccess edge computing architecture, the vertical search task computing model of multidimensional resources in English discipline is constructed to realize the offline vertical search of attribute information. The following results can be obtained through the experiment:

- (1) When the total number of pages of English resources for educational English resources was 123242, the access ratio of edge calculation method was 88.96%. The total number of pages of art English resources is 103524, and the access ratio of edge calculation method is 95.31%, indicating that the method in this paper can obtain relatively considerable access ratio for different topic resources, and the index effect is better.
- (2) When the amount of resource data of English subject is 50 MB, the recall rate of multidimensional resource data of English subject in edge calculation method is 97%, which indicates that the recall rate of

multidimensional resource data of English subject in this paper is relatively high.

- (3) When the amount of resource data is 55 MB, the search time of multidimensional resource data of English subject by edge calculation vertical index method is only 39 ms, which indicates that the multidimensional resource data search efficiency of English subject proposed in this paper is relatively high.

Based on the above analysis, we can see that the proposed method can effectively improve the performance of the search algorithm. The edge computing is an efficient tool for vertical search method of multidimensional resources in English discipline. In the future, our main work will be to continue using the edge computing method to further improve the search efficiency, so that it can be applied.

Data Availability

The data used to support the findings of this study are available from the corresponding author upon request.

Conflicts of Interest

The author declares that there are no conflicts of interest regarding the publication of this paper.

References

- [1] Y. Fang, "Construction of vertical retrieval system of scientific and technological projects based on elastic stack," *Information Research*, vol. 1, no. 1, pp. 87–91, 2018.
- [2] Y. Li, X. Tang, W. Cai, J. Tong, X. Liu, and G. Wang, "Resource-efficient index shard replication in large scale search engines," *IEEE Transactions on Parallel and Distributed Systems*, vol. 30, no. 12, pp. 2820–2835, 2019.
- [3] Y. Yao, Y. Zhang, T. Zhou et al., "Research and development of medical vertical search engine," *Science and Technology and Innovation*, vol. 109, no. 13, pp. 23–26, 2018.
- [4] L. Luo, "Research on the legal issues involved in the vertical search service on the internet -- taking the image vertical search service as an example," *Science and Technology and Law*, vol. 1, no. 3, pp. 39–45, 2018.
- [5] F. Xu, Q. pan, X. Yu et al., "Wine traceability based on internet vertical search," *China Strategic Emerging Industries*, vol. 140, no. 8, pp. 226–227, 2018.
- [6] Z. Gao, H. Xue, and S. Wan, "Multiple discrimination and pairwise CNN for view-based 3D object retrieval," *Neural Networks*, vol. 125, 2020.
- [7] H. Y. Xioa, H. He, Z. Huang, and C. A. I. Zhao-yang, "Research on employment vertical search engine based on nutch," *Computer Technology and Development*, vol. 29, no. 2, pp. 207–211, 2019.
- [8] S. Wan, X. Xu, T. Wang, and Z. Gu, "An intelligent video analysis method for abnormal event detection in intelligent transportation systems," *IEEE Transactions on Intelligent Transportation Systems*, vol. 5, 2020.
- [9] Z. Xia, "Research on vertical search engine for big data subject based on lucene," *Scientific and Technological Innovation*, vol. 1, no. 31, pp. 96–97, 2019.

- [10] Y. Zheng, E. Zheng, and Z. Ming, "Research and optimization of employment theme search engine based on Heritrix and Solr," *Journal of Qiqihar University (Natural Science Edition)*, vol. 34, no. 4, pp. 13–20, 2018.
- [11] Y. Liu, X. Wang, G. Boudreau, A. B. Sediq, and H. Abou-Zeid, "A multi-dimensional intelligent multiple access technique for 5G beyond and 6G wireless networks," *IEEE Transactions on Wireless Communications*, vol. 20, no. 2, pp. 1308–1320, 2021.
- [12] K. Xie, X. Wang, G. Xie et al., "Distributed multi-dimensional pricing for efficient application offloading in mobile cloud computing," *IEEE Transactions on Services Computing*, vol. 12, no. 6, pp. 925–940, 2019.
- [13] X. Xu, Q. Wu, L. Qi, W. Dou, S.-B. Tsai, and M. Z. Alam Bhuiyan, "Trust-aware service offloading for video surveillance in edge computing enabled Internet of vehicle," *IEEE Transactions on Intelligent Transportation Systems*, vol. 6, 2020.
- [14] X. Xie, J. Mao, Y. Liu et al., "Modeling user behavior for vertical search: images, apps and products," in *Proceedings of the 43rd International ACM SIGIR Conference on Research and Development in Information Retrieval*, Xi'an, China, July 2020.
- [15] Y. B. Yu, S. L. Huang, N. Tashi, and H. Zhang, "A survey about algorithms utilized by focused web crawler," *Journal of Electronic Science and Technology*, vol. 16, no. 2, pp. 35–44, 2018.
- [16] P. Procházka, M. Kocián, J. Drdák et al., "Vertical search blending: a real-world counterfactual dataset," in *Proceedings of the 42nd international ACM SIGIR conference*, Koln, Germany, April 2019.
- [17] W. Bae, S. Lee, Y. Lee et al., "Resource optimized neural architecture search for 3D medical image segmentation," in *Proceedings of the International Conference on Medical Image Computing and Computer-Assisted Intervention*, Springer, Cham, Switzerland, September 2019.
- [18] F. Lu, "Research on lucene Mongolian word segmentation technology based on vertical search engine," *Journal of Inner Mongolia University of Science and Technology*, vol. 37, no. 3, pp. 162–167, 2018.
- [19] X. Xu, X. Zhang, X. Liu, J. Jiang, L. Qi, and M. Z. A. Bhuiyan, "Adaptive computation offloading with edge for 5G-envisioned internet of connected vehicles," *IEEE Transactions on Intelligent Transportation Systems*, vol. 11, pp. 1–10, 2020.
- [20] S. Ding, S. Qu, Y. Xi, and S. Wan, "Stimulus-driven and concept-driven analysis for image caption generation," *Neurocomputing*, vol. 398, pp. 520–530, 2020.
- [21] T. Zhang, "A search algorithm based on chinese word segmentation," *Computer Applications and Software*, vol. 35, no. 10, pp. 9–12, 2018.
- [22] A. S. Yüksel and M. A. Karabiyik, "Vertical search engine for academic publications," in *Proceedings of the International Conference on Cyber Security and Computer Science*, Karabük, Turkey, October 2018.
- [23] Y. Cao, N. Ma, W. Fuchang, and X. He, "Research and design of cross-language vertical search engine for special agricultural E-commerce platform," *MATEC Web of Conferences*, vol. 176, 2018.
- [24] S. Li, Z. Du, H. Yu et al., "A robust multi-circle detector based on horizontal and vertical search analysis fitting with tangent direction," *International Journal of Pattern Recognition and Artificial Intelligence*, vol. 33, no. 4, pp. 1–20, 2019.
- [25] M. Doro, F. Bellini, S. Brigadoi et al., "A bilateral N2pc (N2pcb) component is elicited by search targets displayed on the vertical midline," *Psychophysiology*, vol. 57, no. 3, pp. 22–32, 2020.
- [26] A. Murrieta-Mendoza, L. Ternisien, B. Beuze et al., "Aircraft vertical route optimization by beam search and initial search space reduction," *Journal of Aerospace Information Systems*, vol. 12, no. 6, pp. 1–15, 2018.
- [27] E. Kacprzak, L. Koesten, L. D. Ibáñez, T. Blount, J. Tennison, and E. Simperl, "Characterising dataset search—an analysis of search logs and data requests," *Journal of Web Semantics*, vol. 55, no. 5, pp. 37–55, 2019.
- [28] M. C. W. Janssen, "Vertical contracts in search markets," *International Journal of Industrial Organization*, vol. 70, no. 15, pp. 18–27, 2019.
- [29] J. Arguello and B. Choi, "The effects of working memory, perceptual speed, and inhibition in aggregated search," *ACM Transactions on Information Systems*, vol. 37, no. 3, pp. 1–34, 2019.
- [30] N. Rick, "Vertical resolution, channel count lead users' wish lists," *EE: Evaluation Engineering: The Magazine of Electronic Evaluation*, vol. 57, no. 4, pp. 6–11, 2018.
- [31] Z. Li, "Research and implementation of electronic information vertical search engine," *Digital World*, vol. 1, no. 2, pp. 200–220, 2018.
- [32] Z. Ge, Z. Zhang, and L. Bo, "Application of water conservancy data vertical search based on knowledge map," *Shandong Water Resources*, vol. 1, no. 5, pp. 1–2, 2018.
- [33] Y. Pan, J. Zhou, Y. Peng et al., "Optimization of machine learning hyperparametric debugging through dynamic cloud resource allocation system—a case study of heart sounds," *TANet 2018 Taiwan Internet Symposium*, vol. 20, pp. 1270–1275, 2018.
- [34] S. Wan, Z. Gu, and Q. Ni, "Cognitive computing and wireless communications on the edge for healthcare service robots," *Computer Communications*, vol. 149, pp. 99–106, 2020.
- [35] X. Deng, H. Shao, C. Hu, D. Jiang, and Y. Jiang, "Wind power forecasting methods based on deep learning: a survey," *Computer Modeling in Engineering & Sciences*, vol. 122, no. 1, pp. 273–301, 2020.
- [36] Y. Xi, Y. Zhang, S. Ding, and S. Wan, "Visual question answering model based on visual relationship detection," *Signal Processing: Image Communication*, vol. 80, 2020.

Research Article

A Multipath Processing Technology Based on Multiparameter-Combined Observation in GNSS

T. Y. Zhou^{1,2} and B. W. Lian¹ 

¹School of Electronics and Information, Northwestern Polytechnical University, Xi'an 710129, China

²School of Information, Hunan University of Humanities Science and Technology, Loudi 417000, China

Correspondence should be addressed to B. W. Lian; bwlian@126.com

Received 25 February 2021; Revised 8 April 2021; Accepted 29 April 2021; Published 17 May 2021

Academic Editor: Chi-Hua Chen

Copyright © 2021 T. Y. Zhou and B. W. Lian. This is an open access article distributed under the Creative Commons Attribution License, which permits unrestricted use, distribution, and reproduction in any medium, provided the original work is properly cited.

In the Global Navigation Satellite System (GNSS), the multipath error affected by many aspects is the main error source that affects satellite navigation, and it is difficult to establish a much more accurate model to analyze it. Based on the ground multipath reflection model, it firstly deeply studies the influence of GNSS satellite orbit parameters on multipath fading frequency and establishes a multipath signal model related to satellite orbit parameters. Secondly, the influence of carrier phase cycle slip, receiver clock adjustment, and GNSS satellite orbit on multiparameter- (MP-) combined observations is analyzed in detail based on the measured data. Finally, aiming at the common phenomenon of code-carrier divergence in the Beidou system, the elevation-based pseudorange correction model and a sidereal filtering are built to correct the MP errors; experiments with measured data show that there is a fluctuation range reduction of 35.7% after sidereal filtering when the receiver reaches a steady state.

1. Introduction

The satellite navigation system has become one of the most important technical means in modern navigation and positioning measurement [1, 2]. To pursue more accurate positioning results, it is necessary to analyze the reasons that affect the accuracy of a satellite navigation system and take targeted measures to reduce and correct the relevant errors and obtain a better positioning performance [3, 4]. There are many factors which will affect the positioning error of satellite navigation, among which ionospheric error and tropospheric error can be eliminated by differential technique or some mathematical methods [5, 6]. However, the multipath error is affected by many aspects, and it is difficult to establish a more accurate model for it and eliminate it by the general method, so multipath error has become the main error source that affects satellite navigation [7, 8]. As early as the GPS demonstration test, the influence of the multipath effect on satellite ranging performance and positioning results was considered by the designers. The mathematical relationship between the multipath effect and pseudorandom code tracking derived by

Hagerman in 1973 is the basis of multipath effect analysis. In the late 1970s, the researchers tested the multipath effect and its effect on the receiver [9, 10]. The influence of the multipath effect on short baseline carrier phase differential positioning was studied by MIT and Draper laboratories in the early 1980s. For GPS systems, the effect of the multipath effect on carrier phase differential positioning can be reduced to several centimeters by averaging the observation results greater than 1 hour [11, 12]. Since then, with the deepening of the research, the research on multipath effect in the field of satellite positioning and navigation mainly focuses on the environment and channel modelling, multipath measurement technology, anti-multipath antenna, anti-multipath receiver digital signal processing technology, anti-multipath data postprocessing method, and multipath research under the new signal system and evaluation of anti-multipath performance. Based on the traditional antenna design, an antenna technology with a standing wave ratio below 1.5 m is studied by using L feed and double-layer structure in [4]. A technique of adding parasitic circular metal patch as the top-loaded antenna is studied based on a prefeed network in [11].

2. Literature Review

Multipath is the main systematic error of the GNSS short baseline positioning. Multipath error cannot be eliminated by the double-differenced technique and is difficult to parameterize, which severely restricts the high-precision GNSS positioning application. A correlation reconstruction algorithm for energy compensation under the BOC system is studied in [13]. A time-division multiplexing dual reference waveform multipath suppression algorithm for TmBOC signals is studied in [14]. Based on Bayesian estimation, a multipath estimation technique of the particle filter algorithm is studied in [15]. Based on maximum likelihood estimation, an off-line mesh search and online iteration method is studied in [16] to suppress short multipath delay. In [17], the authors propose a new multipath mitigation strategy in the coordinate domain that shakes off the formation mechanism of multipath; a convolutional neural network (CNN) long short-term memory (LSTM) method is used to mine the deep multipath features in GNSS coordinate series. An advanced receiver autonomous integrity monitoring (ARAIM) method is proposed to evaluate GNSS integrity in [18], which mainly focuses on validating whether the multipath error model in the ARAIM algorithm is conservative enough for GEO satellites. In [19], the authors address the problem of GNSS multipath mitigation using antenna arrays, in which a new data-dependent beamforming technique is proposed, which is based on the well-known Capon beamformer. This technique aims to avoid the typical cancellation phenomenon between signal and correlated multipaths, by exploiting the known power of the direct signal at the receiver. To this effect, a measure of the correlation between the signal and multipaths is obtained in the matrix form, and it is then subtracted from the spatial correlation matrix of the received signal. This results in a new spatial correlation matrix that is used for the final Power-Based Capon beamformer. The behaviour of this technique is justified mathematically, and it is supported by several numerical results.

Here, this paper establishes a much more accurate multipath signal model, and the basic ideas can be concluded as follows: firstly, the influences of GNSS satellite orbit parameters on multipath fading frequency are studied and analyzed, and a multipath fading frequency model related to satellite orbit parameters is established. Secondly, the MP-combined observations are extracted by the code subtraction carrier phase, and the influences of carrier phase cycle slip, receiver clock correction, and GNSS satellite orbit to MP observations are analyzed by measured data. Finally, the elevation correlation pseudorange correction model and sidereal filtering are used to correct the common code-carrier divergence phenomenon in the Beidou system. The rest of the paper is organized as follows. In Section 3, the mathematical model of multipath signals is established. In Section 4, the MP-combined observations are analyzed. In Section 5, the suppression of MP signals is discussed. Finally, in Section 6, we conclude our work.

3. Mathematical Model of the Multipath Signal

3.1. Fading Frequency of the Multipath Signal. Considering generality, assume that the satellite signal reaches the receiver at the same time as the reflected signal, and the received synthetic signal $s(t)$ can be described as

$$s(t) = p(t)\sin(\omega_0 t) + |\Gamma|p(t - \Delta t)\sin(\omega_0 t + \Delta\phi_m(t)), \quad (1)$$

where $p(t)$ is the signal amplitude (or spread spectrum code or message), $|\Gamma|$ is the attenuation coefficient, Δt is the multipath delay (s), ω_0 is the angular frequency of the direct signal and contains the influence of the doppler shift $\Delta\omega_0 = 2\pi\Delta f_0$, $\Delta\phi_m(t) = \Delta\varphi_m + (\Delta\omega_m - \Delta\omega_0)t$ is the phase difference between the reflected signal and the direct signal, where $\Delta\varphi_m$ is the initial phase of the reflected signal, $(\Delta\omega_m - \Delta\omega_0)$ is the Doppler frequency difference between the reflected signal and the direct signal, and $|\Gamma|$, Δt , and $\Delta\phi_m(t)$ describe the basic characteristics of the synthesized signal.

Due to the relative motion between the antenna of the ground receiver and the satellite, the multipath delay Δt and phase difference $\Delta\phi_m(t)$ will change randomly with time, which will cause the change of the carrier frequency of the reflected wave and produce an increment $\Delta f_m(t)$ on the carrier nominal frequency, which is called multipath fading frequency. According to the relationship between the frequency and phase of the sinusoidal signal, $\Delta f_m(t)$ can be expressed in [10]:

$$\Delta f_m(t) = \frac{1}{2\pi} \frac{d\Delta\phi_m(t)}{dt} = \frac{1}{2\pi} \frac{d[\Delta\varphi_m + (\Delta\omega_m - \Delta\omega_0)t]}{dt}. \quad (2)$$

It can be seen from equation (2) that $\Delta f_m(t)$ depends on the Doppler frequency difference $(\Delta\omega_m - \Delta\omega_0)$; when it changes rapidly with time, the relative speed between the ground receiving antenna and the satellite will be relatively fast, and $\Delta f_m(t)$ will be larger.

3.2. Multipath Reflection Model. The multipath reflection model (see Figure 1), in which $\theta^s(t)$ is the elevation angle of the

satellite at t time in the Earth-centered Earth-fixed (ECEF) coordinate system. A is the phase center of the user receiver, whose height from the ground is h , R is the incident point of the reflected signal, and $L_{\text{LOS}}(t)$ and $L_{\text{NLOS}}(t)$ represent the propagation path length of the direct signal and reflected signal, respectively.

Since the satellite is far from the satellite, it is generally considered that the direct signal is parallel to the reflected signal, and the vertical line of the direct signal and the reflected signal is made at R ; with the vertical foot is D , the multipath geometric distance delay of the reflected signal relative to the direct signal $L(t)$ can be expressed as follows:

$$L(t) = |L_{\text{NLOS}}(t) - L_{\text{LOS}}(t)| = |AR|(1 - \cos 2\theta^s(t)) = \frac{h}{\sin \theta^s(t)} \cdot 2 \sin^2 \theta^s(t) = 2h \cdot \sin \theta^s(t). \quad (3)$$

According to equation (3), $L(t)$ is a function of antenna height h and satellite elevation angle $\theta^s(t)$. According to the theory of electromagnetic wave propagation, the relative phase of multipath $\Delta\phi_m(t)$ is explained in [11]:

$$\Delta\phi_m(t) = \frac{2\pi L(t)}{\lambda} = \frac{4\pi h \cdot \sin \theta^s(t)}{\lambda}, \quad (4)$$

where λ is the signal wavelength.

Combine equations (4) with (2), the multipath fading frequency $\Delta f_m(t)$ can be rewritten as

$$\Delta f_m(t) = \frac{1}{2\pi} \frac{d\Delta\phi_m(t)}{dt} = \frac{2h}{\lambda} \cdot \frac{d[\sin \theta^s(t)]}{dt}. \quad (5)$$

3.3. Satellite Orbital Parameters. In ECEF coordinates, the geometric relationship between the satellite orbits and Earth (see

Figure 2, in which, R_e is the radius of the Earth whose center is O , and the GNSS receiver antenna is placed at A , a point on the ground (which can fall at any point in the sphere; for easy drawing, it is placed at the north pole, the vector OA point to zenith). P is the level plane where the user A is, S represents the spatial position of the satellite relative to the Earth at t time, whose projection point on the horizontal P is D , $r(t) = \|AS\|$ is the line of sight distance between the user and the satellite, $R_s = \|OS\|$ represents the geometric distance between the geocentric center O and the satellite, and the satellite elevation angle $\theta^s(t)$ is the angle between AS and AD at time t .

According to the geometric relation shown in Figure 2 and the cosine theorem, it can be obtained that

$$\sin \theta^s(t) = \frac{R_s^2 - R_e^2 - r^2(t)}{2R_e \cdot r(t)}. \quad (6)$$

where α is the inclination angle of the satellite's orbit, w_e is the rate of the Earth's self-rotation, w is the distance of the orbit near the Earth's angle, and w^s is the angular rate of the satellite.

For the convenience of analysis, we define a Kepler multipath fading (Kepler Multipath Fading, KMPF) factor $\kappa(t)$:

$$\kappa(t) = \frac{e \sin f^s}{\sqrt{1 + e^2 + 2e \cos f^s}} V \cos \alpha. \quad (13)$$

Combine (5) with (6), then $\Delta f_m(t)$ can be represented as

$$\Delta f_m(t) = -\frac{2h}{\lambda} \left(\frac{1}{R_e} + \frac{\sin \theta^s(t)}{r(t)} \right) r'(t), \quad (7)$$

where h , λ , R_e , $\theta^s(t)$, and $r(t)$ can be regarded as known, that is, $\Delta f_m(t)$ mainly depends on the unknown $r'(t)$, which can be understood as the relative velocity in the direction of the signal propagation.

Let $K = -(2h/\lambda)((1/R_e) + (\sin \theta^s(t)/r(t)))$, equation (7) can be simplified as

$$\Delta f_m(t) = Kr'(t). \quad (8)$$

For a ground static receiver, let \vec{v}^s represent the satellite velocity and \vec{I} represent the unit observation vector, then $r'(t)$ can be regarded as the projection of the satellite velocity on \vec{I} , that is [10],

$$r'(t) = v^s \cdot \cos \beta, \quad (9)$$

where β is the angle between \vec{v}^s and \vec{I} and satisfies

$$\cos \beta = \frac{e \sin f^s}{\sqrt{1 + e^2 + 2e \cos f^s}} \cos \gamma, \quad (10)$$

where f^s is the true near point angle of the satellite and γ is the angle between the satellite observation vector and geocentric distance vector.

Based on the transformation theory of the coordinate system, v^s can be expressed as

$$v^s = \frac{R_s}{\sqrt{2}} V, \quad (11)$$

where

$$V = \sqrt{(w_e^2 + w^{s2})(1 + \cos^2 \alpha) - 4w_e w^s \cos^2 \alpha + [w_e^2 \cos 2(w^s t + w) + w^{s2}] \sin^2 \alpha}, \quad (12)$$

Combine equations (8)-(10) and (13), we can conclude

$$\Delta f_m(t) = K\kappa(t)R_s \cos \gamma \cos^{-1} \alpha. \quad (14)$$

4. MP-Combined Observations

4.1. Extraction of MP. GNSS pseudorange and carrier phase observation equations can be expressed, respectively, as [12]

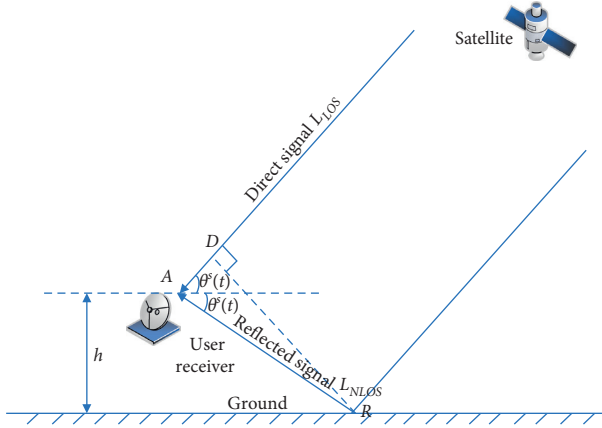


FIGURE 1: A multipath reflection model.

$$P = \rho + c(dt_r - dT^s) + c(T + I + M_p + v_p + HW) + URE + \varepsilon_p, \quad (15)$$

$$\begin{aligned} \Phi = \lambda f = \rho + c(dt_r - dT^s) + c(T - I + M_\phi + v_\phi + HW) \\ + URE + \varepsilon_\phi + \lambda N, \end{aligned} \quad (16)$$

where M_p and M_ϕ are the specular reflection of pseudorange and carrier phase, respectively, v_p and v_ϕ are the diffuse reflection of pseudorange and carrier phase, respectively, HW is the time delay of the processor, and URE is the deviation of the satellite orbit.

Ignore the carrier phase errors ε_ϕ , v_ϕ , and M_ϕ with very small values; the difference between pseudorange and carrier phase observation at the same frequency, also named as multiparameter(MP)-combined observation, can be obtained as follows:

$$(P - \Phi)_{\text{adj}} = c(2I + v_p + M_p) + \varepsilon_p - \lambda N, \quad (17)$$

where the ionospheric delay $2cI$ can be modified with a double-frequency ionospheric correction method described in [13].

The carrier multipath error can be ignored, for its maximum multipath error is much smaller than that of code multipath error [14]. Hence, the MP-combined observation is usually used to describe the multipath signal. According to the method mentioned above, the modified MP_{f_i} of f_i frequency with dual-frequency ionospheric method can be described as

$$MP_{f_i} = (P_{f_i} - \phi_{f_i})_{\text{adj}} - 2cI_{f_i} = \varepsilon_p + c(v_p + M_p) - \lambda N. \quad (18)$$

Since the transformation factor between time and distance is a constant c , there is no distinction between the two different physical quantities representing time and distance without confusion in the GNSS positioning field. Therefore, equation (18) can be further simplified as follows:

$$MP_{f_i} = (P_{f_i} - \phi_{f_i})_{\text{adj}} - 2cI_{f_i} = \varepsilon_p + v_p + M_p - \lambda N. \quad (19)$$

4.2. Effect of Carrier Phase Cycle Slip on MP Observations. If there are cycle slips in the carrier phase of the observations, the calculated carrier phase ionospheric delay is inaccurate, which will, in turn, affect the MP value; in particular, a continuous small cycle slip will cause fluctuations in the MP values. Hence, it is necessary to analyze and detect the influence of the carrier phase slip on MP values. The dual-frequency carrier phase method and ionospheric residual method are generally used to detect the cycle slip [15]. Here, the double-frequency pseudorange observations are used for cycle slip detection.

For the convenience of analysis, the smaller error term in the phase measurement equation is ignored, and the carrier phase measurement equation described in equation (16) can be simplified as follows:

$$\phi = \rho + c(\delta t_u - \delta t^u) + c(T - I) + \lambda N. \quad (20)$$

The phase observations of two adjacent epochs at times t and $t + 1$ are calculated; most of the ionospheric and tropospheric delays can be eliminated without the carrier phase slip [16], and the carrier phase difference $\Delta\phi$ can be expressed as

$$\Delta\phi = \phi^{t+1} - \phi^t = \Delta\rho + c[(\delta t_u^{t+1} - \delta t^{u(t+1)}) - (\delta t_u^t - \delta t^{u(t)})]. \quad (21)$$

The two-frequency phase observations for GPS $L1$ and $L2$ satisfies

$$\Delta\phi_{L1}\lambda_1 - \Delta\phi_{L2}\lambda_2 = 0. \quad (22)$$

Let

$$v = \Delta\phi_{L1} - \frac{\lambda_2}{\lambda_1} \Delta\phi_{L2}. \quad (23)$$

Technically, the cycle slip search of MP observations can be carried out in two steps: firstly, the severe cycle slips and signal tracking interruption are detected with a threshold of 5σ or above [20], where σ is the mean square error (MSE) of carrier phase difference, marked in the output results and repaired in sections. According to the all-day data collected from Beidou on January 3rd in 2018, the cycle slips and their influences on MP of SV5 B1 are shown in Figure 3.

In Figure 3, the X axis represents epoch time (s) or samples and (a) and (b) show the first difference of ionospheric residuals before and after cycle slip repair, respectively, whose Y axis represents the ionospheric residual (m). The red horizontal line in (a) is the severe cycle slip search threshold, while the blue pulse is the severe cycle slip and tracking interruption that needs to be repaired. The green horizontal line in (b) is the position where the small cycle slips appear. The threshold is chosen according to [21]. (c) is the ionospheric residual curve, in which the Y axis represents the ionospheric residual value, the red asterisk is the location of the severe cycle slip and tracking interrupt, and the green circle is the location where the small cycle slips occur. (d) is the final MP observations, where the blue and red curves correspond to $B1$ and $B2$ frequencies, respectively.

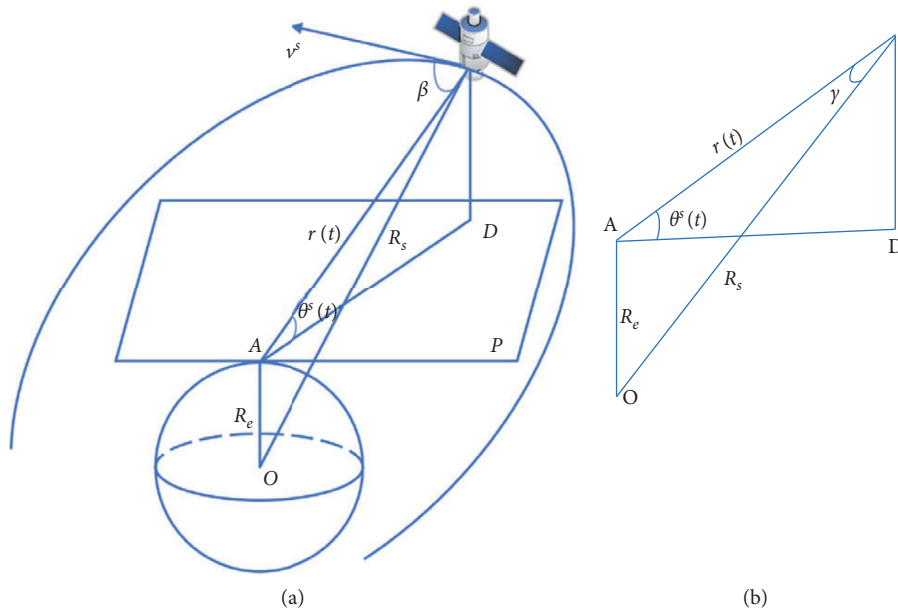


FIGURE 2: Geometric relationship between the Earth and the satellite orbits. (a) 3D model. (b) Local Magnification Diagram.

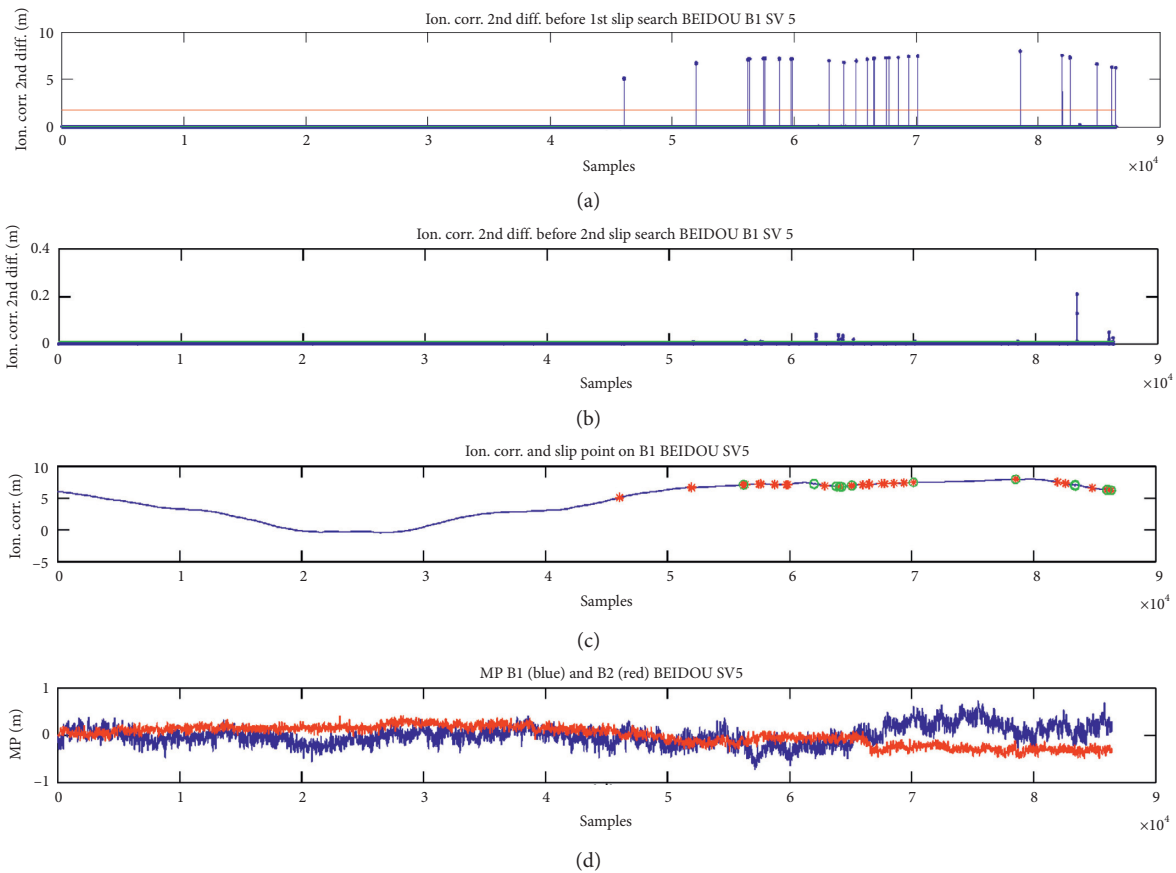


FIGURE 3: Effect of the carrier phase cycle slip on MP observations.

4.3. *Effect of Receiver Clock Adjustment on MP Observations.* There are usually two methods for the receiver to deal with the local clock [21]: one is to use an interval clock adjustment

when the cumulative error reaches a certain threshold (such as 0.5 ms), the local clock is set back or forward twice the threshold (1 ms), and the other is to use a continuous clock

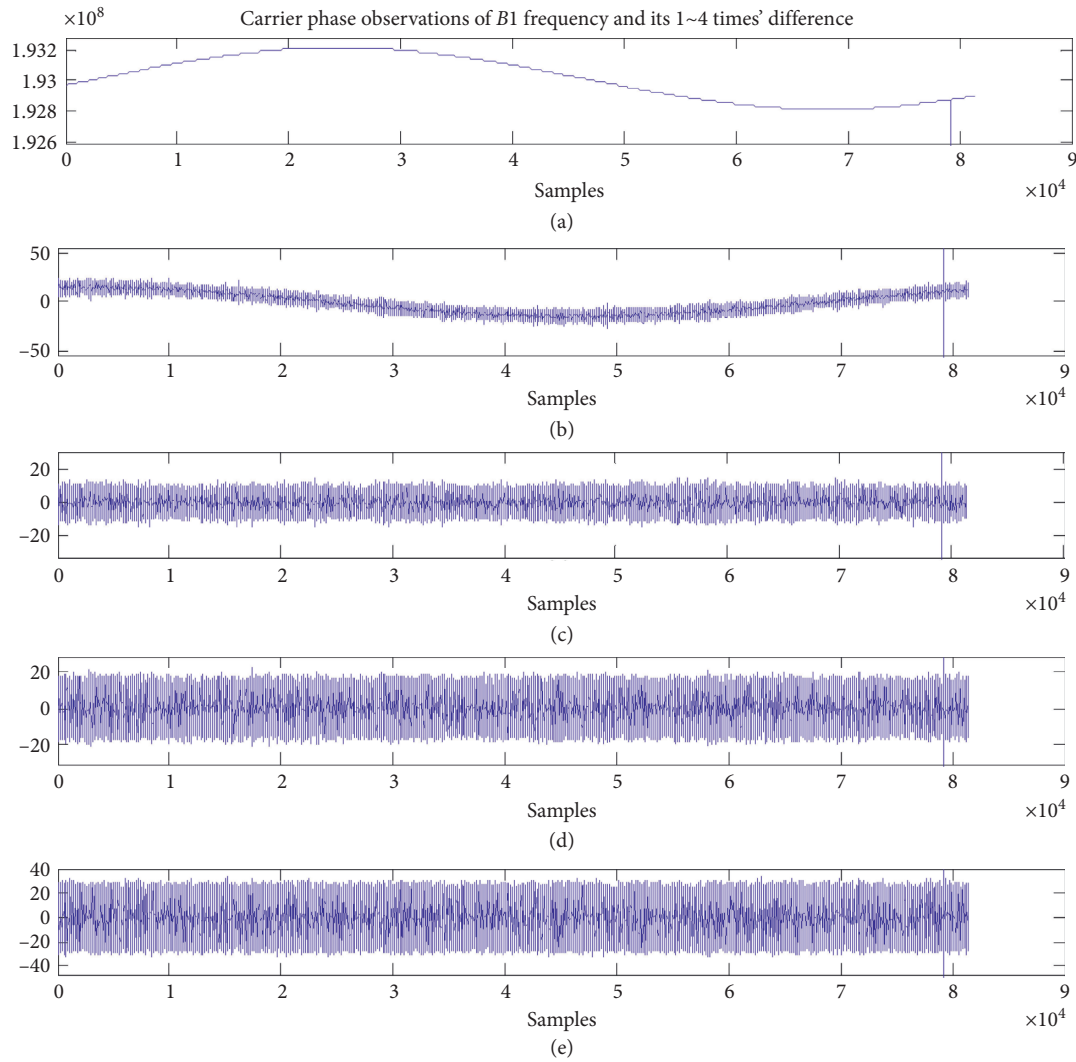


FIGURE 4: The all-day carrier phase observations of B1 frequency.

adjustment, which adjusts the local clock immediately after the completion of positioning, keeping synchronization with the satellite. The effects of clock adjustment on MP observations in the Aerospace Star receiver are shown in Figures 4 and 5.

In Figure 4, X-axis represents epoch time (s) or samples, Y-axis represents the carrier phase observations of B1 frequency (m) and (a)–(e) are the carrier phase observations of B1 frequency and its 1–4 times' difference, respectively.

In Figure 5, the X-axis represents epoch time (s) or samples, (a) and (b), Y-axis represents the ionospheric residual (m), which is the first difference of ionospheric residuals before and after the cycle slip repairment, respectively, where the red and green horizontal lines are the cycle slip detection thresholds. (c) is the ionospheric residual curve, where the red mark indicates the location of the cycle slip, and (d) is the final MP observations. It can be seen from Figures 4 and 5 that there is no serious cycle slip with the ionospheric residuals, and the high order difference results of the carrier phase are stable within ± 20 cycles.

4.4. MP Observations of IGSO/MEO/GEO Satellites

4.4.1. MP Observations of IGSO/MEO Satellites. There exists code and carrier divergence in the MP observations of Beidou IGSO/MEO satellites which is related to the elevation angle. In the process of satellite transits, the MP decreases gradually with the increase of the elevation angle, and conversely, the MP value increases with the falling of the elevation angle [21]. According to the MP measurement theory, the reason for the decrease of the MP is that the pseudorange measurements are small or the carrier phase measurements are too large. The all-day MP observations of Beidou IGSO (PRN6~10) and MEO (PRN11/14) satellites collected with the Zhongda receiver at the self-built station of Northwest Polytechnic University on June 7th in 2015 are shown in Figure 6.

The MP observations of SV193 L1 frequency and Beidou PRN6 B1 frequency of Quasi-Zenith Satellite System (QZSS) observed at IGS JFNG and IGS XMIS stations on January 3rd in 2016 are shown in Figure 7.

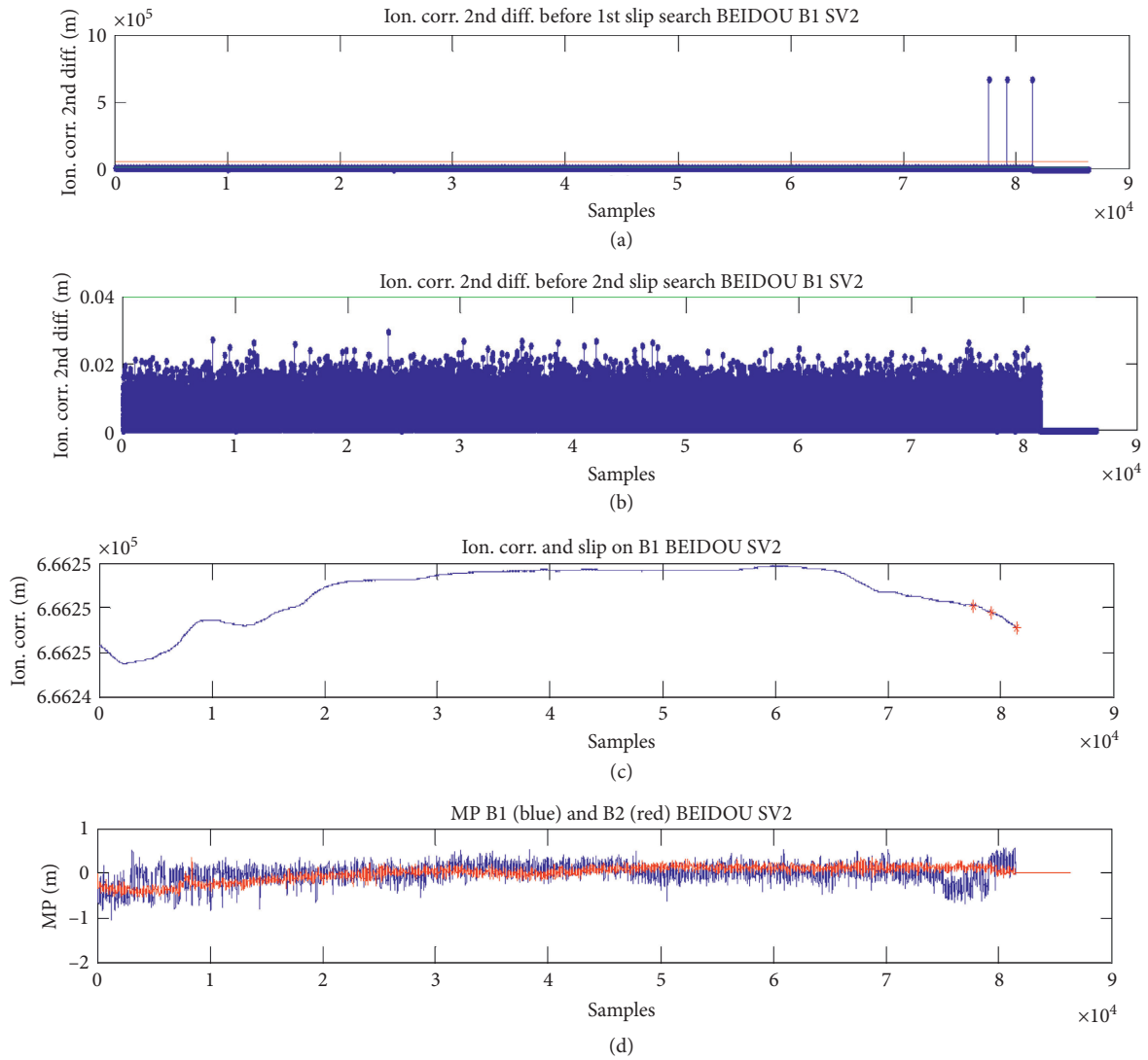


FIGURE 5: The ionospheric residuals and MP observations before and after cycle slip repair.

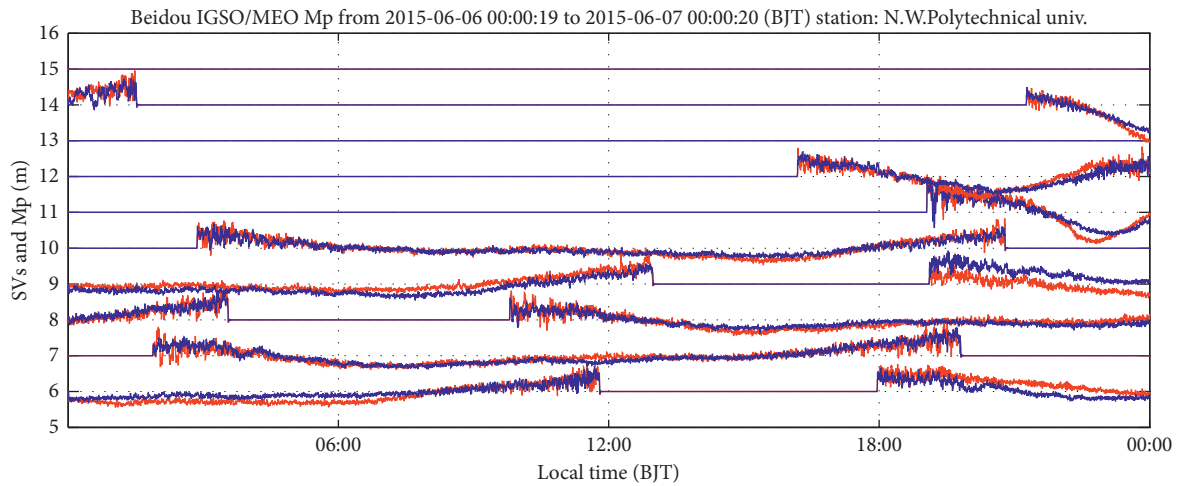


FIGURE 6: MP observations of Beidou IGSO/MEO satellites (red: B2 frequency; blue: B1 frequency).

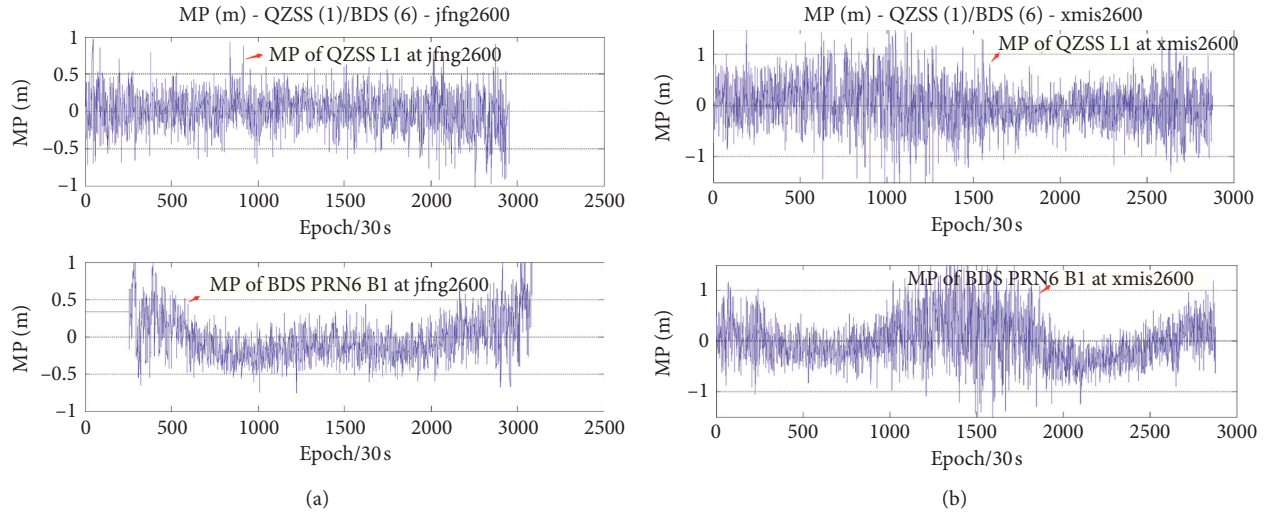


FIGURE 7: MP observations of Beidou PRN6 and QZSS. (a) MP observations of QZSS L1 and Beidou PRN6 B1 at IGS JFNG station. (b) MP observations of QZSS L1 and Beidou PRN6 B1 at IGS XMIS station.

All the data in Figures 6 and 7 are collected with the same receiver. The analysis of the IGS MEGX data shows that there are no obvious changes related to the elevation angle in the MP observations of QZSS, which is independent of the multipath environment and its surrounding area and more inclined to come from the satellite itself.

4.4.2. MP Observations of GEO Satellites. MP observations of GEO satellites are more complex than that of IGSO; the GEO satellites of the Satellite-Based Augmentation System (SBAS) also emit L1 and L5 dual-frequency signals. The MP change law of the SBAS system is different from that of Beidou GEO satellites. MP observations of SBAS S127 collected at CUT0, JFNG, and MAYG stations with an elevation of 16°, 17°, and 71°, respectively, are shown in Figure 8.

The MP values after the 2500 epoch in Figure 8 change strongly for both L1 and L5, and the fluctuation period of L5 is 2 hours at the same time in the receiver of the three different stations, which is caused mainly by the satellite signals. The fluctuation of L1 decreases with the increase of the elevation angle.

5. Suppression of MP Signals

5.1. Pseudorange Correction Model Based on Elevation. MP observations of Beidou satellites show a change related to elevation, which is called the code-carrier divergence phenomenon [21]. In Section 4, a mathematical model of pseudorange multipath error is established, which can be applied to MEO, IGSO, and GEO satellites. But it does not consider the code-carrier divergence phenomenon of the Beidou satellite, so a statistical model based on elevation can be used to describe the code and carrier divergence of Beidou IGSO and MEO satellites. Instead of considering the cause of code and carrier divergence, the model only repairs it statistically. The GPS SVN49 satellite launched in March 2009

also showed a code and carrier divergence; different from that of Beidou, the code and carrier divergence of the L1 frequency of SVN49 is not obvious when the elevation is less than 40°; otherwise, it increases with the elevation; however, the code and carrier divergence of L2 frequency will decrease first and then increase when the elevation exceeds 40°. Hauschild et al. [22] collected the orthogonal signal of GPS SVN49 with a high gain antenna, separated the delay, relative amplitude, and phase difference of the multipath signal on L1 and L2 by impulse response and chip shape, explained the origin of the multipath by the GPS satellite antenna parameters and radiofrequency circuit structure, and, finally, reproduced the MP fluctuation and code-carrier divergence with these parameters.

Using the above model, the simulation results of MP fluctuation of the GEO satellite are illustrated (see Figure 9).

Based on the statistical analysis of the measured MP, an elevation-based pseudorange correction model is established with B1, B2, and B3, three frequencies, using the continuous observations for several cycles, which is shown in detail (see Table 1).

Because of the ambiguity of carrier phase observation, the MP value is a relative quantity, and its average value is artificially set to zero. Therefore, the absolute value of the pseudorange correction cannot be obtained when the elevation pseudorange correction model is established based on the MP observations. That is, if a constant is added to the pseudorange correction Δp in the model, the modified MP value remains unchanged, but the location results may change.

5.2. Sidereal Filtering Based on Satellite Elevation. Usually, the multipath error period of the GEO satellite is between 86184 and 86201 seconds, which is very close to a stellar day period (86164 seconds). Therefore, to weaken the influence of multipath error on positioning, a sidereal filtering is often used to correct the pseudorange observation.

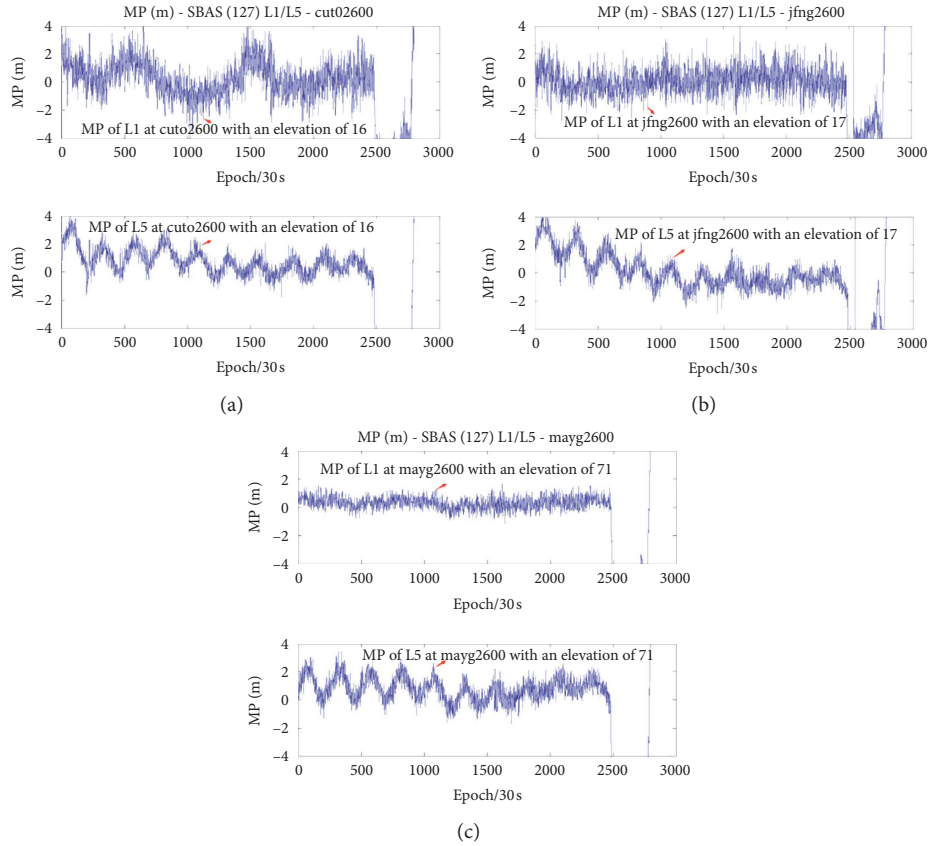


FIGURE 8: MP observations of SBAS S127. (a) CUT0 Station. (b) JFNG Station. (c) MAYG Station.

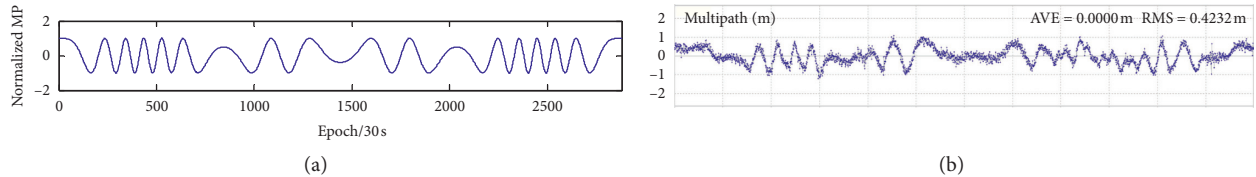


FIGURE 9: MP observations of the GEO satellite. (a) Simulation data. (b) Measured data.

TABLE 1: Pseudorange correction Δp (m) [21].

Elevation (deg)	B1: MEO	B2: MEO	B3: MEO	B1: IGSO	B2: IGSO	B3: IGSO
0	-0.47	-0.40	-0.22	-0.55	-0.71	-0.27
10	-0.38	-0.31	-0.15	-0.40	-0.36	-0.23
20	-0.32	-0.26	-0.13	-0.34	-0.33	-0.21
30	-0.23	-0.18	-0.10	-0.23	-0.19	-0.15
40	-0.11	-0.06	-0.04	-0.15	-0.14	-0.11
50	0.06	0.09	0.05	-0.04	-0.03	-0.04
60	0.34	0.28	0.14	0.09	0.08	0.05
70	0.69	0.48	0.27	0.19	0.17	0.14
80	0.97	0.64	0.36	0.27	0.24	0.19
90	1.05	0.69	0.47	0.35	0.33	0.32

The main principle of the sidereal filtering is to use the strong correlation of the two consecutive days' data to correct the multipath error. Usually, the data features of the first day are extracted to correct the data for the second day. Due to the difference of 236 seconds between a stellar day

and a solar day, it is necessary to translate the previous day's data when using a sidereal filtering [23]. The principle of the sidereal filtering is shown in Figure 10.

The pseudorange MP fluctuation of Beidou GEO and IGSO satellites can be alleviated with a sidereal filtering. In

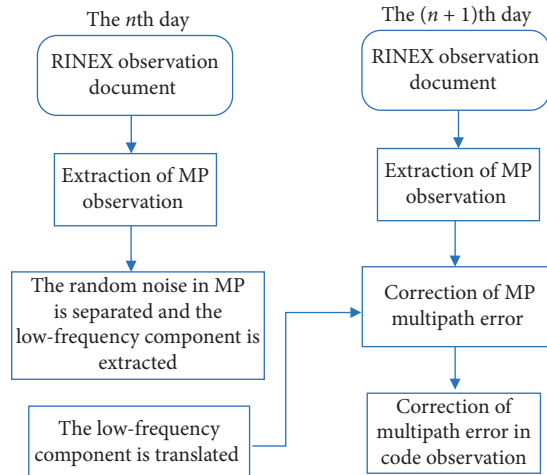


FIGURE 10: Working principle of the sidereal filtering.

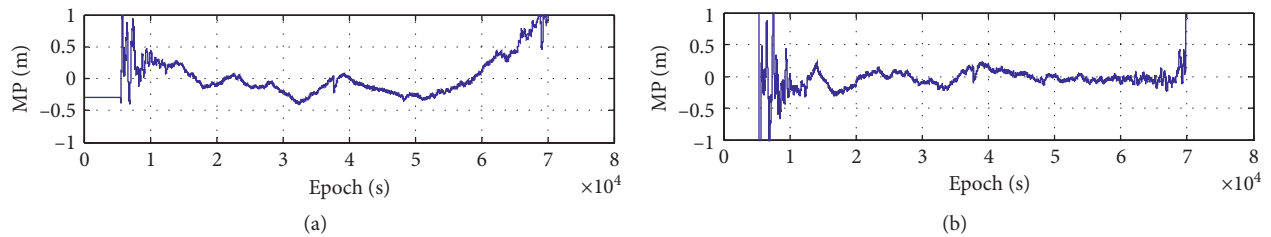


FIGURE 11: MP observations before and after the correction of sidereal filtering. (a) Original MP observations. (b) Revised MP observations after sidereal filtering.

the elevation-based pseudorange correction model, the mean value of the all-day pseudorange measurement must remain unchanged; the pseudorange measurement noises of the two consecutive days are independent, even if the low-pass filter has filtered out the high-frequency component of the noise; the cost of the sidereal filtering is the increase of the measurement noise.

Data of Beidou C06 collected with the Trimble BD930 receiver on October 7th and 8th in 2018 is used for analysis; the MP observations before and after the correction of sidereal filtering are shown in Figure 11, where the MP observations range within $(-0.4, 1)$ m before sidereal filtering, but after sidereal filtering, the MP observations range within $(-0.3, 0.2)$ m with a fluctuation range reduction of 35.7% when the receiver reaches a steady state.

6. Conclusions

In GNSS systems, satellite multipath interference is a non-negligible factor restricting the overall performance of the satellite navigation systems. Based on the ground multipath reflection model, it deeply studies the influence of GNSS satellite orbit parameters on multipath fading frequency and establishes a multipath signal model related to satellite orbit parameters. Through collecting the measured data of different stations and satellites, the influence of carrier phase cycle slip, receiver clock adjustment, and GNSS satellite orbit on MP observation is analyzed in detail. The

statistical analysis of the measured data shows that the multipath fading characteristics of the IGSO satellite and the MEO satellite are related to the satellite elevation, and there is a code-carrier divergence phenomenon, which is not obvious in the GEO satellite. Finally, aiming at the common phenomenon of code-carrier divergence in the Beidou system, the elevation-based pseudorange correction model and a sidereal filtering are built to correct the MP errors, and finally, the measured data are used to verify the model. The MP model built in this paper explains the source of the periodic fluctuation of the MP value but does not explain the phenomenon of Beidou satellite code-carrier divergence. Also, the elevation model and sidereal filtering can be used to repair code-carrier divergence in precise single point positioning, but its practical application is very limited. So it is necessary to study the cause of code-carrier divergence and establish a widely used MP model in the future.

Data Availability

The data used to support the findings of this study are included within the article.

Conflicts of Interest

The authors declare that there are no conflicts of interest regarding the publication of this paper.

Acknowledgments

This work was supported in part by the National Major Fundamental Research Program of China (Grant no. GFZX0301040115), National Natural Science Foundation of China (Grant no. 61571188), and Construct Program of the Key Discipline in Hunan Province.

References

- [1] Y. Liu, B. Lian, and T. Zhou, "Gaussian message passing-based cooperative localization with node selection scheme in wireless networks," *Signal Processing*, vol. 156, pp. 166–176, 2019.
- [2] A. Kumar and A. K. Singh, "A novel multipath mitigation technique for GNSS signals in urban scenarios," *IEEE Transactions on Vehicular Technology*, vol. 69, no. 3, pp. 2649–2658, 2020.
- [3] T. Y. Zhou, Y. Cheng, and B. W. Lian, "Research on high-precision passive localization based on phase difference changing rate," *Concurrency and Computation Practice & Experience*, vol. 31, no. 23, Article ID e4492, 2019.
- [4] C. Chen, G. Chang, N. Zheng, and T. Xu, "GNSS multipath error modeling and mitigation by using sparsity-promoting regularization," *IEEE Access*, vol. 7, pp. 24096–24108, 2019.
- [5] T. Y. Zhou, B. W. Lian, S. Q. Yang et al., "Improved GNSS cooperation positioning algorithm for indoor localization," *Computer, Materials & Continue*, vol. 56, no. 2, pp. 225–245, 2018.
- [6] C. H. Chen, F. Y. Song, F. J. Hwang et al., "A probability density function generator based on neural networks," *Physica A: Statistical Mechanics and Its Applications*, vol. 541, Article ID 123344, 2020.
- [7] Y. Y. Liu, B. W. Lian, and T. Y. Zhou, "Gaussian message passing-based cooperative localization with node selection scheme in wireless networks," *Signal Processing*, vol. 156, pp. 166–176, 2018.
- [8] T. Y. Zhou, B. W. Lian, D. D. Yang et al., "Research on GPS geometry-based observational stochastic error model," *Journal on Communications*, vol. 40, no. 9, pp. 1–12, 2019.
- [9] Y. Wang, Y. Wu, and Y. Shen, "Joint spatiotemporal multipath mitigation in large-scale Array localization," *IEEE Transactions on Signal Processing*, vol. 67, no. 3, pp. 783–797, 2019.
- [10] P. Wu, B. Lian, Y. Song, and Z. Yue, "Study on multipath effect of GEO satellite in bei dou navigation satellite system," in *Proceedings of the China Satellite Navigation Conference (CSNC) 2016 Proceedings*, pp. 347–358, Singapore, April 2016.
- [11] H. Ko, B. Kim, and S.-H. Kong, "GNSS multipath-resistant cooperative navigation in urban vehicular networks," *IEEE Transactions on Vehicular Technology*, vol. 64, no. 12, pp. 5450–5463, 2015.
- [12] C.-H. Chen, "A cell probe-based method for vehicle speed estimation," *IEICE Transactions on Fundamentals of Electronics, Communications and Computer Sciences*, vol. 103, no. 1, pp. 265–267, 2020.
- [13] D. Li, P. Zhang, J. Zhao et al., "MP mitigation in GNSS positioning by GRU neural networks and adaptive wavelet filtering," *IET Communications*, vol. 13, no. 17, pp. 1–10, 2019.
- [14] W. Mu, Z. Wang, L. Guo, and Y. Liu, "A framework of multipath mitigation with joint multipath-Doppler diversity for RF relative measurement," *Institute of Electrical and Electronics Engineer Access*, vol. 8, pp. 166839–166851, 2020.
- [15] J. Park, S. V. Veetil, M. Aquino, L. Yang, and C. Cesaroni, "Mitigation of ionospheric effects on GNSS positioning at low latitudes," *Navigation*, vol. 64, no. 1, pp. 67–74, 2017.
- [16] G. Hu, L. Ni, B. Gao, X. Zhu, W. Wang, and Y. Zhong, "Model predictive based unscented kalman filter for hypersonic vehicle navigation with INS/GNSS integration," *Institute of Electrical and Electronics Engineer Access*, vol. 8, pp. 4814–4823, 2020.
- [17] Y. Tao, C. Liu, T. Chen et al., "Real-time multipath mitigation in multi-GNSS short baseline positioning via CNN-LSTM method," *Mathematical Problems in Engineering*, vol. 2021, Article ID 6573230, 12 pages, 2021.
- [18] J. Chang, X. Zhan, Y. Zhai, S. Wang, and K. Lin, "Analysis of BDS GEO satellite multipath effect for GNSS integrity monitoring in civil aviation," *Aerospace Systems*, vol. 23, 2021.
- [19] M. M. Caballú, A. L. Swindlehurst, and G. S. Granados, "Power-based capon beamforming: avoiding the cancellation effects of GNSS multipath," *Signal Processing*, vol. 180, pp. 1–9, 2020.
- [20] L. Wanninger and S. Beer, "BeiDou satellite-induced code pseudorange variations: diagnosis and therapy," *GPS Solutions*, vol. 19, no. 4, pp. 639–648, 2015.
- [21] B. W. Parkinson, *Multipath Effects Global Positioning System* American Institute of Aeronautics and Astronautics, Washington, DC, USA, 1996.
- [22] A. Hauschild, O. Montenbruck, S. Thielert, S. Erker, M. Meurer, and J. Ashjaee, "A multi-technique approach for characterizing the SVN49 signal anomaly, part 1: receiver tracking and IQ constellation," *GPS Solutions*, vol. 16, no. 1, pp. 19–28, 2012.
- [23] S. Thielert, M. Meurer, S. Erker, O. Montenbruck, A. Hauschild, and P. Fenton, "A multi-technique approach for characterizing the SVN49 signal anomaly, part 2: chip shape analysis," *GPS Solutions*, vol. 16, no. 1, pp. 29–39, 2012.

Research Article

Design of Enterprise Management System Based on Edge Computing Architecture

Yongzhong Yang,¹ Zheng Mei,¹ Benxia Zheng,² and Shuoli Qiu ¹

¹School of Sichuan University, Chengdu Sichuan 610041, China

²Sichuan Vocational College of Finance and Economics, Sichuan Chengdu 610101, China

Correspondence should be addressed to Shuoli Qiu; hujiheng@stu.scu.edu.cn

Received 9 February 2021; Revised 23 March 2021; Accepted 24 April 2021; Published 3 May 2021

Academic Editor: Hsu-Yang Kung

Copyright © 2021 Yongzhong Yang et al. This is an open access article distributed under the Creative Commons Attribution License, which permits unrestricted use, distribution, and reproduction in any medium, provided the original work is properly cited.

In the current enterprise management system, the coupling relationship between enterprise management and operation and maintenance database is not considered, which leads to many system vulnerabilities, slow running speed, and long response time. An enterprise management system based on edge computing architecture is designed. According to the characteristics of mobile edge computing, we design the architecture of the edge computing platform, integrate the MEC virtualization infrastructure layer, MEC platform layer, and MEC application layer, construct the edge computing model, reflect the coupling relationship between enterprise management and operation and maintenance database, calculate the delay vector of the enterprise management server, and complete the parameter calculation of enterprise management and operation and maintenance system. This paper analyzes the feasibility, objectives, and users and functional requirements of the enterprise management system, designs the functional structure of the system, realizes the design of the public module, function menu module, and login module, adopts the SQL database management system, and designs the database and data table, so as to realize the design of the enterprise management system based on edge computing architecture. Experimental results show that the proposed method has fewer system vulnerabilities and can effectively speed up the system operation speed and shorten the system response time.

1. Introduction

Enterprise informatization is an important means to improve the speed of modernization. In order to speed up the informatization construction and modernization process of the government and enterprises, government departments need to introduce the office automation system to improve the office efficiency and transparency of government staff [1]. It is not enough for an enterprise to only introduce a system. It also needs to introduce a complete and comprehensive information management platform, increase the depth and strength of enterprise informatization, and strive to make the enterprise develop healthily and rapidly in the fierce international market competition under the guidance of information, so as to play a positive role in the industrialization and modernization of the enterprise [2]. The introduction of the information management platform is the best choice for enterprises and companies, especially for

production and sales enterprises, to realize their information strategy. Through the introduction of the information enterprise management platform, we can introduce the most advanced modern management ideas and methods in the world. Therefore, the enterprise information management platform is a powerful tool to help enterprises develop, make enterprises step into the modern enterprise management mechanism, and strengthen the market competitiveness of enterprises. Although there is a great demand for information management software in the current market, the information management software obtained according to the previous development method has to be redeveloped when the business changes or the demand changes slightly, resulting in a huge waste of human and financial time [3]. Therefore, how to improve the software productivity and software quality of the information management platform, on the basis of realizing complex software requirements and improving software quality, to improve software

productivity has become the consistent pursuit of many information management platform developers.

The process of enterprise management informatization is accelerating, and the application of the information system has a profound impact on enterprise management. The competition among enterprises is becoming more and more fierce. More and more enterprises realize the importance of information and management system in improving the enterprise management level, reducing enterprise operating costs, improving service quality, and meeting customer needs. At present, the research on the enterprise management system has also made great progress. Ducq et al. [4] proposed the design of the enterprise performance measurement system, using a group of specific performance indicators, and grouping them in the coherent system of the performance measurement system. The design objectives and basis are different, and each method has its advantages and disadvantages. It can measure the performance optimally. In this paper, the main concepts of various methods are described. Introduce as many new methods as possible, describe them in detail, and compare them so that decision makers can choose one or more methods that suit their needs. The system can effectively achieve the global goal of PMS design and implementation. The authors of [5] proposed the management design of the last planner system in the enterprise construction stage, studied and discussed the designers, engineers and managers sharing their knowledge and solving design related problems during the site meeting, the influence of using LPS in the design stage on the site meeting discussion in the construction stage, and the video records of 17 site meetings in the BIM transformation project to share their professional knowledge to solve the outstanding problems. This method can develop more collaborative design management methods and practices. However, the above method does not consider the coupling relationship between enterprise management and operation and maintenance database, which leads to many system vulnerabilities, slow running speed, and long response time. The growing computing power on intelligently connected things and devices requires the decentralization of cloud computing to avoid unnecessary latency and take full advantage of the available computing power at the edge of the network. Literature [6] analyzes existing works to identify their role in decentralized cloud and future computing development. Growing service demands for terminal devices may overwhelm installed MECs, and cost constraints limit the increase in installed MEC computing and data storage capacity. Literature [7] divides the device-enhanced MEC mechanism into computational offload mechanism and cache mechanism and further subdivides the offload mechanism and cache mechanism according to the target performance target. In addition, literature [7] identifies the main limitations of the existing device-enhanced MEC mechanism and outlines future research directions.

The Mobile Cloud Computing (MCC) [8] is a precedent for edge and fog computing. It defines the concept of a proximal cloud, which provides tighter computing power to avoid latency on the mobile devices it serves. Many writers have taken advantage of this connection. Examples are Bilal

et al. [9], Satyanarayanan [10], and Satyanarayanan et al. [11]. The first steps towards decentralization of cloud computing are being achieved through the emergence of fog [12] and edge computing [13]. These are believed to be rooted MCC [9, 11]. The OpenFog Consortium in its reference architecture refers to the fact that fog computing is often misnamed as edge computing and debates the different levels of cloud interaction, layers, and aspects handled. A recent publication of the OpenFog Consortium blog expands this definition, arguing that fog computing is a continuum or range from cloud computing and edge computing to device computing.

To solve the above problems, the enterprise management system based on edge computing architecture is designed. By designing the edge computing platform architecture and integrating the MEC virtualization infrastructure layer, MEC platform layer, and MEC application layer, the edge computing model is constructed, and the server delay vector is calculated. This paper analyzes the requirements of the enterprise management system, designs the system function structure, realizes the design of the public module, function menu module, and login module, adopts the SQL database management system, designs the database and data table, and realizes the design of the enterprise management system based on edge computing architecture. The system has fewer loopholes, which can effectively speed up the operation of the system and shorten the response time of the system.

2. Edge Computing Technology

2.1. Concept and Characteristics of Edge Computing. Mobile edge computing (MEC) technology refers to the deployment of general servers on the wireless access side, which provides it with cloud computing capabilities for the wireless access network [14]. MEC technology allows direct mobile communication between edge core network and mobile terminal enterprise users. Each mobile terminal enterprise user has its corresponding MEC core network. The wireless access network thus has the ability of low delay, high bandwidth transmission, and open wireless network information perception, avoiding bottlenecks and system failures. At the same time, the computing task and data sink, i.e., localization deployment, can effectively reduce the computing load and storage load of the mobile system, so as to realize the purpose of optimizing the operation cost of the mobile network. In addition, mobile operators can form a new industrial chain with mobile cloud platform, application developers, and network equipment manufacturers to cooperate and benefit together through the mobile edge computing platform.

According to the white paper published by the European Telecommunication Standardization Association, the characteristics of mobile edge computing are as follows:

- (1) Locality: MEC platform can access local resources and run independently from other parts of the core network. This isolation from other parts of the network also makes the MEC network less vulnerable to external attacks.

- (2) Proximity: mobile edge computing intelligent base station is deployed in the nearest location from the mobile terminal, which has the advantage of acquiring, analyzing, and mining big data. Accordingly, it is also beneficial to the need for computer computing power.
- (3) Reduce latency: the mobile edge computing intelligent base station service is deployed in the nearest location from the mobile terminal equipment, which can isolate the core network from the mobile network data. Therefore, this isolation brings high bandwidth, low latency, and high-quality enterprise user experience.
- (4) Location awareness: distributed devices under the jurisdiction of the mobile edge computing intelligent base station can use low-level signaling to realize information sharing with the intelligent base station, so as to find the location of each distributed device.
- (5) Network context information: mobile edge computing can be applied to the business model of some specific applications, which can benefit from both application service providers and application service enterprise users. Based on the real-time information of the wireless access network, the congestion degree and bandwidth occupation degree of the wireless cellular network can be estimated, which will assist such applications to make decisions to improve the quality of service.

2.2. Architecture Design of the Edge Computing Platform. The MEC system platform in this paper integrates the MEC virtualization infrastructure layer, MEC platform layer, and MEC application layer. The architecture of the mobile edge computing platform is shown in Figure 1.

In the MEC virtualization infrastructure layer, edge devices are connected through a variety of networks (such as mobile cellular network, local network, and external network), and enterprise management data interaction is realized through a variety of communication methods. In the MEC platform layer, virtualization infrastructure and MEC applications are integrated. Virtualization infrastructure has the function of infrastructure service, which provides diversified and efficient runtime and hosting environment for the application of the enterprise management data program [15]. Its infrastructure service controller can control the work of the enterprise management platform, give full play to its application advantages, and provide more secure and reliable enterprise management application resources and safe program running environment. In this facility, a virtual device application is installed in the virtual device, which can run on top of the enterprise management infrastructure service. In the above system, the enterprise management platform service facilities have strong compatibility in the application platform services and are suitable for a variety of services to smoothly complete the collection, analysis, application, and processing of enterprise management data.

The MEC application layer is an important layer in the MEC platform, including the ME host set in operator network architecture and ME algorithm model necessary for enterprise management ME application, which can allocate MEC tasks and control the operation of the whole enterprise management system [16]. By using MEC technology, it can provide highly distributed computing environment and information storage function in the enterprise information management platform, so as to effectively reduce network delay and improve the quality of enterprise user experience.

2.3. Edge Computing Model. In edge computing, the algorithm can directly reflect the coupling relationship between different parameters in the enterprise management database and operation and maintenance database and edge computing system. In practical application, analyzing the requirements of enterprise management application scenarios and mapping them to the parameters of the classification model can help enterprise users quickly select the best edge computing system of target application scenarios. The structural characteristics of the edge computing model are shown in Figure 2.

When calculating the enterprise management and operation and maintenance system, it includes the following steps: firstly, obtain the data information in the enterprise management database and the enterprise operation and maintenance system database information, the data information includes the enterprise management ability and operation level, and the enterprise management ability data includes the load data and transfer data. Operation level data includes comprehensive index data, equipment level data, and equipment operation status data [17]. When measuring enterprise management and operation, we usually measure the resource consumption required by the data enterprise application server to start a session, and delay information about the start of the MEC server.

Next, by constructing the resource consumption and enterprise application service delay model required by the enterprise application server to start the session, the session delay vector d_{ijm} of the enterprise application service can be further calculated. When calculating the session delay vector, the model is constructed as follows:

$$d_{ijm}(c_i) = \frac{\varphi_i}{1 + \sigma_i e^{-\omega_i c_i}}. \quad (1)$$

In formula (1), d_{ijm} is the time delay for data calculation when the program i is running in the jm enterprise management server in the mobile edge computing network m . φ_i , σ_i , and $e^{-\omega_i c_i}$ are represented as the first, second, and third regression parameters, respectively, i is the program startup session, and c_i is the amount of CPU resources required by the edge device for program startup calculation i .

When calculating the delay vector of the enterprise management server, for the convenience of calculation, it is represented by the letter $d_{i,mjm,p}$, and the formula calculation model is

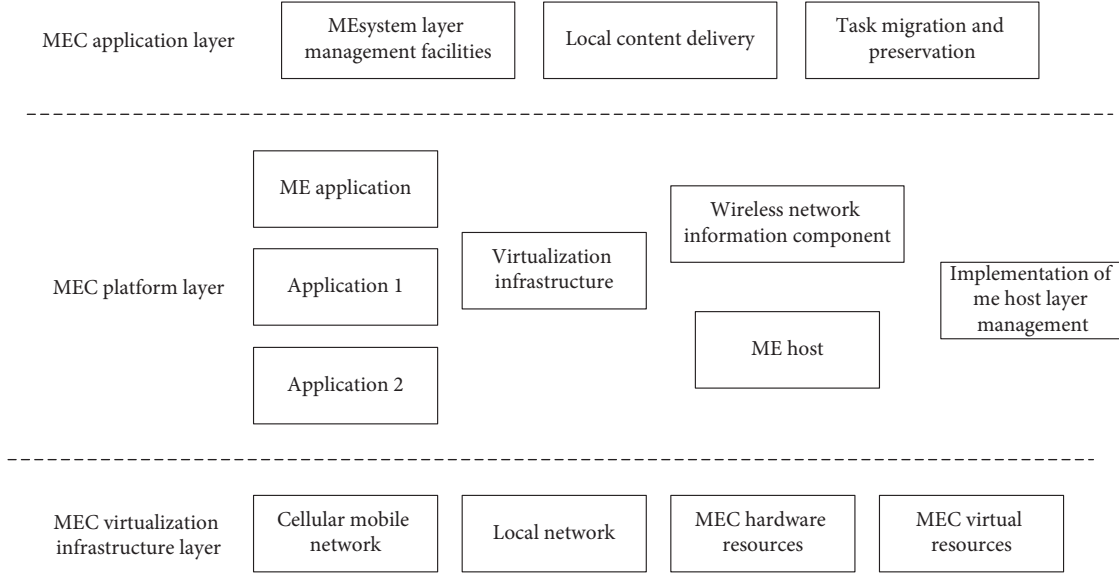


FIGURE 1: Architecture of the edge computing platform.

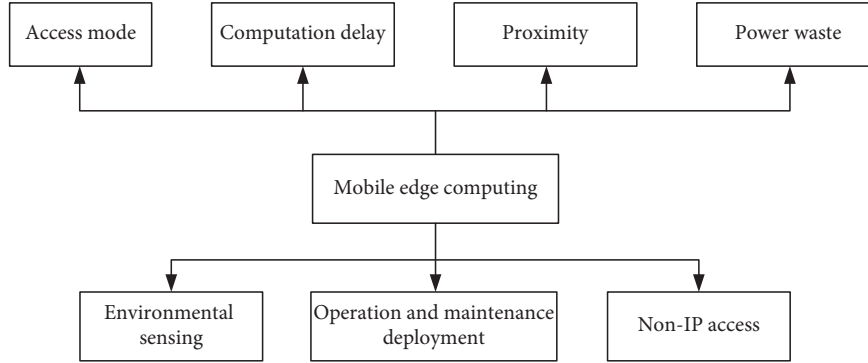


FIGURE 2: Structural features of the edge computing model.

$$d_{i,mjm,p} = \frac{1}{2} \left[\left(\text{RTT}_{i,jm,p} - \text{RTT}_{i,m,p} \right) - \left(T_{jm,s} - T_{jm,a} \right) \right]. \quad (2)$$

In formula (2), $d_{i,mjm,p}$ is the network delay of enterprise management operation. More specifically, the delay is the time delay for connecting the core switch m and the enterprise management server jm to start the session i in the enterprise management, in the m information communication network, and in the p data communication path [18]. $\text{RTT}_{i,m,p}$ is the round-trip delay for the i session between the controller used in the network configuration and the m switch in the p path. $\text{RTT}_{i,jm,p}$ is the round-trip delay of the i session between the controller used by the network configuration and the enterprise management server jm in the p path. $T_{jm,s}$ is the sending time of the enterprise management server jm message, and $T_{jm,a}$ is the arrival time of the message.

When calculating the delay vector of the enterprise management server group, it is represented by $d_{i,mm,p}$, and the model formula is

$$d_{i,mm,p} = T_{\alpha} - T_s - \frac{1}{2} \left(\text{RTT}_{i,n,p} - \text{RTT}_{i,m,p} \right). \quad (3)$$

In formula (3), $d_{i,mm,p}$ is the network delay, that is, in the p communication path, and the core switch m is connected to the core switch n to start the network delay of the session i . $\text{RTT}_{i,m,p}$ is the round-trip delay of the i session between the controller and switch m in the p communication path, and $\text{RTT}_{i,n,p}$ is the round-trip time of the i session between the controller and switch n in the p path extension. T_{α} is the time from the controller to switch m , and T_s is the time sent by switch n .

Then, express the relationship between the session delay vector, the enterprise management server delay vector, and the enterprise management server group delay vector through the objective function. The function is expressed as

$$O_{\text{total}} = \sum_{i=1}^{N_{gm}} \sum_{j=1}^{N_{sm}} \sum_{m=1}^{N_m} \left[\alpha_i \left(\sum_{p=1}^{N_{pm}} d_{i,mjm,p} x_{i,mjm,p} \right) \right] + \left[\beta_i \left(\sum_{p=1}^{N_{p,mm}} d_{i,mm,p} y_{i,mm,p} \right) + \gamma_i d_{ijm} z_{ijm} \right]. \quad (4)$$

In formula (4), N_m is the number of networks m used for mobile edge computing, N_{sm} is the number of enterprise management servers s used in the mobile edge computing network m , and N_{gm} is the mobile edge computing network m , where the enterprise management server starts the number of sessions i , N_{pm} is the number of p paths between the switch and the enterprise management server in the mobile edge computing network m , and $N_{p,mm}$ is the number of p paths between the mobile edge computing network m and n . α_i , β_i , and γ_i are expressed as the first, second, and third weighting factors of the objective function, where γ_i is obtained according to $1 - \alpha_i - \beta_i$, and $x_{i,mjm,p}$, $y_{i,mm,p}$, and z_{ijm} are expressed as the first, second, and third decision variables. Through the above formula calculation, the calculation of various parameters in the enterprise management and operation and maintenance system is realized.

3. Requirement Analysis of the Enterprise Management System

Requirement analysis refers to the detailed investigation of the objects to be dealt with, clear user needs, to determine the purpose of new system functions [19]. Requirement analysis is the first stage of the database structure design, and it is also a very important stage. In this stage, it is mainly to investigate, collect, and analyze the information requirements, processing requirements, and security and integrity requirements of users in data management. Information requirement refers to the content and nature of information users need to obtain from the database.

3.1. System Feasibility Analysis. In order to realize the better management of the enterprise, the enterprise needs to have a good management system, realize the scientific and effective management of employees, check the inventory status in real time, adjust the quantity of inventory materials, supply materials for the production of products, and feed back the completion of the plan in time after the completion of the products. The enterprise management system is designed based on the edge computing framework. This system integrates the database technology and edge computing technology, makes the database system an important organic part, and realizes the organic combination of database technology and edge computing technology. The system can be analyzed from three aspects: economic feasibility, technical feasibility, and operation feasibility:

- (1) Operation feasibility: because this system is an information system developed for enterprise employees, although these employees may not have used a similar system, with the friendly interface of Windows and the good security settings of this system, users can quickly master the operation

method of the system under the guidance and help of the navigation column of the enterprise management website. At the same time, users can learn to use the system correctly according to the detailed “user manual.”

- (2) Technical feasibility: from the current popular database development and management software point of view, for the information management system related to the database, using edge computing architecture development and MySQL in the database, is the most appropriate solution in practical application. The development members are very skilled in using this technology and can develop this system well from the technical point of view.
- (3) Economic feasibility: the main way to improve the management level is to update the ideas of managers and enhance the scientific understanding of management activities [20]. At the same time, the use of mature information technology, the development of the network office system, is an effective measure to deepen the reform of enterprise management. Enterprises need to build their own company management personnel management system. In order to make the system development smoothly, it provides a lot of financial support.

3.2. System Objective Requirement Analysis. As an enterprise personnel management platform, the enterprise management system should meet the following goals in design:

- (1) Based on mature technology to create the system: whether the construction goal of the enterprise management system can be achieved and whether the whole investment of the system can play its due benefits will ultimately depend on whether the system is reliable and practical. Therefore, mature and reliable technology should be adopted in the system, and the design principle and implementation method of productization should be implemented.
- (2) Conducive to the improvement of the information resource-sharing rate: the enterprise management system is based on LAN or Internet, striving to achieve high-level information resource sharing and cross-platform information resource access. Due to the different platforms and databases of network information systems and resource subsystems, the system structure must have the mechanism of cross-platform access to different data sources to solve the information sharing of different resource subnets and improve the occupancy rate of information resource sharing.
- (3) The system is simple, easy to use, and maintain: the design of the enterprise personnel management

system should meet the needs of enterprise management, with complete and practical functions and an easy to learn, friendly, and clear interface. The network structure should be simple, clear, and easy to manage. These measures can fully realize the management functions of the product company. It provides a convenient and quick information query function for users.

- (4) Safe and reliable performance: the enterprise management system should have a safe and efficient communication mechanism, identity authentication, and authority check to solve the security and confidentiality problems of the system and prevent information leakage and illegal intrusion into confidential information.
- (5) High quality information service: on the basis of information standardization and normalization, we should make a reasonable layout of information and provide high-quality and efficient business management and transaction processing. At the same time, the system runs stably, safely, and reliably.

3.3. System User Analysis. The reasonable design of user rights is the basis to ensure the normal operation of the system and the maximum efficiency of the system. The personnel management system involves trade secrets to a certain extent, so it has higher requirements for the user authority design [21]. The system administrator is the owner of the highest authority, who not only can complete the operation of the general administrator but also can manage the information of the general administrator. Ordinary users can only log in to the system for basic operation after the administrator registers for them. System users include ordinary users, general administrators, and general administrators.

Functions of ordinary users: the functions of ordinary users are to manage the basic information of their own employees, modify their own passwords, query basic information of the department, query the type of attendance information, query their own daily attendance and monthly attendance information, query their own basic salary and subsidies information, query your own past and current salary information, manage your own personal communications and query company communications, query rewards and punishments information, query job change information, and send and receive emails.

Functions of general administrators: general administrators can query the basic files of management employees, but cannot modify the passwords of other ordinary employees, manage basic information of the department, manage attendance information, query the daily attendance and monthly attendance of themselves and other ordinary employees information, manage basic salary and subsidy information, generate employee salary, manage employee position change information, manage files, manage employee reward and punishment information, manage personal address book, and recruit and train employee management.

The function of the system administrator: the function of the system administrator is to query the basic information of the management staff, but cannot modify the passwords of other ordinary employees and the basic information of the management department, manage the attendance information, query the daily attendance and monthly attendance of themselves and other ordinary employees information, manage basic salary and subsidy information, and generate employee salaries, administrator information management, system event query, system decision-making and statistics, security management, database management, and file management.

3.4. System Function Analysis. The function of the system must be able to meet the user's information requirements, processing requirements, and security and integrity requirements. The goal of the enterprise management system is to build a brand-new modern enterprise management system according to the requirements of enterprise management, realize the automation, digitization, and intellectualization of employee management, purchase, warehouse management, distribution management, and other activities through computer, network, and other modern science and technology, and build an information platform for enterprise management [22]. This paper proposes that the enterprise management system based on edge computing technology mainly includes three modules, namely, enterprise personnel management, enterprise inventory management, and system maintenance. The enterprise personnel management system also includes employee management, department management, attendance management, salary management, and other submodules. The enterprise inventory management also includes commodity warehousing management, commodity inventory management, commodity sales management, data statistics and reports, and other submodules.

- (1) The main work content of employee management is to add, modify, delete, and query employee information, as well as detailed records of employee transfer, including the adjustment of department, position and title, and employee turnover.
- (2) The main work of department management is to add, modify, delete, and query departments.
- (3) The main work content of attendance management is to add and modify daily attendance records. It focuses on the function of adding and modifying daily attendance records according to all employees, department employees and selected employees, so as to facilitate user operation. In addition, it can add, modify, delete, and query employees' daily leave information.
- (4) The main work content of salary management is batch addition, modification, deletion, and query of monthly salary information. In addition, it focuses on the export function of salary data, which can be exported in the form of Excel file or online banking file.

- (5) Commodity warehousing management is the planning and organization of various business activities such as unloading, checking, acceptance, and handling warehousing procedures when receiving warehousing goods according to the commodity warehousing voucher. Its basic requirement is to ensure that the quantity of goods in storage is accurate and the quality meets the requirements. Its main work content is goods storage and storage query.
- (6) Inventory management includes warehouse management and inventory control. Warehouse management includes warehouse planning, goods in and out management, and warehouse quality management. Inventory control mainly refers to the control of inventory quality. Its main work content is commodity lending, commodity lending query, commodity return, commodity return query, commodity inventory, and inventory query.
- (7) Commodity sales management is a software used to help users manage the commodity sales process. Users can easily realize the management of commodity sales process by inputting the goods, orders, sellers, and other data involved in the sales process. Its main work content is commodity sale and sale inquiry.
- (8) Statistical report is to provide basic statistical data from the bottom to the top according to unified form, unified submission procedure, and report time. Its main work content is in and out of warehouse day statistics, in and out of warehouse year statistics, out of warehouse report, and inventory report.

The system maintenance module is a functional module mainly for maintaining system security. Its main work contents are operator management, password modification, operator permission setting, data backup, data recovery, data cleaning, log viewing, and log cleaning.

4. Enterprise Management System Design

The goal of the enterprise management system design is to design a practical, easy-to-use, extensible, easy to maintain, stable, and efficient enterprise management system to adapt to the current situation of enterprise management and to design a general enterprise management system suitable for the current management situation of most enterprises through this system [23]. The design process of the enterprise management system must strictly abide by the software engineering development process, and the design should follow the principles of practicability, security, ease of use, efficiency, stability, easy maintenance, and scalability of the system.

4.1. System Function Structure Design. According to the analysis of the functional requirements of the enterprise management system, the enterprise management system is

divided into three functional modules, namely, enterprise personnel management, enterprise inventory management, and system maintenance. The enterprise personnel management system also includes employee management, department management, attendance management, salary management, and other submodules. The enterprise inventory management also includes commodity warehousing management, commodity inventory management, enterprise management, commodity sales management, data statistics and reports, and other submodules. The functional structure of the system is shown in Figure 3.

4.1.1. Enterprise Personnel Management Module. Enterprise personnel management is one of the information management systems that must be owned by modern enterprises and institutions to manage employees, wages, and daily attendance. It should include the addition, deletion, modification and check of personnel information, personnel transfer and resignation, printing and output of personnel information, daily attendance management, wage management, and welfare management. The enterprise personnel management module includes employee management, department management, attendance management, salary management, and other four submodules. The main work of employee management is to add, modify, delete, and query employee information, as well as detailed records of employee transfer, including the adjustment of department, position and professional title, and employee turnover. The main work content of department management is the addition, modification, deletion, and query of department staff. It mainly includes two submodules: adding department information and modifying department information. The main work content of attendance management is to add and modify daily attendance records. It focuses on the function of adding and modifying daily attendance records according to all employees, department employees and selected employees, so as to facilitate users to add, modify, delete, and query employees' daily leave and leave information. It mainly includes three submodules: attendance information setting, adding and modifying attendance records, and employee leave. The main work content of salary management is batch addition, modification, deletion, and query of monthly salary information. In addition, it focuses on the export function of salary data, which can be exported in the form of Excel file or online banking file. It mainly includes three submodules: salary information management, overdue data processing, and salary export.

4.1.2. Enterprise Purchase, Sale, and Inventory Management Module. The enterprise purchase, sale, and inventory management module can realize the information management of the enterprise's purchase, sale, inventory, and other businesses. It is a necessary condition for the steady development of small- and medium-sized enterprises in the modern society. It can improve the management level and work efficiency of enterprises and minimize the mistakes of manual operation. The enterprise purchase, sale, and inventory management module includes four submodules:

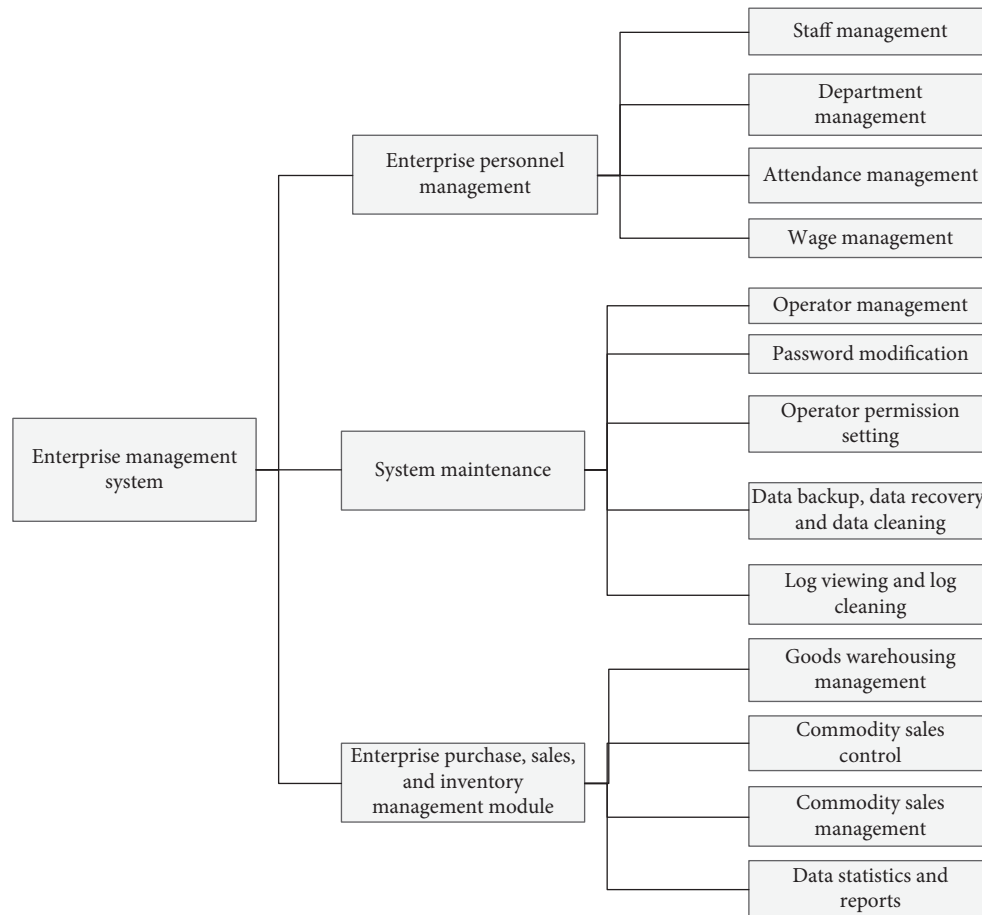


FIGURE 3: System function structure diagram.

commodity storage management, commodity inventory management, commodity sales management, and data statistics and reports. Before using this system, enterprises need to establish the basic information of enterprises in the system, including commodity information setting, warehouse information setting, and initial inventory setting. Commodity warehousing management is the plan and organization of various business activities such as unloading, checking, acceptance, and handling warehousing procedures when receiving warehousing goods according to the commodity warehousing voucher. Its basic requirement is to ensure that the quantity of goods in storage is accurate and the quality meets the requirements. It mainly includes goods warehousing, warehousing query, and so on. Inventory management includes warehouse management and inventory control. Warehouse management includes warehouse planning, goods in and out management, and warehouse quality management. Inventory control mainly refers to the control of inventory quality. The commodity inventory management module is mainly to complete the work of commodity lending, commodity lending query, commodity return, commodity return query, commodity inventory, inventory query, etc. Commodity sales management is a module used to help users manage the commodity sales process. Users can easily realize the management of commodity sales process by inputting the goods, orders, sellers,

and other data involved in the sales process. The commodity sales management is mainly to complete the commodity sales and sales inquiry. Statistical report is to provide basic statistical data from the bottom to the top according to unified form, unified submission procedure, and report time. The data statistics and report module is mainly used to complete the daily statistics of in and out of warehouse, annual statistics of in and out of warehouse, out of warehouse report, inventory report, etc.

4.1.3. System Maintenance Module. The system maintenance module is a functional module mainly to maintain system security, which mainly includes operator management, password modification, operator permission setting, data backup, data recovery, data cleaning, log viewing, and log cleaning.

4.2. Database Design

4.2.1. Data Table Design. According to the system function structure design, a number of data tables are established. They are employee information table, department table, salary table, attendance record table, inventory information table, commodity warehousing information table, commodity outbound table, and other related data tables.

- (1) Employee information table: employee information table records the basic information of employees, including employee ID number, employee name, employee gender, employee ID card number, employee birth date, employee participation time, employee entry time, staff working age, and other information
- (2) Department table: it is mainly used to record the department information of an enterprise, including department number, department name, department manager, department address, and department telephone number
- (3) Payroll: the payroll is used to store the detailed salary information of each employee every month, including the salary month, employee number, employee name, employee basic salary, employee overtime pay, employee seniority salary, employee pension insurance, employee medical insurance, employee salary payable, employee salary deduction, and employee actual salary
- (4) Attendance record table: it is used to record the daily attendance of employees, including employee number, employee name, employee commuting situation, employee commuting time, date, whether abnormal, abnormal time, and other information
- (5) Inventory information table: the inventory information table is used to store the relevant information of commodity inventory, including commodity number, commodity name, commodity specification, commodity unit, commodity receipt quantity, commodity unit price, and commodity receipt date
- (6) Commodity warehousing information table: it is used to store relevant information of commodity warehousing, including commodity number, commodity name, supplier number of commodity, supplier name of commodity, commodity specification, commodity quantity, commodity unit price, commodity amount, commodity warehousing date, commodity warehouse year, commodity warehousing month, handler, modifier, and modification date
- (7) Commodity delivery table: commodity delivery table is used to store the delivery information of commodities, including delivery number, commodity number, commodity name, unit of measurement, quantity of delivered commodities, delivery date, delivery year, delivery month, delivery company, delivery person, handler, modifier, and modification date

4.2.2. Common Module Design. When designing the system, those functions that may be reused should be written as general procedures or functions and stored in standard modules. This not only reduces the amount of code but also facilitates future maintenance. In addition, in the standard module, you can also define some common variables, which can facilitate the mutual transfer of values between the

functional windows. Before using a standard module, you should first create it by selecting the “Project”/“Add Module” command to create a new module, using the default name Module 1.

4.2.3. Function Menu Design. The realization of various functions of the system is realized through the operation of the menu and supports the operation of the keyboard and the mouse at the same time. The menu has a first-level menu, a second-level menu, and a third-level menu. The menu of this system is mainly designed through the menu editor. First, select the “Project”/“Menu Editor” command in the project, open the “Menu Editor” dialog box, and design in it. After the menu is designed, you need to add code to its Click event, that is, the code to call each functional form. Use the Load statement to load the required form into the memory, and then, use the Show method to display the form.

4.2.4. Design of the Login Module. In order to prevent illegal users from using the system, the system login module is provided in the server of the enterprise management system. The module is the portal for users to enter the system. Only through the login module can the user be authenticated and enter the main interface of the system. In order to verify whether the user name and password are correct, it is necessary to query the user information from the database according to the user name and password entered by the user. If the user information is correct, it will enter the main interface of the system; otherwise, there will be corresponding prompt information.

First, create a new form in the project, name it frm_xtld, and set the StartUpPosition property to “2-screen center,” the BorderStyle property to 0-None, and the Picture property to the specified picture. Second, add a PictureBox control on the form and set its AutoSize property to true, which is consistent with the size of the picture. Set the Picture property to the specified picture. Finally, add a ListView control and an ImageList control. These two controls are ActiveX controls, not Visual Basic standard controls, so you need to select the “Project”/“Parts” command and check the check box in the pop-up “Parts” Microsoft Windows Common Controls 6.0 (SP6) dialog box. Add the ListView control and ImageList control to the toolbox. Set the BorderStyle property of the ListView control to 0-ccNone, and set the ListView control to have no border, and it can be embedded in the picture seamlessly, and at the same time, add pictures to the ImageList control. Through the above steps, the enterprise management system design is realized.

5. System Test Results and Analysis

5.1. Setting System Test Environment. In order to test the effectiveness of the enterprise management system based on the edge computing architecture, the system is tested and deployed in the WEB environment, and the system performance is tested through the enterprise’s internal network and Internet client terminals. The system is a Windows

Server 2018 server, configured as Intel Pentium 4 3.0 GHz or higher dual CPU, 8 GB memory, SCSI dual hard disk mirroring, and SQL Server 2003. The configuration on the client is Intel Pentium 4 3.0 GHz or higher and WindowsXP/ Vista operating system. The test indicators are the proportion of system bugs, the system CPU occupancy rate, and the system response time. The method in [4, 5] and the proposed method are used to compare the system performance of the proposed method.

5.2. System Vulnerability Test and Analysis. Bug is in this system program development process; there are some hidden defects or problems that have not been found, that is, vulnerability. The higher the proportion of system bugs, the more system vulnerabilities. On the contrary, the lower the proportion of system bugs, the less the system vulnerabilities. In the system unit test phase, integration test phase, and acceptance test phase, the method in [4, 5] and the proposed method are used to test, respectively, and the number of system bugs of different methods is compared, as shown in Figure 4.

According to Figure 4, in the system unit test phase, integration test phase, and acceptance test phase, the system bugs of the method in [4] account for 32%, 28%, and 21%, respectively, and the system bugs of the method in [5] account for 39%, 33%, and 42%, respectively, while the system bugs of the proposed method account for 9%, 11%, and 7%, respectively. Therefore, the number of system bugs of the proposed method is relatively low, and the system vulnerabilities are less.

5.3. System Running Speed Analysis. CPU occupancy is the CPU resources occupied by running programs. The higher the CPU occupancy is, the slower the system runs. Conversely, the lower the CPU occupancy is, the faster the system runs. In order to verify the running speed of the enterprise management system based on the edge computing architecture, the number of clients is set to 400, and the method in [4, 5] and the proposed methods are used to test, respectively. The CPU occupancy rate of different methods is compared, and the results are shown in Figure 5.

As can be seen from Figure 5, with the increase of the number of system clients, the CPU occupancy of the system with different methods increases. Among them, when the number of clients reaches 400, the CPU occupancy rate of the method in [4] is 68%, the CPU occupancy rate of the method in [5] is 43%, and the CPU occupancy rate of the proposed method is only 21%. Therefore, compared with the method in [4, 5], the CPU occupancy of the proposed method is lower and the running speed is faster.

5.4. System Response Time Analysis. On this basis, the response time of the enterprise management system based on the edge computing architecture is further verified. The method in [4, 5] and the proposed method are used to compare the system response time of different methods, as shown in Figure 6.

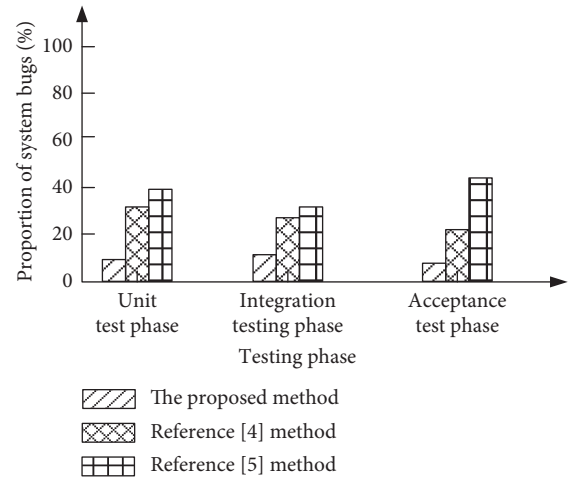


FIGURE 4: Comparison results of the number of system bugs by different methods.

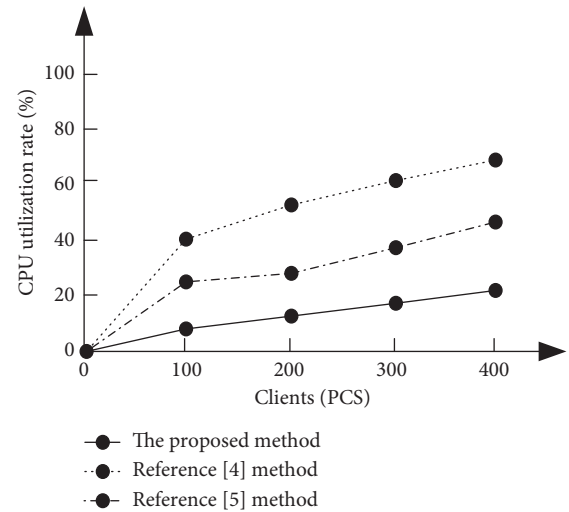


FIGURE 5: Comparison results of system CPU usage of different methods.

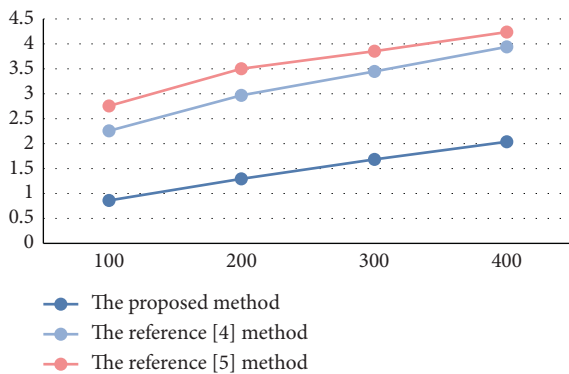


FIGURE 6: System response time comparison of different methods.

According to the data in Figure 6, with the increase of the number of clients, the system response time of different methods increases. When the number of clients is 400, the system response time of the method in [4] is 3.95 s, that of

the method in [5] is 4.23 s, and that of the proposed method is only 2.04 s. Therefore, compared with the method in [4, 5], the system response time of the proposed method is shorter.

6. Conclusion

According to the characteristics of mobile edge computing, this paper designs an enterprise management system based on edge computing architecture, designs an edge computing platform architecture, integrates the MEC virtualization infrastructure layer, MEC platform layer, and MEC application layer, constructs an edge computing model, reflects the coupling relationship between enterprise management and operation and maintenance database, and realizes the parameter calculation of enterprise management and operation and maintenance system. Analyze the requirements of the enterprise management system, design the system function structure, database, and data table, and realize the design of the enterprise management system based on edge computing architecture. The system can effectively reduce the system vulnerabilities, speed up the system operation speed, and shorten the system response time. But in the enterprise management system, we should further improve the function of the system and verify the superiority of the system in practical application. Therefore, in the next step of research, the system is applied to specific engineering application projects to further verify the effectiveness of the enterprise management system.

Data Availability

The datasets used and/or analyzed during the current study are available from the corresponding author upon reasonable request.

Conflicts of Interest

The authors declare that there are no conflicts of interest.

References

- [1] Y. Liu, F. R. Yu, X. Li, H. Ji, and V. C. M. Leung, "Decentralized resource allocation for video transcoding and delivery in blockchain-based system with mobile edge computing," *IEEE Transactions on Vehicular Technology*, vol. 68, no. 11, pp. 11169–11185, 2019.
- [2] W. Li, Y. Wang, Q. Ren et al., "Design and implementation of digital control system based on PAC architecture for large-capacity pulse power supply," *IEEE Transactions on Plasma Science*, vol. 47, no. 12, pp. 5339–5344, 2019.
- [3] C. Valor, C. Escudero, V. Labajo, and R. Cossent, "Effective design of domestic energy efficiency displays: a proposed architecture based on empirical evidence," *Renewable and Sustainable Energy Reviews*, vol. 114, no. OCT, pp. 109301.1–109301.11, 2019.
- [4] M. S. Ravelomanantsoa, Y. Ducq, and B. Vallespir, "A state of the art and comparison of approaches for performance measurement systems definition and design," *International Journal of Production Research*, vol. 57, no. 15–16, pp. 5026–5046, 2019.
- [5] T. Mäki and H. Kerosuo, "Design-related questions in the construction phase: the effect of using the Last Planner System in design management 1," *Canadian Journal of Civil Engineering*, vol. 47, pp. 290–382, 2020.
- [6] A. J. Ferrer, J. M. Marquès, and J. Jorba, "Towards the decentralised cloud," *ACM Computing Surveys*, vol. 51, no. 6, pp. 1–36, 2019.
- [7] M. Mehrabi, D. You, V. Latzko, H. Salah, M. Reisslein, and F. H. P. Fitzek, "Device-enhanced MEC: multi-access edge computing (MEC) aided by end device computation and caching: a survey," *IEEE Access*, vol. 7, pp. 166079–166108, 2019.
- [8] M. Satyanarayanan, B. Paramvir, R. Caceres, and N. Davies, "The case for VM-based cloudlets in mobile computing," *IEEE Pervas Computing*, vol. 8, pp. 4–23, 2009.
- [9] K. Bilal, O. Khalid, A. Erbad, and U. K. Samee, "Potentials, trends, and prospects in edge technologies: fog, cloudlet, mobile edge, and micro data centers," *Computing Network*, vol. 2017, 2017.
- [10] M. Satyanarayanan, "The emergence of edge computing," *Computer*, vol. 50, pp. 1–30, 2017.
- [11] M. Satyanarayanan, P. Simoens, Yu Xiao et al., "Edge analytics in the internet of things," *IEEE Pervas Computing*, vol. 14, pp. 2–31, 2015.
- [12] F. Bonomi, R. Milito, Z. Jiang, and S. Addepalli, "Fog computing and its role in the internet of things," in *Proceedings of the 1st Edition of the MCC Workshop on Mobile Cloud Computing*, Helsinki, Finland, August 2012.
- [13] P. Garcia Lopez, A. Montresor, D. Epema et al., "Edge-centric computing," *ACM SIGCOMM Computer Communication Review*, vol. 45, pp. 5–42, 2015.
- [14] Y. Ma, C. Lu, B. Sinopoli, and S. Zeng, "Exploring edge computing for multi-tier industrial control," *IEEE Transactions on Computer-Aided Design of Integrated Circuits and Systems*, vol. 39, no. 11, pp. 648–653, 2020.
- [15] M. S. C. Inguva and J. B. Seventiline, "Implementation of FPGA design of FFT architecture based on CORDIC algorithm," *International Journal of Electronics*, vol. 18, no. 10, pp. 750–759, 2020.
- [16] R. Zhang, J. Wu, R. Wang, R. Yan, Y. Zhu, and X. He, "A novel battery management system Architecture based on an isolated power/data multiplexing transmission bus," *IEEE Transactions on Industrial Electronics*, vol. 66, no. 8, pp. 5979–5991, 2019.
- [17] C. Li, J. Tang, and Y. Luo, "Scalable replica selection based on node service capability for improving data access performance in edge computing environment," *The Journal of Supercomputing*, vol. 75, no. 11, pp. 7209–7243, 2019.
- [18] D. Marmsoler and L. Eichhorn, "On the impact of architecture design decisions on the quality of blockchain-based applications," *The Knowledge Engineering Review*, vol. 35, pp. 193–199, 2020.
- [19] B. Y. Kong, "Multi-touch detector architecture based on efficient buffering of intensities and labels," *Electronics Letters*, vol. 56, no. 1, pp. 884–892, 2020.
- [20] P. Bellavista, D. Belli, S. Chessa, and L. Foschini, "A social-driven edge computing architecture for mobile crowd sensing management," *IEEE Communications Magazine*, vol. 57, no. 4, pp. 68–73, 2019.
- [21] L. Nie, "Visual design of marine architecture in coastal cities based on "BIM + VR"" *Journal of Coastal Research*, vol. 112, no. sp1, pp. 2112–2118, 2020.

- [22] F. Li, D. Li, and W. Li, "Research and design of load balancing algorithm for edge coverage network storage," *Computer Simulation*, vol. 37, no. 11, pp. 390–393, 2020.
- [23] R. T. Tiburski, C. R. Moratelli, S. F. Johann et al., "Lightweight security architecture based on embedded virtualization and trust mechanisms for IoT edge devices," *IEEE Communications Magazine*, vol. 57, no. 2, pp. 67–73, 2019.

Research Article

A Supply Chain Information Pushing Method for Logistics Park Based on Internet of Things Technology

Zhongqiang Zhang 

School of Management, Xuzhou University of Technology, Xuzhou 221018, China

Correspondence should be addressed to Zhongqiang Zhang; zzq@xzit.edu.cn

Received 1 February 2021; Revised 19 March 2021; Accepted 22 April 2021; Published 29 April 2021

Academic Editor: Hsu-Yang Kung

Copyright © 2021 Zhongqiang Zhang. This is an open access article distributed under the Creative Commons Attribution License, which permits unrestricted use, distribution, and reproduction in any medium, provided the original work is properly cited.

The existing push methods of supply chain information in logistics parks stay on the analysis of data surface, which leads to higher Mae value. Therefore, this paper proposes a push method of supply chain information in logistics parks based on the Internet of Things technology. Firstly, RFID structure is designed by introducing RFID, GPS, infrared, and other Internet of Things technologies to encode the materials in the logistics warehouse; secondly, the supply chain model of the logistics park is established to obtain the general ontology element model of the node enterprises in the supply chain of the park and the interaction business situation model between the node enterprises in the supply chain of the park. Finally, the average value of the node score is subtracted from the score of the node to calculate the information centralized scoring, as well as the establishment of Spark operation framework, to achieve the logistics park supply chain information pushing. In the simulation experiment, the international land port logistics park of a city is selected as a case to test. The experimental results show that the information pushing method of logistics information park supply chain based on Internet of Things technology has higher recommendation accuracy and better performance.

1. Introduction

Logistics park is the result of spatial agglomeration of logistics enterprises, which is a form of logistics industry collaboration and an important part of regional economic structure. There are nearly 1000 large-scale logistics parks in China. After the completion of the logistics park, the preferential policies and location advantages enjoyed by enterprises in the park have been basically fixed, and the appreciation space has been very limited. However, high-quality information service is an important way for enterprises in the park to provide value-added services. This study provides active and personalized logistics services for the supply chain nodes of the park, so as to improve the efficiency of integrated utilization and optimal allocation of social logistics resources in the logistics park, promote logistics enterprises to gather in the park, and promote the coordinated development of logistics industry and regional economy [1, 2]. Since the concept of “Internet of Things” is first proposed, it has experienced more than 10 years of development and improvement. The Internet of Things has

been gradually developed into a strategic plan of various countries and regions, gradually recognized by the international community, and even reached a consensus. The Internet of Things is considered to be the third wave of the world information industry after the computer, Internet, and mobile communications and will promote a new round of development of technological innovation. A supply chain is a network of retailers, distributors, transporters, storage facilities, and suppliers that participate in the production, delivery, and sale of a product to the consumer. It is typically made up of multiple companies who coordinate activities to set themselves apart from the competition. There are three key parts to a supply chain: Supply focuses on the raw materials supplied to manufacturing, including how, when, and from what location. Manufacturing focuses on converting these raw materials into finished products. Distribution focuses on ensuring that these products reach the consumers through an organized network of distributors, warehouses, and retailers. The U.S. government has made a positive response to the “smart Earth” concept proposed by IBM, believing that the smart Earth is the core

area of national development after the Internet; in June 2009, the European Commission releases the European Internet of Things Action Plan, which describes the future application of Internet of Things technology and proposes that EU governments should strengthen the management of Internet of Things and eliminate various factors that hinder the development of Internet of Things. In August 2009, Premier Wen Jiabao proposed establishing China's "perception of China" center as soon as possible. In the government work report in March 2010, the development of the Internet of Things was really promoted to the national strategic height and included in the revitalization plan of key industries. The Internet of Things (IOT) technology obtains and processes the relevant information about the environment of logo users through modern information and communication technologies (ICT) such as Wi-Fi, RFID, information sensing, and network services, so as to further understand the user's behavior choice motivation. It provides an important direction for improving user experience training, "active service design," especially in the user personalized service demand response. Therefore, it can provide users with more accurate active push service.

The main contributions of our work include the three following points:

- (1) This paper proposes a push method of supply chain information in logistics park based on Internet of Things technology
- (2) RFID structure is designed by introducing RFID, GPS, infrared, and other Internet of Things technologies
- (3) The supply chain model of the logistics park is established to obtain the general ontology element model of the node enterprises in the supply chain of the park

This paper is divided into 5 sections. Section 2 introduces the related works about supply chain information pushing for logistics park based on Internet of Things technology. Section 3 discusses the supply chain information pushing method. Section 4 describes the experimental results. Section 5 concludes this paper with contributions, limitations, and future works.

2. Related Work

Modern logistics park is a place where multiple logistics entities are concentrated in space, and it is the assembly point of comprehensive logistics service and management facilities with a certain scale. Among them, information construction plays an increasingly prominent role in building a modern logistics park integrating business flow, information flow, and capital flow [3, 4]. With the support of modern information technology, integrating the supply, storage, transportation, distribution, information processing, and other links of the park, optimizing the business process of enterprises, and reasonably allocating and scheduling the relevant logistics resources have become the inevitable trend and urgent requirement of the sustainable

development of the logistics park. At present, the former domestic logistics park has made some achievements in the level of information construction, but, due to the problems of asymmetric information, frequent mobile tasks, and highly professional division of labor, it is still in a passive position in the logistics resource scheduling and integration. Due to the increasingly huge resource data, the existing information pushing methods can only stay on the surface of data analysis, resulting in higher Mae value. Therefore, this paper proposes a supply chain information pushing method for logistics park based on Internet of Things technology.

Based on the technology of Internet of Things, this paper studies the information pushing method of supply chain in logistics park. According to the task environment of supply chain nodes in the park, it introduces the perception training calculation analysis model of Internet of Things, abstracts the behavior of information collaborative management in logistics park into "role, event, process, result," and other elements, and constructs a multidimensional and multilevel information collaborative mechanism, in order to solve the problem of low precision and weak timeliness of logistics service information pushing.

2.1. Push Supply Chain Strategies. A push model supply chain is one where projected demand determines what enters the process. For example, warm jackets get pushed to clothing retailers as summer ends and the fall and winter seasons start. Under a push system, companies have predictability in their supply chains, since they know what will come and when long before it actually arrives. This also allows them to plan production to meet their needs and gives them time to prepare a place to store the stock they receive.

2.2. Pull Supply Chain Strategies. A pull strategy is related to the just-in-time school of inventory management that minimizes stock on hand, focusing on last-second deliveries. Under these strategies, products enter the supply chain when customer demand justifies it. One example of an industry that operates under this strategy is a direct computer seller that waits until it receives an order to actually build a custom computer for the consumer. With a pull strategy, companies avoid the cost of carrying inventory that may not sell. The risk is that they might not have enough inventory to meet demand if they cannot ramp up production quickly enough.

2.3. Push/Pull Strategies. Technically, every supply chain strategy is a hybrid between the two. A fully-push-based system still stops at the retail store where it has to wait for a customer to "pull" a product off of the shelves. However, a chain that is designed to be a hybrid flips between push and pull somewhere in the middle of the process. For instance, a company may choose to stockpile finished product at its distribution centers to wait for orders that pull them to stores. Manufacturers might choose to build up inventories of raw materials, especially those that go up in price,

knowing that they will be able to use them for future production.

3. Design of Supply Chain Information Pushing Method for Logistics Park Based on Internet of Things Technology

3.1. Introduction of Internet of Things Technology. Internet of Things technology can be said to represent a new generation of information technology. Internet of Things technology uses advanced information technology such as radio frequency identification technology and global positioning technology to connect and communicate objects with the network. Therefore, Internet of Things technology can also be said to be the further development of the Internet. Now the Internet of Things technology has been applied in many fields, such as medical and health field and environmental monitoring field. In this paper, in the process of pushing the supply chain information of the logistics park, the Internet of Things technologies are used, including radio frequency identification technology, GPS technology, and infrared technology [5, 6]. Radio frequency identification (RFID) technology is a noncontact automatic identification technology that can use the principle of radio frequency signal and spatial coupling transmission. RFID technology is composed of two parts, namely, RFID tag and information processing system. RFID tag is mainly used as the carrier of data, RFID tag, and reader. It has the advantages of noncontact identification. The reader reads the tag by radio frequency, long service life, and strong signal penetration. The reader reads the tag data by radio frequency and transmits the read data to the reader information processing system. In the business process optimization of commercial vehicles, RFID technology mainly realizes the marking of vehicles and the preservation of some vehicle information.

In the push supply chain information in logistics park, the real-time update of material information is the basis of accurate push. The Internet of Things is an extension of the Internet. Through the combination of wireless or wired networks and the Internet, RFID, which can store material information, is also known as radio frequency identification technology. Noncontact sensing technology is gradually maturing. In the current logistics warehouse, the main identification technologies include optical identification and bar code identification. RFID technology has its unique characteristics and is more suitable for the daily application of logistics warehouse. Table 1 lists the main parameters of these identification methods.

In the logistics and transportation industry, RFID technology can automatically identify a single object and then has the ability to identify object coding. This technology can quickly, real-time, and accurately collect and process cargo information in the logistics warehouse and can manage the cargo in the warehouse more conveniently. In order to apply the intelligent positioning method in this paper, the framework of RFID identification technology is designed, and the structure is shown in Figure 1.

REID can read and write data through wireless identification. It is encapsulated in a closed shell. The external water, ash, and other adverse conditions have little impact on it, and they have high adaptability to the environment. Labels on materials can be miniaturized and diversified, which is different from traditional barcode and QR code [7, 8]. The traditional bar code can only identify the types of goods. Based on RFID technology, the method in this paper develops a set of its own coding rules. As the unique "ID" for identifying materials, the code can realize the identification and tracking of single object. The material coding structure is shown in Figure 2.

According to the coding rules, the outsourcing classes can be classified and coded with high confidentiality, which provides a good technical basis for the intelligent positioning of the automated logistics warehouse. Through the application of the Internet of Things technology in the warehouse, the data and information flow transmission efficiency of the automated warehouse is ensured. Figure 2 shows the material code of logistics warehouse. Material code is the unique identification code for materials in the warehouse system. It represents a kind of material by a group of codes. The material code must be unique; that is, a material cannot have multiple material codes, a material code cannot have a variety of materials, and the relationship between them is one-to-one correspondence.

GPS (Global Positioning System) is a technology used to determine the target location. It can realize the real-time management of goods in the logistics park. For the commodity logistics vehicle, its transportation process is a moving process. If it can realize the real-time management, it will be of great help to the scheduling of logistics vehicles and the selection of transportation routes. In addition, the use of GPS technology can effectively combine all aspects of the supply chain of commercial vehicle transportation, so that managers can master the operation of vehicles in real time, so as to improve the service level of the supply chain of commercial vehicle transportation. Infrared ray is a kind of light with a wavelength of 0.76 to 400 μm . It is an invisible light. Its ability to pass through clouds is stronger than that of visible light. It has a wide range of applications in communication, detection, medical treatment, military, and so on. Infrared technology is a kind of automatic control device realized by using infrared. It uses infrared transmitting and receiving device to realize an infrared loop. When the infrared receiving line is blocked, the receiving device can immediately send out a warning. In this paper, infrared technology is used to realize the control of transport vehicles in the logistics park, as well as the antitheft control of commodity vehicles.

3.2. Supply Chain Modeling of Logistics Park. The supply chain of logistics park is similar to a huge "magnetic field" system, which is composed of personnel, capital, technology, information, goods, and other basic elements. A simple index evaluation system cannot fully reflect the concept of logistics park. Therefore, it needs a strict and scientific perspective to determine the boundary of logistics park. On

TABLE 1: Comparison of several identification technical parameters.

Parameter	Optical recognition	Bar code	RFID identification
Data volume	1-100 B	1-100 B	16-64 KB
Read mode	Photoelectric conversion	Laser scanning	Wireless communication
Recognition distance	Very close	Near	Far
Recognition speed	Less than 3S	Less than 4S	Less than 4S
Artificial intelligence	Probably	Restricted	Impossible
Machine recognition	Good	Good	Good
Confidentiality	Nothing	Nothing	Good
Light masking effect	Invalid	Invalid	No impact
Moisture effects	Serious	It is serious	No impact
Azimuth effect	Small	Small	No impact
Multitarget recognition	No	No	Can

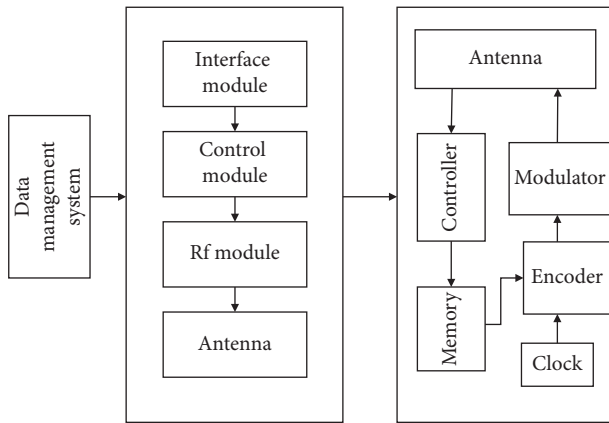


FIGURE 1: RFID structure.

the whole, the existing research on the boundary of logistics park has achieved some results, but there are still some defects in the data collection and quantitative methods. Therefore, in the specific operation, it is needed to select certain representative indexes pertinently and follow the principles of comprehensiveness, feasibility, scientificity, contrast, and orientation when selecting the boundary index system based on theory and practice [9, 10]. The boundary of logistics park is easily affected by internal and external factors. Because this study is based on the following premise, that is, the determination of the boundary of the logistics park is before the determination of the scale of the logistics park, it is difficult to obtain the internal factors that affect the strength of the logistics park center in the planning stage. There are many internal indicators of the logistics park, such as logistics capacity, facilities and equipment, cargo turnover, service quality, and logistics modernization. In this paper, the author describes in detail the internal impact indicators of nonlogistics park and evaluates it. The author defines the scope of regional logistics park according to the situation. For example, if the park to be analyzed is in different cities, then the city is regarded as the “region” in the “regional logistics park”; if it is in a city, then the “region” can be understood as different urban areas.

Combined with the previous comprehensive researches, based on the availability and rationality of the data obtained by the logistics park and the characteristics of the planning period of the logistics park, this paper evaluates it according

to two indicators: the first is to evaluate the comprehensive ability of its location, and the second is to evaluate the impact of its region on the park.

- (1) Ability evaluation of logistics park location: the evaluation is aimed at the evaluation of social, economic, and natural environment of the location selected by the logistics park, and the ability of the logistics park should be evaluated according to the evaluation. In general, the better the economic development, the greater the demand for logistics, and the stronger the ability of the logistics park in a certain aspect.
- (2) Evaluation of the impact of logistics park location on the park: the main body of the index is the fit degree between the logistics park and its location, which can be measured by the estimation of logistics volume and the support degree of regional policies and guidelines to the park [11, 12]. Under normal circumstances, the greater the degree of fit between the park and its location is, the more support it can get from the outside world, and the larger its boundary becomes.

Ontology can be used to solve the problems of information organization, information retrieval, and the interoperability of heterogeneous information systems. Based on the basic business of the park, such as warehousing, transportation, and freight forwarding, this paper constructs the situation ontology meta model of the park around the user needs of the park management committee, logistics demanders, logistics suppliers, government departments, logistics intermediaries, and auxiliary service providers, as shown in Figure 3.

At the same time, aiming at the interactive business between different node enterprises in the park supply chain, the scenario model of interactive business between node enterprises is established, as shown in Figure 4.

In the intelligent information push service of park supply chain, context is used to describe the collection of user characteristic information, including “role, environment, and event.” Role includes node enterprise and its post role of park logistics service chain. Environment information includes park resource distribution, resource status, and resource usage. Event includes interactive business, other events, historical transaction, and customer files.

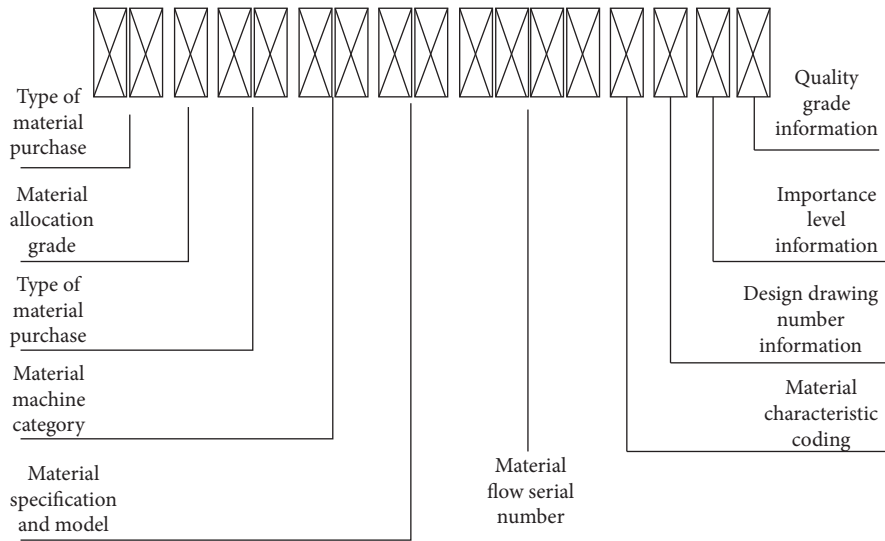


FIGURE 2: Material code of logistics warehouse.

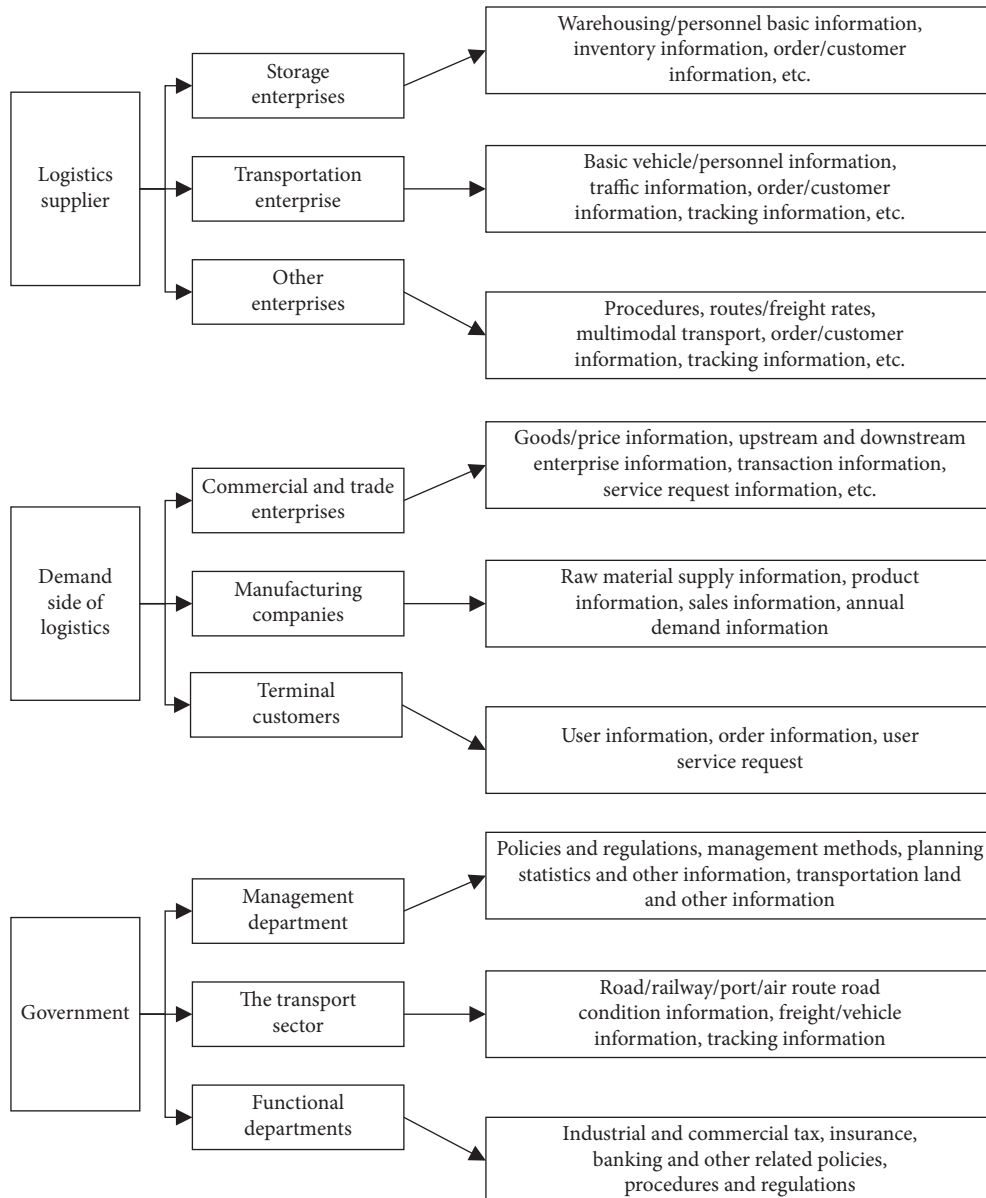


FIGURE 3: General ontology meta model of supply chain node enterprises in park.

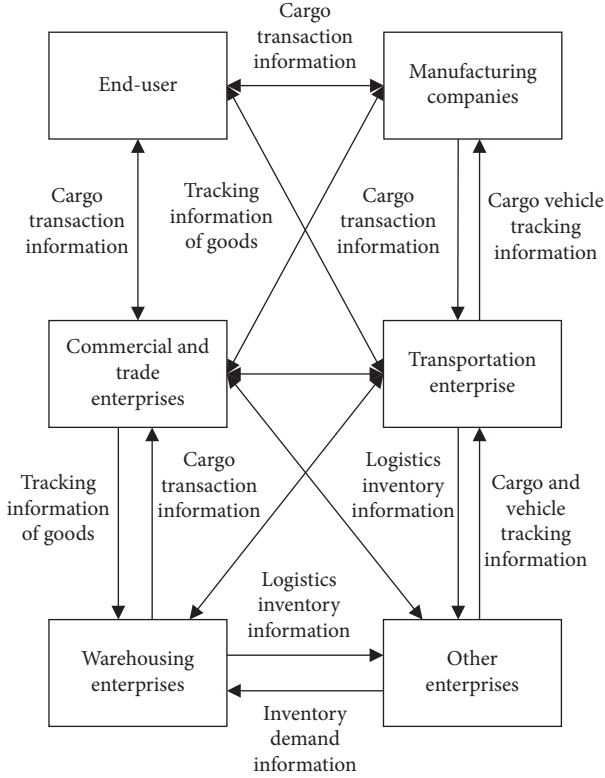


FIGURE 4: Interactive business scenario model between node enterprises in park supply chain.

3.3. Realization of Supply Chain Information Pushing for Logistics Park. On the basis of the established logistics park supply chain model, in order to achieve the accurate push supply chain information, it is needed to rely on the information balance between nodes to make predictions, and the neighboring nodes need to compare the similarity for selection. Therefore, in the calculation of similarity, it is needed to be able to correctly measure the similarity between node information and node demand, so as to ensure the accuracy of information push. In the traditional algorithm, cosine similarity is used, but cosine similarity ignores the problem that the information is graded. Therefore, it needs to be modified. The average value of the node's score minus the information's score is used for centralized scoring. The calculation formula is as follows:

$$\text{sim}(i, j) = \frac{\sum_{u \in U(i) \cap U(j)} (T_{u,i} - \bar{T}_u)(T_{u,j} - \bar{T}_u)}{\sqrt{\sum_{u \in U(i)} (T_{u,i} - \bar{T}_u)^2} \sqrt{\sum_{u \in U(j)} (T_{u,j} - \bar{T}_u)^2}} \quad (1)$$

In the above formula, $\text{sim}(i, j)$ represents the similarity of supply chain information i and j , $U(i)$ represents all nodes that score supply chain information i , $U(j)$ represents all nodes that score supply chain information j , $U(i) \cap U(j)$ represents all nodes that score i and j , $T_{u,i}$ and $T_{u,j}$ represent the scores of node u on supply chain information i and j , respectively, and \bar{T}_u and \bar{T}_u represent the average scores of two supply chain information [13, 14]. There is a certain

distance between a single resource information and the set of all information, which is the minimum distance between them. The distance between a single node and the set of nodes can also be obtained by the same principle. In the collaborative filtering algorithm based on MOOC supply chain information, the selection of similarity has an important impact on the accuracy of the algorithm as a whole. The optimization of similarity calculation in collaborative filtering of supply chain information is realized.

In order to achieve accurate recommendation of MOOC supply chain information, spark architecture is needed. Spark is a fast and general cluster computing engine. In the research of recommended algorithm in this paper, memory based data abstraction design is adopted to save the results of the middle part of Spark task. The specific framework is shown in Figure 5.

Spark framework includes SQL query, text processing, machine learning, and other functional components. These components are tightly integrated in Spark, and their computing performance is better. Especially in the working environment of mass information analysis and iteration, the advantages of Spark framework are more prominent. When spark architecture runs in the cluster, the driver first completes the supply chain information application through the supply chain information manager. After the manager allocates the supply chain information, it starts the executor on the corresponding node. After completing the task submitted by the driver, the node finally submits the feedback to the driver. The running process is shown in Figure 6.

The spark architecture is introduced into the algorithm, which can filter a large amount of supply chain information in the process of operation and make deep information prediction score for the remaining supply chain information. The prediction score mainly uses the similarity of supply chain information and the neighbor set $N(i)$ of supply chain information i to evaluate the score of a node on the target supply chain information. The specific information evaluation method is shown in

$$P_{u,i} = \bar{R}_i + \frac{\sum_{j \in N(i)} (R_{u,j} - \bar{R}_j) * (\text{sim}(i, j))}{\sum_{j \in N(i)} |\text{sim}(i, j)|} \quad (2)$$

In formula (2), $P_{u,i}$ represents the similarity prediction score of node u for supply chain information i , \bar{R}_i represents the average score of supply chain information i , $N(i)$ represents the neighbor set of supply chain information i , $R_{u,j}$ represents the score of node u for supply chain information j , \bar{R}_j represents the average score of supply chain information j , and $\text{sim}(i, j)$ represents the similarity between supply chain information i and supply chain information j . The higher the similarity prediction score obtained by the formula, the higher the accuracy of the algorithm. According to the score value of node u on the nearest neighbor set $N(i)$ of supply chain information i , the score of node u on supply chain information i is predicted by using formula (2), and the supply chain information recommendation list is generated, which realizes the accurate push supply chain information in logistics park.

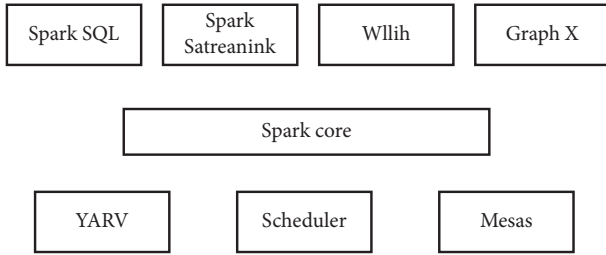


FIGURE 5: Framework of Spark.

In the last three years, many methods were proposed to handle the supply chain information pushing; here we introduce four outstanding methods: FPGA-IoT [15], ESS [16] Blockchain-IoT [17], and AI-IoT [18], which can be used to solve the related works taking different kinds of Internet of Things work structures. FPGA-IoT is a graph-based network that builds connections between different risk nodes so as to improve the speed of different nodes' communications; and ESS uses a specific loss structure to keep the costs of nearest nodes as lower as possible and decrease the total costs of overall parks [19, 20]. Blockchain-IoT is the basic model that needs more computation consumption to obtain the desired performances and can only keep the information pushing smooth; and AI-IoT uses the deep learning structure to capture the features and assess the distance of different nodes and give the different weights of each pair of nodes according to their importance. However, these methods have their disadvantages, respectively. The first two are too slow, the third is so complicated, and the last one also needs more spaces. Compared with these methods, our proposal can consider both time consumption and calculation speed, so we compared them together [21].

In this paper, we utilize the entropy loss function to build the model for our research problems. It can be defined as follows: $\text{loss}(x, y) = \sum_{i=1}^n -p_i \log(1 - p_i)$. The bigger the value of the loss was, the worse our proposal performed; and our proposal is used to train a model that fits the real and predicted values, so that the machine can perform well [22, 23].

Compared with the three methods, our proposal can deal with the problems easily and we also need a smaller computation space to build our model. However, our model may obtain a relatively lower accuracy than others sometimes, which may lead to unstable prediction [24].

4. Experiment

4.1. Case Overview. In order to verify the effectiveness of the supply chain information pushing method for logistics park based on Internet of Things, its performance needs to be verified. The case selected in this paper is an international inland port logistics park with a planning area of 60 square kilometers, covering 3 square kilometers of A town, B17 square kilometers, and the planning area of the core area of 30 square kilometers [25, 26]. The international land port logistics park gives full play to the advantages of location, industry, and multimodal transport and focuses on the construction of cross-border trade e-commerce industrial

park, cross-border e-commerce town, and other projects. The planning plan establishes the "four in one" international trade channel of high seas, air, and rail from 2015 to 2025 and strives to build a 100 billion level commercial logistics industrial cluster. The planning plan is shown in Figure 7.

In this paper, the development plan of an international inland port logistics park in the next 10 years is taken as a simulation case. The simulation data comes from the management committee of the international land port logistics park, the management committee of the cross-border trade e-commerce industrial park, and other units and departments. Some data are obtained through field research. Due to the need of commercial secrets and simulation, the data obtained in this paper are preprocessed in advance, so that the cellular automata (CA) model can be directly applied [27, 28].

4.2. Experimental Preparation. For the accurate push supply chain information, it is needed to evaluate the results of the push supply chain information. In order to truly and objectively evaluate the accuracy of information pushing, this paper constructs an index system to evaluate the informatization level of international land port logistics park based on the principles of science, system, and strong operability. In the selection of evaluation method, this paper uses the analytic hierarchy process (AHP). Firstly, the push results to be analyzed are hierarchical; secondly, according to the nature of the problem and the overall goal to be achieved, the problem is divided into different elements, and, according to the correlation between these elements and the relationship between them, the elements are combined according to different levels, so as to build a multilevel analysis structure model. Finally, compare the advantages and disadvantages of the push results and score them.

First of all, according to the evaluation index system mentioned above, the first level index mainly includes 6 items: infrastructure, development, and use of information resources, application of information technology, utilization and cultivation of logistics informatization talents, logistics informatization policies, regulations and standards, and sustainability of logistics informatization development. The average score of each index is taken. In this way, the index weight of each item can be obtained, as shown in Table 2.

The above method can be used to calculate the weight of each secondary index. Due to the layout problem, we will not list them one by one here. So far, the preparation of experimental data is completed.

4.3. Simulation Experiment Scheme. Under the above experimental preparation, it starts to build the experimental test environment of the supply chain information pushing method for logistics park based on the Internet of Things technology. Firstly, a Spark cluster with 6 virtual machines is built, one of which is set as the master node, and the other five are set as slave nodes. The parameters are shown in Table 3.

In the information pushing method of this paper, the main collaborative filtering algorithm uses the mean

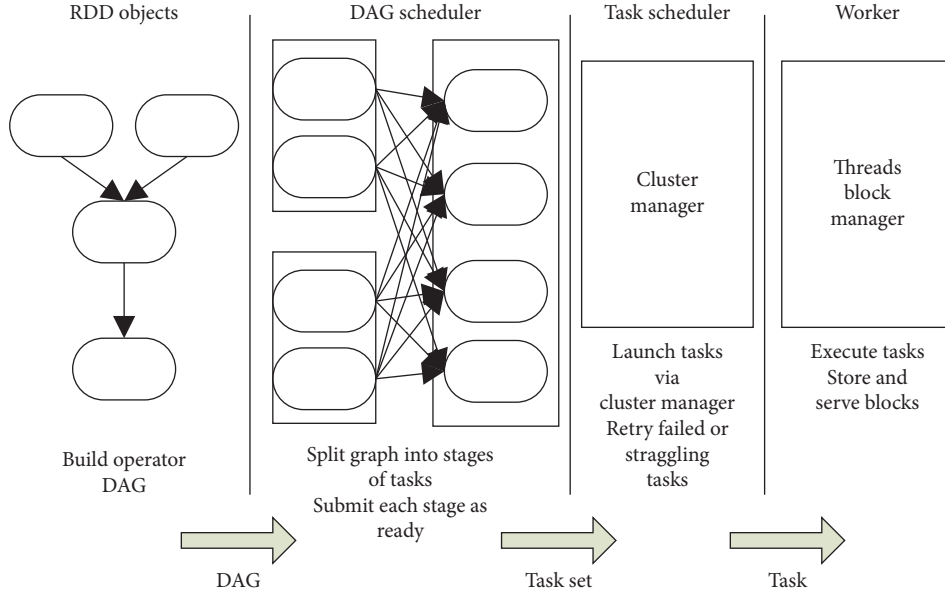


FIGURE 6: Operation architecture of Spark.

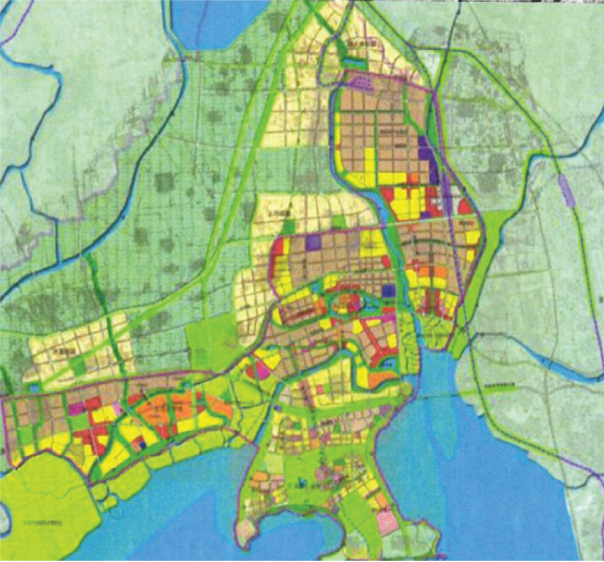


FIGURE 7: The planning plan of a city's international inland port logistics park.

absolute error MAE as the accurate evaluation index of the algorithm, which is different from the others that use the average values as the accurate evaluation. The calculation formula is defined as follows:

$$\text{MAE} = \frac{\sum_{i=1}^N |p_i - q_i|}{N} \quad (3)$$

In formula (3), N represents the amount of information, p_i represents the actual score of information, and q_i represents the prediction score of information. The smaller the MAE value is, the higher the accuracy of recommendation is. The proportions of training set and test set are 6:4, 7:3, 8:2, and 9:1, respectively. Based on the

relevant research data and literature model of international land port logistics park, the relevant parameters are set: the initial number of enterprises in the international land port logistics park is 1000, the status update interval is 10 days, the boundary of the model is periodic, the simulation time is 3600 days, and the relationship between the Internet of Things and these influencing factors is set as linear correlation. On this basis, the simulation model of the formation and development process of Qingdao international land port logistics park is developed.

4.4. Experimental Results and Analysis. Under the above experimental environment parameters, the traditional push method and the push method in this paper are used for experiments, and the push results of supply chain information of this method and the traditional method are obtained in the simulation software, as shown in Figure 8.

The experimental results show that, with the increase of the proportion of training set and test set, the MAE values of the three algorithms are decreasing, and the accuracy is improving. In the case of each proportion, the MAE value of the proposed algorithm is lower than those of the three traditional methods, which shows that the recommendation accuracy and performance of the proposed method based on the Internet of Things technology are higher.

Figure 8 shows the simulation results of the two methods when the ratio of training set and test set is 6:4. Figure (1) shows the simulation results obtained by the traditional method, and Figure (2) shows the simulation results obtained by this method. In order to facilitate comparison, this paper quantizes the simulation results and obtains the experimental results under different training set and test set proportions, as shown in Table 4.

TABLE 2: Index weight.

Index	R_1	R_2	R_3	R_4	R_5	R_6	W_1	Test
R_1	1	0.75	2	1.33	1.33	1.33	0.23	$C_r = 0.0214, < 0.1$; therefore, the consistency is satisfied
R_2	0.75	1	0.67	1	1	1	0.15	
R_3	0.5	0.67	1	0.67	0.67	0.67	0.13	
R_4	0.75	1	1.5	0.67	0.75	0.5	0.15	
R_5	0.75	1	1.5	1.33	0.67	0.67	0.26	
R_6	0.75	1	1.5	1	1.5	1.33	0.49	

TABLE 3: Parameters of software and hardware in the experiment.

Experimental parameters	Master node	Slave node
Operation platform	OpenStack cloud platform	OpenStack cloud platform
Virtual core	4 cores	2 cores
Running memory	64 G	16 G
Hard disk	128 G	128 G
JAVA	Java-7-oracle	Java-7-oracle
Linux	Ubuntu 12.04	Ubuntu 12.04
Spark	1.0.0	1.0.0

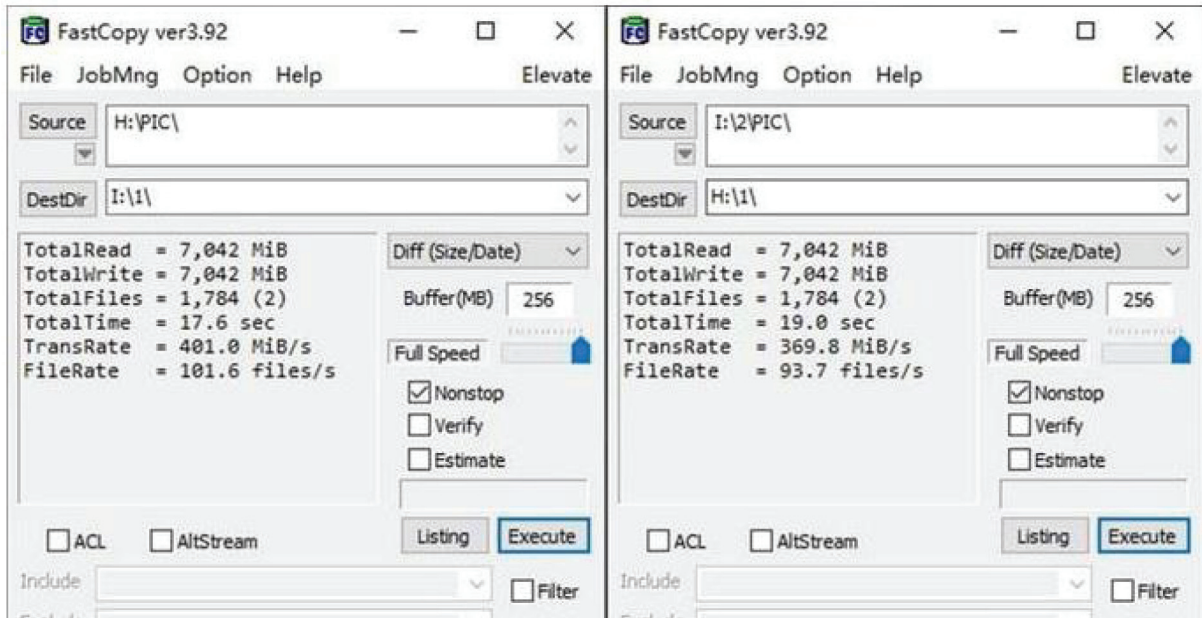


FIGURE 8: Simulation results of different pushing methods.

TABLE 4: MAE of different proportions of training set and test sets.

Proportions of training set and test set	MAE value				
	FPGA-IoT	ESS	Blockchain-IoT	AI-IoT	Our method
6:4	0.859	0.896	0.955	0.855	0.763
7:3	0.854	0.832	0.841	0.832	0.741
8:2	0.852	0.811	0.845	0.811	0.726
9:1	0.847	0.766	0.823	0.803	0.709

5. Conclusion

Through the Internet of Things technology, according to the difference of task environment of different users, the task context-aware information processing model of logistics park is constructed, which provides data exchange and

distribution services, carries out intelligent push service of business information, and enhances the timeliness and adaptability of the system to meet the needs of complex task environment. At present, aiming at the problems of existing information pushing methods, this paper designs a supply chain information pushing method for logistics park based

on Internet of Things technology. The simulation results show that the proposed method can effectively improve the recommendation accuracy. Although this method has achieved some results, there are still two problems. One is the failure to achieve intelligent resource information acquisition, and intelligent resource information acquisition events trigger push information events. Another problem is that the mining of user demand information is not deep enough. If the user need information cannot be completely obtained, then the role of information pushing is not obvious or even cannot push any information.

In the future research, it is necessary to study the following aspects:

- (1) Further study the related algorithms of information mining in push technology, and improve the establishment of demand tree by combining scenario modeling and collaborative filtering technology.
- (2) According to the nature of each node in the Internet of Things, improve the system code, and combine the information collection event with the push system.
- (3) Expand the Internet of Things platform, so that it is not only suitable for simple information pushing service but also suitable for a variety of Internet of Things push methods, such as client tools, web push, and microblog push.

Data Availability

The data used to support the findings of this study are available from the corresponding author upon request.

Conflicts of Interest

The author declares that there are no conflicts of interest.

Acknowledgments

This research was supported by the major projects of Natural Science Research in Colleges and Universities of Jiangsu Province (no. 17KJA413002).

References

- [1] M. Mayer and A. J. Baemner, "A megatrend challenging analytical chemistry: biosensor and chemosensor concepts ready for the internet of things," *Chemical Reviews*, vol. 119, no. 13, pp. 7996–8027, 2019.
- [2] X. Zhong, L. Li, S. Zhang, and R. Lu, "ECOR: an energy aware coded opportunistic routing for cognitive radio social internet of things," *Wireless Personal Communications*, vol. 110, no. 1, pp. 1–20, 2020.
- [3] M. A. Carlos-Mancilla, L. F. Luque-Vega, H. A. Guerrero-Osuna, G. Ornelas-Vargas, Y. Aguilar-Molina, and L. E. González-Jiménez, "Educational mechatronics and internet of things: a case study on dynamic systems using MEIoT weather station," *Sensors*, vol. 21, no. 1, p. 181, 2020.
- [4] Q. L. Kweh, W.-M. Lu, F. Lin et al., "Impact of research and development tax credits on the innovation and operational efficiencies of Internet of things companies in Taiwan," *Annals of Operations Research*, pp. 1–25, 2021, (prepublish).
- [5] H. Wei, H. Luo, and Y. Sun, "Mobility-aware service caching in mobile edge computing for internet of things," *Sensors*, vol. 20, no. 3, pp. 610–630, 2020.
- [6] A. Qaffas Alaa, H. Rakibul, and A. Najah, "The internet of things and big data analytics for chronic disease monitoring in Saudi arabia," *Telemedicine Journal and E-Health: The Official Journal of the American Telemedicine Association*, vol. 27, no. 1, 2020.
- [7] G. Lyu, L. Chen, and B. Huo, "The impact of logistics platforms and location on logistics resource integration and operational performance," *The International Journal of Logistics Management*, vol. 30, no. 2, pp. 549–568, 2019.
- [8] C. Han, J. Otto, and M. Dresner, "A typological analysis of US transportation and logistics jobs: automation and prospects," *Transportation Journal*, vol. 58, no. 4, pp. 323–341, 2019.
- [9] N. Pushpamali, D. Agdas, T. M. Rose, and Rose, "A review of reverse logistics: an upstream construction supply chain perspective," *Sustainability*, vol. 11, no. 15, p. 4143, 2019.
- [10] R. Yates, N. Power, and J. Buckley, "Characterizing the transfer of program comprehension in onboarding: an information-push perspective," *Empirical Software Engineering*, vol. 25, no. 1, pp. 940–995, 2020.
- [11] J. W. Fowler, S.-H. Kim, L. Dan, and Shunk, "Design for customer responsiveness: decision support system for push-pull supply chains with multiple demand fulfillment points," *Decision Support Systems*, vol. 123, pp. 113071.1–113071.14, 2019.
- [12] U. Rehmat, R. Muhammad Atif Ur, and B. S. Kim, "Hierarchical name-based mechanism for push-data broadcast control in information-centric multihop wireless networks," *Sensors (Basel, Switzerland)*, vol. 19, no. 14, pp. 1914–3034, 2019.
- [13] P. Basu, Q. Liu, and J. Stallaert, "Supply chain management using put option contracts with information asymmetry," *International Journal of Production Research*, vol. 57, no. 6, pp. 1772–1796, 2019.
- [14] J. Van Eeden, M. Bvuchete, and S. S. Grobbelaar, "Best practices for demand-driven supply chain management in public healthcare sector: a systematic literature review," *South African Journal of Industrial Engineering*, vol. 31, no. 2, 2020.
- [15] Z. Zhou, Y. Liu, H. Yu, and Q. Chen, "Logistics supply chain information collaboration based on FPGA and internet of things system," *Microprocessors and Microsystems*, vol. 80, Article ID 103589, 2021.
- [16] Z. Zhang, Y. Xue, J. Li et al., "Supply chain logistics information collaboration strategy based on evolutionary game theory," *IEEE Access*, vol. 8, pp. 46102–46120, 2020.
- [17] Y. Zhou and X. Xu, "Intelligent supply chain information system based on internet of things technology under asymmetric information," *Symmetry*, vol. 11, no. 5, p. 656, 2019.
- [18] A. Q. Song, Y. Chen, Y. Zhong et al., "A supply-chain system framework based on internet of things using Blockchain technology," *ACM Transactions on Internet Technology*, vol. 21, no. 1, pp. 1–24, 2021.
- [19] H. Fu and Y. Ma, "Optimization and coordination of decentralized supply chains with vertical cross-shareholding," *Computers & Industrial Engineering*, vol. 132, pp. 23–35, 2019.
- [20] F. Wen, Y. Zhao, M. Zhang, and C. Hu, "Forecasting realized volatility of crude oil futures with equity market uncertainty," *Applied Economics*, vol. 51, no. 59, pp. 6411–6427, 2019.
- [21] J. Cao and F. Wen, "The impact of the cross-shareholding network on extreme price movements: evidence from China," *Journal of Risk*, vol. 22, no. 2, pp. 79–102, 2019.

- [22] B. Javier and M. C. Juan, "Neural networks in distributed computing and artificial intelligence," *Neurocomputing*, vol. 272, 2018.
- [23] H. C. C. Carneiro, C. E. Pedreira, F. M. G. França, and P. M. V. Lima, "A universal multilingual weightless neural network tagger via quantitative linguistics," *Neural Networks*, vol. 91, pp. 85–101, 2017.
- [24] C. James, J. Matti, H. K. Janne, and B. Mark, "Bayesian network structure learning with integer programming: polytopes, facets and complexity," *Journal of Artificial Intelligence Research*, vol. 58, pp. 85–229, 2017.
- [25] A. Burduk, "Artificial neural networks as tools for controlling production systems and ensuring their stability," *Lecture Notes in Computer Science*, vol. 8104, pp. 487–498, 2017.
- [26] Y. Gao, A. Xu, P. J.-H. Hu, and T.-H. Cheng, "Incorporating association rule networks in feature category-weighted naive Bayes model to support weaning decision making," *Decision Support Systems*, vol. 96, pp. 27–38, 2017.
- [27] S. Bouaafia, R. Khemiri, F. E. Sayadi, and M. Atri, "Fast CU partition-based machine learning approach for reducing HEVC complexity," *Journal of Real-Time Image Processing*, vol. 17, no. 1, pp. 185–196, 2020.
- [28] S. Hoochang, H. R. Roth, M. Gao et al., "Deep convolutional neural networks for computer-aided detection: CNN architectures, dataset characteristics and transfer learning," *IEEE Transactions on Medical Imaging*, vol. 35, no. 5, p. 1285, 2016.

Research Article

Research on Biomechanical Simulation and Simulation of Badminton Splitting and Hanging Action Based on Edge Computing

Bo Zhang 

College of Sports and Health, Guangzhou Sport University, Guangzhou 510500, China

Correspondence should be addressed to Bo Zhang; 51073@gzsport.edu.cn

Received 9 February 2021; Revised 15 April 2021; Accepted 17 April 2021; Published 27 April 2021

Academic Editor: Hsu-Yang Kung

Copyright © 2021 Bo Zhang. This is an open access article distributed under the Creative Commons Attribution License, which permits unrestricted use, distribution, and reproduction in any medium, provided the original work is properly cited.

Sports biomechanics refers to the science of the laws of mechanical motion produced in the process of biological movement. Its essence is to systematically and digitally reconstruct the fundamental attributes and characteristics of motion. At present, the research of sports biomechanics mainly focuses on the theoretical research of basic aspects and lacks the new technology of sports biomechanics digital simulation innovation and data measurement. This article takes the badminton chopping action as the research object and carries out biomechanical simulation and simulation research with the help of edge computing and genetic algorithm. First of all, this paper constructs a badminton chopping and hanging action system framework based on edge computing, so as to facilitate simulation and improve data transmission efficiency. Secondly, genetic algorithm is used in biomechanics simulation and simulation optimization and data analysis process. System testing and simulation verify the excellent performance of the biomechanical simulation of badminton chopping and hanging action established in this paper. The research will provide a reference for the academic circles to explore the field of sports biomechanics.

1. Introduction

Sports biomechanics refers to the science of the laws of mechanical motion produced in the process of biological motion [1]. Its essence is to systematically and digitally reconstruct the fundamental attributes and fundamental characteristics of sports. Broadly speaking, sports biomechanics is the characteristics and evaluation of the state and attributes of all sports, and it is a comprehensive evaluation and analysis of all aspects of sports [2, 3]. In a narrow sense, sports biomechanics is a study on the state of human motion. The object and main purpose of the study is human, and the mechanics in the basic category of physics is introduced into the concept of research. In short, sports biomechanics in the narrow sense is actually to simplify and objectify the connection activities of nerves, muscles, and joints in the process of human motion, as the gear link in the overall driving system, and only discuss the effects of this system [4, 5]. The resulting force changes are analyzed and simulated in the digital form.

It is worth noting that the current sports biomechanics not only is a pure subject attribute and subject characteristic but also covers human anatomy, human biology, mechanics within the physical category, and psychology and other related fields. It is a comprehensive and academic direction with a multidisciplinary nature [6–8]. That is, from the perspective of fundamental properties, the essence of sports biomechanics is the combination of mathematics and mechanics, and its main research is to capture, reconstruct, analyze, and then judge the action based on the construction of mathematical models, computer, or model simulation [9]. Through the analysis of the force and angle in the athlete's sports state, the overall sports performance can be evaluated and improved [10–12]. The development of sports biomechanics is an emerging discipline with broad prospects for development. In the current academic circles, the interest in sports biomechanics is very high, showing a positive state of affairs [13]. According to the results of our previous literature research, through the synthesis of a large number of domestic and

foreign literatures related to the research direction of sports biomechanics, from the current research status, the current research on sports biomechanics mainly focuses on basic theoretical research. Actions in actual training sports require multiple simulations and guidance in postures and motion states. Research and discussion on teaching methods, etc., involving a series of sports factors including athletes, movements, and sports equipment [14, 15].

At present, the research of sports biomechanics mainly focuses on the theoretical research of basic aspects and lacks the new technology of sports biomechanics digital simulation innovation and data measurement [16]. This article takes the badminton chopping action as the research object and carries out biomechanical simulation and simulation research with the help of edge computing and genetic algorithm. The research will provide a reference and reference for the academic circles to explore the field of sports biomechanics.

2. Related Overview

2.1. Edge Computing. As an emerging technology, mobile edge computing was first proposed by ETSI and has now become a research hotspot in academia and industry [17, 18]. In recent years, research on task scheduling strategies in mobile edge computing has also achieved certain results. Research on task scheduling can be roughly divided into device task offloading strategy, edge cloud task scheduling strategy, and task coordination scheduling strategy between the device and the edge cloud. In the MEC network architecture, computing and storage capabilities are delegated to the edge of the mobile network, such as base stations and wireless access points [19, 20]. Mobile devices can offload application tasks to nearby computing nodes for processing, thereby obtaining low-latency and high-reliability computing services. In the 5G mobile network, the basic network architecture of MEC consists of three parts: mobile devices, edge cloud, and core network [21–23].

In addition to the breakthrough of basic theory and the reform of digital simulation technology, the innovation in the field of sports biomechanics in my country has also made breakthroughs in the practical application of sports biomechanics. Biomechanics diagnosis technology is the innovation of its application model. Based on big data platform and high-speed networked information means, it realizes the collection of information on the competition venue and training venue and the evaluation of the overall sports state of athletes [24, 25]. Figure 1 shows the innovation path of biomechanical diagnosis technology based on edge computing.

At present, sports biomechanics diagnosis technology is integrated with multiple disciplines, such as the development of wearable devices, visual analysis, and smart monitoring based on big data, which can achieve precise and personalized diagnosis for different competition types and different sports people [26].

2.2. Overview of the Development of Sports Mechanics. The development of sports biomechanics has experienced the initial generalization of simple motor functions with

anatomy and mechanics as the core [27, 28]. Later, in the 18th century, there has been an exploration of the essence and principle of specific forms of motion, until the exploration of forms of motion with human sports as the core. In fact, the study of human body motion biomechanics relies on the rise of sports, the expansion of fast-developing computer technology, and the breakthrough of simulation experiment technology. The research covers athletes' technical movement simulation research, technical analysis research, conceptual connotation research, mechanics principal research, digital simulation technology research, theoretical practice research, training research, teaching research, etc. [29, 30]. The biomechanical research content of badminton chopping and hanging action is shown in Figure 2.

The development of modern sports mechanics does not use the nervous system, muscle system, and bone and joint system as the main research methods [31, 32]. The research also actively introduced quantifiable mathematical elements, using space, numbers, and motion trajectories as elements to construct a mathematical model, using coordinates as the evaluation of the human body's front, back, left, and right torso directions, and using numbers as an explanation of the movement process [33, 34]. The dynamic equation model is used for comprehensive analysis and query. This method is essentially a simulation and analysis method of the actual human motion, and it is the main direction of current development. Through a large number of literature searches in the early stage, from the current research situation, the current development of sports mechanics is still concentrated on the simulation and comprehensive analysis of athletes' technical movements and the in-depth research on the basic concepts and basic theories of sports biomechanics [35]. The research involves sports equipment research, sports biomechanics training methods, and sports biomechanics teaching methods. Figure 3 shows the framework of the biomechanical innovation model of badminton splitting and hanging.

In the field of physiology, the current innovative research includes differentiated and refined analysis of the individual body physique [36]. It mainly proposes that, in addition to real-time monitoring of basic physiological indicators such as muscle tension, heartbeat, blood pressure, blood lipids, and blood sugar, it is specifically proposed for the monitoring of blood lactic acid, to comprehensively evaluate the athletes' anaerobic glycolysis and acid tolerance, to evaluate the impact of exercise intensity and exercise duration on human blood lactic acid levels, and to pay attention to blood lactic acid levels during normal training and competition. The specific differences: in the field of mechanics, the most innovative research currently is the study of muscle mechanics. After breaking through the limitations of Newtonian mechanics in vitro sports mechanics, muscle mechanics is mainly based on muscles as the main research object, with the Hill equation as the main calculation formula, muscle tension and muscle strength as measurement indicators to explore the in-body muscles during exercise the model of mechanics, explore its synergy and recovery effect, etc., and to try new fields of mechanics. We have introduced

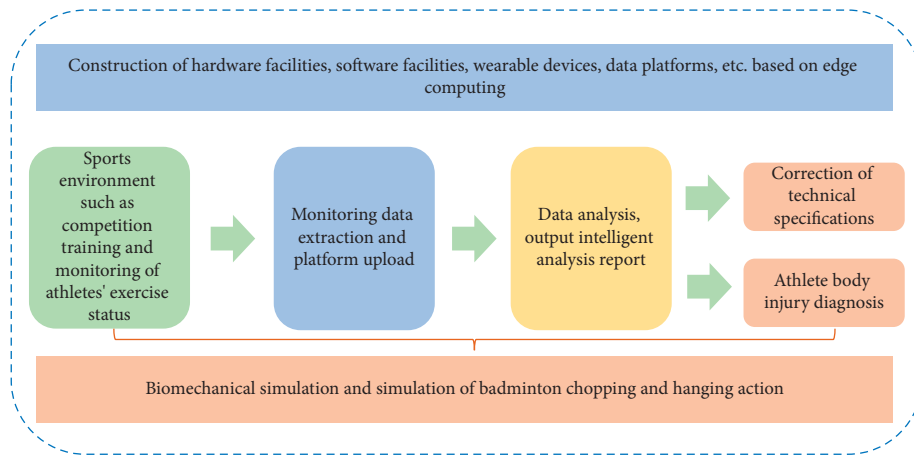


FIGURE 1: Innovation path of biomechanical diagnosis technology based on edge computing.

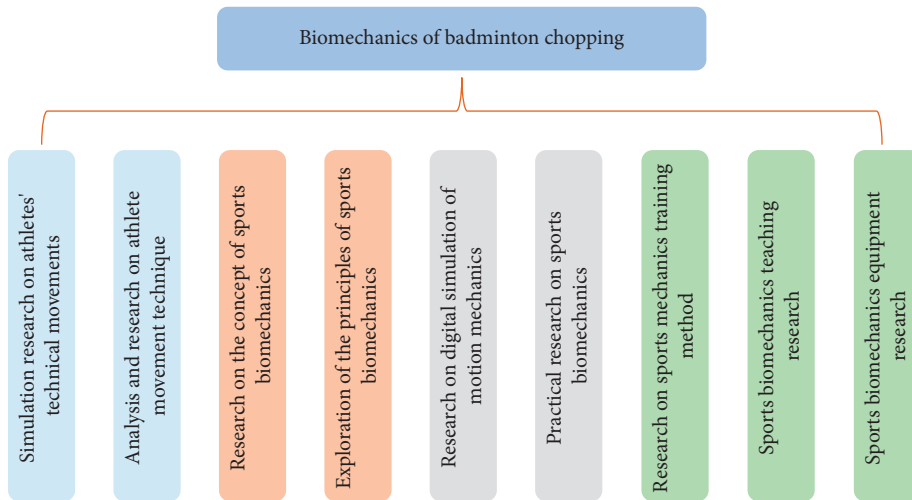


FIGURE 2: Biomechanical research content of badminton chopping and hanging action.

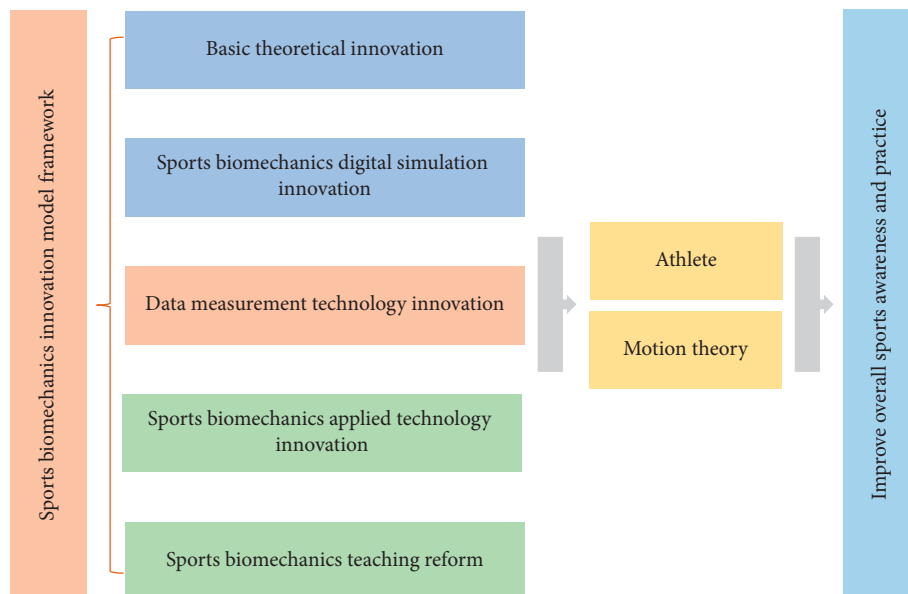


FIGURE 3: Framework of the biomechanical innovation model of badminton chopping and hanging.

the content of sports biomechanics and the current status of development.

3. Biomechanical Simulation of Badminton Chopping and Hanging Action Based on Genetic Algorithm

Sports biomechanics digital simulation innovation is mainly based on new mathematical functions, mathematical formulas, new computer algorithms, and matrix equations as the main research objects. The fusion smoothing algorithm of the unscented Kalman filter is currently a representative digital simulation innovation. In the traditional algorithm, two-dimensional coordinates are mainly used for tracking and analysis. However, the tracking and practice of motion needs to be simulated and analyzed by a three-dimensional algorithm. There must be nonlinear changes and digital modeling under the guidance of nonlinearities. The variables that exist in the measurement of the human body's motion state include state variables and random variables. The distribution of variables will take into account the Gaussian distribution and the nonlinear distribution and cover the phenomenon of matrix transition and mean shift. The introduction of innovative algorithms can accurately and steadily track the human body's posture in the process of complex calculations, reflect the motion characteristics in real time, and achieve accurate assessment of the human motion state.

The basic idea of the genetic algorithm is to start with a set of feasible solutions to the optimization problem, according to the principle of survival of the fittest and survival of the fittest, and evolve from generation to generation to produce better and better feasible solutions. In each generation, according to the fitness of the feasible solution, a part of the good body is selected to be copied to the next generation, and operations such as crossover are performed to generate a set representing the new solution. The optimal individual in the whole process is the optimal solution. Design a new task pricing scheme according to the requirements of the topic, that is, a problem of eliminating the factors of small relevance. Therefore, when designing the fitness function [5], the original objective function value is used as the fitness value to ensure that excellent individuals have a large adaptation value. The target value can be converted into a fitness value through the scale transformation of the following formula, namely,

$$\text{Fitness}(I) = \frac{D_{\max} - D_i + \alpha}{D_{\max} - D_{\min} + \alpha}, \quad (1)$$

where I is the first chromosome of the current population, $\text{Fitness}(I)$ is the fitness function value, D_{\max} is the minimum target value of the current population, is the minimum target value of the current population, D_{\min} is the target value to be converted, and D_i is the open interval $(0, 1)$ positive real numbers within.

The roulette operation is used to select the fitness value. First, generate a random number $\alpha(0 \leq \alpha \leq 1)$ and then choose according to the following formula:

$$\sum_{j=1}^n \frac{f(x^{j-1})}{\sum_{n=1}^{\text{pop-size}} f(x^{j-1})} \leq \alpha \leq \sum_{j=1}^n \frac{f(x^j)}{\sum_{n=1}^{\text{pop-size}} f(x^j)}. \quad (2)$$

Through this operation, the parent population that needs to be reproduced can be selected. Using single-point crossover and uniform mutation operators, the calculation expressions for crossover and mutation probability are as follows:

$$P_c \begin{cases} k_2, & f' \leq f_{\text{avg}}, \\ \frac{k_1(f_{\max} - f')}{f_{\max} - f_{\text{avg}}}, & f' \geq f_{\text{avg}}, \end{cases} \quad (3)$$

$$P_m \begin{cases} k_4, & f \leq f_{\text{avg}}, \\ \frac{k_3(f_{\max} - f)}{f_{\max} - f_{\text{avg}}}, & f \geq f_{\text{avg}}, \end{cases} \quad (4)$$

where f_{\max} is the largest fitness value in the group, f_{avg} is the average fitness value of each generation of the group, f' is the larger fitness value of the two individuals to be crossed, and f is the fitness value of the individual to be mutated.

$$X_{ij} = \sum_{n=1}^5 X_{ijne}. \quad (5)$$

The evaluation index of all evaluation experts is V_{ij} , and the gray evaluation right of the first evaluation gray category is r_{ije} :

$$r_{ije} = \frac{X_{ijne}}{X_{ij}}. \quad (6)$$

Evaluation index V_{ij} is the gray evaluation weight vector $rij = (rij1, rij2, rij3)$ for each category. Synthesize the gray evaluation weight vector, and obtain the gray evaluation weight matrix R_i :

$$R_i = \begin{Bmatrix} ri1 \\ ri2 \\ \dots \\ rij \end{Bmatrix} = \begin{Bmatrix} ri11 & ri12 & ri13 \\ ri21 & ri22 & ri23 \\ \dots & \dots & \dots \\ rij1 & rij2 & rij3 \end{Bmatrix}. \quad (7)$$

If the difference in fitness values between chromosomes is large, the fitness value ratio selection is adopted; if the interval is relatively small, the selection tends to be randomly selected among competing chromosomes. Next, focus on the current innovative research in sports biomechanics, try to build an innovative model framework covering new ideas and methods, and achieve breakthroughs in the field of sports biomechanics from multiple dimensions and multiple system levels. Our overall framework mainly covers basic theoretical innovation, sports biomechanics digital simulation innovation, sports biomechanics data measurement and measurement technology, sports biomechanics application technology innovation, sports biomechanics teaching reform, etc. and strives to achieve the depth of sports biomechanics innovation the study.

4. Badminton Biomechanics Test Analysis

In the study of sports biomechanics, data capture and measurement technology is the most critical. Only by realizing the data-based capture and measurement in the early stage can the subsequent digital modeling, matrix analysis, algorithm evaluation, and other series of sports mechanics research be realized. The innovation of sports biomechanics measurement data currently includes balance force testing technology, muscle tension testing technology, stress testing technology, electrophysiological testing technology, medical testing technology, infrared testing technology, and ultra-high-speed motion capture technology. Figure 4 shows the biomechanical test results of badminton splitting and hanging.

At present, the research field of athlete’s technical action simulation in our country is mainly based on camera photography capture technology as the main method. Explore the capture of athletes’ movements by different equipment and equipment, as well as possible problems and improvement methods in the process. Figure 5 shows the impact performance test of the badminton split-hanging system.

Sports biomechanics digital simulation technology: the connotation of sports biomechanics is for the study of physiology and mechanics during exercise. Its main research method is to introduce mathematical models or mathematical formulas for deduction. Therefore, digital simulation technology is sports biology. The focus of mechanic’s research: at present, the main research focuses on the exploration of classical algorithms, matrix models, and measurement methods in mathematics and the introduction of artificial intelligence, high-speed computers, and simulation technology to enrich the research in this field. Figure 6 shows the simulation test result of the spatial distribution of badminton splitting and hanging motion.

Research on basic concepts and basic theory of sports biomechanics: in the research of kinematics and zoology, the research involving basic concepts and basic theoretical knowledge is also extremely rich. The basic research of sports biomechanics is basically based on the body’s physical motor functions including the nervous system, muscle tissue, and skeletal joint system, as well as the categories of gravity, friction, force, and reaction in the field of physics. It is basically a further expansion of the field of mechanics and physiology. Figure 7 shows the simulation results of muscle tension performance of badminton splitting and hanging.

Research on sports biomechanics training methods: theoretical research and breakthroughs are to better guide practice and application, so training methods based on competition and fitness as the main purpose are also the focus of current sports biomechanics research. Under the guidance of sports biomechanics theory, professional athletes in sports competitions are trained to improve the scientific, durability, and explosive power of athletes’ sports and, at the same time, take into account the physical and psychological state of athletes. The comparison between genetic algorithm and Bi-LSTM, gradient descent decision tree, and other methods is shown in Figure 8.

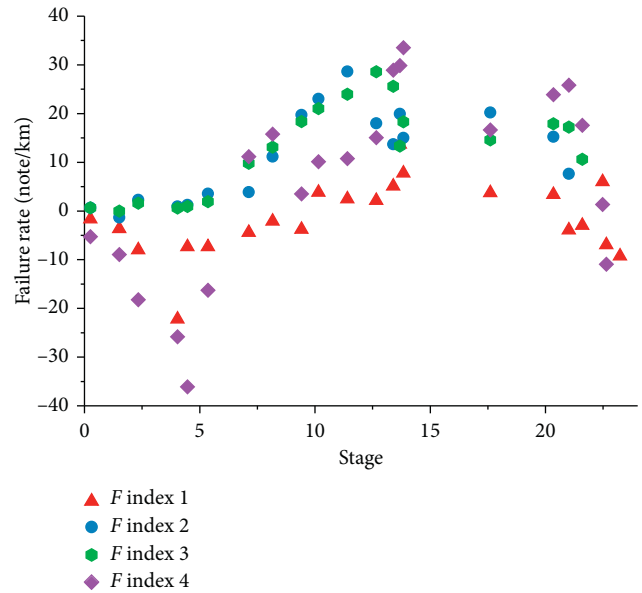


FIGURE 4: Badminton splitting and hanging balance mechanics test results.

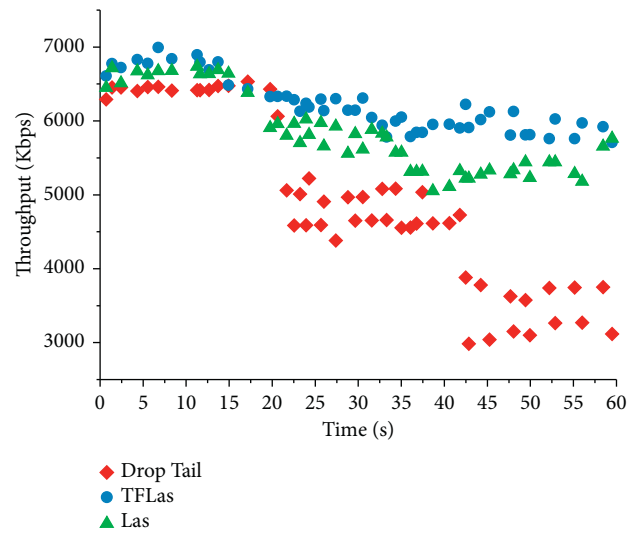


FIGURE 5: Impact performance test of badminton split-hanging system.

In this paper, genetic algorithm is applied to biomechanical simulation, simulation optimization, and data analysis optimization process. In addition, the method is compared with Bi-LSTM, gradient descent decision tree, and other methods. We use the data optimization accuracy rate as an indicator, and the comparison result is shown in Figure 7. Genetic algorithm is better than Bi-LSTM and gradient descent decision tree in the direction of sports biomechanics data optimization [37, 38]. System testing and simulation verify the superiority of the method established in this paper. The biomechanical simulation of badminton cutting and suspension motion established by this method has excellent performance.

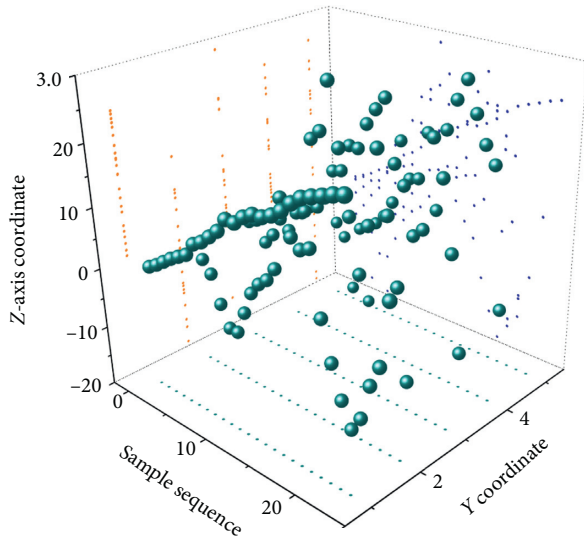


FIGURE 6: Simulation test of the spatial distribution of badminton splitting and hanging movement.

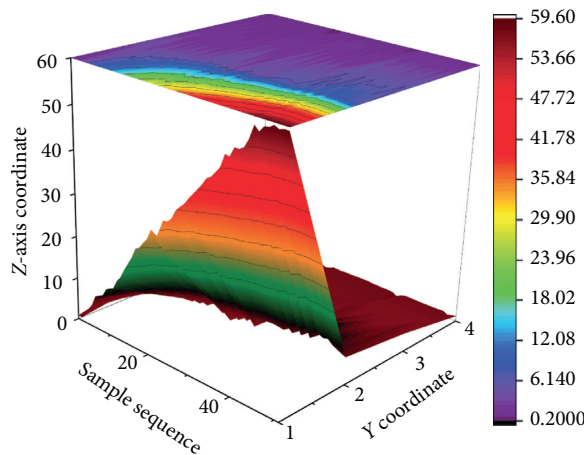


FIGURE 7: Simulation results of muscle tension performance of badminton splitting.

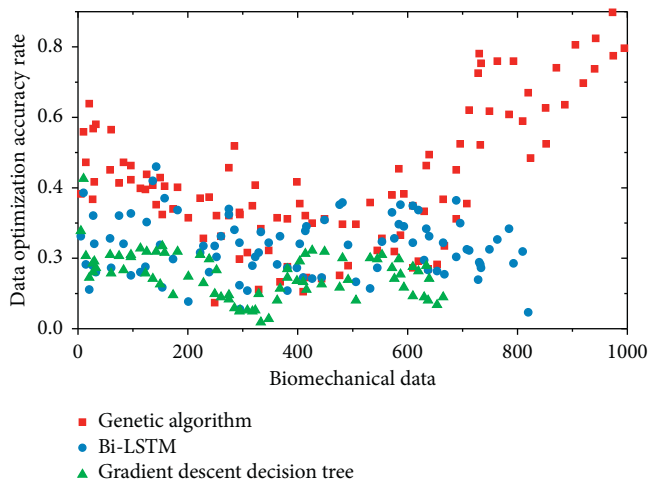


FIGURE 8: Comparison of genetic algorithm with Bi-LSTM, gradient descent decision tree, and other methods.

5. Conclusion

At present, a large number of new methods and methods have emerged in the teaching reform of sports biomechanics, mainly focusing on breakthroughs in teaching methods. At present, the importance of sports biomechanics in sports education is increasing day by day, but there are problems such as single teaching methods, solid thinking, and unmatched hardware and software equipment. In short, the innovation of teaching methods allows athletes to have a deep understanding of the biomechanical principles of their own sports and to better realize the evaluation of sports status and the cultivation of athletic ability. In the current research field of sports biomechanics, thanks to the vigorous development of high-precision technology and continuous breakthroughs in biophysiological theory, multidisciplinary can be integrated with sports biomechanics for innovation and development, such as virtual simulation technology and artificial intelligence. It can be combined with sports biomechanics to continuously open up new research fields and realize the development and application of new technologies and methods. We propose a good development prospect for the application of this field in the actual sports process, the changes in the physiological function of the athlete's overall sports state, and the expansion of various sports fields and sports trends, which are conducive to continuous breakthroughs in the field of sports biomechanics.

Data Availability

The datasets used and/or analyzed during the current study are available from the corresponding author on reasonable request.

Conflicts of Interest

The author declares that he has no conflicts of interest.

References

- [1] C. Michie, I. Andonovic, C. Davison, A. Hamilton, and M. Gilroy, "The Internet of Things enhancing animal welfare and farm operational efficiency," *Journal of Dairy Research*, vol. 87, no. 1, pp. 1–8, 2020.
- [2] N. Matheusara, L. Hernández-Ramos José, and F. Skarmetaantonio, "Baldinagianmarco, A survey of cybersecurity certification for the internet of things," *Acm Computing Surveys*, vol. 23, no. 3, pp. 233–245, 2020.
- [3] M. Tozakidou, I. Apine, K. U. Petersen et al., "Comparison of different iterative CT reconstruction techniques and filtered back projection for assessment of the medial clavicular epiphysis in forensic age estimation," *International Journal of Legal Medicine*, vol. 134, no. 1, pp. 355–361, 2020.
- [4] S. Luo, L. Zheng, S. Luo, N. Gu, and X. Tang, "Data sustained misalignment correction in microscopic cone beam CT via optimization under the Grangeat Epipolar consistency condition," *Medical Physics*, vol. 47, no. 2, pp. 45–58, 2020.
- [5] J. Liu, H. R. Zhao, H. L. Wei et al., "Efficacy of bronchoalveolar lavage as adjunct therapy in the treatment of neonatal severe pneumonia: a prospective case-control study," *Journal of Tropical Pediatrics*, vol. 34, no. 5, pp. 532–546, 2020.

- [6] J. Liu, H. R. Zhao, H. L. Wei, C. Chen, and Y. Q. Gao, "Efficacy of bronchoalveolar lavage as adjunct therapy in the treatment of neonatal severe pneumonia: a prospective case-control study," *Journal of Tropical Pediatrics*, vol. 19, no. 34, pp. 612–625, 2020.
- [7] F. Liu, L. Lei, L. Haitao, S. Liping, and P. Longkai, "The level of plasm donor-derived cell-free dna in kidney transplant patients with severe pneumonia," *Transplantation*, vol. 12, no. 9, pp. 154–167, 2020.
- [8] F. Kassem and G. Kang, "Shin, security and privacy in the internet of things," *Computer*, vol. 43, no. 13, pp. 765–778, 2019.
- [9] H. Jiang, Z. Xiao, Z. Li, J. Xu, and D. Wang, "An energy-efficient framework for internet of things underlying heterogeneous small cell networks," *IEEE Transactions on Mobile Computing*, vol. 22, no. 99, pp. 413–425, 2020.
- [10] J. Huang, J. Guo, H. Li, W. Huang, and T. Zhang, "Efficacy and safety of adjunctive corticosteroids therapy for patients with severe community-acquired pneumonia: a systematic review and meta-analysis," *Medicine*, vol. 98, no. 13, pp. 235–246, 2019.
- [11] P. Guilpain, C. L. Bihan, V. Foulongne, P. Taourel, and V. L. Moing, "Rituximab for granulomatosis with polyangiitis in the pandemic of covid-19: lessons from a case with severe pneumonia," *Annals of the Rheumatic Diseases*, vol. 2020, pp. 537–549, 2020.
- [12] M. D. Greg Zaharchuk and S. Guido Davidzon, "AI for optimization and interpretation of PET/CT and PET/MR images-ScienceDirect," *Seminars in Nuclear Medicine*, vol. 43, no. 11, pp. 127–134, 2020.
- [13] L. Fichera, G. Li-Destri, and N. Tuccitto, "Fluorescent nanoparticle-based Internet of things," *Nanoscale*, vol. 32, no. 14, pp. 212–234, 2020.
- [14] H. Eric and J. Paulina, "Internet of things: energy boon or bane?" *Science*, vol. 43, no. 14, pp. 323–344, 2019.
- [15] A. M. Dimmitt, J. A. Pelz, M. E. Albertson et al., "Evaluation of adaptive statistical iterative reconstruction-V reconstruction algorithm vs filtered back projection in the detection of hypodense liver lesions: reader performance and preferences," *Journal of Computer Assisted Tomography*, vol. 43, no. 12, pp. 231–245, 2019.
- [16] Z. Deng, H. U. Yuxing, P. Yang, P. Zheng, and X. Tian, "Diagnosis and treatment of an acute severe pneumonia patient with COVID: case report," *Journal of Medical Virology*, vol. 63, no. 14, pp. 412–424, 2020.
- [17] Z. Deng, Y. Hu, P. Yang et al., "Diagnosis and treatment of an acute severe pneumonia patient with COVID-19: case report," *Journal of Medical Virology*, vol. 17, no. 13, pp. 2405–2412, 2020.
- [18] K. Cho, J. Chae, R.-Y. Kwon, S.-C. Bong, and K.-S. Cho, "The application of the filtered backprojection algorithm to solar rotational tomography," *The Astrophysical Journal*, vol. 895, no. 1, pp. 55–67, 2020.
- [19] W.-C. Chen, J.-S. Niu, I.-P. Liu et al., "Study of a palladium (Pd)/Aluminum-Doped zinc oxide (AZO) hydrogen sensor and the kalman algorithm for internet-of-things (IoT) application," *IEEE Transactions on Electron Devices*, vol. 67, no. 10, pp. 4405–4412, 2020.
- [20] J. Chauhan and P. Goswami, "An integrated metaheuristic technique-based energy aware clustering protocol for Internet of Things based smart classroom," *Modern Physics Letters B*, vol. 12, no. 1, pp. 205–220, 2020.
- [21] V. Chang, V. M. Muoz, and M. Ramachandran, "Emerging applications of internet of things, big data, security, and complexity: special issue on collaboration opportunity for IoTBDS and COMPLEXIS," *Computing*, vol. 43, no. 2, pp. 323–341, 2020.
- [22] R. Ceipek, J. Hautz, A. D. Massis, K. Matzler, and L. Ardito, "Digital transformation through exploratory and exploitative internet of things innovations: the impact of family management and technological diversification," *Journal of Product Innovation Management*, vol. 23, no. 7, pp. 143–156, 2020.
- [23] D. T. Braddock, P. R. Stabach, K. Zimmerman, D. Kavanagh, C. T. Sauei, and K. J. Yarema, "Protein engineering and glycan optimization improves pharmacokinetics of an enzyme biologic 10-fold," *Faseb Journal*, vol. 33, no. 12, pp. 125–136, 2019.
- [24] R. Boudewijns, Z. Wang, J. V. Weyenbergh, S. Kaptein, and H. J. Thibaut, "STAT2 signaling restricts viral dissemination but drives severe pneumonia in SARS-CoV-2 infected hamsters," *Nature Communications*, vol. 11, no. 4, pp. 58–74, 2020.
- [25] D. Blez, A. Soulier, F. Bonnet, E. Gayat, and M. Garnier, "Monitoring of high-flow nasal cannula for SARS-CoV-2 severe pneumonia: less is more, better look at respiratory rate," *Intensive Care Medicine*, vol. 13, no. 4, pp. 160–184, 2020.
- [26] M. Beckmann, P. Maass, and J. Nickel, "Error analysis for filtered back projection reconstructions in Besov spaces," *Inverse Problems*, vol. 37, no. 1, 2020.
- [27] O. Barker, "Realizing the promise of the internet of things in smart buildings," *Computer*, vol. 53, no. 2, pp. 76–79, 2020.
- [28] M.-P. Hosseini, T. X. Tran, D. Pompili, K. Elisevich, and H. Soltanian-Zadeh, "Multimodal data analysis of epileptic EEG and rs-fMRI via deep learning and edge computing," *Artificial Intelligence in Medicine*, vol. 104, 2020.
- [29] M. A. Guillén, A. Llanes, B. Imbernón, R. Martínez-Espaa, and J. M. Cecilia, "Performance evaluation of edge-computing platforms for the prediction of low temperatures in agriculture using deep learning," *Journal of Supercomputing*, vol. 77, no. 9, pp. 145–153, 2021.
- [30] M. Gairing and R. Savani, "Computing stable outcomes in symmetric additively separable hedonic games," *Mathematics of Operations Research*, vol. 12, no. 3, pp. 321–330, 2019.
- [31] J. J. Fyfe and J. P. Loenneke, "Interpreting adaptation to concurrent compared with single-mode exercise training: some methodological considerations," *Sports Medicine*, vol. 48, no. 2, pp. 289–297, 2018.
- [32] R. Du, Y. Liu, L. Liu, and W. Du, "A lightweight heterogeneous network clustering algorithm based on edge computing for 5G," *Wireless Networks*, vol. 26, no. 3, pp. 145–153, 2020.
- [33] R. Du, Y. Liu, L. Liu, and W. Du, "A lightweight heterogeneous network clustering algorithm based on edge computing for 5G," *Wireless Networks*, vol. 26, no. 3, pp. 145–153, 2020.
- [34] P. Derbeko, S. Dolev, and E. Gudes, "Wavelet-based dynamic and privacy-preserving similitude data models for edge computing," *Wireless Networks*, vol. 23, pp. 1–16, 2020.
- [35] C.-H. Huang, L.-I. Hsu, T.-K. Chang et al., "Stress distribution of the patellofemoral joint in the anatomic V-shape and curved dome-shape femoral component: a comparison of resurfaced and unresurfaced patellae," *Knee Surgery, Sports Traumatology, Arthroscopy*, vol. 25, no. 1, pp. 263–271, 2017.

- [36] P. E. Boyle, M. D. Richardson, M. C. Savin, D. E. Karcher, and D. A. Potter, "Ecology and management of earthworm casting on sports turf," *Pest Management Science*, vol. 75, no. 8, pp. 145–153, 2019.
- [37] H. Zheng, F. Lin, X. Feng, and Y. Chen, "A hybrid deep learning model with attention-based conv-LSTM networks for short-term traffic flow prediction," *IEEE Transactions on Intelligent Transportation Systems*, vol. 99, pp. 1–11, 2020.
- [38] Y. Wei, M.-M. Zhao, M. Hong, M.-J. Zhao, and M. Lei, "Learned conjugate gradient descent network for massive MIMO detection," *IEEE Transactions on Signal Processing*, vol. 68, pp. 6336–6349, 2020.

Research Article

The Bidirectional Information Fusion Using an Improved LSTM Model

Tianwei Zheng , Mei Wang , Yuan Guo, and Zheng Wang

Xian University of Science and Technology, Xian 710054, China

Correspondence should be addressed to Mei Wang; wangm@xust.edu.cn

Received 15 January 2021; Revised 21 February 2021; Accepted 12 April 2021; Published 21 April 2021

Academic Editor: Hsu-Yang Kung

Copyright © 2021 Tianwei Zheng et al. This is an open access article distributed under the Creative Commons Attribution License, which permits unrestricted use, distribution, and reproduction in any medium, provided the original work is properly cited.

The information fusion technology is of great significance in intelligent systems. At present, the modern coal-fired power plant has the fully functional sensor network. However, many data that are important for the operation of a power plant, such as the coal quality, cannot be directly obtained. Therefore, the information fusion technology needs to be introduced to obtain the implied information of the power plant. As a practical application, the soft measurement of coal quality is taken as the research object. This paper proposes an improved LSTM model combined with the bidirectional deep fusion, alertness mechanism, and parameter self-learning (DFAS-LSTM) to realize online soft computing for the coal quality analyses of industries and elements. First, a latent structure model is established to preprocess the noisy and redundant sensor network data. Second, an alertness mechanism is proposed and the self-learning method of the activation function parameters is used for the data feature extraction. Third, a deeply bidirectional fusion layer is added to the long short-term memory neural network model to solve the problem of the insufficient accuracy and the weak generalization. Using the historical data of the sensor network, the DFAS-LSTM model is established. Then, the online data of the sensor network is input to the DFAS-LSTM model to implement the online coal quality analyses. Experiment shows that the accuracy of the coal quality analyses is increased by 1%–2.42% compared to the traditionally bidirectional LSTM.

1. Introduction

Long short-term memory (LSTM) neural network is a variant model of the recurrent neural network [1, 2]. In recent years, there have been many studies on the LSTM. Reference [3] proposed a novel DC-Bi-LSTM model. Reference [4] developed a selective multimode long short-term memory network. Reference [5] studied a novel layered network to solve the problem of the pedestrian trajectory prediction. Besides, aiming at the problem of the 3D motion recognition, reference [6] introduced a new gating mechanism into LSTM to increase the reliability of the sequential input data and to adjust the effect on updating the long-term context information stored in the memory cell.

For the past few years, neural network models based on the bidirectional long short-term memory (Bi-LSTM) networks have achieved excellent application performance in their respective fields and have shown a vitality of the

Bi-LSTM in the field of the sequential data processing [7, 8]. Therefore, the basic research of the bidirectional long short-term memory network is of a great significance for the performance upgrading of the neural network model based on it as well as the development of a new neural network model in specific application field.

In recent years, neural network technology has shown excellent performance in pattern recognition, automatic control, signal processing, auxiliary decision-making, and other fields [9, 10]. In particular, the coal is an important energy in the world, and the way of the coal energy utilization still has a great improvement space. Meanwhile, neural network technology has the practical value for adjusting the energy utilization way. According to the data provided by BP p.l.c. in 2019, world's total primary energy consumption is 583.88 EJ, of which coal consumption is 157.86 EJ. The coal plays an important role in the consumption of the primary energy [11]. The main utilization

mode of the coal is combustion in coal-fired power plants [12]. The types of the coal used in coal-fired power plants are complex and changeable. In coal-fired power plants, the boiler combustion system is the heart. The change of the coal quality directly affects the combustion state of the boiler, as well as the stability, safety, and economy of the boiler combustion system. The timely acquisition of the coal quality information is of a great significance for ensuring the smooth operation and the adequacy of the fuel combustion in the boiler.

At the same time, it can also provide power for improving the economic benefits of the coal-fired power plant and the energy utilization rate of the coal-fired industry. So far, the coal quality measurement technologies include neutron activation analysis, laser-induced breakdown spectroscopy, and near-infrared spectroscopy [13, 14]. The above technologies realize the real-time measurement of the coal quality in coal-fired power plants, but all rely on expensive hardware facilities.

For the application, an improved LSTM model with the bidirectional fusion, alertness mechanism, and parameter self-learning (DFAS-LSTM) is used for coal quality computing in coal-fired power plants. The real-time coal quality computing method is not yet found in publications, and the soft computing of the coal quality in coal-fired power plant is a major challenge for many years. However, coal-fired power plants generally have a certain degree of intelligence. They have a strong sensor network composed of edge devices and central processing systems. In the sensor network, there are a large number of sensors with complete categories, which provide a wealth of the edge data for the system. These edge data contain rich information about coal-fired power plants systems. Some of the information, such as coal quality information, is hidden in the edge data in the form of the high-dimensional data features. The way to realize element analyses of the coal quality through edge data mining can avoid the interference to the system operation as well as the cost increase caused by the addition of the hardware facilities. It is cheap and convenient as well. To achieve this goal, this paper proposes a DFAS-LSTM model, which is used to mine coal quality-related information in the edge data of the coal-fired power plants. At the same time, this paper uses the alertness mechanism for the alerting abnormal data information, the improved activation function, and the deeply bidirectional fusion structure of the LSTM for improving the performance of the model. The logic diagram of the soft computing system is shown in Figure 1.

The following parts of this paper include related work, data set and its latent structure, establishment of the alertness mechanism, deeply bidirectional fusion LSTM modeling, experiment and result analyses, and conclusions.

2. Related Work

This section discusses the development trend of the efficient use of energy in the world and the related work of scholars on the optimization of the LSTM structure and the coal utilization from various countries.

At present, the world is in a trend of economic transformation and efficient use of energy. The sustainable development trend of the economy puts forward higher requirements for the rational and efficient use of the primary energy. According to the statistics of the International Energy Agency (IEA), the energy intensities of some countries are shown in Figure 2.

Among primary energy sources, coal is mainly used for power generation in coal-fired power plants. The coal-fired power plants are facing increasingly severe challenges. The introduction of the intelligent technologies and methods is necessary for them to adapt to the historical trend of the efficient energy utilization.

In recent years, the generation capacity of wind and solar power has continued to grow. However, due to the high volatility of the renewable energy from wind and solar power generation, coal-fired power plants must be used to cover the gap between renewable energy generation and load to maintain the stability of the frequency and the power supply stability [15]. Therefore, the method of the coal-fired power generation is still irreplaceable.

According to the survey data from BP p.l.c., driven by the wind and solar energy, the growth of the renewable energy has reached a record level, accounting for more than 40% of the primary energy growth in 2019 [16]. This also means that the ever-changing energy structure places higher demands on coal-fired power generation technology.

2.1. Optimization of the LSTM Model. Aiming at increasing the depth in the time dimension, reference [17] extended a highway LSTM (HW-LSTM) model by adding highway networks inside an LSTM and used it for language modeling. As an application of the recursive neural network, reference [18] studied the capture of the behavior trajectory through a large context window and achieved the purpose of solving the data sparseness and improving the robustness. Combined with the attention mechanism and the character-level convolutional neural network, reference [19] proposed several new classification architectures based on the long short-term memory (LSTM) language model and the gated recurrent unit (GRU) language model. Reference [20] formulated precipitation nowcasting as a spatiotemporal sequence forecasting problem. By extending the fully connected LSTM (FC-LSTM) to have convolutional structures in both the input-to-state and state-to-state transitions, they proposed the convolutional LSTM (ConvLSTM) and used it for the precipitation nowcasting problem. Reference [21] presented a novel unified framework (LSTM-E) for exploring the learning of the LSTM and visual-semantic embedding. In order to solve the problem of the energy load forecasting, reference [22] presented a novel forecasting model based on long short-term memory algorithms. Reference [23] designed an architecture with the purpose of serving as a model which can generate sequence samples, while simultaneously classifying a given sequence.

2.2. Optimization of the Coal Energy Utilization. At present, the process of the power plant intelligence is constantly

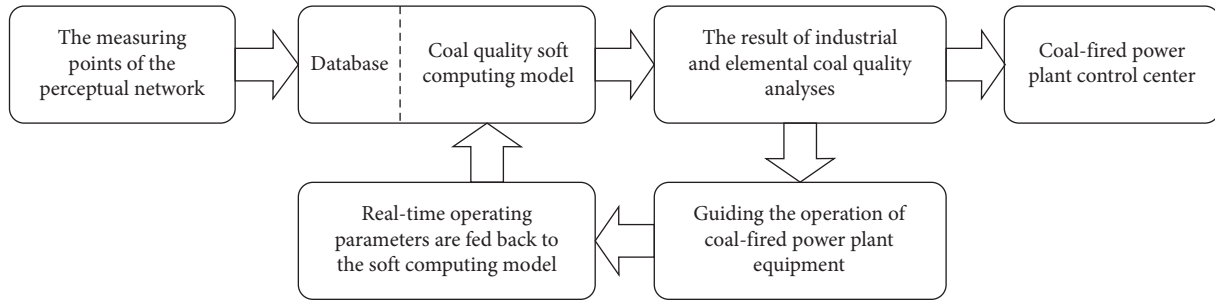


FIGURE 1: The logic diagram of the soft computing system for the industrial and the elemental coal quality analyses.

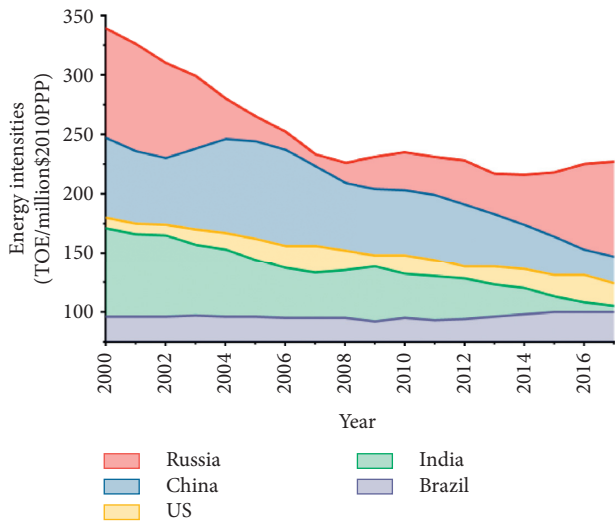


FIGURE 2: Energy intensities of some countries.

advancing. Reference [24] developed a dynamic model of the drum-boiler using NARX neural networks, which can forecast the actual pressure and water level of the drum-boiler. Reference [25] proposed a pilot program aiming at developing a comprehensive knowledge base for power plants by using principal component analysis and artificial neural networks. The program used the principal component analysis method to filter noise in the prediagnosis stage and evaluated the neural network model based on representative data of the power plant. Reference [26] developed a diagnosis system of the power plant gas turbine to detect the deterioration of the turbine. By using artificial neural network, the system can be used for predicting the deterioration of the main component. Reference [27] proposed a new method for predicting the output of a power plant by using a feedforward neural network. The network used ambient temperature, atmospheric pressure, relative humidity, and vacuum as the input parameters to predict the average hourly output of the power plant.

At present, coal quality information of a coal-fired power plant cannot be obtained in real time. As a result, untimely coal quality information lacks guiding value for the optimization of coal combustion, which leads to the underutilization of the coal in coal-fired power plants. As a method to improve the utilization of the coal, an online soft measurement model

for coal quality is proposed in this paper. The system framework is shown in Figure 3.

3. Data Set and Its Latent Structure

This section discusses the data acquisition and preprocessing including the selection of conventional measurement points, principal component analysis, and independent component analysis.

3.1. Selection of Conventional Measurement Points. In the sensor network of a coal-fired power plant, there are many kinds of conventional measurement points, and the redundancy among the measured data is serious. Most of the conventional measurement points have no obvious correlation with coal quality. These points lack the guidance for the coal quality soft computing. Therefore, it is necessary to screen the conventional measurement points of the coal-fired power plant and obtain the effective data from the monitoring points.

The operation process of a coal-fired power plant includes complex physical and chemical reaction processes. The existing operation mechanism research of the coal-fired power plant provides a basis for the selection of conventional measurement points [28]. According to the laws of the energy conservation, material conservation, and the actual process flow in the operation of a coal-fired power plant, 190 conventional measurement points related to the coal quality are determined from the sensor network of the coal-fired power plant. Some relevant measurement points used in soft computing of the coal quality are shown in Table 1.

In coal-fired power plants, the sensors used in conventional measurement points have various working principles and complex working environment; these result in the serious data redundancy and noise. At the same time, the range and accuracy of the data from different measuring points are significantly different, as well as the correlation with coal quality. In order to ensure the performance of the model, it is necessary to preprocess the data of conventional measurement points in coal-fired power plants.

For the monitoring data coming from conventional measurement points in coal-fired power plants, the bad points in the data are eliminated first. The data preprocessing model realizes this function mainly through the following steps:

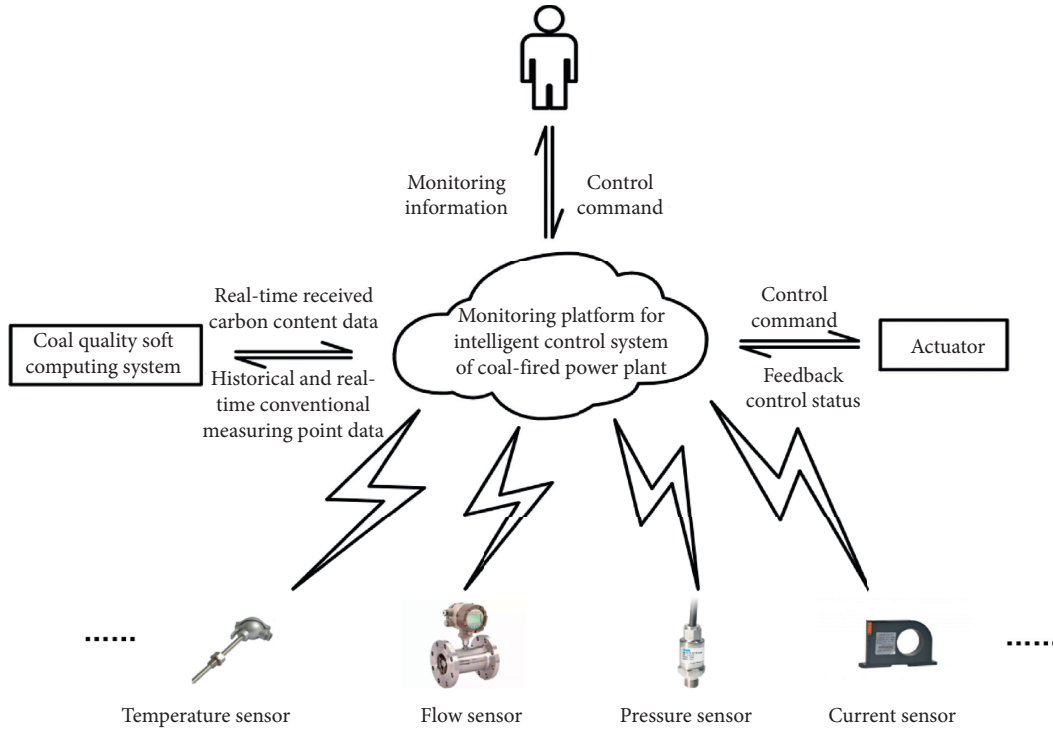


FIGURE 3: The system framework.

TABLE 1: Some relevant measurement points used in soft computing of the coal quality.

No.	Name/unit
1	Active power of the generator (MW)
2	Total power of the generator (MW)
3	Total coal supply (T/h)
4	Current of the coal feeder (A)
5	Current of the coal mill (A)
6	Primary air volume at mill inlet (T/h)
7	Primary air temperature at mill inlet (°C)
8	Steam temperature at the outlet of the final reheater (left side) (°C)
9	Steam temperature at the outlet of the final superheater (left side) (°C)
10	Flow of the feed water (T/h)
11	Temperature of the feed water (°C)
12	Pressure of the feed water (MPa)
13	Drum pressure (MPa)
14	Drum water level (mm)
15	Secondary air flow rate (T/h)
16	Desuperheating water temperature of the superheater (°C)
17	Outer wall temperature of the high-pressure cylinder (°C)
18	Inner wall temperature of the high-pressure cylinder (°C)
19	Inlet air temperature of the secondary heater (°C)
20	Primary air pressure at outlet of the air preheater (MPa)
21	Secondary air pressure at the inlet of the air preheater (MPa)
22	Outlet air pressure of the forced draft fan (MPa)
23	Current of the supply fan (A)
24	Current of the primary fan (A)
25	Outlet air pressure of the primary fan (MPa)
26	Differential pressure between the secondary air box and the furnace (MPa)
27	Inlet air temperature of the primary fan (°C)
28	Outlet air temperature of the primary air heater (°C)
29	Inlet air temperature of the primary air heater (°C)
30	Negative pressure at the outlet of the extension end low-temperature superheater (MPa)
31	Negative pressure at the outlet flue of the fixed end superheater (MPa)

TABLE 1: Continued.

No.	Name/unit
32	Temperature of the primary air (°C)
33	Temperature of the hot secondary air (°C)
34	Primary air duct pressure of the furnace (MPa)
35	Main pipe pressure of the hot primary air (MPa)
36	Outlet pipe temperature of the reheater (left side) (°C)
37	Outlet pressure of the reheater (left side) (MPa)
38	Working environment temperature of the coal mill (°C)
39	Inlet temperature of the reheater desuperheater (left side) (°C)
40	Desuperheating water flow of the reheater (left side) (T/h)
41	Primary air pressure at mill inlet (MPa)
42	Pressure of the reheater inlet (MPa)
43	Inlet steam temperature of the low-pressure cylinder (_C)
44	Exhaust temperature of the high-pressure cylinder (_C)
45	Exhaust pressure of the high-pressure cylinder (MPa)
46	Outlet air temperature of the secondary heater (_C)
47	Steam pipe pressure of the high and intermediate pressure cylinder (MPa)
48	Steam pipe temperature of the high and medium pressure cylinder (_C)
49	Differential pressure between the secondary air box and the furnace (MPa)
50	Oxygen concentration at chimney inlet (%)
51	Outlet flue gas temperature of the air preheater (_C)
52	Outlet flue gas pressure of the air preheater (kPa)
53	Flue gas temperature at the inlet of the air preheater (_C)
54	Inlet flue gas pressure of the air preheater (kPa)
55	Main motor current of the air preheater (A)
56	The current of the induced draft fan (A)
57	Flue gas pressure at the inlet of the induced draft fan (kPa)
58	Low-pressure cylinder exhaust temperature (_C)
59	Inlet flue pressure of the fixed end economizer (MPa)
60	Feed water temperature at economizer inlet (_C)
61	Pressure of the main water supply pipe at economizer inlet (MPa)
62	Inlet flue pressure of the economizer at expansion end (MPa)

- (1) According to the measurement range information of each measurement point, remove the measurement point data which obviously deviates from the measurement range
- (2) Combined with the actual operation experience of the power plant, remove the data which obviously deviates from the experience value under the current working condition

At the same time, in order to shorten the time of the data processing and remove redundant information from the monitoring data, this paper proposes a feature extraction method based on the latent structure model for the monitoring data. Two common methods, principal component analysis (PCA) [29, 30] and independent component analysis (ICA) [31, 32], are used in this latent structure model.

3.2. Principal Component Analysis. In coal-fired power plants, there are many conventional measurement points. The soft computing method, by which we obtain the coal quality-related information through edge data mining, requires the processing of the high-dimensional data. The principal component analysis method is a commonly used data dimensionality reduction method, which aims at maximizing the variance of the data after dimensionality reduction. The PCA algorithm is used to map the raw data to

the low-dimensional feature space with most of the information saving. At the same time, the algorithm realizes the data compression and avoids too many parameters of the following neural network.

In this paper, the data of the conventional measurement points and the coal quality test are used as the test data of the model. Set the data set of the conventional measurement points of the coal-fired power plants after data preprocessing as U .

$$U = \begin{bmatrix} X_{0,t_0} & X_{0,t_1} & \cdots & X_{0,t_{N-1}} \\ X_{1,t_0} & X_{1,t_1} & \cdots & X_{1,t_{N-1}} \\ \vdots & \vdots & \vdots & \vdots \\ X_{M-1,t_0} & X_{M-1,t_1} & \cdots & X_{M-1,t_{N-1}} \end{bmatrix}, \quad (1)$$

where $\{X_{M-1,t_0}, X_{M-1,t_1}, \dots, X_{M-1,t_{N-1}}\}$ is the data of the M th coal-fired power plants' conventional measuring points at the sampling time of the t_0, t_1, \dots, t_{N-1} , respectively. N is the number of samples, and M is the total number of the conventional measuring points. The correlation matrix R of the U^T is calculated by

$$R = E[U^T U]. \quad (2)$$

Find the eigenvalue λ_{ij} of the R , queue the eigenvalues from the big to the small, select the first d bigger eigenvalues,

and calculate the eigenvectors corresponding to the d eigenvalues. After normalization, record them as $U_j, j = 1, 2, \dots, d$. The transformation matrix A is composed of the U_j .

$$A = (U_1, U_2, \dots, U_d). \quad (3)$$

K - L transformation is applied to the sample set U^T . If the transformed matrix is I , then

$$I = A^T U^T, \quad (4)$$

where vector I is the low-dimensional data obtained after principal component analysis, and the data dimension is reduced to d dimension. After the principal component analysis, the correlation of the data is removed by using the two-order statistical information, the processed data may still have higher order redundant information, and the components of the data may not have mutual independence. Therefore, the independent component analysis is used to obtain the independent component of the data after the principal component analysis.

3.3. Independent Component Analysis. Independent component analysis (ICA) is a data analysis method that aims at the independence of the processed data components. Taking Fast-ICA algorithm as an example, this paper describes the implementation of the ICA algorithm. Fast-ICA algorithm, also known as fixed point algorithm, is a kind of the fast optimization iterative algorithm, which has forms based on kurtosis, likelihood, and negative entropy. In this section, taking Fast-ICA algorithm based on negative entropy as an example, suppose the data to be processed is X ; then the Fast-ICA algorithm determines the separation matrix W by observing the data X . The data result Y of the independent component analysis is shown in

$$Y = WX. \quad (5)$$

According to the information theory, among random variables with the same variance, Gaussian random variables have the largest differential entropy. According to the central limit theorem, the stronger the non-Gaussianness of the Y , the greater its negative entropy and the stronger its independence. The decision basis for the Fast-ICA algorithm based on negative entropy is the maximization of the negative entropy. The definition of the negative entropy is given in

$$J_g(Y) = H(Y_{\text{Gauss}}) - H(Y), \quad (6)$$

$$H(Y) = - \int p(Y) \lg p(Y) dY, \quad (7)$$

where $J_g(Y)$ is the negative entropy, Y_{Gauss} is a Gaussian random variable with the same variance as Y , and $H(Y_{\text{Gauss}})$ is the entropy of the random variable. In practical applications, in order to avoid using the unknown probability density distribution function of the variable Y , the approximate formula of the negative entropy is shown in

$$J(Y) \approx [E\{G(Y)\} - E\{G(Y_{\text{Gauss}})\}]^2, \quad (8)$$

where E is the mean calculation and G is a nonlinear function.

Because the data is generally standardized before being analyzed by Fast-ICA algorithm, the constraint is given by in

$$\|WX\| = \|W\| = 1. \quad (9)$$

From equation (8), combined with the method of the Lagrange multipliers, equation (10) can be obtained as follows:

$$E\{XG(WX)\} + \beta W = 0, \quad (10)$$

where β is the Lagrangian multiplier.

In practical applications, the iterative algorithm and equation (10) can be combined to realize the processing of the independent component analysis on the data.

4. Establishment of the Alertness Mechanism

The basic theory of the alertness mechanism originates from philosophy, cognitive psychology, social science, and linguistics. It is a new mechanism to strengthen the key information of the data based on prior knowledge [33]. The data used for online measurement of the coal quality is the actual operation data of a coal-fired power plant. In the actual operation of a coal-fired power plant, due to the segmented control behavior of the control system or the subjective operation of the operators, the regularity of the raw data in the time series will be destroyed in some places. Because this kind of the damage will reduce the accuracy of the model, and according to the prior knowledge, it has a certain alertness feasibility. In this paper, the alertness mechanism is introduced to data processing for the purpose of optimizing the model. The specific implementation process is as follows:

- (1) According to the prior knowledge of the operation in a coal-fired power plant, determine the data location of conventional measurement points that need the active alert, such as the changing points of the total coal input of the coal mill, plant load, and boiler water level.
- (2) The active alert matrix C is defined. The alert matrix is a sparse matrix. The value of each element in the matrix is the alert weight. The data position weight that needs alert is not 0, and the rest position elements are 0.

$$C \triangleq \begin{bmatrix} 0 & 0 & \dots & 0 \\ 0 & W_{j,t_1} & \dots & 0 \\ W_{i,t_0} & 0 & \dots & 0 \\ 0 & 0 & \dots & W_{h,t_{N-1}} \\ \vdots & \vdots & \vdots & \vdots \\ 0 & 0 & \dots & 0 \end{bmatrix}, \quad (11)$$

where $W_{i,t_0}, W_{j,t_1}, \dots, W_{h,t_{N-1}}$ are alert weights and subscripts $i, j, h, t_0, t_1, t_{N-1}$ indicate the location and time of the alert data.

- (3) Modify the data; introduce the alertness mechanism to the feature vector extracted by the latent structure model. Let the input of the alertness mechanism be matrix I ,

$$I = \{I_{t_0}, I_{t_1}, \dots, I_{t_{N-1}}\}, \quad (12)$$

where $I_{t_0}, I_{t_1}, \dots, I_{t_{N-1}}$ are d -dimensional eigenvectors. The data after the introduction of the alertness mechanism are shown in equation (13), where N is the number of samples, $I_{t_0}, I_{t_1}, \dots, I_{t_{N-1}}$ represent the sampling time series, I is the original data, and W is the alert weight.

$$I_A \triangleq I + C \times I = \begin{bmatrix} I_{0,t_0} & I_{0,t_1} & \cdots & I_{0,t_{N-1}} \\ I_{1,t_0} & \vdots & \cdots & I_{1,t_{N-1}} \\ \vdots & (1 + W_{j,t_1}) \times I_{j,t_1} & \cdots & I_{2,t_{N-1}} \\ (1 + W_{i,t_0}) \times I_{i,t_0} & I_{j+1,t_1} & \cdots & \vdots \\ I_{i+1,t_0} & I_{j+2,t_1} & \cdots & (1 + W_{h,t_{N-1}}) \times I_{h,t_{N-1}} \\ \vdots & \vdots & \vdots & \vdots \\ I_{d-1,t_0} & I_{d-1,t_1} & \cdots & I_{d-1,t_{N-1}} \end{bmatrix}. \quad (13)$$

- (3) The object of the alertness mechanism is some specific discrete data points, while attention mechanism introduces attention mechanism to all or part of the data.
- (4) The purpose of introducing alertness mechanism to data in the model is to reduce the damage caused by the subjective operation behavior of operators or the segmented control behavior of the control system in coal-fired power plants, while the general purpose of the attention mechanism is to pay attention to the key information in data and enhance the ability of the neural network to data mining.

The introduction of the alertness mechanism enhances the stability of the training model and suppresses the influence of the abnormal data fluctuation on the accuracy of the model output. To a certain degree, it reduces the damage of the unpredictable factors to the data regularity and optimizes the performance of the DFAS-LSTM model proposed in this paper.

5. Deeply Bidirectional Fusion LSTM Modeling

This section discusses the establishment of the deeply bidirectional fusion LSTM including improved activation function of parameters self-learning, structure of the deeply bidirectional fusion LSTM, and Encoder-Decoder framework with attention mechanism.

- (4) The output of the alertness mechanism is the input of the long short-term memory neural network in the model. With the training process, the weight of the alertness mechanism and the neural network parameters are modified by the gradient descent method.

The alertness mechanism proposed in this paper refers to the mechanism of the attention mechanism in neural network, and it is obviously different from attention mechanism [34, 35]. The main differences between alertness mechanism and attention mechanism are as follows:

- (1) The initial setting of the alertness mechanism's weight is based on the prior knowledge of practical problems, while attention mechanism does not need the support of the prior knowledge.

5.1. Improved Activation Function of the Parameter Self-Learning. Long short-term memory (LSTM) is a variant of the recurrent neural network. Different from the traditional recurrent neural network, LSTM neural network uses three gate controllers: input gate, output gate, and forgetting gate. On the basis of the original short-term memory, memory units are added to maintain long-term memory. Reference [36] studied the recent LSTM variants, summarized the results of 5400 experiments, and found that the forgetting gate and output activation function are the most critical components. Compared with the traditional recurrent neural networks model, the long short-term memory neural network uses gate structure, which enhances the selective memory ability of the neural network and overcomes the problem that the traditional recurrent neural networks are prone to gradient explosion and gradient dispersion in dealing with long-term sequential problems. Therefore, it has a unique advantage in dealing with long-term sequential problems. Activation function is an indispensable part of the long short-term memory neural network, and the activation function of its input gate plays an important role in the mapping process from input to neuron state [37]. Tanh function is a commonly used activation function of the bidirectional long short-term memory neural network. The expression is given in equation (14).

$$\tanh(x) = \frac{e^x - e^{-x}}{e^x + e^{-x}}. \quad (14)$$

The tanh activation function and its derivative curve are shown in Figure 4.

As shown in Figure 4, tanh function has a wide saturation region, in which the derivative of the tanh function is almost zero. Because the neural network uses the gradient descent method to modify the network weight, when the activation function enters the saturation region, the modification of the weight will be very slow. When tanh is selected as the activation function, if there is a large number of the data input, the weight parameters may be congested due to the slow correction of the weight, resulting in a longer training time or even inability to train. To solve the above problems of the tanh activation function, this paper proposes an improved multiparameter hyperbolic tangent activation function $f(x)$, whose expression is given by

$$f(x) = \lambda \tanh(\gamma h) + \eta x, \quad (15)$$

where λ regulates the output amplitude of the activation function, γ regulates the scale of the independent variable, and η regulates the gradient of the activation function, reflecting the gradient limit of the activation function. The function curve of the improved activation function $f(x)$ is shown in Figure 5.

λ , γ , and η are adjustable parameters in neural network, and their values affect the performance of the neural network model. In this paper, λ , γ , and η are set as optimization variables. After the initial value is set, with the training process, the gradient descent method is used to optimize the values of λ , γ , and η . After the training, the appropriate values of λ , γ , and η are determined and solidified into the model. In the model training process, the value optimization process of λ , γ , and η is shown in Figure 6.

It can be seen from Figure 6 that the parameters λ , γ , and η in the improved activation function of the multiparameters self-learning realize self-learning with the training process. The parameter correction process is relatively slow, and the parameter correction of λ , γ , and η in this model tends to be stable after about 50000 steps. After training convergence, the activation function parameters λ , γ , and η in this model are about: $\lambda = 0.2442114$, $\gamma = 2.82857346$, and $\eta = 0.01878586$. The improved hyperbolic tangent activation function avoids the difficulty due to gradient saturation during training. At the same time, this method realizes the process of the independent optimization in the model. The influence of the subjective parameters on the performance of the neural network is weakened. The parameter self-learning method proposed in this paper is also suitable for some common superparameters and provides a new idea for the optimization of the superparameters in neural network.

5.2. Structure of the Bidirectional Deep Fusion LSTM. When using deep learning methods to deal with sequence problems, RNN is a common and effective method. During the operation of a coal-fired power plant, it takes a long time for the material and energy of the coal to be completely converted. Data on coal quality is scattered over a long time series. As a kind of the RNN, LSTM has better performance in dealing with long sequence problems than traditional RNN. Bidirectional long short-term memory (Bi-LSTM) networks,

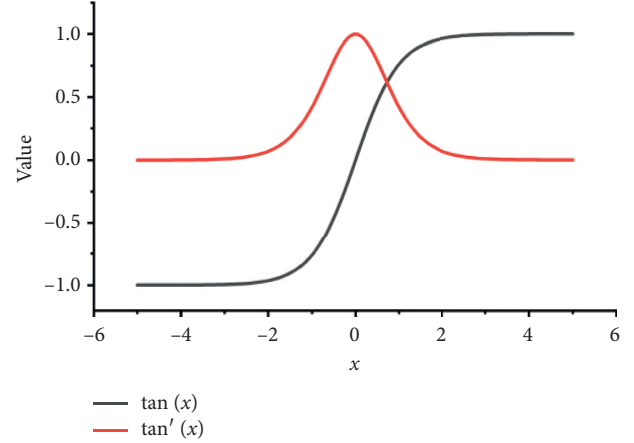


FIGURE 4: The tanh activation function and its derivative curve.

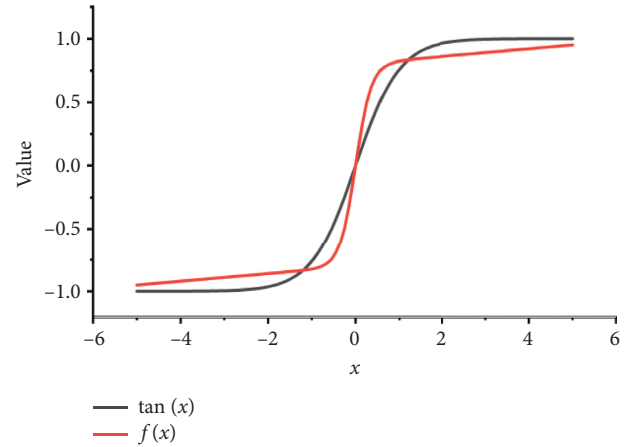


FIGURE 5: Curve of the improved activation function $f(x)$.

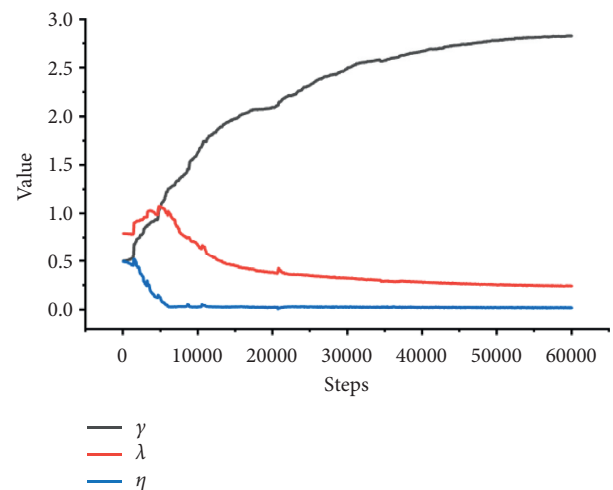


FIGURE 6: Curve of the activation function parameter as training converges.

compared with unidirectional long short-term memory networks, consider the relevance of the data in the reverse direction, which helps to fully mine the relevance of the data

in the forward and reverse direction [38]. On the basis of the Bi-LSTM, this paper proposes a structure of the deeply bidirectional fusion LSTM model. The structure of the deeply bidirectional fusion LSTM model is shown in Figure 7.

The structure of the deeply bidirectional fusion LSTM is an important part of the DFAS-LSTM proposed in this paper. It uses the fusion layer to realize the fusion of the forward and the reverse data in the hidden layer of the model. Compared with the deeply bidirectional fusion LSTM, the traditional bidirectional LSTM is essentially two independent unidirectional LSTM networks, and there is no bidirectional data fusion in the hidden layer of the network. The structure design of the forward and reverse data splitting hinders the ability of the hidden layer in the neural network to extract bidirectional data features. In this paper, the deeply bidirectional fusion LSTM structure constructed by DFAS-LSTM model overcomes the defect of the traditional bidirectional LSTM by fusion structure, which makes the neural network structure have stronger ability of the data feature representation. Deeply bidirectional fusion LSTM structure is the core structure of the DFAS-LSTM model, which consists of the input layer, forward LSTM layer, reverse LSTM layer, bidirectional data fusion layer, and output layer. Among them, the fusion layer is the key structure to realize bidirectional data fusion in DFAS-LSTM model and also the key to distinguish the deeply bidirectional fusion LSTM from the traditional deeply bidirectional LSTM.

In the fusion layer, bidirectional fusion weight, sigmoid function, and Encoder-Decoder unit are set. In this structure, the input of this structure is the output of the upper bidirectional LSTM neuron, and the output is the input of the lower LSTM neuron. After the data enters the fusion layer, the forward and reverse neuron output data are given fusion weights. After bidirectional data superposition, sigmoid function is used to output the fused vector. This vector outputs the vector data of the specified dimension through the Encoder-Decoder framework that introduces the attention mechanism. This output is connected to the bidirectional LSTM neuron node of the lower layer. The structure of the bidirectional data fusion layer is shown in Figure 8.

In order to visually characterize the working process of the fusion layer, mathematical expressions are given. Suppose the input of the fusion layer, that is, the output of the previous layer, is \mathbf{Y}_f and \mathbf{Y}_b , respectively. Then, the mathematical operation process of the fusion layer is shown in equations

$$\mathbf{Y} = \text{sigmoid}(\mathbf{Y}_f \times \mathbf{W}_f + \mathbf{Y}_b \times \mathbf{W}_b), \quad (16)$$

$$\mathbf{Y}_f = [y_{f1}, y_{f2}, y_{f3}, \dots, y_{fn}], \quad (17)$$

$$\mathbf{W}_f = [w_{f1}, w_{f2}, w_{f3}, \dots, w_{fn}], \quad (18)$$

$$\mathbf{Y}_b = [y_{b1}, y_{b2}, y_{b3}, \dots, y_{bn}], \quad (19)$$

$$\mathbf{W}_b = [w_{b1}, w_{b2}, w_{b3}, \dots, w_{bn}], \quad (20)$$

where \mathbf{Y} is the input of the Encoder-Decoder framework, \mathbf{Y}_f is the forward output matrix, \mathbf{Y}_b is the reverse output matrix,

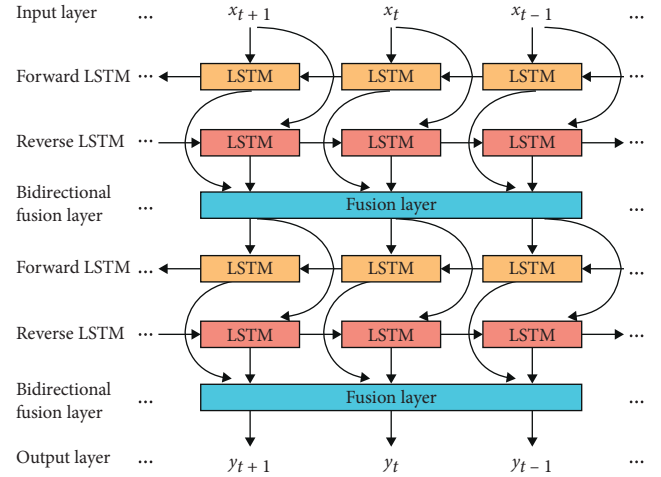


FIGURE 7: Structure of the deeply bidirectional fusion LSTM model.

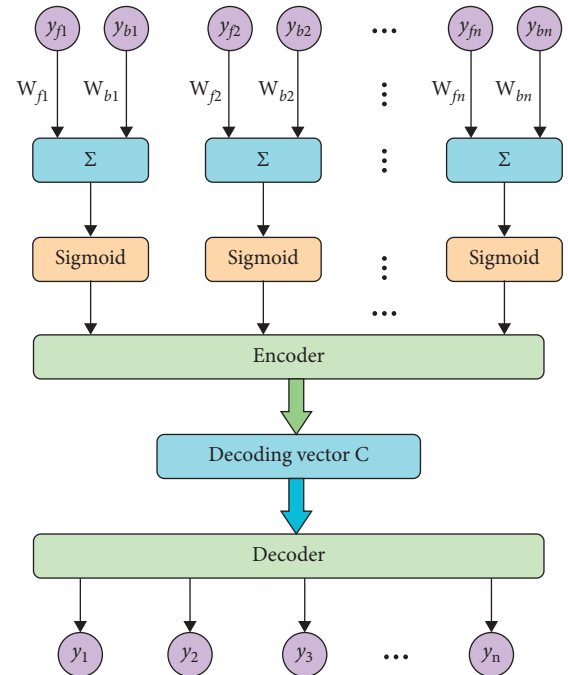


FIGURE 8: Structure of the bidirectional data fusion layer.

\mathbf{W}_f is the forward fusion weight, and \mathbf{W}_b is the reverse fusion weight. Sigmoid function enhances the nonlinear fitting ability of the fusion layer, adjusts the fusion result range, and enhances the representation ability of the model.

5.3. Encoder-Decoder Framework with Attention Mechanism. As shown in Figure 8, the fusion layer uses the Encoder-Decoder framework to adjust the data after bidirectional data fusion. The working mechanism of the Encoder-Decoder framework is as follows: use encoder to map the input to the specified dimension space, get the fixed dimension decoding vector C , and then use decoder structure to decode the decoding vector C . This structure realizes the function of the data feature acquisition and data structure adjustment.

In this paper, the fusion layer of the DFAS-LSTM model is constructed based on Encoder-Decoder framework, and attention mechanism is added. The attention mechanism in deep learning is essentially similar to the selective visual attention mechanism of the human beings. Its core goal is to select the primary and secondary information of the current task, so as to achieve the purpose of paying attention to the primary information and ignoring the secondary information. Compared with the traditional Encoder-Decoder framework, the encoder structure of the Encoder-Decoder framework which introduces attention mechanism encodes the input into a vector sequence. At the same time, each vector in the vector sequence obtains different attention weights according to its importance to the target output. Then, the decoder structure decodes the vector sequence with attention weight. In the fusion layer, the Encoder-Decoder framework of this structure can effectively obtain the key information in the bidirectional fusion data and improve the data feature extraction ability of the fusion layer. The Encoder-Decoder framework with attention mechanism is shown in Figure 9.

6. Experiment and Result Analyses

This section discusses the performance of the DFAS-LSTM in coal quality computing. Content includes presetting and training, metrics soft computing of the industrial coal quality analyses, and soft computing of the elemental coal quality analyses.

6.1. Presetting and Training. Our algorithm is implemented in Tensorflow-1.12.0 with the Python wrapper and using eight cores of a 3.6 GHz Intel Core i7-7700 CPU and two NVIDIA GeForce GTX 1080 Ti GPUs. The data for model training and testing comes from actual operating data of a coal-fired power plant. Among them, the coal quality data comes from the laboratory data of a coal-fired power plant. Coal quality data includes industrial analyses data and elemental analysis data. The soft computing method proposed in this paper can realize industrial analyses and element analyses of the coal quality based on these data. Among them, the industrial analyses of the coal quality include low calorific value, total moisture, ash content, and volatile; the elemental analysis of the coal quality includes carbon content, hydrogen content, oxygen content, nitrogen content, and sulfur content.

The DFAS-LSTM model is used to solve the problem of the coal quality soft computing. The framework of the DFAS-LSTM model for coal quality soft computing is shown in Algorithm 1.

6.2. Metrics. In order to intuitively represent the ability of the model, this paper uses the fitting index and root mean square error as the evaluation index of the model. Equation (21) shows the expression of the fitting index.

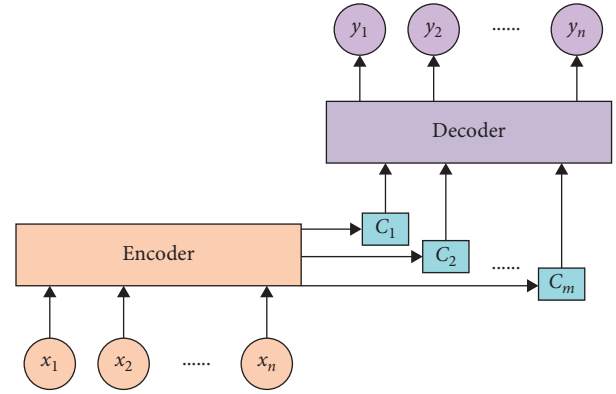


FIGURE 9: Encoder-Decoder with attention mechanism.

$$R_f = 1 - \sqrt{\frac{\sum_i^n (y_i - y_{ip})^2}{\sum_i^n y_i^2}}, \quad (21)$$

where R_f is the fitness index, y_i is the real value of the sample, and y_{ip} is the output value of the model.

The model proposed in this paper belongs to regression model, using root mean square error as the loss function of the model; the loss function can evaluate the deviation degree between the model output and the real value, and the smaller the value, the better the robustness of the model. The expression of the RMSE loss function is given in

$$\text{RMSE} = \sqrt{\frac{1}{n} \times \sum_i^n (y_i - y_{ip})^2}, \quad (22)$$

where RMSE is the root mean square error, n is the number of samples, y_i is the true value of samples, and y_{ip} is the output value of the model.

6.3. Soft Computing of Industrial Coal Quality Analyses. Industrial analyses of the coal, also called technical analysis or practical analysis of the coal, is the basis for evaluating coal quality and an important indicator for understanding coal quality. In this section, soft computing of the industrial analyses is carried out, which includes low calorific value, total moisture, ash content, and volatile. The specific meaning of each industrial analysis involved is as follows:

- (1) Low calorific value: the low calorific value of the coal refers to the heat produced by the combustion of the coal under atmospheric pressure, after deducting the vaporization heat of the moisture in the coal, the remaining heat that can actually be used
- (2) Total moisture: it is the moisture that the coal sample loses when it is in the air and reaches equilibrium with air humidity
- (3) Ash content: the ash content of the coal refers to the residue left after the coal is completely burned
- (4) Volatile: the volatile of the coal is the content heated by insulation at a certain temperature, and

Input: Data of the historical conventional measurement points of the coal-fired power plants X_h ; Real-time conventional measurement data of the coal-fired power plants X_r ; Coal quality test data of the coal-fired power plants y_r ;

Output: Real-time coal quality data in the furnace of the coal-fired power plants y ;

- (1) Remove noise from historical data X_h and filter it;
- (2) Standardize the data, process the standard data by PCA and ICA algorithm to obtain data X_i ;
- (3) Initialize weight parameters, batch the data to get X_{ib} , and input X_{ib} into DFAS-LSTM;
- (4) Use alertness mechanism to process data X_{ib} and obtain data X_a ;
- (5) Data X_a input to LSTM, which is based on improved activation function and fusion structure;
- (6) Use the coal quality test data y_r to compare with the output of the neural network to obtain the cost function C ;
- (7) Use the optimizer to optimize the cost function C by updating the weight parameters of the neural network;
- (8) After the model is stable, the optimization ends and the model parameters are solidified;
- (9) Take X_r as input, output coal quality information y in real time.

ALGORITHM 1: The soft computing of the coal quality analyses by using DFAS-LSTM model.

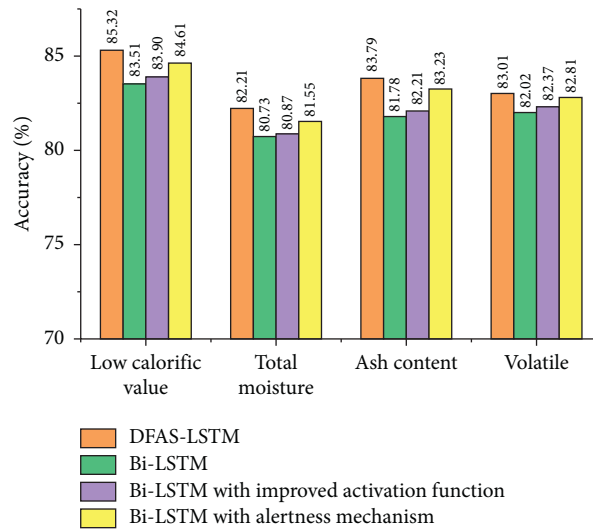


FIGURE 10: Statistical results of the industrial analyses accuracy.

the moisture is subtracted from the escaped material

In order to verify that the DFAS-LSTM model proposed in this paper has advantages, in this section, based on the data, soft computing of the industrial analyses is realized by using DFAS-LSTM, conventional Bi-LSTM model, Bi-LSTM model with improved activation function, and Bi-LSTM with alertness mechanism. Each model runs 20 times, the accuracy obtained is averaged, and the statistics are shown in Figure 10.

Using the DFAS-LSTM model proposed in this paper, based on the conventional measurement points data of a coal-fired power plant, the soft computing of the above industrial analyses' information is realized. In chronological order, 20 data points were selected at random time to show the actual value of industrial analyses and the soft

computing result for comparison. The result is shown in Figure 11.

6.4. Soft Computing of Elemental Coal Quality Analyses.

In this section, DFAS-LSTM model is used to achieve soft computing for elemental analysis of the coal. Elemental analysis of the coal is to detect and analyze the element content in coal. The element content in coal is an important indicator of the coal quality. The element analyses data used in this paper is based on the received basis. In this section, elemental analysis specifically includes carbon content, hydrogen content, oxygen content, nitrogen content, and sulfur content. Similarly, elemental analysis soft computing is realized by using DFAS-LSTM, conventional Bi-LSTM model, Bi-LSTM model with improved activation function, and Bi-LSTM with alertness mechanism. Each model runs 20 times, the accuracy obtained is averaged, and the statistics are shown in Figure 12.

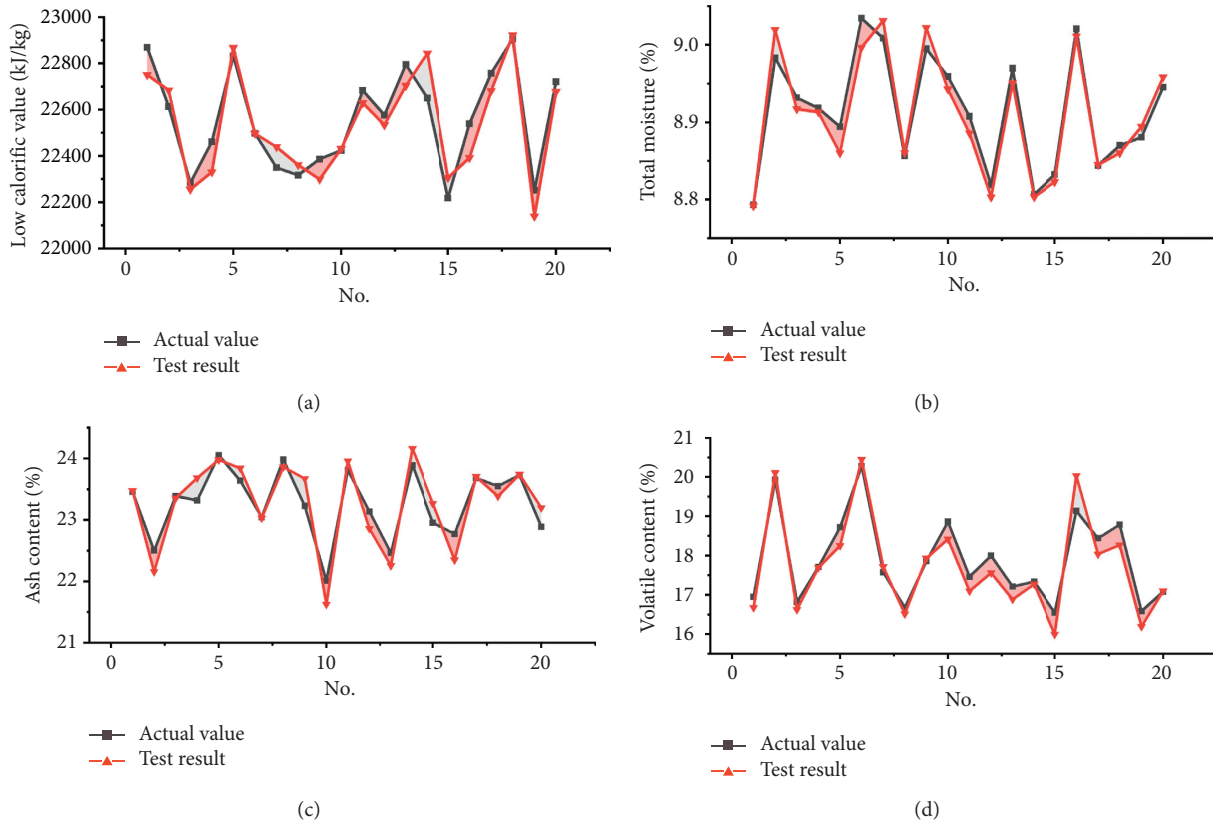


FIGURE 11: The results of industrial analyses by using DFAS-LSTM model: (a) the actual and test value of the low calorific value; (b) the actual and test value of the total moisture; (c) the actual and test value of the ash content; (d) the actual and test value of the volatile.

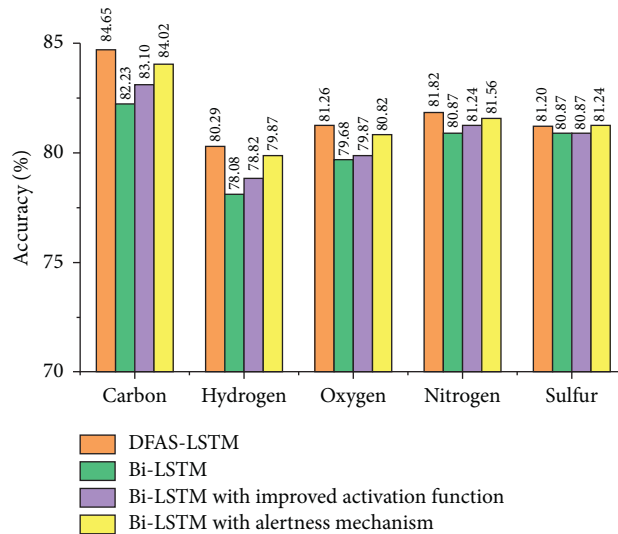


FIGURE 12: Statistical results of the elemental analyses accuracy.

For elemental analyses of the coal, the same work has been done as industrial analyses. Using the DFAS-LSTM model proposed in this paper, the soft computing of the above elemental analyses is realized. In chronological

order, 20 data points were selected at random time to show the actual value of the elemental analyses and the soft computing result for comparison. The result is shown in Figure 13.

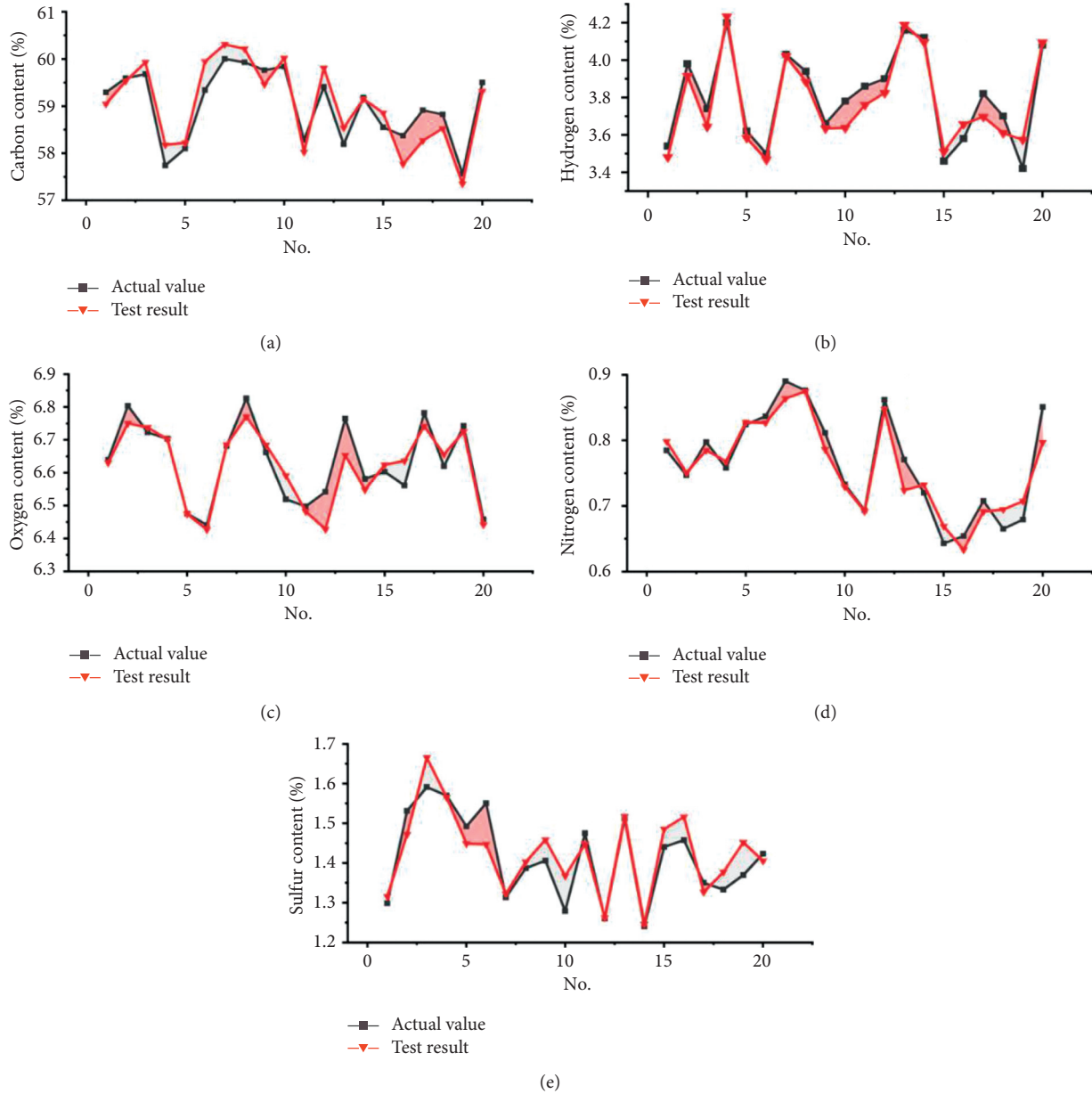


FIGURE 13: The results of elemental analyses by using DFAS-LSTM model: (a) the actual and test value of the carbon content; (b) the actual and test value of the hydrogen content; (c) the actual and test value of the oxygen content; (d) the actual and test value of the nitrogen content; (e) the actual and test value of the sulfur content.

7. Conclusions

In this paper, the information fusion technology applied in the coal-fired power plant is discussed. As a practical application, the soft measurement of the coal quality in the power plant is achieved by the information fusion method. Combining the sensor network of a coal-fired power plant, an improved LSTM model with the bidirectional fusion, alertness mechanism, and parameter self-learning (DFAS-LSTM) is proposed to realize the soft computing of the coal quality. The use of the alertness mechanism can suppress the interference information; the use of the improved activation function of parameters self-learning can improve the accuracy of the model; the use of the bidirectional fusion structure can improve the accuracy and the

generalization ability of the model. In order to verify the superiority of the DFAS-LSTM model proposed in this paper, the model is compared with conventional Bi-LSTM model, Bi-LSTM model with improved activation function, and Bi-LSTM with alertness mechanism. For the test of the model, the data of the coal-fired power plant is used to achieve the industrial and elemental analyses of the coal quality. To be specific, the industrial analyses include low calorific value, total moisture, ash content, and volatile. The accuracies of industrial analyses using DFAS-LSTM model are 85.32%, 82.21%, 83.79%, and 83.01%. The elemental analyses include carbon content, hydrogen content, oxygen content, nitrogen content, and sulfur content. The accuracies of the elemental analyses using DFAS-LSTM model are 84.65%, 80.29%, 81.26%, 81.82%, and 81.20%. The

verification shows that the DFAS-LSTM model proposed in this paper basically completes the functions of industrial and elemental analyses, which provides support for online analyses of the coal quality in coal-fired power plants. Traditional measurement methods rely on expensive equipment and cannot achieve coal quality analyses in real time. The soft measurement method proposed in this paper avoids the weakness of the traditional measurement methods and saves the cost. In the future, the correlation between conventional measurement points and coal quality will be further analyzed. By removing the measurement points with low correlation, the data dimension will be further reduced. The model parameters and the time consumed for analyses will reduce at the same time.

Data Availability

The data used to support the findings of this study are available from the corresponding author Mei Wang, whose e-mail is wangm@xust.edu.cn.

Conflicts of Interest

The authors declare that they have no conflicts of interest regarding the paper.

Acknowledgments

This work was supported by the Shaanxi Province Science and Technology Project (2016GY-040) and the National Natural Science Foundation of China (51804249).

References

- [1] S. D. Kumar and D. Subha, "Prediction of depression from EEG signal using long short-term memory (LSTM)," in *Proceedings of the 3rd international conference on trends in electronics and informatics (ICOEI)*, pp. 1248–1253, Tirunelveli, India, April 2019.
- [2] O. Barut, L. Zhou, and Y. Luo, "Multitask LSTM model for human activity recognition and intensity estimation using wearable sensor data," *IEEE Internet of Things Journal*, vol. 7, no. 9, pp. 8760–8768, 2020.
- [3] Z. Ding, R. Xia, J. Yu, X. Li, and J. Yang, "Densely connected bidirectional LSTM with applications to sentence classification," *Natural Language Processing and Chinese Computing*, vol. 1, pp. 278–287, 2018.
- [4] Y. Huang, W. Wang, and L. Wang, "Instance-aware image and sentence matching with selective multimodal LSTM," in *Proceedings of the IEEE Conference on Computer Vision and Pattern Recognition*, pp. 2310–2318, 2017.
- [5] H. Xue, D. Q. Huynh, and M. Reynolds, "A Hierarchical LSTM model for pedestrian trajectory prediction," in *Proceedings of the 2018 IEEE Winter Conference on Applications of Computer Vision (WACV)*, pp. 1186–1194, Lake Tahoe, NV, USA, March 2018.
- [6] J. Liu, A. Shahroudy, D. Xu, and G. Wang, "Spatio-temporal LSTM with trust gates for 3D human action recognition," *Computer Vision - ECCV 2016*, vol. 40, pp. 816–833, 2016.
- [7] S. O. Sahin and S. S. Kozat, "Nonuniformly sampled data processing using LSTM networks," *IEEE Transactions on Neural Networks and Learning Systems*, vol. 30, no. 5, pp. 1452–1461, 2019.
- [8] B. Liu, N. Liu, G. Chen, X. Dai, and M. Liu, "A low-cost vehicle anti-theft system using obsolete smartphone," *Mobile Information Systems*, vol. 2018, Article ID 6569826, 16 pages, 2018.
- [9] H. Lu, M. Zhang, X. Xu, Y. Li, and H. T. Shen, "Deep fuzzy hashing network for efficient image retrieval," *IEEE Transactions on Fuzzy Systems*, vol. 29, no. 1, pp. 166–176, 2020.
- [10] B. Siegel, "Industrial anomaly detection: a comparison of unsupervised neural network architectures," *IEEE Sensors Letters*, vol. 4, no. 8, pp. 1–4, 2020.
- [11] C. Zou, Q. Zhao, G. Zhang, and B. Xiong, "Energy revolution: from a fossil energy era to a new energy era," *Natural Gas Industry B*, vol. 3, no. 1, pp. 1–11, 2016.
- [12] Y. Zhu, R. Zhai, H. Peng, and Y. Yang, "Exergy destruction analysis of solar tower aided coal-fired power generation system using exergy and advanced exergetic methods," *Applied Thermal Engineering*, vol. 108, pp. 339–346, 2016.
- [13] J. Singh and S. Thakur, *Laser-induced Breakdown Spectroscopy*, Elsevier, Amsterdam, Netherlands, 2020.
- [14] Z. Zang, X. Qiu, Y. Guan, E. Zhang et al., "Determining moisture content of traditional Chinese medicines using a near-infrared LED-based moisture content sensor with spectrum analysis," *Optical and Quantum Electronics*, vol. 51, no. 5, pp. 51–133, 2019.
- [15] H. Schwarz and X. Cai, "Special issue: development of renewable energy and smart grid," *Frontiers in Energy*, vol. 11, no. 2, pp. 105–106, 2017.
- [16] B. Looney, *BP Statistical Review of World Energy: BP Statistical Review*, Baker Library, Hanover, NH, USA, 2020.
- [17] G. Kurata, B. Ramabhadran, G. Saon Sathy, and A. Sathy, "Language modeling with highway LSTM," in *Proceedings of the 2017 IEEE Automatic Speech Recognition and Understanding Workshop (ASRU)*, pp. 244–251, Okinawa, Japan, December 2017.
- [18] S. Y. Tseng, S. N. Chakravarthula, B. R. Baucom, and P. Georgiou, "Couples behavior modeling and annotation using low resource LSTM language models," *Interspeech*, vol. 12, no. 1, pp. 898–902, 2016.
- [19] B. Athiwaratkun and J. W. Stokes, "Malware classification with LSTM and GRU language models and a character-level CNN," in *Proceedings of the 2017 IEEE International Conference on Acoustics, Speech and Signal Processing (ICASSP)*, pp. 2482–2486, New Orleans, LA, USA, March 2017.
- [20] X. Shi, Z. Chen, H. Wang et al., "Convolutional LSTM network: a machine learning approach for precipitation nowcasting," *Advances in Neural Information Processing Systems*, vol. 2015, pp. 802–810, 2015.
- [21] Y. Pan, T. Mei, T. Yao et al., "Jointly modeling embedding and translation to bridge video and language," 2016, <https://arxiv.org/abs/1505.01861>.
- [22] K. Amarasinghe, D. L. Marino, and M. Manic, "Deep neural networks for energy load forecasting," in *Proceedings of the 2017 IEEE 26th International Symposium on Industrial Electronics (ISIE)*, pp. 1483–1488, Scotland, UK, June 2017.
- [23] D. L. Marino, K. Amarasinghe, and M. Manic, "Simultaneous generation-classification using LSTM," in *Proceedings of the 2016 IEEE Symposium Series on Computational Intelligence (SSCI)*, pp. 1–8, Athens, Greece, December 2016.
- [24] E. Oko, M. Wang, and J. Zhang, "Neural network approach for predicting drum pressure and level in coal-fired subcritical power plant," *Fuel*, vol. 151, pp. 139–145, 2015.
- [25] A. Ayodeji, Y.-k. Liu, and H. Xia, "Knowledge base operator support system for nuclear power plant fault diagnosis," *Progress in Nuclear Energy*, vol. 105, pp. 42–50, 2018.

- [26] M. Talaat, M. H. Gobran, and M. Wasfi, "A hybrid model of an artificial neural network with thermodynamic model for system diagnosis of electrical power plant gas turbine," *Engineering Applications of Artificial Intelligence*, vol. 68, pp. 222–235, 2018.
- [27] M. Rashid, K. Kamal, T. Zafar et al., "Mathavan. Energy prediction of a combined cycle power plant using a particle swarm optimization trained feedforward neural network," in *Proceedings of the 2015 International Conference on Mechanical Engineering, Automation and Control Systems (MEACS)*, pp. 1–5, Novosibirsk, Russia, December 2015.
- [28] J. Li, Z. Wu, K. Zeng, G. Flamant, A. Ding, and J. Wang, "Safety and efficiency assessment of a solar-aided coal-fired power plant," *Energy Conversion and Management*, vol. 150, pp. 714–724, 2017.
- [29] H. Chen, W. Rong, X. Ma et al., "An extended technology acceptance model for mobile social gaming service popularity analysis," *Mobile Information Systems*, vol. 2017, Article ID 3906953, 12 pages, 2017.
- [30] S. Liu, L. Feng, J. Wu, G. Hou, and G. Han, "Concept drift detection for data stream learning based on angle optimized global embedding and principal component analysis in sensor networks," *Computers & Electrical Engineering*, vol. 58, pp. 327–336, 2017.
- [31] Z. Uddin, A. Ahmad, M. Iqbal et al., "Adaptive step size gradient ascent ICA algorithm for wireless MIMO systems," *Mobile Information Systems*, vol. 2018, Article ID 7038531, 9 pages, 2018.
- [32] T. Venkatakrishnamoorthy and G. U. Reddy, "Cloud enhancement of NOAA multispectral images by using independent component analysis and principal component analysis for sustainable systems," *Computers & Electrical Engineering*, vol. 74, pp. 35–46, 2019.
- [33] J. Bowler and P. Bourke, "Facebook use and sleep quality: light interacts with socially induced alertness," *British Journal of Psychology*, vol. 110, no. 3, pp. 519–529, 2019.
- [34] D. K. Jain, R. Jain, Y. Upadhyay, A. Kathuria, and X. Lan, "Deep Refinement: capsule network with attention mechanism-based system for text classification," *Neural Computing and Applications*, vol. 32, no. 7, pp. 1839–1856, 2020.
- [35] Y. Wang, C. Hu, K. Chen et al., "Self-attention guided model for defect detection of aluminium alloy casting on X-ray image," *Computers & Electrical Engineering*, vol. 88, pp. 1–8, 2020.
- [36] K. Greff, R. K. Srivastava, J. Koutnik, B. R. Steunebrink, and J. Schmidhuber, "LSTM: a search space odyssey," *IEEE Transactions on Neural Networks and Learning Systems*, vol. 28, no. 10, pp. 2222–2232, 2017.
- [37] M. Chammas, A. Makhoul, and J. Demerjian, "An efficient data model for energy prediction using wireless sensors," *Computers & Electrical Engineering*, vol. 76, pp. 249–257, 2019.
- [38] Y. Yao and Z. Huang, "Bi-directional LSTM recurrent neural network for Chinese word segmentation," *Neural Information Processing*, vol. 40, pp. 345–353, 2016.

Research Article

Cloud Classroom Design for English Education Based on Internet of Things and Data Mining

Xiaohua Luo 

School of Nationalities, Lishui University, Lishui 323000, China

Correspondence should be addressed to Xiaohua Luo; lsxyrobin@lsu.edu.cn

Received 2 February 2021; Revised 9 April 2021; Accepted 11 April 2021; Published 19 April 2021

Academic Editor: Hsu-Yang Kung

Copyright © 2021 Xiaohua Luo. This is an open access article distributed under the Creative Commons Attribution License, which permits unrestricted use, distribution, and reproduction in any medium, provided the original work is properly cited.

The Informa ionization of social life and the globalization of economy have made the importance of English increasingly prominent. Building an information-based teaching platform for supplementary teaching under the network environment has become a mainstream teaching method in various basic schools. How to integrate various types of multimedia teaching resources into English classroom teaching has become the main goal of the current college teaching reform. Aiming at the shortcomings of the current English education classroom, this paper designs and develops an English education cloud classroom based on the Internet of Things and data mining methods. First of all, the system adopts a three-tier B/S model, the development platform chooses, NET, the development language, uses ASP.NET, and the database chooses SQL server. Secondly, the data mining method is used to clean and organize the data in the cloud classroom background to explore the course education status behind the data. Finally, the simulation test analysis verifies the efficiency of the English education cloud classroom established in this article.

1. Introduction

Institutions of higher learning are the specific implementation link of our country's talent strategy. In recent years, our country has vigorously promoted educational reform and educational technology application [1, 2]. The application of new technologies such as computer technology, information technology, and network technology has given a more positive development to the prospects of higher education [3, 4]. Through the survey, it is found that the application of most of the network platforms of colleges and universities is relatively single, and most of the network platforms have become educational affairs' platforms or network library platforms of major universities, and the teaching tasks are not completed as expected [5]. From the current technical point of view and teaching task requirements, it is not feasible to completely use the Internet teaching platform to replace manual teaching [6, 7]. However, it is feasible to use the Internet teaching platform as an auxiliary means of manual teaching or even as a teaching platform for elective courses [8, 9].

The use of big data technology can extract laws from massive data [10]. Through the practice of different industries, data mining, sorting, and analysis of massive data can provide effective decision-making reference [11, 12]. The same is true in the education industry. It is effective to introduce data mining technology to the network teaching platform to improve the learning effect and teaching management level of students [13, 14]. Using big data-related technologies to explore the internal laws between students, teachers, courses, grades, and other contents can provide a reference basis for the decision-making level of education and teaching and can also provide a guiding basis for the overall teaching task and teaching plan formulation [15, 16]. After observing the online teaching systems of several colleges and universities, it is found that the current online teaching platforms of colleges and universities are mostly the carriers of students' course selection, score query, and registration information [17]. From a functional point of view, the online teaching platform is more biased towards educational affairs system. Many students' learning information, school status information, course selection information, grades, and other contents are not related to

each other, but in fact, there are connotative rules information that has not been used [18].

From the perspective of the functionality of the online teaching platform, the content of the platform is more static, and its dynamic personalized recommendation and evaluation functions are not yet mature [19, 20]. The Informationization of social life and the globalization of the economy have made the importance of English increasingly prominent. Building an information-based teaching platform for supplementary teaching under the network environment has become a mainstream teaching method in various basic schools. How to integrate various types of multimedia teaching resources into English classroom teaching has become the main goal of the current college teaching reform. Aiming at the shortcomings of current English education classrooms, this paper designs and develops an English education cloud classroom based on the Internet of Things and data mining methods. It is hoped that through the use of association rule algorithms, learning arrangements and teaching management can provide a strong basis to find out the key factors affecting the quality of teaching and provide assistance for improving the level of English teaching. In Section 2, we introduced the basic research of English cloud education classroom and the Internet of Things. In Section 3, we introduced cloud classroom design for English education based on data mining. In Section 4, we introduced relevant examples to verify. In Section 5, we summarize the relevant conclusions and future prospects.

2. Related Work

2.1. English Education Cloud Class. With the gradual deepening of distance education research, English distance education researchers have increasingly realized that comprehensive and systematic learning support services are the core element of maintaining the success of English distance education [21, 22]. Difficulty in interaction, weak learning ability, and lack of time are the three major obstacles hindering the success of distance learners. An important way to solve these difficulties is to develop and provide comprehensive and systematic learning support services for students. As a bridge between English distance education institutions and learners, learning support services aim to develop various services that meet the needs of students and help students solve learning difficulties [23]. With the advent of the era of big data and artificial intelligence, the learning methods, teaching methods, and cognitive methods of English distance education have undergone major changes. The characteristics of the era require new connotations to be injected into learning support services; from the traditional unified, the fixed learning support services have shifted to the development of personalized English teaching design, curriculum management, and learning evaluation services [24]. The conceptual diagram of English education cloud classroom is shown in Figure 1.

With the gradual deepening of research on English distance education, English distance education researchers have increasingly realized that comprehensive and systematic

learning support services are the core elements to maintain the success of English distance education [25, 26]. Compared with full-time students, English distance learners are faced with the following three difficulties in learning under the premise of taking into account work and life. A characteristic of English distance education is that English teachers, students, and teaching institutions are geographically separated. The process of teaching and learning depends on various media and media. Therefore, there is a lack of timely and effective communication between teachers and students and students and students (see [27, 28]). To succeed in English distance education, in addition to the development and provision of well-designed and diverse learning resources by educational institutions, it also requires learners to have high self-learning ability and time-management ability. Secondly, English distance education is mainly based on online autonomous learning, so learners need to have certain computer skills and information technology foundation [29, 30]. English distance learners need to take care of work, study, and life and can only study in their leisure time and holidays, so they need higher learning efficiency. Once students encounter difficulties, they will have corresponding needs [31, 32]. If the needs are not met, these difficulties will cause English learners to lose interest in the course, gradually lose their passion for learning, learning arrangements and plans are chaotic, and ultimately lead to failure.

2.2. Overview of Mobile Information Technology. In recent years, mobile information technology has received extensive attention and development. Technologies such as edge computing and the Internet of Things have received more and more attention from researchers. Definition of the Internet of Things: the Internet of Things (IoT) can be regarded as a far-reaching vision with technical and social significance. From the perspective of technology standardization, IoT can be regarded as the infrastructure of the global information society, providing physical interconnection (physical and virtual) on the basis of existing and emerging interoperable information and communication technologies (ICT) advanced business. Through identification, data capture, processing, and communication capabilities, IoT can make full use of “things” to provide services for various applications, while ensuring security and privacy requirements [33].

The prevailing Internet of Things platform is essentially a centralized structure. Although the traditional Internet of Things is trying to use emerging distributed storage, edge computing, and other technologies, it has not changed its centralized nature [34]. In general, traditional IoT service platforms include server-side service platforms, IoT applications, IoT services, and client-side: full-function IoT devices, IoT gateways, and function-restricted IoT devices. Among them, the core of the “service platform” is network communication capabilities and application and business support capabilities. “Internet of things application” and “Internet of things business” are for the needs of mass users, commerce, and industry and are used to provide specific functional services. The provider is generally a company or

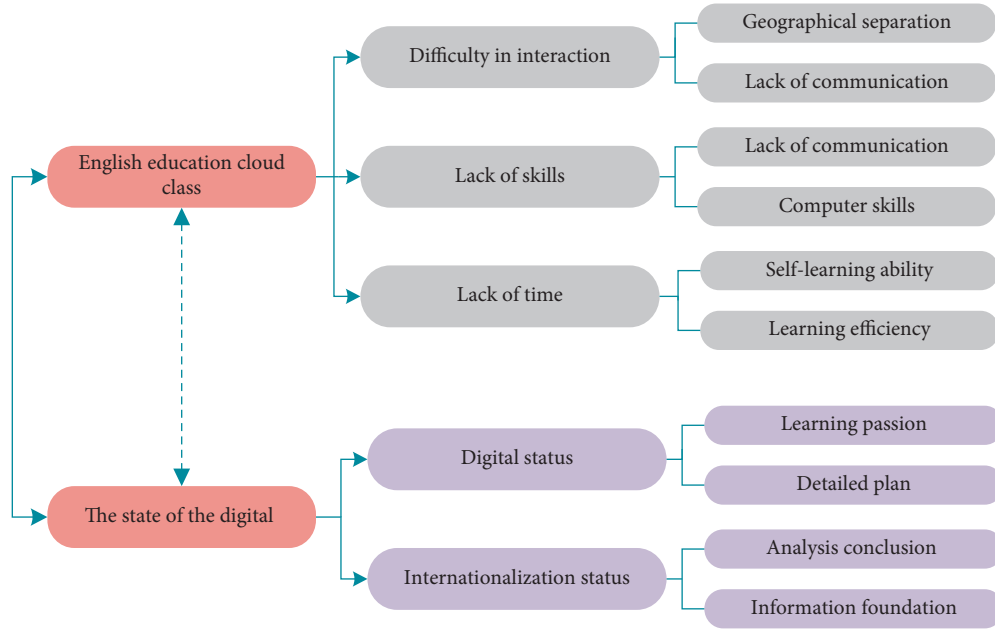


FIGURE 1: Schematic diagram of English education cloud classroom concept.

organization. “Full-featured Internet of Things devices” refer to Internet of Things devices with complete communication and working capabilities, such as smart phones and home electronic devices and industrial equipment that can directly connect to the Internet [35].

3. Cloud Classroom Design for English Education Based on Data Mining

Data mining methods include machine learning methods, statistical methods, neural network methods, and database methods. Among them, machine learning methods include inductive analysis methods (decision trees, rule induction, etc.) and genetic algorithms. Statistical methods include regression analysis (autoregressive, multiple regression, etc.), discriminant analysis (Bayesian discriminant, Fischer discriminant, and nonparametric discriminant), and cluster analysis. Neural network methods include feedforward neural network (BP algorithm) and self-organizing neural network. Database methods include multidimensional data analysis and OLAP methods. Among these methods, the following mining algorithms are commonly used: decision trees, association rules, Bayes, neural networks, rule learning, etc.

Gradient Boosting Decision Tree (GBDT) is a classic boosting algorithm. It is based on the idea of boosting algorithm, and in each iteration, a new decision tree is established in the direction of reducing the gradient of the residual and iteratively improves the generalization ability of the system. The gradient boosting decision tree is essentially a combination of multiple decision trees. The decision tree algorithm based on gradient boosting can identify distinguishable features and feature combinations. In the GBDT algorithm, the path of the decision tree can be directly used as the input features of other models, reducing the steps of

manually selecting and combining features. Therefore, in the context attribute weight calculation, it is possible to identify context attributes that affect user preferences and to obtain the weight results of context attributes based on the relationship between context attributes, so as to dig deeper into user needs and provide users with more personalized Information recommendation. Conceptual diagram of decision tree data mining is shown in Figure 2.

Discretize each context instance under context attributes, convert them into input features, and input them into the gradient boosting decision tree. With the advent of the era of big data and artificial intelligence, the learning methods, teaching methods, and cognitive methods of English distance education have undergone major changes. The characteristics of the era require new connotations to be injected into learning support services; from the traditional unified, the fixed learning support services have shifted to the development of personalized English teaching design, curriculum management, and learning evaluation services. Since the gradient boosting decision tree algorithm is composed of multiple decision trees, each decision tree uses a top-down greedy algorithm to select the attribute with the best classification effect at each node to split:

$$\begin{cases} 1 \longrightarrow \\ 2 \longrightarrow \\ 3 \longrightarrow \\ \vdots \\ m \longrightarrow \end{cases} \begin{pmatrix} x_{11} & x_{12} & x_{13} & \cdots & x_{1n} \\ x_{21} & x_{22} & x_{23} & \cdots & x_{2n} \\ x_{31} & x_{32} & x_{33} & \cdots & x_{3n} \\ \vdots & \vdots & \vdots & & \vdots \\ x_{m1} & x_{m2} & x_{m3} & \cdots & x_{mn} \end{pmatrix}. \quad (1)$$

Therefore, the reference documents of this study measure the contribution degree of the situation instance to the user’s choice based on the average change of the Gini index when each situation instance is used as a split node in each decision tree:

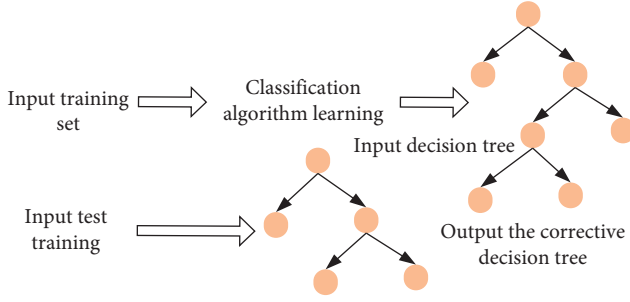


FIGURE 2: Conceptual diagram of decision tree data mining.

$$\text{st.} \begin{cases} \frac{\sum_{r=1}^s u_r y_{rj}}{\sum_{i=1}^m v_i x_{ij}} \leq 1 (j = 1, \dots, n), \\ v_i \geq 0 (i = 1, \dots, m), \\ u_r \geq 0 (r = 1, \dots, s). \end{cases} \quad (2)$$

$$\begin{cases} v_{ij}(t+1) = v_{ij}(t) + c_1 r_1(t)(p_{ij}(t) - x_{ij}(t)) + c_2 r_2(t)(p_{gj}(t) - x_{ij}(t)), \\ m_{ij}(t+1) = m_{ij}(t) + v_{ij}(t+1). \end{cases} \quad (4)$$

The priority of each attribute of the decision tree is usually based on the information gain:

$$Z_1 = -0.002Z_2 - 0.0869Z_3 + 1.6Z_4 + 0.385Z_5. \quad (5)$$

In addition, the Gini index and gain ratio are also commonly used to divide optimal attributes, where the gain ratio is expressed as

$$\max h_{j0} = \frac{\sum_{r=1}^n u_r y_{rj0}}{\sum_{i=1}^m v_r x_{rj0}}. \quad (6)$$

In order to prevent overfitting, decision trees usually adopt pruning methods to improve generalization:

$$t = \frac{1}{\sum_{i=1}^m v_i x_{ij}}, \quad (7)$$

$$w_i = tv_i,$$

$$\mu_r = tu_r.$$

Pruning is divided into prepruning and postpruning. Prepruning is based on the calculation result of information gain to determine in advance whether retaining nodes will increase the generalization of the model. Postpruning is to first generate a complete decision tree model and then proceed upward from the bottom leaf node. Investigate and decide whether to keep each node. For the situation where a sample can belong to multiple categories at the same time, the existence of the degree of membership is used to reflect the degree to which the sample

Assume that M decision trees are obtained through the GBDT algorithm according to the user's preference information for selecting information resources and then the context instance C_k under the context attribute. The degree of contribution to the user's choice of information resources originates from the situational instance C_k :

$$Q = \begin{cases} Y = a_1 x_1 + a_2 x_2 + a_3 x_3 + a_4 x_4 + a_5 x_5, \\ a_1 + a_2 + a_3 + a_4 + a_5 = 1, \\ 0 < a < 1. \end{cases} \quad (3)$$

When M is used as a split node in a decision tree, there is no change in the average value of the Gini coefficient. Among them, the calculation formula for the Gini index of node and node is

belongs to a certain category. Fuzzy mathematics can express the fuzzy nature of things and relationships. On this basis, a fuzzy fault diagnosis model can be constructed to enable fault diagnosis to better handle the complex relationship between fault sources and fault symptoms.

4. Case Study of English Education Cloud Classroom Research

4.1. Case Analysis. The cloud classroom for English education based on data mining is an aid and extension of classroom teaching and is a tool to help students achieve after-class review and consolidate and reduce the workload of teachers. The biggest feature of the system should be reflected in individualization, that is, according to the characteristics of students, the information obtained by data mining should be used to dynamically select and organize the materials to be learned in teaching resources so that students can learn. Individualized guidance can be obtained in the selection of content, the understanding of learning goals, the evaluation of learning effects, and the diagnosis of the learning process, so as to truly realize teaching in accordance with their aptitude. The framework design of the English education cloud classroom system is shown in Figure 3.

The functional roles of the English education cloud classroom system can be divided into three types according to the user's authority, including system administrators, teachers, and students. For the situation where a sample can belong to multiple categories at the same time, the existence

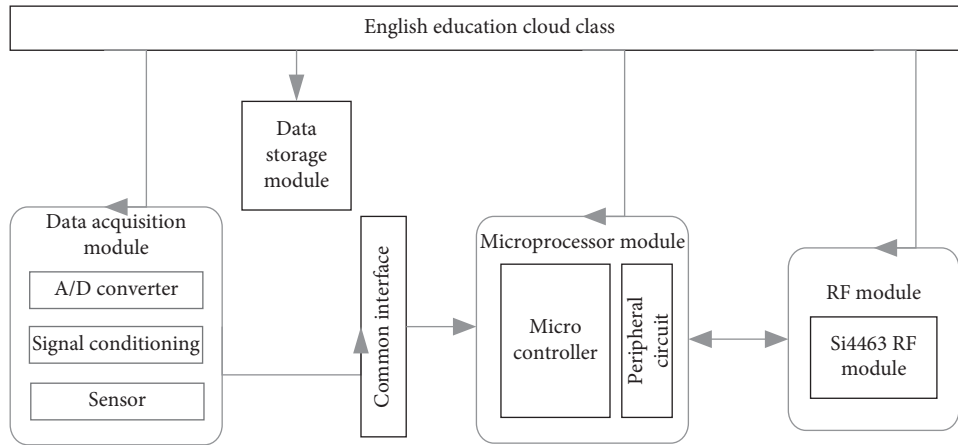


FIGURE 3: Framework design of the English education cloud classroom system.

of the degree of membership is used to reflect the degree to which the sample belongs to a certain category. Fuzzy mathematics can express the fuzzy nature of things and relationships. On this basis, a fuzzy fault diagnosis model can be constructed to enable fault diagnosis to better handle the complex relationship between fault sources and fault symptoms. The responsibilities of the system administrator include the maintenance and management of system information, user information, and user rights; the responsibilities of teachers include the management of teaching resources, through data mining of English student information to analyze and evaluate students' learning behaviors and adjust teaching strategies; students are in the system's personalized learning interface for autonomous learning, practice, testing, and answering questions.

4.2. Technical Testing and Application Effect Evaluation.

In order to verify the impact of the English education cloud classroom system on the learning effect of students, this research applies the system to the undergraduate English exam tutoring course. The effectiveness of the system is tested through three methods: the pass rate of the English unified test, teacher interviews, and student questionnaires, and the application effects of the system are analyzed to find the direction for improvement in the later period. Distribution of score data in English education cloud classroom is shown in Figure 4.

Figure 4 shows the distribution of score data in different courses of English education cloud classroom, such as speaking, reading, and writing. The personalized learning path recommendation system English education cloud classroom system was formally applied to the tutoring process of the undergraduate English test of a university network education. Up to the time of data extraction, two batches of students have used the system. After students enter the English tutoring course for the unified test, they can see the learning path recommended by the system based on their history department data on the homepage, click on the link to get the corresponding learning content and learning resources, and participate in learning activities.

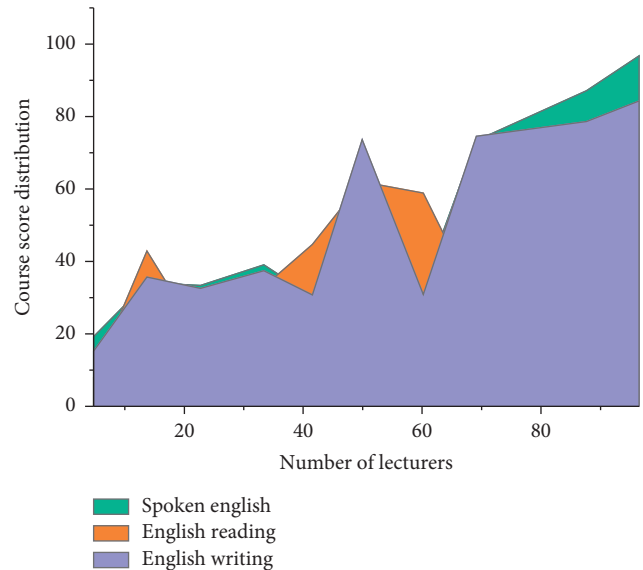


FIGURE 4: Distribution of score data in English education cloud classroom.

After the study is completed, the system will automatically mark the completed content. Teachers can use this system to provide students with personalized learning services and observe and record their learning progress. 75.9% of students think that, after using the system, their learning goals are clearer. This shows that most students agree with the navigation function of the learning path. Secondly, a total of 72.4% of students indicated that their learning time has been reduced after using the system. In contrast, 72.4% of students' learning initiative has been significantly enhanced, 82.8% of students said that the use of the system has mobilized their learning enthusiasm, and the number of logins to the platform has increased significantly. The number distribution of classrooms in different situations is shown in Figure 5.

Figure 5 shows the distribution of the number of classrooms in different situations, such as regular course time, weekend time, and holiday time. The results showed

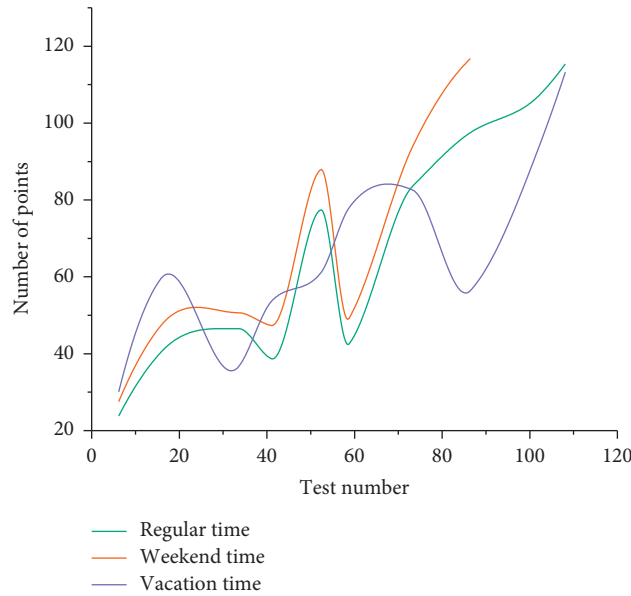


FIGURE 5: The number distribution of classrooms in different situations.

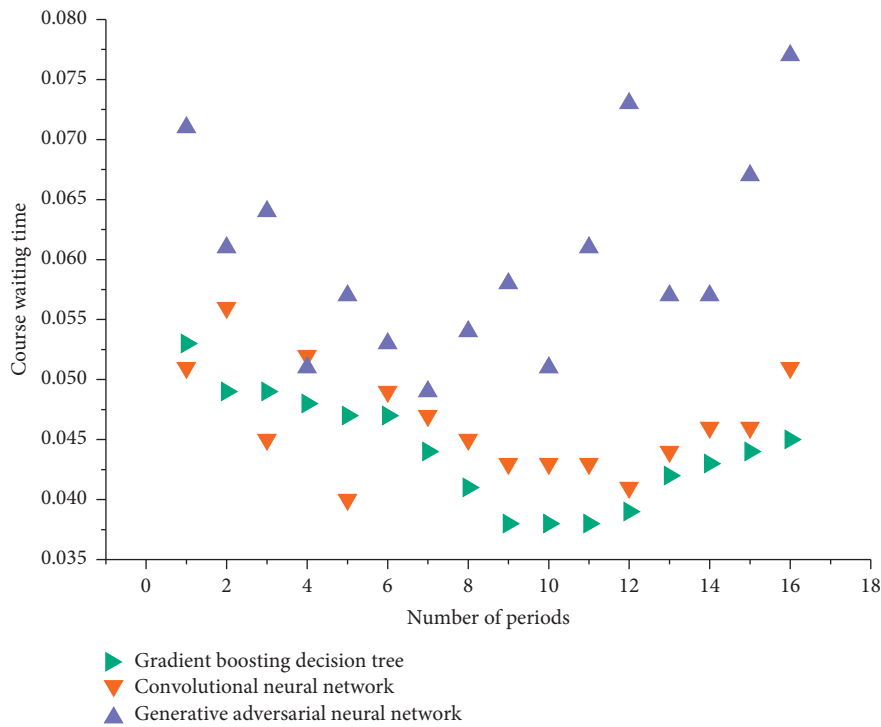


FIGURE 6: Comparison of english classroom based on gradient boosting decision tree and other methods.

that 72.4% of the students did not object to the learning sequence provided by the reference system, and the proportion of students willing to accept it was the highest. The functional roles of the English education cloud classroom system can be divided into three types according to the user's authority, including system administrators, teachers, and students. For the situation where a sample can belong to multiple categories at the same time, the existence of the

degree of membership is used to reflect the degree to which the sample belongs to a certain category. However, the system still has obvious shortcomings. In the GBDT algorithm, the path of the decision tree can be directly used as the input features of other models, reducing the steps of manually selecting and combining features. Therefore, in the context attribute weight calculation, it is possible to identify context attributes that affect user preferences and to obtain

the weight results of context attributes based on the relationship between context attributes, so as to dig deeper into user needs and provide users with more personalized Information recommendation. In addition, a total of 55.2% of students “strongly agree” and “agree” to add more personalized learning support modules to their studies because most students said that it would be difficult for them to only provide a personalized path recommendation function. Feel the convenience and help provided by personalized learning services. The comparison between the English classroom based on the gradient boosting decision tree and other methods is shown in Figure 6.

Figure 6 shows the comparison between the English classroom based on the gradient boosting decision tree and other methods in this paper. Among them, we compare methods such as convolutional neural networks and generative adversarial neural networks. We used the waiting time of the course as an indicator for comparison [36–38]. We found that the gradient boosting decision tree model can maintain less waiting time and run smoothly. In the context attribute weight calculation, this method can identify the context attributes that affect user preferences and obtain the weight results of the context attributes based on the relationship between the context attributes, thereby gaining a deeper understanding of user needs and providing users with more personalized information recommendations. Convolutional neural networks and generative adversarial neural networks have also achieved good results, but due to differences in data samples and model matching, the above methods failed to achieve better results in the test. Although the system obviously helps students reduce the time for resource selection and decision-making and improve their learning motivation, 31% of the students still expressed that they are not optimistic about the probability of passing the exam and the effect of the system cannot be determined before the exam. In summary, the personalized learning path recommendation system provides students with a brand-new and effective learning method, which well demonstrates its goals and path navigation functions. Help students reduce resource search and decision-making time, stimulate students’ interest in learning, and enhance learning initiative. The pointed learning resources and learning activities are not specific and detailed enough, and it does not consider the characteristics of students’ learning styles.

5. Conclusion

From the current technical point of view and teaching task requirements, it is not feasible to completely use the Internet teaching platform to replace manual teaching. However, it is feasible to use the Internet teaching platform as an auxiliary means of manual teaching or even as a teaching platform for elective courses. With the rapid development of network technology, modern teaching has an increasingly urgent need for a mature network teaching platform. Based on this demand, it is necessary to develop and design network teaching systems and gradually apply them to teaching activities. It is necessary to improve the quality of education of. Combining the characteristics of autonomous learning

and collaborative learning, comprehensively considering the needs of teaching management, resource sharing, and multidirectional interaction, this article creates a new type of English education network teaching system that conforms to the 21st century education information construction. The teaching system adopts the three-tier architecture of B/S in the choice of architecture. This choice can make the system’s operating ability more improved and run more smoothly. With the advancement of information technology and network technology, more and more educators realize the importance of network teaching, and more and more network teaching systems are applied to teaching. Therefore, a new network teaching system that fully meets the needs of teachers and students can achieve more long-term development.

Data Availability

The datasets used and/or analyzed during the current study are available from the corresponding author on reasonable request.

Ethical Approval

This article does not contain any studies with human participants or animals.

Disclosure

All authors agree to submit this version and claim that no part of this manuscript has been published or submitted elsewhere.

Conflicts of Interest

The author declares that he has no conflicts of interest.

References

- [1] S. Zhang, X. Xiaoming, and J. Peng, K. Huang and Z. Li, Physical layer security in massive internet of things: delay and security analysis,” *IET Communications*, vol. 13, no. 1, pp. 93–98, 2019.
- [2] Y. Ye, T. Li, D. Adjero, and S. S. Iyengar, “A survey on malware detection using data mining techniques,” *ACM Computing Surveys*, vol. 50, no. 3, pp. 1–40, 2017.
- [3] N. Ye, “A reverse engineering algorithm for mining a causal system model from system data,” *International Journal of Production Research*, vol. 55, no. 3-4, pp. 828–844, 2017.
- [4] S. Venkatraman, B. Surendiran, and P. Arun Raj Kumar, “Spam e-mail classification for the internet of things environment using semantic similarity approach,” *The Journal of Supercomputing*, vol. 76, no. 2, pp. 756–776, 2020.
- [5] L. Varpio, J. Frank, J. Sherbino, L. S. Snell, and M. Young, “Research environments: can the cloud supplement bricks and mortar?” *Medical Education*, vol. 52, no. 9, pp. 891–893, 2018.
- [6] J. B. Varley, A. Miglio, V. A. Ha, M. J. V. Setten, G. M. Rignanes, and G. Hautier, “High-throughput design of non-oxide p-type transparent conducting materials: data mining, search strategy, and identification of boron phosphide,” *Chemistry of Materials*, vol. 29, no. 6, pp. 2568–2573, 2017.

- [7] J. R. R. Dorea and G. J. M. Rosa, "748 mining farm-and animal-level data to optimize beef cattle production," *Journal of Animal Science*, vol. 95, 2017.
- [8] P. Spachos, L. Papapanagiotou, and K. N. Plataniotis, "Microlocation for smart buildings in the era of the internet of things—a survey of technologies, techniques, and approaches," *IEEE Signal Processing Magazine*, vol. 35, no. 5, pp. 140–152, 2019.
- [9] H. R. Pourghasemi, S. Yousefi, A. Kornejady, and A. Cerdà, "Performance assessment of individual and ensemble data-mining techniques for gully erosion modeling," *Science of the Total Environment*, vol. 609, no. 3, pp. 764–775, 2017.
- [10] V. Radonjić Đogatović, M. Đogatović, M. Stanojević, and N. Mladenovic, "Revenue maximization of internet of things provider using variable neighbourhood search," *Journal of Global Optimization*, vol. 78, pp. 375–396, 2020.
- [11] S. A. Naghibi, D. D. Moghaddam, B. Kalantar, B. Pradhan, and O. Kisi, "A comparative assessment of GIS-based data mining models and a novel ensemble model in groundwater well potential mapping," *Journal of Hydrology*, vol. 548, pp. 471–483, 2017.
- [12] C. Michie, I. Andonovic, C. Davison et al., "The internet of things enhancing animal welfare and farm operational efficiency," *Journal of Dairy Research*, vol. 87, no. 1, pp. 20–27, 2020.
- [13] M. Mayer and A. J. Baumner, "A megatrend challenging analytical chemistry: biosensor and chemosensor concepts ready for the internet of things," *Chemical Reviews*, vol. 119, no. 13, pp. 7996–8027, 2019.
- [14] S. N. Matheu, J. L. Hernández-Ramosjosé, A. F. Skarmetaantonio, and G. Baldini, "A survey of cybersecurity certification for the internet of things," *ACM Computing Surveys*, vol. 53, no. 6, pp. 26–33, 2020.
- [15] M. T. Baldassarre, D. Caivano, G. Dimauro, E. Gentile, and G. Visaggio, "Cloud computing for education: a systematic mapping study," *IEEE Transactions on Education*, vol. 61, no. 3, pp. 234–244, 2018.
- [16] M. Hauben, V. Patadia, C. Gerrits, L. Walsh, and L. Reich, "Data mining in pharmacovigilance: the need for a balanced perspective," *Drug Safety*, vol. 28, no. 10, pp. 835–842, 2018.
- [17] L. Khalafi, P. Doolittle, and J. Wright, "Speciation and determination of low concentration of iron in beer samples by cloud point extraction," *Journal of Chemical Education*, vol. 95, no. 3, pp. 463–467, 2018.
- [18] U. L. Igbokwe, K. C. N. Onyechi, C. S. Ogbonna et al., "Rational emotive intervention for stress management among English education undergraduates: implications for school curriculum innovation," *Medicine*, vol. 98, no. 40, Article ID e17452, 2019.
- [19] U. L. Igbokwe, E. N. Nwokenna, C. Eseadi et al., "Intervention for burnout among English education undergraduates: implications for curriculum innovation," *Medicine*, vol. 98, no. 26, Article ID e16219, 2019.
- [20] F. Hufsky and S. Bocker, "Mining molecular structure databases: identification of small molecules based on fragmentation mass spectrometry data," *Mass Spectrometry Reviews*, vol. 36, 2016.
- [21] H. He, T. Zhao, H. Guan et al., "A water-evaporation-induced self-charging hybrid power unit for application in the internet of things," *Science Bulletin*, vol. 64, no. 19, pp. 1409–1417, 2019.
- [22] S. M. Ghaffarian and H. R. Shahriari, "Software vulnerability analysis and discovery using machine-learning and data-mining techniques," *ACM Computing Surveys*, vol. 50, no. 4, pp. 1–36, 2017.
- [23] R. M. Geilhufe, A. Bouhon, S. S. Borysov, and A. V. Balatsky, "Three-dimensional organic dirac-line materials due to nonsymmorphic symmetry: a data mining approach," *Physical Review B*, vol. 95, no. 4, Article ID 041103, 2017.
- [24] L. Fichera, G. Li-Destri, and N. Tuccitto, "Fluorescent nanoparticle-based internet of things," *Nanoscale*, vol. 12, 2020.
- [25] H. Eric and J. Paulina, "Internet of things: energy boon or bane?" *Science*, vol. 364, no. 6438, pp. 326–328, 2019.
- [26] W. English, P. Vulliamy, S. Banerjee, and S. Arya, "Surgical training during the COVID-19 pandemic—the cloud with a silver lining?" *British Journal of Surgery*, vol. 107, no. 9, 2020.
- [27] J. R. R. Dorea, G. J. M. Rosa, K. A. Weld, and L. E. Armentano, "Mining data from milk infrared spectroscopy to improve feed intake predictions in lactating dairy cows," *Journal of Dairy Science*, vol. 101, no. 7, pp. 5878–5889, 2018.
- [28] Y. Djenouri, D. Djamel, and Z. Djenouri, "Data-mining-based decomposition for solving MAXSAT problem: towards a new approach," *IEEE Intelligent Systems*, vol. 99, p. 1, 2017.
- [29] W.-C. Chen, J.-S. Niu, I.-P. Liu et al., "Study of a palladium (Pd)/aluminum-doped zinc oxide (AZO) hydrogen sensor and the kalman algorithm for internet-of-things (IoT) application," *IEEE Transactions on Electron Devices*, vol. 67, no. 10, pp. 4405–4412, 2020.
- [30] J. Chauhan and P. Goswami, "An integrated metaheuristic technique based energy aware clustering protocol for internet of things based smart classroom," *Modern Physics Letters B*, vol. 34, no. 22, Article ID 2050360, 2020.
- [31] R. Ceipek, J. Hautz, A. D. Massis, K. Matzler, and L. Ardito, "Digital transformation through exploratory and exploitative internet of things innovations: the impact of family management and technological diversification*," *Journal of Product Innovation Management*, vol. 14, no. 5, pp. 142–165, 2020.
- [32] B. Delibašić, P. Marković, P. Delias, and Z. Obradović, "Mining skier transportation patterns from ski resort lift usage data," *IEEE Transactions on Human-Machine Systems*, vol. 47, no. 3, pp. 417–422, 2017.
- [33] A. Bate, M. Lindquist, I. R. Edwards, and R. Orre, "A data mining approach for signal detection and analysis," *Drug Safety*, vol. 25, no. 6, pp. 393–397, 2002.
- [34] L. Barolli, F. Hussain, and M. Takizawa, "Special issue on intelligent edge, fog, cloud and internet of things (IoT)-based services," *Computing*, vol. 103, pp. 357–360, 2021.
- [35] O. Barker, "Realizing the promise of the internet of things in smart buildings," *Computer*, vol. 53, no. 2, pp. 76–79, 2020.
- [36] W. Li, X. Zhang, Y. Peng, and M. Dong, "Spatiotemporal fusion of remote sensing images using a convolutional neural network with attention and multiscale mechanisms," *International Journal of Remote Sensing*, vol. 42, no. 6, pp. 1973–1993, 2021.
- [37] Z. Liu, S. Zhong, Q. Liu et al., "Thyroid nodule recognition using a joint convolutional neural network with information fusion of ultrasound images and radiofrequency data," *European Radiology*, vol. 12, no. 5, pp. 16–20, 2021.
- [38] M. Mardani, E. Gong, J. Y. Cheng et al., "Deep generative adversarial neural networks for compressive sensing MRI," *IEEE Transactions on Medical Imaging*, vol. 38, no. 1, pp. 167–179, 2019.

Research Article

Gated Recurrent Unit with RSSIs from Heterogeneous Network for Mobile Positioning

Junxiang Wang,¹ Canyang Guo,² and Ling Wu ^{2,3}

¹School of Information and Intelligent Transportation, Fujian Chuanzheng Communications College, Fuzhou City, Fujian Province, China

²College of Mathematics and Computer Science, Fuzhou University, Fuzhou City, Fujian Province, China

³Key Laboratory of Intelligent Metro of Universities in Fujian, Fuzhou University, Fuzhou, China

Correspondence should be addressed to Ling Wu; wuling1985@fzu.edu.cn

Received 13 December 2020; Revised 10 March 2021; Accepted 2 April 2021; Published 13 April 2021

Academic Editor: Hsu-Yang Kung

Copyright © 2021 Junxiang Wang et al. This is an open access article distributed under the Creative Commons Attribution License, which permits unrestricted use, distribution, and reproduction in any medium, provided the original work is properly cited.

Recently, research studies on Location-Based Services (LBSs) based on networks including cellular network and Wi-Fi network have gradually become popular. Received Signal Strength Indicators (RSSIs) from the network can be detected and collected by mobile devices to estimate the locations without adopting the Global Positioning System (GPS). Previous research studies utilized the RSSIs of only cellular network or only Wi-Fi network to estimate location, which leads to a two-fold predicament involving error limits of cellular network-based methods and environmental constraints of Wi-Fi network-based methods. In addition, accommodating a highly temporal dependence of RSSI series data, this paper proposed a mobile positioning system based on Gated Recurrent Unit (GRU) with RSSIs from the heterogeneous network. GRU learns the temporal correlation of RSSIs and the relationship between RSSIs and GPS coordinates to estimate the locations of mobile devices. A large number of real experiments have been carried out to verify the performance of the proposed method, and experimental results demonstrate that the proposed method has lower errors (i.e., 5.86 m and 75% of errors within 4 m) compared with Neural Network (NN), Recurrent Neural Network (RNN), and Long Short-Term Memory (LSTM).

1. Introduction

The rapid development of the cellular network, Wi-Fi network, and mobile devices has promoted the Location-Based Services (LBSs) which can provide positioning services under the current locations of mobile devices by Global Positioning System (GPS) or network positioning method [1–3]. GPS is widely equipped in many mobile devices such as smartphones, cars, airplanes, and so on and shows excellent location performance [4]. However, there are some disadvantages with GPS for it may not work well in the situations of the indoor environment, urban roads, or multipath propagation of wireless signals [5]. In addition, higher power consumption is another reason that researchers take significant focus on other positioning methods including cellular network signal-based [1, 6] and Wi-Fi network signal-based [7–12] positioning methods.

For cellular network signals, they can be analysed to estimate the locations of mobile devices and are widely employed in outdoor environments where cellular network covered. However, positioning methods adopting cellular network signals may cause larger errors compared with the methods of adopting Wi-Fi network signals [8]. Therefore, the methods based on Wi-Fi network signals are usually utilized to detect and analyse the Received Signal Strength Indicators (RSSIs) from Wi-Fi access points (APs) for accurate locations of the indoor environment [8]. They utilize machine learning algorithms including Neural Network (NN), Convolutional Neural Network (CNN), and Recurrent Neural Network (RNN) to analyse the correlation between coordinates of GPS and RSSIs to extract features to estimate the locations of mobile devices [5, 7, 9, 13]. None is perfect, although Wi-Fi-based methods can provide accurate positioning, they may be invalid in outdoor environments where there are no or rare APs [9].

Considering of two-fold predicament involving error limits of the cellular network-based method and environmental constraints of the Wi-Fi network-based method, this paper adopts a positioning method based on heterogeneous network, which considers RSSIs from cellular network and Wi-Fi network. In addition, to accommodate the temporal dependence of RSSIs, the Gated Recurrent Unit (GRU) is utilized to extract the temporal characteristics of RSSI sequence and the correlation between RSSIs and GPS coordinates to estimate the locations of mobile devices. In summary, this paper aims to propose a mobile positioning system based on GRU with RSSIs from the heterogeneous network, which can provide accurate locations if there are network signals no matter cellular network signals or Wi-Fi network signals. A large number of experiments have been carried out in this paper, and experimental results show that the proposed method has better estimation performance (i.e., 5.86 m and 75% of errors within 4 m) than comparative methods.

The remainder of this paper is organized as follows. Section 2 represents the related work. Section 3 proposes a mobile positioning system based on GRU with RSSIs from the heterogeneous network. The practical experimental results and discussion are illustrated in Section 4. Section 5 elaborates the conclusions and future research directions.

2. Related Work

LBS is based on the network positioning method adopting machine learning techniques to estimate the locations of mobile devices by RSSIs from networks. Firstly, these methods utilize mobile devices to detect and collect data including coordinates of GPS and RSSIs from cellular network or Wi-Fi network and store them in the fingerprinting database [14–16]. Secondly, machine learning models are employed to capture the correlation between GPS coordinates and RSSIs. Finally, real-time RSSIs obtained by mobile devices are input to the trained model to estimate coordinates in real scenes.

Positioning model plays a critical role in the above methods, and how to develop an appropriate model has been widely studied by researchers. Wang et al. proposed a Wi-Fi fingerprint positioning method, which utilized the k -nearest neighbors algorithm to choose near reference points to improve positioning performance [17]. Although this method had lower errors, it would cost a lot of computation when estimating locations. Dai et al. proposed an indoor positioning method based on NN with RSSIs from Wi-Fi network, which learned the relationship among received signal strength signals transforming section, the raw data denoising section, and the node locating section to estimate locations by multilayer NN [18]. Zhang and Yi proposed a CNN-based Wi-Fi fingerprint positioning method which utilized a convolutional layer to extract the local feature of RSSIs to estimate locations [6]. Different structures of CNN and k -nearest neighbors were performed on public datasets, and experimental results showed that CNN-based method had lower errors with the accuracy of 90.83% correct positioning.

Although NN and CNN can estimate the locations effectively, they ignore the temporal characteristics of RSSIs. Therefore, researchers adopted the RNN-based method to learn the temporal dependence of RSSIs series data to improve the performance of positioning estimation [9, 13, 16]. Shi et al. proposed an indoor positioning method based on Long Short-Term Memory (LSTM) with RSSIs from Wi-Fi APs [19]. They chose appropriate APs for learning temporal features of RSSIs by LSTM, and the proposed method had been demonstrated to have better performance in experimental environments. Hoang et al. [12] compared the indoor positioning performance of multiple types of RNN with various inputs and outputs. Experimental results proved that LSTM with inputs including RSSIs and previous predicted location to predict multiple locations obtained the best performance. Although this method had estimation for the indoor environment, it would be invalid where there were no Wi-Fi signals. Therefore, this paper aims to propose a mobile positioning system based on GRU with RSSIs from the heterogeneous network, which can provide accurate locations if there are network signals no matter cellular network signals or Wi-Fi network signals.

3. Positioning System

3.1. Positioning Server. This paper proposes a mobile positioning system (shown in Figure 1) based on GRU with RSSIs from the heterogeneous network (i.e., cellular network and Wi-Fi network). The system consists of a mobile station, positioning server, database server, and model server, which will be introduced in the following.

3.1.1. Mobile Station. In the training stage, the function of the mobile station is to detect and receive the coordinates from GPS and RSSIs from cellular network and Wi-Fi network, and the received data are transmitted to the positioning server for positioning model training. In the testing stage, the function of the mobile station is to detect and receive RSSIs from the cellular network and Wi-Fi network and transmit the received data to the positioning server to estimate the positioning coordinates.

3.1.2. Positioning Server. In the training stage, the positioning system transmits the received data to the database server for storage. The estimation model will be trained by these data stored in the model server. In the testing stage, the positioning system can download the trained model from the model server to provide location estimation.

3.1.3. Database Server. The function of the database server is to keep the data including coordinates of GPS and RSSIs from the cellular network and Wi-Fi network for the training of the estimation model.

3.1.4. Model Server. The function of the database of the model server is to store the trained model. When

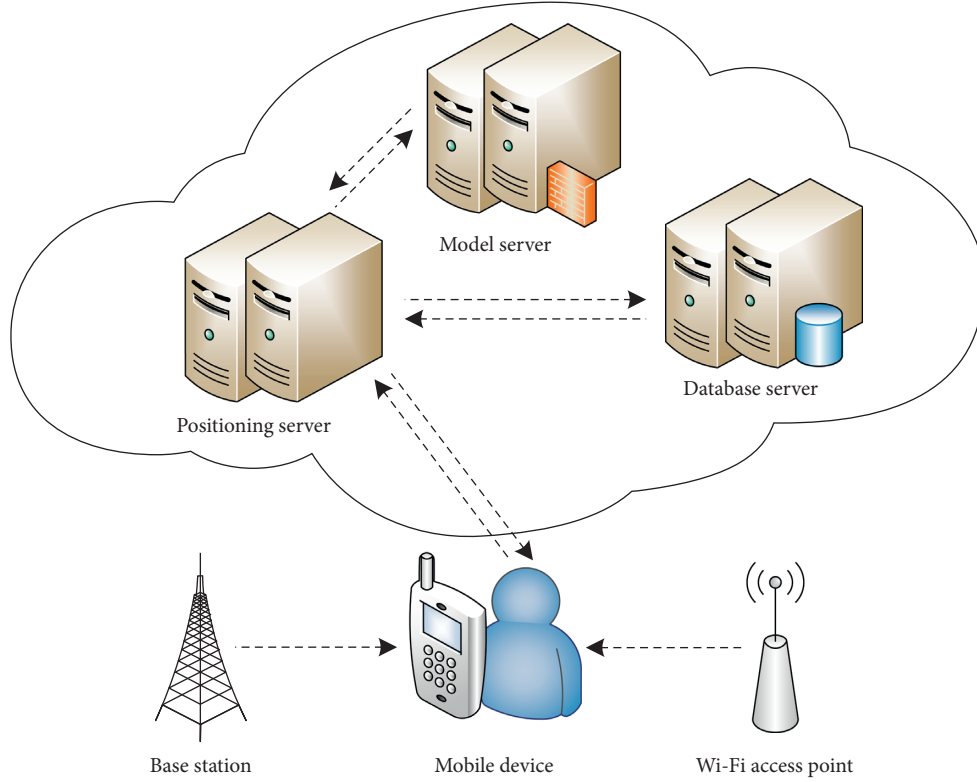


FIGURE 1: Proposed positioning system.

positioning, the positioning server can download the trained model from the model server.

3.2. Positioning Model

3.2.1. Data Preprocessing. The dataset collected by the mobile station is divided into the training set D_1 and testing set D_2 . D_1 and D_2 are made up of m and n labeled samples, which are expressed as $\{(R^{(i)}, l^{(i)})\}_{i=1}^m$ and $\{(R^{(i)}, l^{(i)})\}_{i=1}^n$. Among them, $R^{(i)}$ denotes i -th RSSI (expressed as equation (1)), which consists of cellular network signals $R_c^{(i)}$ (expressed as equation (2)) and Wi-Fi network signals $R_w^{(i)}$ (expressed as equation (3)). $l^{(i)}$ is the i -th coordinate of GPS including longitude $l_x^{(i)}$ and latitude $l_y^{(i)}$ (expressed as equation (4)).

$$R^{(i)} = \{R_c^{(i)}, R_w^{(i)}\}, \quad (1)$$

$$R_c^{(i)} = \{r_{c,1}^{(i)}, r_{c,2}^{(i)}, \dots, r_{c,p}^{(i)}\}, \quad (2)$$

$$R_w^{(i)} = \{r_{w,1}^{(i)}, r_{w,2}^{(i)}, \dots, r_{w,q}^{(i)}\}, \quad (3)$$

$$l_i = \{l_x^{(i)}, l_y^{(i)}\}, \quad (4)$$

where p and q denote the number of base stations and APs.

Considering that some road segments are not covered by Wi-Fi network signals, the corresponding encodings of these network signals are expressed with 0. Also, this paper adopts the max-min function to normalize the RSSI data and coordinates of GPS, which is expressed as follows:

$$\text{normalized}_i = \begin{cases} \frac{\text{observe}_i - \text{observe}^{(-)}}{\text{observe}^{(+)} - \text{observe}^{(-)}}, & \text{if } \text{observe}_i \neq 0, \\ 0, & \text{otherwise,} \end{cases} \quad (5)$$

where observe_i is the observed value (e.g., longitude, latitude, and RSSIs) in the i th record and normalized_i is the normalized value of observed values. $\text{observe}^{(+)}$ and $\text{observe}^{(-)}$ represent the maximum and minimum of corresponding data category, respectively.

3.2.2. Positioning Model Based on Gated Recurrent Unit with Heterogeneous Network. Considering that the outputs of NN are only related to the current inputs, this mechanism makes NN unable to process time-series data. RNN is a kind of variant of NN, which is usually employed in the scene of processing time-series data. Accommodating the gradient disappearance of RNN, LSTM is proposed by researchers to extract the long-term time-series data [19, 20]. GRU is a variant of LSTM, which is provided with the capability of dealing with long-term dependency and cheaper structure compared with LSTM (about a third of the parameters reduced) [18, 21–23].

This paper embeds the RSSIs data from the cellular network or Wi-Fi network and coordinates of GPS in the input layer and the output layer of the GRU model, respectively, and develops an effective positioning method whose structure is shown in Figure 2.

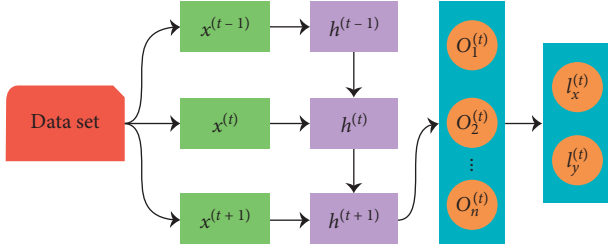


FIGURE 2: Proposed positioning model.

The input of the proposed method is a two-dimensional matrix, and each of the dimensions denotes memory length t and RSSIs data, which is expressed as follows:

$$x^{(i)} = \begin{Bmatrix} r_{c,1,1}^{(i)}, r_{c,2,1}^{(i)}, \dots, r_{c,p,1}^{(i)}, r_{w,1,1}^{(i)}, r_{w,2,1}^{(i)}, \dots, r_{w,p,1}^{(i)} \\ r_{c,1,2}^{(i)}, r_{c,2,2}^{(i)}, \dots, r_{c,p,2}^{(i)}, r_{w,1,2}^{(i)}, r_{w,2,2}^{(i)}, \dots, r_{w,p,2}^{(i)} \\ \vdots \\ r_{c,1,t}^{(i)}, r_{c,2,t}^{(i)}, \dots, r_{c,p,t}^{(i)}, r_{w,1,t}^{(i)}, r_{w,2,t}^{(i)}, \dots, r_{w,p,t}^{(i)} \end{Bmatrix}. \quad (6)$$

GRU contains a reset gate r_j and an update gate z_j to deal with past, present, and future information. The calculation formula of the reset gate is expressed as follows:

$$r_j = \sigma([W_r x]_j + [U_r h_{t-1}]_j), \quad (7)$$

where W_r and U_r are the weights of the reset gate, which will be optimized in the training stage, x and h_{t-1} denote the current input and previous hidden state, respectively, j is the j -th element of vectors, and σ denotes activation function, namely, sigmoid, which is computed as follows:

$$\sigma(a) = \frac{1}{1 + e^{-a}}. \quad (8)$$

The calculation formula of the update gate is expressed as follows:

$$z_j = \sigma([W_z x]_j + [U_z h_{t-1}]_j). \quad (9)$$

The hidden unit of time t is computed as follows:

$$h_j^t = z_j h_j^{t-1} + (1 - z_j) \tilde{h}_j^t. \quad (10)$$

The formula of \tilde{h}_j^t is expressed as follows:

$$\tilde{h}_j^t = \phi([W x]_j + [U(r \odot h_{t-1})]_j), \quad (11)$$

where ϕ denotes tanh function as shown in the following equation:

$$\phi(a) = \frac{e^a - e^{-a}}{e^a + e^{-a}}. \quad (12)$$

In equation (11), the reset gate is utilized to weigh the impacts of previously hidden layer information and current input layer information on the current hidden layer. The greater the reset gate r_j , the greater the influence of previously hidden layer information. In equation (10), the update gate z_j controls the effect of previously hidden layer information on the current hidden layer.

The output of the proposed method is a one-dimensional matrix containing a set of latitude and longitude coordinates. After denormalization, it can be expressed as follows:

$$y^{(i)} = \{I_{x,t}^{(i)}, I_{y,t}^{(i)}\}. \quad (13)$$

In addition, the loss function of the proposed method adopts quadratic loss, which is expressed as follows:

$$J(W, b) = \frac{1}{m} \sum_{i=1}^m L(W, b; \hat{x}^{(i)}, \hat{y}^{(i)}) \quad (14)$$

$$= \frac{1}{m} \sum_{i=1}^m (\hat{y}^{(i)} - y^{(i)})^2,$$

where $\hat{x}^{(i)}$ and $\hat{y}^{(i)}$ are the i -th observed values of RSSIs and coordinates of GPS.

The purpose of training is to obtain the parameters W and b which can minimize the value of the loss function. This paper utilizes the backpropagation algorithm to optimize the proposed model, and the optimization process is shown in Algorithm 1.

4. Practical Experimental Results and Discussion

4.1. Practical Experimental Environments. The dataset including GPS coordinates and RSSIs from cellular and Wi-Fi network utilized in this study is collected by an Android application installed on a mobile station (i.e., Redmi 5 running Android platform 7.1.2). The researcher carried the mobile station eight times across a 5.6 km road at Fuzhou University in China and collected data each second. Finally, 4525 records are collected, and each record consists of 59 RSSIs from base stations in a long-term evolution network, 582 RSSIs from Wi-Fi APs, and a set of longitude and latitude coordinates from GPS. Among them, 2263 records are selected as the training set and the others are regarded as the testing set. For cellular network-based methods or Wi-Fi network-based methods, only cellular network signals and GPS data or Wi-Fi network signals and GPS data are utilized to estimate the locations of the mobile device. For heterogeneous network-based method, two types of network signals and GPS data are utilized for the experiments. Among them, the availability of cellular network signals is 100%, while for Wi-Fi signals, the availability is 96% because some road segments are not covered by Wi-Fi signals.

For evaluating the effectiveness of the proposed method, other deep learning models (e.g., NN, RNN, LSTM, Triple RNN, Triple LSTM, Triple GRU, and Ensemble method) are regarded as comparative models. Among them, Triple RNN denotes an ensemble model, which integrates three RNNs by a weighted average method, so do Triple LSTM and Triple GRU. Moreover, the ensemble model consists of RNN, LSTM, and GRU. Both the proposed method and comparative methods are trained on Keras framework with TensorFlow backend, and the trained models are employed in the real scene to estimate the location. Keras is an advanced neural

```

(1) Require: loss function  $J(W,b)$ , initial parameter  $W, b$ 
(2) Normalize the features of input: equation (5)
(3) While  $J$  not converged Do
(4)   Select  $k$  samples from the training set randomly
(5)   For each sample Do
(6)     Input layer: equation (6)
(7)     Hidden layer: equations (7)–(12)
(8)     Output layer: equation (13)
(9)     Compute the loss function: equation (14)
(10)  End For
(11)  Compute the gradients of weights
(12)  Update the weights
(13) End While
(14) Return  $W, b$ 

```

ALGORITHM 1: Training of GRU.

network API written in Python. It can run with TensorFlow, CNTK, or Theano as the backend. Keras’s development focus is to support fast experiments, which can convert your ideas into experimental results with minimal delay. The distance between observed coordinates and estimated coordinates is utilized as evaluation index, whose unit is meter, and the formula is expressed as follows:

$$\text{error}_i = R * \arccos[\cos(\hat{y}^{(i)}) * \arccos(y^{(i)}) * \cos(\hat{x}^{(i)} - x^{(i)}) + \sin(\hat{y}^{(i)}) * \sin(y^{(i)})], \quad (15)$$

where R is the radius of the Earth. For the sake of fairness, the study sets the same training parameters as shown in Table 1.

4.2. Discussion

4.2.1. Memory Length Comparison. This section presents a detailed research of selecting appropriate memory for RNN, LSTM, and GRU with RSSIs from different networks (i.e., cellular network, Wi-Fi network, and heterogeneous network) as shown in Table 2. Remarkably, when RSSIs consist of only cellular network, the positioning performance of RNN, LSTM, and GRU improves with the increase of memory length, and the errors are far greater than that of Wi-Fi network and heterogeneous network. In addition, the positioning error can reach the level of 5 to 7 m with the memory length increased when the RSSIs contain Wi-Fi network signals. Among them, the proposed method obtains minimum positioning error (5.58 m) while memory length is 2 s.

4.2.2. Model Comparison. Table 3 presents the experimental results of each deep learning technique with RSSIs from different networks when the memory length is equal to 2 s. Clearly, when the network signals are heterogeneous, the GRU model obtains superior performance compared with NN, RNN, LSTM, Triple RNN, Triple LSTM, Triple GRU, and the Ensemble model. When the RSSIs consist of only

TABLE 1: Training parameters.

Parameters	Value
Memory length	2
Number of hidden layers	1
Number of neurons of hidden layer	30
Optimizer	Adam
Learning rate	0.001
Decay rates	0.9, 0.999
Training epoch	20000
Batch size	5
Loss function	Quadratic loss

cellular network signals, the Triple LSTM model obtains the best performance. Moreover, the Ensemble model has superior positioning error than other models when the RSSIs consist of only Wi-Fi network signals. In the experimental results, GRU with RSSIs from heterogeneous networks obtains the average error of 5.86 m and 75% of errors within 4 m, which is better than other methods. Therefore, the proposed method is selected as the positioning model of the proposed positioning system for further research.

4.2.3. Optimizer Comparison. This section presents a detailed study of optimizer comparison among Stochastic Gradient Descent (SGD), Adaptive Moment Estimation (Adam), and Nesterov-Accelerated Adaptive Moment Estimation (Nadam) [24, 25] for GRU with RSSIs from different network signals, and the experimental results are shown in Table 4. The learning rates of these optimizers are set to default values. Generally, GRU optimized by Adam obtains lower positioning errors than that of others when the compositions of the RSSIs are only Wi-Fi network or heterogeneous (i.e., Wi-Fi: 6.28 m and Cell + Wi-Fi: 5.86 m), and 5.86 m is the best performance of all. In addition, Nadam obtains the lowest errors if RSSIs are made up of only cellular network (i.e., 12.96 m). Among these optimizers, SGD gets the worst performance in the experiments. Therefore, Adam is selected as the optimizer in this paper.

TABLE 2: Positioning error comparison of deep learning techniques with different memory lengths and RSSIs from different networks.

Memory length (s)	RNN			LSTM			GRU		
	Cell	Wi-Fi	Cell + Wi-Fi	Cell	Wi-Fi	Cell + Wi-Fi	Cell	Wi-Fi	Cell + Wi-Fi
1	12.43	8.00	7.63	11.42	7.23	9.06	11.18	7.10	7.16
2	14.16	7.16	9.43	15.00	7.85	10.22	13.59	6.28	5.86
3	24.66	9.75	10.89	24.61	9.69	12.98	20.00	9.14	7.12
5	13.13	7.16	7.36	11.55	7.14	7.30	11.24	7.18	7.08
10	11.76	7.48	7.76	6.88	7.18	7.28	10.01	6.78	7.06
15	11.68	6.77	7.73	6.74	6.76	6.80	6.86	6.73	6.74

TABLE 3: Positioning error of deep learning techniques with RSSIs from different networks when memory length is equal to 2 s.

Network	RNN	LSTM	GRU	Triple RNN	Triple LSTM	Triple GRU	Ensemble
Cell	14.16	15.00	13.59	14.36	14.52	12.36	12.69
Wi-Fi	7.16	7.85	6.49	7.09	6.90	7.73	6.04
Cell + Wi-Fi	9.43	10.22	5.85	8.41	7.46	7.61	6.93

TABLE 4: Performance comparison of SGD and Adam optimizing GRU with RSSIs from different networks.

Network	Cell			Wi-Fi			Cell + Wi-Fi		
	SGD	ADAM	Nadam	SGD	ADAM	Nadam	SGD	ADAM	Nadam
Error (m)	22.54	13.59	12.96	9.67	6.28	6.91	9.28	5.86	6.44

TABLE 5: Positioning error comparison of activation functions with RSSIs from different networks.

Network	Cell			Wi-Fi			Cell + Wi-Fi		
	Relu	Sigmoid	tanh	Relu	Sigmoid	tanh	Relu	Sigmoid	tanh
Error (m)	12.78	13.59	11.93	8.71	6.28	7.23	7.54	5.86	6.51

4.2.4. *Activation Function Comparison.* For selecting the appropriate activation function to transfer information between layers, this paper compares the performance of three activation functions, and Table 5 shows the experimental results of activation function comparison among relu, sigmoid, and tanh for GRU with RSSI from different networks. Clearly, sigmoid obtains superior performance compared with relu and tanh when RSSIs are collected through Wi-Fi network and heterogeneous network (i.e., Wi-Fi: 6.28 m and heterogeneous: 5.86 m). 5.86 m is the best positioning result of all, and sigmoid is selected as the activation function.

5. Conclusions

LBSs based on network positioning method adopting machine learning techniques estimate the locations of mobile devices by RSSIs from networks. For positioning method based on the cellular network, it can provide location estimation where there exist base stations. However, larger errors will be obtained when considering only cellular network signals. Compared with this method, the positioning method based on Wi-Fi network has lower location errors, but it can be employed where Wi-Fi signals can be accessed. In addition, due to the highly temporal dependence of RSSI series data, this paper proposed a mobile positioning system based on GRU with RSSIs from the heterogeneous network. Mobile devices detect and collect GPS coordinates and RSSIs from both cellular network and Wi-Fi network for the training of

the GRU model. A large number of real experiments have been carried out to verify the performance of the proposed method, and experimental results demonstrate that the proposed method has lower errors (i.e., 5.86 m and 75% of errors within 4 m) compared with NN, RNN, and LSTM. Furthermore, important parameters including optimizer, activation function, and memory length of the proposed model have been discussed in detail.

This paper takes all RSSIs of cellular network and Wi-Fi network into account, which not only costs a lot of computing power but also easily leads to overfitting. In the future, feature selection based on knowledge engineering [26] can be applied in RSSIs to reduce training costs and improve location performance. Furthermore, distributed computing [27] and cloud computing [28] can be applied to improve the effectiveness of the mobile positioning method. For optimization, more optimization methods [29] can be considered and adopted to reduce the errors of estimated locations.

Data Availability

The data used to support the findings of this study are available from the corresponding author upon request.

Conflicts of Interest

The authors declare that they have no conflicts of interest.

Acknowledgments

This study was partially supported by the National Natural Science Foundation of China (no. 62002063), Fujian Natural Science Funds (no. 2020J05112), Funds of Science and Technology Department of Fujian Province (no. 650634/JAT190026), and Fuzhou University (no. 510872/GXRC-20016).

References

- [1] C. H. Chen, B. Y. Lin, C. H. Lin, Y. S. Liu, and C. C. Lo, "A green positioning algorithm for campus guidance system," *International Journal of Mobile Communications*, vol. 10, no. 2, pp. 119–131, 2012.
- [2] C. Wu, Z. Yang, Y. Xu, Y. Zhao, and Y. Liu, "Human mobility enhances global positioning accuracy for mobile phone localization," *IEEE Transactions on Parallel and Distributed Systems*, vol. 26, no. 1, pp. 131–141, 2014.
- [3] E. Goldoni, L. Prando, A. Vizziello, P. Savazzi, and P. Gamba, "Experimental data set analysis of RSSI-based indoor and outdoor localization in Lora networks," *Internet Technology Letters*, vol. 2, no. 1, p. e75, 2019.
- [4] R. Liu, J. Zhang, S. Chen, and C. Arth, "Towards slam-based outdoor localization using poor GPS and 2.5 d building models," in *Proceedings of the 2019 IEEE International Symposium on Mixed and Augmented Reality*, pp. 1–7, IEEE, Beijing, China, October 2019.
- [5] K. Cho, B. Van Merriënboer, C. Gulcehre et al., "Learning phrase representations using RNN encoder-decoder for statistical machine translation," 2014, <https://arxiv.org/abs/1406.1078>.
- [6] T. Zhang and M. Yi, "The enhancement of wifi fingerprint positioning using convolutional neural networks," in *Proceedings of the 2018 International Conference on Computer-Communication and Network Technology*, Jiangxing, China, 2018.
- [7] K. Chen, C. Wang, Z. Yin, H. Jiang, and G. Tan, "Slide: towards fast and accurate mobile fingerprinting for wi-fi indoor positioning systems," *IEEE Sensors Journal*, vol. 18, no. 3, pp. 1213–1223, 2017.
- [8] C.-H. Chen, J.-H. Lin, T.-S. Kuan, and K.-R. Lo, "A high-efficiency method of mobile positioning based on commercial vehicle operation data," *ISPRS International Journal of Geo-Information*, vol. 5, no. 6, p. 82, 2016.
- [9] E. Mok and B. Cheung, "An improved neural network training algorithm for wi-fi fingerprinting positioning," *ISPRS International Journal of Geo-Information*, vol. 2, no. 3, pp. 854–868, 2013.
- [10] S. Xia, Y. Liu, G. Yuan, M. Zhu, and Z. Wang, "Indoor fingerprint positioning based on wi-fi: an overview," *ISPRS International Journal of Geo-Information*, vol. 6, no. 5, p. 135, 2017.
- [11] M. Lan, Y. Zhang, L. Zhang, and B. Du, "Global context based automatic road segmentation via dilated convolutional neural network," *Information Sciences*, vol. 535, pp. 156–171, 2020.
- [12] M. T. Hoang, B. Yuen, X. Dong, T. Lu, R. Westendorp, and K. Reddy, "Recurrent neural networks for accurate RSSI indoor localization," *IEEE Internet of Things Journal*, vol. 6, no. 6, pp. 10639–10651, 2019.
- [13] X. M. Yu, H. Q. Wang, and J. Q. Wu, "A method of fingerprint indoor localization based on received signal strength difference by using compressive sensing," *EURASIP Journal on Wireless Communications and Networking*, vol. 2020, no. 1, p. 72, 2020.
- [14] L. Zheng, B.-J. Hu, J. Qiu, and M. Cui, "A deep-learning-based self-calibration time-reversal fingerprinting localization approach on wi-fi platform," *IEEE Internet of Things Journal*, vol. 7, no. 8, pp. 7072–7083, 2020.
- [15] T. Koike-Akino, P. Wang, M. Pajovic, H. Sun, and P. V. Orlik, "Fingerprinting-based indoor localization with commercial mmwave wifi: a deep learning approach," *IEEE Access*, vol. 8, pp. 84879–84892, 2020.
- [16] L. Wu, C.-H. Chen, and Q. Zhang, "A mobile positioning method based on deep learning techniques," *Electronics*, vol. 8, no. 1, p. 59, 2019.
- [17] B. Wang, X. Gan, X. Liu et al., "A novel weighted KNN algorithm based on RSS similarity and position distance for wi-fi fingerprint positioning," *IEEE Access*, vol. 8, pp. 30591–30602, 2020.
- [18] H. Dai, W. H. Ying, and J. Xu, "Multi-layer neural network for received signal strength-based indoor localisation," *IET Communications*, vol. 10, no. 6, pp. 717–723, 2016.
- [19] X. Shi, J. Guo, and Z. Fei, "Wlan fingerprint localization with stable access point selection and deep LSTM," in *Proceedings of the 2020 IEEE 8th International Conference on Information, Communication and Networks*, pp. 56–62, Xi'an, China, August 2020.
- [20] S. Bai, M. Yan, Q. Wan et al., "DL-RNN: An Accurate Indoor Localization Method via Double RNNs," *IEEE Sensors Journal*, vol. 20, no. 1, pp. 286–295, 2020.
- [21] S. Hochreiter and J. Schmidhuber, "Long short-term memory," *Neural Computation*, vol. 9, no. 8, pp. 1735–1780, 1997.
- [22] T. N. Sainath, O. Vinyals, A. Senior, and H. Sak, "Convolutional, long short-term memory, fully connected deep neural networks," in *Proceedings of the 2015 IEEE International Conference on Acoustics, Speech and Signal Processing*, pp. 4580–4584, South Brisbane, Australia, April 2015.
- [23] R. Dey and F. M. Salemt, "Gate-variants of gated recurrent unit (GRU) neural networks," in *Proceedings of the IEEE International Midwest Symposium on Circuits & Systems*, pp. 1597–1600, Dallas, TX, USA, August 2017.
- [24] L. Lyu, J. Yu, K. Nandakumar et al., "Towards fair and privacy-preserving federated deep models," *IEEE Transactions on Parallel and Distributed Systems*, vol. 31, no. 11, pp. 2524–2541, 2020.
- [25] L. Lyu, J. C. Bezdek, X. He, and J. Jin, "Fog-embedded deep learning for the internet of things," *IEEE Transactions on Industrial Informatics*, vol. 15, no. 7, pp. 4206–4215, 2019.
- [26] X. Xue, "A compact firefly algorithm for matching biomedical ontologies," *Knowledge and Information Systems*, vol. 62, no. 7, pp. 2855–2871, 2020.
- [27] H. Chen, H. Jin, and S. Wu, "Minimizing inter-server communications by exploiting self-similarity in online social networks," *IEEE Transactions on Parallel and Distributed Systems*, vol. 27, no. 4, pp. 1116–1130, 2016.
- [28] H. Y. Kung, T. H. Kuo, C. H. Chen, and Y. L. Hsu, "Two-stage cloud service optimisation model for cloud service middle-ware platform," *The Journal of Engineering*, vol. 2018, no. 3, pp. 155–161, 2018.
- [29] P. Hu, J. S. Pan, and S. C. Chu, "Improved binary grey wolf optimizer and its application for feature selection," *Knowledge-Based Systems*, vol. 195, no. 11, Article ID 105746, 2020.

Research Article

Research on the Application of Multimedia Elements in Visual Communication Art under the Internet Background

Wenli Liu 

Jiaozuo University, Jiaozuo 45400, China

Correspondence should be addressed to Wenli Liu; liuwenli@jzu.edu.cn

Received 27 January 2021; Revised 17 March 2021; Accepted 27 March 2021; Published 8 April 2021

Academic Editor: Hsu-Yang Kung

Copyright © 2021 Wenli Liu. This is an open access article distributed under the Creative Commons Attribution License, which permits unrestricted use, distribution, and reproduction in any medium, provided the original work is properly cited.

With the rapid development of Internet technology, the dissemination of information is undergoing rapid changes. The Internet has become an indispensable part of people's study, work, and life. In the context of the Internet, this paper analyzes the application of multimedia elements in visual communication art design, elaborates the basic concepts, visual features, and design principles of the visual communication art design, and analyzes the multifaceted aspects of multimedia elements. This paper discusses the basic methods and general rules of the application of multimedia elements in visual communication art design under the background of the Internet, as well as the research on the emotional factors and interactions of multimedia elements on people. Brain-like computing is the meaning of imitation brain. First is the structure, then the function, then from the structure design and analysis of the brain, and finally use the brain's thinking ability to solve problems. It summarizes the text, graphic images, and colors in the Internet background. The innovative application of multimedia elements such as page layout and animation in visual communication art design explains the influence of multimedia elements on the overall visual effect in visual communication art design. It explores how visual information can be conveyed more reasonably and effectively. In the context of the Internet, the application of multimedia elements has brought a new possibility for developing visual communication art design, providing a new platform for the traditional visual communication art design.

1. Introduction

Nowadays, with the rapid development of Internet technology, online media has become an emerging medium that genuinely integrates into our lives [1]. Compared with other traditional media, network media has its characteristics in technology and communication [2]. On the platform of this new information transmission supported by network technology, the visual communication design will have a new visual communication design expression suitable for it. In 1994, with the help of Michael Detrusors of the MIT (Massachusetts Institute of Technology) Computer Laboratory, Berners-Lee founded the World Wide Web (WWW), which laid the foundation for technical standards and development research for the development of web pages [3]. The brain-like computing system mainly simulates the human brain's calculation function, analyzes and processes various data, obtains the best processing model through long-term training, and can do brain

stimulation, understand brain mechanisms, treat brain diseases, etc. The rapid development of the Internet in the 1990s promoted the Internet's rapid evolution [4]. Braun proposed the cropping and composition features of the changed image and obtained the image's relevant information by using the image algorithm to extract the information quickly [5]. Paiva et al. proposed a memory-guided probability saliency model based on video data sets. This model memorizes changed video images, then extracts information in the background, and then conducts information fusion analysis to obtain relevant image information [6]. The Internet network architecture provided a technical platform for the development of web pages. The emergence and development of web pages also drove the modern information industry's growth and realized the Internet as a society [7]. Development goals are an essential part of the economy and life.

A web page is the basic information publishing logic unit in the World Wide Web. This publishing method displays

multimedia elements such as text, pictures, sound effects, and animations, which are the main elements of information exchange through the terminal screen, giving people convenient access to information and communication [8]. In terms of physical properties, web pages are computer-based information carriers and a collection of thousands of networks worldwide [9]. From its social role, people will naturally regard the network as the fourth media after newspapers, radio, and television. It is not only another new media, but an information exchange, information integration, and resource return [10]. With a diversified platform for class and processing, people's wisdom and ideals are displayed on the maximum opportunity platform.

This paper takes website visual art design as the starting point. Firstly, it studies and discusses the five basic multimedia elements that constitute the visual art of web interface and summarizes the general rules of web interface visual design based on five basic elements [11]. The web page sample outlines the visual styles of different types of web page interfaces, analyzes the application of multimedia elements in visual communication art design under the background of the Internet, and summarizes the development trend of the visual communication art design contemporary web page interface [12].

The specific contributions of this paper include the following:

- (1) The application of multimedia elements in visual communication art design is analyzed
- (2) This paper expounds on the basic concept, visual characteristics, and design principles of the visual communication art design
- (3) The principle of brain-like computing is introduced
- (4) The influence of multimedia elements on the overall visual effect in visual communication art design is explained

The rest of this paper is organized as follows. Section 2 discusses related work, followed by color elements in the web interface in Section 3. Color elements in the web interface are discussed in Section 4. Section 5 concludes the paper with a summary and future research directions.

2. Related Work

The essence of visual communication art design is the transmission of information. Graphics, text, image, and color are the carriers of information. Every change in the way of information transmission will have an impact on visual communication design. With the changes in the media environment, the media vocabulary will also follow [13]. The increases in the visual communication design process have a very close relationship with the media. It can be said that the media change has promoted the development of the design. The changes in media and the evolution of visual communication design are shown in Table 1 [14].

Before we can visually design the web interface, we must first understand the factors that need to be paid attention to in the web interface's visual design [15]. The visual design of

the web interface has its characteristics. Unlike traditional media, the web interface includes new multimedia elements such as sound, video, and animation except for text, images, and colors, and various interactions realized by programming in code language. The effect of the web interface increases the vividness and complexity of the web interface and also makes the web designer need to consider the arrangement and optimization of more page elements [16]. This chapter will explore the five basic multimedia elements of the text like graphics, color, dynamic effects, and composition and layout of the web interface visual design to find a specific law. It can be understood as a general term for various media such as text, graphics, images, animation, sound, and videos that directly affect human senses, that is, the expression and transmission of various information carriers [17].

2.1. Elements and Characteristics of Multimedia Elements

- (1) Text is a form of information expressed by words and various special symbols. It is the most used information storage and transmission method in real life. Conveying information in the text gives people a rich imagination. It is mainly used for the descriptive representation of knowledge, such as expounding concepts, definitions, principles, and problems and displaying titles, menus, and so on [18].
- (2) Image is one of the most important forms of information representation in multimedia software. It is a critical factor in determining the visual effect of multimedia software.
- (3) Animation uses human visual persistence characteristics to quickly play a series of graphic images of continuous motion changes, including special effects such as zooming, rotating, transforming, fade-in, and fade-out. Animation can visualize abstract content, making many incomprehensible teaching contents vivid and exciting. Reasonable use of animation can achieve twice the result with half the effort.
- (4) Sound is one of the most convenient and familiar ways people use to convey information and exchange feelings. In the multimedia courseware, according to its expression, the sound can be divided into three categories: explanation, music, and effect.
- (5) Video images have time series and rich information connotations, which are often used to explain the development of things. The video is very similar to the movies and TVs we are familiar with, and it plays an essential role in multimedia.

Because communication media is different from traditional media, its design focusing on multimedia visual communication design has also changed. It is mainly reflected in the new artistic expressions displayed by information design and interactive design. Knowledge can be expressed in the information, and information is defined in data. This is the causal relationship among data,

TABLE 1: Media transformation and visual communication design evolution.

Information revolution	Information media	Visual communication design development
The first information revolution	Language communication	Decorative paintings
The second information revolution	Text communication	Text, books
The third information revolution	Print communication	The rise of modern design
The fourth information revolution	Analog electronic propagation	Film and television advertising design
The fifth information revolution	Digital information dissemination	Multimedia, web page, interactive advertising

information, and knowledge (see Figure 1). The information conversion process is shown in Figure 1.

Good information organization is the foundation of visual communication success. In the network-based multimedia visual communication design, visual communication's success depends not only on the information related to every single page but on the information relationship between each page. Therefore, the visual communication design information organization in the network is richer and more complex, and the art form has the characteristics of multiple integrations and logical gradual progress. Figure 1 clearly shows the design and transformation process of information [19].

2.2. Text Elements in the Web Interface. Text is the essential carrier of Internet information, so the text's design plays a pivotal role in the web page. In addition to transmitting information, the text displays the website's content, enhances the visual communication effect, increases the appeal of the web page, and enhances the aesthetic value of the web page [20]. The quality of the text directly affects the quality of the entire page. Handling the relationship of the text is a problem that the designer should pay special attention to in the web page's visual communication design. The visual characteristics of web page text include the following:

- (1) *Uniqueness.* The recognizability of the font is reflected in the unique style and strong personality impression. Create fonts of different personalities based on differences in information management concepts, cultural backgrounds, and industry characteristics.
- (2) *Readability.* The font should convey clear information, and the content is brief and easy to read. This is in line with the speed of modern information, which has the instant effect of visual communication [21].
- (3) *Modeling.* Whether the font design is successful or not, the modeling factor is the decisive condition. Under the premise of observing the principles and rules of styling, innovation, intimacy, and beauty are pursued. The font conveys the personality characteristics of the information through its morphological characteristics and strives to achieve the beauty of the communication, create a beautiful image, and improve communication efficiency.

2.3. Dynamic Effects in the Web Interface. Web design based on static text and images uses Gif animation to express a part of the line-of-sight effect. A variety of interactive techniques

based on Flash-based motion animation (Motion) to induce user response have been produced. The dynamic effect (Dynamic Effect) gradually appeared. The form of motion animation is the design of time and space, which is beyond the static scope [22]. However, in the digital environment based on computers and networks, the new media has two-way interactive features that greatly support the new environment's interaction. Dynamic effects can be divided into three types according to different interaction representation methods: interactive navigation, storytelling, and user interaction created by scripts.

Story narrative design is not only a simple performance effect but a way of designing ideas, which needs to have a plotting ability. Storytelling design also requires designers to have capabilities of narrative style and creative ideas that convey the theme. For example, Hillman Curtis, the first-generation leader in motion graphics design, used motion graphics to create illustrations of illustrator Craig Frazier. These illustrations express lyrical themes through peaceful and gentle storytelling, as shown in Figure 2.

2.4. Graphic Elements in the Web Interface. Although graphics creation has a certain degree of independence, once placed on a page, the meaning of graphics programming is to find a suitable visual relationship between graphics and other graphics and other page elements [23].

- (1) *Processing of Graphics.* The image processing includes the modification and improvement of the color, structure, and size of the image. For the layout design, the meaning of image processing is to uniformly edit the proportional relationship of the images in the layout surface, to highlight the image body at the center of the vision, and to coordinate the style between the image and other orchestration elements.
- (2) *Combination of Graphics.* The combined relationship of images mainly includes juxtaposition, primary and secondary relations, and prosody relations. The parallel connection refers to the combination of the same information level and visual form image in the layout; the primary and secondary relationship refers to the image combination with different information levels and visual forms in the layout; the prosody relationship refers to the overlap formed by the images according to certain visual laws, spiral, launch, and gradient combinations. In the page of multiple image combinations, the analysis of image information level and visual meaning is beneficial to

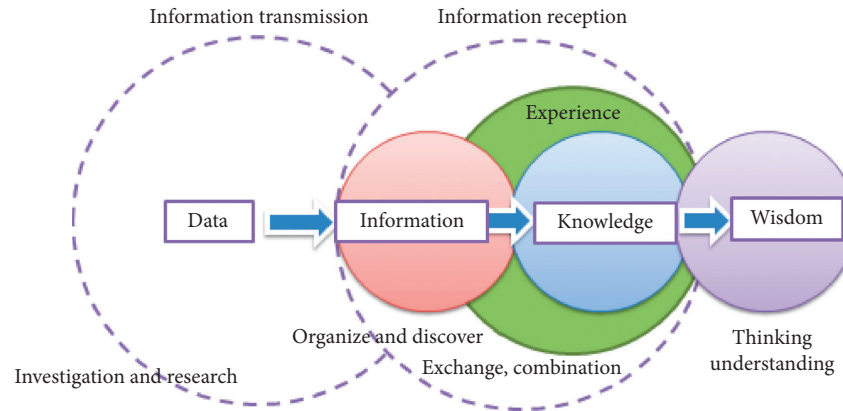


FIGURE 1: Information conversion process.

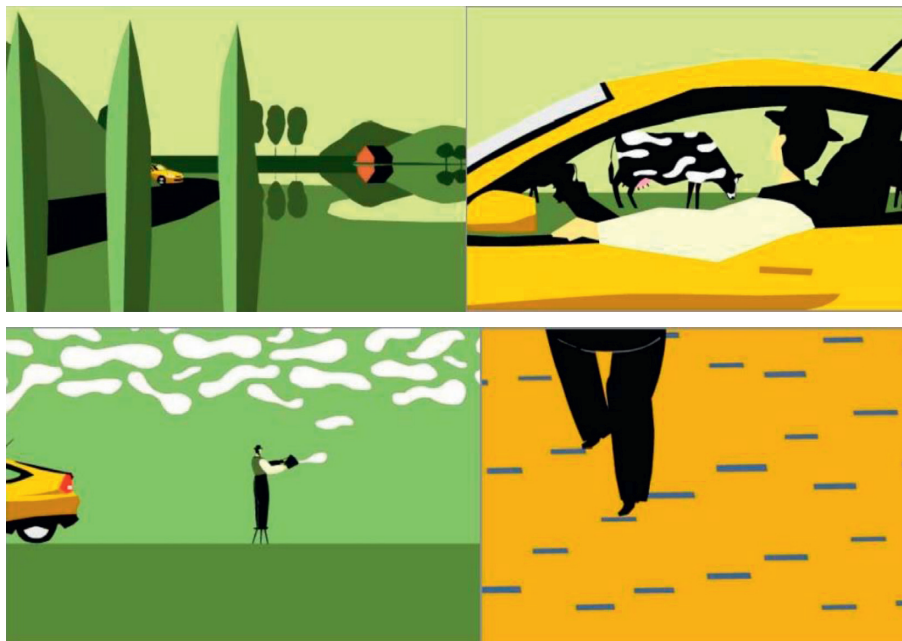


FIGURE 2: Website by Hillman Curtis.

find the internal relationship between images. The combination relationship between such images often determines the overall structure of the page [24].

- (3) *The Composition of the Graphics*. Whether it is photographic images or creative graphics, the graphic always has the visual structure formed by the creator's subjective consciousness. For the layout page, the graphic composition itself is an important factor affecting the overall layout. The graphic composition with obvious structural style and directionality is an important reminder of the layout structure. With this feature, graphics and other elements in the page can be formed. The overall and organic connection between them creates the integrity and interest of the layout vision [25].

The motion graphic display design content can make up for the lack of two-dimensional performance in visual communication design, but for designers, there is a greater challenge.

3. Color Elements in the Web Interface

In the context of the new media era, digital technology and high-speed mobile information dissemination have changed our traditional visual communication methods. The expansion of new media to convey visual symbols is even more exciting. Due to the fast speed of information, the dissemination of new media is not affected by regions. The symbolic semantics of different cultural backgrounds will interact. The visual language nature of the image is more penetrating, with clearer visual semantics and symbolism.

The mobile information system is a relatively mature technology. Based on a comprehensive communication platform composed of modern mobile communication technology and mobile Internet technology, it realizes management services and application analysis through the interactive communication of information on multiple platforms such as handheld terminals, servers, and personal computers—terminal design. The interface design of mobile

terminals has developed rapidly. From the earliest pure text and symbol design to the brilliant IOS and Android systems, the three major design elements of color, text, and graphics have been successfully integrated, which has not only changed people's terminals [26]. Usage habits have also changed the development direction of the terminal. This article discusses the visual design of mobile terminals and, at the same time, puts forward a new point of view on the future interface visual communication design, namely, dynamic, intelligent window design. This visual communication method can play a good role in image analysis and visual analysis—the practical effect [27].

3.1. The Role of Color in Web Design. The direct psychological effect of color comes from the direct influence of physical light stimulation of color on human physiology. Psychologists have done many experiments on this. They found that, in an environment with red color, people's pulse will speed up, their blood pressure will rise, and their emotions will be excited. In an environment with blue color, the pulse will slow down, and the mood will be quieter. Some scientists have found that color can affect brain waves; brain waves are alert to red and relaxed to blue. Since the middle of the 19th century, psychology has moved from philosophy to science, and psychologists have focused on the color psychological effects verified by experiments [28]. The psychological feelings of color give people a sense of warmth, lightness, and melancholy, excitement and calmness, gorgeousness and simplicity, comfort and fatigue, positive and negative feelings, etc. [29].

Traditionally, we know that a color image has a three-dimensional vector $[R, G, B]$, called RGB space, in which both the color and brightness information of the image are included, such as the traditional image enhancement method for color and image transformation. While enhancing the image's brightness, the color information will change, and supersaturation or color distortion will occur if the two pixels in the space are proportional, i.e.,

$$\lambda = \frac{R_1}{R_2} = \frac{G_1}{G_2} = \frac{B_1}{B_2}. \quad (1)$$

The two points of color information in the description space are the same but have different brightness. Taking an $N \times M$ color image $f(x, y)$ as an example, consisting of a single pixel, its brightness value is within $[0, 255]$. The histogram can directly reflect the grayscale brightness information distribution of the image. The closer to the brightness of 255, the higher the area's brightness, otherwise the lower. Therefore, we can separate the three primary colors, R , G , and B , separately calculate the three channels' histogram distribution, and select the maximum value as the brightness gain. Then, formula (1) changes to

$$\lambda = \max \frac{1}{NM} \left\{ \sum_{k=0}^{L-1} f_k^r(x, y), \sum_{k=0}^{L-1} f_k^d(x, y), \sum_{k=0}^{L-1} f_k^b(x, y) \right\}, \quad (2)$$

where $\sum_{k=0}^{L-1} f_k^r(x, y)$ represents the gray histogram of the red channel, $\sum_{k=0}^{L-1} f_k^d(x, y)$ represents the gray histogram of the green channel, and $\sum_{k=0}^{L-1} f_k^b(x, y)$ represents the gray histogram of the blue channel [30].

The obtained λ value is inverted as the primary color coefficient $\lambda' = 255 - \lambda$, and the primary color is mixed with the remaining two-channel values of the original image to obtain a new layer, which is defined as

$$g^i(x, y) = \lambda' f^i(x, y), \quad (3)$$

where i corresponds to the remaining two channels after the original color image is removed from the maximum brightness value channel. According to the above formula, we change the RGB value of the original image pixel, and the obtained new pixel value and the original image pixel value are mixed by formula (4) to obtain the last enhanced image.

$$f(a, b) = 255 - (255 - a) * (255 - b), \quad (4)$$

where a is the original image and b is the new layer obtained after the change. Substituting equations (2) and (3) into (4), the enhanced image is expressed as

$$f(f^i(x, y), g^i(x, y)) = 255 - (255 - f^i(x, y)) * (255 - g^i(x, y)). \quad (5)$$

3.2. Basic Design Principles for Web Page Color. Different colors have different symbolic meanings, giving people different psychological feelings. The color design of the web page should be targeted and should reflect its own characteristics. The web page's color is unique and has its unique style, making the personality stand out and leave a deep impression on the viewer. Visual communication design mainly uses visual media to transmit information. An all-around audio-visual experience is an important form of digital media communication. For the way of digital multimedia is transmitted, visual communication design not only transmits information through vision but also integrates it into multisensory representation. The comprehensive experience of multimedia technology can be unified by editing and processing of graphics, images, text, sound, animation, and other media forms, bringing people a full range of audio-visual effects. A lot of research proved that multisensory memory is better than a single sensory memory, and the memory of the same information if perceived only by visual perception, after some time, will be less than 10%, while multisensory memory is five times that of the former, as shown in Figure 3.

It can be said that digital media communication enriches the communication effect of visual communication design, enabling designers to break through the limitations of paper media in design thinking and open up the creative space of design. The comprehensive sensory application of digital media can enable the audience to participate in information exchange actively. In the activity, it will mobilize all the perceptions of people and realize the blending of emotions and scenery to achieve the effect of efficient and interactive information dissemination.

3.3. Composition and Layout of the Web Interface. The visual characteristics of human beings determine the formation of visual processes. Because of the physiological structure of the human eye's crystal structure, only one focus can be produced, and the line of sight cannot be kept at two or more places at the same time. The existence of many visual elements in a complicated layout makes the organization and scheduling of information difficult. According to the layout information level, reasonable classification and the complex page elements are summarized into several groups of visual level, which is the primary way to form an adequate visual level. So how do we classify page elements? First, we need to understand how humans organize visual aspects. Gestalt psychology explains this phenomenon for us. Gestalt psychology explains how humans organize visual elements as shown in Figure 4.

As shown in Figure 4, first, for proximity, similar objects in spatial locations are referred to as near or close relationships. Gestalt believes that the closer the distance between two visual elements, the easier it is for people to think of them as a whole. Therefore, the closer the page's distance and position in the page, the more overall the visual orientation. Second, for similarity, in the actual layout design, the visual elements are often of various origins, with different visual features, finding the formal laws among these visual elements or creating uniform or similar visual features in different visual elements, which can be effective. Promote the relationship between the layout elements and form the visual whole of the layout. Third, continuity refers to a visual tissue with continuous motion or direction. Gestalt believes that a continuous visual image can direct the line of sight to form a visual whole. In page layout, continuous visual organization, especially continuous patterns with specific patterns, can often connect and closely visualize the layout to establish a specific visual order. Closedness is based on a kind of human temperament—people tend to perceive a part with intrinsic connections as a whole visual image.

4. Application Analysis of Multimedia Elements in Web Design Style Positioning-Taking Shopping Website as an Example

This article uses the Internet to search the required cases and conduct a sample selection of shopping websites. Mainly based on well-known shopping websites at home and abroad, the principle of sample selection is the homepage with diverse visual styles. First, the researcher subjectively selects 100 homepages. Through the five postgraduates with professional backgrounds, a total of 40 eligible shopping catalogs were chosen in a classified manner. Then, through the preliminary test, the cluster sample analysis divides the homepage sample into several clusters and selects 17 representative homepage samples, as shown in Table 2, for subsequent semantic difference analysis experiments.

Exploring the image semantics commonly used by users to describe web pages' style and the relationship between image semantics, firstly refer to the 84 groups of imagery semantics summarized by Zhang Jiancheng, select 50 groups

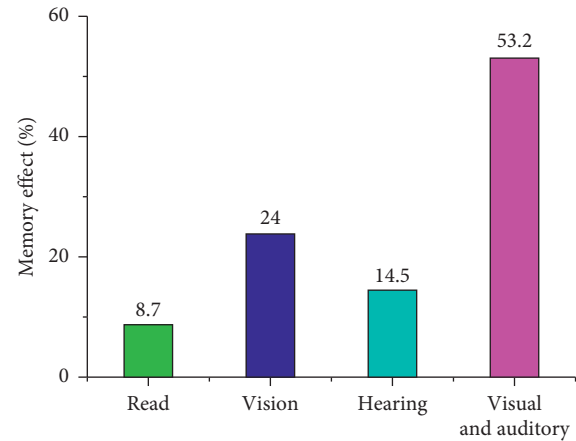


FIGURE 3: Different sensory memory contrast.

of adjectives, and filter out 13 sets of image semantics. Then, the 13 groups of image semantics were initially screened. According to the preliminary questionnaire, the final screening of the shopping website's style was carried out, and the image semantics was reduced to 9 groups, as shown in Table 3.

The homepages of the 17 shopping websites selected were analyzed with the analysis of the researchers and the type attributes defined by the literature. Firstly, the first-page design factor of the shopping website is extracted. A total of seven design factors are removed: page layout, title design, navigation design, promotional image, product display area, web content, and color combination. The next step is to analyze different categories of each design factor. To avoid quantitative I-type analysis's complexity, the shopping site is divided into three types, as shown in Table 4.

In order to verify the effectiveness of the visual analysis method proposed in this paper, this paper defines the technique proposed in the paper as A and then compares with other methods, including method B: multimedia design based on dynamic information model [13]; method C: based on e-learning continuity image analysis model [14]; method D: analysis method based on discriminative visual elements [16]; method E: analysis method based on reactive calculation as a model [20]; method F: based on subjective VoIP quality evaluation model [21]; method G: analysis model based on collision design optimization [23]. Except for method A, the other methods are commonly used visual analysis methods. Finally, the proportions in the image semantics of various methods are obtained through simulation as shown in Figure 5.

From the simulation analysis in Figure 5, it can be seen that each method can obtain image information, but method A is faster than other methods to obtain information, and the image converges faster. It can match the image in visual image analysis.

Taking stability and activity as an example, the design factors that have larger effects are the promotional image (*D*), the color combination (*G*), the product display area (*E*), the button shape (*C*), navigation design (*B*), and page layout (*A*). The influence of design factors is second, and the influence of web content (*F*) design factors is low. The analysis of the remaining experimental results is shown in Table 5.

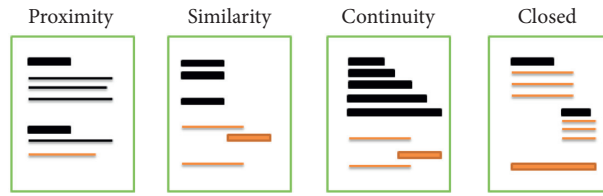


FIGURE 4: Gestalt psychology explains how humans organize visual elements.

TABLE 2: Shopping website homepage sample.

(1) Galante.pl	(2) Taobao	(3) Tootoo	(4) Fugitive toys	(5) Cellyshop	(6) DDB
(7) Macys	(8) Evel	(9) Freeshop	(10) Habitat	(11) Junglecrazy	(12) Habitat
(13) Lallepuesta	(14) Somethingl's	(15) Like	(16) Vondutch	(17) Catwalk	

TABLE 3: Shopping website semantic analysis adjectives.

<i>Exquisite-rough</i>	Rustic-beautiful	Stable-lively	Native-international
<i>Volkswagen-professional</i>	Conflict-reconciled	Classical-popular	Inherited-creative
<i>Concise-rich</i>			

TABLE 4: Shopping website design factor attributes and type coding annotations.

Design factor	Design factor form		
A. Page coding	a1. Up and down menu + right or left menu	a2. Up and down menu + multisegment menu	a3. Other forms of menu
B. Title design	b1. Pure logo	b2. Logo + text	b3. Logo + graphic
C. Navigation design	c1. Graphic + text	c2. Border + text	c3. Plain text
D. Promotional graphics	d1. Single picture	d2. Looping pictures	d3. No
E. Product showcase	e1. Image + text list	e2. Text list only	e3. Video playback window
F. Web content	f1. Single content	f2. Multicell	f3. Single/multiple cells
G. Color combination	g1. Moderate color	g2. Enthusiastic and bright color	g3. Fresh and elegant color

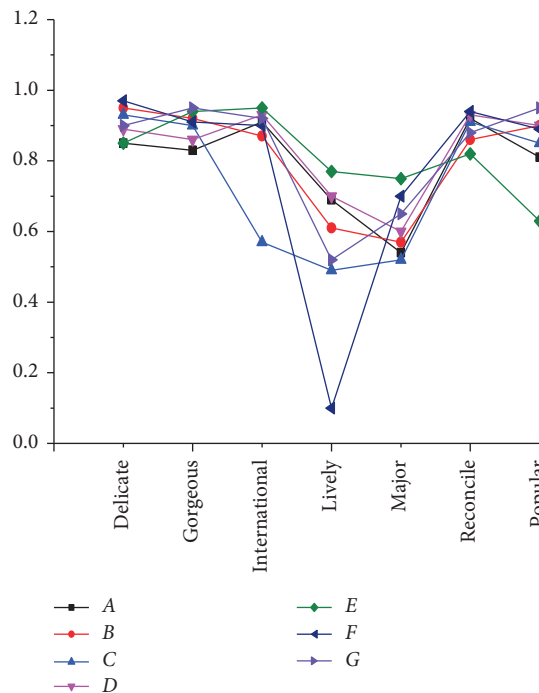


FIGURE 5: The proportion of each design factor in the style intention.

TABLE 5: The proportion of web design attributes in each semantic meaning.

Semantic meaning	Design factor gravity ordering
Exquisite	$A > D > G > E > C > B > F$
Beautiful	$A > G > F > B > C > E > D$
International	$D > G > E > A > F > C > B$
Lively	$D > G > E > C > B > A > F$
Professional	$F > G > A > C > D > E > B$
Reconcile	$G > D > E > C > A > B > F$
Popular	$D > E > C > B > F > A > G$
Creative	$C > D > A > G > F > E > B$
Rich	$G > A > D > E > F > C > B$

TABLE 6: Different design patterns for shopping site style image benefit value.

The value of the design factor form for the intentional value of the style							
	Design factor form	Exquisite	Beautiful	Lively	Professional	Creative	Rich
Page layout	a1	-0.60	-0.52	-0.57	-0.30	0.16	-0.54
	a2	0.22	0.10	0.03	0.42	0.09	0.13
	a3	0.80	0.95	-0.95	-0.50	0.22	0.15
Title design	b1	1.24	0.76	-1.30	-0.35	0.78	-0.66
	b2	-0.12	0.13	0.10	0.17	0.53	0.13
	b3	-0.50	0.70	0.58	0.15	-0.75	-0.02
Navigation design	c1	0.16	0.69	0.70	-0.28	0.02	-0.58
	c2	1.70	-0.87	0.31	-0.20	-0.58	0.1
	c3	-0.50	-0.09	0.53	0.33	-0.70	0.33
Promotional graphics	d1	1.17	0.07	0.30	0.06	0.75	0.76
	d2	-0.16	1.90	0.67	0.17	-0.58	1.33
	d3	-0.19	-0.55	-0.30	-0.40	-0.76	-0.76
Product showcase	e1	-0.65	1.29	-0.10	0.03	-0.78	0.37
	e2	1.40	-0.08	0.40	0.76	0.09	0.12
	e3	-0.62	-1.10	0.55	-0.45	0.28	-0.02
Web content	f1	0.50	-0.44	0.58	-0.45	-0.55	-0.36
	f2	-0.19	0.47	1.33	-0.36	0.98	0.79
	f3	-0.51	-0.41	-0.70	0.38	-0.23	-0.22
Color combination	g1	-0.97	-1.05	-0.79	-0.08	0.85	-0.55
	g2	1.60	2.25	-0.50	0.70	1.79	0.26
	g3	2.10	-0.06	0.73	-0.23	-0.66	-0.23

It can be seen from Table 5 that the proportion of various design factors varies with the style of the web page, which also shows that various design attributes play different roles in a different image of style web pages. Different web design factor patterns have different effects on web page style. Some factor patterns have positive effects, and some factor types have negative effects. Table 6 shows the impact of the shopping site on the design factors for various image semantics. Due to the different proportions of each design factor type, if the sample design factor type is changed, the web page's design style will change. Different design patterns for shopping site style image benefit value is shown in Table 6.

The principal component analysis was performed using the main component analysis method, and the results of the subjects' subjective assessment results were used for principal component analysis. The results are shown in Table 7.

It can be found from Table 7 that the nine descriptive words in the semantic difference analysis method can be reduced to two factors axially. For the theme, the first factor is expressed as "popular, refined, lively, creative, rich, and beautiful," which is mainly used to identify the homepage of the shopping website by the theme, so it is called the "evaluation factor." The second factor is expressed as "professional, international, reconciliation" and so on. This stage's meaning is to describe the image of the shopping website in the entire use and layout process, so it is called "structural factors." In total, the above two main factors can explain 73.75% of the variation in the axial direction.

This chapter takes 17 homepages of shopping websites as an example to select the leading website style of competitive web pages and analyzes its characteristics, components, and image positioning. The main conclusions are as follows:

TABLE 7: Main factors guiding the perception of shopping websites.

Factor guide	Intentional semantics	Factor one	Factor two
Evaluation factor	Exquisite	0.97	0.06
	Lively	0.95	0.18
	Popular	0.90	0.35
	Creative	0.88	0.22
	Rich	0.85	0.35
	Beautiful	0.84	0.11
Structural factor	Professional	0.43	0.88
	International	0.26	0.85
	Reconcile	0.10	0.84
Explain the amount of variation		54.05%	19.70
Cumulative interpretation of variation		54.05%	73.75

- (1) For the image positioning of the shopping website and the user, the shopping websites with prominent attribute characteristics of the structural factor will have a better positioning. The common feature of these websites is that the top of the page uses a high-definition product promotion picture that is looped, which indicates that it is an important indicator of whether there is a looping product promotion picture on the shopping website.
- (2) On the website with leading factors of evaluative factors, the design of the website's product display area has become an advantage in the competition of the website. In the research data, it is found that the image display of the leading group web page product display area of the evaluation factor and the page color matching are two important indicators. Such websites have a large number of rich product display images and colorful web pages, which stimulate people's vision and the desire to buy. However, at the same time, due to the excessive amount of information, users often cause confusion and frustration in the use process, making the time spent on the site reduced, so sites with leading structural factors cannot be a leader in the positioning of evaluative factors.
- (3) The color combination of the website is also an important indicator for the shopping website. In color, the user prefers the website style of the evaluative factor, and the web page based on it uses the enthusiastic and bright color; the color is rich, and the warm color is dominant, but this is actually not suitable for shopping. The color of the website, the website's structural style, the web page based on it are simple in color design, and the color matching is higher, the color is less, fresh, and elegant, and it is a more rational color, with a color scheme that is more suitable for use in shopping websites.

5. Conclusion

The Internet's speed has grown tremendously, and it has been amid many media in just a few decades. As the carrier

of Internet communication information, the web interface must meet people's practical needs and pay attention to the unity and integrity of the situation and content. The visual communication art design is a creative activity that blends technology and art harmoniously. It must not only consider the principle of the first nature of information transmission but also reflect the aesthetic function of the interface and the psychological and accepting forms of information received from the content and form of the page. The innovative use of multimedia elements in web interface design is a new trend in developing web interface design in the future. This paper analyzes the multimedia elements in the web interface, mainly including text, graphic images, colors, animations, and layout relationships. This paper explores various innovative methods for applying multimedia elements in web interface and visual communication art design. It also introduces the principle of web interface functionality and artistic harmony and has helped people further understand it.

Although the findings of this article have achieved stage results, the method lacks a solid theoretical foundation and efficient calculation methods. Therefore, in future work, we will work to make up for some of the theoretical flaws of this method and the efficiency of the algorithm.

Data Availability

The data used to support the findings of this study are available from the corresponding author upon request.

Conflicts of Interest

The authors declare that there are no conflicts of interest regarding the publication of this paper.

References

- [1] Y. W. Hao and Y. Wei, "Expression methods of visual communication design in multimedia design," *Advanced Materials Research*, vol. 811, pp. 293–296, 2013.
- [2] V. Rakocevic, "Congestion control for multimedia applications in the wireless internet," *International Journal of Communication Systems*, vol. 17, no. 7, pp. 723–734, 2004.
- [3] K. Shin, T. Abdelzaher, S. Han, J. Reumann, and E. Abram-Profeta, "Multimedia-friendly server and communication design," *IEEE Multimedia*, vol. 6, no. 2, pp. 84–90, 1999.
- [4] M. Vojnovic, N. Rozic, D. Begusic, J. Ursic, and H. Dujmic, "Multimedia dictionary network application: design and implementation," *IEEE Communications Magazine*, vol. 38, no. 2, pp. 130–137, 2000.
- [5] R. Braun, "Internet protocols for multimedia communications. II. Resource reservation, transport, and application protocols," *IEEE Multimedia*, vol. 4, no. 4, pp. 74–82, 1997.
- [6] M. A. C. Paiva, R. A. Silva, and C. A. Fleury, "Design of a novel architecture signaling network to provide internet multimedia subsystem services through aeronautical passenger communication," *IEEE Latin America Transactions*, vol. 13, no. 7, pp. 2356–2365, 2015.
- [7] C. Bae, J. Seok, and Y. Choe, "Multimedia data processing elements for digital TV and multi-media services in home

- server platform,” *IEEE Transactions on Consumer Electronics*, vol. 49, no. 1, pp. 64–70, 2003.
- [8] X. Xin, A. Nagar, G. Srivastava, Z. Li, F. Fernandes, and A. K. Katsaggelos, “Large visual repository search with hash collision design optimization,” *IEEE Multimedia*, vol. 20, no. 2, pp. 62–71, 2013.
- [9] X. Li, M. Larson, and A. Hanjalic, “Geo-distinctive visual element matching for location estimation of images,” *IEEE Transactions on Multimedia*, vol. 20, no. 5, p. 1, 2017.
- [10] S. Nick, “CHEMnet: analysis of the use of special features and multimedia elements of an online chemistry course,” *Journal of Chemical Education*, vol. 83, no. 83, pp. 1099–1102, 2006.
- [11] N. H. Narayanan and M. Hegarty, “Multimedia design for communication of dynamic information,” *International Journal of Human-Computer Studies*, vol. 57, no. 4, pp. 279–315, 2002.
- [12] B. Stiller, C. Class, M. Waldvogel, G. Caronni, and D. Bauer, “A flexible middleware for multimedia communication: design, implementation, and experience,” *IEEE Journal on Selected Areas in Communications*, vol. 17, no. 9, pp. 1580–1598, 1999.
- [13] M. Park and J. Yoo, “Effects of perceived interactivity of augmented reality on consumer responses: a mental imagery perspective,” *Journal of Retailing and Consumer Services*, vol. 52, Article ID 101912, 2020.
- [14] P. Jones, A. Turney, H. Georgiou, and W. Nielsen, “Assessing multimodal literacies in science: semiotic and practical insights from pre-service teacher education,” *Language and Education*, vol. 34, no. 2, pp. 153–172, 2020.
- [15] M. Aubry, B. C. Russell, and J. Sivic, “Painting-to-3D model alignment via discriminative visual elements,” *ACM Transactions on Graphics*, vol. 33, no. 2, pp. 1–14, 2014.
- [16] S. Sittig, J. Wang, and S. Iyengar, “Incorporating behavioral trigger messages into a mobile health app for chronic disease management: randomized clinical feasibility trial in diabetes,” *JMIR mHealth and uHealth*, vol. 8, no. 3, Article ID e15927, 2020.
- [17] C. Wu, Q. Peng, Y. Xia et al., “Online user allocation in mobile edge computing environments: A decentralized reactive approach,” *Journal of Systems Architecture*, vol. 113, Article ID 101904, 2021.
- [18] Z. Hu, H. Yan, T. Yan, H. Geng, and G. Liu, “Evaluating QoE in VoIP networks with QoS mapping and machine learning algorithms,” *Neurocomputing*, vol. 386, pp. 63–83, 2020.
- [19] J. Wei, X. Yang, and Y. Dong, “User-generated video emotion recognition based on key frames,” *Multimedia Tools and Applications*, vol. 10, pp. 1–19, 2021.
- [20] M. L. Falcidieno, E. Bistagnino, and M. E. Ruggiero, “Interactive actions between project and communication: new ideas for passenger orientation on board,” *International Journal on Interactive Design and Manufacturing (IJIDeM)*, vol. 14, no. 1, pp. 89–101, 2020.
- [21] K. Iigaya, S. Yi, and I. A. Wahle, “Aesthetic preference for art emerges from a weighted integration over hierarchically structured visual features in the brain,” *Neuroscience*, vol. 3, 2020.
- [22] M. Modesto-Mata, M. C. Dean, and R. S. Lacruz, “Short and long period growth markers of enamel formation distinguish European Pleistocene hominins,” *Scientific Reports*, vol. 10, no. 1, pp. 1–12, 2020.
- [23] S. Wu, Z. Cao, and F. Shi, “Investigation of the prognostic role of neutrophil-to-lymphocyte ratio in idiopathic sudden sensorineural hearing loss based on propensity score matching: a retrospective observational study,” *European Archives of Oto-Rhino-Laryngology*, vol. 277, no. 7, pp. 2107–2113, 2020.
- [24] Z. Gomolka, B. Twarog, and E. Zeslawska, “Cognitive investigation on pilot attention during take-offs and landings using flight simulator,” in *Proceedings of the International Conference on Artificial Intelligence and Soft Computing*, pp. 432–443, Springer, Cham, Switzerland, June 2017.
- [25] C.-H. Chen, “An arrival time prediction method for bus system,” *IEEE Internet of Things Journal*, vol. 5, no. 5, pp. 4231–4232, October 2018.
- [26] G. Li, L. Deng, D. Wang et al., “Hierarchical chunking of sequential memory on neuromorphic architecture with reduced synaptic plasticity,” *Frontiers in Computational Neuroscience*, vol. 10, p. 136, 2016.
- [27] B. Zhang, L. P. Shi, and S. Song, “Creating more intelligent robots through brain-inspired computing, special supplement: brain-inspired intelligent robotics: the intersection of robotics and neuroscience sciences,” *Science*, vol. 354, no. 6318, p. 1445, 2016.
- [28] Z. Luo, C. Xiong, X. Zhang, Z.-G. Guo, J. Cai, and X. Zhang, “Extremely large magnetoresistance at low magnetic field by coupling nonlinear transport effect and anomalous hall effect,” *Advanced Materials*, vol. 28, pp. 2760–2764, 2016.
- [29] G. Li, “Temperature based restricted Boltzmann machines,” *Scientific Reports*, vol. 6, p. 19133, 2016.
- [30] Z. Luo, X. Zhang, C. Xiong, and J. Chen, “Silicon-based current-controlled reconfigurable magnetoresistance logic combined with non-volatile memory,” *Advanced Functional Materials*, vol. 25, pp. 158–166, 2015.

Research Article

Research on Business English Translation Framework Based on Speech Recognition and Wireless Communication

Leida Wu¹ and Lianguan Wu ²

¹Cangzhou Medical College, Cangzhou 061001, China

²Beijing Wohaole Technology Co. Ltd., Beijing 100071, China

Correspondence should be addressed to Lianguan Wu; chenhm2015@cumt.edu.cn

Received 26 January 2021; Revised 15 March 2021; Accepted 25 March 2021; Published 8 April 2021

Academic Editor: Hsu-Yang Kung

Copyright © 2021 Leida Wu and Lianguan Wu. This is an open access article distributed under the Creative Commons Attribution License, which permits unrestricted use, distribution, and reproduction in any medium, provided the original work is properly cited.

In order to improve the accuracy of English translation, reduce the error rate of translation results, and increase the correction rate of translation, this paper proposes a business English translation architecture design based on speech recognition and wireless communication. The architecture is partitioned according to the functions of the overall system design, and the voice acquisition module, voice processing module, and peripheral circuit module are designed according to functional requirements. Among them, speech recognition helps users to perform language translation to reduce the possibility of errors in the translation process. At the same time, it uses wireless communication technology to construct a business English translation corpus to meet the personal needs of users. The paper also uses an improved translation model for translation error correction and intelligent proofreading, which improves the reliability of translation results. Experimental results show that the system has a high error correction rate and error correction rate, and the translation results have a certain degree of reliability, which fully verifies the effectiveness and application value of the system.

1. Introduction

As a specialized English, business English contains a rich culture, including business traditions and customs in different countries and business etiquette habits [1]. For the business English translation, national cultural images are often lost or distorted, which may cause people to misunderstand other cultures and lead to transaction failures. Therefore, it is urgent to solve the problem of misplaced business English translation [2, 3]. At present, a number of high-quality dictionary and translation types of software have emerged on the mobile platform, providing complete Chinese-English translation, word query, and other functions, but they are still limited to the traditional text translation field and have not touched the increasing demand urgent voice translation function [4, 5]. Although some foreign translation software provides text-to-speech services, there are few translation tools to provide voice-to-text function, which still cannot fully meet the diversified

translation needs of users [6]. Therefore, it is of great significance to study a multifunctional business English translation tool.

The authors of [7] designed a translation system based on deep learning and proposes a deep learning system for context-aware blind assessment. It is superior to traditional English translation tools in retaining the meaning of the text (translation adequacy), and the fluency of the translation system has been significantly improved. However, the translation results of the system are close to the quality of human translation and even have the problem of low error correction rate to some extent, which cannot effectively obtain the optimal translation results. The authors of [8] presented the results of an empirical study on translation productivity in interactive translation prediction (ITP) with an underlying neural machine translation (MT) system (NITP). The results show that over half of the professional translators in the study translated faster with NITP compared to PE and most preferred it over PE. This paper also

examined differences between PE and ITP in other translation productivity indicators and translators' reactions to the technology. Reference [9] introduced the development from computer-aided translation (CAT) to neural network machine translation (NMT). With the real cases completed by Transn Company, it unveils the characteristics of engineering industry translation and the application of human-computer interaction platform in engineering translation. Furthermore, it is shown that the capacity gathering and adaptation through accurate projections can greatly save time and enhance the ability of translators in the engineering industry. The authors of [10] improved the translation quality of the neural machine translation compression model by using monolingual data and extracted implicit bilingual knowledge from monolingual data, thus improving the translation quality of small and low precision neural machine translation model (student model). This paper proposes a pseudobilingual data teaching method, which improves the student model by using the synthetic bilingual data obtained from the monolingual data translated by the teacher model, and then takes the probability distribution of the target language words obtained by the teacher model as the knowledge, so as to improve the translation quality of the model under the framework of knowledge distillation. The experimental results show that the proposed method improves the generalization performance of the translation model, but there is a problem that the grammar error correction module is not effective.

Aiming at the problems existing in the traditional English translation system, this paper studies and analyzes the rapid development of speech recognition technology and wireless communication technology. Combined with the functional requirements of the system, a language database is built in the system to improve the comprehensiveness of the translation results. The system has certain technical difficulties and innovations. This paper introduces the design and implementation of several core modules, such as the voice acquisition module, voice processing module, and peripheral circuit module, systematically solves the technical difficulties encountered in the development, and then effectively tests the system to demonstrate the feasibility and availability of the system.

The research innovations of this paper mainly include the following aspects:

- (1) This paper proposes a business English translation architecture design based on speech recognition and wireless communication.
- (2) It divides according to the functions of the overall system design and designs voice acquisition modules, voice processing modules, and peripheral circuit modules according to functional requirements.
- (3) At the same time, it uses wireless communication technology to construct a business English translation corpus to meet the personal needs of users.
- (4) Translation error correction and intelligent proof-reading are carried out through an improved

translation model, which improves the reliability of translation results.

The rest of this paper is organized as follows. Section 2 presents the architecture of the business English translation based on speech recognition and wireless communication. Section 3 proposes the strategy to improve the effect of business English translation. Test instances and performance metrics will be given in Section 4. In this section, the experimental results are also presented and analyzed. Finally, Section 5 sums up some conclusions and gives some suggestions as the future research topics.

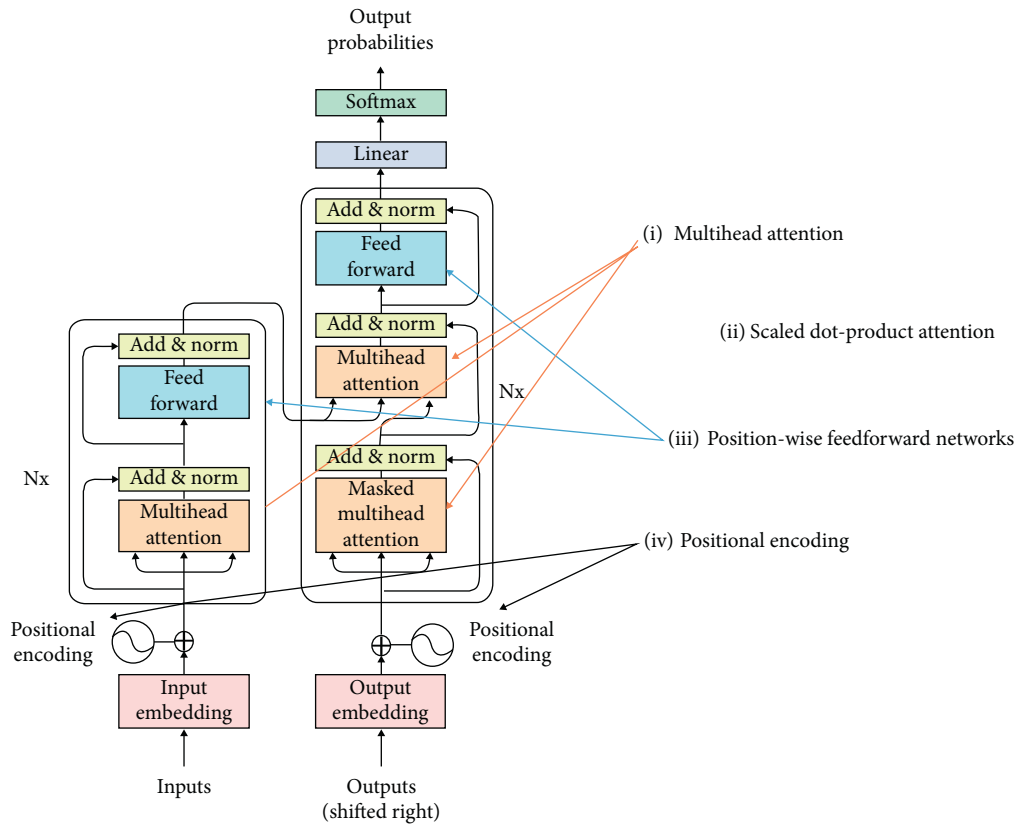
2. Business English Translation Architecture Based on Speech Recognition and Wireless Communication

This chapter introduces in detail the relevant knowledge needed to construct the business English translation framework, designs the overall system architecture and system functions, and elaborates the functions of each module of the system. Finally, it introduces the basic concept of business English translation architecture and the software and hardware architecture, which paves the way for the design and implementation of English translation functions.

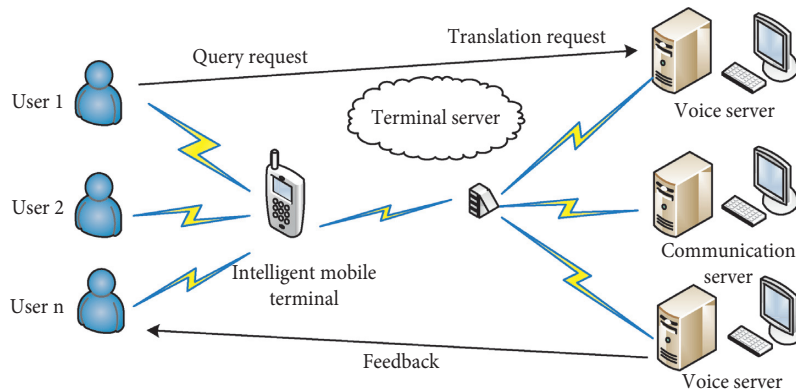
2.1. Overall System Architecture Design. The process of business English translation can be regarded as a process of applying knowledge for reasoning, and knowledge is the basis of this process. The knowledge representation forms used in translation are divided into internal knowledge and external knowledge. Among them, external knowledge is the knowledge stored in the knowledge base and managed by language workers, such as dictionaries and rule bases [11]; internal knowledge is generated temporarily in the process of translation, which is used to describe the grammar and semantic features of translated sentences, such as tree graph, feature structure, and semantic network. The architecture of MT and overall structure of business English translation are shown in Figure 1.

2.2. System Function Design. According to the overall structure of business English translation, the system function is analyzed. The system platform is based on speech recognition technology and wireless communication technology and uses B/S (Browser/Server) structure. Users can complete online real-time division of roles, role identification, collection and analysis of translation resources, testing, discussion, questioning, and submitting exercises and assignments. Users can cooperate through words, sounds, or graphics [12].

In the system platform, the former translation tools provide users with basic word and text translation functions, which are not flexible and comprehensive. Because of the small screen of mobile devices and the trouble of text input, the practicability of these translation tools is limited. With the development of speech recognition technology and wireless communication technology, the network access



(a)



(b)

FIGURE 1: The overall structure of business English translation. (a) Architecture of MT. (b) Structure of business English translation.

ability and accessible services of mobile devices are greatly enhanced. Using some open public translation and voice processing cloud services can add some more practical functions to the translation system [13]. On this basis, the translation system is mainly designed for business negotiation application scenarios. The functional design of the system mainly focuses on the following points:

- (1) To achieve a more rapid and accurate text translation function;
- (2) The basic functions of text translation used to realize more complex functions such as document translation and short message translation;

- (3) Providing voice translation function to improve user experience.

In order to provide special tool services for business negotiation scenarios, the main functions of the existing translation software in the market are examined and improved. Combined with the main functions mentioned above, the system function use case diagram as shown in Figure 2 is obtained.

According to Figure 2, users send requests to the server according to their own needs, such as requests for translation of relevant content or speech recognition translation. Therefore, the business English translation system should

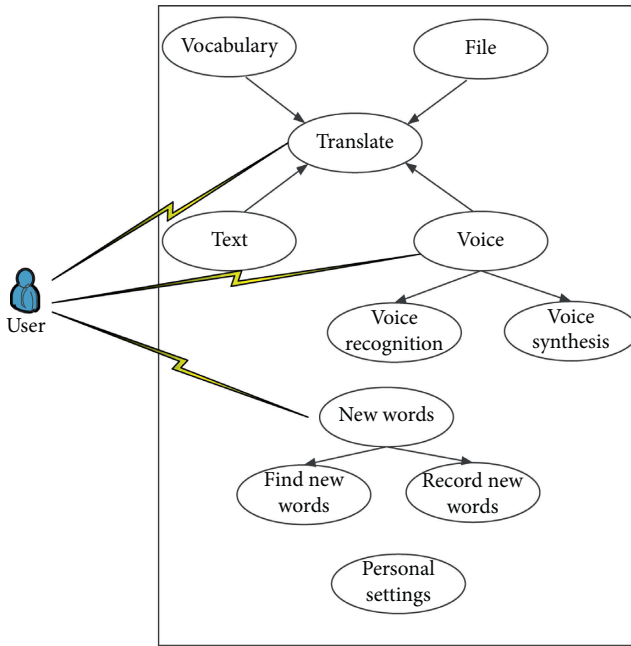


FIGURE 2: System function use case diagram.

contain a variety of translation resources, such as text, graphics and images, sound, video, and animation. When the server receives the request, it will send the relevant information to the user's browser, and users can translate through the browser [14]. If a user wants to discuss a problem with another remote user, he can log in to the discussion module in the system. The system receives the discussion information input by the user and broadcasts it to all users participating in the discussion. After the user discusses the module, other users in the system can be seen.

2.3. System Module Analysis

2.3.1. Voice Acquisition Module. The main function of this module is to realize the acquisition of voice signal and realize signal filtering, endpoint detection, and data normalization. Among them, the voice acquisition module is designed by using WM8731 on the DE2 board. After setting with the I2C bus, it can work in the setting mode to realize the voice acquisition function. The acquisition unit mainly includes a PLL, I2C bus controller, and voice acquisition controller [15]. The system uses voice acquisition module to convert the voice data collected by the voice chip into 16-bit PCM code. The voice data is transmitted to the memory and saved, realizing the setting of 4 s recording time. The user can input 3 isolated words at one time, input the processed data into the subsequent memory address for storage, and store the detected words in the first address.

2.3.2. Voice Processing Module. Speech translation is one of the innovative functions of this system, and its core content is speech processing. Speech processing related to speech translation includes speech recognition and speech synthesis. Speech recognition function refers to the

transformation of user's voice input into text form with the assistance of voice cloud and can ensure high translation accuracy [16]. When the user wants to use the voice translation function, first press the start button to trigger the voice recognition function. After finishing the speech, confirm the end. At this time, the system will transfer the recording file of the user's speech to the voice cloud for analysis and return the specific text after recognition. When users need speech translation, the system can combine the speech processing function with the translation function; that is, the text to be translated is obtained through the speech recognition function, the translated text is obtained through the translation function, and the pronunciation of the translated text is obtained through the speech synthesis function.

Audio interface chip uses codec chip, which has a low price and can support wire control standard. It is the most commonly used full-duplex audio chip in an embedded system. Because of the timeliness of speech signal processing and a large number of recorded and played voice signals, if the voice transmission and reception use the first-in-first-out queue for buffering, according to the terminal, data will be sent to the system. If the cost is high and the sound recording and playing cannot be guaranteed reliably, then the audio recording and playing should be realized by DMA [17]. Using this method to record and play the data can realize the setting of the destination address, data source address, and length and can also automatically send buffer to realize filling. Until the specified length of data is achieved, the system can apply for interruption. Multiple buffers are created through memory to record and play audio data effectively. The controller developed by Samsung company is used in the design of voice processing module. The core structure of the ARM processor is shown in Figure 3.

Generally, the auxiliary functions of the speech processing module are processing, recording, and transmission, but the computer and natural language are quite different. How to accurately recognize the difference between the two languages is a problem that needs to be solved in the recognition process of translation software. Feature extraction is the most basic content of modern speech recognition systems. It can effectively extract features of English language, send accurate language signals to the translator, and improve the accuracy of computer translation work [18]. The speech recognition system requires matching corresponding modules, which can assist the user's language translation and reduce the probability of errors in the translation process.

2.3.3. Peripheral Circuit Module. Flash memory can realize the function of electric erasure in the system, the information will not be lost after power failure, and the capacity is large, so it is widely used in various systems. Nand memory with high performance is used in the integrated controller of the system, the data storage capacity is 64 MB, and the storage management is realized by block page. SDRAM chip has large capacity, low cost, and fast access speed. It is widely used in crisis management system. SDRAM can store variables and codes, which refers to the memory accessed after

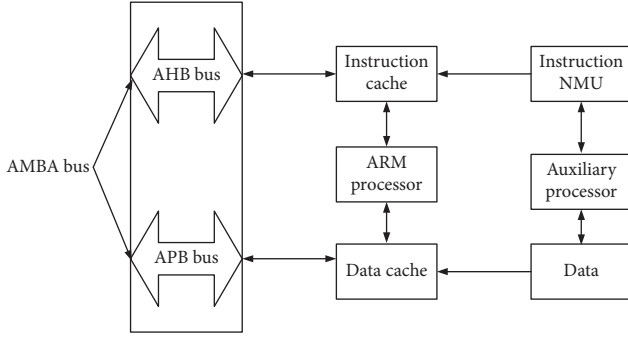


FIGURE 3: Speech processing module ARM processor core structure.

the system is started [19]. Because SDRAM should be able to refresh regularly, so as to ensure the accuracy of stored data, the microprocessor requires the function of refreshing control logic. In this paper, S2C2410 microprocessor chip is used to realize the setting to meet the actual needs of speech recognition system, and Samsung chip is used to create memory system. Figure 4 is the schematic diagram of peripheral circuit module.

3. Improving the Effect of Business English Translation Based on Wireless Communication Technology

In the era of mobile big data, the rapid development of wireless communication technology and mobile Internet has strengthened the carrying capacity of wireless networks and has a wider coverage, which in turn enables people to realize mobile learning anytime, anywhere through mobile communication devices such as mobile phones and tablets. Mobile learning can realize the three-dimensional access between people and people, people and things, and things and things in different scenarios and is more and more popular among young people. This provides a brand new platform for the application of business English translation system design. Based on wireless communication technology, a business English translation corpus is constructed, and the errors in business English translation are corrected in time. In order to further ensure the accuracy of translation results, the translation model is used for intelligent proof-reading of translation results, so as to realize the overall design of business English translation framework based on speech recognition and wireless communication.

3.1. Construction of Business English Corpus Database Based on Cloud Architecture. Through the development of business English major and the goals and requirements of application scenarios, the basic selection principle of corpus can be obtained: “starting from the cultivation of the ability to distinguish and adjust sounds, the training of listening, pronunciation, and oral expression is closely combined, emphasizing the training of basic functions and paying attention to practice” [20]. The construction of business

English multimedia corpus database mainly includes the following aspects:

(1) Basic Knowledge and Content of Phonetic Training

(1) The comprehensive training of English phoneme’s correct pronunciation method, distinguishing ability, and imitation ability is as follows:

$$z_i^k = z_i^{k+1} + v_i^{k+1}, \quad (1)$$

where z_i^k represents the basic knowledge of voice training; z_i^{k+1} represents the pronunciation standard; v_i^{k+1} represents the voice recognition ability [21].

(2) For the teaching and training of the basic laws, expression forms, and ideographic functions of English word stress and sentence stress, the following specific calculation formulas are given:

$$K_{ik} = z_i^k \left(\frac{\tau_n}{d\tau_i} - \frac{\tau_m}{d\tau_i} \right), \quad (2)$$

where τ_n and τ_m represent the more frequently used and less frequently used words in business English translation, respectively; τ_i represents the total amount of English elements in the corpus; d represents the space storage capacity of the corpus.

(3) The rhythm, basic characteristics, basic elements of English language flow, and training of strong and weak reading styles.

(4) The peculiar pronunciation, intonation structure, function of business English, and its use in communication.

(2) Business English Translation Content

Incorporate teaching materials of basic English, reading, listening, and speaking courses into the corpus to create a good environment for the English translation and improve the effect of the English translation [22].

(3) Business English Training Content Based on Network Resources

Construct English multimedia materials, and perform English translation exercises by storing voice training content as different forms of corpus resources and effectively enhancing the real time and effectiveness of obtaining English translation information. Among them, the effective resources in the corpus can be expressed by the following formula:

$$h_{ik} = \frac{h_i - h_n}{h_a} - \frac{h_i - h_m}{h_b}, \quad (3)$$

where h_n represents the correct English translation result; h_m represents the wrong English translation result; h_a represents the effective language element in the corpus; h_b represents the invalid language element in the corpus [23].

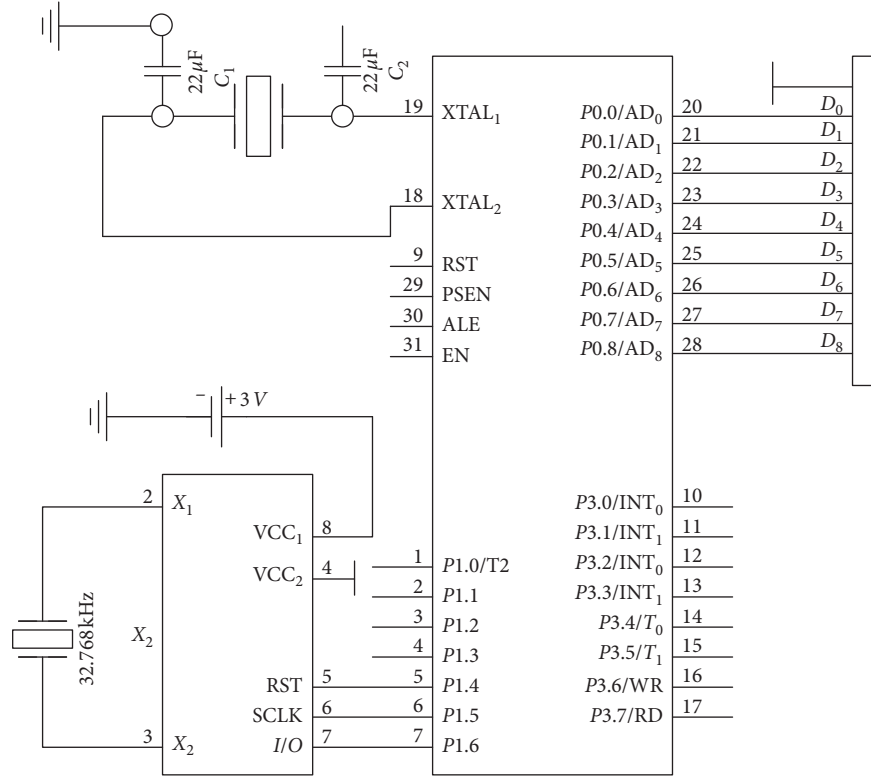


FIGURE 4: Schematic diagram of peripheral circuit module circuit.

- (4) The establishment of personalized business English translation corpus; that is, users can collect English materials that are suitable for their own language level and content and interest to carry out independent translation training. It can meet the users' personal needs and make full use of the corpus.

3.2. Correction of Translation Errors. It is based on a cloud-based business English corpus database, in order to improve the accuracy of business English translation results, improve translation effects, and correct errors in translation.

According to the content to be translated, the semantic similarity estimated by Jiang-Conrath is used to roughly select a part with relatively similar semantics from the database to form a similar set. The Jiang-Conrath method used for semantic similarity is a method based on corpus statistical analysis and WordNet to calculate the semantic similarity between words. The accuracy of this method is close to the upper limit of manual judgment. Assuming that there are two words p and q , the semantic distance $\text{dist}(p, q)$ between them is defined as

$$\text{dist}(p, q) = x_i + \rho_t^I (x_{p_{\max}} - x_{p_{\min}})(x_{q_{\max}} - x_{q_{\min}}). \quad (4)$$

Among them, $x_{p_{\max}}$ and $x_{p_{\min}}$, respectively, represent the words with the largest and smallest similarity features with p ; $x_{q_{\max}}$ and $x_{q_{\min}}$, respectively, represent the words with the largest and smallest similarity features with q ; x_i represents the amount of statistical information in the corpus, and it is calculated by the following formula:

$$x_i = \sum_{i=1}^N w_i \text{dist}(p, q). \quad (5)$$

where N represents the feature similarity coefficient; w_i represents the probability value of the invalid language element in the corpus [24].

The semantic similarity is the inverse of the semantic distance; that is,

$$P(k) = \sum_{i=1}^N [1 - w(k)]^i = \text{dist}_{\min}(p, q) \frac{1}{(1 - (1/L_k))^{k-1}}, \quad (6)$$

where $w(k)$ represents the element set after excluding invalid language elements; L_k represents the corpus difference coefficient.

In the process of judging the similarity of business English corpus, the similarity is defined as the sum of the semantic similarity between words and the semantic similarity between sentences:

$$T_{ab} = pq_N + cv_N, \quad (7)$$

where pq_N represents the semantic similarity between words; cv_N represents the semantic similarity between sentences. Through the similarity measurement results, the invalid language elements are removed to realize the preliminary correction of translation errors [25].

3.3. Intelligent Proofreading Method for Translation Errors Based on Improved Translation Model. As there are a large

number of language elements in the corpus, only the invalid language elements can be eliminated through Section 3.2, which cannot guarantee the accuracy of the translation results. Therefore, the intelligent proofreading method based on the improved phrase translation model is further used to correct the translation errors and realize the accurate output of the translation results. The transformation from one form of text to another is the common ground of English translation and English translation proofreading. Therefore, the process of intelligent proofreading of English translation errors is actually to compare and replace the results of proofreading and initial translation, so as to realize the intelligent proofreading of the English translation.

Definition H represents the wrong English translation result, and H' represents the correct English translation result. The process of transforming H into H' is the process of translation error proofreading. The content to be proofread is expressed in the form of a collection:

$$U = \{u_1, u_2, \dots, u_n\}. \quad (8)$$

In the above equation, u_n represents the total amount of content to be proofread.

First, construct a judgment matrix U' to judge the importance of business English translation:

$$U' = \begin{bmatrix} u_{11} & u_{12} & \cdots & u_{1n} \\ u_{21} & u_{22} & \cdots & u_{2n} \\ \vdots & \vdots & \ddots & \vdots \\ u_{n1} & u_{n2} & \cdots & u_{nm} \end{bmatrix}. \quad (9)$$

According to formula (9), the accuracy of vocabulary translation in the results obtained by traditional English translation methods needs to be improved. Therefore, when designing an intelligent proofreading method, the accuracy of vocabulary translation should be corrected. The specific method is as follows.

If the weight (or authority) of each evaluation factor is represented by a fuzzy set, then the comprehensive evaluation result of the thing is

$$b_i = \min \sum_{i=1}^m \omega_i \times s_{ij}. \quad (10)$$

In the above equation, ω_i represents the weight of the accuracy of the word translation result; s_{ij} represents the probability of translation error.

In order to facilitate the expression of the computer intelligent proofreading method based on the improved phrase translation model, it will be used as the vocabulary to be proofread, and the proofreading completed vocabulary is represented by J_k . It is defined that z characters exist in J , denoted by J_z , and these characters correspond to the vocabulary in the English translation model; at the same time, there are r characters in J_k , denoted by J_{kr} .

Divide J_z into g character strings randomly, where the character strings correspond to the vocabulary in the English translation model. Similarly, divide J_k into g' character strings randomly to achieve the corrected result:

$$PN = \frac{P - \min(g)}{\max(g) - \max(g')}. \quad (11)$$

In the process of intelligent proofreading of business English translation results, the key point is to find a method suitable for dividing the words to be proofread and proofread the words to be proofread in turn and arrange the proofreading results so as to be used in the later translation. By improving the translation model, the intelligent proofreading of English translation errors is realized, which lays a solid foundation for the reliability of business English translation results.

In conclusion, based on speech recognition technology and wireless communication technology, the overall architecture and module design of business English translation systems are realized. On this basis, the intelligent correction of translation results is realized by relying on the business English corpus database and improved translation model.

4. Experiment

In order to verify the application effect of a business English translation framework based on speech recognition and wireless communication, the simulation experiment is carried out. In the experiment, design a translation system based on deep learning [7], an interactive English-Chinese translation system based on feature extraction algorithm [8], and a system based on joint minimum Bayesian fusion [9] as a comparison.

4.1. System Verification Environment Design. Figure 5 shows the architecture diagram of the simulation experiment environment.

Figure 5 shows the system structure of the system simulation experiment environment. From the structure, it can be seen that different sensors and experimental structures have different effects on the simulation experiment. The specific hardware configuration parameters of the server in Figure 5 are shown in Table 1.

Specific experimental operations are performed in the simulation experimental environment architecture shown in Figure 5. In order to save experimental time, the method of manually inputting the target English terms is not used for the experiment, but an automatic input program is written through the Java language. The search results are formed into massive Internet data clusters, and experiments are carried out in this environment. Search 500 translation instruction tasks in the massive Internet data cluster to obtain the effect of error correction modules of different systems, the probability of repeated translation, the probability of missing translation, and the accuracy of translation results.

Data preprocessing is an important step in ASR. So, the first step of this experiment is to process the original data. The preprocessing includes preemphasis and framing. The purpose of preemphasis is to enhance the high frequency part of speech, remove the influence of lip radiation, and increase the high frequency resolution of speech. Generally,

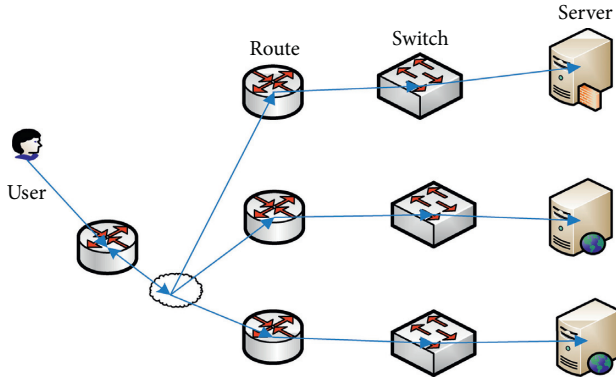


FIGURE 5: Simulation experiment environment architecture.

TABLE 1: Server hardware configuration.

Hardware	Specific configuration
CPU	Frequency above 850 Hz
RAM	1 T
Motherboard	ATX architecture
Graphics card	AGP
Network card	100 Mb/s
Hard disk	60 Gb

the transfer function is a first-order FIR high-pass digital filter. The purpose of framing is to divide the data into convenient data frames.

4.2. Evaluation Criteria. Since the presentation of translation results of different systems is different, different evaluation criteria are used for the evaluation of test results. The error correction effect, that is, the error correction rate, is used as an evaluation indicator, and the results submitted by different systems are compared with the correct answers referenced. Specifically, formula (12) is used to evaluate the effect of error correction, which is defined as

$$\text{Precision} = \frac{\sum_{i=1}^n |g - g'|}{\sum_{i=1}^n \max(g) - \max(g')}. \quad (12)$$

In the above equation, $|g - g'|$ represents the number of translations that meet the reference correct answer after correcting the answer.

Another indicator, Recall, evaluates the system's correction ratio for all errors that should be corrected, that is, the correction rate, which is defined as

$$\text{Recall} = \frac{\sum_{i=1}^n |g \cap g'|}{\sum_{i=1}^n |g|}. \quad (13)$$

In the above equation, $\sum_{i=1}^n |g|$ represents the number of correct corrections.

4.3. Experimental Results and Discussion

4.3.1. Comparison of Error Correction Rate and Total Error Rate. Before the experiment, users' behavior habits were

analyzed, and it was known that users usually only looked at the search results of the previous pages when using the search system. Therefore, a program to automatically calculate the average value was written in Java language. The error correction results of the designed system, the system in [7], the system in [8], and the system in [9] were counted. The results are shown in Table 2.

Analysis of the data in Table 2 shows that the error correction rate reaches 97.3% and the total correction rate reaches 98.5% when using the designed system to correct translation errors, while the error correction rate and correction rate of the system in [7], the system in [8], and the system in [9] are significantly lower than those of the designed system. Moreover, the response time of the designed system is the shortest and the search efficiency is higher, which not only improves the correction rate and error correction rate of the system but also improves the operation efficiency of the system. Through the data comparison, it can be seen that the designed system can effectively correct the errors in English translation, and the correction results are more reliable. This is because the method sends accurate language signals to the translator based on speech recognition technology, which improves the accuracy coefficient of computer translation, and can assist users in language translation and reduce the probability of errors in the translation process. Thus, the error correction probability is higher, and the correction result has the advantage of comprehensiveness.

4.3.2. Comparison of the Probability of Repeated Translation.

In principle, repeated results in translation results are not allowed to exist. However, in massive Internet data clusters, there are some differences in data structure characteristics between repeated results. It is impossible to completely eliminate duplicate results, which can only be extremely reduced. Therefore, the repeated translation probabilities of different systems are compared, and the results are shown in Figure 6.

As shown in Figure 6, although there are repeated translations in the designed system, there are not many repeated results, and the probability of repeated translation is low. However, the repetition rate of the system in [7], the system in [8], and the system in [9] is much higher than the strategy proposed in this paper. So, we can draw that the proposed strategy has certain advantages in terms of the repetition translation probability.

4.3.3. Comparison of the Probability of Missing Translation.

Similar to the repeated translation probability, the omission result in the translation result is not allowed to exist in principle. Therefore, the probability of missing translation is the lower the better. Figure 7 gives the comparison of missing translation probability.

The result of Figure 7 shows that the missing translation probability of the designed system is always lower than that of the other three strategies, and the highest value of the missing translation probability of this scheme is less than 0.2. Compared with the other three strategies, the proposed

TABLE 2: Comparison of error correction effects of different systems.

System	Response time (s)	Error correction rate (%)	Correction rate (%)
Designed system	0.09	97.3	98.5
Reference [7] system	0.15	59.6	75.2
Reference [8] system	0.28	64.2	68.3
Reference [9] system	0.19	71.0	70.1

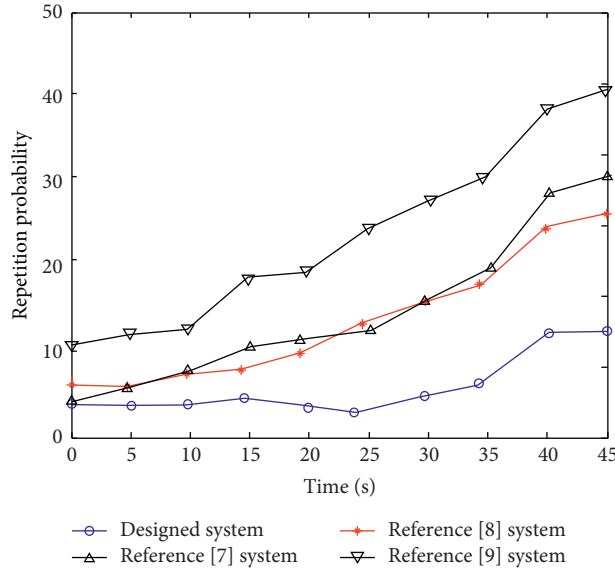


FIGURE 6: Comparison of repeated translation probability.

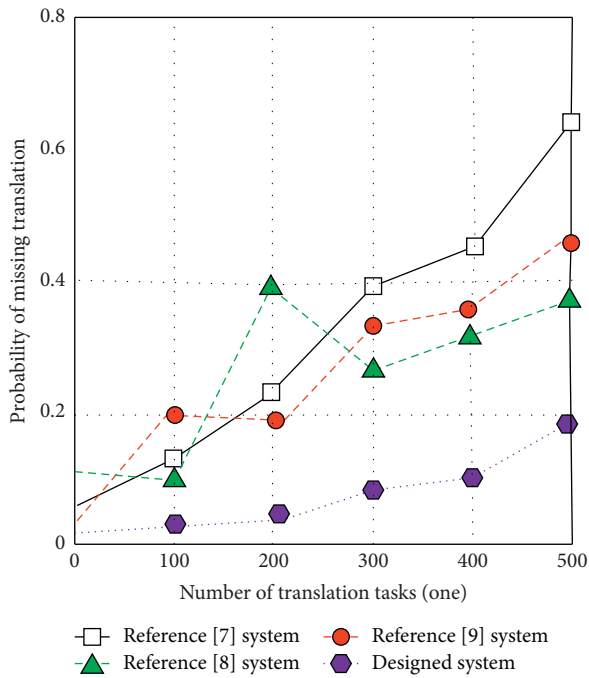


FIGURE 7: Comparison results of missing translation probability.

scheme has obvious advantages in the aspect of missing translation. The reason is that, in the design process, this system can help to obtain the similarity between different English languages and can help to remove the invalid language elements.

4.3.4. Comparison of Accuracy of Translation Results. The accuracy of translation results of different systems is shown in Figure 8.

It can be seen from Figure 8 that the translation accuracy of the proposed scheme is much higher than that of the other three strategies, but it is only slightly higher than that of the strategy proposed in [9]. The main reason is that the method proposed in this paper overcomes the problem of inability to solve the problem of lexical error correction by the similarity relationship between words. According to the experimental results, the designed system has certain advantages in evaluating the accuracy of business English translation.

In addition, the experimental results of this system are evaluated based on reference sentences generated by bilingual human experts. The reference sentences cover all linguistic variants of English taxonomy. The result of 0.78 and 0.10 was obtained by the BLEU and WER, respectively.

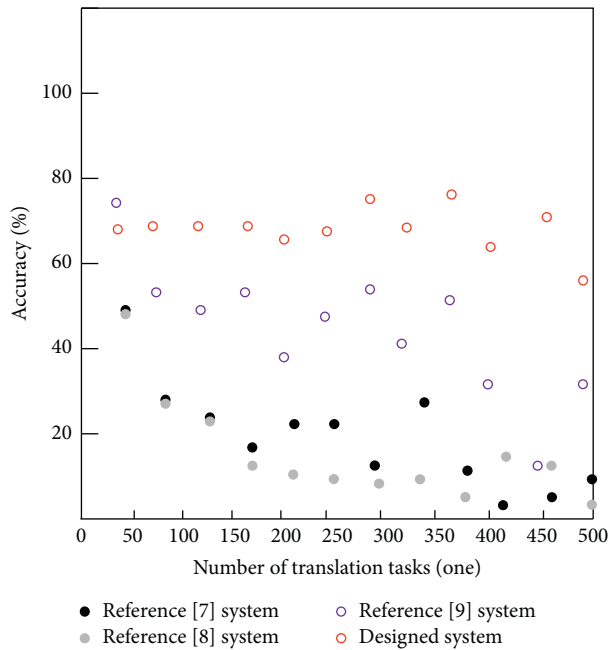


FIGURE 8: Comparison of accuracy of translation results.

5. Conclusion

To solve the problems of low accuracy of business English translation results and low correction rate and error correction rate of traditional methods, a business English translation framework based on speech recognition and wireless communication is designed. The use of speech recognition technology can convert the user's voice input into text form and can ensure a high translation accuracy, which effectively solves the problem of low error correction rate in the traditional system in the translation process. After the realization of speech recognition, the corpus and intelligent proofreading method of translation errors are designed by wireless communication technology, which can effectively identify the errors in translation and further improve the translation effect. The experimental results show that the error correction rate of the system is 97.3%, and the correction rate is 98.5%. The accuracy of the translation results is higher, which fully verifies the comprehensiveness and reliability of the system.

Data Availability

The data used to support the findings of this study are available from the corresponding author upon request.

Conflicts of Interest

The authors declare that there are no conflicts of interest regarding the publication of this paper.

References

[1] A. Pathak and P. Pakray, "English-mizo machine translation using neural and statistical approaches," *Neural Computing and Applications*, vol. 31, no. 2, pp. 1–17, 2019.

[2] J. Joseph, Z. E. H. Moore, D. Patton, O. Tom, and E. N. Linda, "The impact of implementing speech recognition technology on the accuracy and efficiency (time to complete) clinical documentation by nurses: a systematic review," *Journal of Clinical Nursing*, vol. 3, no. 4, p. 29, 2020.

[3] V. V. R. Vegesna, K. Gurugubelli, and A. K. Vuppala, "Application of emotion recognition and modification for emotional Telugu speech recognition," *Mobile Networks and Applications*, vol. 24, no. 1, pp. 193–201, 2019.

[4] N. S. Khan, A. Abid, and K. Abid, "A novel natural language processing (NLP)-based machine translation model for English to Pakistan sign language translation," *Cognitive Computation*, vol. 12, no. 2, pp. 1–18, 2020.

[5] S. Singh, M. Anand Kumar, K. P. Soman et al., "Attention based English to Punjabi neural machine translation," *Journal of Intelligent & Fuzzy Systems*, vol. 34, no. 3, pp. 1551–1559, 2018.

[6] M. Tassavor and Y. Y. Chen, "Lost in translation: caring for limited English proficiency patients," *Journal of the American Academy of Dermatology*, vol. 80, no. 3, pp. 829–831, 2018.

[7] M. Popel, M. Tomkova, J. Tomek, and Ľ Kaiser, "Transforming machine translation: a deep learning system reaches news translation quality comparable to human professionals," *Nature Communications*, vol. 11, no. 1, p. 4381, 2020.

[8] R. Knowles, M. Sanchez-Torron, and P. Koehn, "A user study of neural interactive translation prediction," *Machine Translation*, vol. 33, no. 1-2, pp. 135–154, 2019.

[9] C. Wei, "A review of constructivism learning theory," *Academic Exchange*, vol. 21, no. 10, pp. 12–14, 2007.

[10] X. Li, Y. Liu, W. Chen, and Q. Liu, "Improving the translation quality of compressed neural machine translation models with monolingual data," *Journal of Chinese Information Processing*, vol. 33, no. 7, pp. 46–55, 2019.

[11] D. Kamińska, "Emotional speech recognition based on the committee of classifiers," *Entropy*, vol. 21, no. 10, pp. 1–17, 2019.

[12] T. Wesarg, S. Arndt, K. Wiebe et al., "recognition in noise in single-sided deaf cochlear implant recipients using digital remote wireless microphone technology," *Journal of the American Academy of Audiology*, vol. 30, no. 7, pp. 607–618, 2019.

[13] T. Laszig, A. Klis, and M. Igras-Cybulska, "Speech emotion recognition based on voice fundamental frequency," *Archives of Acoustics*, vol. 44, no. 2, pp. 277–286, 2019.

[14] C. Andy and S. Kumar, "An appraisal on speech and emotion recognition technologies based on machine learning," *International Journal of Automotive Technology*, vol. 8, no. 5, pp. 2266–2276, 2020.

[15] M. Alam, M. A. Jan, L. Shu, X. He, and Y. Chen, "Editorial: current and future trends in wireless communications protocols and technologies," *Mobile Networks and Applications*, vol. 23, no. 3, pp. 377–381, 2018.

[16] T. Raisanen, "The use of multimodal resources by technical managers and their peers in meetings using English as the business lingua franca," *IEEE Transactions on Professional Communication*, vol. 63, no. 2, pp. 172–187, 2020.

[17] M. K. Glatz, "Conceptualising English as a business lingua franca," *European Journal of International Management*, vol. 12, no. 2, p. 46, 2018.

[18] K. A. Darabkh, L. Haddad, S. Z. Sweidan, M. Hawa, R. Saifan, and S. H. Alnabelsi, "An efficient speech recognition system for arm-disabled students based on isolated words," *Computer Applications in Engineering Education*, vol. 26, no. 2, pp. 285–301, 2018.

- [19] H. H. Gu, "Multi-band anti-noise speech recognition method simulation based on multi-core learning," *Computer Simulation*, vol. 36, no. 10, pp. 364–367, 2019.
- [20] C.-H. Chen, F. Song, F.-J. Hwang, and L. Wu, "A probability density function generator based on neural networks," *Physica A: Statistical Mechanics and its Applications*, vol. 541, Article ID 123344, 2020.
- [21] B. D. Nye, "Intelligent tutoring systems by and for the developing world: a review of trends and approaches for educational technology in a global context," *International Journal of Artificial Intelligence in Education*, vol. 25, no. 2, pp. 177–203, 2015.
- [22] A. A. Genlott and Å. Grönlund, "Closing the gaps-improving literacy and mathematics by ICT-enhanced collaboration," *Computers & Education*, vol. 99, pp. 68–80, 2016.
- [23] J. I. Liontas, "Reading and multimedia applications: going beyond bells and whistles, hotlinks and pop-up windows," *IALLT Journal of Language Learning Technologies*, vol. 33, no. 1, 2017.
- [24] A. Öman and S. Sofkova Hashemi, "Design and redesign of a multimodal classroom task-implications for teaching and learning," *Journal of Information Technology Education: Research*, vol. 14, no. 1, pp. 139–159, 2015.
- [25] S. Fraihat and Q. Shambour, "A framework of semantic recommender system for e-learning," *Journal of Software*, vol. 10, no. 3, pp. 317–330, 2015.

Research Article

Research on Sports Performance Prediction Based on BP Neural Network

Sitong Yang ¹, Lina Luo,¹ and Baohua Tan²

¹*School of Physical Education, Hubei University of Technology, Wuhan, Hubei 430068, China*

²*School of Science, Hubei University of Technology, Wuhan, Hubei 430068, China*

Correspondence should be addressed to Sitong Yang; sitongyang@hbut.edu.cn

Received 21 January 2021; Revised 16 March 2021; Accepted 23 March 2021; Published 7 April 2021

Academic Editor: Hsu-Yang Kung

Copyright © 2021 Sitong Yang et al. This is an open access article distributed under the Creative Commons Attribution License, which permits unrestricted use, distribution, and reproduction in any medium, provided the original work is properly cited.

Artificial neural network has the advantages of self-training and fault tolerance, while BP neural network has simple learning algorithms and powerful learning capabilities. The BP neural network algorithm has been widely used in practice. This paper conducts research on sports performance prediction based on 5G and artificial neural network algorithms. This paper uses the BP neural network algorithm as a pretest modelling method to predict the results of the 30th Olympic Men's 100m Track and Field Championships and is supported by the MATLAB neural network toolbox. According to the experimental results, the scheme proposed in this paper has better performance than the other prediction strategies. In order to explore the feasibility and application of the BP neural network in this kind of prediction, there is a lot of work to be done. The model has a high prediction accuracy and provides a new method for the prediction of sports performance. The results show that the BP neural network algorithm can be used to predict sports performance, with high prediction accuracy and strong generalization ability.

1. Introduction

The artificial neural network is a kind of network information processing system inspired by a human brain. It has high nonlinear dynamic processing ability and does not need to know the distribution form and variable relation of data [1, 2]. When the input and output relationships of hybrid systems are too complex to be expressed in general terms, it is easy to realize their highly nonlinear mapping relationships by the God-Jing network [3, 4]. A neural network has achieved good results in pattern recognition, automatic control, and many other fields. In recent years, the neural network model has been successfully applied to economic prediction. For this reason, we use the BP learning algorithm of an artificial neural network to study the prediction of sports achievement [5, 6].

According to the existing sports results, the prediction of the sports results will be used in large-scale games, such as the Olympic Games, the Asian Games, the National Games, and so on. This prediction not only provides clear training and competition goals for athletes and coaches, at the same time, we

can track and judge the development law and characteristics of sports achievement [7]. Therefore, this kind of forecast is always in an important position in the sports achievement forecast research. The more accurate the prediction of this kind of sports achievement is, and the direct influence is on the formulation of training and training objectives. This paper conducts research on sports performance prediction based on 5G and artificial neural network algorithms [8]. This paper uses the BP neural network algorithm as a pretest modelling method to predict the results of the 30th Olympic Men's 100m Track and Field Championships and is supported by the MATLAB neural network toolbox. According to the results of forecasting research, artificial neural networks have advantages. In order to explore the feasibility and application of BP neural networks in this kind of prediction, there is a lot of work to be done [9].

The results show that the BP neural network algorithm can be used to predict sports performance with high prediction accuracy and strong generalization ability. It is also on the discovery of the law of achievement development and the characteristics of sports development [10]. However, due to the small amount of data on which this kind of prediction

is based, the randomness of the data in the process of producing the data is large and there are many hidden influencing factors, which make the data information very uncertain [11]. Therefore, it is difficult to ensure the accuracy of this kind of prediction. Therefore, the selection of a suitable, high-precision prediction method will be the key to prediction.

How to evaluate the performance of sports is an issue worth studying, and many scholars have studied the evaluation method for course performance. The usual method is to make scoring rule, in which the judge marks according to the completion of the rule and adds up the scores. However, this method is greatly affected by the experience and level of the judge. The AHP method is widely used in various types of performance evaluation [12]. In comparison with the traditional direct scoring method, this method achieves significant progress, combining the qualitative evaluation with the quantitative evaluation and improves the accuracy of the evaluation. The BP (back propagation) network was proposed by the scientist team headed by Rumelhart and McClelland in 1986 [13, 14], which is a multilayer feed-forward network trained by using the error back-propagation algorithm. In this paper, we will take advantage of the BP network to establish a prediction model, which can improve the prediction performance.

The BP network is currently one of the most widely applied neural network models. The BP network can learn and store a large number of input-output model mapping without disclosing or describing the mathematical equation of this mapping in advance. This method has wide application prospect in the performance evaluation of sports aerobics. The BP algorithm can better describe the nonlinear relationship between sports performance and various factors [15]. Neural networks prediction, however, is limited in our research due to its large requirement on training samples and weak generalization ability.

Above all, although there are many methods to deal with sports performance prediction, the prediction time and prediction accuracy cannot meet the technical requirements. Therefore, a new prediction algorithm is needed to improve the prediction performance. On this basis, we use the BP neural network algorithm to predict the sport performance.

The contributions of this paper are summarized as follows:

- (1) This paper proposes a new pretest modelling method which combines the BP algorithm and 5G
- (2) This paper uses the combined algorithm as a pretest modelling method to predict the results of the 30th Olympic Men's 100m Track and Field Championships and is supported by the MATLAB neural network toolbox

This paper is organized as follows. Section 2 presents some related work. Section 3 gives the method to establish the prediction network. In Section 4, experiment is

presented and analyzed. Section 5 gives the training result and result analysis. Finally, Section 6 sums up some conclusions and gives some suggestions as the future research topics.

2. Related Work

Based on the existing sports performance, the prediction of sports performance will be used in the Olympic Games, Asian Games, National Games, and other major sports events [16, 17]. This prediction not only provides clear training and competition goals for athletes and coaches, at the same time, we can track and judge the development laws and characteristics of sports achievements. In the 1940s, an artificial neural network was first proposed [18]. It formed a new machine learning method theory by imitating the process of human brain processing problems and the method of solving problems. From the structural point of view, the artificial neural network is composed of some neurons, mainly simulating the interaction between these neurons and embedding the action mode into the network structure [19].

The main feature of artificial neural networks is parallel data processing. Although the structure of a single neuron is relatively simple, the structure formed by combining a large number of neurons is still very complicated. Yan et al. [20] provided a basis for the application of neural network modelling in biomechanics and opened up a broad prospect for research in this area. They took a shot put as an example and used neural network technology to establish a transformation model between feature quantity and original information [21]. In addition, some scholars have explored the generalized inverse transformation of sports biomechanics information [22]. The original data restoration effect is better. Essentially speaking, the neural network eventually acquires knowledge through learning, so it can be used to establish a more complex model of causality in human motion.

3. Methods

The BP neural network is a multilayer pre-error feedback neural network, which belongs to the error back-propagation algorithm [23, 24]. It consists of an input layer, an output layer, and several hidden layers, each of which has several nodes, each node representing a neuron, and the upper and lower nodes are connected by weight. The nodes between the layers are all interconnected, and there is no correlation between the nodes in each layer [25, 26].

3.1. Information Forward Propagation Process. In the BP neural network, the differentiable function of sigmoid strong bending type, that is, strict incrementally, can make the output show a better balance between linearity and non-linearity, so the nonlinear mapping between input and

output can be realized. It is suitable for medium- and long-term forecasts. It has the advantages of a good approximation effect, fast calculation speed, and high precision [27, 28]. At the same time, its theoretical basis is solid, the derivation process is rigorous, the formula is symmetrical and graceful, and it has a strong nonlinear fitting ability. The neural network model of the hidden layer is a linear or nonlinear regression model. It is generally believed that increasing the number of hidden layers can reduce network error. Of course, it also complicates the network and increases the training time and the tendency of “overfitting.” Therefore, a 3-layer BP network (that is, 1 hidden layer) was used in this study [29, 30].

The number of nodes in the hidden layer is not only related to the number of nodes in the input and output layers but also to the complexity of the problem to be solved, the type of transfer function, and the characteristics of the sample data. The condition of determining the number of hidden layer nodes is that the number of nodes in and out layer and hidden layer must be less than $n-1$ (where n is the number of training samples) [31]. The input and output of all kinds of training samples in this study are all 5 and 1, so the number of nodes in the hidden layer is determined to be 3. On the basis of determining various parameters, a neural network was established, and through the training of the neural network, the results of 100,200,400 people in the 30th Olympic Games were predicted, and the results of 7 events were predicted by the following methods: rolling prediction [32, 33]. That is to say, the results of the 23rd and 27th sessions are used to predict the results of the 28th session, the 2400th session to predict the results of the 29th session, and the 25th session of the 29th session to predict the results of the 30th session so as to form the rotation training and repeat it until the full precision requirement of prediction is fulfilled [34, 35]. And the achievement that satisfies the accuracy, namely, the forecast result that wants to obtain for the forecast is shown in Figure 1.

3.2. BP Development Research. The mechanism of artificial neurons and biological neurons is similar. The input accepts the n -dimensional input vector x or receives the output of other neurons. The output can be denoted by the following formula:

$$o = f(wx). \quad (1)$$

The interconnection between two neurons is like the “axon-dendritic” model of information transmission pathway [29, 30], which can be calculated as follows:

$$f_1(x) = \frac{1}{1 + e^{-\lambda x}}, \quad (2)$$

$$f_1'(x) = \lambda f_1(x)[1 - f_1(x)].$$

The weight of the connection indicates the degree of interaction between the two interconnected neurons as follows:

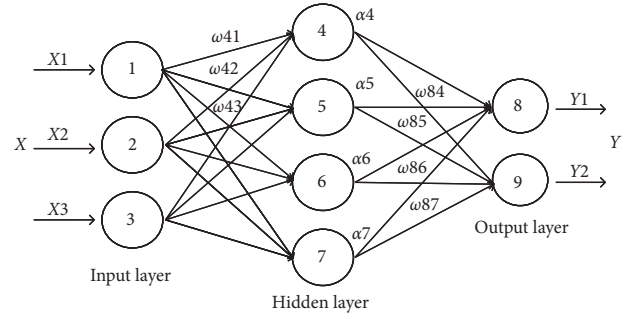


FIGURE 1: A 3-layer fully connected neural network.

$$\Delta w_{ji} = \eta \delta_j x_{ji}, \quad (3)$$

$$w_{ji} = w_{ji} + \Delta w_{ji}.$$

The artificial psychic network is composed of several units like biological neurons and the dense connection between each unit. Each unit can accept numeric input and output [36, 37].

$$E(w) = \frac{1}{2} \sum_{k \in \text{outputs}} (t_k - o_k)^2. \quad (4)$$

One of the motivations of artificial neural network systems is to obtain this highly parallel algorithm based on distributed representation, and it is as follows:

$$\delta_k = o_k'(t_k - o_k) = o_k(1 - o_k)(t_k - o_k). \quad (5)$$

Although artificial neural networks mimic the human brain nervous system as much as possible, in fact, artificial neural networks do not fully exhibit complex features in the biological nervous system.

$$\delta_k = o_k' \sum_{k \in \text{outputs}} w_{kh} \delta_k = o_k(1 - o_k) \sum_{k \in \text{outputs}} w_{kh} \delta_k. \quad (6)$$

In the artificial neural network, we only consider the invariant value of each unit output one but not the real biological nervous system time and impulse information [38]. The neural network model requires a large amount of data for input-output training. The more data, the more accurate the model.

3.3. Error Back-Propagation Process. Morning pulse refers to the number of pulses when you wake up in the morning (per minute); the morning pulse of each person is relatively stable. Therefore, we can determine whether exercise is appropriate by measuring the morning pulse the next day after exercise [39, 40]. Morning pulse testing is an important parameter basis for athletes in match and training, and this kind of measurement is very effective at present, and it also plays an important role in training regulation. Systemic circulation arterial blood pressure is referred to as blood pressure [41]. Parameter test architecture in sports training is shown in Figure 2.

Blood pressure is the pressure on the blood vessel wall when blood flows in the blood vessel; it is also the driving

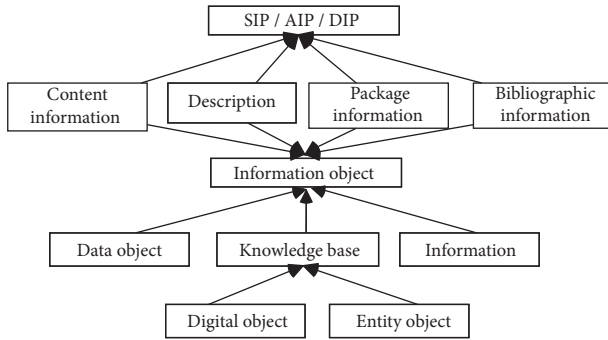


FIGURE 2: Parameter test architecture in sports training.

force of blood flow in the blood vessel. We know that blood vessels can be divided into arteries, veins, and capillaries, so blood pressure should also be divided into arterial blood pressure, venous blood pressure, and capillary pressure [42, 43]. What we usually mean by blood pressure is arterial blood pressure. Oxygen saturation is the percentage of the volume of oxygenated hemoglobin in the blood, that is, the concentration of oxygen in the blood, which is an important physiological parameter of respiratory circulation. It is an important index to maintain the normal physiologic function of the human body. The oxygen saturation of normal arterial blood was 9.8% that of venous blood was 75% [44, 45].

3.4. G Technology and Mobile Information System. The key technologies of 5G include large-scale antenna technology, ultra-dense heterogeneous network deployment, advanced spectrum utilization technology, and flexible physical access technology [46, 47]. Large-scale antenna technology improves the spectrum efficiency of the entire system through multiple antennas with multiple inputs and multiple outputs; ultra-dense networking achieves a substantial increase in capacity through the high-density deployment of base stations; advanced spectrum utilization technologies such as full spectrum access technology can effectively use spectrum resources. Flexible physical access technologies, such as nonorthogonal multiple access technology, simultaneous same-frequency full-duplex technology, and new modulation and coding technology, can bring about a significant improvement in user experience and spectrum efficiency. Among these technologies, ultra-dense heterogeneous networking is the main research technology of this article [48]. On the one hand, all the data used in this prediction model can be obtained from the terminal used to collect the original data by the wireless communication system. On the other hand, we can transmit the predict result to the terminal who is interested to it by this wireless communication system too. The basic model of the data transmission system is shown in Figure 3.

3.5. Numerical Test of Dynamic Performance Prediction. In the process of constructing the neural network model, it is necessary to set the parameters. The appropriate parameter setting can not only guarantee the accuracy of the model

construction but also the best prediction effect and reduce the error. At the same time, the running time can be greatly reduced. The number of neurons in the input layer of the network is the number of characteristic factors of the system, and the number of nodes in the output layer is the number of the target of the system [49, 50]. At present, there is no specific basis for determining the number of hidden layer nodes, which can only be determined by experience and trial and error [51, 52]. The number of hidden layer nodes is usually set to 7.5% of the number of nodes in the input layer. The initial weights are generally determined by experience and cannot be set to a set of values that are completely equal. The training rate is set. In the classical BP algorithm, the training rate is determined by experience. The higher the training rate is, the larger the weight will be and the faster the convergence rate will be. If the training rate is too large, it may cause the system to oscillate. Therefore, the training rate is set on the premise of no oscillation, the larger the better [53].

4. Experiment

The first step of establishing a reliable neural network model is to determine the structure of the neural network [54]. Based on this, the parameters are as follows: the transfer function of the hidden layer is t ensign, the transfer function of the output layer is t ensign, the training function is putt, the display interval is 10, the learning rate of the network is 0.001, the maximum training frequency is 50000, and the target error is $0.65 \cdot 10^{-11}$. In order to prevent overfitting during the antistop experiment, the prediction performance of the network model is low, and the generalization ability is weak.

4.1. Difference Test. In this study, we also analyzed the relationship between the performance of the 3,000-meter dash and oxygen saturation. The results showed that there was a strong correlation between them. In medicine, it is generally believed that the positive oxygen saturation should not be less than 9.4%, but below 94%, we consider this condition to be insufficient oxygen supply. Another group of researchers believed that when oxygen saturation was 90, it could be considered hypoxemia. And they think that when the oxygen saturation is greater than 70, the accuracy can reach ± 2 .

It is also considered that there is a certain error when the oxygen saturation is below 70%. In clinic, oxygen saturation readings can be directly used to reflect the respiratory function of the human body. In actual training, we found that when athletes appear stable and with high oxygen saturation level, they tend to have higher results. When the saturation of blood oxygen decreases obviously, the result of the competition will also decline by a large margin, which is like the degree of decline of saturation of blood oxygen. At the same time, with the gradual improvement of the saturation of blood oxygen, there will be a corresponding improvement in the performance of the athletes. This point has very important reference significance for training, adjustment, and competition.

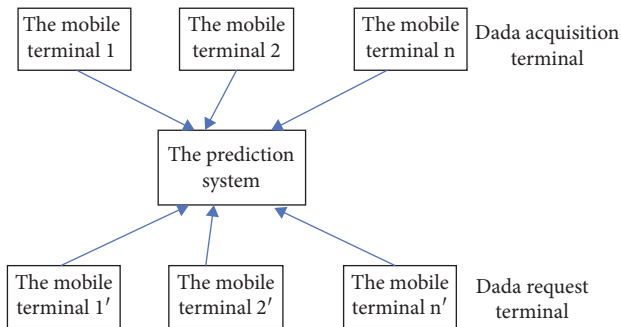


FIGURE 3: Basic model of the data transmission system.

4.2. Correlation Test. As one of the most widely used neural network models, the BP neural network can be used as the research of classification, clustering, pretest, and so on. At present, the BP neural network has been successfully used in the aspects of athlete's competitive state, sports score prediction, the prediction of the special performance of the link and shot, and the comprehensive evaluation of the athlete's sprint ability. Classification of sports performance predictions under different methods is shown in Figure 4.

In Figure 4, sample size is the number of sample, and category classification is the time of classification. Category 1 is the scheme proposed in this paper. Category 2 is the CAO (colony of ant optimization) strategy which is proposed by Shiraishi et al. [55]. Category 3 means the MEPSO (multi-exemplar particle swarm optimization) proposed in [56]. Category 4 means the OSVM (optimized support vector machine) which is proposed by Mahmood and Qasim [57]. Category 5 means the LRFAR (linear regression factor analysis regression) scheme [58].

By Figure 4, it can be seen that the classification of different methods is very different for the analysis of athletes' performance, and classification research must be carried out according to the characteristics of athletes. In order to deal with the instability of the existing performance evaluation method, an artificial neural network-based evaluation model of 3000 m obstacle running performance is proposed, and then the neural network evaluation model is established by the physiological and biochemical indexes and the sports scores of the 3000-meter obstacle running athletes in Ningxia. The results show that the prediction value and the real value obtained by the BP neural network are much better than those of the other four schemes.

4.3. Posterior Error Test. In this paper, a model of the artificial intelligence network is established, in which the physical quality of 3000-meter obstacle runners is related to their special achievements. This method does not need to determine the expression of the mathematical model in advance and can reflect the relationship between the quality and special achievement of 3000-meter obstacle runner intelligently and scientifically. Classification of sports performance predictions under different standards is shown in Figure 5. In this figure, sample size is the number of sample, and category classification is the time of classification. In addition, Category 1, Category 2, Category 3, Category 4,

and Category 5 are with the same mean as they are in Figure 4.

A scientific analysis of the relationship between the performance of the 3000-meter obstacle course and the morning pulsation has been carried out. It is pointed out that when the athlete's morning pulsation is relatively stable, the results tend to perform well. When the athlete's morning pulsation fluctuates, the athlete is prone to unstable and poor performance. From the experimental results, we can conclude that the classification of sports performance predictions of the proposed scheme is much better than those of the other four strategies. With the prediction method proposed in this paper, the coaches and athletes can accurately grasp the development trend and provide a more reasonable mechanism.

5. Training Result and Result Analysis

This paper makes a scientific analysis of the relationship between the results of the 3000-meter obstacle race and systolic and diastolic blood pressure and points out that when the athlete's systolic pressure is lower and the diastolic pressure is higher, it is easier to get better results. When the systolic pressure is high, the athletes' fatigue degree is larger and the body is more uncomfortable. The accuracy of sports performance prediction under different methods is shown in Figure 6.

Figure 6 shows the accuracy of sports performance prediction for different methods. We compare the BP neural network in this paper with the MEPSO algorithm, CAO algorithm, and OSVM algorithm in this figure. It can be seen from the simulation in Figure 6 that the performance of the athletes under different standards is parabolic, which has a great relationship with the physical strength of the athletes. From the simulation in Figure 6, it can be seen that the performance of the athletes under different standards is parabolic. It has a lot to do with the athlete's physical strength. This article scientifically analyses the relationship between the results of the 3000-meter race and the weight and points out that there is no correlation between the 3000-meter race and the weight, as shown in Figure 7. Although the performance of the BP neural network algorithm is worse than that of the other three algorithms at the beginning, the average level of efficiency is almost the same as other three algorithms.

Figure 7 gives the accuracy of sports performance prediction under different standards for the proposed scheme. In this figure, the standard test means that the original test data originate different specified times, and standard test a, standard test b, standard test c, and standard test d mean the sample of the test data, and the specific value varies with each sampling. It can be seen from the simulation in Figure 7 that the performance of athletes under different standards fluctuates, but the overall trend is to moderate. This paper makes a scientific analysis of the relationship between the results of the 3000-meter obstacle race and the saturation of the blood oxygen and points out that the saturation of the blood oxygen has a strong correlation when the athletes appear stable with high saturation of the blood oxygen; it is

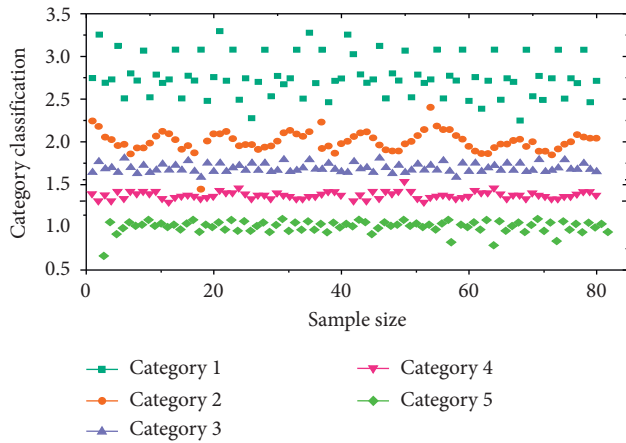


FIGURE 4: Classification of sports performance predictions under different methods.

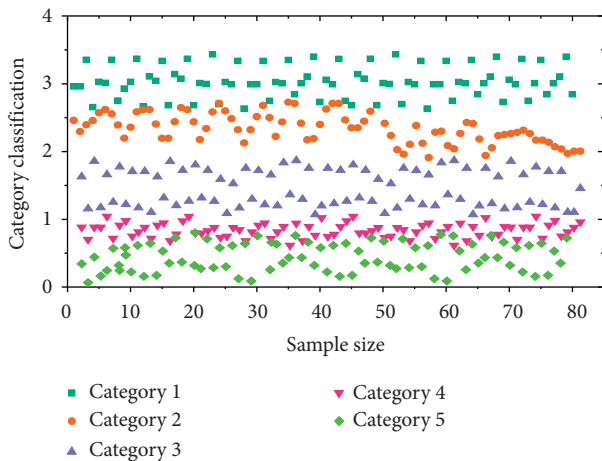


FIGURE 5: Classification of sports performance predictions under different standards.

easy to get high results. At the same time, with the gradual improvement of the athletes' oxygen saturation level, their performance will also be improved.

6. Results and Discussion

Based on the BP neural network model and the scientific analysis of the relationship between the results of the 3000-meter obstacle race and morning, pulse systolic blood pressure is different from diastolic blood pressure weight and oxygen saturation. We have come to the following conclusion: during training and competition, attention should be paid to maintain the morning pulse and systolic blood pressure of the athletes. The diastolic blood pressure is relatively stable. Currently, the athletes have the lowest degree of fatigue, the body is active, and the functional state is the best. In general, in this case, athletes who participate in major competitions can create better results. When athletes have higher pressure and fatigue, unnecessary training should be reduced. Because of the strong correlation between the saturation of blood oxygen, when the athletes

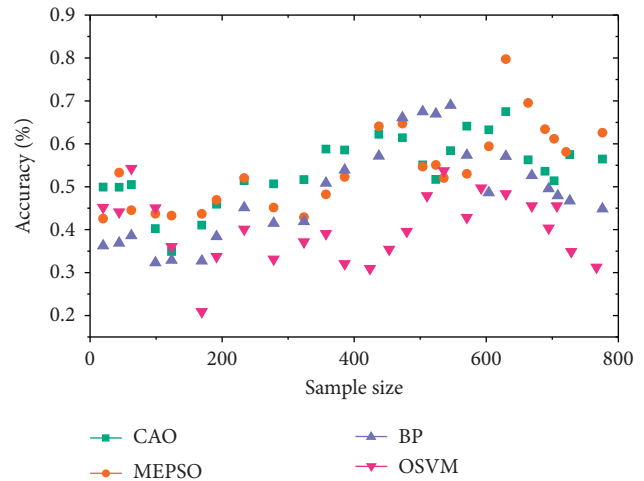


FIGURE 6: The accuracy of sports performance prediction under different methods.

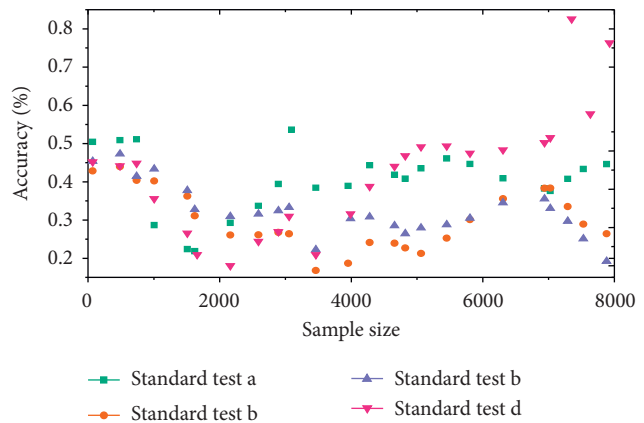


FIGURE 7: The accuracy of sports performance prediction under different standards.

appear stable and with high oxygen saturation level, it is easy to have a higher performance. During actual training and competition, attention should be paid to keep the athlete's high oxygen saturation.

Therefore, the BP neural network algorithm can be used to predict sports performance. At the same time, the MATLAB neural network toolbox brings great convenience to the prediction of sports performance and improves the efficiency of modelling and the accuracy of prediction. The prediction of sports performance is to realize nonlinear mapping, and the BP network can also be regarded as a nonlinear mapping from input to output.

The two characteristics of the BP neural network algorithm can solve the problems and difficulties of predicting the uncertain factors of sports performance. The first is that the BP network algorithm can learn and store many input/output pattern mapping relationships without revealing the mathematical equation describing the mapping relationship in advance. Secondly, the BP network algorithm has good adaptive and self-organizing ability. Therefore, this article establishes an artificial neural network model to predict

sports performance. Numerical experiments show that the prediction accuracy of this method is high, and it has certain practical reference value for studying the development trend of various sports performances in the future and can assist in decision-making and determining the training and development goals of competitive athletes.

Data Availability

Data sharing is not applicable to this article as no datasets are generated or analyzed during the current study.

Conflicts of Interest

The authors declare that they have no conflicts of interest.

Acknowledgments

This work was supported by the Hubei University of Technology (grant nos. 61675164 and 61827827).

References

- [1] Y. Zou, Y. Chen, J. He, G. Pang, and K. Zhang, "4D time density of trajectories: discovering spatiotemporal patterns in movement data," *ISPRS International Journal of Geo-Information*, vol. 7, no. 6, p. 212, 2018.
- [2] Z. Zhao, Q. Xu, and M. Jia, "Improved shuffled frog leaping algorithm-based BP neural network and its application in bearing early fault diagnosis," *Neural Computing & Applications*, vol. 27, no. 2, 2016.
- [3] K. Zhang, J. Guo, D. Nie, F. Yuan, and Z. Xiao, "Diagnosis model for transformer fault based on CRO-BP neural network and fusion DGA method," *High Voltage Engineering*, vol. 42, 2016.
- [4] Z. Wu and H. Wang, "Super-resolution reconstruction of sar image based on non-local means denoising combined with bp neural network," *Geoscience*, vol. 12, 2016.
- [5] J. Wang, P. Shi, P. Jiang et al., "Application of BP neural network algorithm in traditional hydrological model for flood forecasting," *Water*, vol. 9, no. 1, p. 48, 2017.
- [6] J. Wang and J. Jeong, "Wavelet-content-adaptive BP neural network-based deinterlacing algorithm," *Soft Computing*, vol. 22, 2017.
- [7] B. Wang, X. Gu, L. Ma, and S. Yan, "Temperature error correction based on BP neural network in meteorological wireless sensor network," *International Journal of Sensor Networks*, vol. 23, no. 4, p. 265, 2017.
- [8] B. Wang, X. Gu, M. Li, and S. Yan, *Temperature Error Correction Based on BP Neural Network in Meteorological Wireless Sensor Network*, Springer International Publishing, Berlin, Germany, 2016.
- [9] J. Velay and D. Beaubaton, "Influence of visual context on pointing movement accuracy," *Cahiers De Psychologie Cognitive Current Psychology of Cognition*, vol. 6, no. 5, pp. 447–456, 2018.
- [10] X. Tongle, W. Yingbo, and C. Kang, "Tailings saturation line prediction based on genetic algorithm and BP neural network," *Journal of Intelligent & Fuzzy Systems*, vol. 30, no. 4, pp. 1947–1955, 2016.
- [11] W. Shouxiang, Z. Na, Wu Lei, and W. Yamin, "Wind speed forecasting based on the hybrid ensemble empirical mode decomposition and GA-BP neural network method," *Renewable Energy*, vol. 94, 2016.
- [12] X. Shen, L. Wang, and D. Han, "Application of BP neural network optimized by artificial bee colony in intrusion detection," *Computer Engineering*, vol. 16, 2016.
- [13] Y. Safarpour and B. Jabbari, "Botulinum toxin treatment of movement disorders," *Current Treatment Options in Neurology*, vol. 20, no. 2, p. 4, 2018.
- [14] L. I. Ru-Ping, L. Zhu, W. U. Fang-Shen, and X. U. Zhen-Yu, "BP neural network algorithm improvement and application research," *Journal of Heze University*, vol. 6, 2016.
- [15] T. Ren, S. Liu, G. Yan, and H. Mu, "Temperature prediction of the molten salt collector tube using BP neural network," *IET Renewable Power Generation*, vol. 10, no. 2, pp. 212–220, 2016.
- [16] G. E. Pérez, A. Conte, E. J. Garde, S. Messori, R. Vanderstichel, and J. Serpell, "Movement and home range of owned free-roaming male dogs in Puerto Natales, Chile," *Applied Animal Behaviour Science*, vol. 205, Article ID S0168159118302612, 2018.
- [17] D. Ma, T. Zhou, J. Chen, S. Qi, M. Ali Shahzad, and Z. Xiao, "Supercritical water heat transfer coefficient prediction analysis based on BP neural network," *Nuclear Engineering and Design*, vol. 320, pp. 400–408, 2017.
- [18] Da Luciano, C. Fontoura, C. Leandro, and D. Cintra, "An integrated approach to the characterization of cell movement," *Cytometry Part A*, vol. 8, 2019.
- [19] L. Liang, S. Zhang, and Z. Rui, "CoMP in the sky: UAV placement and movement optimization for multi-user communications," *IEEE Transactions on Communications*, vol. 99, 2018.
- [20] M. Li, B. Wang, S. Yan, and X. Gu, "Temperature error correction based on BP neural network in meteorological wireless sensor network," *International Journal of Sensor Networks*, vol. 23, no. 4, p. 265, 2017.
- [21] D. Li, G. Wu, J. Zhao, W. Niu, and Q. Liu, "Wireless channel identification algorithm based on feature extraction and BP neural network," *Journal of Information Processing Systems*, vol. 13, no. 1, pp. 141–151, 2017.
- [22] P. Lantto, "Actions, organization and collaboration: strategies of the Sami movement in Sweden during the 20th century," *Cell Metabolism*, vol. 6, no. 6, p. 431, 2018.
- [23] P. Joanny and C. F. Brue, "Hyperbaric oxygen: effects on metabolism and ionic movement in cerebral cortex slices," *Science*, vol. 164, 1970.
- [24] G. Jiang, M. Luo, K. Bai, and S. Chen, "A precise positioning method for a puncture robot based on a PSO-optimized BP neural network algorithm," *Applied Sciences*, vol. 7, no. 10, p. 969, 2017.
- [25] S. H. Fox, R. Katzenschlager, S. Y. Lim et al., "International Parkinson and movement disorder society evidence-based medicine review: update on treatments for the motor symptoms of Parkinson's disease," *Movement Disorders Official Journal of the Movement Disorder Society*, vol. 33, 2018.
- [26] G. M. Findlay and A. S. W. Defreitas, "DDT movement from adipocyte to muscle cell during lipid utilization," *Applied Sciences*, vol. 7, no. 10, p. 969, 2017.
- [27] A. K. Davison, C. Lansley, N. Costen, K. Tan, and M. H. Yap, "SAMM: a spontaneous micro-facial movement dataset," *IEEE Transactions on Affective Computing*, vol. 9, no. 99, pp. 116–129, 2018.
- [28] K. Cui and X. Qin, "Virtual reality research of the dynamic characteristics of soft soil under metro vibration loads based on BP neural networks," *Neural Computing & Applications*, vol. 29, 2017.

- [29] V. Citovsky, "Tobacco mosaic virus: a pioneer of cell-to-cell movement," *Philosophical Transactions of the Royal Society of London*, vol. 1383, pp. 637–643, 2018.
- [30] M. S. Boyce, J. Pitt, J. M. Northrup et al., "Temporal auto-correlation functions for movement rates from global positioning system radiotelemetry data," *IEEE Transactions on Affective Computing*, vol. 9, no. 99, pp. 112–134, 2017.
- [31] H. Vuojala, M. Mustonen, X. Chen et al., "Spectrum access options for vertical network service providers in 5G," *Telecommunications Policy*, vol. 44, 2020.
- [32] A. Shahmansoori, G. E. Garcia, G. Destino, G. Seco-Granados, and H. Wymeersch, "Position and orientation estimation through millimeter-wave MIMO in 5G systems," *IEEE Transactions on Wireless Communications*, vol. 17, no. 3, pp. 1822–1835, 2018.
- [33] S. Sekander, H. Tabassum, and E. Hossain, "Multi-tier drone architecture for 5G/B5G cellular networks: challenges, trends, and prospects," *IEEE Communications Magazine*, vol. 56, no. 3, pp. 96–103, 2018.
- [34] H. A. Obeidat, R. Asif, N. T. Ali et al., "An indoor path loss prediction model using wall correction factors for WLAN and 5G indoor networks," *Radio Science*, vol. 53, no. 3-4, pp. 544–554, 2018.
- [35] M. Matinmikko, M. Latva-Aho, and P. Ahokangas, "On regulations for 5g: micro licensing for locally operated networks," *Telecommunications Policy*, vol. 42, 2018.
- [36] S. Kim, "5G network communication, caching, and computing algorithms based on the two-tier game model," *Etri Journal*, vol. 40, no. 1, pp. 61–71, 2018.
- [37] T. G. Khanh, S. Hidekazu, and S. Kei, "User satisfaction constraint adaptive sleeping in 5G mmWave heterogeneous cellular network," *Ieice Transactions on Communications*, vol. 101, 2018.
- [38] Y. Jifu, R. Christopher, X. Hain, J. Zhan, and M. Dong, "Technological trends for 5G networks influence of E-health and IoT applications," *Journal of Hydrology*, vol. 9, 2019.
- [39] Chih-Lin, Li Han, K. Jouni, H. Jinri, and H. Liuyan, "RAN Revolution with NGFI (xhaul) for 5G," *Journal of Lightwave Technology*, vol. 23, 2018.
- [40] S. Chen, Q. Fei, H. Bo, L. Xi, Z. Chen, and J. Liu, "User-centric ultra-dense networks for 5g: challenges, methodologies, and directions," *IEEE Wireless Communication*, vol. 23, 2018.
- [41] N. Betzalel, P. Ben Ishai, and Y. Feldman, "The human skin as a sub-THz receiver - does 5G pose a danger to it or not?" *Environmental Research*, vol. 163, pp. 208–216, 2018.
- [42] A. Anand and G. D. Veciana, "Resource allocation and HARQ optimization for URLLC traffic in 5G wireless networks," *IEEE Journal on Selected Areas in Communications*, vol. 36, 2018.
- [43] M. Alzenad, M. Z. Shakir, H. Yanikomeroglu, and M. S. Alouini, "FSO-based vertical backhaul/fronthaul framework for 5G+ wireless networks," *IEEE Communications Magazine*, vol. 56, 2018.
- [44] I. Afolabi, A. Ksentini, M. Bagaa, T. Taleb, M. Corici, and A. Nakao, "Towards 5G network slicing over multiple-domains," *Ieice Transactions on Communications*, vol. 100, no. 11, pp. 1992–2006, 2018.
- [45] L'amministrazione Trump vuole nazionalizzare la rete 5G.. *Technology Review* (2018).
- [46] A. Poordavoodi, M. Reza Moazami Goudarzi, A. Rahmani, A. M. Rahmani, and M. Izadikhah, "Toward a more accurate web service selection using modified interval DEA models with undesirable outputs," *Computer Modeling in Engineering & Sciences*, vol. 123, no. 2, pp. 525–570, 2020.
- [47] C. Zhang, X. Guo, X. Guo et al., "Machine learning model comparison for automatic segmentation of intracoronary optical coherence tomography and plaque cap thickness quantification," *Computer Modeling in Engineering & Sciences*, vol. 123, no. 2, pp. 631–646, 2020.
- [48] X. Xu, B. Shen, X. Yin et al., "Edge server quantification and placement for offloading social media services in industrial cognitive IoV," *IEEE Transactions on Industrial Informatics*, vol. 17, 2020.
- [49] X. Xu, X. Zhang, X. Liu, J. Jiang, L. Qi, and B. Md Zakirul Alam, "Adaptive computation offloading with edge for 5G-envisioned internet of connected vehicles," *IEEE Transactions on Intelligent Transportation Systems*, vol. 10, 2020.
- [50] Y. Li Z Gao and S. Wan, "Exploring deep learning for view-based 3D model retrieval," *ACM Transactions on Multimedia Computing, Communications, and Applications*, vol. 16, 2020.
- [51] Y. Xi, Y. Zhang, S. Ding, and S. Wan, "Visual question answering model based on visual relationship detection," *Signal Processing: Image Communication*, vol. 80, Article ID 115648, 2020.
- [52] A. Zhou, S. Wang, S. Wan, and L. Qi, "LMM: latency-aware micro-service mashup in mobile edge computing environment," *Neural Computing and Applications*, vol. 32, pp. 1–15, 2020.
- [53] S. Wan, Z. Gu, and Q. Ni, "Cognitive computing and wireless communications on the edge for healthcare service robots," *Computer Communications*, vol. 149, pp. 99–106, 2020.
- [54] S. Ding, S. Qu, Y. Xi, and S. Wan, "Stimulus-driven and concept-driven analysis for image caption generation," *Neurocomputing*, vol. 398, pp. 520–530, 2020.
- [55] M. Shiraishi, R. Takeuchi, H. Nakagawa, S. I. Nishimura, A. Awazu, and H. Nishimori, "Diverse stochasticity leads a colony of ants to optimal foraging," *Journal of Theoretical Biology*, vol. 465, pp. 7–16, 2019.
- [56] W. Song and Z. Hua, "Multi-exemplar Particle Swarm optimization," *IEEE Access*, vol. 8, no. 8, pp. 176363–176374, 2020.
- [57] S. A. Mahmood and Q. Q. Qasim, "Big data sentimental analysis using document to vector and optimized Support vector machine," *UHD Journal of Science and Technology*, vol. 4, no. 1, pp. 18–28, 2020.
- [58] D. Sharma and P. Chandra, "Linear regression with factor analysis in fault prediction of software," *Journal of Interdisciplinary Mathematics*, vol. 23, no. 1, pp. 11–19, 2020.

Research Article

Web-Based Human-Machine Interfaces of Industrial Controllers in Single-Page Applications

Shyr-Long Jeng ¹, Wei-Hua Chieng,² and Yi Chen²

¹Department of Mechanical Engineering, Lunghwa University of Science and Technology, Taoyuan 333326, Taiwan

²Department of Mechanical Engineering, National Chiao Tung University, Hsinchu 300, Taiwan

Correspondence should be addressed to Shyr-Long Jeng; aetsl@gm.lhu.edu.tw

Received 31 October 2020; Revised 12 March 2021; Accepted 19 March 2021; Published 7 April 2021

Academic Editor: Hsu-Yang Kung

Copyright © 2021 Shyr-Long Jeng et al. This is an open access article distributed under the Creative Commons Attribution License, which permits unrestricted use, distribution, and reproduction in any medium, provided the original work is properly cited.

Advances in conventional industrial controllers have led to new technologies such as multilanguage use, cross-platform applications, and remote monitoring and control. However, the human-machine interfaces (HMIs) of conventional industrial controllers and mobile devices cannot directly transmit instant messages to each other. This study describes a simple method of upgrading the HMIs of conventional industrial controllers into controllers capable of Web-based remote access. The study began with the development of a model-view-controller architecture consisting of Hypertext Markup Language, Cascading Style Sheets, and JavaScript and proceeded to the implementation of a single-page application (SPA) method through AJAX and WebSocket, which communicates with the back-end Node.js server to transfer data. Future advancements will enable information to flow through cross-platform devices across various operating systems and Web browsers, allowing users to remotely monitor and control machines from mobile smart devices. We demonstrated the simplicity of the SPA method by transforming a conventional personal computer-based industrial controller, WINPC32, to an all-purpose Web-based HMI for industrial use with the graphic user interface software, GPX.

1. Introduction

With the advancement of the Internet of Things (IoT) and changes in industrial demand, the platform used for the monitoring of many industrial applications has gradually shifted to web pages and mobile devices [1, 2]. Enterprises have developed mobile apps that enable communication among their various devices while human-machine interfaces (HMIs) are important tools for industrial monitoring. The motivation behind this study was to offer a solution that allows the HMIs of traditional industrial controllers to be executed on mobile devices. The challenge was that HMIs require cross-platform functions to be executable on different operating systems (Windows, iOS, and Linux) and devices (desktops, laptops, tablets, and smartphones). One aesthetically satisfying solution is to embed the HMI of the monitoring system on a browser-based web page and to use Extensible Markup Language (XML) as the format of the system configuration file.

The objective of this study was to describe a form of Web-based remote accessibility for conventional industrial controllers that connect supervisory control and data acquisition (SCADA) control with programmable logic controllers (PLCs). Phuyal et al. [3] proposed a Web-based remote-access real-time laboratory using SCADA control. They used a PLC to control the operation of the system and installed a SCADA system to monitor and control the process. The Web interface was designed in Visual Studio with ASP.NET and allowed students to access the lab and information regarding the experiment. The remote laboratory allowed for users to control an induction motor; this was used as an example to demonstrate its effectiveness. Kondratenko et al. [4] proposed monitoring and automating control processes in specialized pyrolysis complexes (SPCs) to utilize municipal polymeric waste. They described the functional structure and the main components of their generalized SPC Web SCADA system. They also presented an example of the application they proposed for the SPC

Web SCADA system. Rather than focusing on the previously mentioned applications, we focused on industrial controllers that are top-tier SCADA and PLC devices arranged in a typical structure: an industrial controller, SCADA, and PLC connected via Modbus. Industrial controllers with an open platform communications (OPCs) server and client-based architecture use the Internet, whereas conventional controllers without OPC capabilities are standalone and detached from the Internet. Qasim et al. [5] described a model of an HMI for Android mobile devices that uses model-to-text transformation to take the domain model as an input model for generating the complete mobile Android HMI code and uses Widgets Designer (.axml) code for applications. Caiza et al. [6] proposed a Web platform for creating HMIs that uses low-cost devices to integrate shop floor information through the OPC unified architecture (UA) protocol and PLC-based automation. These works, which arose in contexts similar to that of this study, have exhibited a simple path for a conventional controller to enter Web-based HMIs. XML and JavaScript Object Notation (JSON) enable information to flow through cross-platform devices on a variety of operating systems and Web browsers.

This study used a single-page application (SPA) architecture [7] to transmit conventional industrial controller information across various cross-platform devices, operating systems, and browsers. The Asynchronous JavaScript and XML (AJAX) can also be used to implement multiple user usage scenarios. Re-encoding conventional industrial controller data into XML helps reduce file size, improves system performance, and enhances the ease of maintenance, and such information stream can be combined with browser-style Web applications to increase system development efficiency. Remote monitoring through the Internet allows users to instantly control on-site system equipment from a distance. This method can substantially reduce the cost of equipment and labor as well as the time required to convert conventional industrial controllers into Web-based controllers.

The first academic article addressing SPAs and single-page Web applications was a technical report by Mesbah and Deursen [8] in which the authors responded to a problem Web technology faced at the time: "Web applications have suffered from poor interactivity and responsiveness towards end-users." The reason for the problem was that traditional Web design relied on postbacks, which required that pages be continuously refreshed and divided websites into several different design structures. This type of design pattern is called a "multipage application." Several of the multiuser applications had obvious flaws, such as low immediacy, slowness, poor Web interaction, and poor user experience. The SPA design pattern was proposed as a solution to these problems. The shift from multipage to single-page design did not merely reduce multiple pages to a single page but provided users with an experience akin to desktop applications by moving the user interface (UI) from the server side to the client side and implementing application logic on the client side [9, 10].

The concept of SPAs arose from the popularity of AJAX technology. Technologies such as jQuery and Bootstrap and

front-end frameworks such as React.js, Vue.js, and Angular.js can be used to implement single-page design. jQuery is a minimalist system primarily used to manipulate existing Document Object Model structures. IBM Dojo's package system simplifies the management of large-scale HMI development projects and incorporates high-performance implementations of common utilities into its core. Whereas Dojo uses standard Cascading Style Sheets (CSS) 3 queries, jQuery features a hybrid XML Path (XPath)-CSS query language and offers a wide range of options and operations for the results of these queries. jQuery incorporates AJAX, effects, and other utilities into its small core. Useful benchmarks for several packages were described in [11]. With respect to user experience, front-end development has seen a trend of UIs that operate similarly to desktop applications [12, 13]. The websites most frequently developed with SPA design are Web-managed web pages, in which the UI is usually a dashboard with top or side content navigation bars. Web pages, Google's Gmail, Google Drive, and Azure Portal are examples of SPAs.

In data management, graphical monitoring interfaces present information more effectively than digitally based interfaces. Chynal and Sobecki [14] analyzed users' visual focus to understand the strengths and flaws of several current web pages and suggested effective methods for developers to present data. For example, line and waveform graphs are intuitive methods for presenting changes in the voltage of a sensor, and supplementing them with pie charts or bar graphs can allow users to see statistics from a certain period of time at a glance. These graphical effects can be achieved through Web applications. These methods make quantitative data easy to interpret and more aesthetically pleasing and accurate than the old, unwieldy interfaces of traditional hardware displays [15].

The model-view-controller (MVC) software design pattern has become the mainstream Web design architecture. MVC prioritizes separating concerns and clearly distinguishing the roles of data, display, and logic, which is a particularly crucial part of HMI development. MVC can also simplify large programs into small modules or objects, making programs easily reusable, a feature which accommodates the design and development of modern SCADA-HMI systems [16]. Wang [17] analyzed two approaches to data serializing used in Web applications: XML and JSON. The results revealed that the transmission of Web application data was secure and powerful in the XML approach and fast and convenient in the JSON approach. Nurzhan et al. [18] compared two formats for data interchange currently used for industrial applications. The results revealed that JSON was faster and used fewer resources than its counterpart, XML. With the evolution of data lightweighting technology, the XML format has been replaced by the JSON format for data transmission, not only reducing the amount of data being transmitted but also increasing the transmission speed and improving the performance of the web page. In addition to MVC, a remote monitoring system enables developers to efficiently divide work, ensuring that the development of business logic and UIs remains separate.

This method was used to develop the Web application for the IoT-based toll system [19].

The component system approach subdivides an application into multiple components to construct an entire application or web page, with a component as the smallest unit. Development frameworks based on component systems have become a trend in modern Web development technology; examples are Java-based Web development frameworks such as Tapestry, Jakarta Server Faces, and Wicket [20]. Web front-end frameworks based on JavaScript include Vue.js, Angular.js, React.js, and Backbone.js. [21, 22]. The biggest advantage of component systems is that each component can be modularized and reused to achieve separation, allowing each component to perform its respective duties. Web applications built with component systems are easy to maintain, and developers can easily add new features or components to a template. Papcun et al. [23] described the evolution of HMIs and provided examples of solutions and case studies for each stage of this evolution. HMI 2.0 remote visualization and control on personal computers (PCs) can only work with networking. HMI 3.0 was applied to Internet connectivity and Web servers in companies, thereby opening the possibilities of Web and mobile applications. The integration of easy-to-access and open-source software, such as AJAX and the Node.js server, enables conventional industrial controllers to increase IoT connectivity.

After substantial development, the IoT has come to play the vital role of enforcing security and privacy policies to avoid a variety of vulnerabilities and threats to systems. IoT security requirements are classified into the following categories: authentication, access control, maintainability, resilience, data security and data sharing, security monitoring, and network security [24]. One approach to security is to use a virtual private network (VPN)—a secure connection between a device and a VPN server over the Internet. VPN private networks create secure communication channels between two points over public networks [25–27]. Because OPC UA did not use a VPN, its ability to provide security for industrial process control systems was compromised. Hackers obtained usernames and passwords and gained access to the system. OPC UA servers [28] were then outfitted with additional security features, such as server certificates for signing and encryption, authentication certificates for logging in, and a trust-reject function for controlling access (signing procedure) and identifying who can connect to the server.

In this study, we developed a general-purpose industrial controller HMI for browsers. Figure 1 displays the controller's architecture. We used an SPA design based on an MVC architecture and a component system using Vue.js to remotely monitor the industrial controllers and created a back-end server based on AJAX, WebSocket applications, and Node.js to manage data transmissions. The industrial controller developed in this study is based on the WINPC32 (Windows-Based Programmable Controller) industrial controller software, and the results of the development output by WINPC32's graphic control software, GPX, were converted into an SPA by a parser. The controller allows

users to achieve cross-platform remote monitoring. By transforming a conventional PC-based industrial controller with the WINPC32 graphical user interface (GUI) software, GPX, into a general-purpose Web-based HMI for industrial use, we demonstrated the simplicity of the SPA methodology. The cyber-physical systems of Industry 4.0 [29] can be implemented to perform remote diagnoses or collect data for machine learning through the Internet.

1.1. Development of SPA Architecture

1.1.1. WINPC32 and GPX. As Figure 2 shows, WINPC32 is a programmable control and HMI platform developed by Hurco Automation Ltd. [30]. Built on this foundation is a suite of soft-programmable industrial-control modules that encompass Soft-PLC, process PID, Soft-Motion, industrial networking, and machine vision. The manner in which the remote data included in the WINPC32 system are implemented is by the SCADA engine through communication drivers or OPC UA servers via communication master cards or direct serial link through COM or Ethernet ports once the input and output (I/O) is configured. On top of those real-time soft modules is an HMI module, which provides advanced HMI functions and network connectivity to Web, LAN, the major field bus, and PLC controls. The Soft-PLC complies with IEC61131-3 and offers the main types of PLC editing languages. The programming environment of all other modules, such as motion and HMI, is also compatible with major industry standards. The hardware I/O supported in WINPC32 includes the local ones assigned from various PC-Based Add-On cards, including a digital I/O module, analog I/O module, process proportional-integral-derivative (PID) interface module, motion interface module for motion, and data acquisition module, and remote ones supported from the various field bus slave I/O and device nodes or controls like PLC or temperature controller. Soft-PLC Editor offers three major PLC programming languages: Ladder Diagram, Instruction List, Function Block (FB), and Structured Text. In addition, WINPC32 also offers standard C language for logic programming. The C programming can be used for partial (just a customized function) or entire logic controls. PID software configures the I/O of each PID loop corresponding to I/O or other variables. In addition, PID software establishes control parameters, such as PID gains for on-off, or proprietary control loops. GPX is a visualization development tool with which to edit GUI and recipes, program flow control logic, configure alarm logs, and establish security and remote monitoring. The run-time engine includes the Global Data Exchange Server (GDS). The GDS is responsible for executing the hardware and software modules the user has selected and configured as a hybrid system at a predefined priority and timing.

The GPX Windows graphics control software is an HMI-editing software for the PC-based general-purpose industrial controller WINPC32. With its integration and application of WINPC32 and various control modules, GPX offers a wide range of applications for both traditional and high-tech industries.

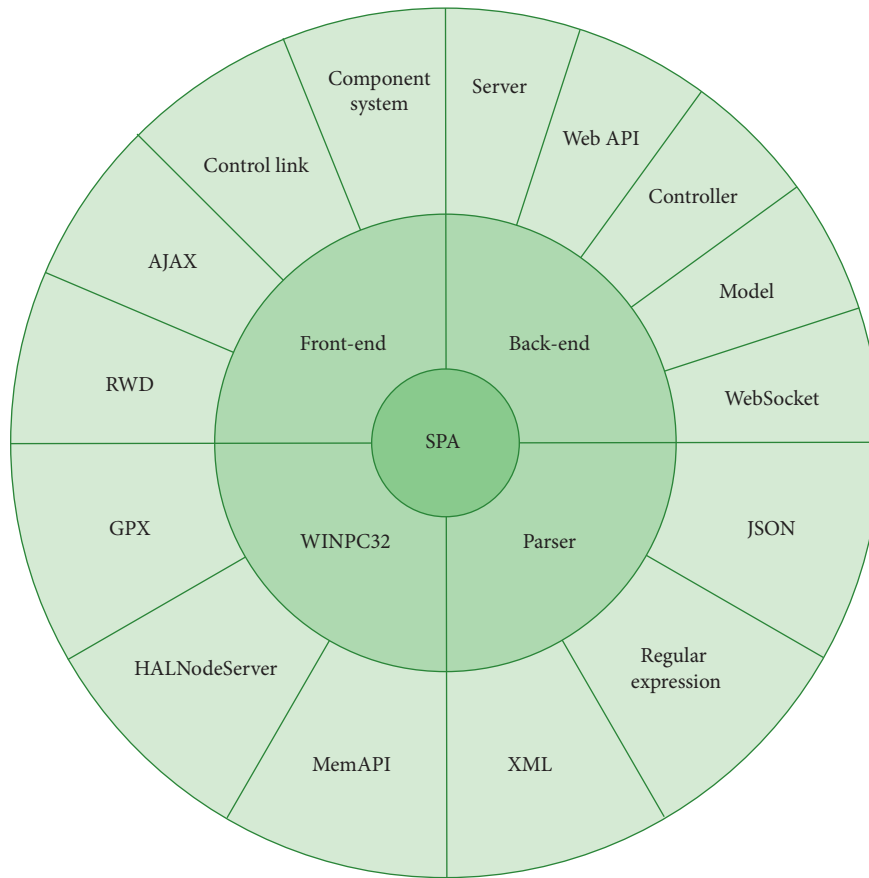


FIGURE 1: Architecture of the general-purpose Web-Based HMI for an industrial controller.

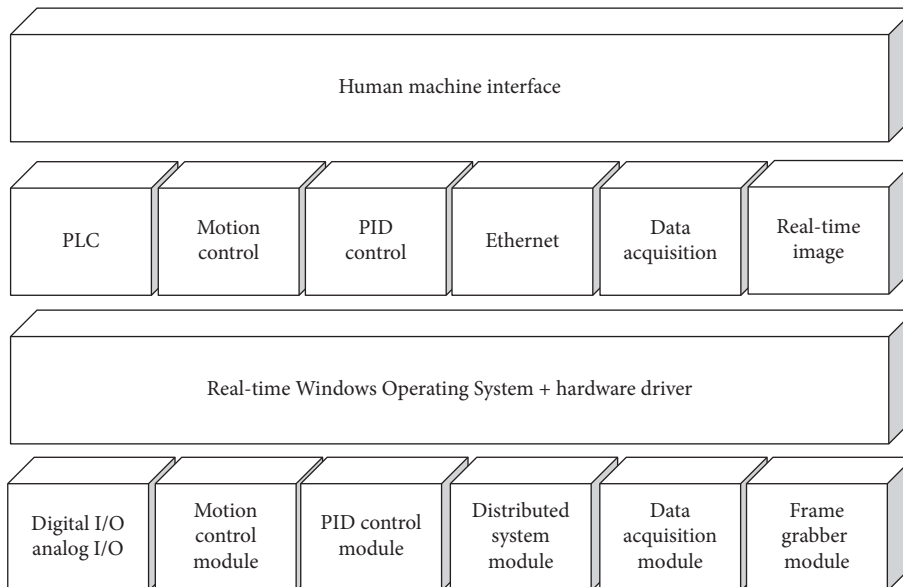


FIGURE 2: The system architecture of WINPC32.

GPX contains two main programs: Windows Maker for developing the controller HMI and Windows Viewer for presenting the results. Developers use GPX’s graphical interface to develop and design HMIs because the program

makes it easy to adjust the component control style and set the memory address mapped to the hardware. After the development phase, GPX exports the files in XML. Figure 3 shows an example of a project created with GPX. The main

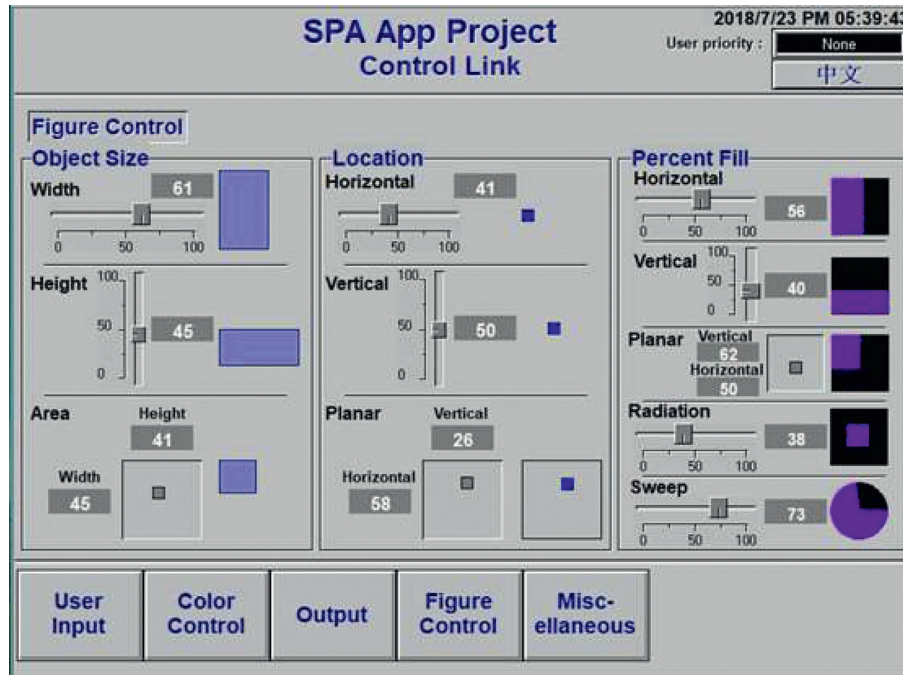


FIGURE 3: SPA project in GPX.

purpose of this study was to translate the data from the original desktop application to the Web application executed on the browser in an XML file.

1.2. Front-End and Back-End. As Web technology has progressed, website functions have become increasingly complex. The structure of web pages increasingly tends toward the division of responsibilities and designs that separate concerns, as in the MVC architecture. To improve user experience, several developers have developed their own Web applications for their websites. SPAs are widely used in websites that require real-time interaction with users and several modern Web technologies, such as AJAX, WebSocket, Webpack, and the Web application programming interface (API), to run efficiently. Large-scale Web projects often require a team of developers.

To equally distribute labor, the architecture of modern Web development is usually divided into two parts: the front-end and back-end. Front-end engineers are mainly responsible for the appearance of user pages in the browser, including the web page style, page layout, user experience, and application functions. Back-end engineers are mainly responsible for server-side data access, database management, API design, website analysis, and website optimization.

The main languages for front-end Web development are Hypertext Markup Language (HTML), CSS, and JavaScript. Depending on the situation, developers can use jQuery, Bootstrap, or other extension libraries and front-end Web development frameworks such as Angular.js, React.js, and Vue.js to create a website. Modular and component-based development makes programs not only easy to build but also easy to maintain. The range of options for back-end server

languages is broad. Developers can use ASP.NET C#, Visual Basic, Java, PHP: Hypertext Preprocessor, Python, Ruby, and Go, among many others. If developers use Node.js as the server, they can use JavaScript for the project's architecture to develop both the front-end and the back-end.

1.3. MVC Architecture. The components of MVC are as follows: "model" refers to data related to the application's business logic and processing of the data and can directly access data in locations such as databases. "View" represents the display logic and the rendering of the page. "Controller" represents control of the flow of Web applications and response to the various events related to user behavior and changes to the model.

Figure 4 displays a diagram of the network architecture in an MVC design. Operations are executed in the following steps: (1) the client uses the browser to send a request, (2) the server accepts the request and sends the command to the corresponding controller, (3) and (4) the controller accesses the model data, (5) the controller sends the data to the view to render the display page, (6) the viewer renders the rendered page back to the controller in HTML, (7) the controller encapsulates and generates the response data to the browser, and (8) the final display page is returned to the browser by the server.

Without dividing the front-end and the back-end, the architecture of the MVC design displays page contents by using server-side rendering to dynamically update the web page through ASP.NET MVC and Ruby on Rails, meaning that a combination of data access and page demonstration is performed on the server side. Each request by the client is regarded as an action, and the method corresponding to a page is generated by the controller.

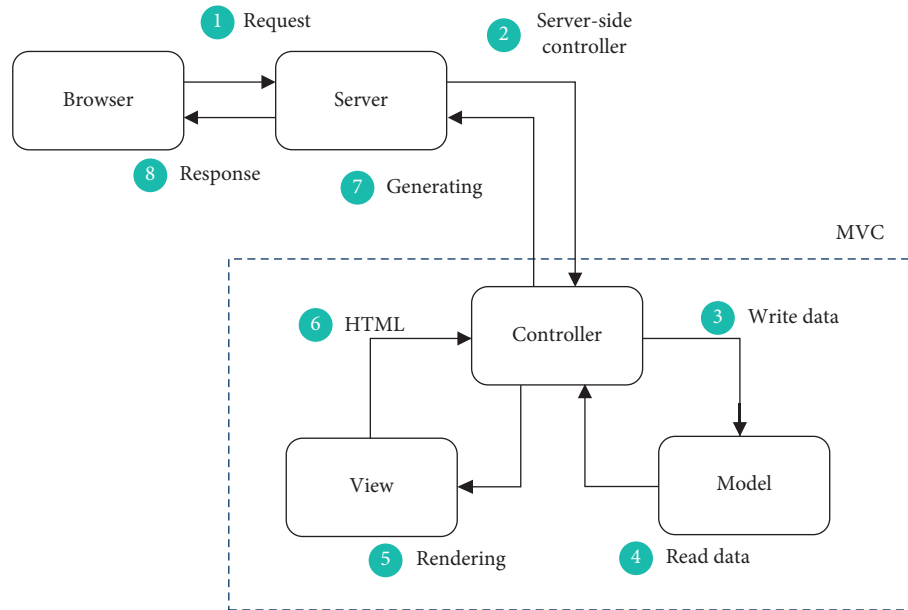


FIGURE 4: Web development architecture of MVC.

Although logic and data can be separated in this structure, labor responsibilities cannot be easily allocated because the engineers responsible for data access and UI design must complete the entire project to debug and develop the program—the engineer responsible for the UI must set up the database and the server. For this reason, the division of labor in this structure becomes unclear.

1.4. Client-Side Rendering. In practice, the view must be extracted from the MVC on the server side. The extracted view is processed by the client’s browser: the page and the data are combined in the browser, a process known as “client-side rendering.” As a result, the server focuses on returning data instead of returning the entire page’s HTML file to the browser to separate the front-end and the back-end. This structure represents the design of modern web page architecture separating concerns and duties.

Making the server focus on returning data instead of returning the entire page’s HTML file to the browser is common practice in modern Web design to separate duties between the front-end and the back-end. However, this approach increases the complexity of the front-end project. Figure 5 displays the web page architecture rendered by the client.

Another simple method can be implemented into the front-end as part of the “view” section of the MVC. In this method, a router processes routing problems on the front-end. The front-end route is usually distinguished from the back-end route by the “#” symbol, as in the uniform Resource Identifier, “http://localhost/#/Home/Gpx.” The corresponding controller handles the flow of data, and the model requests the data from the server through the back-end API. The server returns a response containing only data and a few headers and then temporarily stores the data in the front-end, performs logical operations, and submits a

display logic of the view to render the final view to the user. Although front-end engineering has become complicated, it greatly improves the separation of duties, program maintenance, and development flexibility and reduces the resource burden on the server at high traffic.

1.5. Component Systems. Component systems are an integral part of modern Web design. Component systems begin with the root component. Then, countless reusable subcomponents can be used to construct an entire web page, which can be abstracted into a component tree with trunks and branches. Figure 6 displays a tree diagram of the component system. The relationship between the components can be easily identified as parent-child or sibling-sibling. Component systems can be implemented without special development tools. Component systems are commonly implemented by using a front-end framework, such as Angular.js, React.js, or Vue.js. The development of front-end projects is modular and supports front-end routing and state management functions that make the development of SPAs smoother. In this study, we used Vue.js to develop the component system.

When using Vue.js, the data are transferred between the parent and child components through event emitting and props passing. Vuex can use a public interface to call each component in the parent layers, thereby managing the state of each component in the entire web page. Data can be transferred between sibling components through the `$root.$emit()` and `$root.$on()` functions in the Vue root component, as shown in Figure 7.

1.6. Software Development. The concept of regular expression in computer science is a key tool for writing parser programs. Regular expressions use a single string to describe a series of strings that conform to certain syntax rules. In several text editors, regular expressions are often used to

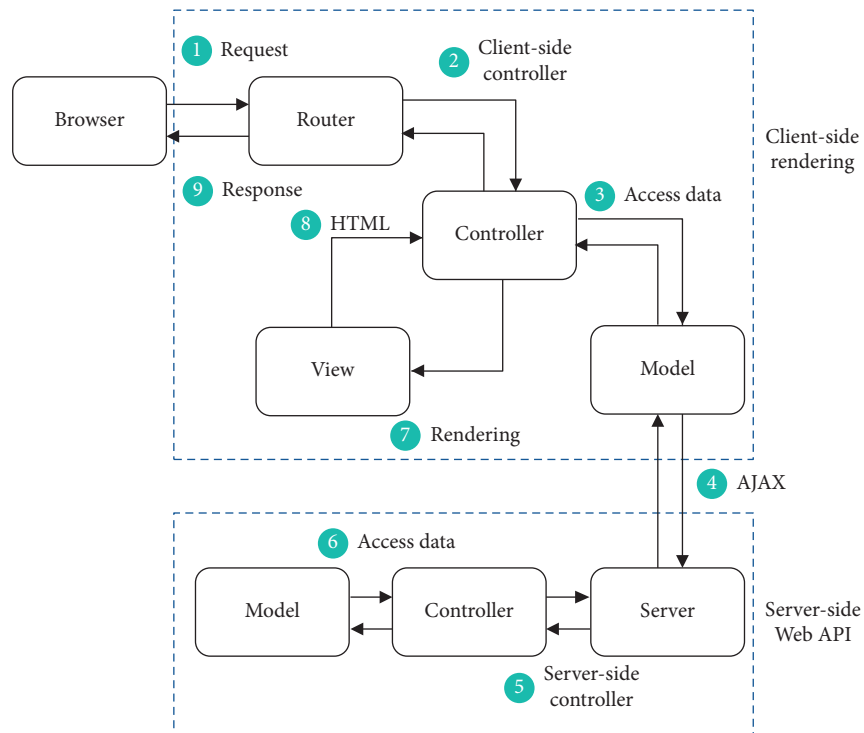


FIGURE 5: MVC architecture with client-side rendering.

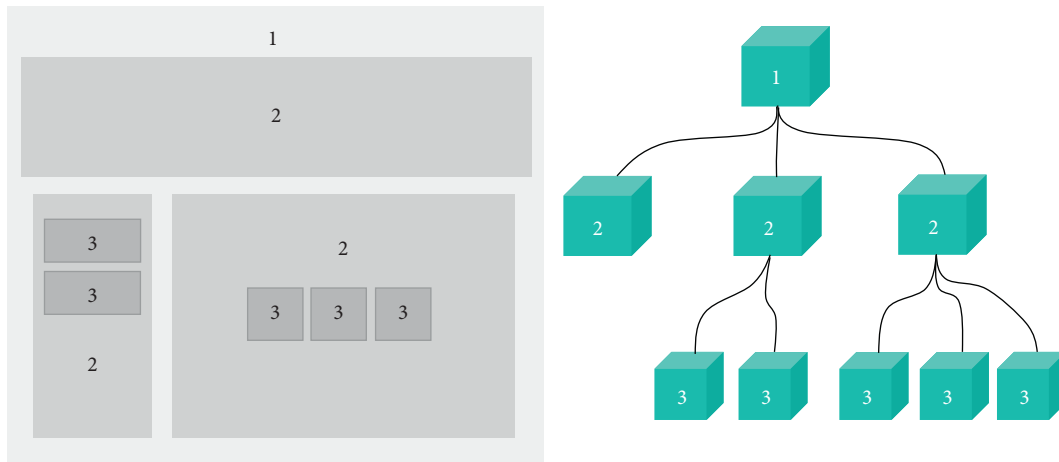


FIGURE 6: Tree diagram of the component system.

retrieve, filter, and replace text that matches a specific pattern. In this study, we used regular expressions to filter out the placement of individual objects, the members of each object, and the real-time data. The data could then be stored in the GPX object generated by JavaScript. When the data had been extracted, the GPX object was output as a module.exports object, allowing it to be imported into other JavaScript programs, such as server.js; by compiling GPX into JSON and defining the Web API, the front-end can access the data at any time. Figure 8 presents the main block diagram of the parser.

Two main tasks were involved in the implementation of the front-end project. The first task was to design and convert

the GPX object from the back-end into various components that could interact with the Web users and completely transplant the GPX HMI to the web page. The second task was to realize the communication interface between the control elements and the AJAX Hypertext Transfer Protocol (HTTP) request. The request sent to the back-end is wrapped in the event handler of each component and is triggered by the event to execute the user’s command.

The implementation of the back-end project also had two main goals. The first goal was to compile the output object of the GPX parser into JSON data and send them to each client to render the GPX style. The second goal was to design a Web API to release the data access capability of WINPC32.

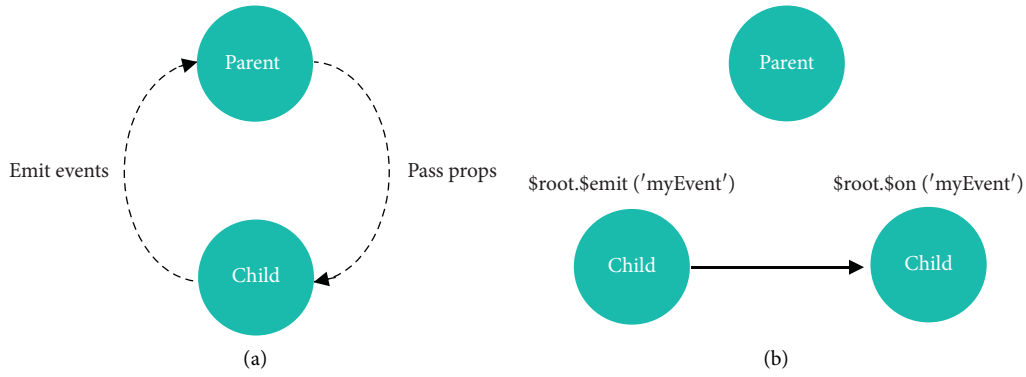


FIGURE 7: Communication among components. (a) Parent-child and (b) sibling-sibling.

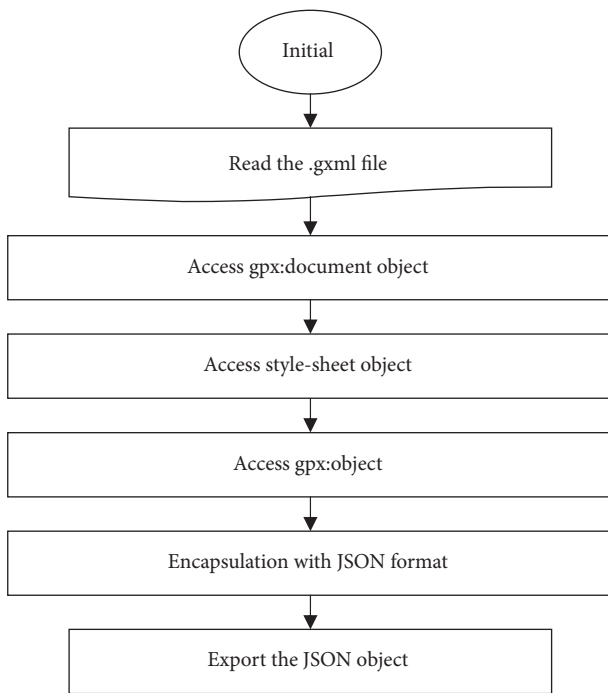


FIGURE 8: Main block diagram of the parser.

The API uses ClientSubscription() and ServerPublish() functions to execute industrial functions so that front-end components can call the controller to run the corresponding processing.

2. Results

Using WINPC32, we implemented the SPA of the GPX window graphics control software, converted XML files into JavaScript objects for web development, implemented object data as the HMI of the Web application, and executed different applications with the back-end WIMPC32 API. The process consisted of three parts:

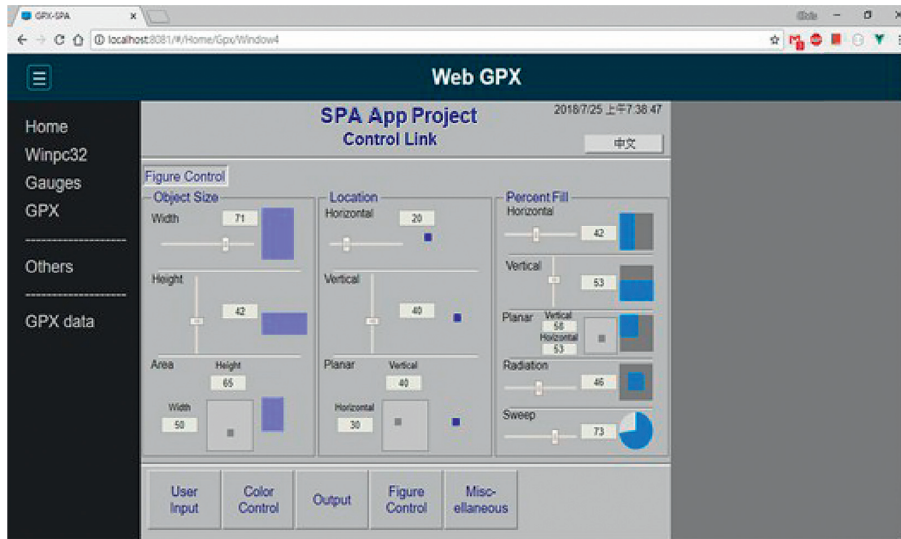
- (1) GPX Parser: converted XML data of GPX objects into JSON for Web development.
- (2) Front-end tasks: the front-end involved two main tasks. The first task was to convert the GPX objects

from the back-end into the web page. The second task was to implement the communication interface for the control components to send AJAX HTTP requests to the back-end. The communication interface was wrapped in the event handler for each component and triggered events to execute the functions of the HMI. The user input command was then sent to the back-end.

- (3) Back-end tasks: the back-end project involved two main tasks. The first task was to compile the output objects of the GPX parser into JSON data and send them to each client to render the GPX style. The second was to design a Web API that integrated WINPC32. The data access function in the front-end control component called the controller for function processing in the form of API to achieve industrial control.

The GPX application project, depicted in Figure 3, was used as the input source for the implementation software shown in Figure 9(a). The reason for selecting this project as an example project was that it included a large number of common control components, which are necessary when designing a general-purpose HMI. After the XML file output by the sample project was read, it was converted into a Web application. Figure 9(b) displays additional SPA implementation corresponding to the classic GPX components. The control link of GPX in the WINPC32 system was running in the software’s real-time mode, in which the SPA had the lowest priority of all the control processes in the controller. Thus, the latency in the data obtained through Internet communication was not considered a serious concern.

2.1. Industrial Controller Case Study. This case study was supported by Taiwan’s Ministry of Science and Technology and involved a quasicontinuous wave (QCW) laser-cutting machine, as shown in Figure 10(a), that used a conventional industrial controller. The control parameters of the QCW laser-cutting machine included laser power, pulse width, repetition frequency, and speed of the laser head movement, which required adjustment for different processing and material specifications. Variation in the laser vaporization



(a)



(b)

FIGURE 9: Web-based HMI results of the SPA project. (a) SPA example project. (b) Other mapping from GPX (left column) to the SPA page (right column).

zone is a determining factor of the accuracy and quality of laser processing. Therefore, real-time in situ monitoring, which conventional controllers lack, should be added to improve the temperature distribution of laser cutting. The user must also change the control parameters according to the temperature distribution of the remote site.

We added an infrared thermal imager to the QCW laser-cutting machine to monitor the material vaporization temperature. The QCW laser-cutting machine had an XY machine table and a Z-axis assembled with an IPG Photonics 1-kW laser head. We used the QCW machine to perform stealth laser dicing of the gallium nitride (GaN) on a silicon wafer, as shown in Figure 10(b). We fixed the value of the numerical aperture to 2.5 cm and changed the focal length of the various focusing lenses. When the focal point was 2.5 cm,

as Figure 10(c) shows, the temperature inside the wafer changed drastically. With such a high-value aperture mirror, the laser beam radius had a high focusing effect inside the wafer. At first, the laser energy was small, and the temperature near the focus area rose. As the upper absorption coefficient increased, the laser light energy caused a sharp rise in temperature above the focus, resulting in damage to the material and creating scars. However, throughout processing, the surface temperature of the GaN layer did not substantially rise.

The motion control on the XY table required to displace the wafer from the focus of the laser and the focus length control required on the Z-axis were performed using a hard real-time control system, WINPC32. The software was written in FB in accordance with IEC61131-3 standards.

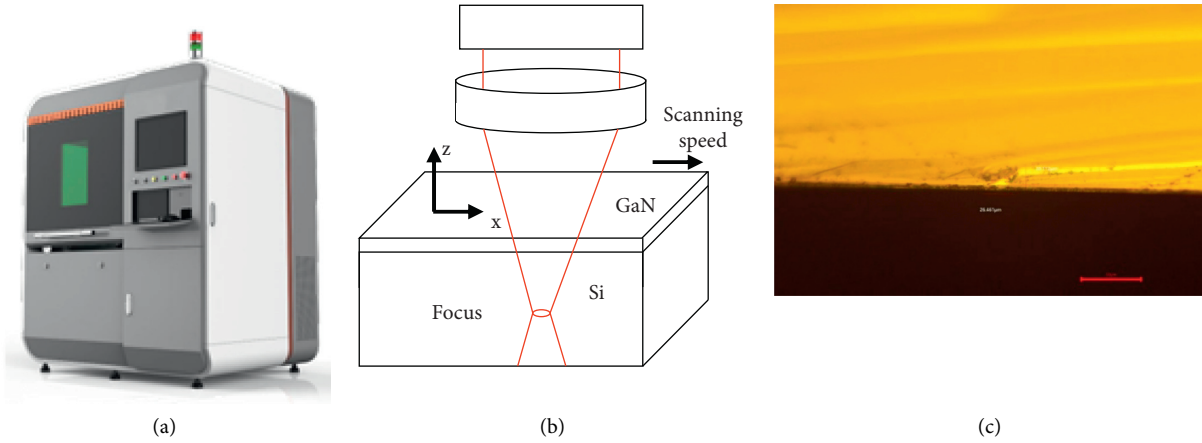


FIGURE 10: Stealth laser dicing using QCW laser. (a) QCW laser-cutting machine. (b) Laser position control. (c) Microscopic images of GaN on silicon control.

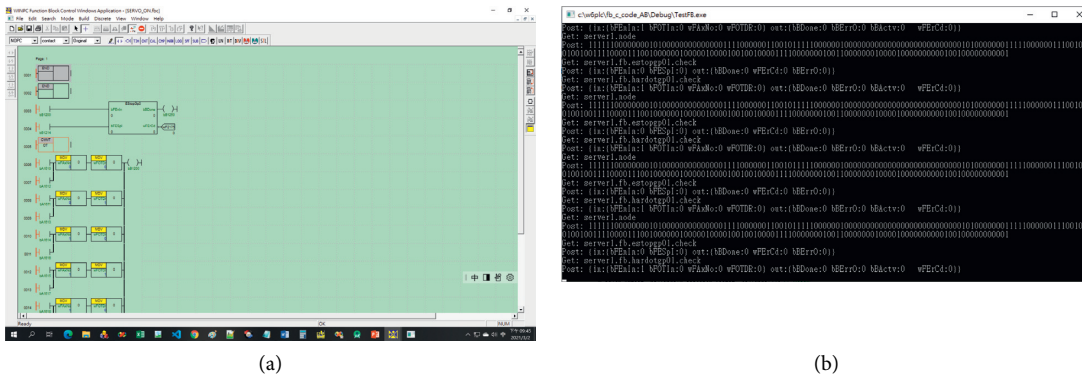


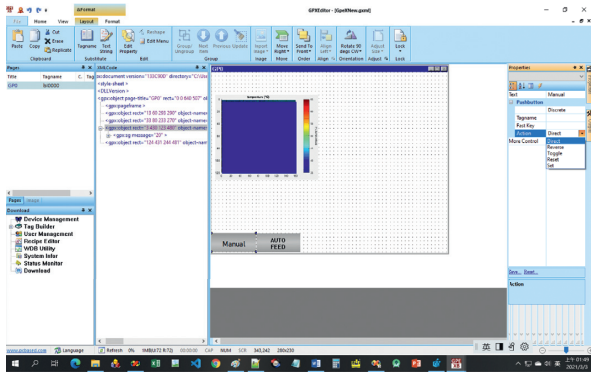
FIGURE 11: JASON data streaming from the PLC. (a) FB for logic and motion control. (b) Data subscription and publishing.

The program flow, as shown in Figure 11(a), is processed between the SPA and the internal PLC controller through the Node.js server. The digital I/O map can be transferred into a series of 0's and 1's. The analog data of the FBs transferred into JSON are shown in Figure 11(b) as an example. The SPA page following the component conversion from the GPX page can utilize the JSON data streaming to simultaneously display the controller and the sensor statuses on smartphones by using the MVC architecture and the client-side rendering, as shown in the flowchart in Figure 5. The PLC was running in a hard real-time environment and using real-time kernels, including RTX from Microsoft. The JSON data streaming publishes the hard real-time control data into software real-time monitoring data that the client SPA page is subscribing.

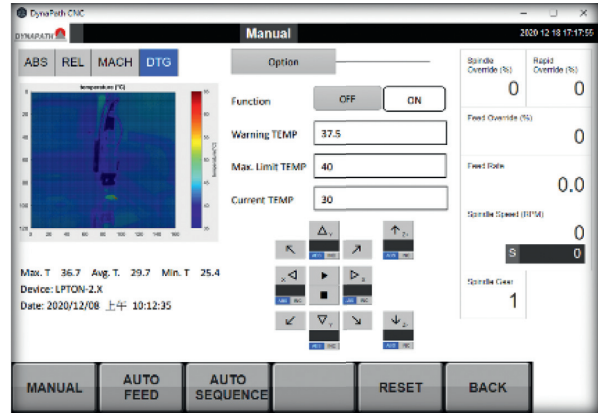
A new control page corresponding to the material vaporization temperature monitoring with an infrared thermal imager was added to the conventional controller. The execution of the Web-based HMI on the SPA technology for the QCW laser-cutting machine is shown in Figure 10. We first edited the control page on GPX in WINPC32 and then converted it into web page

components with the structure displayed in Figure 6. Figure 12(a) shows the process of adding the HMI components one by one to the GPX page. Each component is linked to one of the hard real data defined in the FB, as shown in Figure 12(b). A thermal image was taken at 10 fps and was encoded through the vfw32.lib in a soft real-time process. The receipt download for the laser-cutting control can be implemented in a soft real-time process, as shown in Figure 12(c). The Web-based SPA can be accessed through Node.js.

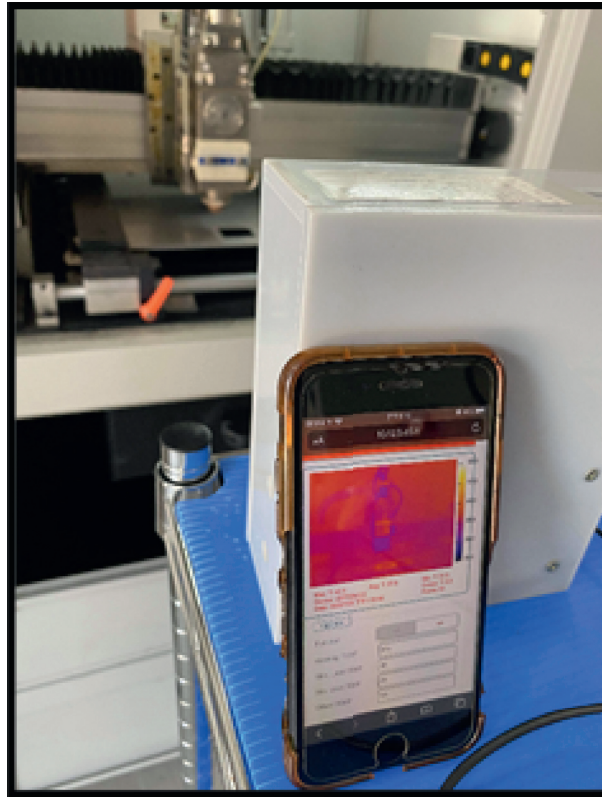
SPAs on smartphones enable users to remotely monitor the laser-cutting process in real time. With SPAs, experts at remote sites can adjust the corresponding control parameters on a web page and monitor the temperature distribution changes of the laser vaporization zone subject to control adjustment in real time. This is a breakthrough for QCW laser machines, which up until now had not allowed remote users to access measurement data and control parameters. The studies reported in [3, 4] entail the transfer of data from the traditional SCADA or PLC to a PC. Our study implemented Web-based technology in PC-based industrial controllers without altering the original Modbus



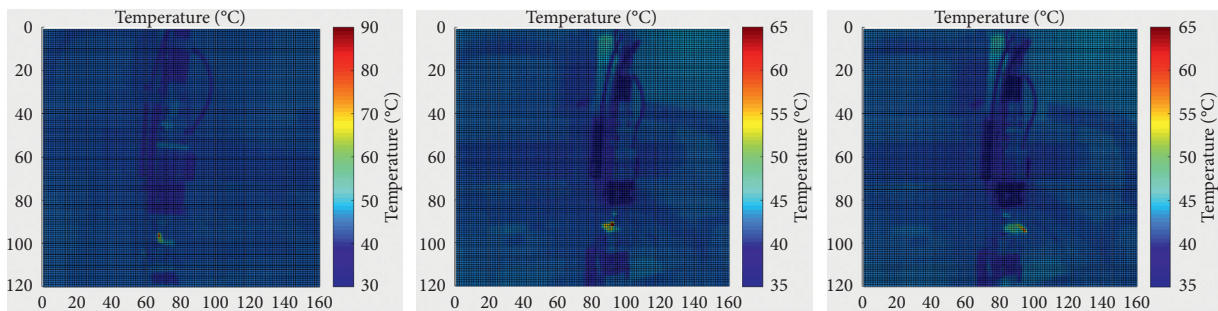
(a)



(b)



(c)



(d)

FIGURE 12: Example of Web-based HMI using SPA on the QCW laser machine. (a) Implementation of GPX. (b) Example of control. (c) SPA on web page. (d) Thermal images of laser dicing.

communication arrangement. Our general-purpose Web-based HMI developed for an industrial controller has the following features:

- (1) Direct conversion of the XML file output by the GPX maker to the Web version of the HMI
- (2) Use of browsers on different operating systems to process real-time data streaming
- (3) Remote real-time monitoring and control for conventional industrial controllers
- (4) Simplified program maintenance and automatic adjustment of the web page view on mobile devices

3. Conclusions

Millions of industrial controllers around the world still require IoT technology to transmit controller instant messages across platforms. The first step for software engineers, which may also be the most difficult step, is to find a simple solution to connect conventional controllers to the Internet without rearranging the device's wiring. This study demonstrated a simple strategy for conventional controllers to enter Web-based applications. The solution was to convert the necessary control pages from the conventional controller's HMI into a Web-based HMI. The control pages must be converted into XML at the beginning of the process. XML and JSON enable the information to flow through cross-platform devices across a variety of operating systems and Web browsers. Data flow can be controlled and monitored by using SPAs implemented through AJAX and WebSocket, which can communicate with the back-end Node.js server to transfer data. As reported in the "Results" and "Industrial controller case study" sections of this paper, we converted a number of commonly used control components from conventional industrial controllers to Web-based HMIs. We demonstrated that conventional machines that had not allowed remote users to access measurement data and control parameters could be viewed and controlled through the Internet. The integration of easy-to-access and open-source software such as AJAX and the Node.js server enabled the transformation, making conventional industrial controllers compatible with popular IoT. The results of our research can serve as a reference for software programmers seeking to modernize standalone conventional industrial machines and their controllers. OpenVPN has implemented many features for authentication, encryption, and management that may allow us to use VPN communication in the future to secure network traffic in our system.

Data Availability

The XML format data used to support the results of this study were originally exported by GPX Windows graphics control software. The JSON format data used for web development are generated by GPX Parser and can be obtained from the corresponding author upon request.

Conflicts of Interest

The authors declare that they have no conflicts of interest.

Acknowledgments

This work was supported by Ministry of Science and Technology, Republic of China, under Grant no. MOST 109-2622-E-262-005-CC3. This manuscript was edited by Wallace Academic Editing.

References

- [1] H. Boyes, B. Hallaq, J. Cunningham, and T. Watson, "The industrial internet of things (IIoT): an analysis framework," *Computers in Industry*, vol. 101, pp. 1–12, 2018.
- [2] W. Z. Khan, M. H. Rehman, H. M. Zangoti, M. K. Afzal, N. Armi, and K. Salah, "Industrial internet of things: recent advances, enabling technologies and open challenges," *Computers & Electrical Engineering*, vol. 81, Article ID 106522, 2020.
- [3] S. Phuyal, D. Bista, D. Bista, J. Izykowski, and R. Bista, "Design and implementation of cost efficient SCADA system for industrial automation," *International Journal of Engineering and Manufacturing*, vol. 10, no. 2, pp. 15–28, 2020.
- [4] Y. Kondratenko, O. Kozlov, O. Gerasin, A. Topalov, and O. Korobko, "Automation of control processes in specialized pyrolysis complexes based on web SCADA systems," in *Proceedings of the IEEE 9th International Conference on Intelligent Data Acquisition and Advanced Computing Systems: Technology and Applications (IDAACS)*, Bucharest, Romania, September 2017.
- [5] I. Qasim, M. W. Anwar, F. Azam, H. Tufail, W. H. Butt, and M. N. Zafar, "A model-driven mobile HMI framework (MMHF) for industrial control systems," *IEEE Access*, vol. 8, pp. 10827–10846, 2020.
- [6] G. Caiza, A. Nuñez, C. A. Garcia, and M. V. Garcia, "Human machine interfaces based on open source web-platform and OPC UA," *Procedia Manufacturing*, vol. 42, pp. 307–314, 2020.
- [7] R. Sood, G. Singh, and S. K. Chawla, "Single page application: architecture and application," *Recent Trends in Programming Languages*, vol. 6, no. 1, pp. 27–30, 2019.
- [8] A. Mesbah and A. Deursen, "Migrating multi-page web applications to single-page AJAX interfaces," in *Proceedings of the 11th European Conference on Software Maintenance and Reengineering (CSMR'07)*, pp. 181–190, Amsterdam, The Netherlands, April 2007.
- [9] M. Uehara, "Experiences with a single-page application for learning programming," in *Proceedings of the International Conference on Broadband and Wireless Computing, Communication and Applications*, pp. 55–66, Yonago, Japan, October 2020.
- [10] J. Gunawan and R. R. Kosala, "Genie enterprise resource planning for small medium enterprises implementing single page web application," *E&ES*, vol. 426, no. 1, Article ID 12170, 2020.
- [11] <https://dojotoolkit.org/reference-guide/1.7/quickstart/introduction/whydojo.html>.
- [12] F. Shahzad, "Modern and responsive mobile-enabled web applications," *Procedia Computer Science*, vol. 110, pp. 410–415, 2017.
- [13] S. Deshmukh, D. Mane, and A. Retawade, "Building a single page application web front-end for E-learning site," in

- Proceedings of the 2019 3rd International Conference on Computing Methodologies and Communication (ICCMC)*, pp. 985–987, Erode, India, March 2019.
- [14] P. Chynał and J. Sobiecki, “Eyetracking evaluation of different chart types used for web-based system data visualization,” in *Proceedings of the IEEE Conference Network Intelligence Conference (ENIC)*, pp. 159–164, Wroclaw, Poland, September 2016.
- [15] S. Scepanovic, T. Vujicic, and P. Radunovic, “Web application for lightning activity monitoring system (LAMS),” in *Proceedings of the IEEE Conference Information System and Technologies (CISTI)*, pp. 1–4, Lisbon, Portugal, June 2017.
- [16] A. Voinov, C. W. Yang, and V. Vyatkin, “Automatic generation of function block systems implementing HMI for energy distribution automation,” in *Proceedings of the IEEE 15th International Conference on Industrial Informatics (INDIN)*, pp. 706–713, Warwick, UK, July 2017.
- [17] G. Wang, “Improving data transmission in web applications via the translation between XML and JSON,” in *Proceedings of the 2011 Third International Conference on Communications and Mobile Computing*, pp. 182–185, Qingdao, China, April 2011.
- [18] N. Nurseitov, M. Paulson, R. Reynolds, and C. Izurieta, “Comparison of JSON and XML data interchange formats: a case study,” *Caine*, vol. 9, pp. 157–162, 2009.
- [19] B. Cvijić, D. Pašalić, D. Bundalo, and Z. Bundalo, “Cloud based web application supporting vehicle toll payment system,” in *Proceedings of the IEEE, 5th Mediterranean Conference on Embedded Computing (MECO)*, pp. 489–492, Bar, Montenegro, June 2016.
- [20] V. Okanovic, “Web application development with component frameworks,” in *Proceedings of the IEEE 37th International Convention on Information and Communication Technology, Electronics and Microelectronics (MIPRO)*, pp. 889–892, Opatija, Croatia, May 2014.
- [21] N. G. Obbink, I. Malavolta, G. L. Scoccia, and P. Lago, “An extensible approach for taming the challenges of JavaScript dead code elimination,” in *Proceedings of the IEEE 25th International Conference on Software Analysis, Evolution and Reengineering (SANER)*, pp. 291–401, Campobasso, Italy, March 2018.
- [22] G. Zhang and J. Zhao, “Scenario testing of AngularJS-based single page web applications,” in *Proceedings of the International Conference on Web Engineering*, pp. 91–103, Daejeon, Republic of Korea, June 2019.
- [23] P. Papcun, E. Kajáti, and J. Koziorek, “Human machine interface in concept of industry 4.0,” in *Proceedings of the 2018 World Symposium on Digital Intelligence for Systems and Machines (DISA)*, pp. 289–296, Kosice, Slovakia, August 2018.
- [24] K. Tange, M. De Donno, X. Fafoutis, and N. Dragoni, “A systematic survey of industrial internet of things security: requirements and fog computing opportunities,” *IEEE Communications Surveys & Tutorials*, vol. 22, no. 4, pp. 2489–2520, 2020.
- [25] M. Iqbal and I. Riadi, “Analysis of security virtual private network (VPN) using openVPN,” *International Journal of Cyber-Security and Digital Forensics*, vol. 8, no. 1, pp. 58–65, 2019.
- [26] Q. Zhang, J. Li, Y. Zhang, H. Wang, and D. Gu, “Oh-Pwn-VPN! security analysis of OpenVPN-based Android apps,” in *Proceedings of the International Conference on Cryptology and Network Security*, pp. 373–389, Hong Kong, China, December 2017.
- [27] A. Skendzic and B. Kovacic, “Open source system OpenVPN in a function of virtual private network,” in *IOP Conference Series: Materials Science and Engineering*, vol. 200, no. 1, p. 12065, 2017.
- [28] L. Roepert, M. Dahlmanns, I. B. Fink, J. Pennekamp, and M. Henze, “Assessing the security of OPC UA deployments,” 2020, <https://arxiv.org/abs/2003.12341>.
- [29] A. Napoleone, M. Macchi, and A. Pozzetti, “A review on the characteristics of cyber-physical systems for the future smart factories,” *Journal of Manufacturing Systems*, vol. 54, pp. 305–335, 2020.
- [30] <http://hacontrols.com.tw/Products/Product-typeA-2.asp?nplSinuYwbaIxJ6ZkoZI>.

Research Article

Research on Mining of Applied Mathematics Educational Resources Based on Edge Computing and Data Stream Classification

Liping Lu ¹ and Jing Zhou²

¹*School of Statistics and Mathematics, Henan Finance University, Zhengzhou 451464, China*

²*Data Analytics Department, Cabin John Consulting Corp., Arlington, VA 22202, USA*

Correspondence should be addressed to Liping Lu; luliping@hafu.edu.cn

Received 27 January 2021; Revised 10 March 2021; Accepted 14 March 2021; Published 26 March 2021

Academic Editor: Hsu-Yang Kung

Copyright © 2021 Liping Lu and Jing Zhou. This is an open access article distributed under the Creative Commons Attribution License, which permits unrestricted use, distribution, and reproduction in any medium, provided the original work is properly cited.

Facing the massive data of higher education institutions, data mining technology is an intelligent information processing technology that can effectively discover knowledge from the massive data and can discover important information that people have previously ignored from the huge data information. This article is dedicated to the development of applied mathematics education resource mining technology based on edge computing and data stream classification. First of all, this article establishes a resource system architecture suitable for existing applied mathematics education through edge computing technology, which can effectively improve the efficiency of data mining. Secondly, the data stream classification algorithm is used for information extraction and classification integration of massive applied mathematical education data. This method provides potential and valuable information for decision-makers and education practitioners. Finally, the simulation and performance test of the system verify that it has the functions of mathematical information mining and data processing. This system will provide strong support for applied mathematics education reform.

1. Introduction

In recent years, with the rapid development of education, colleges and universities have also developed by leaps and bounds [1, 2]. Colleges and universities are not only expanding the scale of running schools but also increasing the scale of enrollment. With the increase in the number of teachers and the number of students in school, most of the traditional teaching management models have been unable to adapt to the development of schools [3]. In order to effectively improve the efficiency and level of education management, various colleges and universities have increased their investment in informatization, and various information management systems have been continuously used, such as educational administration management system, student achievement management system, student status management system, university personnel management system, and

library information management system [4, 5]. The use of information system greatly improves work efficiency and level [6]. The system saves manpower and material and financial resources and greatly facilitates the daily management of colleges and universities [7]. However, various database systems have accumulated a large amount of data in their use. Over time, these historical data have not been used well. On the contrary, they have become junk files and have been deleted and abandoned [8, 9]. The reason is that these management systems can realize the functions of data entry, query, and modification, but they cannot discover the internal connections and corresponding rules between these data [10].

With the rapid development of database technology and the wide application of database management systems, how to make full use of data and dig out useful information and knowledge is a question of great concern to organizations with large amounts of data [11, 12]. Derived from ancient

data analysis and statistics technology plus modern artificial intelligence, database, and statistics-related technologies, the collection of the above methods realizes interdisciplinary database knowledge discovery, namely, “data mining” [13, 14]. At present, the application of data mining technology in the field of education management has not yet completed, and universities mainly stay in the use of databases in terms of information construction. Really use data mining technology to mine useful information for education, and obtain very little valuable information [15]. However, with the continuous use of various information management systems in colleges and universities, the amount of data storage is increasing, and the application of data mining technology in the teaching management of colleges and universities must become a trend [16, 17].

If the data from the grassroots can be effectively used, the valuable information hidden in the data can be mined, and the value of the data can be improved, which will provide decision-makers with a better factual basis and basis, thereby changing management methods and formulating better management and formulation to improve the quality and level of running schools [18, 19]. Facing the massive data of higher education institutions, data mining technology is an intelligent information processing technology that can effectively discover knowledge from the massive data and can discover important information that people have previously ignored from the huge data information. This article is dedicated to the development of applied mathematics education resource mining technology based on edge computing and data stream classification. We discussed the research progress on mathematics education in the second part. The third part discusses the related applications and research of edge computing. The fourth part describes the mining methods of applied mathematics education resources. The fifth part is the actual verification of the case and the performance analysis of the model. In the sixth part, we summarized the full text and looked forward to the future.

2. Overview of Applied Mathematics Education

As the main front of mathematics education, ecological research in mathematics classrooms has received more and more attention [20, 21]. The previous open teaching of mathematics was mostly limited to the construction of open questions and the development of classroom operations and seldom aimed at the overall research as a model. The development of the application of ecology in the field of education provides us with a new perspective on open teaching [22, 23]. Therefore, the author combines the research history of education ecology and open teaching of mathematics, analyzes and discusses mathematics classroom teaching from the perspective of ecology, deeply excavates the ecological characteristics of open mathematics teaching, and expounds the feasibility and necessity of mathematics open teaching research. It puts forward a construction strategy and specific implementation process [24, 25]. The conceptual diagram of applied mathematics education mining is shown in Figure 1.

In educational resources, question banks are very important to educational resources, while traditional question banks focus on providing educators or students with exercises and statistical analysis of students’ learning through the right or wrong or scores of the exercises [26, 27]. In order to evaluate the learning situation of students, it cannot conduct effective evaluation and evaluation for individual students nor can it specifically understand the degree of mastery of knowledge points of different students [28, 29]. Therefore, the traditional question bank system cannot provide effective tutoring functions for individual students. In order for the question bank resources to effectively guide students and improve their learning and thinking ability in the process of doing questions, the question bank resources need to contain more knowledge information, so useful knowledge information needs to be dug out from the question bank [30, 31]. The schematic diagram of the applied mathematics education mining system architecture is shown in Figure 2.

Process ontology is a subtype of ontology. It describes related process models in the domain in a declarative way and needs to express concepts and relationships such as processes, activities, and timing in the domain [32, 33]. Foreign research on process ontology mainly includes the help of OWL description language, proposes a layered network ontology language business-OWL, and applies this language to the decomposition and formulation of dynamic business processes [34]. Celentano et al. proposed the application of process ontology to the exam business process specification framework, which realized the semantic capture and sharing in the B2B e-commerce model and was able to perform knowledge deduction and knowledge reasoning on shared information [35]. Professor Fan Yuxin of Tsinghua University and others proposed a design process description metamodel based on extensible markup language XML and process ontology. The model constructs the description rules of the core elements of the process definition language based on extensible markup language to realize the multidisciplinary design optimization process and information. It can be seen that the research of process ontology is closely related to application, but the process ontology constructed in different application fields is also different in representation and structure [36].

3. Overview of Edge Computing Technology

The ultralarge bandwidth and extremely low-latency service access of 5G puts new demands on the network [37]. The traditional network structure is a tree structure, and the business layer needs to be converted to a central node for processing, but when facing big data business scenarios, problems arise [38]. When all services are deployed to the central node, the network load is greatly increased and the network delay time is longer, which puts forward higher requirements on network bandwidth and delay performance. In order to solve the problem of limited computing storage space and power consumption of mobile terminals, we believe that it is necessary for i to migrate high-complexity, high-energy-consuming computing tasks to the

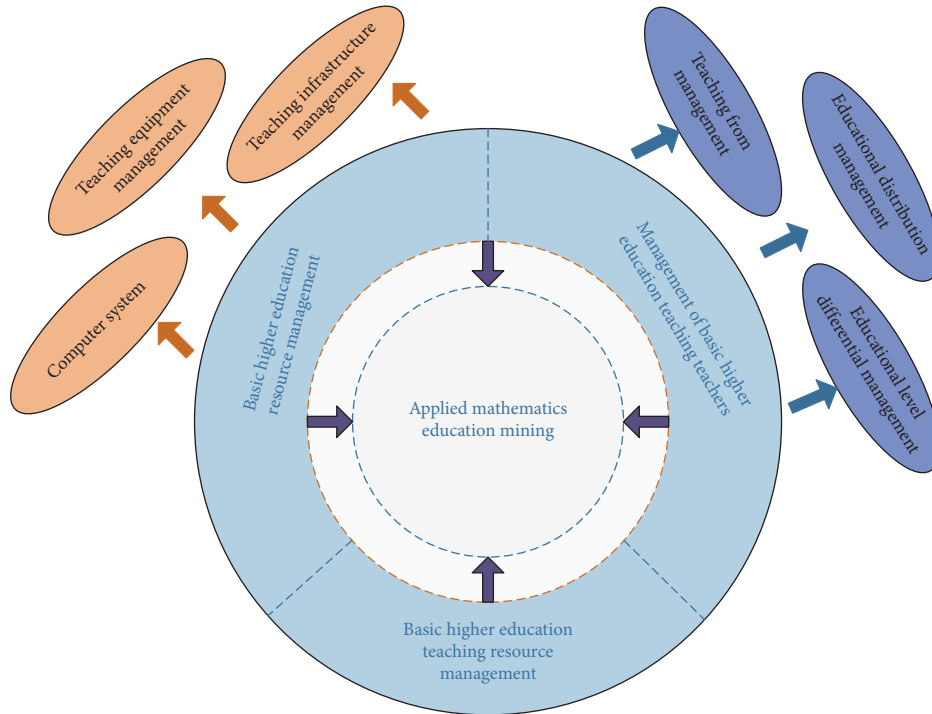


FIGURE 1: Schematic diagram of applied mathematics education mining concept.

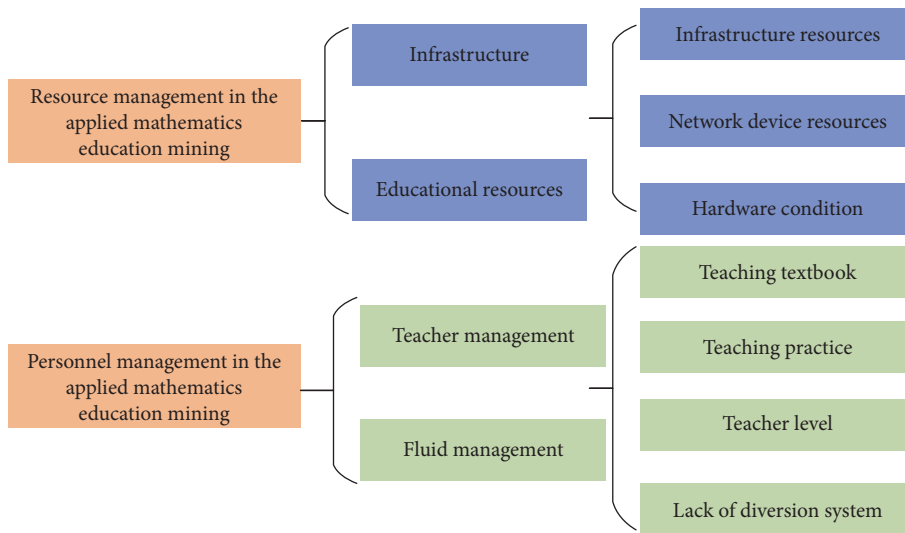


FIGURE 2: Schematic diagram of applied mathematics education mining system architecture.

server side of the cloud computing center to reduce energy consumption. This technology can consume mobile terminals and extend their standby time. However, the method of migrating computing tasks to cloud computing centers also increases the data transmission delay, which has a certain impact on delay-sensitive business applications and QoS. Mobile edge computing provides great possibilities for service innovation at the edge of the network. The conceptual diagram of mobile edge computing is shown in Figure 3.

Mobile edge computing (MEC) can be defined as an implementation of edge computing, which introduces

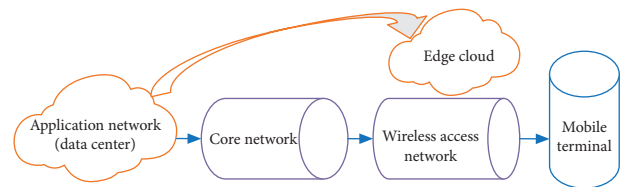


FIGURE 3: Conceptual diagram of mobile edge computing.

computing and storage functions to the edge of the radio access network, thereby reducing waiting time by moving the cloud and service platform to the edge of the network. As

shown in Figure 3, using servers deployed at the edge of the network, mobile operators can provide suitable production and operating environments for various upper-layer applications, and “sink” services down to mobile terminals to reduce network congestion. Deploying the application server at the edge of the wireless network can make full use of redundant computing resources at the edge of the network, and mobile devices and IoT devices can achieve low completion delays for computing tasks.

4. Mining of Applied Mathematics Education Resources

4.1. Data Stream Classification. Classification technology is the study of how to assign observed samples to predefined categories. In recent years, there have been more and more researches on data stream mining. Compared with static data, data stream data have the characteristics of high speed, unlimited, concept drift, concept evolution, and a small number of tags. According to the type of classifier used, the data stream is classified into a single classification model and an integrated classification model. The data stream contains a lot of information [39].

The concept drift phenomenon in the unstable data stream seriously reduces the classification accuracy, so this paper proposes a dynamic weighting scheme to solve this problem. This scheme explains in detail how to assign weights to all training examples in the data block. The higher the weight of the example, the greater the impact on the classifier training process:

$$\Pr[A(X) \in \hat{D}] \leq e^{[X, X']} \Pr[A(X') \in \hat{D}],$$

$$\tilde{p}(n, m) = p(n, m) * h(n) = \sum_{L=-N_1}^{N_1} p(n-L, m)h(L). \quad (1)$$

In this way, you can directly control which instances at the current moment should be set with higher weights so that the trained classifier can better adapt to the current concept:

$$\left. \begin{aligned} \tilde{p}(0) &= h(-255)p(-255) + \dots + h(0)p(0) + \dots + h(255)p(255), \\ \tilde{p}(1) &= h(-255)p(-255) + \dots + h(0)p(1) + \dots + h(255)p(255), \\ &\vdots \\ \tilde{p}(255) &= h(-255)p(-255) + \dots + h(0)p(255) + \dots + h(255)p(255), \end{aligned} \right\} \quad (5)$$

$$\delta_i^{(n_i)} = \frac{\partial}{\partial z_i^{(n_i)}} J(W, b; x, y) = \frac{\partial}{\partial z_i^{(n_i)}} \frac{1}{2} \|y - h_{w,b}(x)\|^2 = -(y_i - a_i^{(n_i)}) \cdot f'(z_i^{(n_i)}).$$

$$= \left(\sum_{j=1}^{S_{sq}} W_{ji}^{n_i-1} \delta_j^{(n_i)} \right) f'(z_i^{n_i-1}).$$

$$\delta_i^{(n_i)} = \frac{\partial}{\partial z_i^{(n_i)}} J(W, b; x, y),$$

$$\delta_i^{(n_i)} = \frac{\partial}{\partial z_i^{(n_i)}} \frac{1}{2} \|y - h_{w,b}(x)\|^2 = -(y_i - a_i^{(n_i)}) \cdot f'(z_i^{(n_i)}). \quad (2)$$

The biggest difference between data flow and other data is that data flow is time-sensitive; that is, only newer instances can reflect the trend of data changes. Therefore, the importance of the examples in the data stream for training the classifier will change over time; especially in the case of a nonstationary environment, if a concept drift occurs, the data distribution at the current moment will be significantly different from the previous distribution:

$$\delta_i^{(l)} = \left(\sum_{j=1}^{S_{l+1}} W_{ji}^{(l)} \delta_j^{(l+1)} \right) f'(z_i^{(l)}), \quad (3)$$

$$\tilde{P}_2 = s \cdot P_2 \cdot R + L.$$

When processing data streams, it is necessary to consider the problem of data stream processing in nonstationary environments. At this time, it is often not feasible to use only naive Bayes classifiers because in nonstationary situations, it is not enough to just deal with the incoming instances. It is also necessary to consider the problem of concept drift and make appropriate responses to it:

$$v_{ij}^{e+1} = W + V_{IJ}^e + C_1 * R_1 * (pBest_{ij} - P_{ij}^e) + C_2 * R_2 * (gBest_{ij} - P_{ij}^e), \quad (4)$$

$$s = tr(P_{K1}^T \cdot P_{k2} \cdot R) / tr(P_{K2}^T \cdot P_{k2}).$$

Since the naive Bayes classifier has no concept drift detection mechanism and the ability to adapt to concept drift, it is not suitable for processing data streams with concept drift. In this case, the classification accuracy of the naive Bayes classifier will be significantly reduced:

With the arrival of data blocks, new tag data may be generated. The appearance of the new mark may be a set of feature values that have not been seen before, or a known mark that has not been seen before, or both. Therefore, both feature and mark space are taken into consideration.

4.2. Mining of Applied Mathematics Educational Resources Based on Data Stream Classification. Among educational resources, the question bank is very important to educational resources. The traditional question bank focuses on providing exercises for educators or students, and statistical analysis of students' learning through the scores of the exercises. But it can only be used to evaluate the learning status of students as a whole. It cannot effectively evaluate and evaluate individual students, nor can it specifically understand the degree of mastery of knowledge points of different students.

The displacement of the center of gravity is used to describe the effect of applying mathematical mining under different data stream classification indicators. The classic barycentric coordinate is a coordinate defined on a plane polygon, not limited to a specific coordinate system. The points in the polygon are expressed linearly by the vertices of the polygon, and the combination coefficient is the center of gravity coordinate. In order to generalize the construction method of GBCs, this paper understands the barycentric coordinates from the perspective of linear algebra from the recursion, discusses the restriction conditions when recursing the barycentric coordinates from the two-sided polygon to the $n+1$ polygon, and gives a method for constructing the barycentric coordinates kind of new ideas. It is not limited to those functions that have geometric meaning, as long as a function that satisfies the inequality relationship is constructed, a set of centers of gravity coordinates can be obtained. The displacement of the center of gravity is used as an index to measure the effect of applying mathematics mining under different data stream classification indexes, as shown in Figure 4.

As shown in Figure 4, under different data stream classification indicators, there are great differences in the application of mathematical mining. Therefore, the importance of example data in training the classifier will change over time, especially in nonstationary environments. If a concept drift occurs, the data distribution at the current moment will be different from the previous one. The distribution is significantly different [40].

We have added relevant citations to the revised manuscript. In order to compare the effectiveness and efficiency of the model established in this paper, we compare the model established in this paper with the methods in recent international references [40–42]. Most of the existing data stream adaptive classification models usually assume that the true label can be obtained after the data are input into the classification model to obtain the predicted label. However, this assumption is unreasonable in some cases because data labeling is usually expensive and time-consuming.

Therefore, we use the accuracy of the model as a comparison index to compare the particle swarm and the neural network optimized by ADAM [43, 44]. The application mathematics mining effect of these three models on the three sample sets is shown in Figure 5.

The experimental data in Figure 5 reflect some of the problems in information mining in applied mathematics education. Compared with static data, data stream data have the characteristics of high speed, unlimited, concept drift, concept evolution and a small number of tags. According to the type of classifier used, the data stream is classified into a single classification model and an integrated classification model. The data stream contains a lot of information. The concept drift phenomenon in the unstable data stream seriously reduces the classification accuracy, so this paper proposes a dynamic weighting scheme to solve this problem. Therefore, the lack of necessary authentication information during the automatic authentication process will cause the automatic authentication to fail. According to data analysis, the most important problem is mainly because the computer cannot effectively understand the information provided by the exercise.

5. Case Analysis of Mining of Applied Mathematics Educational Resources

5.1. Sample Data Collection. In educational resources, question banks are very important to educational resources, while traditional question banks focus on providing exercises for educators or students and statistical analysis of students' learning conditions through the correctness and wrongness or scores of the exercises. Through the above research on the edge computing and data stream classification model, the network throughput of the applied mathematics education resource mining system is summarized.

The largest network power consumption is when a large amount of data are sent and received. In order to reduce the power consumption of the terminal device, in actual applications, the data should be sent in a short time as much as possible to avoid frequent waking up of the wireless network card. Based on the above research, we propose a scheme to test the network throughput of the applied mathematics education resource mining system. Figure 6 shows the network test of applied mathematics education system resources in different network environments.

It can be seen from Figure 6 that, under different network environments, the error rate of predicting applied mathematics education system resource network sample datasets is low. It can be seen that the data stream classification technology has effectively improved the quality and classification of original applied mathematics education information data samples. Figure 7 shows the simulation results of applied mathematics education system resource throughput under different test standards.

It can be seen from Figure 7 that, under different test standards, the error rate of predicting the applied

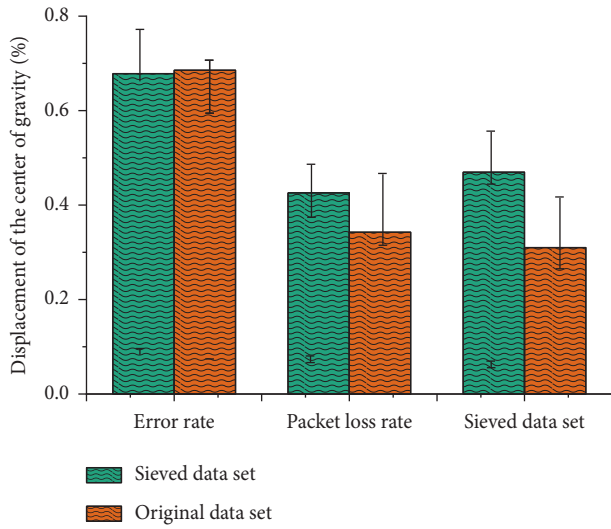


FIGURE 4: Effect of applied mathematics mining under different data stream classification indicators.

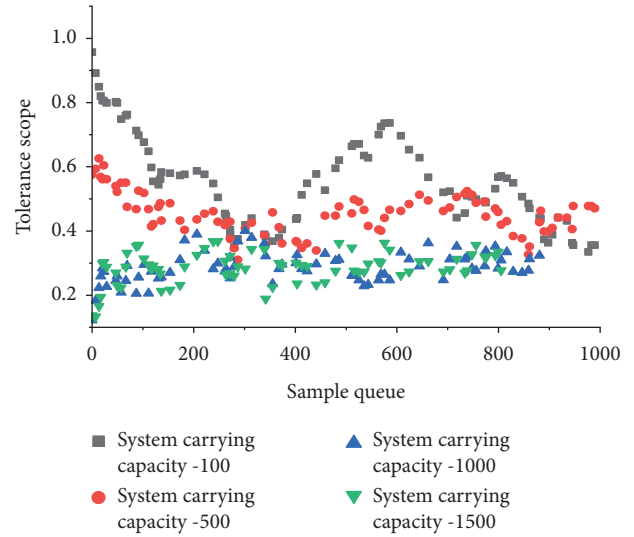


FIGURE 6: Network test of applied mathematics education system resources under different network environments.

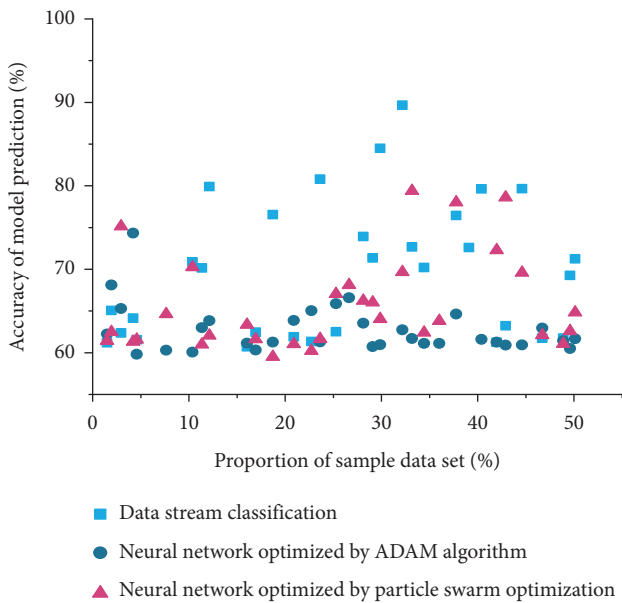


FIGURE 5: Application of mathematics mining effect under different data flow models.

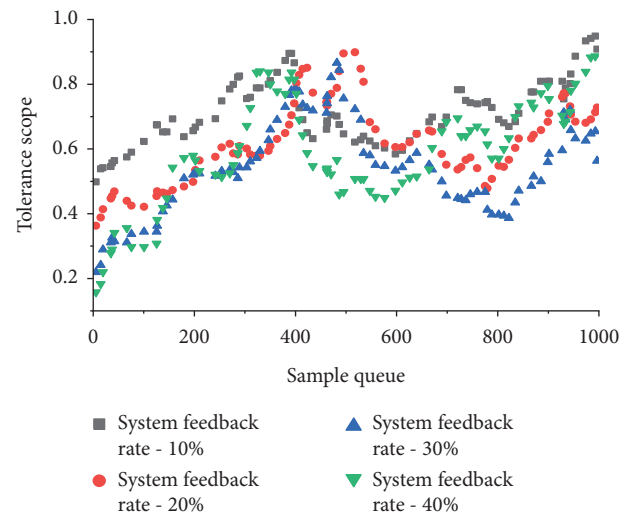


FIGURE 7: Simulation of resource throughput of applied mathematics education system under different test standards.

mathematics education system resource network sample dataset is low. It can be seen that the data stream classification technology has effectively improved the quality and classification of original applied mathematics education information data samples. If the data from the grassroots can be effectively used, the valuable information hidden in the data can be mined, and the value of the data can be improved, which will provide decision-makers with a better factual basis and basis, thereby changing management methods and formulating better management and formulation to improve the quality and level of running schools.

6. Conclusion

With the rapid development of database technology and the wide application of database management systems, how to make full use of data and dig out useful information and knowledge is a question of great concern to organizations with large amounts of data. At present, the application of data mining technology in the field of education management has not yet completed, and universities mainly stay in the use of databases in terms of information construction. This article is dedicated to the development of applied mathematics education resource mining technology based on edge computing and data stream classification. Due to the

limitations of our own knowledge, we will be committed to further exploring new mechanisms and methods in related fields to improve the level and quality of existing applied mathematics education resources mining. Facing the massive data of higher education institutions, data mining technology is an intelligent information processing technology that can effectively discover knowledge from the massive data and can discover important information that people have previously ignored from the massive data.

Data Availability

The datasets used and/or analyzed during the current study are available from the corresponding author on reasonable request.

Disclosure

This article does not contain any studies with human participants or animals performed by any of the authors. This paper did not receive any funding. All authors agree to submit this version and claim that no part of this manuscript has been published or submitted elsewhere.

Conflicts of Interest

The authors declare that there are no conflicts of interest.

References

- [1] J. Zhang, L. Zhou, F. Zhou et al., "Computation-efficient offloading and trajectory scheduling for multi-UAV assisted mobile edge computing," *IEEE Transactions on Vehicular Technology*, vol. 69, no. 2, pp. 2114–2125, 2020.
- [2] K. Yue and C. Tayler, "Choosing educational resources to build interprofessional, palliative care competency: a replicable review methodology," *Journal of Palliative Care*, vol. 13, no. 8, pp. 415–428, 2020.
- [3] B. Yang, X. Cao, J. Basse, X. Li, and L. Qian, "Computation offloading in multi-access edge computing networks: a multi-task learning approach," 2020, <https://arxiv.org/abs/2006.16104>.
- [4] R. L. Vicente-Vicente, M. Prieto, M. Pescador et al., "The TOX-OER project: learning toxicology through open educational resources. An international experience in permanent education," *Toxicology Letters*, vol. 280, p. S304, 2017.
- [5] N. Tratnik, "Generalized cut method for computing the edge-Wiener index," *Discrete Applied Mathematics*, vol. 282, pp. 222–233, 2020.
- [6] G. Tatiana, G. Z. Choleva, D. L. Tsogas, and E.C. Giokas, "An edge-iot framework and prototype based on blockchain and smart contracts," *Talanta*, vol. 6, pp. 4719–4732, 2019.
- [7] A. Tanious, J. D. Brooks, L. J. Wang, M. L. Shames, and D. L. Dawson, "Educational resources for vascular laboratory education in vascular surgery residencies and fellowships: survey of Vascular Surgery Program Directors," *Journal of Vascular Surgery*, vol. 69, no. 6, 2019.
- [8] Z. Sun, C. L. Liu, J. Niu, and W. Zhang, "Discriminative structure learning of sum-product networks for data stream classification," *Neural Networks*, vol. 123, 2019.
- [9] N. Shaikh, R. U. De Azevedo, A. Rajesh, and D. R. Farley, "Re: lack of online video educational resources for open colorectal surgery training," *Anz Journal of Surgery*, vol. 89, no. 5, p. 618, 2019.
- [10] M. Pratama, W. Pedrycz, and G. I. Webb, "An incremental construction of deep neuro fuzzy system for continual learning of nonstationary data streams," *IEEE Transactions on Fuzzy Systems*, vol. 28, no. 7, pp. 1315–1328, 2020.
- [11] L. Peng, H. Zhang, H. Hassan, Y. Chen, and B. Yang, "Accelerating data gravitation-based classification using GPU," *The Journal of Supercomputing*, vol. 75, no. 6, pp. 2930–2949, 2019.
- [12] B. Olav, W. A. Ueland, J. Espen et al., "Acoustic classification in multifrequency echosounder data using deep convolutional neural networks," *Ices Journal of Marine Science*, vol. 4, p. 4, 2020.
- [13] S. Nizamuddin, A. De, R. Aashish, and R. David, "Lack of online video educational resources for open colorectal surgery training," *Anz Journal of Surgery*, vol. 23, no. 13, pp. 523–533, 2020.
- [14] T. T. Nguyen, T. T. T. Nguyen, A. V. Luong, Q. V. H. Nguyen, W. C. Liew, and B. Stantic, "Multi-label classification via labels correlation and one-dependence features on data stream," *Pattern Recognition*, vol. 90, 2019.
- [15] D. Muthukrishna, G. Narayan, K. S. Mandel, R. Biswas, and R. Hložek, "RAPID: early classification of explosive transients using deep learning," *Publications of the Astronomical Society of the Pacific*, vol. 131, no. 105, pp. 118–131, 2019.
- [16] H. Melyssa, H. Michael, and M. Sonya, "Educational resources for global health in otolaryngology," *Otolaryngologic Clinics of North America*, vol. 51, no. 3, pp. 563–574, 2018.
- [17] G. M. Machado, V. Maran, G. M. Lunardi, L. K. Wives, and J. P. M. D. Oliveira, "AwARE: A framework for adaptive recommendation of educational resources," *Computing*, 2021.
- [18] J. L. Lobo, I. Oregi, A. Bifet, and J. D. Ser, "Exploiting the stimuli encoding scheme of evolving Spiking Neural Networks for stream learning," *Neural Networks*, vol. 14, no. 43, pp. 124–156, 2019.
- [19] H. Li, H. Xu, C. Zhou, L. Xing, and Z. Han, "Joint optimization strategy of computation offloading and resource allocation in multi-access edge computing environment," *IEEE Transactions on Vehicular Technology*, no. 99, 2020.
- [20] R. Levy, E. Chow, B. Kwon, K. Socha, M. McCarthy, and P. R. Turner, "SIAM education subcommittee report on undergraduate degree programs in applied mathematics," *Siam Review*, vol. 59, no. 1, pp. 199–204, 2017.
- [21] C. Lee, S. Hong, S. Hong, and T. Kim, "Performance analysis of local exit for distributed deep neural networks over cloud and edge computing," *Etri Journal*, vol. 42, no. 5, 2020.
- [22] O. Laurenium, D. Norbert, C. Octavian, E. Marius, and M. Costel, "Edge computing in space: field programmable gate array-based solutions for spectral and probabilistic analysis of time series," *Review of Scientific Instruments*, vol. 90, no. 11, p. 114501, 2019.
- [23] N. Kilarkaje, H. Al-Hussaini, and R. Ettarh, "Millennial students study alone using mixed educational resources," *Faseb Journal*, vol. 33, no. S1, 2019.
- [24] R. S. Kantar, A. R. Alfonso, E. P. Ramly, J. R. Diaz-Siso, and R. L. Flores, "Educational resources in craniofacial surgery: the case for user-friendly digital simulators," *Journal of Craniofacial Surgery*, vol. 31, 2020.
- [25] J. H. Huh, "Reefer container monitoring system using PLC-based communication technology for maritime edge computing," *Journal of Supercomputing*, vol. 76, 2020.
- [26] Y. Huang, X. Song, F. Ye, Y. Yang, and X. Li, "Fair and efficient caching algorithms and strategies for peer data sharing

- in pervasive edge computing environments,” *IEEE Transactions on Mobile Computing*, p. 1, 2019.
- [27] M.-P. Hosseini, T. X. Tran, D. Pompili, K. Elisevich, and H. Soltanian-Zadeh, “Multimodal data analysis of epileptic EEG and rs-fMRI via deep learning and edge computing,” *Artificial Intelligence in Medicine*, vol. 104, Article ID 101813, 2020.
- [28] X. Hong, L. Liang, X. Jie, and A. Nallanathan, “Joint task assignment and resource allocation for d2d-enabled mobile-edge computing,” *IEEE Transactions on Communications*, vol. 99, 2019.
- [29] S. H. Hallett and S. P. Caird, “Soil-Net: development and impact of innovative, open, online soil science educational resources,” *Soil Science*, vol. 182, no. 5, p. 1, 2017.
- [30] S. H. Hallett, S. P. Stephen, and S. P. Caird, “Soil-net,” *Soil Science*, vol. 182, no. 5, pp. 188–201, 2017.
- [31] H. M. Gomes, A. Bifet, J. Read et al., “Correction to: adaptive random forests for evolving data stream classification,” *Machine Learning*, vol. 108, no. 10, pp. 1877–1878, 2019.
- [32] M. Gairing and R. Savani, “Computing stable outcomes in symmetric additively separable hedonic games,” *Mathematics of Operations Research*, vol. 44, 2019.
- [33] R. Du, Y. Liu, L. Liu, and W. Du, “A lightweight heterogeneous network clustering algorithm based on edge computing for 5G,” *Wireless Networks*, vol. 26, no. 3, pp. 1631–1641, 2020.
- [34] S. U. Din and J. Shao, “Exploiting evolving micro-clusters for data stream classification with emerging class detection,” *Information Sciences*, vol. 507, 2019.
- [35] V. Celentano, G. Pellino, and M. G. Coleman, “Lack of online video educational resources for open colorectal surgery training,” *Anz Journal of Surgery*, 2019.
- [36] V. Camel, M. N. Maillard, N. Descharles, E. L. Roux, and I. Billault, “Open digital educational resources for self-training chemistry lab safety rules,” *Journal of Chemical Education*, vol. 98, no. 1, pp. 208–217, 2020.
- [37] S. Ren, W. Zhu, B. Liao et al., “Selection-based resampling ensemble algorithm for nonstationary imbalanced stream data learning,” *Knowledge-Based Systems*, vol. 163, pp. 705–722, 2018.
- [38] A. H. Kleynhans, D. J. Oosthuizen, and V. Hoving, “Emergency medicine educational resource use in Cape Town: modern or traditional?” *Postgraduate Medical Journal*, 2017.
- [39] A. Boukerche and V. Soto, “Computation offloading and retrieval for vehicular edge computing,” *Acm Computing Surveys*, vol. 53, no. 4, 2020.
- [40] S. M. Alvarado and H. Feng, “Representation of dark skin images of common dermatologic conditions in educational resources: a cross-sectional analysis,” *Journal of the American Academy of Dermatology*, vol. S0190-9622, no. 20, 31138 pages, 2020.
- [41] C. Alberto and K. Bartosz, “Evolving rule-based classifiers with genetic programming on GPUs for drifting data streams,” *Pattern Recognition*, vol. 87, pp. 248–268, 2019.
- [42] A. A. Ali, G. Adler, and M. Rapoport, “Session 303 - driving and dementia—an introduction, educational resources, and international perspectives,” *American Journal of Geriatric Psychiatry*, vol. 25, pp. S19–S20, 2017.
- [43] X. Xiong, K. Zheng, L. Lei, and L. Hou, “Resource allocation based on deep reinforcement learning in IoT edge computing,” *IEEE Journal on Selected Areas in Communications*, no. 99, p. 1, 2020.
- [44] A. Beaufort, F. Moatar, E. Sauquet, P. Loicq, and D. M. Hannah, “Influence of landscape and hydrological factors on stream–air temperature relationships at regional scale,” *Hydrological Processes*, vol. 34, 2020.

Research Article

Network Security Technology of Intelligent Information Terminal Based on Mobile Internet of Things

Ning Sun ^{1,2}, Tao Li,² Gongfei Song,^{2,3} and Haoran Xia⁴

¹Binjiang College, Nanjing University of Information Science & Technology, Nanjing 214105, Jiangsu, China

²CICAEET, School of Automation, Nanjing University of Information Science & Technology, Nanjing 210044, Jiangsu, China

³Key Laboratory of Advanced Control and Optimization for Chemical Processes, Shanghai 200237, China

⁴College of Mechanical & Electrical Engineering, San Jiang University, Nanjing 210012, Jiangsu, China

Correspondence should be addressed to Ning Sun; 001764@nuist.edu.cn

Received 14 October 2020; Revised 21 January 2021; Accepted 12 March 2021; Published 25 March 2021

Academic Editor: Chi-Hua Chen

Copyright © 2021 Ning Sun et al. This is an open access article distributed under the Creative Commons Attribution License, which permits unrestricted use, distribution, and reproduction in any medium, provided the original work is properly cited.

In the process of implementing the Internet of Things, the object itself has identity information and identification equipment and encounters difficulties in communication security during the process of entering the network communication. Just like the Internet and wireless sensor networks, there are security issues in information transmission. Therefore, it is of great significance to study the mobile Internet of Things network security technology depression to protect the communication information in the mobile Internet of Things. This paper mainly studies the network security technology of intelligent information terminal based on mobile Internet of Things. This article will analyze and compare the mainstream encryption algorithms of the current mobile Internet and choose a safer and more secure HASH algorithm. We study the flow of key management, key generation, key distribution, verification key distribution, key update, key storage, key backup, and key validity time setting for mobile Internet of Things, using an existing identity cryptosystem. Based on encryption, the design technology of key management and authentication in this paper is improved. Compared with other methods, the storage consumption of this method on GWN is relatively medium. In the initial stage, the storage is 32 bytes, then in registration stage 1, it reaches 84 bytes, in registration stage 2, it is 82 bytes, and then, in the login authentication phase, the number of bytes rose and reached 356 bytes in authentication phase 3. Experimental results show that this protocol has certain advantages in ensuring safety performance.

1. Introduction

To allow participants in the Internet of Things to avoid the security and privacy issues brought about by the universal network basic platform as much as possible, the Internet of Things must achieve simple and safe completion of various user control behaviors. Networking technology research must fully consider security and privacy. And with the continuous improvement of “object” automation capabilities and autonomous intelligence, the problems of object recognition, identity, stealth, and the role of objects in the role they play will become the focus of academic scholars.

As the Internet of Things is becoming more and more widely used, the number and differences of devices are becoming greater, and the early public key encryption

technology has been unable to meet the information security needs of the Internet of Things [1, 2]. As an important means of protecting nodes in the Internet of Things, key management and authentication methods have become a research hotspot at this stage. How to propose a set of correct keys under the conditions of low-power consumption, low computing, and high security of the nodes Management and authentication methods is of great significance to study the network security technology of intelligent information terminals based on mobile Internet of Things [3, 4].

Raban Y conducts a relatively balanced long-term predictive study to identify the major threat drivers and identify emerging technologies that may have a significant impact on defense and attack capabilities in cybersecurity. The main tools he uses are online scanning and online surveys

conducted by subject matter experts to assess the potential impact of emerging threats and several emerging technologies on network defense capabilities and network attack capabilities. His investigation revealed that network resilience, homomorphic encryption, and blockchain may be considered technologies that primarily contribute to defense capabilities. On the other hand, the Internet of Things, biological hacking, human-machine interface (HMI), and autonomous technologies mainly increase attack capabilities. In the middle, he found that autonomous technology, quantum computing, and artificial intelligence all contribute to defense and attack capabilities, and the impacts on both are roughly similar [5]. *Cavelty MD* used network security research as an empirical research location, which can prove that there are two different ways of understanding network technology in society. The first category of people believe that network technology is nonpolitical, flawed, and important and needs to be repaired to create more security. The other party understands them as political tools in the hands of social participants, without considering technical (possible) possibilities. He suggested focusing on a third understanding to bridge the gap between each other: technology is defined as the embodiment of social knowledge. He believes that, corresponding to this, research on cyber politics will benefit from two innovations: cyber security as the focus of social practice (making and stabilizing by spreading knowledge about vulnerabilities) and the use of practical attention and elimination of these loopholes [6]. *Ahlawat P* studied the problem of node capture from an adversarial perspective. In this view, the enemy intelligently uses various vulnerabilities in the network to establish a cost-effective attack matrix. To resist such attacks, defenders or network designers can construct a similar attack matrix. The defender will identify a set of key nodes and use the key trade-off relationship to assign a key dominance level to each node of the network. The key dominance quantifies the possibility of attacking specific nodes. It is used to determine the length of the hash chain. It can also be used to improve the security of path key establishment and key update of the proposed scheme. The performance of the scheme is analyzed with other existing schemes. His results show that the performance of the scheme is better than the recovery ability of the node capture, the number of hash calculations is reduced, the probability of key leakage of the proxy node is reduced, and the key is updated. The number of links that were revoked during the process decreased [7]. His research provides technical measures and reference programs for this article.

This paper mainly studies the network security technology of mobile Internet of things. According to the seven steps of key generation, key distribution, key validation, key storage, key update, and key validity, the key management of Internet of Things is studied and analyzed. Security analysis, basic theorem and proof, key analysis, authentication analysis, and identity information security analysis of the technical scheme are proposed in this paper. Experimental results show that the proposed protocol has some advantages in security performance.

2. Intelligent Terminal Network Security Technology

2.1. Network Security Key Technology

2.1.1. Establish the Key. The APSZM primitive provides services for establishing a secure link and key management between devices. Each device has an original key, which is set when the device is initially installed [8, 9]. The APSzM primitive performs key exchange and update on the basis of the original key. When a certain device wants to establish a secure communication with another device, it must first establish a secure communication key [10]. Use the security primitive APSZM. MAKELINE. KEY can establish a security key. As shown in Figure 1, it is a timing diagram for key establishment. When two devices want to establish a security key, one acts as the initiator, and the other acts as the responder. The initiator's ZDO will generate an APSZM. MAKELINE. The KEYreq request is sent to the APS layer with the responder's address and the key establishment start method and protocol. The initiator can choose to use the responder's parent node as a contact, just set puse Parent to true in the corresponding parameter, and set the physical address of the parent node in the parameter presParent MAC Addr [11, 12]. After receiving the request, APS will generate a SKKE frame and send it to the network. If a responder receives a request to establish a key, and there is a master key stored in it that is related to the initiator, the APS layer will send an indication primitive to the ZDO layer, which will send a response to the ZDO layer after processing. At the APS layer, this response contains the parameter ACCEPT, which ultimately determines whether to agree to establish a key with the initiator. If agreed, the ASP layer establishes a security key with the initiator through the SKKE protocol [13, 14]. As shown in Figure 1, set the time for the key.

2.1.2. Key Transmission. APSzM's key transmission service plays a key role when the keys need to be transmitted between devices. The key transmission service can transmit the link key, master key, or network key of the program and the master key of the trust center. The key transmission is also composed of an initiator and a responder. When the initiator ZDO layer transmits a key to a responder, it directly generates a primitive for key transmission and sends the primitive to the APS layer. The APS layer is receiving. After the request, the corresponding frame is generated and sent to the network [15, 16]. When the ASP layer of the responder receives the key transmission command frame from the network, it decompresses, decrypts, and authenticates the frame. When the command is confirmed to be legal, it checks whether the address of the command responder is the same, and whether the command has a chain. If road key, master key, and network key are the same, they inform the ZDO layer that a key transmission command has been received [17, 18].

2.1.3. Key Request Service. APSZM provides the key request service to the upper layer. When a device wants to obtain the key of other devices such as the trust center of the current

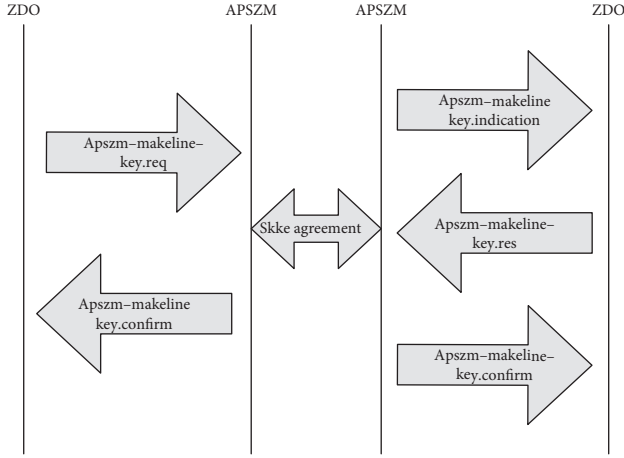


FIGURE 1: Timing of key establishment.

wireless network or the end-to-end master key, it can use the APSZM in the key request service. GET-KEY.req primitives to achieve. The ZDO layer sends this primitive to the APS layer. After receiving the primitive, the APS layer constructs a command frame according to the parameter value. The command in the command frame is APSC GET-KEY, and the data is 0x08 [19, 20]. If the key type is 2, it means that the link key is requested, and if the key type is 1, it means that the network key is requested. The partner address may be 0 or 8 bytes in length. For the application key request, the partner address is the 64-bit physical address of the corresponding device. For network key requests, the partner address is not used.

After the request key frame is constructed, it must go through security processing and then pass NLDE. DATA.req sends the data to the network. When the ASP layer receives a request key command frame, it first decompresses and authenticates the frame data and then sends an instruction to the ZDO layer. After receiving the instruction, the ZDO layer can determine whether to send the command to the sender. Transfer the key, or the key to its partner.

2.1.4. Key Conversion Service. APSZM within APSZM. CHANGE.KEY primitive is used to provide key conversion services to the ZDO layer. When a certain node device (usually a trust center) wants to notify other devices to convert a new network key, some primitives are used. The ZDO layer sends APSZM.CHANGE.KEY primitive, and the APS layer receives the primitive to construct the command frame according to the parameter value and network conditions, through security processing, and then call NLDE-DAI to divide.req sends the data out. When the APS layer of the target device receives the data, it decompresses and authenticates the data. After successful pass, it sends an instruction to the ZDO layer. After receiving the instruction, the ZDO layer replaces the old network key with the key related to KeySeqNumber [21].

2.2. Data Fusion Method. Wireless sensor network, as the main component of the sensing layer of the Internet of

Things, is limited by many factors such as energy, storage capacity, transmission rate, and robustness. Among them, energy limitation is arguably the biggest challenge faced by wireless sensor networks. In wireless sensor networks, energy is mainly consumed in two aspects: transmission consumption and computing consumption. Among them, the energy consumed in the process of data transmission is the most [22]. Therefore, how to carry out complex environmental monitoring and reporting on sensor nodes with limited energy is an important problem to be solved urgently in wireless sensor networks. Since wireless sensor network is a data-centered network, data processing technology in the network can be used to reduce this excessive energy consumption; that is, data fusion technology can be used to solve these problems. Figure 2 shows the location of the data fusion technology in the perception layer.

Through the theoretical analysis and simulation testing, the role of data fusion technology is discussed in detail. The results of the study prove that the ratio of the energy cost of the network when using data fusion technology and not using data fusion technology is as follows:

$$\lim_{d \rightarrow \infty} \frac{N_D}{N_A} = \frac{1}{k}, \quad (1)$$

where d is the distance from the sensor node to the fusion node, k is the number of data collection source nodes, N_D is the number of data transmissions in the network using data fusion, and N_A is the number of data transmissions in the network without data fusion. Formula (1) shows that the larger the overall size of the network (the larger the d), the more energy saved by data fusion technology: the more data source nodes (the larger k), the more energy can be saved by data fusion technology [23, 24]. This shows that the use of data fusion is extremely important to save the energy consumption of wireless sensor network transmission [25].

2.3. Flow Prediction Method. An effective intrusion detection method based on Markov traffic prediction model is introduced. This method performs anomaly detection independently by predicting the traffic of each node, without special hardware support and cooperation between nodes. Suppose that the current state of the sensor node is i , the next state is j , and the transition probability of the state $p_{i,j}$ is expressed by

$$p_{i,j} = p\{X_{m+1} = j | X_m = i\}. \quad (2)$$

The probability that the sensor node transitions from state i to state j once is recorded as $p_{i,j}$, which is called the matrix:

$$P = \begin{Bmatrix} p_{11}, p_{12}, \dots, p_{1N} \\ p_{21}, p_{22}, \dots, p_{2N} \\ \cdot \\ \cdot \\ p_{N1}, p_{N2}, \dots, p_{NN} \end{Bmatrix}. \quad (3)$$

Transfer matrix is for one time (or one step). Suppose that the sensor node in the initial state

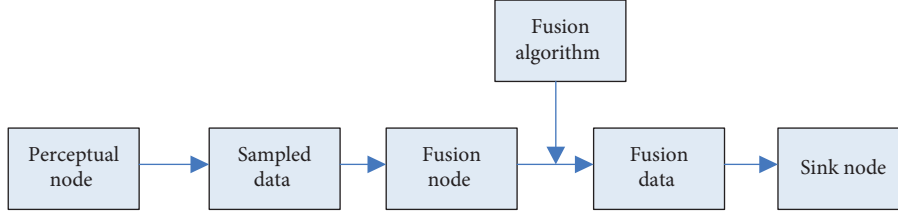


FIGURE 2: Process diagram of data fusion at the perception layer.

$S^{(0)} = (S_1^{(0)}, S_2^{(0)}, \dots, S_N^{(0)})$ of $k=0$ is known, and the state after seven transfers is $S^{(l)} = (S_1^{(l)}, S_3^{(l)}, \dots, S_N^{(l)})$, $k=l, 2, \dots$, then,

$$S^{(k)} = S^{(0)} \begin{bmatrix} P_{11}, P_{12}, \dots, P_{1N} \\ P_{11}, P_{12}, \dots, P_{1N} \\ \vdots \\ P_{N1}, P_{N2}, \dots, P_{NN} \end{bmatrix}. \quad (4)$$

Equation (4) is a Markov prediction model. The state $S^{(k)}$ of the system after k transitions depends only on the initial state $S^{(0)}$ and the transition matrix P . Let B_s represent the number of data packets transmitted by the sensor node in the initial state of S and the interval of Δt , then the number of transmission packets of the node in any state $S^{(k)}$ can be predicted by equation (3), and then by monitoring the sensor node or the deviation of the predicted flow and the actual flow of the cluster head node to detect whether the sensor network has been intruded. The disadvantage of this method is that the node overhead is relatively large.

By using the Genetic Algorithm to optimize the traffic matrix, a method to enhance DDOS attack detection is proposed, and the traffic matrix is improved through the following operations: (1) reconstruction of the hash function to reduce hash conflicts, and (2) the use of packet-based window size. Instead of based on the time window size to reduce the cost of calculation. Then, calculate the variance (Variance, V) through the flow matrix. If $V < T$, an alarm is generated, where T represents the threshold, and V is calculated according to

$$V = \frac{1}{K} \sum_{j=0}^n \sum_{i=0}^n (M_{(i,j)} - u)^2, \quad \text{if } M_{(i,j)} \neq 0, \quad (5)$$

$$u = \frac{1}{K} \sum_{j=0}^n \sum_{i=0}^n (M_{(i,j)})^2, \quad \text{if } M_{(i,j)} \neq 0. \quad (6)$$

Among them, $M(i, j)$ represents the elements in the traffic matrix, and k represents the number of nonzero elements in M .

Intrusion detection system based on neighbor node traffic is introduced. This method considers that nodes that are close to each other in space have similar behavior. If the behavior of a node is significantly different from that of the neighbors, the node is considered a malicious node. This detection technique is regional and unsupervised and adapts to the dynamic changes of the network. Let sensor node $a_i (i = 1, 2, \dots, n)$ monitor its direct neighbor node

$N(a_i) = \{b_{i1}, b_{i2}, \dots, b_{im}\}$, where n represents the number of nodes in the sensor network, and m_i represents the number of neighbor nodes of the a_i node. Let node a_i monitor node $\{b_{i1}, b_{i2}, \dots, b_{im}\}$, and the corresponding attribute vector set is $F(a_i) = \{f(b_{ij}) | j = 1, 2, \dots, m_i\}$. If the Euler distance from $f_k(b_{i,j})$ to the set $\{f_k(b_{i1}), f_k(b_{i2}), \dots, f_k(b_{im})\}$ is greater than δ_k , then the node $b_{i,j}$ is considered as the malicious node by the node a_i . If the attribute value of the node $f_m(b_{i,j})$ is less than γ_m , the node is also regarded as a suspicious node, where γ_m is a threshold set to reduce threats, and the formal definition of the rules is as follows:

$$f_k(b_{i,j}) - \text{AVG}(f_k(b_{i1}), f_k(b_{i2}), \dots, f_k(b_{im})), \quad (7) \\ > \delta_k \text{ and } f_m(b_{i,j}) > \gamma_m.$$

3. Experimental Detection of Terminal Network Security Technology

3.1. Experimental Setup. Hardware selection for this experiment: the user node used is MICAz. The hardware device of the device is the AA size component model that can be modified by the user: MPR2400 and MPR2600. The processor is 8 MHz AtMegal28 L, using IEEE 802.15.4, and the wireless model uses the 2.4 G frequency band. The memory and energy resources are limited, the computing power is underground, the data and storage space is 4K bytes, and the flash memory space is only 128K bytes. Among the IoT application nodes, the overall performance of the node is at a low to medium level, which can relatively represent the capabilities of IoT user terminals.

3.2. Data Set Selection. The experimental data set is a public comment data set. Taking an urban area as an example in the experiment, the map space is limited to a square area of $8 \text{ km} \times 8 \text{ km}$. The entire map space is divided into 80×80 grids, and the area of each grid is $100 \times 100 \text{ m}^2$. The a priori query probability in each grid is obtained by counting the number of comments of all points of interest in the grid. As shown in Table 1, according to the number of points of interest, this article divides the points of interest into the following categories: high-density points of interest, medium-density points of interest, and low-density points of interest. In the experiment, ATM, gas station, and Starbucks were selected as representatives of the above three types of points of interest.

In the experiment, the performance of the proposed algorithm under different density of interest points is

TABLE 1: Types of points of interest.

Types of interest	Quantity	Points of interest	Quantity
High-density points of interest	200	ATM	251
Point of interest	50–200	Gas station	112
Low-density points of interest	50	Starbucks	35

investigated from four different angles: computational cost and communication cost. Since the same interest points are examined in the experiment, the meta-information such as score and average price is almost the same, so this paper only considers the distance factor top-k sorting, but the algorithm in this paper supports the use of multiple factors for top-k sorting. The details of the experimental parameters are shown in Table 2. Examples include appearance of experimental parameters, significance of experimental parameters, and numerical values of experimental parameters.

3.3. Technical Realization. In this paper, this protocol is analyzed experimentally and compared with other related protocols in terms of computing cost, security performance, communication cost, and storage consumption, to prove its effectiveness. In the previous chapter, a key management scheme based on identity is proposed. In this paper, these methods are simulated, quantitative results are given, and the effectiveness of these methods is verified.

For the implemented software environment, MICAz is TinyOS, an operating system based on open source wireless sensors. TinyOS is an embedded open source operating system designed for wireless sensor network design and development. The component-based operating system (component) architecture allows it to be quickly updated, thereby reducing the limitations of code size sensor network storage. TinyOS is a higher professional operating system for low-power wireless devices, mainly used in the field of sensor networks, pervasive computing, personal area networks, smart homes, and smart meters.

TinyOS and its applications are implemented through a language (nesC) for developing component-structured programs. It is a C-based programming language and a mechanism for organizing, naming, and connecting components to become a robust embedded network system. Support bidirectional concurrency.

4. Influence Analysis of Self-Similar Parameters

4.1. Traffic Aggregation without Self-Similarity. Brownian motion is a random process with independent increments that is normally distributed. The mathematical model of Brownian motion can be described by Wiener process. Mandelbrot extended the one-dimensional Brownian motion model $B(t)$ to fractional Brownian motion $B_h(t)$. H represents the Hurst parameter. If the Hurst parameter value of fractal Gaussian noise is greater than 0.5, it will cause the decay of the queue part to become slower. When $H=0.5$, it corresponds to a typical short correlation model. Fractal

Gaussian noise is an incremental process of fractal Brownian motion and has a strict first-order self-similar process. Fractal Gaussian noise can be used to generate data with precise white similar parameters, mean and variance. In this paper, the random number midpoint setting method is used to generate the flow of fractal Gaussian noise. Here, we first generate two types of flows with the same mean, variance and self-similar parameters. Set the mean value $m = 321$, variance $v = 333$, and Hurst = 0.4 to study the characteristics of the aggregated flow after the two types of traffic with the same parameters and without self-similar characteristics are aggregated.

As shown in Figures 3 and 4, after the two types of data traffic with the same mean, variance, and Hurst coefficients and without self-similar characteristics are aggregated, the aggregated traffic still has no self-similar characteristics, and the aggregated traffic Hurst parameter value and composition aggregate traffic Hurst value of the flow source are almost the same.

After data traffic without self-similarity is aggregated, the value of the self-similarity parameter of the aggregated traffic is approximately the same as the value of the traffic source that constitutes the aggregated traffic. Therefore, when the traffic with the same Hurst parameters and no gate similar characteristics is aggregated with the data traffic with the same properties, there is still no self-similarity in aggregated traffic. This is because the suddenness of traffic without self-similarity is extremely small. After traffic aggregation. Although the traffic density increases, it is still relatively stable on the whole and will not produce a sudden burst of traffic in a short time. Therefore, traffic that does not have self-similar characteristics still does not have self-similar characteristics after aggregation.

4.2. Traffic Aggregation with Self-Similar Characteristics. The network traffic has a self-similar characteristic, indicating that the data is not particularly stable and bursty. After the aggregation of bursty traffic, the burstiness of the traffic will be more obvious. It is still due to the mutual influence of each service flow that the burstiness is weakened, and the self-similarity of the traffic is reduced. This is a problem worthy of study. First, there are self-similar characteristics of the aggregated traffic after two types of traffic with the same mean, variance, and Hurst parameters are aggregated. First, generate two kinds of flow with mean value $m = 318$, variance $v = 323$, and self-similarity coefficient $H = 0.8$, and analyze the self-similarity characteristics of the aggregated flow after the two types of flow are aggregated.

As shown in Figure 5, after two types of traffic with the same mean, variance, and Hurst parameters, and with self-citrus-like characteristics are aggregated, the aggregated traffic still has self-similar characteristics.

The self-similarity parameter of the polymerization flow rate is 0.82021, which is much greater than 0.5, slightly less than 0.85, and also greater than the average of the two flow rates of 0.7. The self-similar value of the aggregated flow is equal to the largest of the flow sources, which is different from the conclusion of this article. This is because, after the traffic aggregation, it is no longer a strict second-order self-

TABLE 2: Parameter settings.

Parameter name	Appearance	Meaning	Numerical value
θ	Algorithm a	Similarity threshold	When $k = 1, \theta = 0$; when $k \geq 21, \theta = 1/2$
η	Algorithm b	Number of candidate regions	$5s_i$
λ	Algorithm c	Information entropy threshold	High-density points of interest:1.5; medium-density points of interest:2.5, low-density points of interest:3.5

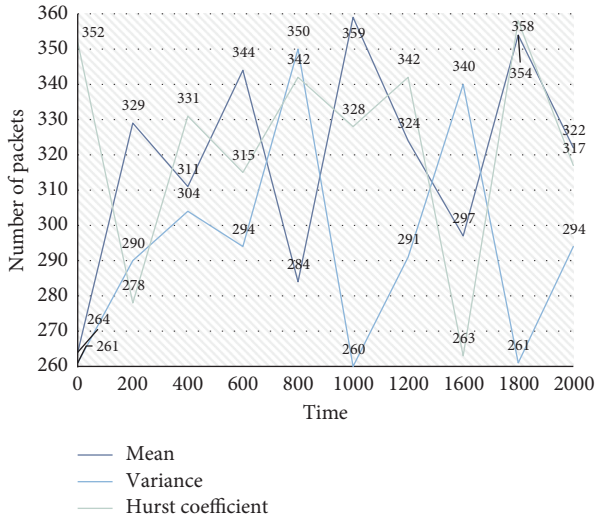


FIGURE 3: Aggregated traffic source 1 data.

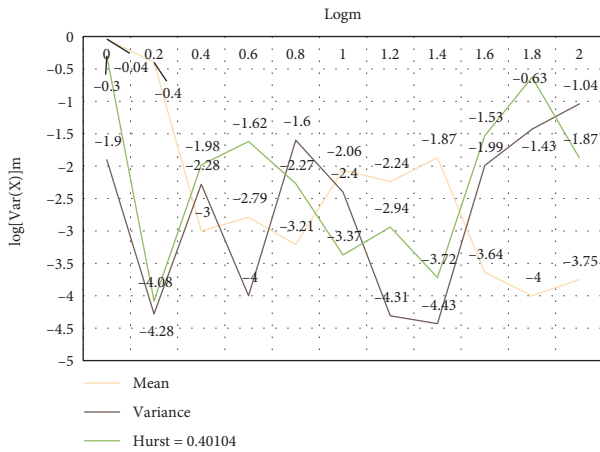


FIGURE 4: Hurst value.

similar process but shows a gradual self-similar characteristic. The H value of the aggregated flow is related to the H value of all flow sources, and the value of the aggregated flow is greater than the largest. It can be seen that when the two types of traffic with self-similar characteristics are aggregated, their mean and variance are the same, but the Hurst parameters are different, and the larger the self-similar parameter, the greater the impact on the aggregated flow.

5. Security Analysis of Network Security Technology

As shown in Figure 6, where the global message set $|I| = 15$, the abscissa is the value of $|GSS|$, the ordinate is the number

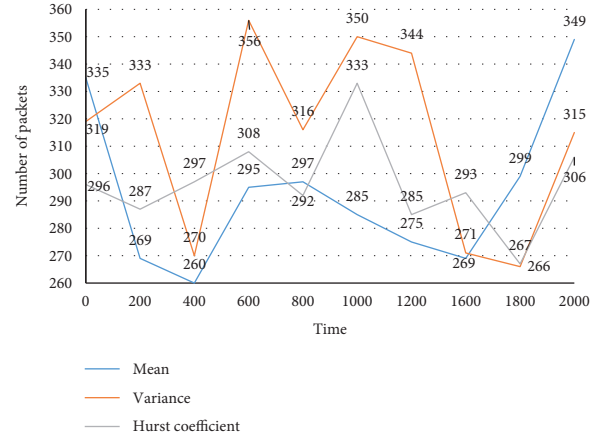
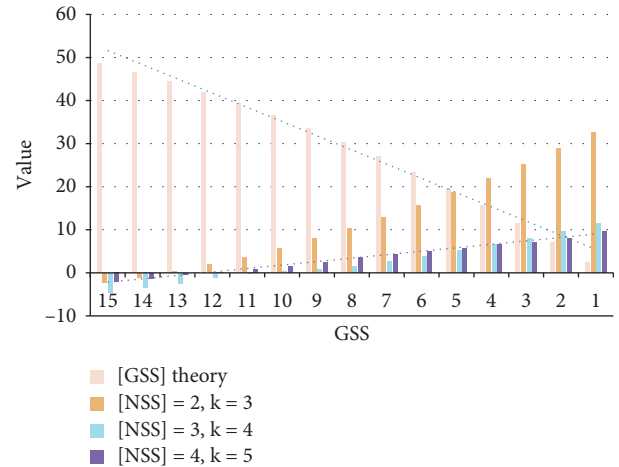


FIGURE 5: Aggregated traffic source 2 data and Hurst values.

FIGURE 6: Comparison of the number of nodes to be captured by a collusion attack when different values of $|GSS|$.

of capture nodes required by the attacker, and $\overline{NSS^l}$ is 2, 3, and 4, respectively. The number of nodes is captured. As can be seen from the figure, after the global message set $|I|$ is determined, the value of $\overline{NSS^l}$ is not as large as possible. The optimal value should be the value of $\overline{NSS^l}$ determined after the anonymous request of k , rounded down or up at the intersection.

On the other hand, by adding round updates of the global secret information set, the scheme will be able to resist statistical analysis attacks at the same time. However, these are only for the security achieved by passive attackers, and the double verification information security data fusion protocol proposed in this section uses the double secret

TABLE 3: Distribution of transmission costs at various levels of the end-to-end solution.

Level	Number of nodes	node transfer bytes (bytes)	End-to-end solution	Number of bytes transmitted by the node in the double verification scheme (bytes)
1	3		2156	14
2	9		736	14
3	27		236	14
4	81		82	14
5	243		32	14
6	729		8	14
7	2187		2	14

information set method, without adding hash calculation, in accordance with the protocol. Its own security features provide the integrity verification of MAX/MIN nonlinear fusion, which can resist the tampering attacks of active attackers, etc., which improves the security of nonlinear fusion and greatly expands its application scenarios.

6. Practical Performance Analysis of Safety Technology

No matter whether it is homomorphic encryption or traditional encryption algorithms, there is no available solution that can support the operation of taking the most value of the ciphertext directly. It did not appear. Data fusion based on the hop-by-hop encryption method always decrypts and exposes the plaintext at the fusion node, which cannot withstand internal node attacks and fails to meet the requirements of secure data fusion. This section compares the simulation energy consumption of the nonfusion method of nonfusion data of double verification, end-to-end encryption, and hop-by-hop encryption fusion on an embedded multinode platform.

Although the energy consumption of the end-to-end scheme is slightly lower than that of the duplex scheme on average to a single node (because the camouflaged data brings additional energy consumption to the duplex scheme), the ciphertext to be transmitted by the end-to-end scheme during the transmission process continues to increase. The more you go to the upper node, the greater the transmission overhead, and the energy consumption will rise sharply. As shown in Table 3 and Figure 7, the end-to-end solution of the 7-layer network topology is compared with the multiple-layer node transmission cost. As can be seen from the table, the overhead of the top node reaches hundreds of the bottom node thousands of times; this will cause the upper nodes to quickly consume electricity and paralyze the network. In the duplex scheme, the transmission cost of a single node at each level is the length of the global information set due to the execution of the maximum value fusion process, which evenly divides the energy consumption of the network.

When nonlinear MAX/MIN fusion is to be performed at the perception layer of the Internet of Things, the double verification of the disguised data security fusion protocol can provide privacy, confidentiality, and fusion of data between nodes while ensuring low transmission overhead and computational complexity. The integrity verification is a safe

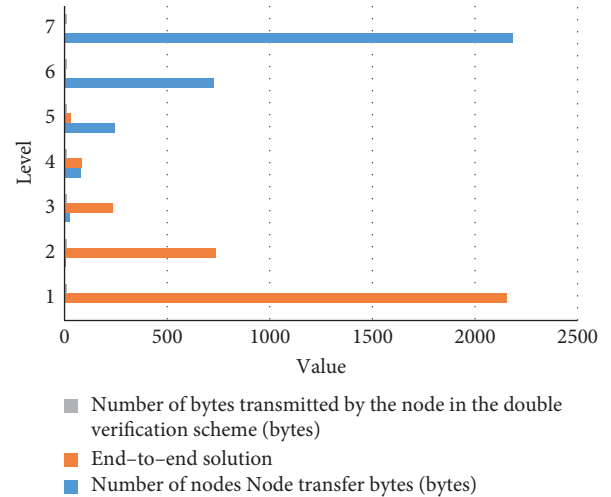


FIGURE 7: End-to-end solution transmission cost distribution at each level.

and efficient nonlinear data fusion scheme suitable for the perception layer of the Internet of Things.

7. Conclusions

This paper aggregates traffic with different characteristics and analyzes the influence of Hurst parameters, variance, traffic density, and human participation on aggregated traffic characteristics. The analysis shows that when the variances are the same, after the aggregation of traffic without self-similar characteristics, the aggregated traffic still has no self-similar characteristics. After the aggregation of traffic with self-similar characteristics, the aggregated traffic still has self-similar characteristics. When the traffic without self-similar characteristics is aggregated with the traffic with self-similar characteristics, the characteristics of the aggregated flow are related to the flow sources that make up the aggregated flow. The self-similar parameters of the aggregated flow increase with the variance of the flows without the self-similar characteristics, and decrease with the variance of service traffic with self-similar characteristics.

When the mean and variance of the flow are the same, the larger the Hurst parameter value, the stronger the influence on the self-similar characteristics of the aggregate flow. The greater the variance of the flow source, the greater the impact on the aggregate flow. We analyzed the flow characteristics of real

Internet traffic, aggregated them with the IoT traffic generated by FGN, and found that when the traffic burst is particularly large, the self-similarity of aggregated traffic will be reduced, but it always has self-similarity. This is because the burstiness of the traffic is too strong, and the aggregated traffic cannot effectively absorb the bursty traffic.

The method proposed in this paper has some advantages in computing power, security, and even storage space. It adopts a lightweight authentication model and USES simple xor and hashing functions to ensure the forward and backward performance of key management and authentication. Considering all objects in the Internet of Things as user nodes improves the scalability of the key management and authentication scheme proposed in this paper.

This paper focuses on the nonlinear security data fusion protocol based on disguised data, so as to enable MAX/MIN data fusion in the Internet of Things system. Aiming at the problems of the existing schemes, the article proposes a double verification nonlinear secure data fusion protocol. By using the method of double global secret information group, the advantage of hidden data bits itself is used to complete the integrity verification of the fusion data results to improve the security of the solution that has been expanded, and the scope of application scenarios of the solution has been widened.

Data Availability

All the data sets used in this paper are from the network traffic audit log data of a power enterprise. At the same time, in order to increase the data of all kinds of intrusion behaviors, a part of security audit data set is added to the data set after analyzing and processing Hadoop platform to form the intrusion detection data set in this paper. This data set uses 2 million network traffics as training data, while the other 1 million data sets are test data sets. There are four types of intrusion: port scanning attack, DoS attack, local user's unauthorized access, and remote host's unauthorized access. Among the 39 types of intrusion attacks found, there are 22 kinds of training data sets provided this time. It is worth mentioning that each record has 53 dimensional attributes, and the last attribute is its category. The data is generally composed of the following four aspects: first, fully consider all the basic characteristics of network connection, such as destination IP address, source IP address, source port, destination port, and other attribute fields. Second, consider the content characteristics of network connection: the data part of the data package contains the user's remote access and operating system sensitive file instructions and login system password and other information. Third, consider the time characteristics of traffic: based on the time correlation of network attacks, some connections with the connection within 2 S before the current connection are counted, assuming the percentage of the same host and service type with the current connection within 2 S, etc. Fourth, fully consider the traffic statistical characteristics of the specified host: the actual network attack behavior will be longer than the time span of 2 S. In order to find out the attack, count the relationships between the 100 connections

before the current connection and the link; for example, count the percentage of the same host and service type between the first 100 connections and the current connection. The format of a normal and an abnormal network connection data is shown below. 192, 112, 211, 25, 202, 206, 187, 45, 4532, 80, 31, 2, tcp, smtp, 0, 1684, 363, 0, 0, 0, 01, 0, 0, 0, 0, 0, 0, 0, 0, 0, 1, 1, 0.00, 0.00, 0.00, 1.00, 0.00, 0.00, 104, 66, 0.63, 0.03, 0.01, 0.00, 0.00, 0.00, 0.00, 0.00, normal. 192, 119, 131, 65, 202, 206, 225, 130, 7642, 25, 24, 0, tcp, private, 1, 0, 0, 0, 0, 0, 0, 0, 0, 0, 0, 0, 0, 0, 0, 0, 0, 0, 38, 1, 0.00, 0.00, 1.00, 1.00, 0.03, 0.55, 0.00, 208, 1, 0.00, 0.11, 0.18, 0.00, 0.01, 0.00, 0.42, 1.00, portsweep. Because the data set contains discrete and continuous data, so, we need to standardize and normalize the data in order to fit the input of neurons and avoid the situation of large numbers eating decimals.

Conflicts of Interest

The authors declare that they have no conflicts of interest.

Acknowledgments

This work was supported by the National Natural Science Foundation of China (61973168, 61973170, and 41675156), and University-Industry Collaborative Education Program of Ministry of Education (201901059005, 201802048012, and 201702177099).

References

- [1] G. Oluwafunmilayo, "An assessment of cybersecurity technologies in the selected universities in southwestern Nigeria," *International Journal of Computer Applications*, vol. 178, no. 50, pp. 11–18, 2019.
- [2] M. Thurber, "CCX Technologies releases cybersecurity hardware," *Aviation International News*, vol. 50, no. 8, p. 6, 2019.
- [3] P. Astromskis, "Legal technologies and cyber security in the singularity age," *Law Review*, vol. 16, no. 2, pp. 34–57, 2017.
- [4] A. A. M. Al-Dherasi and A. Annor-Antwi, "Dependence on blockchain technology for future cybersecurity advancement: a systematic analysis," *Computer Science and Information Systems*, vol. 1, no. 1, pp. 1–13, 2019.
- [5] Y. Raban and A. Hauptman, "Foresight of cyber security threat drivers and affecting technologies," *Foresight*, vol. 20, no. 4, pp. 353–363, 2018.
- [6] M. D. Cavely, "Cybersecurity research meets science and technology studies," *Politics & Governance*, vol. 6, no. 2, p. 22, 2018.
- [7] J. Wider, "C-Suite innovators discuss advances in technology, cybersecurity, interoperability, analytics, and more," *Health Management Technology*, vol. 39, no. 3, pp. 6–9, 2018.
- [8] T. Kasama, "3 cybersecurity technologies :darknet monitoring and analysis:3-1 long-term darknet analysis in NICTER," *Journal of the National Institute of Information & Communications Technology*, vol. 63, no. 2, pp. 25–31, 2016.
- [9] B. Alluhaybi, M. S. Alrahhal, A. Alzhrani et al., "A survey: agent-based software technology under the eyes of cyber security, security controls, attacks, and challenges," *International Journal of Advanced Computer Science & Applications*, vol. 10, no. 8, p. 211, 2019.

- [10] W. Hooper, "Cybersecurity for media technology products," *Smpte Motion Imaging Journal*, vol. 126, no. 1, pp. 1–4, 2017.
- [11] C. D. Calhoun, "Incorporating blended format cybersecurity education into a community College information technology program," *Community College Journal of Research and Practice*, vol. 41, no. 6, pp. 344–347, 2017.
- [12] M. Albettar, "Evaluation and assessment of cyber security based on Niagara framework: a review," *Journal of Cyber Security Technology*, vol. 3, no. 3, pp. 125–136, 2019.
- [13] Q. Ye, "A modular approach for implementation of honeypots in cyber security," *Advances in Computational Ences and Technology*, vol. 11, no. 2, pp. 105–115, 2018.
- [14] S. Suzanne, R. Aftin, C. Seth et al., "The evolving state of medical device cybersecurity," *Biomedical Instrumentation & Technology*, vol. 52, no. 2, pp. 103–111, 2018.
- [15] M. Orcutt, "Venture capitalists chase rising cybersecurity spending," *Technology Review*, vol. 119, no. 2, pp. 72–73, 2016.
- [16] T. Takahashi, "6 security architecture techniques 6-1 cybersecurity information discovery technique and knowledge base," *Journal of the National Institute of Information & Communications Technology*, vol. 63, no. 2, pp. 143–148, 2016.
- [17] C. S. Kruse, B. Frederick, T. Jacobson, and D. K. Monticone, "Cybersecurity in healthcare: a systematic review of modern threats and trends," *Technology and Health Care*, vol. 25, no. 1, pp. 1–10, 2017.
- [18] R. Ganesan, S. Jajodia, A. Shah, and H. Cam, "Dynamic scheduling of cybersecurity analysts for minimizing risk using reinforcement learning," *ACM Transactions on Intelligent Systems and Technology*, vol. 8, no. 1, pp. 1–21, 2016.
- [19] S. T. Hamman, K. M. Hopkinson, R. L. Markham, A. M. Chaplik, and G. E. Metzler, "Teaching game theory to improve adversarial thinking in cybersecurity students," *IEEE Transactions on Education*, vol. 60, no. 3, pp. 205–211, 2017.
- [20] N. Radziwill and M. Benton, "Cybersecurity cost of quality: managing the costs of cybersecurity risk management," *Software Quality Professional*, vol. 19, no. 4, pp. 25–43, 2017.
- [21] T. Butts, "Cybersecurity for broadcasters," *TV Technology*, vol. 37, no. 2, p. 4, 2019.
- [22] W. G. . Wendy, "Measuring information security and cybersecurity on private cloud computing," *Journal of Theoretical & Applied Information Technology*, vol. 97, no. 1, pp. 156–168, 2019.
- [23] D. N. Burrell, "Assessing the value of executive leadership coaches for cybersecurity project managers," *International Journal of Human Capital and Information Technology Professionals*, vol. 10, no. 2, pp. 20–32, 2019.
- [24] Y. Tsuda, N. Kanaya, T. Tomine et al., "4 cyber-security technologies: live network monitoring and analysis technologies 4-1 NIRVANA-kai: a real-time visual siem system Against targeted attacks," *Journal of the National Institute of Information & Communications Technology*, vol. 63, no. 2, pp. 67–75, 2016.
- [25] S. G. Langer, "Cyber-security issues in healthcare information technology," *Journal of Digital Imaging*, vol. 30, no. 1, pp. 117–125, 2017.

Research Article

Matching Sensor Ontologies with Simulated Annealing Particle Swarm Optimization

Hai Zhu ¹, Xingsi Xue ², Aifeng Geng,³ and He Ren ³

¹School of Network Engineering, Zhoukou Normal University, Zhoukou, Henan 466001, China

²Intelligent Information Processing Research Center, Fujian University of Technology, Fuzhou, Fujian 350118, China

³College of Electrical and Power Engineering, Taiyuan University of Technology, Taiyuan 030024, China

Correspondence should be addressed to Xingsi Xue; jack8375@gmail.com

Received 10 February 2021; Revised 12 March 2021; Accepted 15 March 2021; Published 24 March 2021

Academic Editor: Hsu-Yang Kung

Copyright © 2021 Hai Zhu et al. This is an open access article distributed under the Creative Commons Attribution License, which permits unrestricted use, distribution, and reproduction in any medium, provided the original work is properly cited.

In recent years, innovative positioning and mobile communication techniques have been developing to achieve Location-Based Services (LBSs). With the help of sensors, LBS is able to detect and sense the information from the outside world to provide location-related services. To implement the intelligent LBS, it is necessary to develop the Semantic Sensor Web (SSW), which makes use of the sensor ontologies to implement the sensor data interoperability, information sharing, and knowledge fusion among intelligence systems. Due to the subjectivity of sensor ontology engineers, the heterogeneity problem is introduced, which hampers the communications among these sensor ontologies. To address this problem, sensor ontology matching is introduced to establish the corresponding relationship between different sensor terms. Among all ontology matching technologies, Particle Swarm Optimization (PSO) can represent a contributing method to deal with the low-quality ontology alignment problem. For the purpose of further enhancing the quality of matching results, in our work, sensor ontology matching is modeled as the meta-matching problem firstly, and then based on this model, aiming at various similarity measures, a Simulated Annealing PSO (SAPSO) is proposed to optimize their aggregation weights and the threshold. In particular, the approximate evaluation metrics for evaluating quality of alignment without reference are proposed, and a Simulated Annealing (SA) strategy is applied to PSO's evolving process, which is able to help the algorithm avoid the local optima and enhance the quality of solution. The well-known Ontology Alignment Evaluation Initiative's benchmark (OAEI's benchmark) and three real sensor ontologies are used to verify the effectiveness of SAPSO. The experimental results show that SAPSO is able to effectively match the sensor ontologies.

1. Introduction

In recent years, innovative positioning and mobile communication techniques have been developing to achieve Location-Based Services (LBSs) [1, 2]. With the help of sensors, LBS is able to detect and sense the information from the outside world to provide location-related services. To implement the intelligent LBS, it is necessary to develop the Semantic Sensor Web (SSW) [3, 4]; as the kernel technique of the SSW, sensor ontology is a standard information exchange model, which serves as the basis for different machines to understand semantics and implement the sensor data interoperability, information sharing, and knowledge fusion among intelligence systems.

Due to the subjectivity of sensor ontology engineers, they might make use of various concepts to mean the same thing, or one concept might have more than one meaning, yielding the problem of heterogeneity that affects semantic interoperability between ontologies. Ontology matching [5–7] can be seen as a powerful tool to face this challenge, which has been widely applied in different application domains, such as Artificial Internet of Things (AIoT) [8, 9] and biomedical domain [10]. Sensor ontology matching can be used to discover the semantic relationships of different sensor ontologies, which is capable of determining the correspondences between concepts of heterogeneous sensor. The similarity measure is critical for a sensor ontology matching technique. Due to the complicated semantic

relationships among the sensor data, a single similarity measure cannot ensure that it is able to distinguish all the semantically identical entities in any matching context. Thus, several different similarity measures are usually aggregated to enhance the result's confidence. Ontology matching is generally interpreted as how to find a set of appropriate weights and threshold to achieve high-quality ontology alignments.

Particle Swarm Optimization (PSO) [11] is a contributing methodology for determining high-quality ontology alignments [12]. Although PSO converges fast, it is apt to fall into the local optima, which makes it unable to find the global optimal solution. To overcome this drawback, in this work, aiming at various similarity measures, a Simulated Annealing PSO (SAPSO) is proposed to optimize their aggregation weights and the threshold. Particularly, in the process of evolving process, SAPSO introduces a Simulated Annealing (SA) strategy to further enhance the quality of solution. The innovation points of this work are as follows:

- (1) An approximate evaluation metric on ontology alignment is proposed, and an optimization model for the sensor ontology meta-matching problem is constructed.
- (2) To effectively solve the problem of sensor ontology meta-matching, an ontology meta-matching framework and a SAPSO algorithm are proposed.

This paper is organized as follows. Section 2 presents the related work. Section 3 gives the formal definitions on the sensor ontology and similarity measure. Section 4 constructs the optimization model for sensor meta-matching problem. Section 5 presents the SAPSO. Section 6 shows the experimental results and the corresponding analysis. Finally, Section 7 draws the conclusions and puts forward the future research directions.

2. Swarm Intelligence Algorithm-Based Ontology Matching Technique

In different sensor ontologies, due to the subjectivity of the designer, conceptual name in the sensor system may have different naming methods and definition methods, thus causing the problem of communication inconvenience between different sensor ontologies [13, 14]. Due to the complex intrinsic nature of matching two ontologies, swarm intelligence algorithms, such as PSO, Parallel Compact Cuckoo Search Algorithm (PCCSA) [15], Artificial Bee Colony (ABC) algorithm [16], Firefly Algorithm (FA) [10, 17], and Evolutionary Algorithm (EA) [18, 19], have become effective methods to determine the ontology alignments.

Bock et al. [20] used a discrete PSO algorithm to optimize the results of ontology entity matching, which does not require the computation of large similarity matrices. He et al. [16] used the ABC-based matcher to solve the ontology meta-matching problem, whose results can be proved more effective. Xue et al. [17] proposed a Compact Cooperative Firefly Algorithm- (CCFA-) based ontology matching

system, which can improve the search efficiency effectively by using a new mechanism. Xue et al. [12] also proposed a compact multiobjective PSO to solve the matching problem of large-scale biomedical ontology. In addition, they [10] also proposed a Compact Firefly Algorithm (CFA), which greatly reduced the running time and memory consumption by two compact movement operators. Chu et al. [21] first built an ontology model in vector space and proposed a Compact Evolutionary Algorithm (CEA) to solve the ontology matching problem. In this work, we further introduce SA into PSO's evolving process to trade off its exploration and exploitation, which is able to effectively help the algorithm to jump out of the local optima.

3. Sensor Ontology and Similarity Measure

3.1. Sensor Ontology. In the computer and information science field, ontology is a formal list of all the concepts and their relationships in a particular domain [18]. With respect to the SSW, a sensor ontology is used as the most important and extensive model for describing the concepts related to sensors and the IoT [22, 23], such as the sensor's output, observations, observation characteristics, and so on. For ease of description, a set of triples (C, P, I) [24] is used to represent a sensor ontology, where C , P , and I represent the sets of class or concept, property, and instance, respectively. An example of sensor ontology is shown in Figure 1, where an ellipse represents a class and the arrows between the ellipses represent the class' properties. A class is a collection of instances, and each element in I is an instance of a class. Generally, classes, properties, and instances are collectively called entities.

The goal of sensor ontology matching [25] is to establish correspondences between heterogeneous entities and find the set of entity correspondences, the so-called sensor ontology alignment [26]. Here, an entity correspondence is a five-tuple $\langle id, e, e', c, R \rangle$, where id refers to the identifier of entity correspondence; e and e' are the entities of two ontologies, respectively; c is the degree of confidence between e and e' that can be matched, usually at $[0, 1]$; and R is the equivalence relationship between e and e' . The process of matching two sensor ontologies is shown in Figure 2, where O_1 and O_2 , respectively, represent the two sensor ontologies to be aligned, A_I is the input alignment, p is a set of parameters, r represents some external resources, and A_N is the obtained alignment.

A similarity measure uses particular information to calculate to what extent two entities are similar. Generally, the similarity measures can be composed of three types, which are described in detail in Section 3.2.

3.2. Similarity Measure

3.2.1. Syntax-Based Similarity Measure. A syntactic measure calculates the string distance between entities of different ontologies. In our work, we use the N-Gram distance, which is an effective syntactic metric in the ontology matching domain. N-Gram has an obvious advantage in comparing the similarity between two strings [27, 28]. Given two

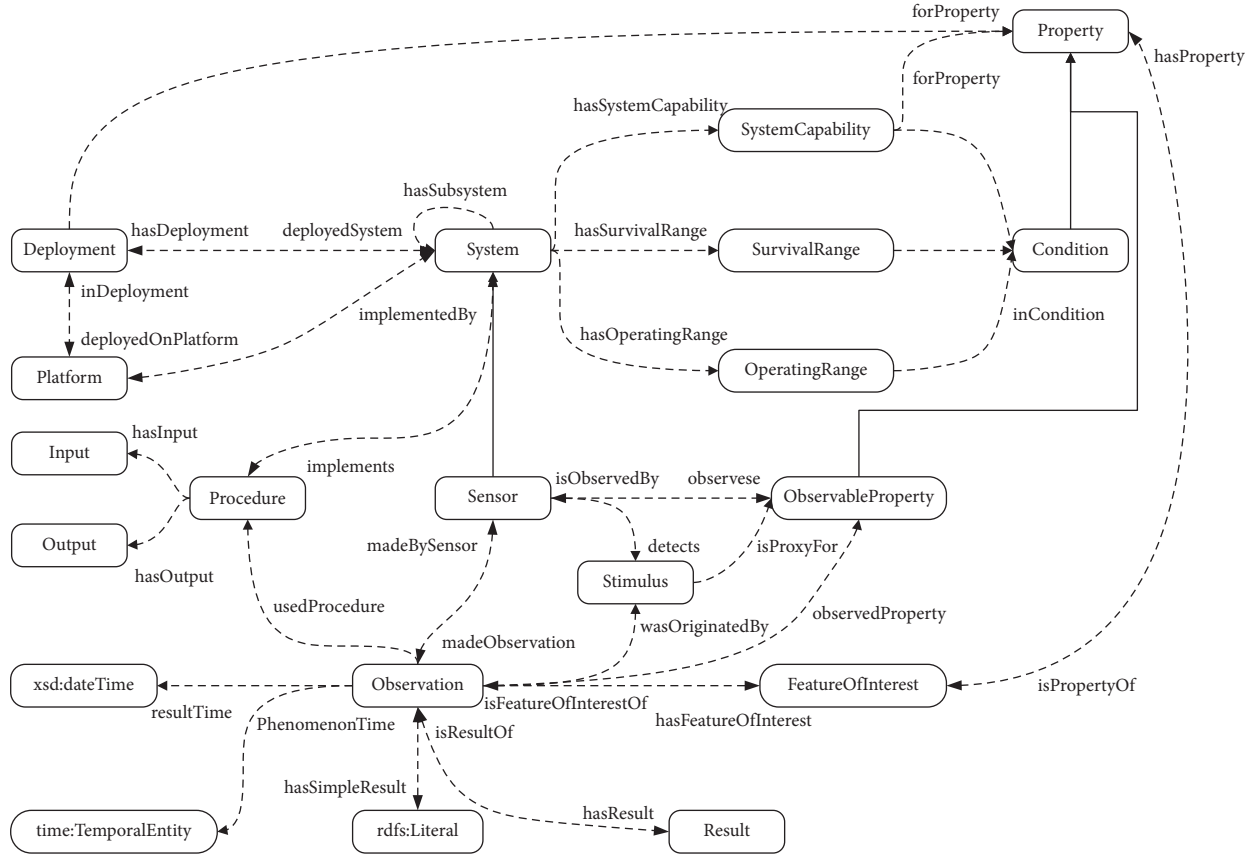


FIGURE 1: An example of sensor ontology.

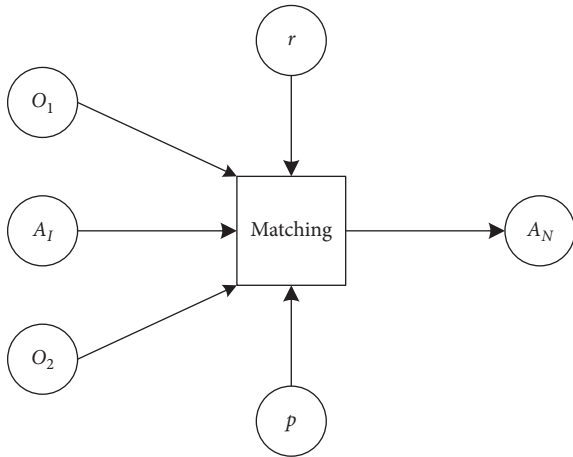


FIGURE 2: The process of sensor ontology matching.

strings, their N-Gram distance is calculated by measuring the number of common substrings they have. To be specific, the N-Gram distance is defined as follows:

$$N - \text{Gram}(s_1, s_2) = \frac{2 \times C(s_1, s_2)}{n_{s_1} + n_{s_2}}, \quad (1)$$

where s_1, s_2 are two strings to be computed, respectively; N stands for the length of each substring after splitting the original string, which is generally set to 2 or 3 (the lower the

value, the higher their similarity; the value of N in this work is 3); $C(s_1, s_2)$ is the number of their common substrings; and n_{s_1} and n_{s_2} are their lengths, respectively.

3.2.2. Linguistic-Based Similarity Measure. Semantic similarity calculates the similarity between entities according to the semantic context. In our approach, we use the Wu-Palmer [29] similarity measure, in particular, it returns a fraction to indicate the degree of similarity between the two words. In this work, we use the WordNet [30], which is an English dictionary based on cognitive linguistics, to calculate the related variables in Wu-Palmer. Here, we choose Wu-Palmer because it is the most popular WordNet-based similarity measure, which calculates the semantic similarity between two strings by considering not only the conceptual depth in the hierarchical semantic structure of WordNet but also their context information. To be specific, it is defined as follows:

$$\text{Wu-Palmer}(s_1, s_2) = \frac{2 \times \text{depth}(lcs(s_1, s_2))}{\text{depth}(s_1) + \text{depth}(s_2)}, \quad (2)$$

where depth denotes the depth of the word in WordNet's hierarchical semantic structure and $lcs(s_1, s_2)$ is the closest common parent concept of s_1 and s_2 .

3.2.3. Structure-Based Similarity Measure. The main idea of structure-based similarity measure is to determine two entities' similarity through neighborhood entities

(superclass and subclass relationship). In general, matched entities have similar structures, that is, they have the same number of superclass and subclass; conversely, if two entities have the same number of superclass and subclass, they are considered similar. In our work, the structure-based

similarity measure that we use is called Out-In degree, which calculates the similarity according to the number of superclasses and subclasses of entities in different ontologies, which is defined as follows:

$$\text{Struc}(s_1, s_2) = \begin{cases} 1, & \text{if two entities have the same number of subclasses and super classes,} \\ 0, & \text{if two entities have different number of subclasses and super classes.} \end{cases} \quad (3)$$

Based on three similarity measures, we can get three similarity matrices, respectively. The similarity matrix is defined as a matrix of $m \times n$, where m and n are, respectively, the number of entities in the original ontology and the target ontology. Each element of the matrix is the similarity value of two corresponding entities determined by the similarity measure. After that, through assigning an aggregating weight for each similarity matrix, we can obtain an aggregated matrix, which is filtered by using a similarity threshold to determine the final matrix. The ontology meta-matching problem can be defined as determining the optimal aggregating weights and the threshold to get a high-quality ontology alignment, which will be formally defined in the following.

4. Sensor Ontology Meta-Matching Problem

In general, optimization problems can be divided into unconstrained optimization problems and constrained optimization problems; the classification criteria are whether there are constraints. In this paper, the problem of sensor ontology meta-matching is modeled as a constrained continuous optimization problem, and its constraints are the sum of the weights and the threshold of the similarity measure, which is explained in more detail in the following. There are three points to consider when building an optimization model: constraint conditions, decision variables, and objective function.

4.1. Constraint Conditions and Decision Variables. For convenience, the process of sensor ontology meta-matching can be described as a seven-tuples $(O_1, O_2, n, M, \omega, \text{thres}, A)$, where O_1 and O_2 represent the source ontology and target ontology, respectively; n represents the number of similarity measures; M represents a set of similarity matrices; ω is the set of aggregating weights; thres is the similarity threshold; and A is the obtained sensor ontology alignment. In particular, M and ω are, respectively, defined as follows:

$$M = \sum_{i=1}^n \omega_i \times M_i, \quad (4)$$

$$\sum_{i=1}^n \omega_i = 1, \quad \omega_i \in [0, 1].$$

The framework of sensor ontology meta-matching is shown in Figure 3, where m_1, m_2, \dots, m_n are the similarity

measures; M_1, M_2, \dots, M_n are the similarity matrices; $\omega_1, \omega_2, \dots, \omega_n$ are aggregating weights on the similarity matrices, respectively; M is the aggregated matrix; A is alignment determined by M ; and thres is the threshold. As can be seen from the figure, the ultimate goal of sensor ontology meta-matching is to find a suitable weight for each similarity matrix and a suitable threshold value for the comprehensive similarity matrix, which is able to ensure the quality of the alignment.

4.2. Objective Function. The quality of the results of sensor ontology meta-matching is usually measured by f -measure, whose value is related to both recall and precision. Traditional recall, precision, and f -measure [9] are defined in equations (5)–(7):

$$\text{recall} = \frac{|R \cap A|}{|R|}, \quad (5)$$

$$\text{precision} = \frac{|R \cap A|}{|A|}, \quad (6)$$

$$f\text{-measure} = \frac{2 \times \text{recall} \times \text{precision}}{\text{recall} + \text{precision}}, \quad (7)$$

where R is the standard alignment; A is the alignment determined by some matching techniques; recall divides true positive correspondences we find by the number of all correct matching pairs, which represents whether the matching results found by us are complete or not; and precision divides the number of true positive correspondences we find by the cardinality of found alignment and represents whether our match is accurate. Their values are between 0 and 1, and the quality of the results is judged by these values, but neither recall nor precision can evaluate the alignment effectively because a high recall value does not mean that our results are accurate and a high precision value does not mean that our results are complete. Therefore, in order to consider the evaluation results of recall and precision, we use f -measure to combine these two indicators. But the traditional evaluation index needs to work with reference matching results, which is impossible to obtain in advance in most cases. To overcome this drawback, in the following, we propose three new quality evaluation metrics [31] on sensor ontology alignment, i.e., ApproximateRecall, ApproximatePrecision, ApproximateFmeasure, to approximate traditional recall, precision, and f -measure:

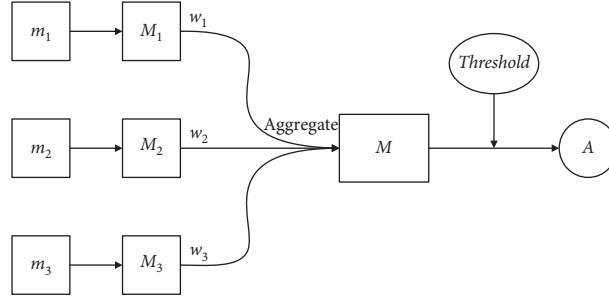


FIGURE 3: Sensor ontology meta-matching framework.

$$\text{Approximate Recall}(M) = \frac{2 \times \sum_{i=1}^m \sum_{j=1}^n \Phi(|M_{ij}|)}{m+n},$$

$$\Phi(|M_{ij}|) = \begin{cases} 1, & \text{when element } M_{ij} \text{ is largest in } i\text{th row and } j\text{th column,} \\ & \text{in } M \text{ matrix, and satisfies threshold criteria,} \\ 0, & \text{otherwise,} \end{cases} \quad (8)$$

where M represents the composite similarity matrix and $|M_{ij}|$ is the value of row i , column j of the composite similarity matrix M .

$$\text{Approximate Precision}(M) = \frac{\sum_{i=1}^m \sum_{j=1}^n |M_{ij}|}{\sum_{i=1}^m \sum_{j=1}^n \Psi(|M_{ij}|)},$$

$$\Psi(|M_{ij}|) = \begin{cases} 1, & \text{when element } M_{ij} \text{ is largest in } i\text{th row and } j\text{th column,} \\ 0, & \text{otherwise,} \end{cases} \quad (9)$$

where M represents the composite similarity matrix and $|M_{ij}|$ is the value of row i , column j of the composite similarity matrix M .

$$\text{ApproximateFmeasure}(M) = \frac{2 \times \text{ApproximateRecall}(M) \times \text{ApproximatePrecision}(M)}{\text{ApproximateRecall}(M) + \text{ApproximatePrecision}(M)}, \quad (10)$$

and finally, the objective function we need to optimize is defined as follows:

$$F(M) = \max \text{ApproximateFmeasure}(M). \quad (11)$$

5. Sensor Ontology Meta-Matching with Simulated Annealing Particle Swarm Optimization

5.1. Particle Swarm Optimization. PSO is an algorithm based on swarm cooperation, which is developed by simulating the birds' foraging behavior [32]. PSO initializes a set of random particles (stochastic solutions) and iteratively searches the

optimal solution; in each iteration, the particles update themselves by tracking two extremes. The formula for updating the speed and position of PSO is as follows:

$$v_i^{t+1} = v_i^t + c_1 \times \text{rand}() \times (\text{pbest}_i^t - \text{present}_i^t) + c_2 \times \text{rand}() \times (\text{gbest}^t - \text{present}_i^t), \quad (12)$$

$$\text{present}_i^{t+1} = \text{present}_i^t + v_i^{t+1}, \quad (13)$$

where i means the i th particle, $i \in [1, n]$, n is the size of population, t is the number of iterations, v is the speed of particles, c_1 and c_2 are learning factors, rand is a random number in $[0, 1]$, pbest is the extremum of an individual, the best solution

found by the particle itself, *gbest* is the global extremum, and present is the current position of the particle. Compared with other swarm intelligence algorithms, PSO has such advantage as only one-way information flow, i.e., all the particles are able to converge quickly, but it tends to fall into the local optima. To solve this problem, the SA strategy is introduced into the evolutionary process of PSO to make it better optimized.

5.2. Encoding Mechanism. A decimal encoding method is used in this work to encode a solution, which encodes a set of weights and a threshold into each particle. With respect to the encoding process on n aggregating weights and one threshold, first, n real numbers are generated in $[0, 1]$ randomly, which are, respectively, denoted as $r_1, r_2, \dots, r_{n-1}, r_n$, represents the encoding information of a particle. Then, the first $n-1$ numbers r_1, r_2, \dots, r_{n-1} are sorted in the ascending order, and we get $r'_1, r'_2, \dots, r'_{n-1}$. In particular, the final number r_n is the threshold for filtering the final alignment. Finally, n aggregating weights are obtained as follows:

$$\omega_t = \begin{cases} r'_1, & t = 1, \\ r'_t - r'_{t-1}, & 1 < t < n, \\ 1 - r'_{n-1}, & t = n. \end{cases} \quad (14)$$

Each particle in the population contains a set of weights and a threshold. An example of encoding process on aggregating weights is shown in Figure 4.

This encoding mechanism on the aggregating weights meets their constraints defined in equation (4), and it is also of help to reduce the solution's dimension, and it ensures that different groups of numbers correspond to different aggregating weights.

5.3. Simulated Annealing. Simulated annealing algorithm is an algorithm that introduces random factors into the search process. The simulated annealing algorithm does not completely reject the worse solution, which greatly improves the probability of getting rid of the local optimal solution. Generally, SA contains two parts, which are metropolis algorithm and annealing process. Metropolis algorithm aims at helping the solution jump out of the local optima, which accepts new solutions with a certain probability. Annealing is a process in which T , the parameter of the probability of accepting the worse solution, decreases with the iteration, so that as the iteration proceeds, the probability of accepting a worse solution gradually decreases. Assuming that a system's previous solution is denoted as $s(n)$ and the current solution is denoted as $s(n+1)$, where n is the current iteration number, the acceptance probability P of the system on changing from $s(n)$ to $s(n+1)$ is

$$P = \begin{cases} 1, & \text{if } F(n+1) \geq F(n), \\ e^{-(F(n)-F(n+1))/T}, & \text{if } F(n+1) < F(n), \end{cases} \quad (15)$$

$$T = \frac{1}{\sqrt{1 + 0.1 \times n}} \times T_0, \quad (16)$$

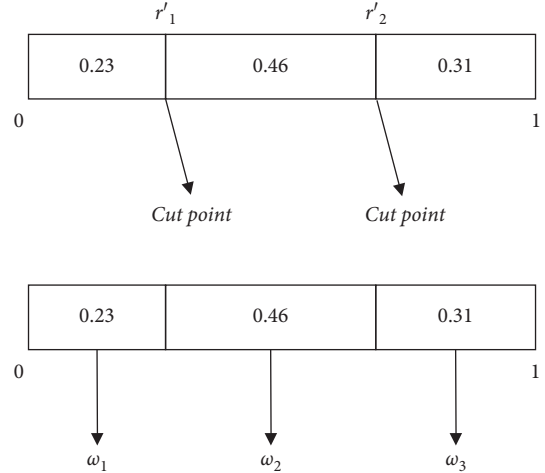


FIGURE 4: An example of encoding process on aggregating weights.

where $F(n)$ and $F(n+1)$ are the fitness of the previous solution and current solution, respectively. T is a parameter that represents the annealing temperature. Here, the initial temperature T_0 should be large, and as the iteration goes on, the temperature T would be gradually reduced, so as to ensure that the probability of state transition is gradually reduced from 1. In such situation, any solution can be accepted at the beginning of the iteration, and the current solution stays unchanged at the end of the iteration. Therefore, SA not only avoids the algorithm falling into local optimization too quick but also guarantees the algorithm's convergence.

For the sake of clarity, the pseudocode of SAPSO is presented in Algorithm 1.

First, the particles are initialized, and each particle generates three random numbers r_1, r_2 , and r_3 on the $[0, 1]$ interval, representing the cut points of the two weights and a threshold, respectively. And each particle also generates three initial velocities. Consider the cut points of weights and a threshold contained by the particle as the best cut points and threshold of individual history for each particle, denoted as $pbest_1, pbest_2$, and $pbest_3$, respectively, and calculate the fitness values for each particle (line 8). The two cut points and one threshold of each particle are denoted as the three dimensions of the particle. Find out the best one of each dimension of all particles, denoted as $gbest_0, gbest_1$, and $gbest_2$, respectively. Initialize the temperature T_0 and calculate/update the annealing temperature T_k (line 16) at the beginning of the iteration based on equation (16), update the cut points and threshold for each particle with the PSO formulas (lines 19 and 20), and get the updated fitness values based on the formulas in Section 4.2 (line 21). Then, there is the key to simulated annealing: if the updated particle has greater fitness than its predecessor, then the solution transition probability is set to 1 (line 23), and the new particle is considered as the *pbest*; otherwise, it is accepted at a certain probability according to equation (15). If the probability condition is satisfied, the new particle is considered as the *pbest* in the next generation to update the velocity and position with PSO (lines 19 and 20). Finally, the

```

(1) Input: Source and target ontologies  $O_1$  and  $O_2$ , number of iteration  $k_{\max}$ , initial temperature  $T_0$ ,
(2) population size  $n$ 
(3) for ( $i = 0; i < n; i++$ )
(4) for ( $j = 0; j < 3; j++$ )
(5)  $v_j[i] = \text{random}(0, 1)$ 
(6)  $r_j[i] = \text{random}(0, 1)$ 
(7)  $\text{pbest}_j[i] = r_j[i]$ 
(8) calculate fitness [ $i$ ]
(9)  $f[i] = \text{fitness}[i]$ 
(10) end for
(11) end for
(12)  $\text{gbest}_0 = \max \{\text{pbest}_0[i]\}$ 
(13)  $\text{gbest}_1 = \max \{\text{pbest}_1[i]\}$ 
(14)  $\text{gbest}_2 = \max \{\text{pbest}_2[i]\}$ 
(15) while  $k < k_{\max}$  do
(16)  $T_k = 1/\sqrt{1 + 0.1 \times k} \times T_0$ 
(17) for ( $i = 0; i < n; i++$ )
(18) for ( $j = 0; j < 3; j++$ )
(19)  $v_j[i] = v_j[i] + c_1 \times \text{random}(0, 1) \times (\text{pbest}_j[i] - r_j[i]) + c_2 \times \text{random}(0, 1) \times (\text{gbest}_j - r_j[i])$ 
(20)  $r_j[i] = r_j[i] + v_j[i]$ 
(21) update fitness [ $i$ ]
(22) if ( $\text{fitness}[i] \geq f[i]$ )
(23)  $P = 1$ 
(24)  $\text{pbest}_j[i] = r_j[i]$ 
(25) else
(26)  $P = e^{-(f[i] - \text{fitness}[i]/T_k)}$ 
(27) if ( $P \geq \text{random}(0, 1)$ )
(28)  $\text{pbest}_j[i] = r_j[i]$ 
(29) end if
(30) end if
(31)  $f[i] = \text{fitness}[i]$ 
(32) end for
(33) end for
(34)  $\text{gbest}_0 = \max \{\text{pbest}_0[i]\}$ 
(35)  $\text{gbest}_1 = \max \{\text{pbest}_1[i]\}$ 
(36)  $\text{gbest}_2 = \max \{\text{pbest}_2[i]\}$ 
(37)  $\text{Gbest} = \max \{f[i]\}$ 
(38) end while
(39) Output Gbest

```

ALGORITHM 1: The pseudocode of SAPSO.

pbest particle whose fitness value is the largest is treated as the global best particle of the population for the next generation of PSO updating. If the end condition is not met, the loop executes the program until the end condition is met and the globally optimal fitness value, f -measure, is output.

5.4. The Flowchart of SAPSO. SAPSO is a method using annealing strategy to avoid the local optimal solution of PSO algorithm. The flowchart of SAPSO is shown in Figure 5.

First, we initialize the entire population, including the parameters of each particle. The second step is to obtain the fitness value for each particle and then judge whether the iteration has reached the max iteration; if the max iteration is reached, the iteration process ends and the results are output; otherwise, the entire population will be optimized using PSO algorithm according to equations (12) and (13), and obtain each particle's new fitness; at this point, we use

“state” to represent all the information that the particle contains, including its fitness value and encoding information, and the particle's fitness is used to indicate the particle's state; *pbest* state and *gbest* states are, respectively, the information of an individual's corresponding local best and the population's global best during the evolutionary process. And then it is going to judge whether the new state is better than that of the previous generation. If the new state is better than the previous generation state, the new state is accepted, which satisfies equation (15), which is the formula for simulated annealing. Using simulated annealing, if the particle accepts the new state, the particle treats the new state as *pbest* state; otherwise, the particle treats the original state as *pbest* state; then, *gbest* state is obtained by comparing the *pbest* state of each particle. The annealing temperature needs to be recalculated according to equation (16) before the next iteration, and then the process is looped until the end condition is met.

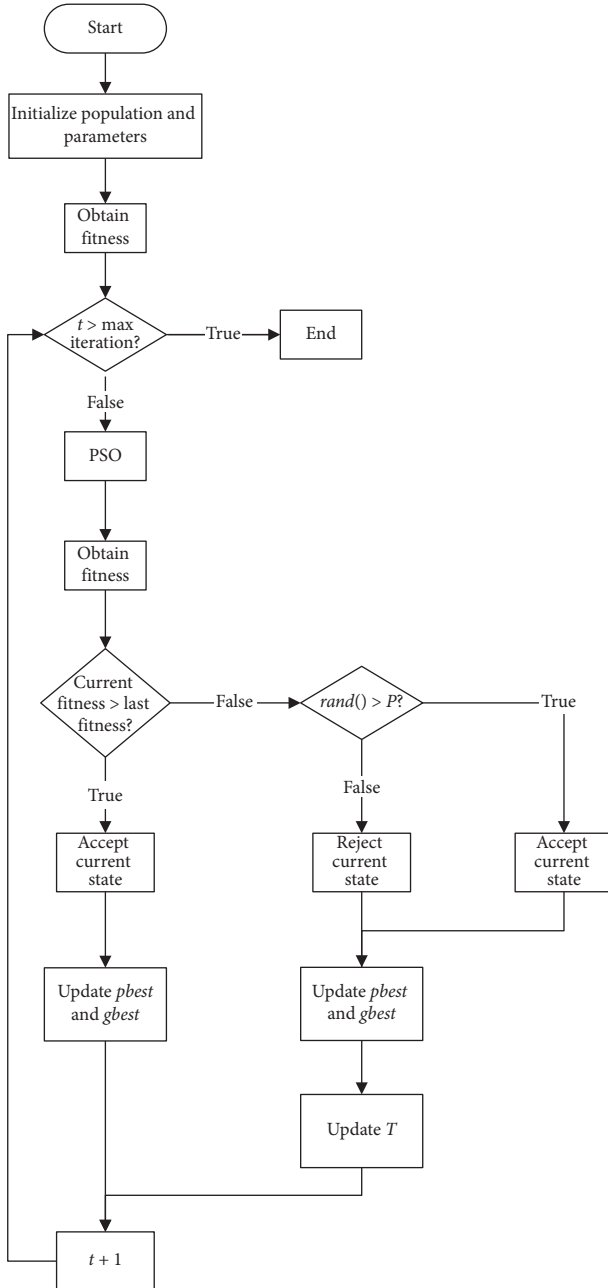


FIGURE 5: The flowchart of SAPSO.

6. Experiment Results and Analysis

In this experiment, to verify the effectiveness of SAPSO, we use the OAEI's benchmark and three real sensor ontologies, i.e., SOSA [33] and new SSN and old SSN ontology [22]. The test results of SAPSO and PSO shown in Tables 1 and 2 are the mean values of 30 independent runs.

6.1. Configuration. Similarity measures used in this experiment:

- Syntactic-based measure: N-Gram
- Linguistic-based measure: Wu-Palmer

Structure-based measure: Out-In Degree

The configuration on SPSO and PSO is as follows:

- Population size: 60
- Maximum number of iterations: 300
- Learning factor c_1, c_2 : 2
- Initial temperature: 10.0

These parameters are determined in an empirical way, which is able to ensure the quality of the alignments in all testing cases.

6.2. Results and Analysis

6.2.1. OAEI Benchmark. The brief description of OAEI's benchmark is presented in Table 3. The first column in Table 3 is the ID of the testing cases, each corresponding to a testing ontology. We divide these test ontologies into five groups according to their specific characteristics, which is described in the second column of the table. We compare SAPSO with PSO-based ontology matching technique and OAEI's participants, i.e., edna, AML [34], LogMap [35], LogMapLt [35], XMap [36], and LogMapBio [35].

In Table 1, SAPSO's results are outperforming all the competitors except XMap on the testing cases 221–247. The reason is that on testing cases 221–247, the source ontology and the target ontology are identical in terms of lexical and semantic features but differ in terms of structural features, and our structure-based similarity measure is not effective, which reduces the f -measure. In particular, on all testing cases, SAPSO's results are all equal to or better than PSO, which shows that the introduction of SA is able to improve PSO's searching ability and improve the solution's quality. From the average of f -measure, SAPSO performs better than others, which shows that SAPSO plays an effective role in improving the quality of ontology matching.

6.2.2. Real Sensor Ontologies. SOSA (<http://www.w3.org/ns/sosa/>), the basic class and property of SSN (<http://www.w3.org/ns/ssn/>) ontology, represents the lightweight core of new SSN ontology. These sensor ontologies describe the function and performance of the sensor. They support many applications and use cases, such as signal detection in large-scale scientific exploration, home infrastructure monitoring, livelihood services, observation-driven ontology engineering, the World Wide Web, sensor data service system, and more [37]. The new SSN differs from the original SSN in that it simplifies the relationship between the device, platform, and system classes on the old SSN. We tested SAPSO on three real sensor ontologies with our sensor ontology meta-matching system and got their f -measure, recall, and precision values. Table 2 shows the matching results of SAPSO.

In Table 2, the first column refers to two matched sensor ontologies, and second, third, and fourth columns are, respectively, f -measure, recall, and precision of the alignments. It can be seen from the table that on the task of matching

TABLE 1: *F*-measure results comparison.

	edna	AML	LogMap	LogMapLt	XMap	LogMapBio	PSO	Our way
101	0.78	0	0.95	0.71	0.97	0.62	1	1
201–201–8	0.315	0.231	0.474	0.345	0.391	0.267	0.808	0.812
221–247	0.831	0.754	0.814	0.726	0.961	0.598	0.952	0.96
248–266	0.318	0.36	0.436	0.338	0.413	0.202	0.5432	0.5487
Average	0.41	0.41	0.51	0.409	0.51	0.28	0.6458	0.6514

TABLE 2: Measurement of *f*-measure, recall, and accuracy of SAPSO on three sensor ontologies.

	<i>F</i> -measure	Recall	Precision
Old SSN-new SSN	0.98	0.97	1.0
Old SSN-SOSA	0.98	0.97	1.0
New SSN-SOSA	1.0	1.0	1.0

TABLE 3: The relevant description of OAEI’s benchmark.

ID	Relevant description
101–104	The two matched ontologies are identical in terms of structural, lexical, and linguistic features
201–210	Two matched ontologies are identical in terms of structural features but differ in terms of lexical and linguistic features
221–247	Two matched ontologies are identical in terms of lexical and linguistic features but differ in terms of structural features
248–266	Two matched ontologies are different in terms of lexical, linguistic, and structural features
301–304	Two matched ontologies are cases from the real world

new SSN and SOSA, SAPSO is able to determine the perfect alignment. With respect to the other two matching tasks, SAPSO’s *f*-measure is also close to 1.0. Since there exist some complex correspondences in the reference alignment, i.e., one source concept corresponds to several target concepts, SAPSO fails to find them, which reduces its *f*-measure. In general, SAPSO is able to effectively match various sensor ontologies.

7. Conclusion and Future Work

LBS’s architecture is widely used in the fields of vehicle speed estimation [38], vehicle travel time prediction system [39], and bus arrival time prediction system [40]. Technologies and applications of LBS cannot be separated from sensors. To implement the intelligent LBS, different sensor ontologies need to be integrated on SSW. To this end, in this work, the new quality evaluation metrics are proposed to evaluate the traditional three evaluation metrics. And a mathematical model on sensor ontology meta-matching problem is constructed; finally, a SAPSO is presented to address the problem, which uses SA to help the algorithm avoid the local optima. To verify the effectiveness of SAPSO, we use the OAEI’s benchmark and three real sensor ontologies. Finally, the experiment proves that SAPSO is an effective method.

In the following work, the quality of the sensor ontology matching results would continue to be enhanced by taking into consideration those complex correspondences. At present, SAPSO still has some defects in determining the entity mappings with heterogeneous characteristics, which

makes its *f*-measure relatively low in those testing cases with heterogeneous structure; at the same time, SAPSO has some limitations, for example, its performance is related to initial value and parameters are sensitive. Last but not least, it is necessary to improve the approximate evaluation metrics on ontology alignment to better guide the algorithm to search for the global optima.

Data Availability

The data used to support this study can be found in <http://oei.ontologymatching.org>.

Conflicts of Interest

The authors declare that they have no conflicts of interest.

Acknowledgments

This study was supported by the National Natural Science Foundation of China (nos. 61801527 and 61103143) and the Natural Science Foundation of Fujian Province (no. 2020J01875).

References

- [1] A. Bröring, J. Echterhoff, S. Jirka et al., “New generation sensor Web enablement,” *Sensors*, vol. 11, no. 3, pp. 2652–2699, 2011.
- [2] D. J. Russomanno, C. R. Kothari, and O. A. Thomas, “Building a sensor ontology: a practical approach leveraging ISO and ogc models,” in *Proceedings of the 2005 International*

- Conference on Artificial Intelligence (IC-AI 2005)*, pp. 637–643, Las Vegas, NV, USA, June 2005.
- [3] A. Bröring, K. Janowicz, C. Stasch, and W. Kuhn, “Semantic challenges for sensor plug and play,” *Web and Wireless Geographical Information Systems*, vol. 5886, pp. 72–86, 2009.
 - [4] J. C. W. Lin, Y. Shao, Y. Djenouri, and U. Yun, “ASRNN: A recurrent neural network with an attention model for sequence labeling,” *Knowledge-Based Systems*, vol. 212, Article ID 106548, 2021.
 - [5] X. Xue and J. Chen, “Using compact evolutionary tabu search algorithm for matching sensor ontologies,” *Swarm and Evolutionary Computation*, vol. 48, pp. 25–30, 2019.
 - [6] X. Xue and Y. Wang, “Using memetic algorithm for instance coreference resolution,” *IEEE Transactions on Knowledge and Data Engineering*, vol. 28, no. 2, pp. 580–591, 2016.
 - [7] X. Xue and J. Chen, “Optimizing ontology alignment through hybrid population-based incremental learning algorithm,” *Memetic Computing*, vol. 11, no. 2, pp. 209–217, 2019.
 - [8] X. Xue and J. Liu, “Collaborative ontology matching based on compact interactive evolutionary algorithm,” *Knowledge-based Systems*, vol. 137, pp. 94–103, 2017.
 - [9] X. Xue and X. Yao, “Interactive ontology matching based on partial reference alignment,” *Applied Soft Computing*, vol. 72, pp. 355–370, 2018.
 - [10] X. Xue, “A compact firefly algorithm for matching biomedical ontologies,” *Knowledge and Information Systems*, vol. 62, no. 7, pp. 2855–2871, 2020.
 - [11] R. Eberhart and J. Kennedy, “A new optimizer using particle swarm theory,” in *Proceedings of the Sixth International Symposium on Micro Machine and Human Science*, pp. 39–43, Nagoya, Japan, October 1995.
 - [12] X. Xue, X. Wu, and J. Chen, “Optimizing biomedical ontology alignment through a compact multiobjective particle swarm optimization algorithm driven by knee solution,” *Discrete Dynamics in Nature and Society*, vol. 2020, Article ID 4716286, 2020.
 - [13] X. Xue and X. Wu, “Optimizing biomedical ontology alignment in lexical vector space,” *Journal of Intelligent & Fuzzy Systems*, vol. 38, no. 5, pp. 5609–5614, 2020.
 - [14] X. Xue and J. Liu, “Optimizing ontology alignment through compact MOEA/D,” *International Journal of Pattern Recognition and Artificial Intelligence*, vol. 31, no. 04, Article ID 1759004, 2017.
 - [15] P. Song, J. S. Pan, and S. Chu, “A Parallel compact Cuckoo search algorithm for three-dimensional path planning,” *Applied Soft Computing*, vol. 94, Article ID 106443, 2020.
 - [16] Y. He, X. Xue, and S. Zhang, “Using artificial bee Colony algorithm for optimizing ontology alignment,” *Journal of Information Hiding and Multimedia Signal Processing*, vol. 8, pp. 766–773, 2017.
 - [17] X. Xue and J. Chen, “Optimizing sensor ontology alignment through compact co-firefly algorithm,” *Sensors*, vol. 20, no. 7, 2020.
 - [18] X. Xue, J. Chen, and J. Pan, *Evolutionary Algorithm Based Ontology Matching Technique*, Science Press, Beijing, China, 2018.
 - [19] X. Xue and J. S. Pan, “An overview on evolutionary algorithm based ontology matching,” *Journal of Information Hiding and Multimedia Signal Processing*, vol. 9, no. 1, pp. 75–88, 2018.
 - [20] J. Bock and J. Hettenhausen, “Discrete particle swarm optimisation for ontology alignment,” *Information Sciences*, vol. 192, pp. 152–173, 2012.
 - [21] S. Chu, X. Xue, J. Pan, and X. Wu, “Optimizing ontology alignment in vector space,” *Journal of Internet Technology*, vol. 21, no. 1, pp. 15–23, 2020.
 - [22] A. Sheth, C. Henson, and S. S. Sahoo, “Semantic sensor Web,” *IEEE Internet Computing*, vol. 12, no. 4, pp. 78–83, 2008.
 - [23] M. Bermudez-Edo, T. Elsaleh, P. Barnaghi, and K. Taylor, “IoT-lite: a lightweight semantic model for the Internet of things and its use with dynamic semantics,” *Personal and Ubiquitous Computing*, vol. 21, no. 3, pp. 475–487, 2017.
 - [24] X. Xue, J. Lu, C. Jiang, and Y. Huang, “Sensor ontology metamatching with heterogeneity measures,” *Wireless Communications and Mobile Computing*, vol. 2020, no. 3, pp. 1–10, 2020.
 - [25] X. Xue, X. Wu, C. Jiang et al., “Integrating sensor ontologies with global and local alignment extractions,” *Wireless Communications and Mobile Computing*, vol. 2021, Article ID 6625184, 2021.
 - [26] X. Xue, C. Yang, C. Jiang et al., “Optimizing ontology alignment through linkage learning on entity correspondences,” *Complexity*, vol. 2021, Article ID 5574732, 2021.
 - [27] V. Mascardi, A. Locoro, and P. Rosso, “Automatic ontology matching via upper ontologies: a systematic evaluation,” *IEEE Transactions on Knowledge and Data Engineering*, vol. 22, no. 5, pp. 609–623, 2010.
 - [28] G. Stoilos, G. Stamou, and S. Kollias, “A string metric for ontology alignment,” *The Semantic Web - ISWC 2005*, vol. 3729, pp. 624–637, 2005.
 - [29] Z. Wu and M. Palmer, “Verb semantics and lexical selection,” in *Proceedings of the 32nd annual meeting on Association for Computational Linguistics*, pp. 133–138, Las Cruces, NM, USA, June 1994.
 - [30] G. A. Miller, “WordNet,” *Communications of the ACM*, vol. 38, no. 11, pp. 39–41, 1995.
 - [31] X. Xue and Y. Wang, “Optimizing ontology alignments through a memetic algorithm using both MatchFmeasure and unanimous improvement ratio,” *Artificial Intelligence*, vol. 223, pp. 65–81, 2015.
 - [32] J. Kennedy and R. C. Eberhart, “Particle swarm optimization,” in *Proceedings of the International Conference on Networks*, vol. 4, pp. 1942–1948, Piscataway, NJ, USA, February 2002.
 - [33] K. Janowicz, A. Haller, S. Cox, D. Le Phuoc SOSA, and M. Lefrançois, “ASOSA: a lightweight ontology for sensors, observations, samples, and actuators,” *Journal of Web Semantics*, vol. 56, pp. 1–10, 2019.
 - [34] F. Daniel, P. Catia, B. Booma et al., “OAEI 2016 results of AML,” in *Proceedings of the Eleventh International Workshop on Ontology Matching*, vol. 1766, Kobe, Japan, October 2016.
 - [35] E. Jimenez-Ruiz, B. Cuenca Grau, and V. Cross, “LogMap family participation in the OAEI 2016,” in *Proceedings of the 11th International Workshop on Ontology Matching Co-located with the 15th International Semantic Web Conference (ISWC 2016)*, Kobe, Japan, July 2016.
 - [36] W. Eddine-Djeddi, M. Tarek-Khadir, and S. Ben-Yahia, “XMap: results for OAEI 2016,” in *Proceedings of the 11th International Workshop on Ontology Matching Co-located with the 15th International Semantic Web Conference (ISWC 2016)*, Kobe, Japan, July 2016.
 - [37] A. Haller, K. Janowicz, S. J. D. Cox et al., “The modular SSN ontology: a joint W3C and OGC standard specifying the semantics of sensors, observations, sampling, and actuation,” *Semantic Web*, vol. 10, no. 1, pp. 9–32, 2019.
 - [38] C.-H. Chen, “A cell probe-based method for vehicle speed estimation,” *IEICE Transactions on Fundamentals of*

- Electronics, Communications and Computer Sciences*, vol. E103.A-A, no. 1, pp. 265–267, 2020.
- [39] C.-H. Chen, F.-J. Hwang, and H.-Y. Kung, “Travel time prediction system based on data clustering for waste collection vehicles,” *IEICE Transactions on Information and Systems*, vol. E102.D, no. 7, pp. 1374–1383, 2019.
- [40] C.-H. Chen, “An arrival time prediction method for bus system,” *IEEE Internet of Things Journal*, vol. 5, no. 5, pp. 4231–4232, 2018.

Research Article

Tourism Destination Preference Prediction Based on Edge Computing

Bin Deng , **Jun Xu**, and **Xin Wei**

Lyceum of the Philippines University, Batangas 4200, Philippines

Correspondence should be addressed to Bin Deng; bindeng@lpubatangas.edu.ph

Received 26 January 2021; Revised 20 February 2021; Accepted 8 March 2021; Published 17 March 2021

Academic Editor: Hsu-Yang Kung; kung@mail.npust.edu.tw

Copyright © 2021 Bin Deng et al. This is an open access article distributed under the Creative Commons Attribution License, which permits unrestricted use, distribution, and reproduction in any medium, provided the original work is properly cited.

In view of the fact that the important characteristics of tourism destination selection preference are not considered in the current prediction methods of tourism destination selection preference, resulting in low prediction accuracy and comprehensive accuracy and long prediction time, a tourism destination selection preference prediction method based on edge calculation is proposed. This paper uses edge computing to construct the characteristics of tourism destination selection preference and uses a random forest algorithm to select important features and carry out preliminary estimation and ranking. Using the multiple logit selection model, the tourists' preference sequence for tourism destination selection is obtained and sorted and the tourism destination selection preference model is obtained. By calculating the weight value of tourism destination selection preference, the weight set of tourism destination selection preference is determined and the tourism destination selection preference is determined according to the link prediction method to realize the tourism destination selection preference prediction. The experimental results show that the comprehensive accuracy of the proposed method is good, which can effectively improve the prediction accuracy of tourism destination selection preference and shorten the prediction time of tourism destination selection preference.

1. Introduction

Tourism is an important part of the modern service industry and a strategic pillar industry of the global economy. It can provide a large number of employment opportunities and good income with strong action and less resource consumption [1]. Promoting the development of tourism is of great practical significance in changing the mode of economic development, adjusting the industrial structure, and expanding domestic demand. The so-called preference is that consumers like one commodity more than another. It is a subjective description method that can reflect a kind of emotion and tendency in people's heart [2]. Preferences have individual characteristics and group characteristics. In other words, a certain group with some common characteristics has similarities in theory. Tourists' preference for tourism destination choice means that some common factors will affect the choice of tourism destination by groups of tourists with specific characteristics. Therefore, there are some similarities in the choice of tourist destinations. That is, they

have similar preferences [3]. Tourism destination preference prediction is an important part of tourism research, tourism planning, and management. Therefore, accurate prediction of tourism destination selection preference can improve the scientific level and effectiveness of tourism research planning and management.

The preference of destination selection directly affects the development trend of outbound tourism. Therefore, it is of great significance to predict the preference of destination selection. At present, a large number of scholars have carried out different degrees of research on the choice of tourism destination and achieved certain theoretical results. In reference [4], a hierarchical Bayesian network with multiple data sources is used to estimate and predict daily source destination tuples. The concept of O-D tuples is proposed. Vehicles in the road network are predicted and tracked by an advanced monitoring system. Aiming at the problem of obtaining the posterior probability of uncertain parameters, a multiprocess hierarchical Bayesian network mechanism in Gaussian space is developed. The model includes the level

and trend components of future traffic volume. This method can meet the demand of forecasting and reduce the uncertainty in the process of estimation and prediction. In reference [5], a destination prediction method based on the initial part of the vehicle trajectory is proposed. The new trajectories are assigned to the most likely clusters, and the similarity grid driven by data is generated by obtaining the trajectory clustering describing user behavior. The final destination of the new trajectory is predicted by using the characteristics of the internal trajectories of the model cluster. The prediction accuracy of this method is high. However, the above methods do not consider the important characteristics of tourism destination selection preference, which leads to the problems of low prediction accuracy and comprehensive accuracy and long prediction time [6].

In view of the above problems, this paper puts forward a prediction method of tourism destination selection preference based on edge computing. It uses the edge calculation to construct the tourism destination selection preference characteristics, uses the random forest algorithm, selects the important features, uses the multiple logit selection model to obtain the tourists' preference sequence for the choice of tourism destinations and sorts them, and obtains the tourism destination selection preference model. By calculating the weight value of tourism destination selection preference, the preference weight set of tourism destination selection is determined, and the tourism destination selection preference prediction is realized. The comprehensive accuracy of the tourism destination preference prediction method is good, which can effectively shorten the prediction time and improve the prediction accuracy [7].

The research contributions of the paper include the following:

- (1) A prediction method based on the preference of tourist destination selection is proposed
- (2) This paper uses edge computing technology to construct tourist destination selection preference features and uses a random forest algorithm to select important features and perform preliminary estimation and ranking
- (3) Using the multiple logit selection model, the preferred sequence of tourists' choice of tourist destinations is obtained and selected, and the model of tourist destination choice preference is obtained
- (4) Determine the weight set of the tourist destination selection preference by calculating the weight value of the tourist destination selection preference and determine the tourist destination selection preference according to the link prediction method to realize the prediction of the tourist destination selection preference

2. Edge Computing

2.1. Concept of Edge Computing. Edge computing is a new computing mode that performs processing data computation at the edge of the network. In edge computing, the

downstream data of the edge represents the cloud service, and the uplink data represents the Internet service of everything. The "edge" of edge computing refers to any computing and network resources between the data source and the cloud computing center path [8]. Edge computing can reduce the request response time, improve the endurance, reduce network bandwidth, and ensure data security and privacy. The edge computing architecture is as shown in Figure 1.

As can be seen from Figure 1, the edge algorithm structure diagram is mainly composed of 4 parts, each part has many branches, and the algorithm is more complicated. User terminals are all kinds of Internet of things devices, such as mobile phones, driverless cars, cameras, etc. These terminals collect a large amount of data and upload the data to the nearest edge device for storage and calculation. Edge devices are a large number of nodes on the edge of the network, such as routers, switches, base stations, or edge servers. These devices store and precalculate the data from the terminal and upload the processed results to the cloud computing center. Cloud Computing Center has powerful computing power, which can perform complex calculations on the acquired data and return the final settlement results to the user terminal [9].

2.2. Relationship between Edge Computing and Cloud Computing. Cloud computing is suitable for nonreal-time, long-period data, and business decision-making scenarios, while edge computing has an irreplaceable role in real-time, short-period data, and local decision-making scenarios [10]. Therefore, the edge computing model and the cloud computing model can complement each other according to different needs.

Edge computing is combined with the existing cloud computing centralized processing model cloud edge collaboration, which migrates part or all of the computing tasks performed by the original cloud computing model to the network edge devices, forming a computing mode of "business application at the edge, management in the cloud," which completes the transformation of computing, network and storage capacity from cloud to network edge. For example, video surveillance is a typical application scenario. Due to the need for social security management and public security, many cameras are deployed in the streets to monitor the crowd in real time. However, due to a large number of cameras and real-time data generation, if all the data are uploaded to the cloud computing center, the network bandwidth and cloud computing center will be under great pressure. Therefore, the collected data can be preprocessed at the nearest storage device of each camera, and the useful data can be filtered out and transmitted to the cloud computing center, which then calculates according to the received data [11]. Therefore, edge computing and cloud computing complement each other to help realize the interconnection of all things.

2.3. Edge Computing Advantages. Edge computing can effectively reduce the delay of computing system, reduce the data transmission bandwidth, relieve the pressure of cloud

computing center, improve availability, and protect data security and privacy [12]. Compared with cloud computing, edge computing has the following advantages:

- (1) Edge computing is the first access to data, which enables edge computing to process a large number of real-time data at the edge of the network, without having to upload all the data to the cloud computing center. This reduces the energy consumption pressure of cloud computing centers and also reduces the load of network bandwidth.
- (2) Edge computing processes data near the edge of the network to reduce network latency and speed up service response.
- (3) Users' private data can be stored and processed on edge devices without network transmission, which reduces the risk of data leakage and improves data security and privacy.

To sum up, the edge computing model is more suitable for processing the data generated by users in the mobile edge terminal. The low latency and high efficiency meet the needs of people in tourism today. For the prediction of tourism destination choice preference, edge computing is undoubtedly the most matching calculation model.

3. Tourism Destination Preference Theory

3.1. Tourist Destination. Tourist destination refers to non-residential area, which is the place where tourists stay and visit for a short time, also known as a tourist destination or tourist resort. The formation of a tourism destination needs six elements: food, housing, transportation, tourism, shopping, and entertainment. Tourism destination is a specific geographical area managed by a unified destination management organization, which can be a specific scenic spot, or a town, or an area of a country, or the whole country, or even a larger place [13]. The common characteristics of tourist destinations are attraction, comfort, and accessibility, a specific area with certain tourism resources, facilities, and transportation conditions, which can attract a certain number of tourists to carry out tourism activities.

3.2. Tourism Preference Theory. Tourism preference refers to the influence of tourists' personality characteristics on tourism behavior. Personality characteristics include interest, hobby, ability, temperament, and personality. The study of tourism preference can be carried out from the aspects of tourists' age, occupation, educational background, gender, and living environment. According to psychology, attitude influences preference [14]. Tourism preference depends on the intensity and complexity of tourists' attitude. The stronger the attitude, the more influence the preference: the more complex the attitude, the easier to form preference. The formation process of tourism preference is as shown in Figure 2.

It can be seen from Figure 2 that the process of forming tourism preferences is more logical, and the strength of tourists' attitudes depends on the needs of

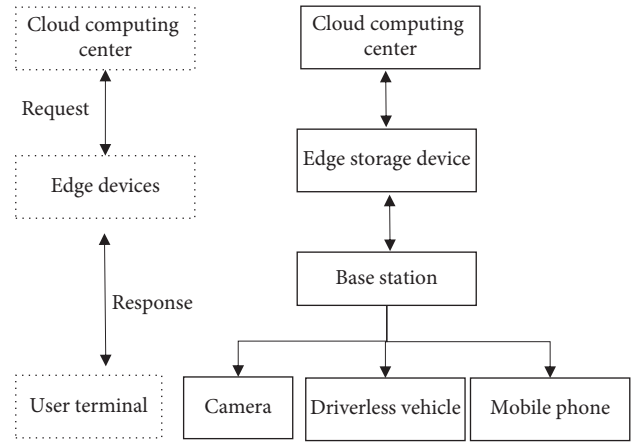


FIGURE 1: Edge computing architecture.

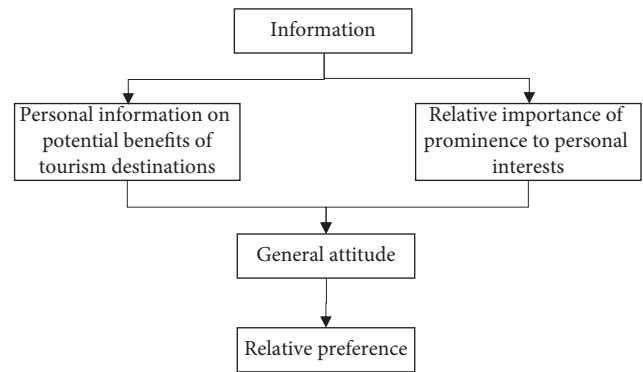


FIGURE 2: Process diagram of tourism preference formation.

tourists and the outstanding attributes of the destination. Once a person has a certain need, he will naturally have a desire, which will affect the strength of his attitude. For example, in a holiday resort, climate, comfort, and environment may be very important for one tourist, but for another tourist, price, transportation, and entertainment facilities are the most important attributes.

The complexity of attitude usually depends on the amount of information about the tourist destination. The more information, the more complex the attitude, the easier it is to form tourism preference, while a simple attitude is difficult to change [15]. For example, if a person has a negative attitude towards outbound tourism, it is difficult to persuade him to form an outbound travel preference.

In the process of forming attitude, two levels should be considered, namely, standard cognition level and interest evaluation level. Through the standard cognition, we can form the feeling and trust to the tourism products; through the benefit evaluation, when a tourist considers the alternative tourist destination, he should first estimate the visible or potential benefits that the destination can give him. After evaluation, plus the salient points of each interest, tourists can decide which tourism destination can fully meet their needs and purposes, and then form corresponding preferences and finally make decisions [16].

3.3. Tourism Destination Mapping Theory. Tourism destination mapping theory, namely tourism destination terrain image theory, refers to the comprehensive image of tourism destination obtained by people directly through tourism activities or indirectly through television, magazines, advertising, Internet, and other media. This image has a certain impact on tourists' choice of destination. Through the construction of the model, the author explores the map of tourist destination from the aspects of tourists' psychological characteristics, experience, perception, demand, education level, media, and marketing, etc., and summarizes and modifies the original image before the start of tourism activities, and finally forms the evaluation image after the tourism behavior combining with the experience image in the process of tourism activities. The formation of the initial impression of a tourist destination depends on the role of advertising, among which the introduction advertising, persuasive advertising, and reminder advertising have a great external impetus to the formation of the image.

3.4. Tourism Decision Theory. Tourism decision-making refers to the process in which tourists select relevant tourism information, formulate tourism plans or tourism plans, and finally put them into practice. The whole process is composed of tourism needs, tourism information, tourism routes, tourism budget, tourism mode, tourism decision, and tourism travel, etc. Among them, the tourism route is the key factor affecting tourism decision-making, which not only determines the division of tourism regions but also determines the tourism budget and tourism experience. Tourists will perceive the tourism information after hoof selection and then make tourism decisions through the influence of other factors such as preference.

The formation of tourism decision-making is the result of the interaction of individual needs, motives, and preferences of tourists and social pressure. The tourism destination selection opportunity group model is as shown in Figure 3.

The optional part is called the overall opportunity group, and the part sensed by tourists is called the induction opportunity group. Due to the limitation of certain conditions, only a part of the induction opportunity that tourists will consider is called the consideration opportunity group [17]. When considering the overlap between opportunity group and opportunity group, which can provide tourists in the market at that time, it is the part selected by tourists, which is called the possibility opportunity group. Therefore, only when the destination (perceived opportunity) is perceived by tourists and the destination (accessibility opportunity) is within the scope of tourists' economic ability can they enter into tourism decision-making and become the real tourism destination (real opportunity).

4. Tourism Destination Preference Prediction Based on Edge Computing

4.1. Edge Computing Prediction Process. The process of edge computing and prediction is mainly divided into two parts:

the cloud processing part and edge prediction part. The operation process of the two parts will be described, respectively.

- (1) Cloud processing: the collected tourism destination selection preference data is preprocessed in the cloud, and the tourism destination selection preference features are constructed. The important features of tourism destination selection preference features are selected by using a random forest algorithm, and preliminary estimation and ranking are carried out. Based on the multinomial logit selection model, the preference sequence of tourist destination choice is obtained, and the preference model of tourist destination selection is sorted. The model is saved and loaded to the edge [18].
- (2) Edge prediction: on the basis of the tourism destination selection preference model, the weight value of tourism destination selection preference is calculated, and the set of tourism destination selection preference weight is determined. Through the link prediction method to determine the tourism destination selection preference, using the tourism destination selection preference prediction formula, the tourism destination selection preference is predicted, thus realizing the tourism destination selection preference prediction. When the preference of tourism destination choice changes, the edge end will call the prediction model corresponding to the new model. When there is a big deviation between the predicted value and the real value, the edge end will make appropriate adjustments.

4.2. Tourism Destination Preference Model

4.2.1. Construct Preference Characteristics of Tourism Destination Selection. Feature construction refers to the generation and selection of features from the original information, also known as feature extraction. In the cognition and prediction of things, the selection feature is particularly prominent. The characteristics of tourism destination selection preference constructed in this paper are as shown in Figure 4.

The characteristics of tourism destination selection preference can be divided into tourist characteristics, tourism destination characteristics, and the interaction between them. The basic characteristics of passenger characteristics are mainly described from the granularity of passenger operation number, passenger expense number, passenger days, and passenger time. Among them, the granularity of passenger operation number mainly represents the number of tourist destination clicks in a specific period of time. The granularity of the number of tourist expenses refers to the number of tourist attractions tickets purchased in a specific period of time. Passenger days granularity refers to the number of days that tourists stay at the destination. Passenger time granularity refers to the time interval between passengers arriving at the destination recently [19].

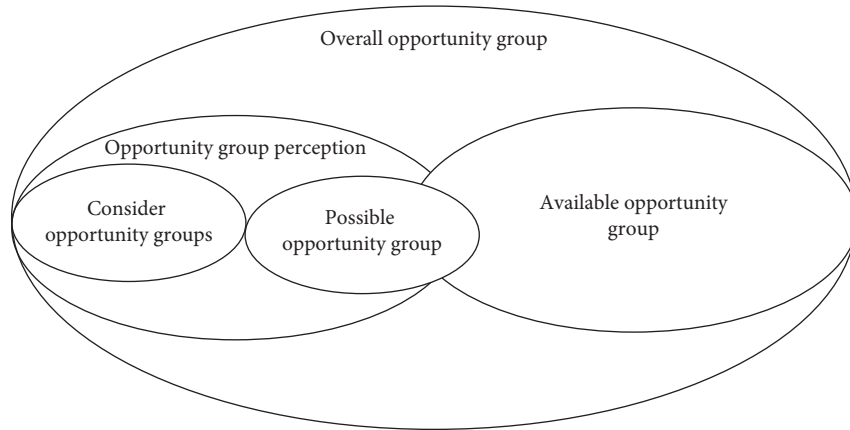


FIGURE 3: Tourism destination selection opportunity group model.

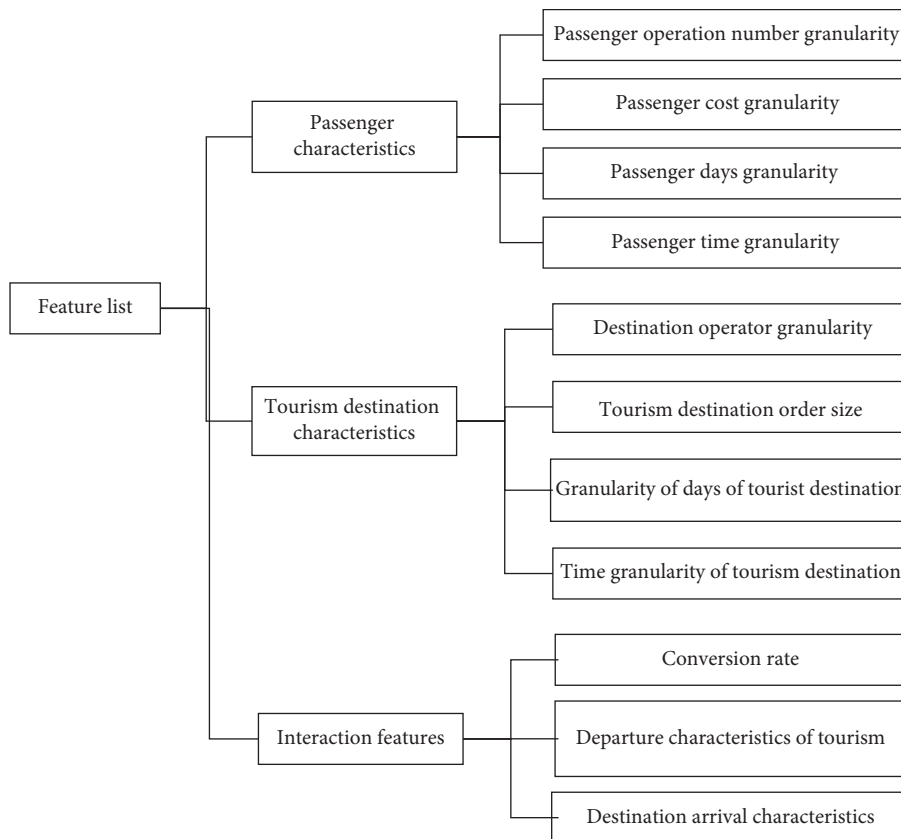


FIGURE 4: Preference characteristics of tourism destination selection.

Tourism destination characteristics are similar to the characteristics of tourists, but the calculation object is changed from tourists to tourism destinations. For example, the tourism destination operands granularity represents the number of times a tourist destination is queried by clicking at a specific time. The granularity of tourism destination order number refers to the purchased quantity of tourism destination in a specific time period, the tourism destination days granularity refers to the arrival days of tourism destination, and the tourism destination time granularity refers

to the time interval between one tourism destination and another.

In addition to the above-mentioned basic characteristics, the interactive characteristics of tourists and tourism destinations also include the conversion rate, the characteristics of departure, and the arrival of tourists' choice of tourism destinations [20]. Among them, the conversion rate refers to the number of times a passenger chooses a tourist destination to set out divided by the number of times a tourist chooses a tourist destination. The characteristics of a

tourist's choice of a tourist destination are mainly expressed as the date and time of departure or arrival.

Because there are many interactive features between tourists and tourist destinations, the most important features must be selected from the large number of features constructed, so as to reduce the number of features, improve the prediction accuracy of the model, and reduce the running time. The goal of the tourist preference sequence is to predict the preference selection model of tourist destination choice. Considering the operation efficiency and prediction accuracy of the algorithm, this paper proposes a pointwise sorting algorithm combining random forest and gradient lifting decision tree. In this paper, we propose a method to fuse a single prediction model and introduce a variety of prediction factors as far as possible, and finally, we can get a more accurate preference prediction model. Therefore, this paper uses a random forest algorithm [21] to select important features, and the steps are as follows:

- (i) Step 1: preliminary estimation and ranking.
 - (1) The characteristic variables of random forest were sorted in descending order according to the importance of variables
 - (2) According to the determined deletion ratio, the unimportant indexes in the current feature variables are eliminated to obtain new features
 - (3) A new random forest is established by using the new features generated, and the importance of each feature is calculated and sorted
 - (4) Repeat the above three steps until m features are left
- (ii) Step 2: according to the feature set obtained in the first step and the established random forest, the out-of-bag error rate is calculated. Finally, the selected feature set is the feature set with the lowest out-of-bag error rate.

According to the input feature training data of interaction between tourists and tourism destination, the first m features of all the features constructed in this paper are selected and input into multiple logit selection model by using the ranking relationship between cross validation method and the importance of the obtained features.

4.2.2. Based on the Multiple Logit Selection Model. The multinomial logit model is a random utility model, which is usually used as the main method to describe the choice of tourist destinations [22]. In the multilogit model, the utility of passenger t choosing a tourist destination j is defined as follows:

$$U_t^j = \mu_t^j + \xi_t^j, \quad j = 0, 1, \dots, n, \quad (1)$$

In formula (1), μ_t^j represents the expected utility constant, and $\xi_t^j, j = 0, 1, \dots, n$ represents independent noise. Generally, the linear model is established to express μ_t^j by the characteristics of tourist destination selected by passenger t . For example,

$$\mu_t^j = \beta^T a_t^j. \quad (2)$$

In formula (2), β represents the parameter vector, and a_t^j represents the characteristics of the tourist destination j selected by the passenger t . Use the tourist destination selection preference feature to construct a_t^j . The noise ξ_t^j is defined as a double exponential distribution. The specific formula is as follows:

$$F_\xi(x) = P(\xi_t^j \leq x) = e^{-(\delta x + \gamma)}. \quad (3)$$

In formula (3), γ represents the Euler constant defined as the Euler constant, and δ represents a positive scale parameter, and is often set to 1. Define $C_t \subset N$ as the preference set of traveler t to choose a tourist destination, and the probability of choosing a tourist destination $j \in C_t$ is as follows:

$$P_t(j) = \frac{e^{\mu_t^j}}{\sum_{i \in C_t} e^{\mu_t^i} + e^{\mu_t^0}}. \quad (4)$$

In formula (4), μ_t^0 represents the nonselection utility, and $e^{\mu_t^i}$ represents the preference weight of the traveler t choice of the travel destination j . Then the probability of the traveler t choosing the travel destination j can be compared with the probability of choosing other preferences—destination selection preference sequence.

4.2.3. Preference Model of Tourism Destination Selection. Aiming at the problem of passengers' preference selection and ranking of tourist destinations, historical data is obtained again to construct the training set D to train the ranking model. The specific solution process is as follows:

- (i) Step 1: in order to make the tourism destination selection preference model get a better evaluation ranking effect, the target ranking value is defined as follows:

$$y_{ij} = 2R_{ij} - 1. \quad (5)$$

In formula (5), R_{ij} represents the predicted probability of tourists' preference for travel destination selection. A training set is obtained as follows:

$$D = [x_s, y_s]. \quad (6)$$

In formula (6), x_s represents the f dimensional characteristics of travelers' choice of destinations.

- (ii) Step 2: establish regression function, which is expressed as follows:

$$\sum_{(x_s, y_s)} [y_s - g(x_s)]^2. \quad (7)$$

The independent variables and dependent variables are continuous variables, and the data obtained from the questionnaire is the score value, which is a linear regression with the mean value of the data (Algorithms 1 and 2)

- (iii) Step 3: use random forest algorithm to train formula (7), and the algorithm process is as follows:
- (iv) Step 4: use the initial training result obtained in the previous step as the initial value input of the tourist destination selection preference model. The algorithm process is as follows:

According to the above method, the tourists' preference model for tourism destination selection is finally obtained.

4.3. Realize the Prediction of Tourism Destination Choice Preference. In order to predict the preference of tourism destination choice, when looking for the sequence of tourists' preference for a tourism destination, this paper combines the trust degree of tourists in tourism destination and the similarity of tourism destination selection preference as the weight value of tourism destination selection preference. The tourism destination selection preference is determined by the link prediction method, and the tourism destination selection preference is predicted by using the prediction formula of tourism destination selection preference. The specific methods are as follows.

4.3.1. Calculate the Preference Weight Value of Travel Destination Selection. In the process of tourism destination selection preference prediction, this paper not only considers the impact of similarity of tourism destination selection preference on the prediction results but also considers the influence of tourists' trust in tourism destination on tourism destination selection preference. The harmonic weight is used to select the weight value of tourism destination selection preference. The harmonic weight is determined by the selection similarity and passenger trust [23]. When the trust degree of tourists to tourism destination is relatively large, the weight value of trust degree is relatively large; when the trust degree of tourists to tourism destination is relatively small, the weight value of similarity is relatively large. Therefore, the calculation formula of harmonic weight is expressed as follows:

$$W(u_i, u_j) = \begin{cases} \alpha_1 \text{sim}(u_i, u_j) + \beta_1 T(u_i, u_j), & T(u_i, u_j) \geq \sigma, \\ \alpha_2 \text{sim}(u_i, u_j) + \beta_2 T(u_i, u_j), & T(u_i, u_j) < \sigma. \end{cases} \quad (8)$$

In formula (8), $W(u_i, u_j)$ represents the reconciliation weight of mobile passenger u_i and mobile passenger u_j , $\text{sim}(u_i, u_j)$ represents the score similarity of mobile passenger u_i and mobile passenger u_j , $T(u_i, u_j)$ represents the trust degree of mobile passenger u_i and mobile passenger u_j , and $\alpha_1, \alpha_2, \beta_1, \beta_2$ represents the reconciliation factor, and $\alpha_1 + \beta_1 = 1$, $\alpha_2 + \beta_2 = 1$, σ represent the trustworthiness threshold.

In determining the preference weight set of tourism destination selection, the $o\%$ harmonic weight is selected as the preference weight set of tourism destination selection. When $o = 0$, the preference weight set of tourism destination selection is empty set; when $o = 100$, the preference weight

set of tourism destination selection includes all passengers in the data set. Therefore, if the value of o is too small or too large, the ideal result can not be obtained. In this paper, the reasonable o value is selected according to the results of many experiments.

4.3.2. Determine the Preference Weight Set of Tourism Destination Selection. The higher the similarity between tourists and tourism destination selection preferences, the greater the possibility of tourists' preference in tourism destination selection. Therefore, when determining the weight set of tourism destination selection preference to be predicted, this paper selects the tourism destination selection preference with correlation degree of $\varepsilon\%$ as the weight set of tourism destination selection preference.

4.3.3. Predict Tourism Destination Preference. Combining the reconciliation weight with the tourism destination selection preference prediction formula, the final weighted average prediction formula is expressed as follows:

$$r_{ui,s} = \bar{r}_{ui} + k \sum_{\substack{u_j \in S_{u_j} \\ s \in N_{ui}}} [W(u_i, s, u_j) \times (r_{ui,s} - \bar{r}_{ui})]. \quad (9)$$

In formula (9), N_{ui} represents the travel destination selection preference weight set of mobile traveler u_i , S_{u_j} represents the travel destination selection preference weight set of mobile traveler u_j , and k represents a standardized factor.

Through the above steps, using edge computing to construct tourism destination selection preference features, using random forest algorithm to select important features of tourism destination selection preference features, and preliminary estimation and ranking, using multiple logit, in this paper, we get the sequence of tourists' preference for tourism destination selection and rank the preference model of tourism destination selection, and then get the preference model of tourism destination choice. This paper calculates the weight value of tourism destination selection preference, determines the weight set of tourism destination selection preference, determines the tourism destination selection preference through link prediction method, and predicts the tourism destination selection preference by using the tourism destination selection preference prediction formula, so as to realize the tourism destination selection preference prediction.

5. Experimental Analysis

5.1. Experimental Environment and Data. In order to verify the effectiveness of the edge computing-based tourism destination selection preference prediction method, the experiment uses a computer configured with Inter E1400 2.0 GHz processor, 8.00 G memory, 800 G hard disk, and 64-bit Windows 10 operating system. In this paper, we obtain the data of about 3000 tourists' preference for tourism destination through a questionnaire and extract the

```

(i) Input: data set  $D = \{(x_1, y_1), \dots, (x_n, y_n)\}$ , parameter:  $K: 0 < K \leq f, M_{RF}: M_{RF} > 0$ 
(ii) for  $t = 1$  to  $M_{RF}$  do
(iii)  $D_t \subseteq D$  #Random sampling sample  $D_t$ , making  $|D_t| = |D|$ .
(iv) #Establish a full tree ( $d = \infty$ )Cart and randomly select  $K$  features when the tree is decomposed downward
(v) end for
(vi)  $T(\cdot) = (1/M_{RF}) \sum_{t=1}^{M_{RF}} h_t(\cdot)$ 
(vii) return  $T(\cdot)$ 

```

ALGORITHM 1: Random forest.

```

(i) Input: data set  $D = \{(x_1, y_1), \dots, (x_n, y_n)\}$ , parameter:  $\alpha, M_B, d, K_{RF}, M_{RF}$ 
(ii)  $F \leftarrow$  Random Forests ( $D_t, K_{RF}, M_{RF}$ )
(iii) Initialization:  $r_i = y_i - F(x_i)$  for  $i = 1$  to  $n$ 
(iv) for  $t = 1$  to  $M_B$  do
(v)  $T_t \leftarrow$  Cart ( $\{(x_1, r_1), \dots, (x_n, r_n), f, d\}$ ) #Build a tree Cart with a depth of  $d$ , and enter all the features  $f$  and  $\{r_i\}$ .
(vi) for  $i = 1$  to  $n$  do
(vii)  $r_i \leftarrow r_i - \alpha T_t(x_i)$  #Update the residual of each sample  $x_i$ .
(viii) end for
(ix) end for
(x)  $T(\cdot) = F(\cdot) + \alpha \sum_{t=1}^{M_B} T_t(\cdot)$ . #Merge the regression tree  $T_1, \dots, T_M$  and the  $F$  obtained by the random forest
(xi) return  $T(\cdot)$ 

```

ALGORITHM 2: Initialize gradient boosted regression trees (squared loss).

historical data of destination preference of these tourists. Taking the above data as a data record of tourists' choice of tourism destination products at different times, the bootstrap method is used to repeatedly sample and generate 1000000 simulated data. Each data include passenger's age, surname, occupation, education background, location, destination selection, travel date, reservation date, etc. The experimental environment is carried out under the joint support of multiple terminal machines.

5.2. Evaluation Index. This article uses mean absolute error (MAE) and F index (F measure) as evaluation indicators. MAE measures the accuracy of prediction by calculating the deviation between the predicted travel destination preference and the actual travel destination preference. The smaller the MAE value, the higher the accuracy of the prediction. Assuming that the predicted tourism destination selection preference set is denoted as $p_i = \{p_1, p_2, \dots, p_n\}$, and the corresponding actual tourism destination selection preference set is denoted as $q_i = \{q_1, q_2, \dots, q_n\}$, then MAE is defined as follows:

$$MAE = \frac{\sum_{i=1}^n |p_i - q_i|}{n} \quad (10)$$

F index is a comprehensive evaluation form of precision rate and recall rate. The larger the F index, the higher the comprehensive accuracy. This article redefines the precision rate and recall rate according to the evaluation standard of experimental results as follows:

The precision rate quantifies the accuracy of the prediction of the preference of tourists to the travel destination. It can be expressed as the ratio of the effective, relevant

preference to all predicted preferences. The precision rate can be expressed as follows:

$$P_z = \frac{N_{rs}}{N_s} \quad (11)$$

The recall rate reflects the comprehensiveness of the tourism destination selection preference prediction. The recall rate is the ratio of the passenger's related tourism destination selection preference to the selection preference of all tourism destinations. Its form can be expressed as follows:

$$R_z = \frac{N_{rs}}{N_r} \quad (12)$$

The F index is expressed as follows:

$$F = \frac{2 \times P_z \times R_z}{P_z + R_z} \quad (13)$$

In order to verify the prediction accuracy of the tourism destination selection preference prediction method based on edge computing, the reference [4] method, the reference [5] method and the proposed method were used to compare the average absolute deviation results of different methods as shown in Figure 5.

It can be seen from Figure 5 that under different tourist destination selection preference sets, the average absolute deviation of reference [4] method is 0.68, the average absolute deviation of reference [5] method is 0.73, and the average absolute deviation of the proposed method only 0.59. Therefore, compared with the reference [4] method and reference [5] method, the average absolute deviation of the proposed method is smaller, and the prediction accuracy of

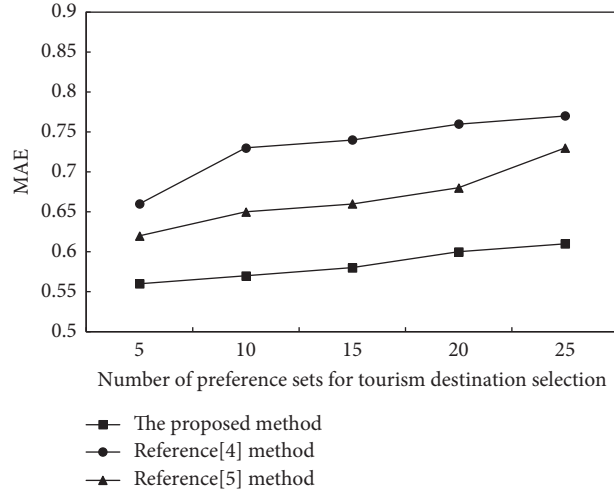
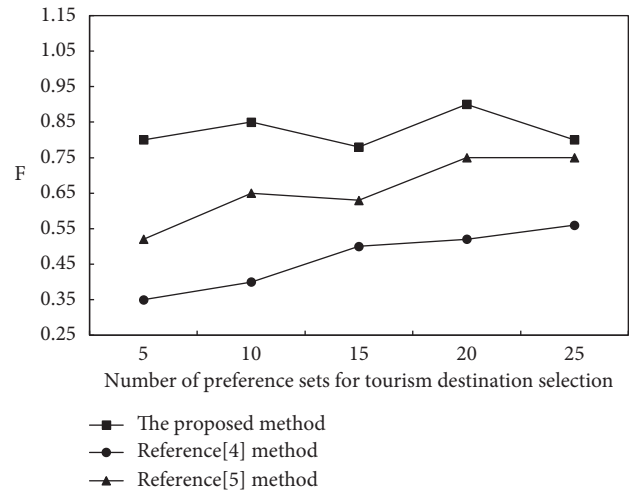


FIGURE 5: Comparison of mean absolute deviation of different methods.

tourism destination preference is higher because the proposed method uses edge computing to construct the characteristics of tourism destination selection preference and determines the weight set of tourism destination selection preference by calculating the value of tourism destination selection preference weight, so as to predict the tourism destination selection preference, which can effectively improve the accuracy of tourism destination selection preference.

5.3. Comparison of Comprehensive Accuracy of Tourism Destination Choice Preference Prediction. To further verify the comprehensive accuracy of the tourism destination selection preference prediction method based on edge computing, reference [4] method, reference [5] method, and the proposed method are used to compare the F index results of different methods as given in Figure 6. Reference [4] is the daily origin-target tuple estimation and prediction using multilayer Bayesian networks. Reference [5] is the destination prediction based on the trajectory distribution model.

It can be seen from Figure 6 that under different tourist destination selection preference sets, the F index of reference [4] method is 0.35, the F index of reference [5] method is 0.68, and the F index of the proposed method is 0.83. Therefore, compared with reference [4] method and reference [5] method, the proposed method has larger F index and higher comprehensive accuracy of tourism destination selection preference prediction because the proposed method calculates the weight value of tourism destination selection preference, determines the weight set of tourism destination selection preference, uses the link prediction method to determine the tourism destination selection preference, and uses the tourism destination selection preference prediction formula to realize the better prediction of tourism destination selection, so as to effectively improve the comprehensive accuracy of tourism destination selection preference.

FIGURE 6: Comparison of F indexes of different methods.

5.4. Comparison of Travel Destination Preference Prediction Time. On this basis, the prediction time of tourism destination selection preference prediction method based on edge computing is verified. Reference [4] method, reference [5] method, and the proposed method are used to compare the prediction time of tourism destination selection preference of different methods as shown in Table 1.

According to the data in Table 1, when the number of experiments reaches 5, the average tourism destination selection preference prediction time of reference [4] method is 6.33 s, and the average tourism destination selection preference prediction time of reference [5] method is 9.15 s, and the average tourism destination preference prediction time of the proposed method is only 3.16 s. It can be seen that compared with reference [4] method and reference [5] method, the tourism destination preference prediction time of the proposed method is shorter. This is due to the proposed method; from a large number of tourism destination selection preference features, a random forest algorithm is used to select the important features of tourism destination

TABLE 1: Comparison of prediction time of tourism destination selection preference with different methods.

Number of experiments	The proposed method	The reference [4] method	The reference [5] method
1	3.34	5.98	8.79
2	3.18	5.87	8.93
3	2.97	5.76	9.65
4	3.23	7.05	9.96
5	3.09	6.99	8.97
Average value	3.16	6.33	9.15

selection preference features; based on multiple logit, the choice model can get the sequence of tourists' preference for tourism destination selection and sort the tourism destination selection preference model to obtain the tourism destination selection preference model, thus effectively shortening the prediction time of tourism destination selection preference.

6. Conclusion

This paper proposes a tourism destination selection preference prediction method based on edge computing, which gives full play to the advantages of edge computing. It can effectively shorten the prediction time of tourism destination selection preference and has high comprehensive accuracy performance. However, in the process of tourism destination selection preference prediction, this method lacks the collection of tourism destination selection preference data and cannot verify the tourism destination selection preference model. Therefore, in the next step of research, we need to collect the data of tourism destination selection preference in real time so as to verify the effect of the tourism destination selection preference model and further improve the model to make the prediction results more accurate.

Data Availability

The datasets used and/or analyzed during the current study are available from the corresponding author upon reasonable request.

Conflicts of Interest

The authors declare that they have no conflicts of Interest.





References

- [1] R. Steiger, E. Posch, G. Tappeiner, and J. Walde, "The impact of climate change on demand of ski tourism - a simulation study based on stated preferences," *Ecological Economics*, vol. 170, Article ID 106589, 2020.
- [2] V. C. Sander, G. C. Caspar, and W. Bert van, "Simulation study on impacts of high aviation carbon taxes on tourism: application of portfolio vacation choice model," *Transportation Research Record*, vol. 2449, no. 1, pp. 64–71, 2018.
- [3] K. Lindner-Cendrowska and K. Błażejczyk, "Impact of selected personal factors on seasonal variability of recreationist weather perceptions and preferences in Warsaw (Poland)," *International Journal of Biometeorology*, vol. 62, no. 1, pp. 113–125, 2018.
- [4] Y. Ma, R. Kuik, and H. Zuylen, "Day-to-Day origin-destination tuple estimation and prediction with hierarchical bayesian networks using multiple data sources," *Transportation Research Record*, vol. 2343, no. 1, pp. 51–61, 2018.
- [5] P. C. Besse, B. Guillouet, J.-M. Loubes, and F. Royer, "Destination prediction by trajectory distribution-based model," *IEEE Transactions on Intelligent Transportation Systems*, vol. 19, no. 8, pp. 2470–2481, 2018.
- [6] D. Li, G. Wu, J. Zhao, W. Niu, and Q. Liu, "Wireless channel identification algorithm based on feature extraction and BP neural network," *Journal of Information Processing Systems*, vol. 13, no. 1, pp. 141–151, 2017.
- [7] X. Tongle, W. Yingbo, and C. Kang, "Tailings saturation line prediction based on genetic algorithm and BP neural network," *Journal of Intelligent & Fuzzy Systems*, vol. 30, no. 4, pp. 1947–1955, 2016.
- [8] R. Zhao, M. Jin, P. Ren, and Q. Zhang, "Stable two-sided satisfied matching for ridesharing system based on preference orders," *Journal of Supercomputing*, vol. 76, no. 10, pp. 1–19, 2016.
- [9] T. Ren, S. Liu, G. Yan, and H. Mu, "Temperature prediction of the molten salt collector tube using BP neural network," *IET Renewable Power Generation*, vol. 10, no. 2, pp. 212–220, 2020.
- [10] M. Lozano-Oyola, F. J. Blancas, M. González, and R. Caballero, "Sustainable tourism tags to reward destination management," *Journal of Environmental Management*, vol. 250, no. Nov.15, pp. 1–11, 2019.
- [11] L. Wu, J. Zhang, and A. Fujiwara, "Dynamic analysis of Japanese tourists' three stage choices: tourism participation, destination choice, and travel mode choice," *Transportation Research Record*, vol. 2322, pp. 91–101, 2018.
- [12] S. Wan, R. Gu, T. Umer, K. Salah, and X. Xu, "Toward off-loading Internet of vehicles applications in 5G networks," *IEEE Transactions on Intelligent Transportation Systems*, vol. 5, pp. 1–9, 2020.
- [13] A. Rossi, G. Barlacchi, M. Bianchini, and B. Lepri, "Modelling taxi drivers' behaviour for the next destination prediction," *IEEE Transactions on Intelligent Transportation Systems*, no. 99, pp. 1–10, 2019.
- [14] Z. Gao, K. X. Xue, and S.H. Wan, "Multiple discrimination and pairwise CNN for view-based 3D object retrieval," *Neural Networks*, 2020, <https://arxiv.org/abs/2002.11977>.
- [15] J. Lv, Q. Sun, Q. Li, and L. Moreira-Matias, "Multi-scale and multi-scope convolutional neural networks for destination prediction of trajectories," *IEEE Transactions on Intelligent Transportation Systems*, vol. 21, no. 8, pp. 3184–3195, 2020.
- [16] X. Xu, B. Shen, X. Yin et al., "Edge server quantification and placement for offloading social media services in industrial cognitive IoT," *IEEE Transactions on Industrial Informatics*, vol. 17, no. 4, pp. 2910–2918, 2020.
- [17] X. Xian, H. Ye, X. Wang, and K. Liu, "Spatiotemporal modeling and real-time prediction of origin-destination traffic demand," *Technometrics*, vol. 63, pp. 1–20, 2019.

- [18] X. Duan, D. Guo, and C. Qin, "Image information hiding method based on image compression and deep neural network," *Computer Modeling in Engineering & Sciences*, vol. 124, no. 2, pp. 721–745, 2020.
- [19] C.-H. Chen, F.-J. Hwang, and H.-Y. Kung, "Travel time prediction system based on data clustering for waste collection vehicles," *IEICE Transactions on Information and Systems*, vol. E102.D, no. 7, pp. 1374–1383, 2019.
- [20] A. Faghih-Imani and N. Eluru, "A finite mixture modeling approach to examine New York City bicycle sharing system (CitiBike) users' destination preferences," *Transportation*, vol. 47, no. 2, pp. 529–553, 2020.
- [21] H. Alibabai and H. S. Mahmassani, "Dynamic origin-destination demand estimation using turning movement counts," *Transportation Research Record*, vol. 2085, no. 1, pp. 39–48, 2018.
- [22] G. Feng, Y. Han, Y. Wang, and J. Cheng, "Modeling and simulation analysis of QoE perception of network quality based on user preferences," *Computer Simulation*, vol. 37, no. 4, pp. 356–360, 2020.
- [23] K. F. Chu, A. Y. S. Lam, and V. O. K. Li, "Deep multi-scale convolutional LSTM network for travel demand and origin-destination predictions," *IEEE Transactions on Intelligent Transportation Systems*, vol. 21, no. 8, pp. 3219–3232, 2019.

Research Article

Detecting Home and Work Locations from Mobile Phone Cellular Signaling Data

Yingkun Yang ^{1,2}, Chen Xiong ^{1,2}, Junfan Zhuo ^{1,2} and Ming Cai ^{1,2}

¹School of Intelligent Systems Engineering, Sun Yat-sen University, Guangzhou 510006, China

²Guangdong Provincial Key Laboratory of Intelligent Transportation System, School of Intelligent Systems Engineering, Sun Yat-sen University, Guangzhou 510006, China

Correspondence should be addressed to Chen Xiong; xiongch8@mail.sysu.edu.cn

Received 29 January 2021; Revised 19 February 2021; Accepted 2 March 2021; Published 12 March 2021

Academic Editor: Chi-Hua Chen

Copyright © 2021 Yingkun Yang et al. This is an open access article distributed under the Creative Commons Attribution License, which permits unrestricted use, distribution, and reproduction in any medium, provided the original work is properly cited.

Obtaining the distribution of home and work locations is essential for city planning, as it defines the structure and mobility pattern of a city. With the development of telecommunication networks, mobile network data, having the advantages of large coverage and strong followability, have produced large amounts of information about human activities. Thus, it has become a popular research subject for human position detection. In this study, we proposed a new method to detect home and work locations based on the extraction of focal points in traces, identifying an individual's working and resting hours, and analyzing the characteristics of city grids using mobile phone cellular signaling data (CSD). At the individual level, we validated the algorithm on ground-truth volunteer data and achieved a small deviation of under 500 and 565 m for home and work location detection 85% of the time. At the aggregate level, we tested it on a city-wide anonymized CSD set and found a high Pearson correlation between our result and the census data of 0.93. Compared to existing studies, this study improved the granularity and location accuracy of home and work location detection, as well as validated the method using both individually labeled ground-truth data and aggregate data for the first time. Applying the algorithm in a city, we captured the population distribution, commuting patterns, and job-housing balance of the city and demonstrated the potential in using mobile network data for urban planning and policy formulation.

1. Introduction

Detecting home and work locations is of great importance to modern city and transportation planning, as it aids the understanding of the relationship of jobs-housing [1], the design of public transportation [2], and the optimization of urban land use [3]. Traditionally, this was accomplished by collecting survey and smart card data [4, 5]. However, survey data have a low update frequency, a small sample size, and a high implementation cost, while smart card data are confined to people using public transportation, which can possibly result in the sample being unrepresentative. To overcome these shortcomings, Global Positioning System (GPS) sensors were introduced to collect human mobility data. Compared to survey data, GPS data provided more accurate data with spatial and temporal details [6]. However, it required users to wear GPS loggers or actively allow GPS

tracking from dedicated applications on their mobile phones, which increased the cost and limited the collection scale.

With the development of telecommunications technology and the increase in the penetration rates of smartphones [7], smartphones have become ideal digital sensors to track human locations. Produced from the interactions between smartphones and telecommunication infrastructures, mobile network data are recorded by telecom operators automatically in the background. Therefore, they can record the carrier's spatiotemporal information at a massive scale with little effort from the carrier. Mobile network data can be classified as event-driven or network-driven data. The former, such as call detail records (CDRs), is produced with the usage of mobile services including calls and texts. The latter, which is generally called cellular signaling data (CSD), is produced from signaling events such as handovers, network

updates, periodic updates, and location area updates [8]. With the advantages, mobile network data have become a research interest in urban structure and human mobility studies [9–11]. Existing studies on home and work locations detection using mobile network data can be classified into two categories.

Studies in the first category defined two timeframes, working hours and resting hours, and selected the locations with the highest frequencies of phone usage or the longest staying times in the two timeframes. If the locations met additional requirements proposed in these studies, they would be identified as home and work locations. The location of a user was determined based on the base station that the user was connected to. The two timeframes were often set as the same for all users, although they could be adjusted based on researchers' knowledge. Kung et al. [12] set daytime and night-time timeframes with the thresholds of 8:00 and 20:00, respectively. In the two timeframes, the user's home and workplace were selected as the locations in which the user spent the maximum time as long as the staying time in such locations accounted for more than 50% of the timeframes. Yan et al. [13] identified the home and work locations as the most frequently visited base stations during the timeframes of 20:00–6:00 and 10:00–16:00, and then calculated the identification confidence and appearance days to determine potential commuters. Ahas et al. [14] developed an anchor point determination model to detect home, work, and multifunctional anchor points. Setting the boundary between the resting time and working time as 17:00, the average start time and the standard deviation of the start time of daily events were considered to distinguish the user's home and work points. The model was validated on a CDR data set in Estonia by comparing the home location identification results with the Estonian Population Register.

Studies in the second category discovered the user's mobility pattern and identified the meaningful places in the user's traces as home and workplace. Previous studies have proved that human trajectories could be mined by trajectory analysis and stay point detection from different kinds of data, including passive recording data like mobile network data [15]. Jiang et al. [16] extracted the stay locations of the user and identified the user's activity types (home, work, shop, etc.) by analyzing features in the trajectories including spatial and temporal regularities. Alexander et al. [17] converted records into clustered locations to identify origin-destination trips and inferred these locations to be home, work, or other considering observation frequency and time. Widhalm et al. [18] presented a filtering and clustering method to detect stay locations and enriched the location sequences with an activity type (work, home, shopping, leisure) inferring from land-use data and time of day. Isaacman et al. [19] clustered recorded locations using the Hartigan algorithm and trained a logistic regression model on CDR data from 18 volunteers to identify their important locations. The model considered the cluster features, including days, durations, and the number of events during working and resting hours. It was validated on data from 19 volunteers and achieved median errors of 0.9 and 0.83 miles

for home and work location detection, respectively. Inspired by this study [19], Zagatti et al. [20] also clustered the user's traces using the Hartigan algorithm. The clusters were then scored depending on the occurrence hours and days of events. The clusters were labelled as daytime clusters, evening time clusters, and undecided clusters depending on their scores, thus identifying the user's home and work clusters.

However, there were limitations in the previous studies. First, in most of the studies, the temporal information was selected as an important feature to detect home and workplace. They set the same working hours and resting hours for every user before identification despite the large differences in the working schedules of people in different occupations (for example, night workers), thereby introducing biases. As the basis of further analysis, defining timeframes with biases may introduce large errors in the identification process. In addition, in the majority of studies, base stations or clusters were selected as the home and work locations. However, the coverage area of base stations differed in urban and rural areas with different base station densities [21]. The spatial resolution of the identification results may range from less than 1 km to more than 10 km, depending on the density of the base stations and the clustering results, which creates concerns about the spatial accuracy of the detection algorithm. Lastly, most of the previous studies lacked validation both at the individual level and the aggregate level. Instead, some simply assessed the algorithms by comparing the identified results with aggregate data, like city-wide censuses or travel surveys, while some did not perform validation. Therefore, the performance of the methods on individual records was seldom reported, which limited their application at a high resolution.

In view of these limitations, this paper proposes a new algorithm to detect home and work locations with a finer resolution using CSD, as well as validates the algorithm at the individual level using ground-truth data and the aggregate level using census data. We first processed the raw CSD and extracted the focal points in active users' traces. Then, we adopted information entropy to measure the activity intensity and used ordered data binning to identify the unique working and resting hours of each user based on the variation of activity intensity of each user. By dividing the study area into grids, we used a regular-grid spatial tessellation to describe the coverages of the base stations, as well as analyzed their geographic, temporal and spatial features. Based on the features selected, multiple attribute decision-making was introduced to construct a selection model to detect work and home grids. We validated the algorithm at the individual level using volunteers' ground-truth data collected by a smartphone app that we developed, as well as at the aggregate level using a city-wide anonymized CSD set. Finally, the algorithm was employed to capture the population distribution, commuting patterns, and job-housing balance in a city, which demonstrated its potential in real practice for policy-makers and urban planners. In contrast to existing works, the main contributions of this work can be summarized as follows:

- (1) Investigating the unique schedule of each user by analyzing the variation of activity intensity of the user, thus distinguishing users with unusual working schedules and avoiding the biases from setting uniform timeframes
- (2) Improving the spatial accuracy of the home and work location detection by comprehensively analyzing the attributes of city grids
- (3) Evaluating the home and work location detection algorithm using both individually labelled ground-truth data and aggregate data for the first time

The rest of the paper is structured as follows. Section 2 presents an overview of the study area and data. Section 3 details the principle of the algorithm developed. Section 4 describes the verification work of the algorithm. Section 5 shows an example application of the model. Section 6 concludes the paper with a brief discussion.

2. Study Area and Data

2.1. Study Area. In this study, we chose Foshan as the study area. Foshan is a southern city in China and covers 3797.72 km². Bordering Guangzhou, which is one of the most-developed cities in China, Foshan is a well-known city of commerce and industry. According to the State Department, Foshan is composed of 5 districts, Chancheng, Nanhai, Shunde, Sanshui, and Gaoming, and it can be further divided into 32 subdistricts.

2.2. Data

2.2.1. Anonymized Cellular Signalling Data (CSD) Data Set. The data were an anonymized CSD set of Foshan and was provided by a large telecom operator in China. It covered the records of 4.9 million users on the operator’s network of 15 weekdays (the weekdays during July 9, 2018, and July 28, 2018). As shown in Table 1, each CSD record contained a user identification (ID) number, information about the user, timestamps of the events, and the connected base station ID number, according to which the longitude and latitude of the base station could be queried. The data set of the studied period contains a total of 8.6 billion interaction records. The number of base stations in the research area of Foshan is 7800. The overall base station density was 1.9 towers per square kilometer, but the spacing between them was not uniform across the city, as shown in Figure 1.

2.2.2. Ground-Truth Volunteer Data. The anonymized CSD set could not be matched to real users for algorithm validation. Therefore, we developed an app for Android phones to collect CSD from the volunteers that were recruited. After installing the app, the volunteer could mark his/her mobility traces and stay locations in the app, while their CSD was collected and uploaded to the database in the background automatically. After collation, the CSD was in the form shown in Table 1.

TABLE 1: Cellular signaling data (CSD) records.

User ID	Gender	Age	Datetime	Base station ID
4117***	M	30	20180715071145	23740
5701***	M	63	20180723053558	25815
5717***	M	20	20180620142020	19086

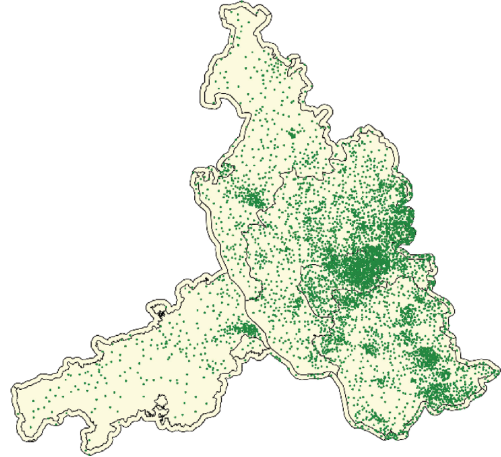


FIGURE 1: Distribution of the base stations.

In this study, a group of 41 volunteers was recruited, consisting of 22 males and 19 females, all of whom were adults aged 25–55 years. They lived and worked in Foshan, the study area, and had no unusual activities, such as moving or changing jobs, during the study period. They gave us permission to collect their CSD for five weekdays and to study the data for research purposes. In addition, they were also asked to provide us with the longitudes and latitudes of their true home and work locations with the help of a web map.

2.2.3. Point of Interest (POI) Data. The POI data consisted of information about the geographical points that represented a particular feature on the map. A POI could be anything closely related to human activities, such as an office building, bus station, or traffic sign. Therefore, the number and types of POIs in an area could reflect the main human activity in the area. The POI information used in this study was downloaded from the API (application programming interface) of a web map service provider. Each POI record contained key information, including the POI ID, type, longitude, and latitude, as shown in Table 2.

Since not all types of POIs are related to the home and workplace, we selected POIs of types closely related to the home and workplace for further analysis, as presented in Table 3. There were approximately 48,544 home-related POIs and 1,578,366 work-related POIs, and their distributions are presented in Figure 2.

3. Method

3.1. Focal Point Extraction. The focal points in a user’s traces were extracted to find the main activity space in his/her life

TABLE 2: POI information.

POI ID	Longitude	Latitude	Type
B02F5077VF	113.210716	22.875081	Culture and education services
B0FFL1FT5P	112.880293	23.180195	Enterprise
B0FFKUJWAO	113.002889	23.240415	Enterprise

TABLE 3: Home- and work-related POI types.

Home/work-related POI	POI type
Home-related POI	Commercial house
	Residential area
	Car services
	Restaurants
Work-related POI	Shopping services
	Life services
	Sports and recreation services
	Accommodation services
	Healthcare services
	Governmental organization
	Culture and education services
	Financial institutions
	Enterprises

for mobility pattern analysis. A typical characteristic of the CSD was that it contained a large amount of noise, and preprocessing was needed. Therefore, in extracting focal points, we aimed to (1) eliminate noise data, including abnormal data and redundant data, (2) filter sparse data to find active users, and (3) cluster spatially close base stations in a user's records.

3.1.1. Eliminating Noise Data. Removing the noise and redundancy in raw data is an essential issue in data preprocessing and help to show clearer information in further analysis. The noise data in the CSD contained abnormal data and redundant data. These are defined as follows:

- (i) *Abnormal Data.* This included records with missing values and records showing unusual behaviors. Records missing users' individual information were filled-in with the corresponding values in neighboring records to maintain data integrity while records missing key information including User ID, Datetime, and Base station ID were deleted. Unusual behaviors included alternate switching between several base stations in a short time and moving at a speed of 120 km/h or higher. In the former case, only records that connected to the most frequent base station in the series were kept. In the latter case, the records were deleted, as we considered it to be signal drifting.
- (ii) *Redundant Data.* As CSD was produced with a high frequency, a large number of records could be generated in a short time at the same place. Such records were merged by only keeping one record that contained the location of the base station, the first

connected time, and the staying time at the base station. In addition, some duplicate records were discarded.

3.1.2. Filtering Sparse Data. Temporal sparsity and inhomogeneous distributions of CSD records in a day could cause identification errors. Figure 3 presents the number of CSD records in each hour of one day from a user. This shows that the records were concentrated within 3 h and were lost for the rest of the day, which led to the incorrect conclusion that the user stayed at one place for a long time, such as between 3:00 and 13:00, thereby introducing errors. Therefore, we filtered out sparse data to obtain data that could reveal the user's mobility patterns. Referencing previous research [22], we divided a day into 48 30 min timeslots. If there were CSD records in at least 16 timeslots (8 h) in a day, the user's records for that day would be kept; otherwise, those records would be deleted. In this study, we selected active users with at least five days of data for further analysis.

3.1.3. Clustering Close Points. Although there were many points in a user's traces, only several points were needed to represent his/her main activity space. To obtain such focal points, we aimed to group together points that were spatially close and filtered out outliers in low-density areas, as they were not regular in the user's life. DBSCAN (density-based spatial clustering of applications with noise) [23], a density-based clustering algorithm, was applied to cluster the base stations connected to the user. It required two parameters: the distance threshold ϵ and the minimum number of points minpts to constitute a cluster. By experimenting with a range of combinations, we found that $\epsilon = 500$ m and minpts = 2 were the most suitable. Figure 4 shows the clustering result of a user's traces. Clusters are represented by blue circles, and their sizes are proportional to the user's staying time at a location. The red lines link the base stations and the clusters they belong to. It shows that the spatially close base stations in the user's traces are clustered and represented by the centroids of the clusters, thus extracting the focal points in the user's traces.

3.2. Schedule Identification. Identifying the schedule of the user helps to distinguish the resting and working hours, and thus detect the home and work location more accurately. Generally, the user's schedule is revealed by his/her unique mobility pattern, which is different in different times of a day and indicates the user's status.

Taking advantage of the characteristics of CSD, we analyzed the activity intensity of the user. In general, people tended to stay in more limited areas and moved less during resting hours, which could be distinguished from other time periods. We proposed adopting the information entropy from information theory to measure the user's activity intensity. Information entropy was first introduced by Shannon [24] to analyze the disorder degree of a system by measuring the uncertainty of information. Calculating the

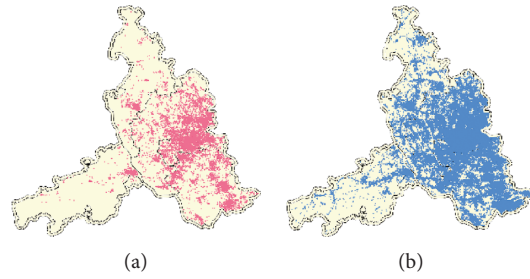


FIGURE 2: (a) Home-related POI distribution; (b) work-related POI distribution.

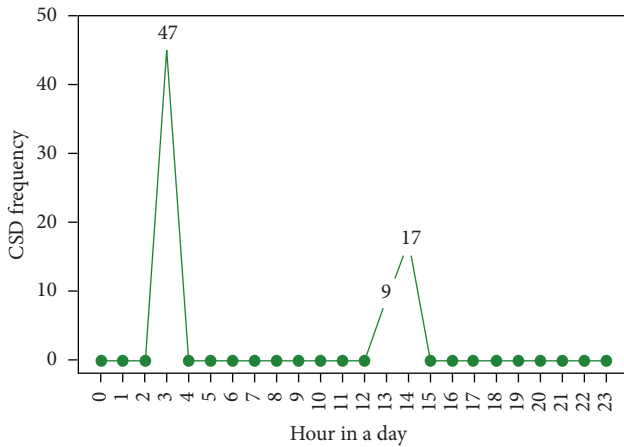


FIGURE 3: Example of the temporal distribution of the CSD.

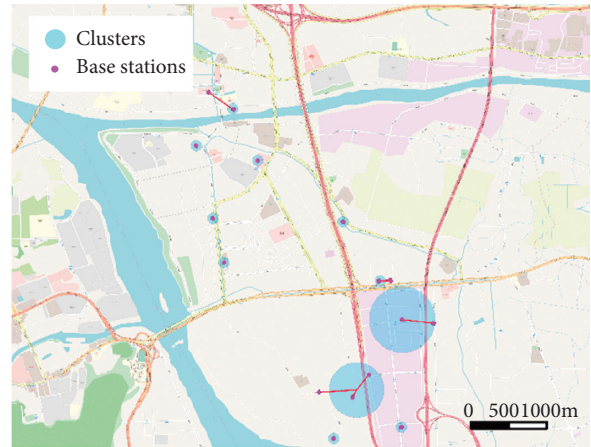


FIGURE 4: Clustering result of a volunteer's traces.

information entropy of a random variable is measuring the difference in the probability of events. The smaller the difference is, the more uncertain the information is, and the higher the information entropy is.

In this paper, the user's information entropy H_{period} during a given period is given by the following:

$$H_{\text{period}} = - \sum_{r=1}^R P_r \ln P_r, \tag{1}$$

$$P_r = \frac{st_r}{st_{\text{period}}},$$

where P_r is the proportion of the user's staying time st_r at location r to the total time st_{period} of the period and R is the number of the locations the user visited during this period.

H_{period} was measured by the difference in the probability that the user stayed at different locations during the period. The probability was represented by the proportion of the user's staying time at each location. A larger entropy means that the difference of the probability is small, thus the user spends his/her time more evenly in several places. On the contrary, a smaller entropy means that the difference of the probability is large, which resulted from the user contacting fewer base stations for longer time and moving less. When the user remains in one location, the information entropy will be 0.

Dividing a day into 24h, we calculated the user's information entropy in each time slot. Figure 5 shows an example of the information entropy in each hour in one day of a single user. The information entropy varied greatly from hour to hour according to the user's mobility pattern. Notably, the information entropy between 0:00 and 7:00 distinguishes from that during the daytime. This may indicate the user's resting time at home.

By measuring the information entropy in different times of a day, we could group time slots with similar activity intensity and divide a day into several timeframes. The time division based on the information entropy of each time slot was a data classification process. The user's day T was composed of 24h $\{t_1, t_2, \dots, t_{24}\}$ and for each hour t_j , its features were its information entropy in m days, which was denoted as $H_j = \{h_{1j}, h_{2j}, \dots, h_{mj}\}$. Based on this, we classified hours with similar features into p classes $\{T_1, T_2, \dots, T_p\}$. In particular, hours in a day could not be disordered in this case, which meant that the time slots in a class must be adjacent. Therefore, we introduced the Fisher-Jenks algorithm [25, 26], an ordered data binning algorithm, to split time slots into contiguous classes without scrambling the order. The key to Fisher-Jenks algorithm was to find the natural breaks in data that minimized the distance between the data points within various classes while maximizing the distance between the classes. It is supposed that the samples of a user could be described as follows:

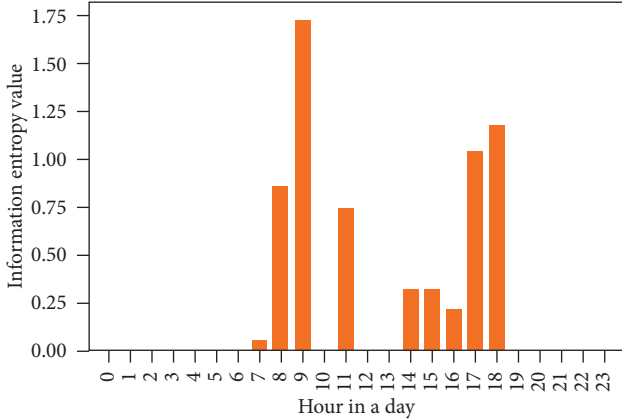


FIGURE 5: Example of the variation of the information entropy over one day.

$$H = \begin{bmatrix} h_{11} & h_{12} & \cdots & h_{1n} \\ h_{21} & h_{22} & \cdots & h_{2n} \\ \cdots & \cdots & \cdots & \cdots \\ h_{m1} & h_{m2} & \cdots & h_{mn} \end{bmatrix} = [H_1, H_2, \dots, H_n], \quad (2)$$

where h_{ij} is the information entropy in day i at hour j and H_n was the information entropy at hour n .

We chose the sum of squares of deviation to measure the data deviation in classes. The algorithm first calculates the distance for all sample pairs after normalizing the matrix H . Then, it computes the minimum deviations of classifying the samples into c classes by dynamically calculating the loss functions and finding the optimal result.

We experimented with a range of classification numbers and found that dividing the time into four classes worked well. The average entropy of a class T_G was calculated as

$$\overline{H}_{T_G} = \sum_{i=1}^m \sum_{j=a}^b h_{ij}. \quad (3)$$

We chose the class with the smallest average entropy as the resting hours of the user. Since most people went to work after the resting hours, we defined the start of the working hours as the end of the resting hours. Considering that the longest working time in a day in China is eight hours according to the labor law, the working time lasted for eight hours for users in our study. Figure 6 shows the information entropy of each hour for five days of one user, and a lighter color represents higher information entropy. According to the variation of information entropy in different times of the days, time was divided into four timeframes, as shown by the red dotted lines. Based on the results, the user was more inactive and remained stable in the first and last timeframe, while the user moved more in the other two timeframes. Using the method described above, the user's resting and working times were defined as 0:00–7:00 and 7:00–15:00.

3.3. Home and Work Grids Detection. Identifying the base stations or clusters as home and work locations resulted in

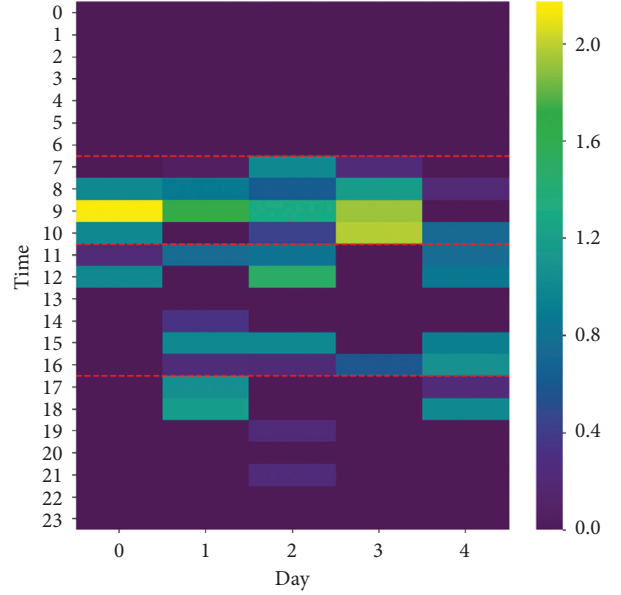


FIGURE 6: Time division using Fisher–Jenks algorithm.

spatial uncertainty of their positioning, as their coverage areas varied. We aimed to improve and stabilize the identification accuracy by extracting home and work grids based on their spatial, temporal, and geographic features.

3.3.1. Inferring Potential Grids. First, we divided the study area into grids and represented the coverage areas of the base stations by grids. As shown in Figure 7, a Voronoi tessellation technique [27] that divided the area into polygons according to the nearest neighbor rule was often used to simulate the coverage areas of base stations. Voronoi diagrams simulate the base station coverages based on the assumption that a mobile phone would connect to its closest base station and that the coverages do not overlap, which contradicts the actual behavior of mobile phones, which connect to the station with the highest signal strength [28]. This approach might underestimate the coverage of base stations. Also, the irregular diagrams might cause difficulties for further analysis in terms of calculation complexity and area segmentation. To solve these problems, we proposed using a regular-grid spatial tessellation to describe the coverages of the base stations. First, the study area was discretized into a mesh of grids with dimensions of $100\text{ m} \times 100\text{ m}$ considering the spatial distribution of the base stations, which achieved a balance between the grid refinement and the calculation efficiency. Then, we drew the circumcircle of each Voronoi polygon and defined the coverage of each base station as the grids that intersected its circumcircle. Figures 8(a) and 8(b) show an example of comparing the coverage areas of six base stations represented by Voronoi polygons and grids, respectively. The red points represent the base station locations and the blue areas represent their coverages. The grids cover more potential areas, and their regular shapes made them suitable for analysis.

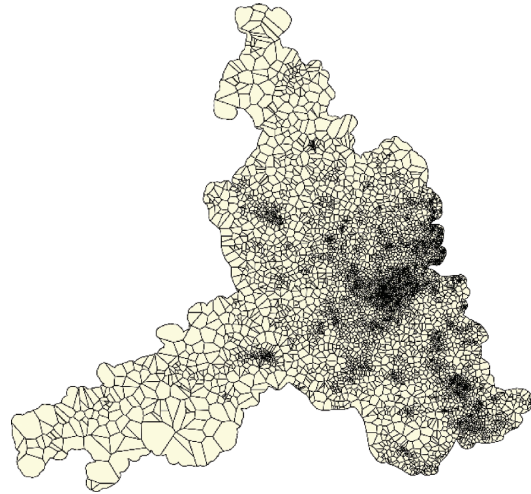


FIGURE 7: Voronoi diagram of the study area.

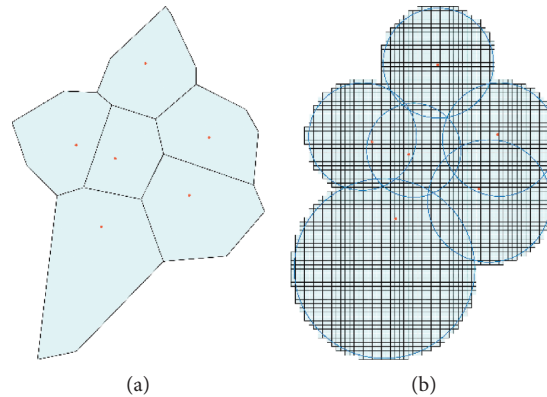


FIGURE 8: Base station coverages represented by (a) Voronoi diagram and (b) grids.

In Section 3.1, we classified the user's traces into different clusters. However, not all clusters were important in the lives of the users. To disregard transitional clusters in the user's traces, we selected the records in the user's resting and working hours, and calculated the staying time in each cluster during the relevant hours. For the two timeframes, we chose the cluster with the longest staying time as the important cluster in it. The grids covered by the base stations in the important clusters were inferred to be potential home or work grids.

3.3.2. Multiple Attribute Decision-Making. For each user, there were many potential grids, but normally, only one of them contained the home or workplace of the user. In this section, we describe how to determine which grid was the home or work grid. Studying the characteristics of the grids, we found that the following three observable factors were key to determining their importance.

(i) *Number of Home-Related or Work-Related POIs.* In general, a user's home and work locations, such as residential areas, apartment buildings, business

buildings, and schools, were recorded as POIs. Since POIs in an area indicated what people tend to do in the area, a grid with home- or work-related POIs with a higher density could more likely cover the user's home or workplace. Instead, if there were no relevant POIs in the grid, it may be located in an irrelevant area, such as a park or a road, and thus, it was less likely to cover the user's home or workplace.

(ii) *Staying Time at the Nearest Base Station.* Without knowing other conditions, such as the building occlusion effect and signal strength, we assumed that the distance between the user's position and base stations was the dominant factor that determined which base station the user connected to. Therefore, the longer the user connected to a base station, the more likely the user was to stay in the nearby grids, and the more likely it was that the grids cover his/her home or workplace.

(iii) *Average Distance to Base Stations in an Important Cluster.* During resting and working hours, the user might have connected to several base stations. This

may have been due to the user moving or the signal drifting inside his/her living and working areas. Therefore, the home and work locations are more likely to be at the center than at the edges of the cluster. This factor reveals the grid's position in the cluster by considering the distribution of the base stations. A grid with a shorter average distance was more likely to cover the home or workplace.

With the factors described above, we constructed a grid selection model based on multiple attribute decision-making to comprehensively analyze the attributes of the grids and select the home and work grids from the potential grids. A multiple attribute decision-making process made optimal decisions from several alternatives depending on their attributes and the relative weights of the attributes. Designing the weights of the attributes was one of the most important parts in the process as it would have a deep influence on the results. To enhance the objectivity of the result, we applied the entropy weight method (EWM) [29] instead of any subjective weighting models to determine the attribute weights. Basically, the EWM measures the importance of an attribute by the amount of useful information it contains. Equal attribute values for all samples does not provide any useful information for differentiating the home or work grid from other grids and such attribute should be given lower importance. We calculated the information entropy of an attribute. The lower the information entropy is, the higher the degree of differentiation of the attribute is, and the more useful it is to the evaluation. Thus, the attribute with lower information entropy will be given a higher weight and vice versa.

In this case, there were three factors and s samples in the evaluation, and y_{ij} was the i^{th} attribute of the j^{th} sample. First, the attributes were standardized as y'_{ij} . The entropy E_i of the i^{th} attribute was calculated as

$$E_i = -\frac{1}{\ln s} \sum_{j=1}^s p_{ij} \ln p_{ij}, \quad (4)$$

where $p_{ij} = y'_{ij} / \sum_{j=1}^s y'_{ij}$.

Larger weights should be given to attributes with higher entropy. The weights are calculated as follows:

$$w_i = \frac{1 - E_i}{\sum_{i=1}^3 (1 - E_i)}. \quad (5)$$

The final score Z_j for grid j is

$$Z_j = \sum_{i=1}^3 y'_{ij} w_i. \quad (6)$$

A user's home or work location was identified as the potential grid with the highest score.

Finally, we checked if the user was a regular resident or worker in the study area. The clusters that covered the home (work) grid in the user's traces were extracted. If they appeared on more than 3/5 of the days of the study period, which meant that the user visited the location on most of the days, the user would be considered to be a regular resident (worker). Otherwise, he/she would be

labelled as not having a regular home (workplace) in the study area.

4. Validation

In this section, we validated the proposed method with a ground-truth volunteer data set and a large-scale anonymized CSD set from the study area, as well as reported the evaluation results.

4.1. Validation on Volunteer Data Set. The algorithm was validated on the volunteer data set to evaluate the algorithm at the individual level. As described in Section 2.2.1, since we had the ground-truth data of individuals, we were able to evaluate the accuracy of the algorithm by measuring the position deviation between the identified locations and the true locations. To comprehensively analyze the result, we also compared our algorithm with two other identification algorithms.

In the first algorithm, called the TimeAccumulation algorithm [12], the resting and working hours were defined as 0:00 to 6:00 and 10:00 to 16:00, based on the typical timeframes of Foshan. A user's home and work locations were identified as the base station that the user was connected to for the longest time during resting and working hours. The second algorithm, called the HomeWorkCluster algorithm [20], clustered the base stations that had interacted with the user. Then, the clusters were scored according to the time of records in the clusters. Records between 8:00 and 17:00 were assigned a score one and those between 19:00 and 7:00 were assigned a score of minus one. The center of the cluster with the highest score was identified as the workplace while the center of the cluster with the lowest score was identified as home. The two algorithms could be classified into the two categories described in Section 1.

Figure 9 shows the cumulative distribution function (CDF) of the deviation between the true home locations and the home locations detected by the algorithm proposed in this paper, the TimeAccumulation algorithm, and the HomeWorkCluster algorithm. For the new algorithm, 85% of the home location deviations were under 500 m. Furthermore, as shown in Table 4, with a mean error of 246 m, the new algorithm outperformed the other two models, whose mean errors were 604 and 600 m, respectively.

Figure 10 shows the deviation between the true work locations and the work locations detected by the three algorithms, and a local enlargement of the figure. For the new algorithm, 85% of the work location deviations were less than 565 m. Although the work deviations were slightly higher than the home location deviations, the new algorithm also achieved a smaller mean error of 566 m, while the mean errors of the other two algorithms were 770 and 868 m, respectively, as shown in Table 4.

4.2. Validation on Anonymized Large-Scale Cellular Signaling Data. To evaluate the performance of our algorithm at the aggregate level, we applied it on the anonymized CSD set of Foshan city and compared the result with the sixth national

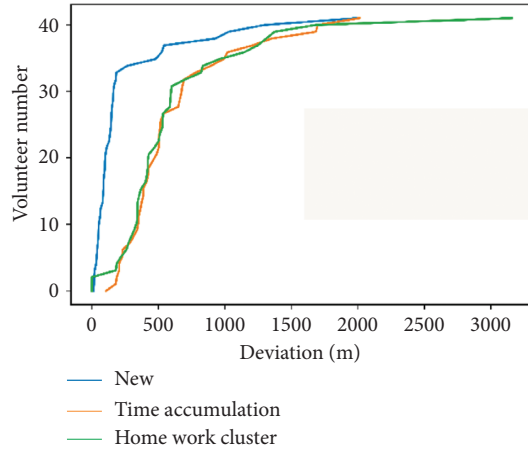


FIGURE 9: Home location deviations of the proposed (new), TimeAccumulation, and HomeWorkCluster algorithms.

TABLE 4: Mean home/work location deviations of the three algorithms.

	New algorithm	TimeAccumulation algorithm	HomeWorkCluster algorithm
Mean deviation of home location	246.47	604.32	599.98
Mean deviation of work location	566.29	769.64	867.74

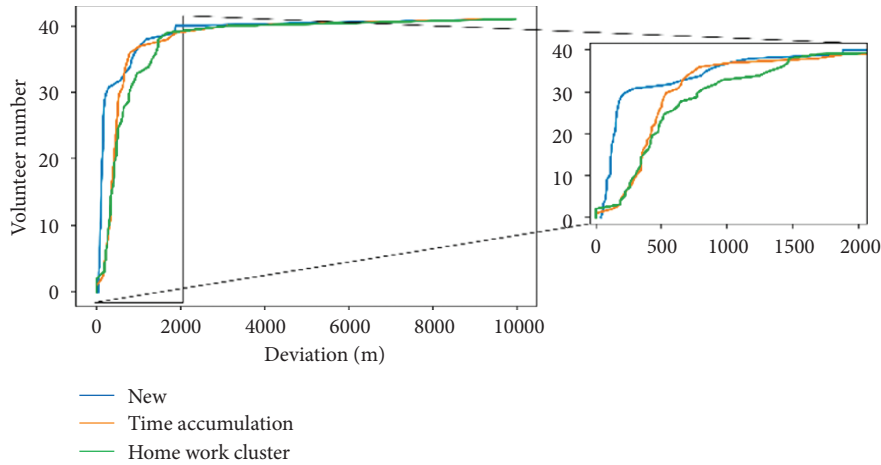


FIGURE 10: Work location deviation of the proposed (new), TimeAccumulation, and HomeWorkCluster algorithms.

census [30] in 2010. Both data sets contained population information of the study area, Foshan. As Foshan could be divided into 32 subdistricts, we inferred users’ home locations from the CSD set using the algorithm and aggregated them in the subdistricts. Figure 11 shows a comparison between the output of our algorithm and the number of residents by subdistrict from the census data. There was a linear relationship between them, indicating that the distribution of residents inferred from the CSD was consistent with the census population, while a few mismatches may have resulted from the different data collecting years and the change of the town borders during the eight-year gap. To further estimate their consistency, we calculated the Pearson correlation coefficient between our result and the census

data, which was $r = 0.93$. The high linear correlation shows that the output of our algorithm reflected the distribution of the population fairly well at the subdistrict level and was reliable for location identification.

5. Case Study

To demonstrate the application of the algorithm in practice, we present a case study in Foshan using the anonymized CSD set. Urban planners pay attention to the commuting between districts and depend on it to analyze land use and transportation connections in the city. Using the algorithm presented in this paper, the home and work locations of the users in Foshan were determined. To analyze the commuting

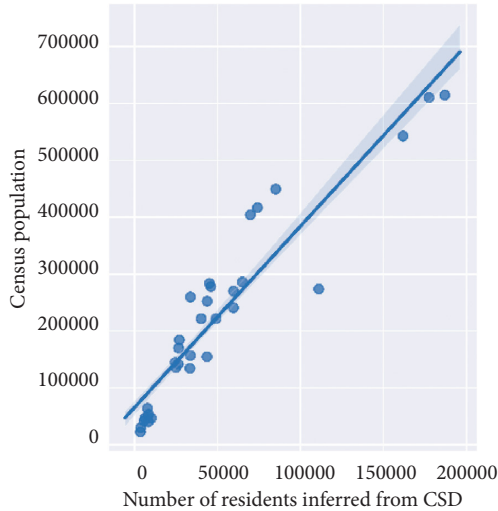


FIGURE 11: Comparison between our inferred residential population from the CSD and the population from the census data.

patterns between districts inside Foshan, we summed up the home and work locations by district and drew the commuting OD (origin-destination) desire lines between the five districts according to the home and work location distribution, as shown in Figure 12. This is a visualization of the commuting matrix of Foshan. The desire lines were drawn between the centroids of the districts and illustrate the flows of commuting people between them. The thicknesses of the lines depend on the number of commuting trips. Figure 12 shows that the majority of interdistrict commuting trips inside Foshan were generated between the Chancheng, Nanhai, and Shunde districts, which made up 86% of the interdistrict commuting trips. This agreed with their role in city planning as the most-developed part of Foshan. In addition, the east side of Foshan borders the heart of Guangzhou, which creates large numbers of job opportunities and attracts residents. In contrast, the other two districts are less economically developed, with lower GDPs (gross domestic products), and the commuting flows into and out of the districts are smaller accordingly.

To further analyze the job and housing situation inside the districts, we narrowed the scope into each subdistrict and calculated the density distribution of homes and workplaces, as presented in Figures 13(a) and 13(b), respectively. The distribution indicates the land-use characteristics in different parts of the city. Figure 13(a) suggests that the home locations are distributed broadly in the city, and the home density was higher on the east side, especially in the city center of the Chancheng district and its surroundings. The highest density reached 3,434 users per square kilometer in the Zumiao subdistrict. Figure 13(b) suggests that the workplace density is relatively high in the eastern portion of Foshan as well, especially in the Zumiao subdistrict, with the highest density of 3,527 users per square kilometer, as Zumiao is the heart of the Chancheng district and a transportation hub of Foshan, where many enterprises, shopping malls, and stations are located.

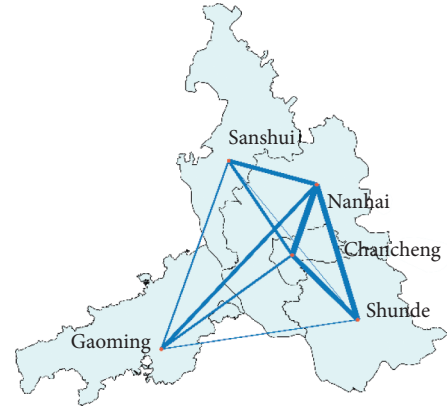


FIGURE 12: Commuting origin-destination (OD) desire lines between districts.

Furthermore, analyzing the traffic demand is essential for transportation planning in cities, and commuting travel is a significant part of the daily traffic demand. From the home and work locations, we could analyze the characteristics of the commuting demand. Considering the reduction of the CSD positioning error as well as the spatial accuracy of the algorithm, as evaluated in Section 4.1, we discretized the city into grids with dimensions of $500\text{ m} \times 500\text{ m}$. We then selected users whose home and workplace were both inside Foshan and allocated their home and work locations into the grids. The commuting distance of each user was calculated as the distance between the centers of their home/work grids. To show the complete distribution of the commuting distance in Foshan, the distribution is presented in double logarithmic coordinates, as shown in Figure 14(a). It shows that with the growth of commuting distance, the percentage of users falls down quickly and the majority of people have relatively small commuting distance. Focusing on this group of people, the pie chart, as presented in Figure 14(b), shows the percentage of users in different commuting distance intervals. About 62% of users' commuting distances were less than 2 km. For this group of people, it was possible to travel in nonmotorized mode. However, almost 5.36% of the users were long commuters whose homes were over 10,000 m from their workplaces, and these groups of people were more likely to travel by car. Overall, the mean commuting distances of the users who lived and worked inside Foshan was about 2,936 m, and about 80% of the users live within 4,000 m from their workplaces. The characteristics of the commuter trips in Foshan showed that people had relatively small commuting distances and might rely more on nonmotorized travel mode or public transport than private cars in their daily commuting. Therefore, for transportation planners and policy-makers of Foshan, more importance should be given to nonmotorized travel infrastructures and public transportation design, including bike-sharing services, bus line planning, and bus scheduling in peak hours.

From the above analysis, we inferred that Chancheng district was the key area of Foshan. Therefore, we focused on analyzing the characteristics of Chancheng, which is located

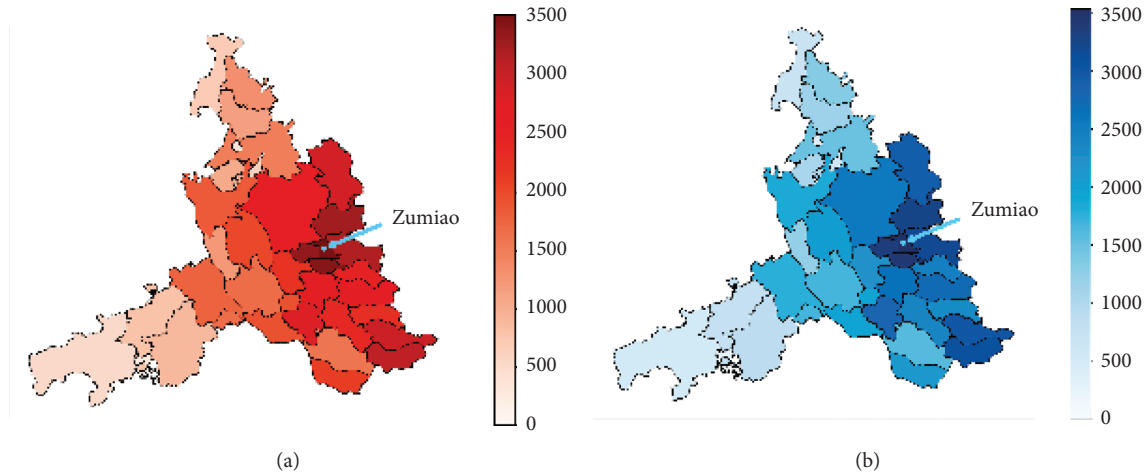


FIGURE 13: (a) Home density distribution in Foshan; (b) workplace density distribution in Foshan.

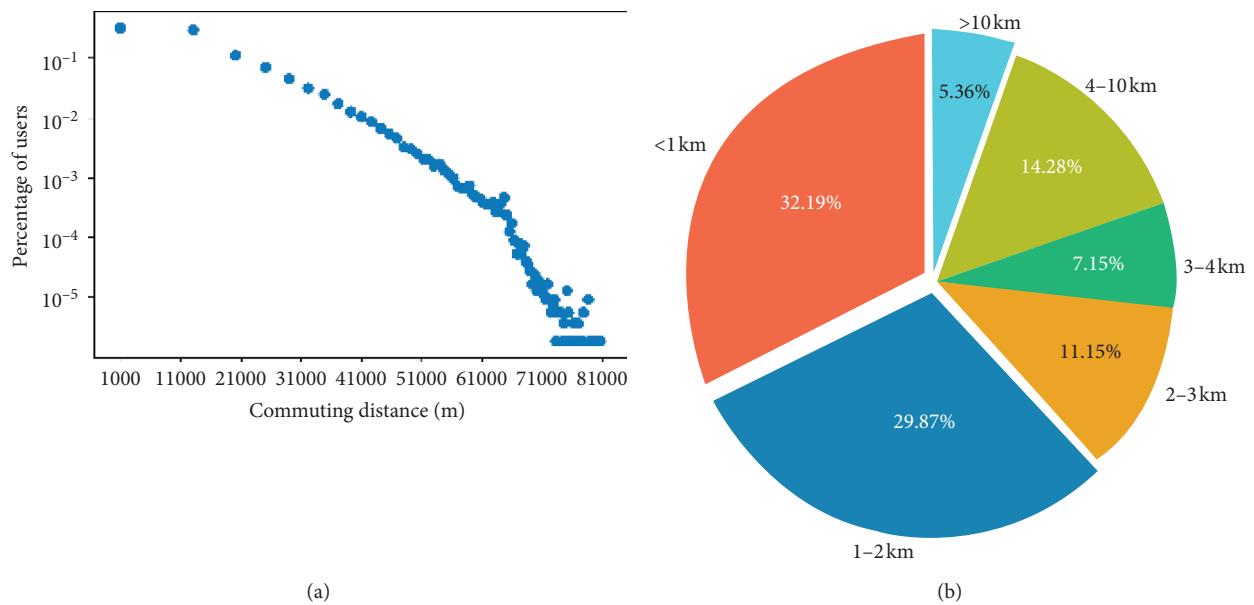


FIGURE 14: (a) The commuting distance distribution in double logarithmic coordinates; (b) the percentage of users in different commuting distance intervals.

at the center of Foshan, covering 154 square kilometers. It is the political, commercial, and cultural center of Foshan and a mixture of office, residential, and industrial areas. First, we focused on the spatial organization of homes and workplaces in Chancheng, as presented in Figures 15(a) and 15(b), respectively. We could see that both the living and working centers were in the east side of the district, while the home and workplace density in the west portion were relatively lower.

To assess the planning and development of the district, we introduced three indices that are often used to evaluate the equitability of job and housing distributions in a region. The first index is the employment self-sufficiency (ESS) [31], which refers to the number of people working and living locally out of the number of local workers. It describes the

self-containment of a region from the supply-side, and a higher ESS indicates that fewer people travel to the region for work. The second index is the employment self-containment (ESC) [31], which refers to the number of people working and living locally out of the number of local residents. It describes the self-containment of a region from the demand-side, and a higher ESC shows that fewer local residents travel to other regions for work. The third index is the job-housing ratio (JHR) [32], which represents the number of workers over the number of residences inside the region. It measures the matching degree between the number of jobs and the number of residences in the region. Table 5 presents the three calculated indices for the Chancheng district.

The ESS of 0.77 showed that 23% of workers were attracted from other districts, and the ESC showed that about

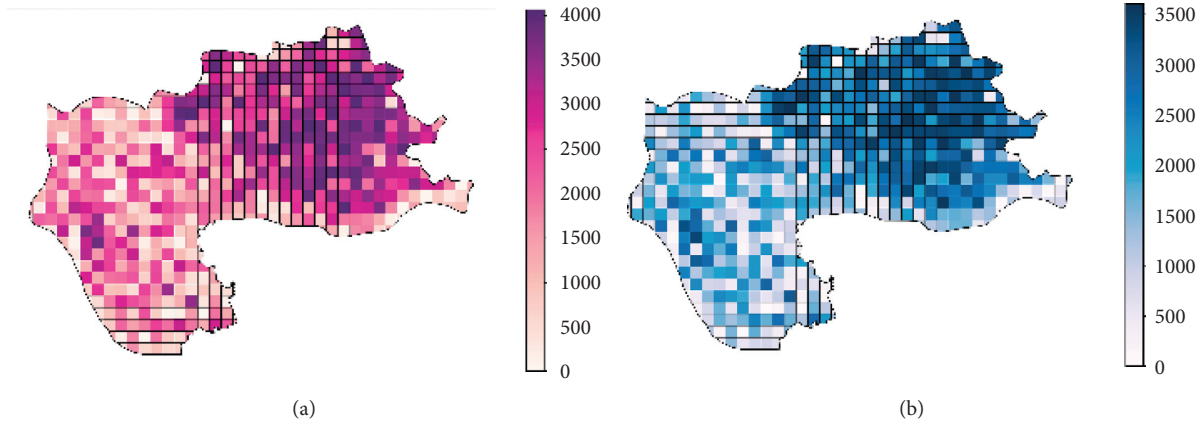


FIGURE 15: (a) Home location distribution in Chancheng; (b) workplace location distribution in Chancheng.

TABLE 5: Employment self-sufficiency (ESS), employment self-containment (ESC), and job-housing ratio (JHR) for the Chancheng district.

Indices	Chancheng district
ESS	0.77
ESC	0.78
JHR	1.01

78% of residents worked inside the district. This indicated that Chancheng, as the heart of Foshan, has great employment appeal for people all over the city and is a one-way attraction for other districts. Furthermore, while the commuting space for local residents is mainly concentrated inside the district, there is a large amount of interdistrict commuting demand to Chancheng that should not be ignored. However, the JHR of Chancheng was 1.01. According to Cervero [32], a value of the JHR between 0.8 and 1.2 indicates a relatively high match between the number of jobs and number of residences, and thus, the Chancheng district reaches a balance between providing job opportunities and housing.

6. Conclusion

Urban and transportation planning relies significantly on obtaining the home and work locations of people. This paper presented a method that could process massive CSD to detect the home and work locations of anonymized phone users. Considering the irregular temporal sampling and uncertain spatial accuracy characteristics of the data, the proposed method analyzed the variation of activity intensity of each user to investigate their schedules and comprehensively considered geographic, temporal, and spatial features of city grids to identify the home and work location. Using ground-truth data from volunteers and census, the study showed that the algorithm had high precision and could be used to detect the home and work locations of people on a large scale with small deviation. At the individual level, the validation results showed that the algorithm could detect users' home and work locations to within 500 and 565 m, respectively, 85% of the time, while at the

aggregate level, the Pearson correlation between our results and the census data was 0.93.

Compared to previous studies, this study is a significant step forward to use mobile phone data for home and work location detection in terms of granularity, location accuracy, and distinction of people with different working schedules. Also, to the best of our knowledge, this is the first study to evaluate the home and work location detection algorithm using both individually labelled ground-truth data and aggregate data.

As the literature suggests, in view of the development of cities, the expansion of the population, and the changing of urban structures and working schedules, the living and working behaviors of people have become more complex. Due to its small sample size and high collection cost, traditional survey data may fail to support the work in city planning and management, and reliable new data sources and methods are needed. Because of their characteristics of wide coverage, large sample size, and strong followability, mobile network data have made it possible to analyze human mobility pattern on a large spatiotemporal scale. By presenting a case study, it was demonstrated that applying our method can help obtain the distribution of home and work locations, extract commuting demand, and assess the job-housing balance in a big city using massive mobile network data. This shows the ultimate goal of the study to help urban planners and policy-makers to derive a new understanding of the city from big data, thus aiding their work in transportation planning for targeted areas, public facility construction to improve service quality, and policy formulations for future urban development.

Data Availability

The data used to support the findings of this study have not been made available because these are anonymized data and are confidential due to volunteer agreement and privacy policies.

Conflicts of Interest

The authors declare that there are no conflicts of interest regarding the publication of this paper.

Acknowledgments

This work was supported by the National Key R&D Program of China (Grant No. 2020YFB1600400) and the Fundamental Research Funds for the Central Universities (Grant No. 19lgpy290).

References

- [1] T. Li, Y. Chen, Z. Wang, Z. Liu, R. Ding, and S. Xue, "Analysis of jobs-housing relationship and commuting characteristics around urban rail transit stations," *IEEE Access*, vol. 7, pp. 175083–175092, 2019.
- [2] G. Qiu, R. Song, S. He, W. Xu, and M. Jiang, "Clustering passenger trip data for the potential passenger investigation and line design of customized commuter bus," *IEEE Transactions on Intelligent Transportation Systems*, vol. 20, no. 9, pp. 3351–3360, 2019.
- [3] Z. Yang, X. Zhu, and D. Moodie, "Optimization of land use in a new urban district," *Journal of Urban Planning and Development*, vol. 141, no. 2, 2015.
- [4] Y. Ji, Y. Cao, Y. Liu, W. Guo, and L. Gao, "Research on classification and influencing factors of metro commuting patterns by combining smart card data and household travel survey data," *IET Intelligent Transport Systems*, vol. 13, no. 10, pp. 1525–1532, 2019.
- [5] J. Huang, D. Levinson, J. Wang, and Z. Wang, "Tracking job and housing dynamics with smartcard data," in *Proceeding of the National Academy of Sciences of the United States of America*, pp. 12710–12715, USA, 2018.
- [6] F. Zhao, F. Pereira, R. Ball et al., "Exploratory analysis of a smartphone-based travel survey in Singapore," *Transportation Research Record*, vol. 2494, Article ID 45e56, 2015.
- [7] M. S. Iqbal, C. F. Choudhury, P. Wang, and M. C. González, "Development of origin-destination matrices using mobile phone call data," *Transportation Research Part C: Emerging Technologies*, vol. 40, no. 1, pp. 63–74, 2014.
- [8] F. Calabrese, L. Ferrari, and V. Blondel, "Urban sensing using mobile phone network data: a survey of research," *ACM Computing Surveys*, vol. 47, no. 2, pp. 1–20, 2014.
- [9] X. Song, Y. Ouyang, B. Du, J. Wang, and Z. Xiong, "Recovering individual's commute routes based on mobile phone data," *Mobile Information Systems*, vol. 2017, 11 pages, 2017.
- [10] M. Ghahramani, M. Zhou, and C. T. Hon, "Mobile phone data analysis: a spatial exploration toward hotspot detection," *IEEE Transactions on Automation Science and Engineering*, vol. 16, no. 1, pp. 351–362, 2019.
- [11] Z. Duan, Z. Lei, M. Zhang, W. Li, J. Fang, and J. Li, "Understanding evacuation and impact of a metro collision on ridership using large-scale mobile phone data," *IET Intelligent Transport Systems*, vol. 11, no. 8, pp. 511–520, 2017.
- [12] K. Kung, G. Kael, S. Stanislav, and C. Ratti, "Exploring universal patterns in human home-work commuting from mobile phone data," *Plos One*, vol. 9, no. 6, Article ID e96180, 2014.
- [13] L. Yan, D. Wang, S. Zhang, and D. Xie, "Evaluating the multi-scale patterns of jobs-residence balance and commuting time-cost using cellular signaling data: a case study in Shanghai," *Transportation*, vol. 46, no. 3, pp. 777–792, 2019.
- [14] R. Ahas, S. Silm, O. Järv, E. Saluveer, and M. Tiru, "Using mobile positioning data to model locations meaningful to users of mobile phones," *Journal of Urban Technology*, vol. 17, no. 1, pp. 3–27, 2010.
- [15] Y. Zheng, "Trajectory data mining," *ACM Transactions on Intelligent Systems and Technology*, vol. 6, no. 3, pp. 1–41, 2015.
- [16] S. Jiang, J. Ferreira, and M. C. Gonzalez, "Activity-based human mobility patterns inferred from mobile phone data: a case study of Singapore," *IEEE Transactions on Big Data*, vol. 3, no. 2, pp. 208–219, 2017.
- [17] L. Alexander, S. Jiang, M. Murga, and M. C. González, "Origin-destination trips by purpose and time of day inferred from mobile phone data," *Transportation Research Part C: Emerging Technologies*, vol. 58, pp. 240–250, 2015.
- [18] P. Widhalm, Y. Yang, M. Ulm, S. Athavale, and M. C. González, "Discovering urban activity patterns in cell phone data," *Transportation*, vol. 42, no. 4, pp. 597–623, 2015.
- [19] S. Isaacman, R. Becker, R. Cáceres et al., "Identifying important places in people's lives from cellular network data," in *Proceedings of the 9th International Conference on Pervasive Computing*, pp. 133–151, Heidelberg, Germany, 2011.
- [20] G. A. Zagatti, M. Gonzalez, P. Avner et al., "A trip to work: estimation of origin and destination of commuting patterns in the main metropolitan regions of Haiti using CDR," *Development Engineering*, vol. 3, pp. 133–165, 2018.
- [21] C. Horn, H. Gursch, R. Kern, and M. Cik, "QZTool—automatically generated origin-destination matrices from cell phone trajectories," *Advances in Intelligent Systems and Computing*, vol. 484, pp. 823–833, 2016.
- [22] C. M. Schneider, V. Belik, T. Smoreda, and M. C. González, "Unravelling daily human mobility motifs," *Journal of The Royal Society Interface*, vol. 10, no. 84, Article ID 20130246, 2013.
- [23] M. Daszykowski and B. Walczak, "Density-based clustering methods," in *Comprehensive Chemometrics*, pp. 635–654, Elsevier, Amsterdam, The Netherlands, 2010.
- [24] C. E. Shannon, "A mathematical theory of communication," *Bell System Technical Journal*, vol. 27, no. 3, pp. 379–423, 1948.
- [25] W. D. Fisher, "On grouping for maximum homogeneity," *Journal of the American Statistical Association*, vol. 53, no. 284, pp. 789–798, 1958.
- [26] G. F. Jenks and F. C. Caspall, "Error on choroplethic maps: definition, measurement, reduction," *Annals of the Association of American Geographers*, vol. 61, no. 2, pp. 217–244, 1971.
- [27] F. Aurenhammer, "Voronoi diagrams—a survey of a fundamental geometric data structure," *ACM Computing Surveys*, vol. 23, no. 3, pp. 345–405, 1991.
- [28] M. Kjaergaard, "Location-based services on mobile phones: minimizing power consumption," *IEEE Pervasive Computing*, vol. 11, no. 1, pp. 67–73, 2011.
- [29] K. Qiu, *Management Decision and Applied Entropy*, Machine Press, Beijing, China, 2002.
- [30] China Statistics Press, *Tabulation on the 2010 Population Census of the People's Republic of China by Township, Population Census Office under the State Council*, China Statistics Press, Beijing, China, 2012.
- [31] K. Martinus and S. Biermann, "Strategic planning for employment self-containment in metropolitan sub-regions," *Urban Policy and Research*, vol. 36, no. 1, pp. 35–47, 2018.
- [32] R. Cervero, "Jobs-housing balance revisited: trends and impacts in the san francisco bay area," *Journal of the American Planning Association*, vol. 62, no. 4, pp. 492–511, 1996.

Research Article

Multiobjective Model and Improved Artificial Raindrop Algorithm for Virtual Network Mapping

Hejun Xuan ¹, Xuelin Zhao,¹ Lei You ^{1,2}, Zhenghui Liu,^{1,2} and Yanling Li^{1,2}

¹School of Computer and Information Technology, Xinyang Normal University, Xinyang 464000, China

²Henan Key Lab. of Analysis and Application of Education Big Data, Xinyang Normal University, Xinyang 464000, China

Correspondence should be addressed to Lei You; lei_perfect_xynu@126.com

Received 9 February 2021; Revised 21 February 2021; Accepted 26 February 2021; Published 12 March 2021

Academic Editor: Chi-Hua Chen

Copyright © 2021 Hejun Xuan et al. This is an open access article distributed under the Creative Commons Attribution License, which permits unrestricted use, distribution, and reproduction in any medium, provided the original work is properly cited.

Network virtualization (NV) can provide the resource according to the request and can improve the flexibility of the network. It has become the key technology of 5G communication. Resource scheduling in virtual network mapping is an important problem faced by NV technology. To enhance the performance of the network, optimal resource scheduling schemes should be determined. In general, maximum index of frequency slots used, energy consumption, and the ratio of used frequency slots are three very important indicators for the network. Based on the previous research studies, we first take these three indicators into the objective of the mathematical model and define a novel multiobjective optimization model. Then, the three objectives are integrated into one objective to be minimized by using the sum weighted strategy. Finally, an efficient algorithm, which integrates the advantages of artificial raindrop algorithm (ARA), particle swarm optimization, and differential evolution, is proposed and denoted as IARA. Moreover, simulation experiments have been conducted in several experimental scenes with other compared algorithms. The experimental results show that the proposed algorithm IARA can obtain better scheduling schemes than the compared algorithms.

1. Introduction

Network virtualization is actually to realize that multiple heterogeneous virtual networks can run in a basic network. By creating a realistic and stable virtual environment, resources reuse of routers, links, and other physical devices can be realized, which greatly improves resource utilization, thus providing support for Internet of Things, cloud computing, and other technologies [1, 2]. Cloud platform is based on the underlying infrastructure of network virtualization technology to achieve the resource sharing, and distributed architecture and the characteristic of being extensible also make cloud platform able to improve the simulation of network scale, but the establishment of the virtual network and dismantling make the demand of the network business change, in order to make the underlying network support heterogeneous virtual network request as much as possible and achieve the efficient scheduling and management of resources [3]. What is more, network virtualization can

accelerate innovation of network architecture. Now there are many different kinds of resources in the network environment, different function, virtual resource distribution is not the same, network heterogeneity and dynamics. The virtual nodes deployed in location and resources to meet the basic requirements of physical nodes and to ensure meeting the resource constraint conditions such as virtual nodes in the path of the physical nodes are linked together, the core problem is the virtual network mapping, there is also an urgent need to solve the key challenge, and the field has become a very popular area of research [4, 5]; it enables network operators to share a physical network in case of different operating virtual optical network and the optical layer to simplify resource management, providing flexible spectrum allocation schemes and secure application services [6]. [7]. Network virtualization as solving the problem of network “rigidity” provides an effective means; it can realize multiple heterogeneous virtual networks sharing the underlying network resources; it not only improves the

utilization rate of network resources but also brings more flexible services; virtual network mapping, as one of the key technologies of network virtualization, has been widely concerned [8–10].

Virtual network mapping has been proved to be an NP-hard problem, and the related solutions have become a research hotspot [11, 12]. Virtual network mapping can be divided into one stage and two stages according to the steps to map, a phase mapping algorithm because of high complexity, low adaptability, now two phase mapping algorithm is the mainstream of the study is the first network all nodes mapping, mapping, and then to link so the node mapping strategy for virtual network mapping plays a key role in success [13]. Node mapping methods mainly include heuristic algorithm [14], linear programming solution [15], and intelligent optimization algorithm [16]. Node sorting has also developed from simple node resource sorting [17] to topological resource joint sorting [18], gradually forming the problem of node multi-index sorting [19]. The authors of [20] put forward a kind of node importance evaluation method based on TOPSIS, and, on the basis of considering the node resources property, the introduction of social network analysis method of the centrality, and approaching degrees centrality, Euclidean distance of TOPSIS method cannot distinguish with positive and negative ideal solution distance equal points, index weight, and node set artificially; subjectivity is stronger. The study in [21] proposed a node ranking method with weighted relative entropy, which can realize the joint perception of virtual topology and physical topology, but its index weight needs to be adjusted manually according to environmental changes, so it relies heavily on experience. The study in [22] introduced the extraction process of the underlying network features and the node sorting method and used the particle swarm optimization method to train the index weight vector. It can automatically determine the parameters in the algorithm for different optimization objectives, but the algorithm complexity is high. The study in [23] proposed a virtual network mapping algorithm based on greedy algorithm. In the node mapping stage, only the CPU resources of the nodes and the bandwidth of the adjacent links were considered, without considering the topological attributes. In order to further improve the mapping efficiency, scholars improve the performance of node mapping algorithm. The study in [24] proposed the optimization model of energy consumption and applied it to the problem of virtual network mapping. The study in [25] designs an optimal backup topology for single link failure in virtual SDN, which improves resource utilization and shortens algorithm execution time. The study in [26] focuses on the problem of network forwarding resources and load balancing and designs an integer linear programming model to solve the problem of online resource allocation of multiple virtual links in SDN environment. The study in [27] proposes a time-sensitive virtualization controller deployment algorithm for SDN controller network delay, which reduces the communication delay between the switch and the controller. However, there are few researches on combinatorial optimization problems, which aim to control delay and balance network load.

In general, maximum index of used frequency slots, energy consumption, and the ratio of used frequency slots are three very important indicators for the network. Based on the previous researches, we first take these three indicators into the objective of the mathematical model and define a novel multiobjective optimization model. Then, the three objectives are integrated into one objective to be minimized by using the sum weighted strategy. Finally, an efficient algorithm, which integrates the advantages of artificial raindrop algorithm (ARA), particle swarm optimization, and differential evolution, is proposed and denoted as IARA. We summarize the major contributions of this paper as follows:

- (i) We first take the three indicators into the objective of the mathematical model and define a novel multiobjective optimization model
- (ii) An efficient algorithm, which integrates the advantages of artificial raindrop algorithm (ARA), particle swarm optimization, and differential evolution, is proposed

The rest of the paper is organized as follows: Section 2 describes the problem and establishes a novel three-objective optimization model. To solve the established mathematical model with high performance, we give the overview of the artificial raindrop algorithm (ARA) and propose an improved artificial raindrop algorithm (IARA) in Section 3. Section 4 presents experimental results and analysis. Conclusions with a summary are drawn in Section 5.

2. Problem Formulation

2.1. Problem Description. Directed graph $G = (V, E)$ denotes a physical network topology. $V = \{v_i | i = 1, 2, \dots, N\}$ is the network nodes set, where N and v_i ($i = 1, 2, \dots, N$) are the numbers of nodes and the optical nodes, respectively. For the node v_i in physical network, there are $c(v_i)$ virtual machines (VMs) in it. $E = \{l_{ij} | i, j \in V\}$ represents optical fiber links set, and $|E|$ is the link number of a network. l_{ij} ($1 \leq i \neq j \leq N$) is the link between physical nodes v_i and v_j in the network topology. Let $F = \{f_u | u = 1, 2, \dots, |F|\}$ denote the set of available frequency slots in each link, and let $|F|$ be the number of frequency slots.

$VON = \{VON^1, VON^2, \dots, VON^M\}$ denotes the set of virtual optical networks (VONs) in network G , where M represents the number of VONs. $V^m = \{v_1^m, v_2^m, \dots, v_{N_m}^m\}$ denotes the set of virtual nodes (VNs) in VON^m , where N_m is the number of VN i in VON^m . In general, we have $N_m \leq N$. Ω_n^m denotes the candidate set v_n^m ($n = 1, 2, \dots, N_m$; $m = 1, 2, \dots, M$) can map to, and the nodes in Ω_n^m are all adjacent to each other. $R^m = \{r_1^m, r_2^m, \dots, r_{|R^m|}^m\}$ is the set of virtual connection requests (VCR) in VON^m . r_k^m ($k = 1, 2, \dots, |R^m|$; $m = 1, 2, \dots, M$) denotes the k^{th} VCR in VON^m . For r_k^m in VON^m , it can be described as $r_k^m = (s_k^m, d_k^m, T_k^m)$. Source node, destination node, and required capacity are s_k^m , d_k^m , and T_k^m , respectively.

For a specific virtual connection request $r_k^m = (s_k^m, d_k^m, T_k^m)$, if VN s_k^m and d_k^m are mapping to nodes $s_{k'}$ and $d_{k'}$ ($s_{k'}, d_{k'} \in V$), respectively, r_k^m would translate into a

physical connection request $r_{k'} = (s_{k'}, d_{k'}, T_{k'})$, where $T_{k'} = T_k^m$. When all the VNs were mapped to nodes, all the VONs are mapping to the network. That is to say, all the VCR are translated to the physical connection requests. $R' = \{r_1, r_2, \dots, r_{|R'|}\}$ denotes the physical connection requests set. Thus, $|R'| = \sum_{m=1}^M |R^m|$ denotes the number of VCRs.

2.2. Multiobjective Mathematical Modeling

2.2.1. Objective Functions

- (1) The first objective is minimizing the maximum index of frequency slots used. The maximum index of frequency slots used is calculated by

$$F_{\max} = \max_{l_{ij} \in E} \left\{ |F_{l_{ij}}| \right\}, \quad (1)$$

where $|F_{l_{ij}}|$ is the maximum index of frequency slots used on l_{ij} . Since $F_{\max} \leq |F|$, the maximum index of frequency slots used can be normalized as

$$f_1 = \frac{\max_{l_{ij} \in E} \left\{ |F_{l_{ij}}| \right\}}{|F|}. \quad (2)$$

Thus, we have $0 \leq f_1 \leq 1$, and the first objective function can be represented as

$$\min f_1 = \min \left\{ \frac{\max_{l_{ij} \in E} \left\{ |F_{l_{ij}}| \right\}}{|F|} \right\}. \quad (3)$$

- (2) The energy consumption is minimized in second objective. Energy consumption for all the connection requests can be calculated by

$$E_{\text{total}} = \sum_{k'=1}^{|R'|} (\lambda_{k'}^q g(Q_{k'}^q)), \quad (4)$$

where $g(Q_{k'}^q)$ denotes the energy consumption of $r_{k'}$ when it occupies the path $Q_{k'}^q$. $\lambda_{k'}^q$ is a Boolean variable; if $r_{k'}$ occupies the q^{th} path in $Q_{k'}$, $\lambda_{k'}^q = 1$; otherwise, $\lambda_{k'}^q = 0$.

Since $\sum_{k'=1}^{|R'|} (\lambda_{k'}^q g(Q_{k'}^q)) \leq \sum_{k'=1}^{|R'|} (g(Q_{k'}^q))$, the total energy consumption can be normalized as

$$f_2 = \frac{\sum_{k'=1}^{|R'|} (\lambda_{k'}^q g(Q_{k'}^q))}{\sum_{k'=1}^{|R'|} (g(Q_{k'}^q))}. \quad (5)$$

Similar to the first objective, we have $0 \leq f_2 \leq 1$. Thus, objective function can be expressed by

$$\min f_2 = \min \left\{ \frac{\sum_{k'=1}^{|R'|} (\lambda_{k'}^q g(Q_{k'}^q))}{\sum_{k'=1}^{|R'|} (g(Q_{k'}^q))} \right\}. \quad (6)$$

- (3) The third objective is maximizing the ratio of frequency slots utilization, and it is defined as

$$\text{RFSU} = \frac{\text{FS}_{\text{total}}}{\text{NL}_{\text{used}} \times |F|}, \quad (7)$$

where FS_{total} and NL_{used} are the total FSs used and number of links used, respectively. Since $\text{FS}_{\text{total}} \leq \text{NL}_{\text{used}} \times |F|$, $0 \leq \text{RFSU} \leq 1$. So, this objective can be expressed by

$$\max \text{RFSU} = \max \left\{ \frac{\text{FS}_{\text{total}}}{\text{NL}_{\text{used}} \times |F|} \right\}. \quad (8)$$

Since the first and second objectives are minimized, we can rewrite the third objective as

$$\min f_3 = 1 - \max \left\{ \frac{\text{FS}_{\text{total}}}{\text{NL}_{\text{used}} \times |F|} \right\}. \quad (9)$$

Obviously, $0 \leq f_3 \leq 1$.

The three objectives can be integrated into one to be minimized by sum weighted strategy; that is,

$$\min f = \min \{ \alpha_1 f_1 + \alpha_2 f_2 + \alpha_3 f_3 \}, \quad (10)$$

where α_1 , α_2 , and α_3 are three weights to adjust the importance of the three objectives, and we have $0 \leq \alpha_1, \alpha_2, \alpha_3 \leq 1$ and $\alpha_1 + \alpha_2 + \alpha_3 = 1$. Since $0 \leq f_1, f_2, f_3 \leq 1$, $0 \leq f \leq 1$. In addition, some constraint conditions should be satisfied. These constraint conditions are given in our previous paper [28]. To solve the multiobjective model, an efficient algorithm, which integrates the advantages of artificial raindrop algorithm (ARA), particle swarm optimization, and differential evolution, is proposed.

3. Overview of Artificial Raindrop Algorithm and Improved Artificial Raindrop Algorithm

3.1. Overview of Artificial Raindrop Algorithm. Artificial raindrop algorithm (ARA) is a kind of nonbiological heuristic algorithm based on population. The algorithm is inspired by the phenomenon of natural rainfall and transplants the effective information processing mechanism contained in the process of natural rainfall into the optimization algorithm design. According to the observation of the natural rainfall process, the whole optimization design cycle is divided into six stages: raindrop formation, raindrop descent, raindrop collision, raindrop flow, raindrop pool renewal, and water vapor renewal. During the optimization process, the location of water vapor or raindrops generated was evaluated using altitude, and the lower elevation positions were recorded in the raindrop pool.

Similar to the most metaheuristic algorithms, ARA searches the optimal solution with an initial population by randomly generating N_p vapors in a limited search space, and each vapor has a corresponding position defined as $v_i = (v_i^1, v_i^d, \dots, v_i^d, \dots, v_i^D)$ $i = 1, 2, \dots, N_p$, where N_p is the population size, D is the dimension of problem, and v_i^d is the position of the i -th vapor in the d -th dimension.

3.1.1. Raindrop Generation. Generally speaking, raindrops are produced by constantly absorbing surrounding water vapor. For simplicity, assume the position of raindrops water

vapor around the geometric center. Therefore, its location can be defined as $RP = (x^1, x^2, \dots, x^d, \dots, x^D)$, where $x^d = (1/N_p) \sum_{i=1}^{N_p} x_i^d$.

3.1.2. Raindrop Descent. When ignoring the impact of external factors, free-falling raindrops from the clouds reach the ground. This means that a component has changed the location of raindrops, and the raindrops will move to a new location representing new raindrops. For raindrops RP, x^{d_j} raindrops at d_j -position on the first dimension, wherein d_j ($j = 1, 2, 3, 4$) from $\{1, 2, \dots, D\}$ set arbitrarily selected. Thus, new raindrop (NRP = $(y^1, y^2, \dots, y^d, \dots, y^D)$), d -th dimension of y^d can be from x^{d_2}, x^{d_3} , and x^{d_4} linear combinations obtained, defined as follows:

$$y^d = \begin{cases} x^{d_2} + \gamma(x^{d_3} - x^{d_4}), & d = d_1, \\ x^d, & \text{otherwise,} \end{cases} \quad (11)$$

where γ is a random number in $(-1, 1)$ and $d = 1, 2, \dots, D$.

3.1.3. Raindrop Collision. When a new raindrop hits the ground, it will split into a large number of small raindrops. These small raindrops (SRP_i , ($i = 1, 2, \dots, N_s$)) fly in all directions. Accordingly, SRP_i can be defined as

$$SRP_i = NRP + \text{sign}(\alpha - 0.5) \cdot \lg(\beta) \cdot (NRP - v_i), \quad (12)$$

where k , which is randomly selected from the set $1, 2, \dots, N_p$, is an index. α and β are two random numbers and are distributed in the range $(0, 1)$ uniformly. $\text{sign}(\cdot)$ represents the sign function.

3.1.4. Raindrop Flowing. Under gravity, SRP_i ($i = 1, 2, \dots, N_p$) will flow to the low altitude and will most eventually stop at a lower altitude from a height position (i.e., a better solution). In the process of evolutionary algorithms, these better solutions can provide more information about the direction of promising progress. Therefore, the design comprising N_{RPO} raindrops pool (textbf RPO) to track these lower positions is found during the search, and textbf RPO update: (1) textbf RPO any feasible solution is to initialize the search space; (2) after each iteration, the optimal solution is added in the current population textbf RPO; and (3) if the size exceeds a threshold RPO value set in advance, in order to maintain the textbf RPO of size stability, reduce the amount of calculation, some solutions of \textbf{RPO} are deleted randomly

What is more, the flowing direction of raindrop $dSRP_i$ for SRP_i ($i = 1, 2, \dots, N_p$) can be constructed based on the linear combination of two vectors $dSRP1_i$ and $dSRP2_i$ as follows:

$$dSRP_i = \tau_1 \cdot \theta_i^1 \cdot dSRP1_i + \tau_2 \cdot \theta_i^2 \cdot dSRP2_i, \quad (13)$$

where τ_1 and τ_2 are two step parameters of SRP_i flowing, and θ_i^1 and θ_i^2 are generated randomly in the range $(0, 1)$. $dSRP1_i$ and $dSRP2_i$ are two vectors and they are defined as follows:

$$\begin{aligned} dSRP1_i &= \text{sign}(F(RPO_{k_1}) - F(SRP_i)) \cdot (RPO_{k_1} - SRP_i), \\ dSRP2_i &= \text{sign}(F(RPO_{k_2}) - F(SRP_i)) \cdot (RPO_{k_2} - SRP_i), \end{aligned} \quad (14)$$

where RPO_{k_1} and RPO_{k_2} ($1 \leq k_1 \neq k_2 \leq N_{rpo}$) are any two of candidate solutions in **RPO**. $F(\cdot)$ denotes the fitness function. Thus, the i -th new small raindrop ($NSRP_i$) can be defined as

$$NSRP_i = SRP_i + dSRP_i. \quad (15)$$

In general, it is necessary to introduce a parameter N_{MF} to control the maximum flow rate. Thus, these new small raindrops will stay in the locations with a lower elevation or evaporate after several flowing because of the parameter N_{MF} .

3.1.5. Vapor Updating. In order to converge ARA, in the water vapor update process, select a new ranking method using the small raindrop and a small steam of N_p as the next best solution vapor population.

3.2. Improved Artificial Raindrop Algorithm (IARA)

3.2.1. Encoding. Four steps are used to solve the problems of mapping VON: (1) physically mapping a virtual node to node, (2) connection request sorting, (3) routing, and (4) spectrum allocation. We randomly sort connection which does not require coding. Accordingly, it only needs to be coded in steps 1, 3, and 4. Therefore, using the virtual node mapping populations, populations and spectrum allocation routing population of these three individuals into the population of these three steps are necessary and reasonable. This paper presents the virtual node mapping and routing of coding schemes and population initialization program [28].

Each gene represents the starting frequency index for each connection request slot on the chromosome. Routing similar population of chromosomes, the chromosome length is carded quantity of connection requests. For example, $z = (z_{k'})_{1 \text{ multiplied } N_{R_i}}$ is a spectral distribution in the population of chromosomes. If $z_{k'} = u$, then u -th is allocated to the $(u + B_{k'} + GF - 1)$ -th frequency slot of the connection request $r_{k'}$. The population of spectrum allocation has been initialized in Algorithm 1.

3.2.2. Improved Raindrop Flowing. In the improved algorithm, flowing direction of raindrop $dSRP_i$ of SRP_i ($i = 1, 2, \dots, N_p$) can be constructed based on the linear combination of three vectors $dSRP1_i$, $dSRP2_i$, and $dSRP3_i$ as follows:

$$dSRP_i = \tau_1 \cdot \theta_i^1 \cdot dSRP1_i + \tau_2 \cdot \theta_i^2 \cdot dSRP2_i + \tau_3 \cdot \theta_i^3 \cdot dSRP3_i, \quad (16)$$

where τ_3 is a step parameter of SRP_i like τ_1 and τ_2 and θ_i^3 also is generated randomly in the range $(0, 1)$. $dSRP3_i = (dSRP3_i^1, dSRP3_i^2, \dots, dSRP3_i^d, \dots, dSRP3_i^D)$ is a vector and it is defined as follows:

```

Input:  $|Q_{k'}|$  for all physical connection requests  $R'$ ,
Population size  $\text{Pop}_{\text{Size}}$ 
Output: Spectrum assignment population RP
(1) for  $p = 1$  to  $\text{Pop}_{\text{Size}}$  do
(2)   for  $k' = 1$  to  $|R'|$  do
(3)     An integer  $u$  is generated randomly between 1
         and  $|F|$ ;
(4)      $\text{SP}(p, k') = u$ ;
(5)   end
(6) end

```

ALGORITHM 1: Spectrum assignment population initialization.

$$\begin{aligned} \text{dSRP}_i^d = & \frac{\text{SRP}_{i,\beta}^d + \text{SRP}_{i,\beta}^d + \text{SRP}_{i,\beta}^d}{3} \\ & + r_3 \cdot (\text{SRP}_{i,\text{best}}^d - \text{SRP}_i^d) + r_4 \cdot (\text{SRP}_j^d - \text{SRP}_i^d), \end{aligned} \quad (17)$$

where r_3, r_4 , and r_5 are three random vectors in $[0, 1]$ and $\text{SRP}_{i,\text{best}}^d$ denotes the best position of i -th raindrop in the past. $\text{SRP}_{i,\beta}^d$, $\text{SRP}_{i,\gamma}^d$, and $\text{SRP}_{i,\delta}^d$ are defined as

$$\begin{aligned} \text{SRP}_{i,\beta}^d &= \text{SRP}_\beta^d - a_1 \cdot |a_2 \cdot \text{SRP}_\beta^d - \text{SRP}_i^d|, \\ \text{SRP}_{i,\gamma}^d &= \text{SRP}_\gamma^d - a_1 \cdot |a_2 \cdot \text{SRP}_\gamma^d - \text{SRP}_i^d|, \\ \text{SRP}_{i,\delta}^d &= \text{SRP}_\delta^d - a_1 \cdot |a_2 \cdot \text{SRP}_\delta^d - \text{SRP}_i^d|, \end{aligned} \quad (18)$$

where a_1 and a_2 are two random numbers in the range $(0, 1)$; SRP_β , SRP_γ , and SRP_δ denote the optimal raindrop, sub-optimum raindrop, and third-optimum raindrop.

4. Experiments and Analysis

In order to prove the effectiveness and efficiency of the proposed algorithm, this section performs several experiments and results are given. In Section 4.1, the parameters used in the algorithm are given. The results are given in Section 4.2. Finally, Section 4.3 presents the analysis of experimental results.

4.1. Parameters Setting. In our simulation experiments, there are three network topologies. NSFNET topology includes 14 nodes and 21 links. CHNNET topology includes 15 nodes and 27 links. ARPANET topology includes 20 nodes and 32 links. Subcarrier modulation level uses 4 kinds: BPSK, QPSK, 8QAM, and 16QAM. Thus, for BPSK, QPSK, 8QAM, and 16QAM different modulation levels, ML 2, 3, and 4 may be selected. The transmission distance of modulation levels are 9600, 4800, 2400, and 1200 km [29]. We assume that each frequency slot is 2.5 GHz. Furthermore, the network topology has 5–10 VMs on each physical node. Each has 4 or 6 VON virtual nodes, a virtual connection request is present between a pair of virtual nodes, and the probability is 0.5. Each virtual node in VONs has between 2–4 candidate nodes in EONs.

4.2. Experimental Results. In order to verify the performance of the proposed algorithm, we compared the proposed algorithm IARA with the ARA proposed in the literature. In addition, we compared the IARA scheme with the DC & TP-EA scheme and considered the energy saving of DCs in node mapping and the energy saving of TPs in link mapping (proposed in [30]) to verify the performance of the IARA scheme. In addition, we also compared the proposed algorithm with the three best-performing algorithms for solving the VONs mapping problem. The first algorithm is expressed as CAN-A and is proposed in [31]. In order to make it more suitable for real networks, CAN-A considers four types of node and link constraints and constructs a subset of candidate substrate nodes and a subset of candidate substrate paths before embedding. LSCD algorithm is map the largest bandwidth requirement virtual links on the shortest distance physical links. The last comparison algorithm is GRC-SVNE proposed in the literature. In the node mapping phase, GRC-SVNE selects some nodes as candidate nodes according to the mapping capacity of all nodes. Then Dijkstra's algorithm is used for link mapping in the second stage.

In order to verify the performance of the algorithm, there are two different experiments to select scenes. In the first experiment scenario, each virtual optical network's virtual section was fixed to 5 points. There is a request to a virtual connection between each pair of virtual nodes, and the probability is 0.5. The number of virtual optical networks from 10 to 20 is selected. In Figures 1–4, the results are given objective function with three network VONs quantity change algorithms. When $\alpha_1 = 1, \alpha_2 = 0, \alpha_3 = 0$, the experimental results obtained by the algorithm are shown in Figure 1. $\alpha_1 = 0, \alpha_2 = 1, \alpha_3 = 0$. The results obtained by the algorithm are shown in Figure 2. Figure 3 shows $\alpha_1 = 0, \alpha_2 = 0, \alpha_3 = 1$. Figure 4 shows $\alpha_1 = 1/3, \alpha_2 = 1/3, \alpha_3 = 1/3$.

In a second experiment scenario, the number of fixed VONs $M = 30$. In each virtual optical network, the number of virtual nodes is from 3 to 7 (Figures 5–8). The results are given objective function with virtual three network nodes change algorithm. $\alpha_1 = 1, \alpha_2 = 0, \alpha_3 = 0$. The results obtained by the algorithm are shown in Figure 5. When $\alpha_1 = 0, \alpha_2 = 1, \alpha_3 = 0$, the experimental results obtained by the algorithm are shown in Figure 6. Figure 7 shows experimental results obtained by the algorithm when

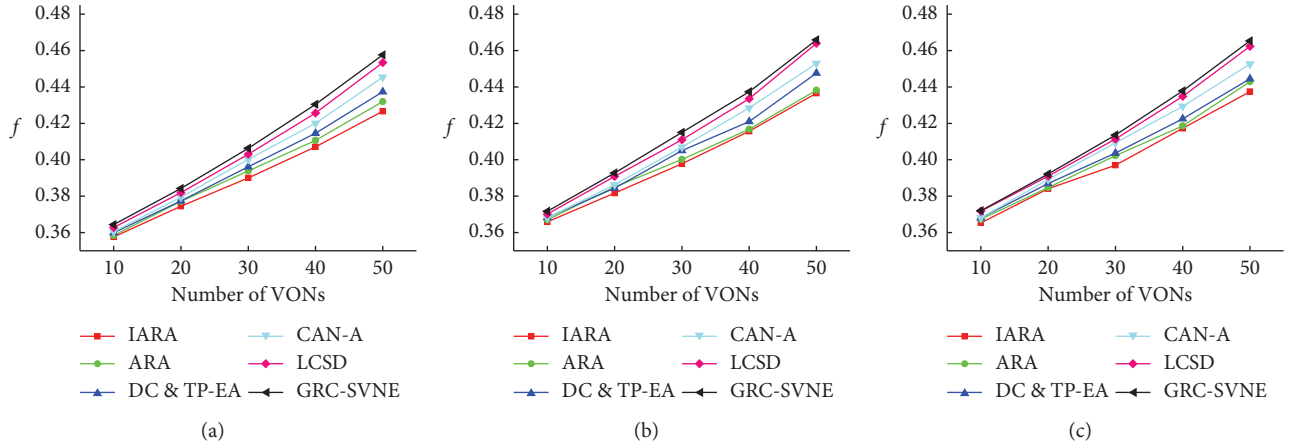


FIGURE 1: Experimental results in the first scene when $\alpha_1 = 1, \alpha_2 = 0, \alpha_3 = 0$. (a) Experimental results in NSFNET. (b) Experimental results in CHNNET. (c) Experimental results in ARPANET.

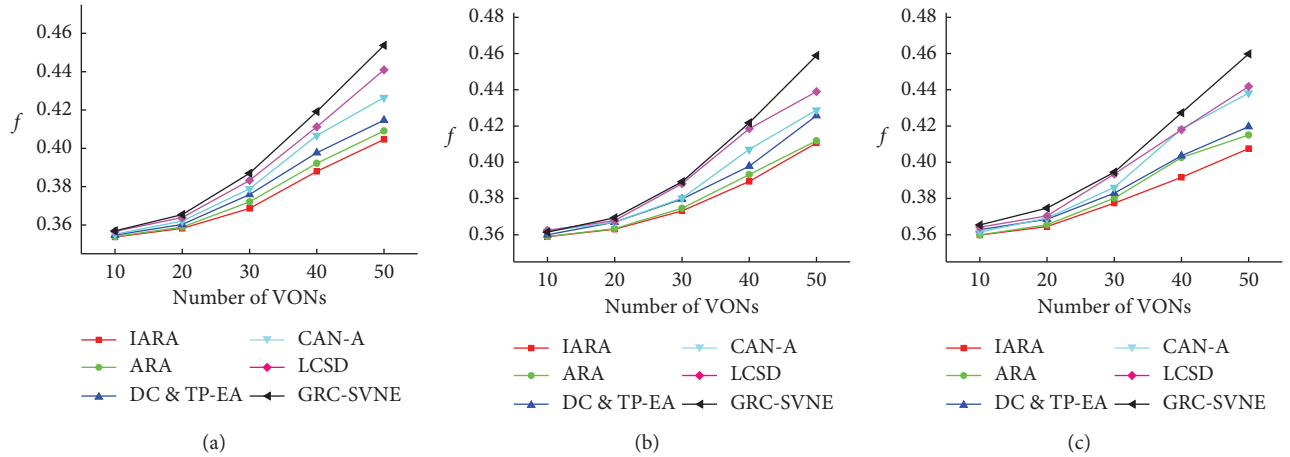


FIGURE 2: Experimental results in the first scene when $\alpha_1 = 0, \alpha_2 = 1, \alpha_3 = 1$. (a) Experimental results in NSFNET. (b) Experimental results in CHNNET. (c) Experimental results in ARPANET.

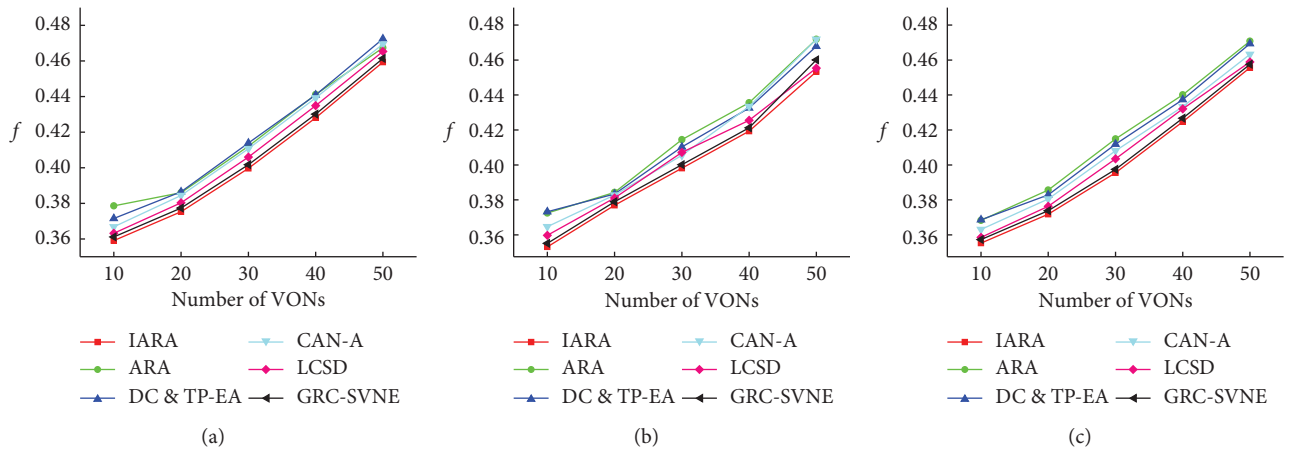


FIGURE 3: Experimental results in the first scene when $\alpha_1 = 0, \alpha_2 = 0, \alpha_3 = 1$. (a) Experimental results in NSFNET. (b) Experimental results in CHNNET. (c) Experimental results in ARPANET.

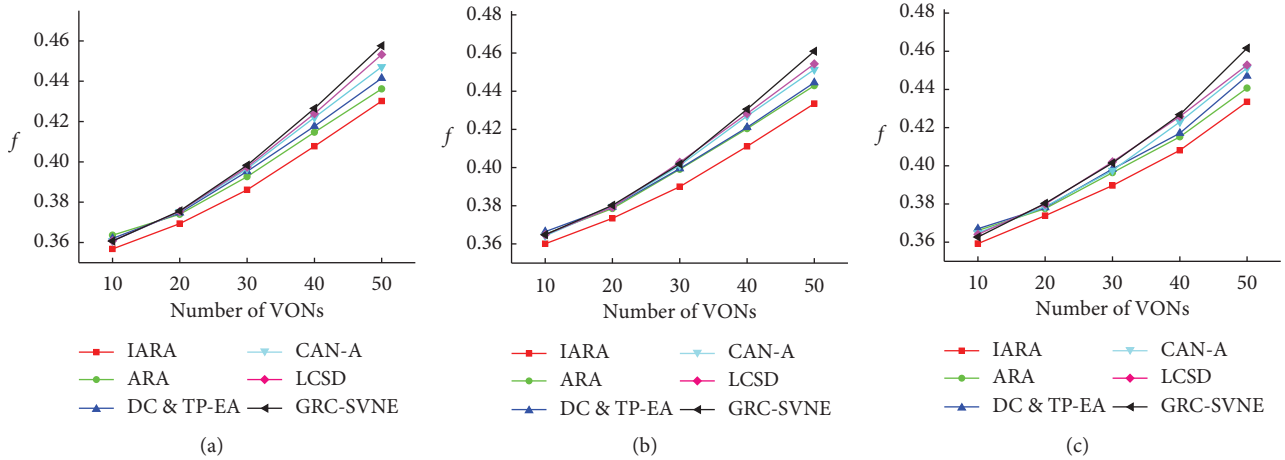


FIGURE 4: Experimental results in the first scene when $\alpha_1 = 1/3, \alpha_2 = 1/3, \alpha_3 = 1/3$. (a) Experimental results in NSFNET. (b) Experimental results in CHNNET. (c) Experimental results in ARPANET.

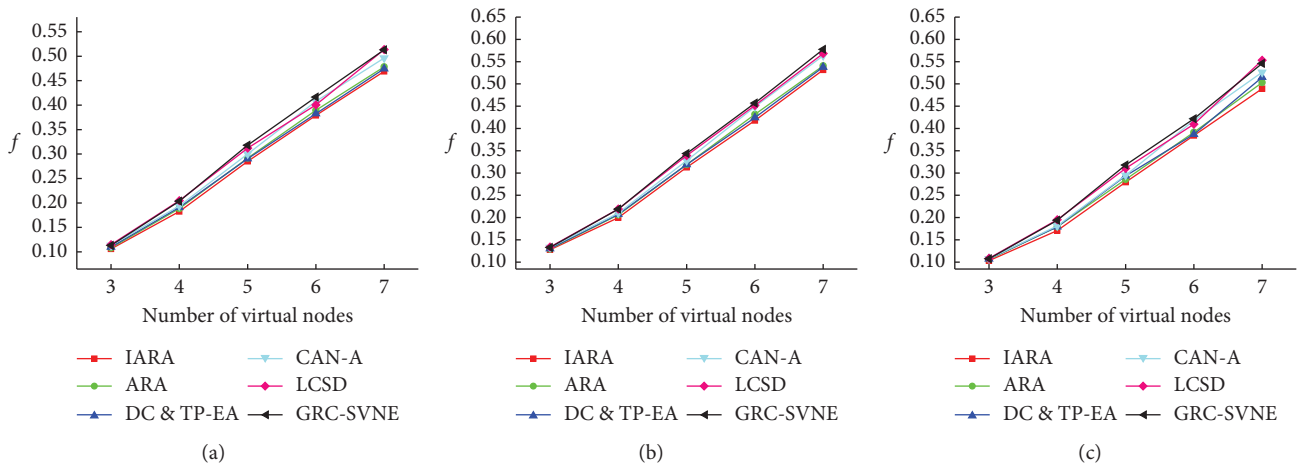


FIGURE 5: Experimental results in the second scene when $\alpha_1 = 1, \alpha_2 = 0, \alpha_3 = 0$. (a) Experimental results in NSFNET. (b) Experimental results in CHNNET. (c) Experimental results in ARPANET.

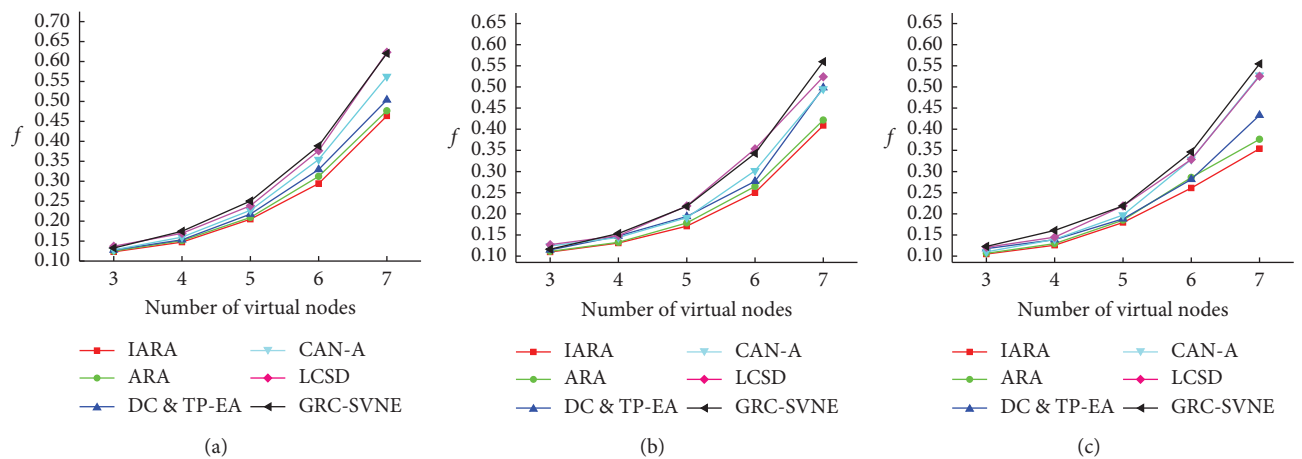


FIGURE 6: Experimental results in the second scene when $\alpha_1 = 0, \alpha_2 = 1, \alpha_3 = 1$. (a) Experimental results in NSFNET. (b) Experimental results in CHNNET. (c) Experimental results in ARPANET.

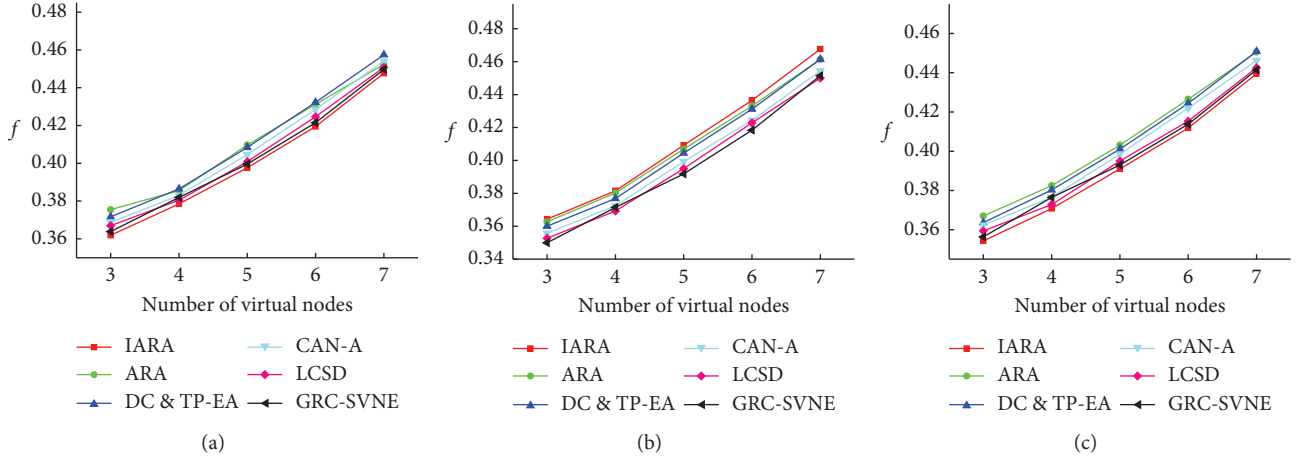


FIGURE 7: Experimental results in the second scene when $\alpha_1 = 0, \alpha_2 = 0, \alpha_3 = 1$. (a) Experimental results in NSFNET. (b) Experimental results in CHNNET. (c) Experimental results in ARPANET.

$\alpha_1 = 0, \alpha_2 = 0, \alpha_3 = 1$. Figure 8 shows the experimental results obtained when $\alpha_1 = 1/3, \alpha_2 = 1/3, \alpha_3 = 1/3$.

4.3. Experimental Analysis. When $\alpha_1 = 1, \alpha_2 = 0, \alpha_3 = 0$, the six kinds of objective function value obtained by the algorithm are shown in Figures 1 and 5 in both different scenarios. From Figure 1, we can see that the value of objective function obtained by proposed algorithm is smaller than those obtained by the compared algorithms with the number of VONs varying from 10 to 50. Similarly, it can be seen from the figure that when the number of VONs is from 3 to 7, the algorithm obtains an objective function value that is less than the objective function value obtained by the comparison algorithm. CAN-A considered four types of constraint nodes and links, wherein the substrate is configured subset of candidate paths and a subset of the candidate nodes in the substrate prior to embedding. GRC-SVNE maps selecting section capacity for all nodes as candidate nodes according to a node. The second stage uses the Dijkstra algorithm downlink map. This can lead to connection requests on a different link imbalance. The algorithm will get a maximum index with greater use of frequency bins. LCS D maximum link bandwidth requirements are mapped to link the shortest distance to reduce network costs, so that the connection request imbalances different links. IARA can search the optimal virtual nodes mapping scheme for all the virtual nodes and optimal routing scheme for all the connection requests using a search operators. In the first experiment scenario, when the number of virtual optical networks is 10, the ratio of the algorithm and the comparison algorithm to obtain the objective function value is 3.9%–7.4%. When the number of VONs is 50, ratio of the algorithm and the comparison algorithm to obtain the objective function value is 5.8%–13.1%. In addition, we can see that, with the increase in the number of VONs, the proposed algorithm can save more frequency slots. In a second experiment scenario, as shown in Figure 5, when the number of virtual nodes is 3, ratio of the algorithm and the comparison algorithm to obtain the objective function value is

4.5%–8.1%. When the number of virtual nodes is 7, ratio of the algorithm and five kinds of the comparison algorithm to obtain the objective function value is 5.2%–10.5%. When $\alpha_1 = 1, \alpha_2 = 0, \alpha_3 = 0$, the goal is to minimize the use of the maximum frequency bin index. Thus, the algorithm in two different experimental scenarios can save more frequency bins.

As can be seen from Figures 2 and 6, the objective function value obtained by the algorithm is less than the objective function value obtained by the comparison algorithm. The algorithm can determine the optimal objective function value with the smallest virtual node mapping and routing scheme. Further, the modulation level may be selected to minimize the objective function value. Thus, the algorithm's objective function value is minimal compared to those of the five kinds of the comparison algorithm. When the number of VONs is 10, the value of objective function by the proposed algorithm is 3.2%–9.8% less than that by the compared algorithms as shown in Figure 2. When the number of the virtual optical networks is 50, the value of the objective function of the algorithm, 5.8%, is smaller than the objective function value of the comparison algorithm, 12.5%. In Figure 6, when the number of nodes in each VON is 3, the value of objective function by the proposed algorithm is 5.1%–11.2%. When the number of nodes in each VON is 7, the value of the objective function of the algorithm is 6.8%–14.3% less than the objective function value of the comparison algorithm. When $\alpha_1 = 0, \alpha_2 = 1, \alpha_3 = 0$, the goal is to minimize the energy consumption (EC). Therefore, the algorithm can save more energy at two different experimental scenarios.

Similarly, when $\alpha_1 = 0, \alpha_2 = 0, \alpha_3 = 1$, the target is $1 - f_3$. That is, the smaller the value of f is, the higher RFSU (frequency slots utilization) is. In Figures 3 and 7, the comparison frequency channel utilization algorithm obtained six kinds of three networks. The proposed algorithm evolution strategy, more balanced in the connection request K candidate path. Therefore, the algorithm can get a higher frequency than the other five algorithms in slot utilization.

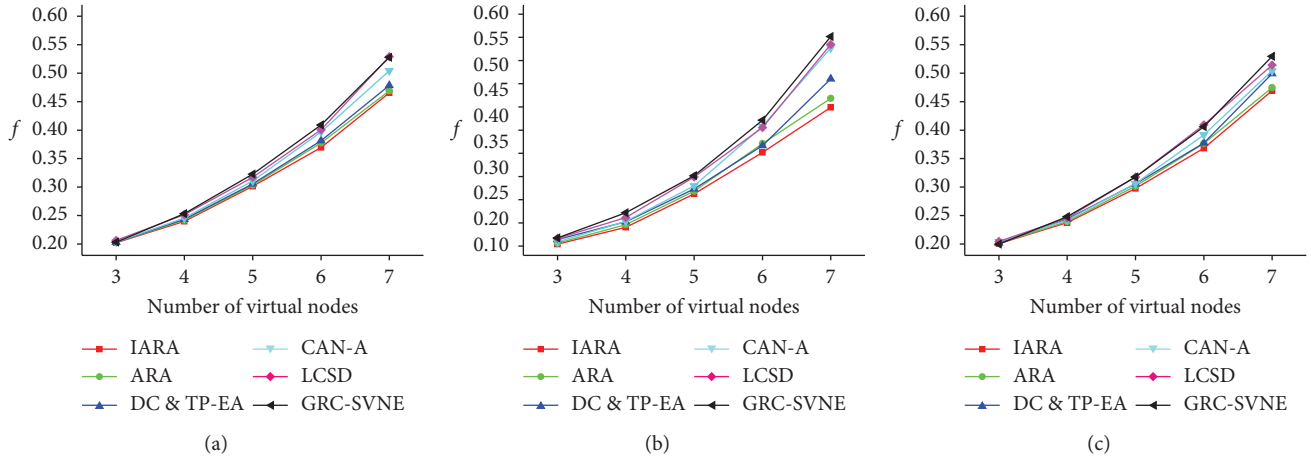


FIGURE 8: Experimental results in the second scene when $\alpha_1 = 1/3, \alpha_2 = 1/3, \alpha_3 = 1/3$. (a) Experimental results in NSFNET. (b) Experimental results in CHNNET. (c) Experimental results in ARPANET.

In Figure 3, in the three networks, when the number of VONs is from 10 to 50, the utilization of the algorithm frequency bins obtained is 42.1 to 49.5%. 35.8% to 48.1%, and 42.6% to 52.4%. In Figure 7, in the three networks, when the number of virtual optical network nodes is from 3 to 7, the utilization of the algorithm frequency bins obtained was 41.8% to 48.2%, 38.7% to 50.4%, and 44.1% to 56.3%. The results showed that, compared with other algorithms, it can improve the utilization rate of frequency bins.

Figures 4 and 8 give the three types in $\alpha_1 = 1/3, \alpha_2 = 1/3, \alpha_3 = 1/3$ comparison of the results of six kinds of experimental algorithm on the network. As can be seen, the objective function value obtained by the algorithm is less than the objective function value obtained by the comparison algorithm. The algorithm can determine the minimum objective function optimal virtual node mapping and routing scheme. As shown in Figure 4, when the number of virtual optical networks is 10, the objective function value obtained by the algorithm in this paper is 4.8%–10.2% smaller than the objective function value obtained by the comparison algorithm. When the number of the virtual optical networks is 50, the objective function value obtained by the algorithm in this paper is 6.7%–14.3% smaller than the objective function value obtained by the comparison algorithm. As shown in Figure 8, when the number of nodes in each virtual optical network is 3, the objective function value obtained by the algorithm in this paper is 5.2%–13.7% less than the objective function value obtained by the comparison algorithm. When the number of nodes in each virtual optical network is 7, the objective function value obtained by the algorithm in this paper is 7.1%–15.9% smaller than the objective function value obtained by the comparison algorithm.

5. Conclusion

We studied VONs mapping problems since generations. We established a maximum frequency bin index and studied the energy consumption of three-minimal-objective model accounting for frequency bin and determined optimum

solution for all connection requests virtual node mapping, routing, and spectrum allocation. In order to effectively solve three-objective optimization model, the weighted sum of the three strategies integrated into a target goal was minimized. Based on the idea of particle swarm optimization and differential evolution, an improved artificial raindrop algorithm (IARA) to effectively solve the biggest model was proposed. In comparison to other algorithms, for the simulation experiments under different test scenarios, test results show the effectiveness of the model and the algorithm proposed. However, the algorithm’s complexity is high, only for static (offline) VONs problem.

Data Availability

All the data are included within the article.

Conflicts of Interest

The authors declare that they have no conflicts of interest.

Acknowledgments

This work was supported by the National Natural Science Foundation of China (nos. 31872704, 62006205, and 62002307), Innovation Team Support Plan of Henan University of Science and Technology (no. 19IRTSTHN014), Foundation of Henan Educational Committee (Contract no. 21A520039), and Nanhu Scholars Program for Young Scholars of XYNU, Youth Sustentation Fund of Xinyang Normal University (no. 2019-QN-040).

References

- [1] X. Xue and J. Chen, “Using compact evolutionary tabu search algorithm for matching sensor ontologies,” *Swarm and Evolutionary Computation*, vol. 48, pp. 25–30, 2019.
- [2] X. Li, T. Gao, L. Zhang, Y. Tang, Y. Zhang, and S. Huang, “Survivable k-node (edge) content connected virtual optical network (kc-von) embedding over elastic optical data center networks,” *IEEE Access*, vol. 6, pp. 38780–38793, 2018.

- [3] H. Cui, S. Tang, F. Sun, Y. Xu, and X. Yang, "Topological embedding feature based resource allocation in network virtualization," *Mathematical Problems in Engineering*, vol. 2014, Article ID 271493, 10 pages, 2014.
- [4] J. Zhao, S. Subramaniam, and M. Brandt-Pearce, "Virtual topology mapping in elastic optical networks," in *Proceedings of the 2013 IEEE International Conference on Communications (ICC)*, pp. 3904–3908, IEEE, Budapest, Hungary, June 2013.
- [5] H. Li, L. Wang, X. Wen, Z. Lu, and J. Li, "MSV: an algorithm for coordinated resource allocation in network function virtualization," *IEEE Access*, vol. 6, pp. 76876–76888, 2018.
- [6] Z. Ding, Z. Xu, X. Zeng, T. Ma, and F. Yang, "Hybrid routing and spectrum assignment algorithms based on distance-adaptation combined coevolution and heuristics in elastic optical networks," *Optical Engineering*, vol. 53, no. 4, Article ID 046105, 2014.
- [7] M. Kalil, M. Youssef, A. Shami, A. Al-Dweik, and S. Ali, "Wireless resource virtualization: opportunities, challenges, and solutions," *Wireless Communications and Mobile Computing*, vol. 16, no. 16, pp. 2690–2699, 2016.
- [8] Z. Li, W. Fei, and Z. Hongli, "QOS-aware resource allocation for network virtualization in an integrated train ground communication system," *Wireless Communications & Mobile Computing*, vol. 2018, Article ID 2653405, 12 pages, 2018.
- [9] B. Chen, J. Zhang, W. Xie, J. P. Jue, Y. Zhao, and G. Shen, "Cost-effective survivable virtual optical network mapping in flexible bandwidth optical networks," *Journal of Lightwave Technology*, vol. 34, no. 10, pp. 2398–2412, 2016.
- [10] J. F. Botero and X. Hesselbach, "Greener networking in a network virtualization environment," *Computer Networks*, vol. 57, no. 9, pp. 2021–2039, 2013.
- [11] A. Khan, A. Zugenmaier, D. Jurca, and W. Kellerer, "Network virtualization: a hypervisor for the internet?" *IEEE Communications Magazine*, vol. 50, no. 1, pp. 136–143, 2012.
- [12] A. Berl, N. Race, J. Ishmael, and H. De Meer, "Network virtualization in energy-efficient office environments," *Computer Networks*, vol. 54, no. 16, pp. 2856–2868, 2010.
- [13] R. Lu and X. Nan, "Survivable multipath routing and spectrum allocation in OFDM-based flexible optical networks," *Journal of Optical Communication and Network*, vol. 5, no. 3, pp. 172–182, 2013.
- [14] P. Zhang, H. Li, Y. Ni, F. Gong, M. Li, and F. Wang, "Security aware virtual network embedding algorithm using information entropy topsis," *Journal of Network and Systems Management*, vol. 28, no. 1, pp. 35–57, 2020.
- [15] B. Farkiani, B. Bakhshi, and S. A. MirHassani, "Stochastic virtual network embedding via accelerated benders decomposition," *Future Generation Computer Systems*, vol. 94, pp. 199–213, 2019.
- [16] P. Zhang, H. Yao, M. Li, and Y. Liu, "Virtual network embedding based on modified genetic algorithm," *Peer-to-Peer Networking and Applications*, vol. 12, no. 2, pp. 1–12, 2017.
- [17] M. Yu, Y. Yi, J. Rexford, and M. Chiang, "Rethinking virtual network embedding," *ACM Sigcomm Computer Communication Review*, vol. 38, no. 2, pp. 17–29, 2008.
- [18] A. Fischer, J. F. Botero, M. T. Beck, H. De Meer, and X. Hesselbach, "Virtual network embedding: a survey," *IEEE Communications Surveys & Tutorials*, vol. 15, no. 4, pp. 1888–1906, 2013.
- [19] E. Amaldi, S. Coniglio, A. M. C. A. Koster, and M. Tieves, "On the computational complexity of the virtual network embedding problem," *Electronic Notes in Discrete Mathematics*, vol. 52, pp. 213–220, 2016.
- [20] L. Gong, H. Jiang, Y. Wang, and Z. Zhu, "Novel location-constrained virtual network embedding LC-VNE algorithms towards integrated node and link mapping," *IEEE/ACM Transactions on Networking*, vol. 24, no. 6, pp. 3648–3661, 2016.
- [21] J. Liao, M. Feng, S. Qing, T. Li, and J. Wang, "Live: learning and inference for virtual network embedding," *Journal of Network and Systems Management*, vol. 24, no. 2, pp. 227–256, 2016.
- [22] Z.-P. Cai, Q. Liu, P. Lü, and Z.-Y. Wang, "Virtual network mapping model and optimization algorithms," *Journal of Software*, vol. 23, no. 4, pp. 864–877, 2012.
- [23] M. He, L. Zhuang, S. Tian, G. Wang, and K. Zhang, "DROI: energy-efficient virtual network embedding algorithm based on dynamic regions of interest," *Computer Networks*, vol. 166, p. 106952, 2020.
- [24] T. Huang, Y. Gu, J. Liu, and Y. Liu, "Time efficient virtual network embedding algorithm," *Intelligent Automation & Soft Computing*, vol. 22, no. 2, pp. 273–280, 2016.
- [25] H. Liu, J. Du, Y. Chen, M. Xiang, and Y. Ma, "A coordinated virtual optical network embedding algorithm based on resources availability-aware over elastic optical networks," *Optical Fiber Technology*, vol. 45, pp. 391–398, 2018.
- [26] M. Pourvali, H. Bai, J. Crichigno, and N. Ghani, "Multicast virtual network services embedding for improved disaster recovery support," *IEEE Communications Letters*, vol. 22, no. 7, pp. 1362–1365, 2018.
- [27] X. Liu, Z. Zhang, J. Li, and S. Su, "Clustering-based energy-aware virtual network embedding," *International Journal of Distributed Sensor Networks*, vol. 13, no. 8, Article ID 15501477, 2017.
- [28] H. Xuan, S. Wei, Y. Feng, H. Guo, and Y. Li, "A new bi-level mathematical model and algorithm for VONs mapping problem," *IEEE Access*, vol. 8, pp. 101797–101811, 2020.
- [29] A. Bocoi, S. Matthias, R. Franz, K. Moritz, B. Christian-Alexander, and S. Bernhard, "Reach-dependent capacity in optical networks enabled by OFDM," in *Proceedings of the OFC (OMQ4)*, pp. 1–3, San Diego, CA, USA, March 2009.
- [30] M. Zhu, Q. Sun, S. Zhang, P. Gao, B. Chen, and J. Gu, "Energy-aware virtual optical network embedding in sliceable-transponder-enabled elastic optical networks," *IEEE Access*, vol. 7, pp. 41897–41912, 2019.
- [31] H. Cao, Y. Zhu, G. Zheng, and L. Yang, "A novel optimal mapping algorithm with less computational complexity for virtual network embedding," *IEEE Transactions on Network and Service Management*, vol. 15, no. 1, pp. 356–371, 2018.

Research Article

Research on the Balanced Relationship between Online Consumer Behavior and E-Commerce Service Quality Based on 5G Network

Yuna Si 

Xijing University, Xi'an 710123, China

Correspondence should be addressed to Yuna Si; siyuna0904@mail.bnu.edu.cn

Received 14 January 2021; Revised 27 January 2021; Accepted 20 February 2021; Published 9 March 2021

Academic Editor: Hsu-Yang Kung

Copyright © 2021 Yuna Si. This is an open access article distributed under the Creative Commons Attribution License, which permits unrestricted use, distribution, and reproduction in any medium, provided the original work is properly cited.

In order to better explore the consumer psychology activities of consumers and reduce the cost control risks of enterprises, this article aims to explore the relationship between online consumer behavior and e-commerce service quality and hopes to study e-commerce by dividing online consumer groups. This article uses 5G technology to track consumer consumption habits and consumption costs. First, according to the existing literature and qualitative interviews with online consumers, it is determined that the e-commerce service quality evaluation factors are the core service quality-related system reliability, efficiency, guarantee and completion, and the quality of after-sales service. Then, based on the data obtained from the questionnaire, SPSS statistical analysis software was used to analyze the reliability of the sample variables, thereby improving the quality of the sample data. We perform descriptive statistical analysis on these measurement items. Each attribute calculates the importance of each dimension. Through the analysis of experimental cases, it can be seen that the use of 5G technology can well match consumers' consumption habits and message needs and can evaluate the quality of e-commerce services more accurately and scientifically.

1. Introduction

The concept of transaction cost was derived from the 1937 paper "The Nature of Business" by Nobel Prize-winning economist Professor Ronald Coase. Coase used this concept to explain the emergence of the company. He pointed out that the market transaction process is costly, and the company appears because its transaction cost is relatively small compared to the market transaction cost. It should be pointed out that before Coase proposed the concept of transaction cost, the study of neoclassical economics was based on the assumption that the transaction cost was zero and thus to some extent lacked persuasiveness to the real world. The presentation of the transaction cost theory specifies constraints on property rights and transaction costs that have a decisive influence on behavior [1]. In the 5G era, there will be no pure e-commerce platform. In other words, any platform related to the cloud will have the attributes of e-commerce. This has already begun to take shape in the latter part of the 4G era, and a final blow to the 5G is still needed to completely disrupt the future. 5G networks can

more quickly explore business opportunities in the e-commerce market, increase the scope and depth of e-commerce services, and capture the market horizontally and vertically.

After Coase, some researchers have differently defined the concept of transaction costs from different research perspectives. For example, Arrow used the "transaction cost" to describe the "cost of economic system operation." It can be seen as a series of institutional costs, including information costs, negotiation costs, the cost of developing and implementing a contract, defining and controlling the cost of property rights, the cost of supervision and management, and the cost of institutional changes, in short, including everything that does not happen directly in the production process [2]. As a master of transaction cost theory, Williamson extends transaction costs to all economic institutional environments. He believes that transaction costs include ex ante transaction costs and ex post transaction costs. Ex ante transaction costs include drafting, negotiating, and maintaining the cost of executing an agreement. The posttransaction costs include unsuitable costs incurred when

the transaction deviates from the required criteria; the cost of controversy; the cost associated with the establishment and operation of the management organization; and the cost of mortgages for which the security guarantee is effective. Although the above scholars have different definitions of transaction costs, they have clearly outlined the basic composition of transaction costs. Obviously, the transaction cost is the sum of the various costs of money, knowledge, time, physical strength, etc. that people pay to complete the transaction. It tells us that both parties to the transaction have a hidden rule, that is, the completion of the transaction depends on whether the revenue is greater than the payment transaction cost. The paper's design method is shown in Figure 1.

The research contributions of this article include the following:

- (1) This article uses 5G technology to track consumer consumption habits and consumption costs.
- (2) We use SPSS statistical analysis software to analyze the reliability of sample variables, thereby improving the quality of sample data.
- (3) We perform descriptive statistical analysis on the measurement items, so that each attribute is well calculated.

The rest of this paper is organized as follows. Section 2 discusses research on the theory of network consumer behavior from the perspective of transaction cost, followed by the research on measurement factors of e-commerce service quality designed in Section 3. Relationship model and empirical research on network consumer behavior and e-commerce service quality are discussed in Section 4. Section 5 concludes the paper with summary and future research directions.

2. Research on the Theory of Network Consumer Behavior from the Perspective of Transaction Cost

2.1. The Application of Transaction Cost Theory in the Interpretation of Online Consumer Behavior. Williams has studied his transaction cost theory in three mutually influential dimensions (i.e., trading uncertainty, asset specificity, and trading frequency) and two main assumptions of human behavior (limited rationality and opportunism). The uncertainty of the transaction mainly refers to the uncertainty that the future situation may not be accurately predicted due to factors such as bounded rationality and information asymmetry, which leads to the uncertainty of the occurrence of incidents; asset specificity refers to the persistence used to support special transactions. In persistent investment, assets are often difficult to use for other purposes; the frequency of transactions refers to the frequency of transactions [3]. Among the human behavior factors, bounded rationality refers to the limited nature of the transaction subject to its own cognitive ability and rationality; opportunism refers to the deceptive strategic behavior adopted by the transaction subject based on the

pursuit of maximization of its own interests. Based on these factors, the transaction cost theory explains why the transaction subject chooses a transaction form. Due to the impact of transaction cost factors on consumer behavior, some scholars have tried to use the transaction cost theory to explain the behavior of consumers engaged in online transactions [4].

2.2. Composition of Network Transaction Costs. The above scholars started with Williams' transaction cost research and proposed the transaction cost factors that may arise in the online transaction process, but they put the research perspective more in the transaction process. We believe that from the perspective of consumers, the cost factors in online transactions can be summarized into the following categories [5].

2.2.1. Asset-Specific Cost. It is the investment of special equipment invested by consumers in order to achieve network transactions, such as computer equipment, network access equipment, and expenses.

2.2.2. Learning Cost. It is the cost that consumers pay for the smooth progress of online transactions and the decision to maximize the effectiveness of the transaction negotiation, such as network knowledge learning, online transaction negotiation skills learning, and lack of knowledge of online transactions in the initial stage of the transaction.

2.2.3. Search Cost. It is the cost of product quality and after-sales service that consumers must provide in order to find suitable products and trading partners.

2.2.4. Time Cost. It is the time cost that consumers pay to make a deal.

2.2.5. Monetary Cost. It is the monetary expenditure of the order, commodity price, distribution, maintenance, etc. paid by the consumer for the purchase of the product.

2.2.6. Risk Cost. It is the risk that consumers bear because of the uncertainty of online transactions.

3. Research on Measurement Factors of E-Commerce Service Quality

3.1. Definition of E-Commerce Service Quality. Broadly speaking, electronic services are based on the exchange of information to provide customers with a better experience. In a narrow sense, electronic services are services based on network delivery. Fan Wang and others proposed five components of electronic services, sorted by importance as follows: core services, convenience services, support services, complementary services, and user interfaces. Compared with the traditional business environment, electronic services are in the special environment of the Internet.

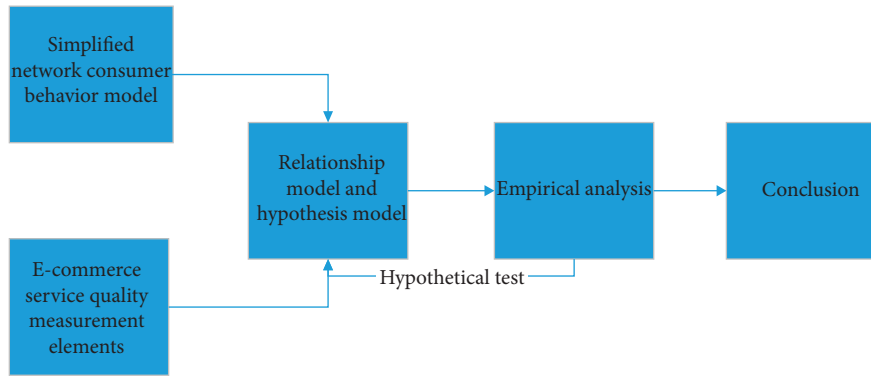


FIGURE 1: The paper design method process.

Electronic service providers deliver services to consumers “online.” It is also composed of a series of activities and is holistic [6].

Generally speaking, the e-service quality in the e-commerce environment is the e-commerce service quality, which refers to the overall evaluation and judgment of the superiority of the service provided by the service provider in the online market. This paper defines the quality of e-commerce service as follows: the sum of the characteristics and characteristics of e-commerce services that can meet the requirements and potential needs, the degree to which e-commerce service can meet the needs of the serviced, and the minimum that the enterprise provides to satisfy the target customers. The service level is also the company that maintains this service level. The theoretical model of the six-dimensional e-commerce service quality of this study is shown in Figure 2.

Compared with the evaluation of traditional service providers, when customers accept e-commerce services, they are more likely to evaluate prepurchase services, purchase services, and postpurchase services throughout the process and results. For online consumers, the primary condition for securing their potential benefits is to develop high-quality e-commerce service quality standards. The openness and sharing characteristics of the network enable network consumers to more easily use the network tools to compare the technical characteristics, product prices, and service quality of e-commerce service providers [7], for example, comparison network [8]. Online reviews and online word of mouth have a major impact on online consumers’ buying decisions. Therefore, e-commerce services play an important role in online consumers. Internet consumers want to demand no lower than the quality of offline services and even higher requirements.

In e-commerce activities, the face-to-face interaction between service personnel and customers has been replaced by website interface, website instant messaging tools, etc., but the quality of service can still be divided into technical quality and functional quality [9]. However, the technical quality and functional quality here no longer refer to the quality of the process and the quality of the results but are given new meaning. Functional quality focuses primarily on the quality of the website itself, while technical quality focuses on the quality of the network service. Functional

quality plays a key role. To improve the technical quality, the actual service provided by the website should be consistent with the promised service, respond to the customer’s needs in a timely manner, and give the correct solution to meet or exceed the customer’s needs or expectations. If the customer is dissatisfied with the technical quality, the customer is likely to be lost and may no longer visit the company website or may not shop from the website. In a networked environment, the cost of replacing an e-commerce service provider is very low, and it is very easy to transfer to a competitor’s website. Therefore, the above situation is very likely.

3.2. Quality of Service Measurement Model. In the traditional environment, the most commonly used quality of service measurement model SERVQUAL model is described below.

American marketing scientist Parasuraman (1985) and others pointed out that perceived service quality is “a comprehensive judgment or opinion made by the customer subjective and related to the quality of the service.” They put forward the “gap theory” on the customer’s measurement of service quality. They believe that the customer’s perceived service quality depends on the degree of difference between the customer’s perception and the customer’s expectations in the service process. When the customer’s actual perceived service quality meets or exceeds their expected service quality, their perceived service quality is good. When they actually felt that the quality of service was not as good as the expected quality of service, their perceived service quality was poor [10]. They conducted an experimental study in 1985 and found ten measurement elements of perceived service quality: perceptibility, reliability, responsiveness, communication, trust, security, competence, sincerity, understanding of customers, and acceptability [11]. These ten factors are further streamlined to five: perceptibility, reliability, responsiveness, assurance, and affection. Perceptibility refers to the “tangible part” of a service product; reliability means that the enterprise can perform reliably and accurately. Responsiveness means that the company is willing to help customers and provide fast service; guaranty refers to the friendly attitude of the service personnel and the ability to do the job; emotionality means that the company should sincerely care about the customers and understand

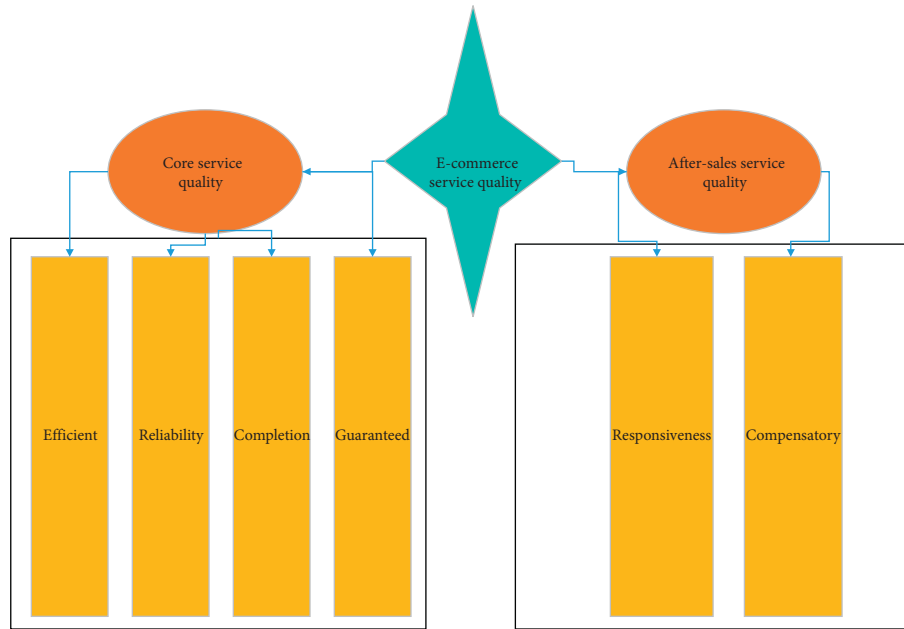


FIGURE 2: The theoretical model of service quality of e-commerce.

their actual needs. On this basis, Parasuraman, Zeithaml and Berry have established a service quality model, SERVQUAL (short for service quality) to measure the quality of service of the enterprise. It uses the difference function to measure the quality of service, i.e., $SERVQUAL = f(\text{perceive an expectation})$. The SERVQUAL model includes a total of 22 measurement indicators (see Table 1).

In general, the quality of electronic service is that the electronic service provider delivers the service to the customer through the special environment of “online,” which includes the overall process, such as the process of browsing the website, the process of goods delivery, and the customer’s overall service. The degree of evaluation and so on are all part of the quality of electronic services [12].

The service quality of e-commerce companies can be divided into two parts: technical quality and functional quality [13]. Moreover, functional quality still plays a key role. For example, enabling customers to quickly find the company’s website is a prerequisite for starting a transaction. Improving technical quality means that the actual service is consistent with the promised service and can meet or exceed customer needs or expectations. Because it is easy for customers to transfer to competitor’s website in the network environment, the above situation is very likely to happen [14].

3.3. Measurement Elements of E-Commerce Service Quality. Based on the SERVQUAL model and reading a large number of documents, combined with the comments of Chinese customers on online shopping, this paper proposes that the measurement elements of e-commerce service quality are mainly efficient, reliable, complete, private, responsive, and compensated. Table 2 shows a description of the significance of PZM to the dimensions in the model [15].

After many studies, this study believes that since responsiveness and contact cover the attitude and efficiency of after-sales service quality, the effects of the two influence each other, so they can be combined into the responsiveness of after-sales service as a whole. Therefore, this study uses two major service areas and six dimensions of the system to study the quality of e-commerce services [16].

3.3.1. Ease of Use. Ease of use includes two main aspects: on the one hand, sufficient functionality, and on the other hand, friendly interface design. Some very useful features, such as search and download capabilities, are necessary for customers to continue to access smoothly. One of the main reasons why customers use the Internet as a purchasing channel is its convenience [17]. In other words, they want to be able to easily complete the transaction on the website [18]. For example, online banking customers want to be able to autopay electronically, view banking conditions for a month, buy stocks and insurance, and avail other financial services. In this sense, having a full range of product lines and service lines can attract a large number of customers to visit their websites. Many customers want to find and discover products and services that are not easily found or not available in traditional local stores [19]. Similarly, customers can view their own transactions at any time and attract customers who are not satisfied with the current service. Therefore, having enough features is one of the keys to a website’s ability to gain customer loyalty [20].

3.3.2. Reliability. Reliability refers to the ability of an enterprise to accurately complete a promised service. This attribute means that the company must deliver the service accurately as promised. Reliability service actually requires the company to avoid mistakes because service errors will

TABLE 1: SERVQUAL measurement scale.

Latitude	Measurement project
<i>Reliability</i>	When a company promises to do something in a certain time, it will keep its promise
	The company tries its best to help customers solve problems when customers encounter problems
	A company provides good service from beginning to end
	A company provides services when it is promised
<i>Responsive</i>	A company informs customers when they start to provide services
	Employees provide prompt and timely service
	A company's employees are always happy to help customers
<i>Guarantee</i>	Employees respond to customer requests in a timely manner no matter how busy
	The behavior of a company's employees is trustworthy
	A company employee should be trustworthy
	A company employee should always treat customers with enthusiasm
<i>Empathy</i>	A company employee should have sufficient knowledge to answer customer questions
	A company gives individual attention to customers
	A company has employees who give individual attention to customers
	A company understands the most interesting things of customers
	A company is very concerned about the personal interests of customers
<i>Perceived</i>	The employees of a company understand the needs of customers
	A company has modern equipment
	The appearance of a company's equipment is attractive
	The employees of a company are dressed properly, clean, and tidy
	Complete information about the services provided
	A company has a convenient time to work

TABLE 2: Explanation of PZM's meaning of the dimension of online service quality.

Online service quality	Meaning of the dimension
Efficiency	The difficulty and speed of access to the site
Fulfillment completion	The commitments provided by the website and related projects are fulfilled
System availability	Station correct technical implementation
Privacy	Website security and customer information
<i>Responsiveness</i>	The degree to which the interest is protected
	Effectively processed and reversed through the website
<i>Compensation</i>	Feed the question
	The website is for the questions that appear
Contact	The degree to which the customer is compensated
	Contact by phone or online way to provide assistance

bring losses to the enterprise, not only direct economic losses but also mean the loss of many potential customers [21].

Some online customers are disappointed with the reliability of the services provided by Internet companies. The reason is mainly because the coordination between the internal and external of the company is not good. Internal cooperation includes communication between different functional departments. External collaboration means collaboration between supply chain partners. In fact, products and services can be regularly checked and updated [22].

Completion requires a good supply of facilities, which is a major task of Internet commerce. Many online retailers use third-party service providers to complete their orders because they often have difficulty controlling the quality and timing of delivery.

3.3.3. *Reactivity*. Responsiveness means being willing to provide consumers with fast and efficient services. In the network environment, because the face-to-face service is gone, it seems difficult to intuitively judge the attitude and performance of the service personnel [23]. In fact, the response is reflected in the response mode and response time of the customer to the customer consultation or complaint, ready to help the customer. The willingness to order comes from the speed of confirmation, allocation, feedback, and delivery. This attribute emphasizes the immediate handling of consumer requests, questions, complaints, and questions. Consumers feel the responsiveness of the service based on the length of time they wait for help from the site staff, answering questions and solving problems. One of the advantages of Internet commerce is that it improves the efficiency of transactions and greatly shortens the processing time of transactions [24]. In order to provide timely service

and help customers solve their problems, this requires timely interaction with customers. Unlike tangible stores, Internet business people often lack timely interaction with customers [2].

3.3.4. Security. Security means ensuring the security of online transactions and the confidentiality of personal privacy. In the bad environment of the Internet, because customers and companies are not in face-to-face contact, customers often think that there are risks in purchasing on the Internet, especially the use of credit cards to make customers more worried about information leakage such as personal privacy or misuse of personal information. For example, the application passwords on the internet are leaked, and the subsequent property is lost; important secrets and business information are revealed; the office system is attacked by hackers, causing economic losses or loss of important data. Therefore, no matter what company is using the Internet to provide customers with perfect and thoughtful service, it must prevent sudden damage.

3.3.5. Customer Care. Customer care, also known as empathy, refers to caring for customers, understanding customer needs, and making the entire service process “human.” Although it is a face-to-face contact, it is necessary to make customers feel valued and cared for [25]. SERVQUAL measurement models and self-service technology research have shown that the company’s concern for customers is an important measure of customer perceived service quality. In the Internet business environment, it is also very important to care for customers and provide humanized services to customers [26]. Foreign studies have found that about two-thirds of customers have abandoned their shopping carts before they check out on the website because they are not cared for. This means that 2/3 of the customers want to trade online, but they give up the deal because they lack enough care. With the development of the economy and the progress of society, more and more customers are pursuing individualized consumption. Whether it is clothing, furniture, electrical appliances, or communication equipment, all show the trend of individualization.

3.3.6. Customer Trust. Customer trust means that one party of the transaction (the customer) believes that the other party of the transaction (online business) is honest and trustworthy. Trust is the most important concept in relationship marketing. The definition of trust is not uniform in academia. According to the commitment-one trust theory, trust is “reliability and loyalty to trading partners.” The above definition of trust points to two dimensions of trust: (1) credibility—the degree of trust in the ability of a trading partner to effectively perform work. Reputation includes ability, consistency, stability, sexual behavior, and other aspects related to the company’s reputation. (2) Benevolence: the degree of belief in the intention and motivation of the

altruistic (the other party) when the trading partner does not consider the situation in the new situation or commitment.

4. Relationship Model and Empirical Research on Network Consumer Behavior and E-Commerce Service Quality

4.1. The Measurement Factors of Business Service Quality. Table 3 summarizes the measurement items for each metric. A total of six elements and 28 measurement items need to be measured.

4.1.1. Research Methods and Research Objects. This study uses the method of issuing questionnaires. In the questionnaires, the judgment sampling method in the nonprobability sampling method is adopted. This method is applicable to exploratory investigations such as market research.

The survey sample includes college students and employees of enterprises and institutions. We only choose people over 18 years old as the research object. This is because these groups generally have certain disposable income and have certain network experience.

4.1.2. Sample Size and Accuracy. In this study, 200 questionnaires were distributed in Changchun in March 2007, and consumers with online consumption experience were invited to fill out the questionnaire. As of April 1, a total of 172 questionnaires were collected, 52 questionnaires that were not carefully completed were removed (if all questions were answered with the same answer or multiple questions were not answered), 120 valid questionnaires were collected, and the effective recovery rate was collected.

When determining the appropriate sample size, we consider three elements:

- (1) The overall size of the difference that can be assured.
- (2) Expected accuracy.
- (3) The confidence required for the estimate.

$$n = \frac{t^2 pq}{e^2}, \quad (1)$$

where n is the sample size; t is the standard error associated with the selected confidence interval; p is the estimated difference of the population; $q = 1 - p$; and e is an acceptable error.

When using the percentage rate method, the biggest difference is that the two answers each account for 50%, which is 50% multiplied by 50%, the maximum possible value. With a 95% confidence interval, $t = 1.96$, the accuracy of this survey sample is

$$e^2 = \frac{t^2 pq}{n} = \frac{1.96^2 * 0.5^2}{120} = 0.008. \quad (2)$$

That is, the sample accuracy of this survey is 92%.

TABLE 3: The measurement factors of business service quality.

Variable	Measurement item
<i>Ease of use</i>	Transaction is easy to complete
	Website is easy to login
	Searching for the information you need is easy
	Service content is easy to understand
	Website content can meet customer needs
	Can check the transaction status at any time
<i>Reliability</i>	Transaction is easy to complete
	Transaction is accurate
	According to personal information record
	Business can fulfill the promise
<i>Reactivity</i>	Product service can be delivered on time
	Can give quick response
	Can solve the problem quickly
	Correct problem solving
	Company personnel have the ability to answer questions
<i>Security</i>	Online company can handle complaints in a friendly way
	Online trading is very safe
	Providing personal information is very safe
<i>Customer Care</i>	Online company will not misuse personal information
	Online company personnel can act according to my requirements
	Online company can record and update my preferences
	Online employees can understand my specific needs
	Online company will tell me some important information soon
	Online company's free service is rich
<i>Customer Trust</i>	Online company personnel can act according to my requirements
	Trust online company
	Online company has a good reputation
	Online company is very honest
	Transaction is fair

$$p_i^j(k) = p_i^j(k-1) - a \frac{\partial e}{\partial p_i^j}, \quad (3)$$

$$\frac{\partial e}{\partial p_i^j} = \frac{(y_d - y_c) a^j}{\sum_{j=1}^n a^j x_i}. \quad (4)$$

In equations (3) and (4), p_i^j is the neural network coefficient; a is the network learning rate; x_i is the network input parameter; and a_j is the product of the input parameter membership. Parameter correction:

$$\begin{aligned} c_i^j(k) &= c_i^j(k-1) - \beta \frac{\partial e}{\partial c_i^j}, \\ b_i^j(k) &= b_i^j(k-1) - \beta \frac{\partial e}{\partial b_i^j}, \end{aligned} \quad (5)$$

where c and b are, respectively, the center and width of the membership function. The conceptual model of relationship between e-commerce service quality and online consumer behavior is shown in Figure 3.

4.2. Data Analysis and Results

4.2.1. Descriptive Analysis of Data. The data collected in this paper are mainly aimed at adults and people of all income

levels. In order to obtain different samples, social workers in formal jobs are mainly selected. In the case of data analysis, it is generally necessary to conduct descriptive statistical analysis of the data to discover its inherent laws and then select a method for further analysis. This step is a prerequisite for correct statistical inference below [2]. This paper conducts a descriptive statistical analysis of e-commerce service quality measurement elements and e-commerce service quality, online consumer attitudes, and behavioral intentions (see Tables 4 and 5). Statistical analysis results are shown in Figures 4 and 5.

It can be seen from the above two figures and two tables that consumers' consumer psychology and consumer behavior have a defined correlation; as a whole, there is a positive proportional relationship, and a linear relationship is also present.

4.3. Correlation Analysis of Data. In an effective indicator system (questionnaire), several indicators under each attribute have a strong linear correlation. However, the correlation of the indicators under each attribute in the initial screening index system is different, so they should be analyzed. Correlation analysis is a measure of the statistical relationship between things. The means and tools of strength and weakness measure the closeness between variables through correlation coefficients. The correlation coefficient is between -1 and 1 .

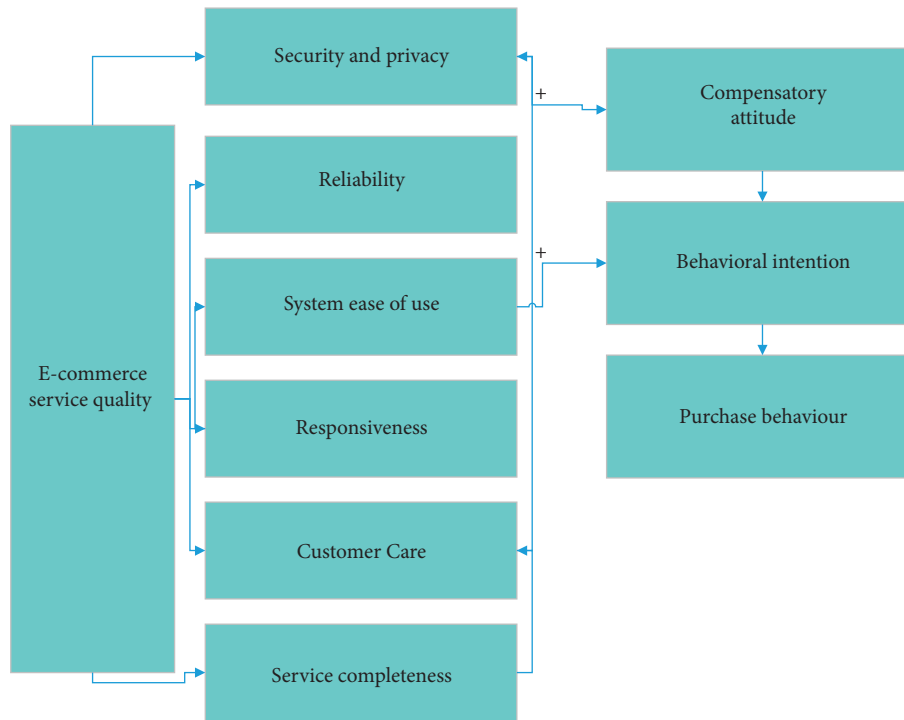


FIGURE 3: Conceptual model of relationship between e-commerce service quality and online consumer behavior.

TABLE 4: Descriptive analysis for measuring the quality of business service quality.

Variables	N	Minimum	Maximum	Mean	Standard deviation
Ease of use	120	2.17	5.00	3.8417	0.61336
Reliability	120	2.00	5.00	3.7188	0.69100
Reactivity	120	1.60	5.00	3.5283	0.67751
Security	120	1.00	5.00	3.1889	0.84872
Customer care	120	1.20	5.00	3.4167	0.70034
Customer trust	120	1.80	5.00	3.5017	0.71054

TABLE 5: Descriptive analysis of business service quality, online consumer attitude, and behavior intention.

Variables	N	Minimum	Maximum	Mean	Standard deviation
E-commerce service quality	120	2.00	5.00	3.8250	0.59285
Attitude	120	2.00	5.00	3.9167	0.76514
Behavioral intention	120	1.67	5.00	3.8472	0.82094
Security	120	1.00	5.00	3.1889	0.84872
Customer care	120	1.20	5.00	3.4167	0.70034
Customer trust	120	1.80	5.00	3.5017	0.71054

The above method is used to analyze the e-commerce service quality measurement factors and the attitudes of network consumers. The results are shown in Table 6 [25].

It can be seen from Table 6 that the correlation coefficient between the six measurement elements of e-commerce service quality and the attitude of network consumers is positive, among which there are four measurement factors of ease of use, reliability, responsiveness, and customer trust and network consumption. The attitude of P value is 0. The 1 level is significantly correlated. The security and online

consumer attitudes are significantly correlated with the P value of 0.05. The correlation between customer care and online consumer attitude is not significant. Relevant analysis diagram of business service quality measurement elements and network consumer attitudes is shown in Figure 6.

4.4. Regression Analysis of Data. Correlation analysis is closely related to regression analysis. They are statistical methods for studying the linear relationship between variables, but there are differences between the two. The

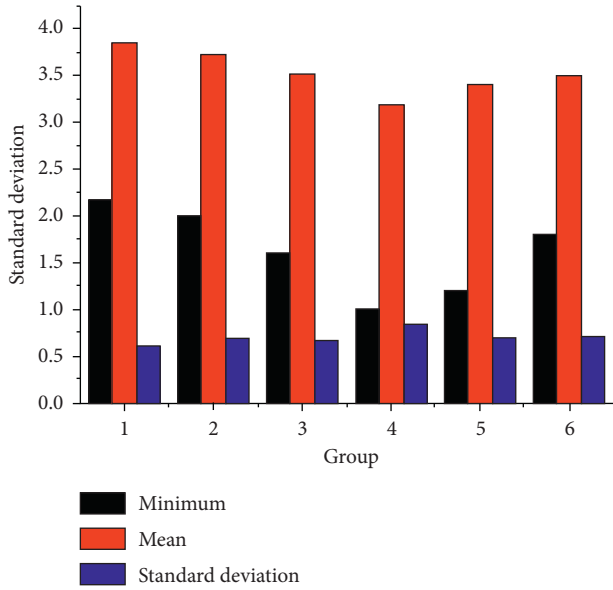


FIGURE 4: Service quality analysis chart.

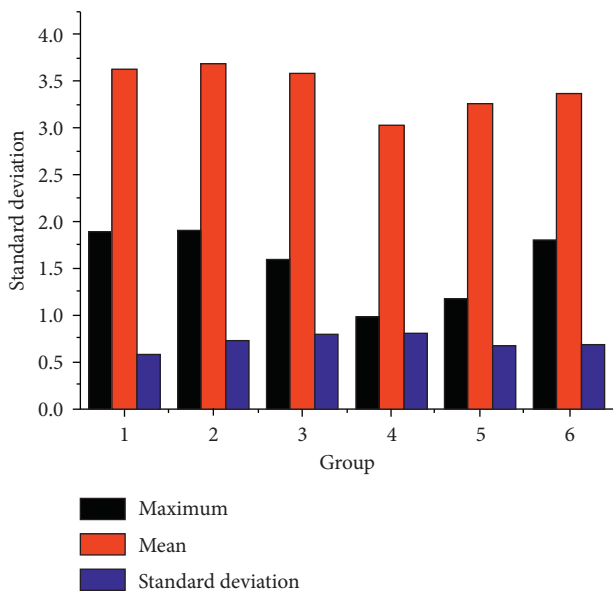


FIGURE 5: Behavioral intention analysis diagram.

TABLE 6: Correlation analysis of measurement elements of business service quality.

Network consumer attitude	Pearson correlation coefficient	Significant sig. (2-tailed)
Ease of use	0.331	0.000
Reliability	0.297	0.001
Reactivity	0.246	0.007
Security	0.188	0.039
Customer care	0.087	0.343
Customer trust	0.237	0.009

variables studied in the correlation analysis are regarded as random variables, and only the linear relationship between the variables is studied, and the variables studied in the

regression analysis are divided into dependent variables and independent variables.

This part uses multiple linear regression analysis to verify the hypothesis of the model through regression analysis of various factors on e-commerce service quality. Regression analysis is carried out on the six measurement elements of e-commerce service quality and e-commerce service quality, so as to obtain the influence of each element on e-commerce service quality, and then the standard regression equation of e-commerce service quality and its measurement elements can be obtained. The regression method used is a combination of methods (stepwise). The results are shown in Table 7 [25].

F test: the larger the *F* value, the better the regression effect; when the Sig. *F* value is < 0.05, it indicates that the independent variable tested can describe the dependent variable.

T test: when $n > 5$, if $\alpha = 0.05$, and then when $t > 2$, it can be judged that the regression coefficient at this time is not 0, and the corresponding variable can be used as an explanatory variable to describe the dependent variable. According to the standard, the regression results from the table show that the equations obtained by regression analysis of the six independent variables designed for the dependent variables satisfy *F*.

The result shows that the regression equation established between the above six independent variables and the dependent variable meets the test requirements. In addition, it can be seen that the complex coefficient (R-square) is 0.21, indicating that the regression equation can explain 21% of the total variation.

4.4.1. Regression Analysis between E-Commerce Service Quality Measurement Factors and Online Consumer Behavior Intentions. As before, we separately analyze the online consumer behavior intention and the e-commerce service quality's six measurement factors. The specific analysis results are shown in Table 7 [26]. Regression analysis diagram of six measurement factors is shown in Figure 7.

Complex decision coefficient (R-square) = 0.211.

F value = 5.030; *p* value = 0.000.

Correct *R*_z (adjusted *R*) = 0.169.

From the regression results, it can be seen that customer care does not enter the equation, indicating that customer care has no significant effect on the online consumer behavior intention. According to the order of the other five factors in the equation, we obtain the regression equation [27, 28]:

$$\begin{aligned} \text{online consumer intent} = & 0.329 * \text{customer trust} + 0.309 \\ & * \text{ease of use} + 0.237 * \text{reactivity} \\ & + 0.193 * \text{reliability} + 0.221 \\ & * \text{security}. \end{aligned} \tag{6}$$

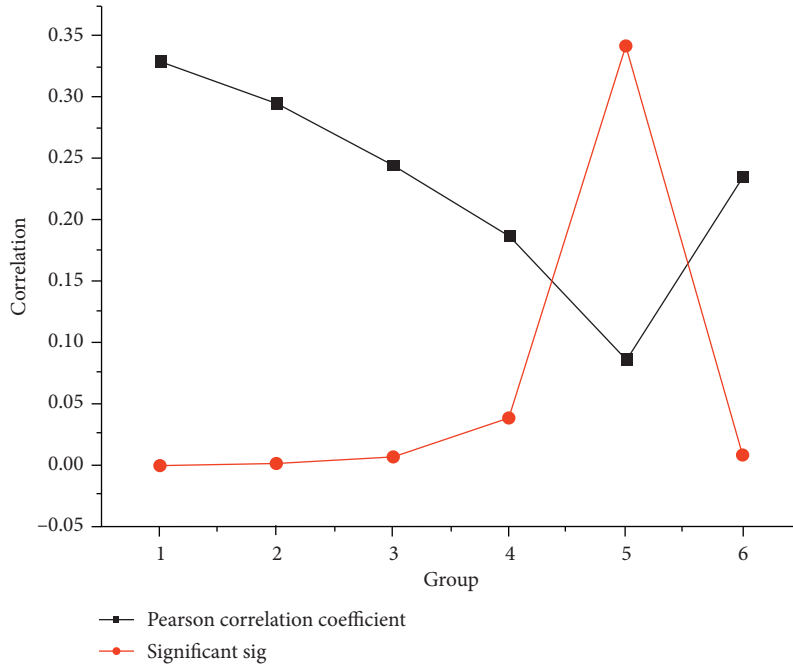


FIGURE 6: Relevant analysis diagram of business service quality measurement elements and network consumer attitudes.

TABLE 7: Regression analysis of e-commerce service quality.

Equations in the variable	Regression coefficient	Standard regression coefficient	T value	Significant probability
Ease of use	0.414	0.309	3.535	0.001
Reliability	0.229	0.193	2.134	0.035
Reactivity	0.287	0.237	2.650	0.009
Security	0.214	0.221	2.466	0.015
Customer care	0.087	0.343	2.569	1.021
Customer trust	0.381	0.329	3.789	0.000

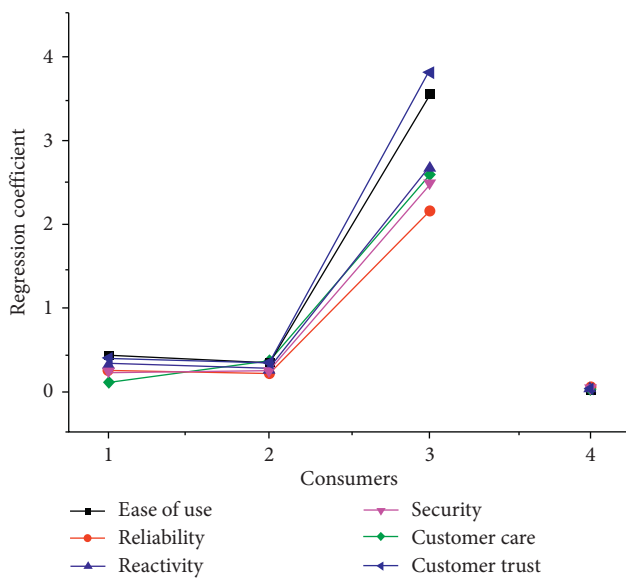


FIGURE 7: Regression analysis diagram of six measurement factors.

The results also show that H3a, H3b, H3c, H3d, and H3f are assumed to be true, assuming that H3e does not hold [29].

4.4.2. The Third Set of Assumptions

H3a: from the results of regression analysis, there is a significant correlation between ease of use and behavioral intentions of online consumers. Empirical studies show that H3a is assumed to be established.

H3b: the empirical results show that there is a positive relationship between reliability and network consumer behavior intention, supporting hypothesis H3b.

H3c: the results of regression analysis show that reactivity has a direct positive impact on the behavioral intention of online consumers, assuming H3c is established.

H3d: the empirical results show that security has a direct positive impact on the behavior of online consumers, supporting hypothesis H3d.

H3e: the empirical results show that customer care has no significant effect on the behavior of online consumers, so it is assumed that H3e is not established.

H3f: the empirical results show that customer trust has a positive correlation between online consumer behavior intentions, supporting hypothesis H3f.

This section is the main part of the thesis. First, we introduce the conceptual model and model hypothesis proposed by us and explain the research design and data collection of this research. Finally, through data analysis, the relationship between online consumer behavior and e-commerce service quality is clarified.

5. Conclusion

This article identifies e-commerce services. The quality measurement elements are ease of use, reliability, responsiveness, safety, customer care, and customer trust, which are meaningful for the company to rationally use limited resources. This paper proposes a simplified relationship model between online consumers based on attitudes and intentions combined with 5G technology to track consumer behavior and e-commerce service quality. On this basis, the hypothesis of e-commerce service quality and online consumer attitudes and behavior intentions is proposed. The analysis verified and clarified the impact of e-commerce service quality on online consumer behavior and provided a basis for companies to better participate in the development of the B2C market.

Data Availability

No data were used to support this study.

Conflicts of Interest

The author declares that there are no conflicts of interest.

Acknowledgments

This study was supported by the Evaluation Research of Comprehensive Competitiveness of Modern Service Industry of Guanzhong-Tianshui Economic Zone on "One Belt One Road" Strategy (XJ150230).

References

- [1] K. J. Li and S. Jain, "Behavior-based pricing: an analysis of the impact of peer-induced fairness," *Social Science Electronic Publishing*, vol. 62, no. 2, pp. 2705–2721, 2016.
- [2] P. Gupta and J. Harris, "How e-WOM recommendations influence product consideration and quality of choice: a motivation to process information perspective," *Journal of Business Research*, vol. 63, no. 9, pp. 1041–1049, 2010.
- [3] E. Carrillo-Álvarez, J. Riera-Romaní, and O. Canet-Vélez, "Social influences on adolescents' dietary behavior in Catalonia, Spain: a qualitative multiple-cases study from the perspective of social capital," *Appetite*, vol. 12, no. 3, p. 289, 2018.
- [4] R. K. Steele, "A perspectival review of rail behavior at the facility for accelerated service testing," *Canadian Metallurgical Quarterly*, vol. 22, no. 3, pp. 353–367, 2014.
- [5] G. Bene and D. Dieks, "A perspectival version of the modal interpretation of quantum mechanics and the origin of macroscopic behavior," *Foundations of Physics*, vol. 32, no. 5, pp. 645–671, 2002.
- [6] Y. Yan, P. Guo, B. Cheng, and Z. Zheng, "An experimental case study on the relationship between workload and resource consumption in a commercial web server," *Journal of Computational Science*, vol. 25, pp. 183–192, 2017.
- [7] J. Li, Z. Zheng, Q. Tian, G. Zhang, F. Zheng, and Y. Pan, "Research on tridiagonal matrix solver designing based on combination of processors," *Computers & Electrical Engineering*, vol. 62, pp. 1–16, 2017.
- [8] X. Li, Z. Lv, Z. Zheng, C. Zhong, I. H. Hijazi, and S. Cheng, "Assessment of lively street network based on geographic information system and space syntax," *Multimedia Tools and Applications*, vol. 76, no. 17, pp. 17801–17819, 2017.
- [9] S. Pan, W. Sun, and Z. Zheng, "Video segmentation algorithm based on superpixel link weight model," *Multimedia Tools and Applications*, vol. 76, no. 19, pp. 19741–19760, 2017.
- [10] S. Shivani, S. Tiwari, K. K. Mishra, Z. Zheng, and K. Arun, "Providing security and privacy to huge and vulnerable songs repository using visual," *Multimedia Tools and Applications*, vol. 77, no. 9, pp. 11101–11120, 2017.
- [11] M. Chahal, S. Harit, K. K. Mishra, A. Sangaiah, and Z. Zheng, "A survey on software-defined networking in vehicular ad hoc networks: challenges, applications and use cases," *Sustainable Cities and Society*, vol. 35, no. 11, pp. 830–840, 2017.
- [12] J. T. Child and D. A. Westermann, "Let's be facebook friends: exploring parental facebook friend requests from a communication privacy management (CPM) perspective," *Journal of Family Communication*, vol. 13, no. 1, pp. 46–59, 2013.
- [13] G. Zhao, "Energy-spectral-efficiency analysis and optimization of heterogeneous cellular networks: a large-scale user-behavior perspective," *IEEE Transactions on Vehicular Technology*, vol. 1, no. 1, p. 99, 2018.
- [14] T. D. Hackenberg, "Realism without truth: a review of Giere's science without laws and scientific perspectivism," *Journal of the Experimental Analysis of Behavior*, vol. 91, no. 3, pp. 391–402, 2013.
- [15] F. Lehner, "Cognitive structure, uncertainty, and the rationality of political action: a synthesis of economic and psychological perspectives," *European Journal of Political Research*, vol. 3, no. 3, pp. 275–291, 2010.
- [16] D. Boonpakdee, W. Surareungchai, and C. Laovorakiat, "Exploring non-linearities of carbon-based micro-supercapacitors from an equivalent circuit perspective," *Journal of Materials Chemistry A*, vol. 6, no. 16, pp. 7162–7167, 2018.
- [17] X. Xu, B. Shen, X. Yin et al., "Edge server quantification and placement for offloading social media services in industrial cognitive IoV," *IEEE Transactions on Industrial Informatics*, vol. 17, no. 4, pp. 2910–2918, 2020.
- [18] X. Xu, X. Zhang, X. Liu, J. Jiang, L. Qi, and M. Zakirul Alam, "Adaptive computation offloading with edge for 5G-envisioned Internet of connected vehicles," *IEEE Transactions on Intelligent Transportation Systems*, vol. 8, pp. 1–10, 2020.
- [19] F. Li, Z. Yu, and C. Qin, "Constructive texture steganography based on compression mapping of secret messages," *CMES-computer Modeling in Engineering & Sciences*, vol. 124, no. 1, pp. 393–410, 2020.

- [20] Z. Gao and S. Wan, "Exploring deep learning for view-based 3D model retrieval," *ACM Transactions on Multimedia Computing, Communications, and Applications*, vol. 16, no. 1, pp. 1–21, 2020.
- [21] C.H. Chen, "An arrival time prediction method for bus system," *IEEE Internet of Things Journal*, vol. 5, no. 5, pp. 4231–4232, 2018.
- [22] Y. Xi, Y. Zhang, S. Ding, and S. Wan, "Visual question answering model based on visual relationship detection," *Signal Processing: Image Communication*, vol. 80, Article ID 115648, 2020.
- [23] A. Zhou, S. Wang, S. Wan, and L. Qi, "LMM: latency-aware micro-service mashup in mobile edge computing environment," *Neural Computing and Applications*, vol. 1–15, 2020.
- [24] F. Yin, Y. Wang, J. Liu, and M. Ji, "Enhancing embedding-based Chinese word similarity evaluation with concepts and synonyms knowledge," *CMES-computer Modeling in Engineering & Sciences*, vol. 124, no. 2, pp. 747–764, 2020.
- [25] S. Wan, Y. Xia, L. Qi, Y. H. Yang, and M. Atiquzzaman, "Automated colorization of a grayscale image with seed points propagation," *IEEE Transactions on Multimedia*, vol. 22, no. 7, pp. 1756–1768, 2020.
- [26] S. Wan, X. Xu, T. Wang, and Z. Gu, "An intelligent video analysis method for abnormal event detection in intelligent transportation systems," *IEEE Transactions on Intelligent Transportation Systems*, vol. 12, pp. 1–9, 2020.
- [27] S. Wan, R. Gu, T. Umer, K. Salah, and X. Xu, "Toward off-loading Internet of vehicles applications in 5G networks," *IEEE Transactions on Intelligent Transportation Systems*, vol. 6, pp. 1–9, 2020.
- [28] Z. Gao, H. Xue, and S. Wan, "Multiple discrimination and pairwise CNN for view-based 3D object retrieval," *Neural Networks*, vol. 125, pp. 290–302, 2020.
- [29] S. Wan and S. Goudos, "Faster R-CNN for multi-class fruit detection using a robotic vision system," *Computer Networks*, vol. 168, Article ID 107036, 2020.

Research Article

Design of Minimizing Expected Energy of Multisource Wireless Cooperative Network Based on Multiobjective Optimization

Shusheng Wang 

Space Star Technology Co, Ltd., Beijing 100095, China

Correspondence should be addressed to Shusheng Wang; wangss@spacestar.com.cn

Received 20 January 2021; Revised 7 February 2021; Accepted 21 February 2021; Published 2 March 2021

Academic Editor: Hsu-Yang Kung

Copyright © 2021 Shusheng Wang. This is an open access article distributed under the Creative Commons Attribution License, which permits unrestricted use, distribution, and reproduction in any medium, provided the original work is properly cited.

In order to solve the problems of high average power consumption, low average throughput, high average energy consumption per unit of data, and short network life cycle in traditional multisource wireless cooperation methods, this paper proposes a multisource wireless cooperative network design method based on multiple goals. We analyze the characteristics of heterogeneous deployment of multisource wireless cooperative networks and the energy consumption of nodes and control the energy consumption of network data transmission through distributed opportunistic transmission scheduling methods according to the analysis results. We use the optimal strategy of minimizing expected energy consumption, transform the problem of data transmission energy consumption, establish a mathematical model, and obtain the optimal solution for minimizing expected energy consumption. According to the optimal stop rule, the minimum expected energy consumption threshold is obtained, and then the optimal solution is obtained on the constraint set of the multiobjective optimization problem through the multiobjective optimization method, so as to achieve the goal of minimizing the expected energy of the network. Experimental results show that this method prolongs the network life cycle, reduces the average power consumption of network data transmission, and improves the average network throughput.

1. Introduction

As an important branch of wireless network, multisource wireless cooperative network is widely used. Especially with the use of intelligent devices, multimedia applications, and intelligent devices, the demand for network data traffic has increased sharply, and the energy consumption of the whole system has reached an unprecedented level. According to related research reports, in a typical multisource wireless cooperative network, the energy consumption caused by the operation of the base station accounts for more than 50% of the entire system [1]. Therefore, how to improve energy efficiency and reduce energy consumption is very important for multisource wireless cooperative networks. In this regard, many scholars in academia have proposed diversified solutions.

At present, the research on node energy consumption of multisource wireless cooperative network mainly focuses on topology control strategy and energy-efficient routing control strategy. The former mainly studies the reduction of

the transmission energy consumption of nodes by adjusting the wireless transmission distance between nodes under the premise of ensuring the normal operation of the network [2]. The latter mainly studies the selection of suitable transmission distances and routes to store energy for sensor nodes by means of node multihop transmission. The commonality of these two types of strategies is that when the wireless transmission interface of the node is in the “active” state of transmitting/receiving information, energy consumption is reduced, but when the node is in the “idle” state, there is still energy consumption, so the sensor node sleep management strategy is put forward. Under the premise of ensuring the normal transmission of the network, this strategy shuts down some temporarily useless nodes, puts them in a “sleep” state, and only activates a few nodes for multihop transmission to save the overall energy consumption of the network [3,4]. Although the above strategy achieves the energy saving of network nodes, there is still the problem of large energy consumption of some nodes.

In order to effectively reduce network latency and energy consumption, reference [5] applies Work Breakdown Structure Number (WBSN) to the Internet of Things. First of all, from the perspective of network architecture, a comprehensive study of energy saving solutions is carried out. Secondly, a mathematical model of the link and interruption probability of the protocol is established. Finally, the end-to-end delay, throughput, and energy consumption are analyzed and studied. The simulation results show that, in general, compared with the direct transmission mode and existing work, this method can obtain better system performance, but the average power consumption of network data is still large after using this method; that is, the energy consumption is large. Prashanth et al. proposed a cluster-based method to minimize the energy consumption of mobile nodes in wireless sensor networks. In order to reduce the moving time of mobile nodes in wireless sensor networks, a node recognition algorithm to determine the optimal path is proposed. The data generated by the cluster members will be aggregated at the identified cluster head, and the ideal path will be determined by connecting all nodes. Experimental results show that this method can reduce node energy consumption to a certain extent, but there is a problem of short network life cycle, and it takes a lot of time to determine the optimal path. Gaujal et al. proposed a dynamic speed scaling method to minimize the expected energy consumption of real-time tasks. The discrete-time Markov decision process method is used to calculate the optimal online speed adjustment strategy to minimize the energy consumption of a single processor that performs limited or infinite multiple task sets under real-time constraints. Experimental results show that this method has better performance without considering job statistics, but the average throughput is lower, and the average energy consumption per unit data is higher.

With the rapid development of wireless network technology, saving energy consumption has become an extremely important topic in building a green wireless network. In this context, aiming at the problems existing in the existing methods, aiming at reducing the network energy consumption, improving the average throughput, and reducing the average power consumption, a multiobjective optimization based design method for multisource wireless cooperative networks is proposed.

The research contributions of this paper include the following:

- (1) A multisource wireless cooperative network design method based on multiple goals is proposed.
- (2) The characteristics of heterogeneous deployment of multisource wireless cooperative networks and the energy consumption of nodes are analyzed, and according to the analysis results, the energy consumption of network data transmission is controlled through the distributed opportunistic transmission scheduling method.
- (3) We use the best strategy to minimize the expected energy consumption, convert the problem of data transmission energy consumption, establish a

mathematical model, and obtain the best solution to minimize the expected energy consumption.

- (4) According to the optimal stopping rule, the minimum expected energy consumption threshold is obtained, and then through the multiobjective optimization method, the optimal solution is obtained for the constraint set of the multiobjective optimization problem, so as to achieve the purpose of minimization.

The remaining organizational structure of the paper is arranged as follows. The second section discusses the design of minimum expected energy of multisource wireless cooperative network, the third section discusses simulation experiment, and the fourth section summarizes the whole paper.

2. Multisource Wireless Cooperative Network Expected Energy Minimization Design

2.1. Heterogeneous Deployment of Multisource Wireless Cooperative Network. For multisource wireless cooperative networks, energy efficiency has inevitably become a concern. Although many strategies have been continuously proposed to improve the power efficiency of the system, most of them are based on homogeneous network scenarios [6]. However, considering the increasing user rate requirements, the structure of the multisource wireless cooperation network has gradually shifted to a heterogeneous network architecture. Figure 1 is an example diagram of the heterogeneous network deployment of the multisource wireless cooperation network.

According to the different network scenarios, the optimization of energy consumption in multisource wireless cooperative networks can be divided into two aspects: the unknown network topology and the known network topology. In the former, base stations are effectively deployed within the specified region to achieve network coverage and reduce energy consumption [7]. If the microbase station is deployed in the macrocell with high density without plan, although it can provide high data rate, it will inevitably lead to a sharp increase in energy consumption.

On this basis, under the condition that the whole network structure is fixed, the performance of the multisource wireless cooperative network and the efficiency of the base station are improved by rational allocation of network resources, so as to achieve the purpose of energy saving.

2.2. Description of Node Energy Consumption Problem. According to the heterogeneous network layout of multisource wireless cooperative network, the energy consumption of multisource wireless cooperative network nodes has time-varying characteristics. In order to meet the receiving power requirements of the receiving terminal, it is necessary to send data with a higher power, which will lead to the decline of energy utilization. A reasonable way to solve this problem is to let some nodes give up this transmission opportunity, and let all nodes compete again, so that the link that successfully obtains

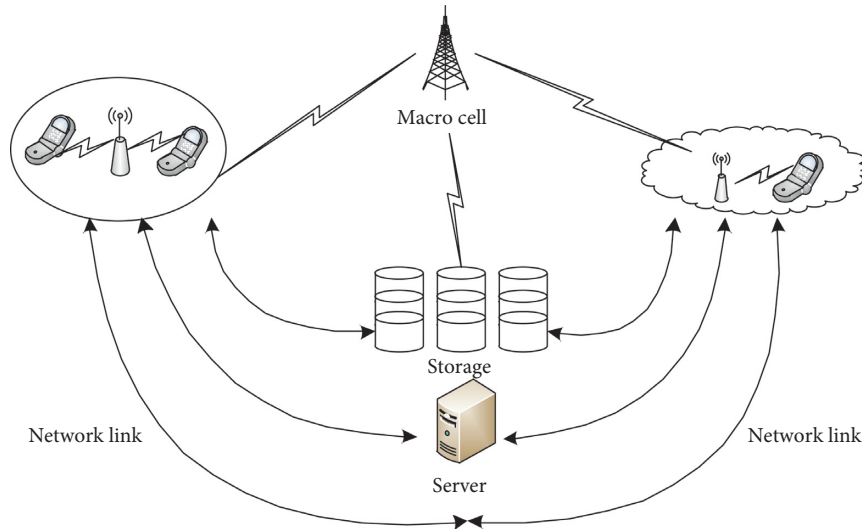


FIGURE 1: Example diagram of heterogeneous layout of multi-source wireless cooperative network.

the channel after recompetition can transmit data in a better channel state [8]. Because different links experience different channel state changes at different times, after further channel detection, it is possible for links to obtain better channel state. Therefore, the diversity of users and the diversity of channel fluctuation can be used to optimize the network performance [9]. On the other hand, each additional channel detection will cause data delay, which is originally used to transmit data. Considering this problem, an optimal stop rule is needed to detect the channel to minimize the network energy consumption.

Assuming that the maximum number of acceptable channel detections in one transmission is m , the upper limit of the time that the sending terminal can delay data transmission is T_{\max} . The calculation formula is

$$T_{\max} = k_1\mu + k_2\mu + \dots + k_m\mu. \quad (1)$$

in which k represents the actual delay; μ represents the external clock. The problem studied in this paper is to determine when it is best to start transmitting data within the time range $[0, T_{\max}]$.

Therefore, according to the optimal stopping theory, the duration of energy minimization is obtained, and the stop moment of energy minimization is set to t , and then the duration of energy minimization is

$$t_s = \sum_{m=1}^n k_i\mu. \quad (2)$$

Among them, n represents the number of links. This duration is the time that the scheduling strategy delays this communication, which is defined as the scheduling delay. If the delayed time arrives at T_{\max} , and the data has not been sent yet, at this time, regardless of the channel status, the multisource wireless cooperative network will send data at time T_{\max} .

To sum up, in the process of two-continuous-channel detection, the communication module of the sending terminal can be set to idle mode or sleep mode to avoid its

continuous work. In this way, the energy consumption can be reduced.

2.3. Distributed Opportunistic Transmission Scheduling.

The main goal of this paper is to minimize the energy consumption of data transmission in a multisource wireless cooperative network. In order to achieve this goal, we use the good timing of the channel to construct a distributed opportunistic transmission scheduling strategy [10]. In a multiuser multisource wireless cooperative network, there are n links, and mutual communication between nodes will cause interference. The nodes access the channel through the carrier sense multiple access/conflict avoidance mechanism. Figure 2 shows the minimization of multiple channels and source wireless collaborative network system model.

Since the analysis in this paper is mainly focused on the energy-efficient communication problem of the wireless link in the entire multisource wireless cooperative network, the system model only considers the impact of small-scale fading on the communication link and assumes that the communication channel will compete successfully for the link. The sending terminal must send data within the specified time range, the delay time of the sending terminal sending data cannot exceed the specified upper limit of time, and the transmission rate is constant; that is, the receiving power of the receiving terminal is fixed [11]. It is stipulated that there is always data that can be transmitted in the communication environment; that is, when the terminal device decides to transmit the data, there is always data that can be obtained. These data can be stored in the device's memory or the device can get it instantly.

2.4. Optimal Strategies for Minimizing Expected Energy Consumption.

Using E to represent the energy consumption of data transmission in a multisource wireless cooperative network, the optimization problem can be expressed as an optimal stopping problem of selecting a stopping rule

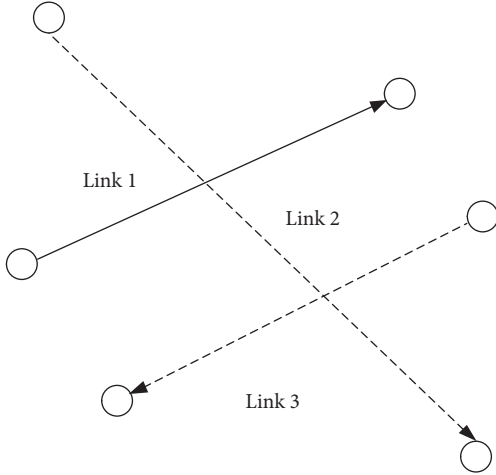


FIGURE 2: Multisource wireless cooperative network system model.

$1 \leq N \leq m$ to minimize the expected energy consumption E_j of the network. In order to make the multisource wireless cooperative network system model more in line with the actual situation, it is assumed that the sending terminal consumes a certain amount of energy during each channel competition, which is defined as E_l . Therefore, the total data transmission energy consumption E in the network is the sum of the total energy consumed by channel detection and the power consumption P_t of transmitting data at time t . Then, E can be expressed as

$$E = \sum_{m=1}^n [t_s \times (E_l - E_j)]^2 - u_e u_t \times G_n. \quad (3)$$

Among them, u_t represents the channel detection time; G_n represents the channel gain sequence, which represents a random variable; u_e represents the energy consumed by the channel detection, and its value is 1 or 0. When it is 0, the link does not participate in channel competition. When it is 1, it means that the link participates in channel competition.

According to formula (3), the optimal stopping rule can be derived from the channel gain sequence and data transmission energy consumption.

The problem of data transmission energy consumption in the multisource wireless cooperative network has been transformed into the problem of minimizing the expected energy consumption, and the corresponding mathematical model has been established [12]. Before solving this problem, it is first necessary to prove that there is an optimal solution to the problem of minimizing expected energy consumption. Therefore, the following propositions are given.

Proposition 1. *Formula (3) has an optimal stopping rule.*

Proof. The optimal stopping rule exists when the following two conditions are met:

$$\begin{cases} S_1 : E[\inf_n E] > -\infty, \\ S_2 : \liminf E \geq E_\infty. \end{cases} \quad (4)$$

Consider these two conditions separately below:

The random variable G_n is independently distributed, and its domains are all finite values. Therefore, $E > -\infty$ is established; that is, the $E[\inf_n E] > -\infty$ condition is satisfied.

When $n \rightarrow \infty$, $E \rightarrow \infty$, and the random variable G_n is independently distributed, and the domains are all finite values, then

$$\liminf E = \liminf \left(\frac{S}{G_n} t + NE \right) = \infty. \quad (5)$$

According to formula (5), it can be known that $E_\infty = \infty$, and then $\liminf E \geq E_\infty$ condition is satisfied. This proves Proposition 1. \square

2.5. Obtaining the Minimum Expected Energy Consumption Threshold Based on the Optimal Stopping Rule.

Comprehensive analysis of node energy consumption and expected energy consumption minimization optimization strategy shows that after the link obtains the channel state at any time, it must decide whether this time is the best stop time for data transmission, and whether to stop or continue detection depends on whether there is a better channel state expectation in the future [13]. The problem of limited scope can usually be solved by backward induction from the final stage to the initial stage. The optimal strategy of expected energy consumption minimization mentioned in the previous section can be deduced by comparing the sending terminal with the threshold sequence in each stage t_k and then deciding whether to transmit data or continue detection. The minimum energy consumption cost of detection channel x at a specific time t_k is given as follows:

$$E_{\min} = \min(P_{t_j}, W_{i-j}) + E_{ij}. \quad (6)$$

Among them, W_{i-j} represents the expected cost that can be obtained by continuing channel detection. It can be seen that formula (6) compares the expected cost from time i to time j with the cost P_{t_j} obtained by stopping at time t and continuing to use the optimal stopping rule and considers the detection energy consumption cost E required by continuing to detect at each stage; W_{i-j} depends only on the number of moments $i - j$ to continue detection. Therefore, the optimal stopping rule is as follows: at time j , if $P_{t_j} \leq W_{i-j}$, the sending terminal stops detecting and transmitting data; otherwise, it gives up this channel transmission opportunity and continues channel detection.

The optimal stopping rule means that, at each moment, j has a transmission power threshold, $j = (W_{i-j})/T$. The "optimal" mentioned in this article means that if the multisource wireless cooperative network stops detection after a certain round of channel detection, then this indicates that it believes that it can obtain it even if it continues to detect the channel until the maximum number of detections. The cost of energy consumption in multisource wireless cooperative network is no less than the cost of data acquisition from base station. Therefore, for multisource wireless cooperative network, the station can obtain the minimum energy consumption in the whole channel detection process, that is, the optimal energy consumption [14].

The real-time energy consumption cost of multisource wireless cooperative network at a certain time is an objective reflection of the channel state and detection times obtained by channel detection, while the expected energy consumption cost obtained by the next channel detection is calculated dynamically according to the current channel state and detection times [15].

Setting P_θ represents the maximum output transmission power of the RF power amplifier of the transmitting terminal, and A_τ represents the cumulative distribution function of transmission power relative to P_θ . In order to ensure that the maximum transmission delay is T_{delay} , when $j = m$, set $A_0 = P_\theta \times T_i$. Then, the W_{i-j} at each stage can be obtained by reverse induction:

$$W_{i-j} = S(m, n)W(i + \tau, j + \tau)dt e^{-j\omega\tau} d\tau. \quad (7)$$

Among them, S represents the network survival time; ω represents the number of cooperative nodes; d represents the network transmission load; τ represents the density of relay nodes.

According to the proposed model, combined with the requirements of the optimal stopping rule, the threshold for minimizing the expected energy consumption at each moment is obtained:

$$P_{rt} = \frac{E(P(u, v))}{W_{i-j}}. \quad (8)$$

Among them, u represents the average energy consumption of data transmission; v represents the data transmission rate. According to the obtained energy threshold, in order to further realize the expected energy minimization of multisource wireless cooperative network, according to the threshold, the multiobjective optimization method is used to obtain the optimal energy minimization threshold.

2.6. Realization of Network Expected Energy Minimization Based on Multiobjective Optimization. At present, the commonly used optimization methods include analytical method, numerical method, hybrid method, and intelligent optimization algorithm. For the objective function and constraints in the optimization mathematical model, if there is a clear mathematical analysis expression, the final result can be obtained by derivative method or variational method according to the necessary conditions of function extremum. Analyze the solution, and then determine the optimal solution of the problem according to the actual physical meaning of the problem. This is the simplest analytical method [16].

If the objective function or constraint conditions are more complicated, or there is no clear mathematical analysis expression, or the existing analytical methods and means cannot be used to obtain the optimization problem of the analytical solution, it can be solved by the numerical solution method.

Currently, with the rapid development of computers in this era, numerical algorithms have shown their superiority. The basic idea is to use a search method to go through a series of iterations, so that the generated sequences can gradually approach the optimal solution of the problem.

Numerical solutions often require experience or experimentation. At the same time, the results also need to be verified by actual problems to be effective [17]. The hybrid solution is a combination of the above two methods, such as a type of solution represented by the gradient method, which is often a combination of analytical and numerical algorithms. If the optimization problem has particularly complex constraints and objective functions, the above solution method can no longer obtain the optimal solution. At this time, a multiobjective optimization method is needed to obtain the optimal solution.

This paper uses a multiobjective optimization method to convert the single objective in the network expected energy minimization problem to multiple objectives and uses a linear accumulation function as the evaluation function to solve the multiobjective optimal result [18].

The linear weighting method is to multiply a set of weight coefficients according to the importance of M objectives and add them as the objective function, and then the objective function is to find the optimal solution on the set of constraints of the multiobjective optimization problem, that is, to construct the following multiobjective optimization problem:

$$E_{\min} = \sum_{i=1}^l \xi_i (w \cdot \varphi(x_i)) + b. \quad (9)$$

Among them, ξ_i represents the total energy consumption of the network; φ represents the network connectivity; x_i represents the node energy consumption balance; b represents the multiobjective optimization function.

By solving the optimal solution of the multiobjective optimization problem, the optimal solution of the multiobjective optimization problem in the sense of linear weighting is obtained:

$$G_{sc} = G_0 + \frac{E_{\min}}{(c_s - aP_n)(1 + (F / F_0))}. \quad (10)$$

Among them, G_0 represents the linear weighted norm; P_n represents the utility function of the node's transmission power; F_0 represents the remaining energy of the node; a represents the node's movement overhead when the network transmits power; c_s represents the weight coefficient. The weight coefficient in formula (10) satisfies the following conditions:

$$c_s = \begin{cases} 1, & |P_k(x, y) - P_0(x, y)|, \\ 0, & \text{others.} \end{cases} \quad (11)$$

Among them, $P_k(x, y)$ represents the weighting coefficient of the network energy function; $P_0(x, y)$ represents the weighting coefficient of the energy distribution. Under the condition that formula (11) is satisfied, the expected energy minimization result of the multisource wireless cooperative network is obtained.

3. Simulation Experiment

In order to verify the feasibility and effectiveness of the multisource wireless cooperative network design method

based on multiobjective optimization, the following simulation experiments are designed.

In order to avoid the singleness of the experimental results and enhance their contrast, this study introduces the idea of comparative experiment and obtains the comparison results between the method and the traditional method. On this basis, the effectiveness of the simulation results is analyzed (Table 1).

3.1. Experimental Environment and Scheme

- (1) Experimental hardware environment setting and parameter setting: the simulation experiment is carried out on a computer with Windows 10 operating system, quad-core 3.75 GHz CPU, 16 GB RAM, and MATLAB 2014a is used to process the experimental data. The specific experimental parameter settings are shown in Table 1.
- (2) Experimental comparison methods: select the network energy minimization method based on WBSN (reference [5] method), cluster-based wireless sensor network mobile node travel time minimizing energy consumption method (reference [19] method), and a method of minimizing expected energy consumption based on dynamic speed scaling to minimize real-time tasks (reference [20] method) as comparison methods.
- (3) Experimental index setting

The average power consumption, network lifetime, average energy consumption per unit data, and average throughput of network data transmission are taken as experimental indexes to verify the application effect of different methods. Among them, the most important evaluation indexes are average power consumption and average throughput. Another key index is the average energy consumption per unit data, which is used to measure whether the system is efficient and energy-saving during data transmission. The lower the index, the higher the energy efficiency of the system, and the lower the energy consumption. The unit of average energy consumption per unit of data is joules per megabyte, that is, watts per megabyte per second. The calculation formula is as follows:

$$P_{cost} = \frac{PC}{THR}. \quad (12)$$

The calculation formula of average power consumption is as follows:

$$PC = \frac{P_n t + E}{\sum_{i=1}^l \alpha_i y_i - P_k(x, y)}. \quad (13)$$

Among them, α_i represents the optimal allocation result of active power; y_i represents the energy consumption of single data transmission.

The average throughput is calculated as follows:

$$THR = \sum_{j=1}^l \alpha_j y_j (a + b). \quad (14)$$

Among them, α_j represents the forward link data throughput; y_j represents the reverse link data throughput.

According to the calculation formula given, calculate the numerical value of each experimental index and compare the application effects of different methods.

3.2. Analysis of Experimental Results

3.2.1. Comparison of Network Life Cycle. Taking the network life cycle as the experimental index, the different methods are compared, and the results are shown in Table 2.

Analysis of the data in Table 2 shows that when the number of iterations is 50, the network life cycle of the proposed method is 16.10, the network life cycle of the method in reference [5] is 7.25, the network life cycle of the method in reference [19] is 7.78, and the network life cycle of the method in reference [20] is 2.82; when the number of iterations is 100, the network life cycle of the proposed method is 20.99, the network life cycle of the method in reference [5] is 10.88, the network life cycle of the method in reference [19] is 9.28, and the lifetime of the network of the method in reference [20] is 4.31. According to the above data analysis results, the network life cycle of the proposed method is significantly higher than that of the traditional method, indicating that the method can improve the life cycle of a multisource wireless cooperative network [21].

3.2.2. Comparison of Average Power Consumption. Take average power consumption as the experimental index, compare different methods, and the result is shown in Figure 3.

Analysis of Figure 3 shows that when the number of iterations is from 0 to 3, the average power consumption of the proposed method is not superior, even higher than that of the traditional method, but since the third iteration, the proposed method has always maintained its superiority [22]. The average power consumption is less than 3000 W, and reference [5] method has a higher average power consumption when the number of iterations is less than 12; although it is reduced later, it is still higher than the proposed method [23]. The method of reference [19] and the method of reference [20] have similar trends but still have a certain gap with the proposed method. This is because the method reduces the average power consumption of the multisource wireless cooperative network through the optimization strategy of expected energy consumption minimization, thereby improving the application effect of the method [24].

3.2.3. Comparison of Average Throughput. Taking the average throughput as the experimental index, the different methods are compared, and the results are shown in Figure 4.

TABLE 1: Experimental parameter settings.

Parameter	Value
Number of links	Article 75
Link capacity	1500 ~ 2000
Number of link requests generated	Article 100 ~ 200
Link resources between the core layer and the aggregation layer	550
Node reading	3
Service request time slot length	5 min
The number of nodes supporting the same function type	8
Number of web services generated	500
Node capacity	1000 ~ 1500

TABLE 2: Comparison of network life cycles under different methods.

Iterations (time)	Network life cycle			
	The proposed method	The method in [5]	The method in [19]	The method in [20]
10	15.52	4.31	6.47	1.58
20	14.88	5.12	6.77	1.63
30	16.96	6.09	7.09	2.45
40	16.37	6.13	7.15	2.74
50	16.10	7.25	7.78	2.82
60	17.93	8.62	8.13	3.19
70	18.52	8.96	8.74	3.25
80	18.58	9.97	9.14	3.95
90	19.69	10.78	9.19	4.05
100	20.99	10.88	9.28	4.31

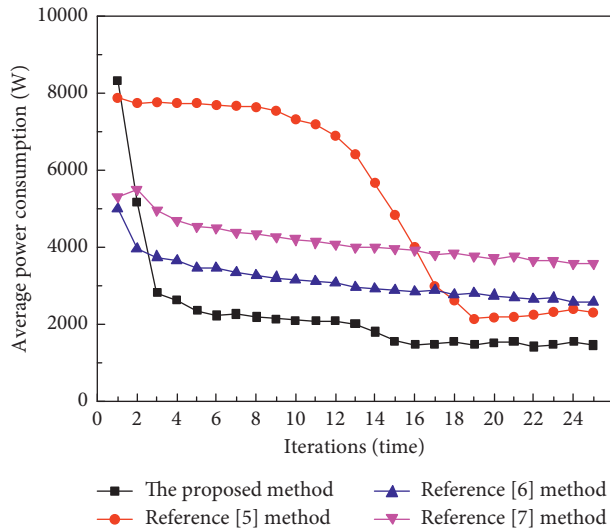


FIGURE 3: Comparison of average power consumption of different methods.

Analysis of Figure 4 shows that the average throughput of the proposed method is always higher than that of the traditional method, and its highest average throughput is close to 300 bit/s, while the highest average throughput of the traditional method is not higher than 250 bit/s. The average throughput is at a low level when the number of iterations is less than 8 times. Through comparison, it can be seen that the proposed method has significant advantages in terms of average throughput [25].

This is because the method uses the distributed opportunistic transmission scheduling method to measure the

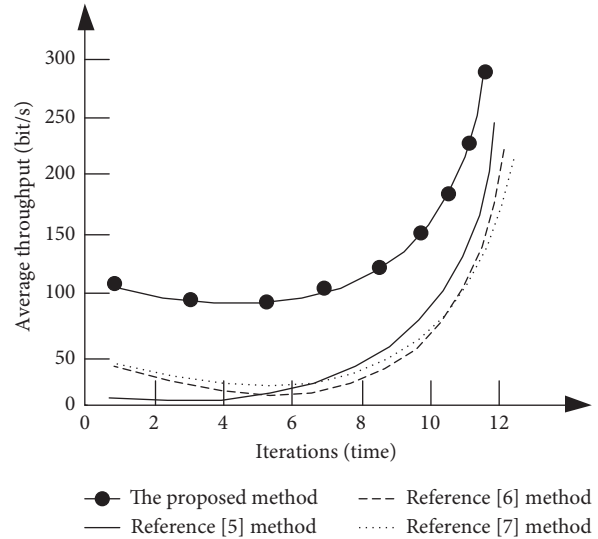


FIGURE 4: Comparison of average throughput of different methods.

energy consumption of data transmission in the multisource wireless cooperative network according to the results of the node energy consumption problem description. Research has improved the average throughput of a multisource wireless cooperative network while ensuring that the receiving terminal's received power is fixed.

3.2.4. Comparison of Average Energy Consumption per Unit Data. Taking the average throughput as the experimental index, the different methods are compared, and the results are shown in Figure 5.

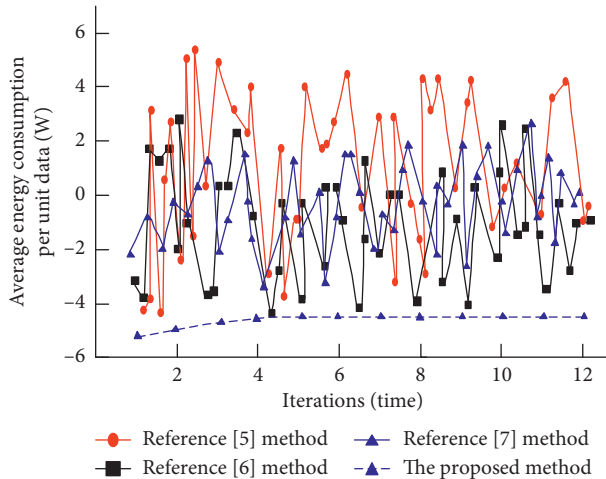


FIGURE 5: Comparison of average energy consumption per unit data of different methods.

Analysis of the results shown in Figure 5 shows that the average energy consumption per unit data of this method is significantly lower than that of the three traditional methods, and this advantage will not weaken with the increase of the number of iterations. However, the average unit energy consumption data of traditional methods show extremely irregular changes. Therefore, the average unit energy consumption data of this method can maintain a relatively stable level, which proves the effectiveness of this method.

The results show that the energy consumption of data processing in multisource wireless cooperative network is low under the proposed method; that is, the method effectively reduces the expected energy of multisource wireless cooperative network and achieves the research purpose of minimizing the expected energy.

In summary, the experimental results show that the proposed method has obvious advantages in average energy consumption per unit data and average throughput. It can optimize the energy of multisource wireless cooperative network, reduce the energy consumption, and realize the network optimization.

4. Conclusion

With the rapid development of wireless networks and data services, how to effectively manage network resources becomes more and more important. In many cases, the battery capacity of wireless devices is limited, especially in the noninfrastructure network composed of wireless devices, there is no continuous power supply, and the mobility of wireless devices reduces the opportunity of power access.

Therefore, it is of great significance to reduce the energy consumption of wireless network, and it is also an important topic to build a green network. Under this background, a design method of multisource wireless cooperative network based on multiobjective optimization is proposed, and the main results of this method are as follows:

- (1) According to the characteristics of heterogeneous distribution of multisource wireless cooperative

network, the energy consumption of nodes is described. According to the analysis results, the distributed opportunistic transmission scheduling method is used to study the energy consumption of network data transmission. This method can improve the average throughput of multisource wireless cooperative network.

- (2) Using the optimization strategy of expected energy consumption minimization, the problem of data transmission energy consumption is transformed into the problem of expected energy consumption minimization, and the mathematical model is established to obtain the optimal solution of expected energy consumption minimization.
- (3) The minimum expected energy consumption threshold is obtained by the optimal stop rule, and then the optimal solution is obtained on the constraint set of the multiobjective optimization problem by the multiobjective optimization method to complete the network expected energy minimization design.
- (4) Experimental results show that the proposed method achieves satisfactory energy-saving effect and significantly improves the network energy efficiency, which is of great significance to the research of wireless network energy efficiency.

Although the design method of this study has achieved some results, due to the limitation of research time, there are some shortcomings in the research. Therefore, in the next research, the design method of this study will be further optimized to further reduce the energy consumption of wireless networks with MIMO links.

Data Availability

The data used to support the findings of this study are included within the article.

Conflicts of Interest

The authors declare that they have no conflicts of interest.

References

- [1] L. C. Mutalemwa, S. Shin, and E. Sciubba, "Secure routing protocols for source node privacy protection in multi-hop communication wireless networks," *Energies*, vol. 13, no. 2, p. 292, 2020.
- [2] M. Mousavi, H. Alshatri, and A. Klein, "Cost sharing games for energy-efficient multi-hop broadcast in wireless networks," *IEEE Transactions on Wireless Communications*, vol. 19, no. 1, pp. 310–324, 2019.
- [3] L. T. T. Hoc, H.-S. Nguyen, Q.-P. Ma et al., "Outage and bit error probability analysis in energy harvesting wireless cooperative networks," *Elektronika ir Elektrotechnika*, vol. 25, no. 5, pp. 69–74, 2019.
- [4] A. Bhowmick, G. C. Das, S. D. Roy, S. Kundu, and S. P. Maity, "Allocation of optimal energy in an energy-harvesting

- cooperative multi-band cognitive radio network,” *Wireless Networks*, vol. 26, no. 2, pp. 1033–1043, 2020.
- [5] A. Alkhayat, A. A. Thabit, F. A. Al-Mayali, and Q. H. Abbasi, “WBSN in IoT health-based application: toward delay and energy consumption minimization,” *Journal of Sensors*, vol. 2019, no. 5, pp. 1–14, 2019.
- [6] J. C. Kwan and A. O. Fapojuwo, “Performance optimization of a multi-source, multi-sensor beamforming wireless powered communication network with backscatter,” *IEEE Sensors Journal*, vol. 19, no. 22, pp. 10898–10909, 2019.
- [7] J. Qadir, A. Khan, M. Zareei, and C. Vargas-Rosales, “Energy balanced localization-free cooperative noise-aware routing protocols for underwater wireless sensor networks,” *Energies*, vol. 12, no. 22, p. 4263, 2019.
- [8] R. M. Rizk-Allah, A. E. Hassanien, and A. Slowik, “Multi-objective orthogonal opposition-based crow search algorithm for large-scale multi-objective optimization,” *Neural Computing and Applications*, vol. 32, no. 17, pp. 13715–13746, 2020.
- [9] A. Rostamian, S. Jamshidi, and E. Zirbes, “The development of a novel multi-objective optimization framework for non-vertical well placement based on a modified non-dominated sorting genetic algorithm-II,” *Computational Geosciences*, vol. 23, no. 5, pp. 1065–1085, 2019.
- [10] K. Kaur, S. Garg, G. Kaddoum, E. Bou-Harb, and K.-K. R. Choo, “A big data-enabled consolidated framework for energy efficient software defined data centers in IoT setups,” *IEEE Transactions on Industrial Informatics*, vol. 16, no. 4, pp. 2687–2697, 2020.
- [11] D. Nguyen Quoc, L. Bi, Y. Wu, S. He, L. Li, and D. Guo, “Energy efficiency clustering based on Gaussian network for wireless sensor network,” *IET Communications*, vol. 13, no. 6, pp. 741–747, 2019.
- [12] L. M. Cruz, D. L. Alvarez, A. S. Al-Sumaiti, and S. Rivera, “Load curtailment optimization using the PSO algorithm for enhancing the reliability of distribution networks,” *Energies*, vol. 13, no. 12, pp. 3236–3251, 2020.
- [13] A. Ouali, D. Allouche, S. De Givry et al., “Variable neighborhood search for graphical model energy minimization,” *Artificial Intelligence*, vol. 278, no. 1, pp. 103194.1–103194.22, 2020.
- [14] P. Hoyingcharoen and W. Teerapabkajornret, “Expected probabilistic detection and sink connectivity in wireless sensor networks,” *IEEE Sensors Journal*, vol. 19, no. 12, pp. 4480–4493, 2019.
- [15] R. Arthi, V. Jagapathi Babu, T. Aditya, and Y. Akshay Kumar, “Queue stability and low energy for energy harvesting cognitive radio networks,” *The International Journal of Electrical Engineering & Education*, vol. 56, no. 4, pp. 338–347, 2019.
- [16] M. Liaqat, K. A. Noordin, T. Abdul Latef, and K. Dimiyati, “Power-domain non orthogonal multiple access (PD-NOMA) in cooperative networks: an overview,” *Wireless Networks*, vol. 26, no. 1, pp. 181–203, 2020.
- [17] C. Wang, “Simulation of energy hole attack suppression in non-uniform node distributed networks,” *Computer Simulation*, vol. 37, no. 4, pp. 322–326, 2020.
- [18] N. Javaid, U. Shakeel, A. Ahmad, N. Alrajeh, Z. A. Khan, and N. Guizani, “DRADS: depth and reliability aware delay sensitive cooperative routing for underwater wireless sensor networks,” *Wireless Networks*, vol. 25, no. 2, pp. 777–789, 2019.
- [19] J. S. Prashanth and S. V. Nandury, “A cluster-based approach for minimizing energy consumption by reducing travel time of mobile element in WSN,” *International Journal of Computers Communications & Control*, vol. 14, no. 6, pp. 691–709, 2019.
- [20] B. Gaujal, A. Girault, and S. Plassart, “Dynamic speed scaling minimizing expected energy consumption for real-time tasks,” *Journal of Scheduling*, vol. 23, no. 10, pp. 1–20, 2020.
- [21] F. Wen, Y. Zhao, M. Zhang, and C. Hu, “Forecasting realized volatility of crude oil futures with equity market uncertainty,” *Applied Economics*, vol. 51, no. 59, pp. 6411–6427, 2019.
- [22] J. Cao and F. Wen, “The impact of the cross-shareholding network on extreme price movements: evidence from China,” *Journal of Risk*, vol. 22, no. 2, pp. 79–102, 2019.
- [23] D. Ciuonzo and P. Salvo Rossi, “Distributed detection of a non-cooperative target via generalized locally-optimum approaches,” *Information Fusion*, vol. 36, pp. 261–274, 2017.
- [24] W.-T. Sung and M.-H. Tsai, “Multi-sensor wireless signal aggregation for environmental monitoring system via multi-bit data fusion,” *Applied Mathematics & Information Sciences*, vol. 5, no. 3, pp. 589–603, 2011.
- [25] X. Cheng, D. Ciuonzo, and P. S. Rossi, “Multibit decentralized detection through fusing smart and dumb sensors based on Rao test,” *IEEE Transactions on Aerospace and Electronic Systems*, vol. 56, no. 2, pp. 1391–1405, 2019.

Research Article

Online Learning Support Service System Architecture Based on Location Service Architecture

Yongyan Zhao ¹ and Shaonan Shan ^{2,3}

¹College of Humanities and Law, Harbin University, Harbin 150086, Heilongjiang, China

²School of Urban Economics and Public Administration, Capital University Economics and Business, Beijing 100070, China

³School of Business Management, Liaoning Vocation Technical College of Modern Service, Shenyang 110000, Liaoning, China

Correspondence should be addressed to Yongyan Zhao; zhaoyongyan@hrbu.edu.cn

Received 16 November 2020; Revised 4 December 2020; Accepted 10 February 2021; Published 26 February 2021

Academic Editor: Hsu-Yang Kung

Copyright © 2021 Yongyan Zhao and Shaonan Shan. This is an open access article distributed under the Creative Commons Attribution License, which permits unrestricted use, distribution, and reproduction in any medium, provided the original work is properly cited.

With the development of network, location-based service architecture is gradually applied to the learning support service system. The purpose of this study is to develop an online learning support system using allocation information service architecture. In this study, the 2019 year of this study was selected as a research material through an online learning support service system within six months. The system architecture of this study is the Browser/Server architecture. Based on this, we analyze the learning result data using the weight setting of the feature attribute and the learning evaluation algorithm. The results show that the improved algorithm based on location-based service architecture can get the best algorithm accuracy when the weight of the whole algorithm is about $\alpha = 0.4$. For the degree of demand for learning guidance, 16.2% thought it was absolutely necessary and 50.7% thought it was more necessary. And 70.6% of the learners thought that the learning system was not very accurate or generally accurate. It is concluded that the learning support service system of this study has a certain role. It provides a new path to improve the quality of online education learning support service and promotes the development of online education.

1. Introduction

Online education can be extended to all fields through the network, and it is very convenient to enjoy the same high level of education. Now, the education mode of “the same place at the same time” can be developed into the education mode of “different places and different times.” Online education is one of the most influential computer technology applications in modern education to establish modern education system and realize learning society. This kind of network communication technology depends on the development of distance education, especially the distance education using network, which will become the direction of education development in the future. Vocational network education system is the development of network education, is the goal of modern education technology and our education system development, and is a main direction.

Based on the measurement, collection, and analysis of the learning process data of online learner, the location-based service architecture and the learning analysis technology establish the learner model and investigate the relation between the learner’s learning characteristic, the teacher education design, and the educational performance and the data education process by establishing base. It provides a comprehensive, personalized, and efficient learning experience to the assessment, diagnosis, forecasting technology system, and learner. Learning center is a large network support and data learning process. The main purpose of this research is to establish a functional model and an evaluation system to provide intelligent and humanitarian support services from data obtained in the process of large-scale network learning and network learning.

In the research of online learning support service system, Wright MK thinks that the online course management software (OCMS) used in pure online undergraduate

courses can not meet the needs of young immature students. Moreover, he believes that these students often lack the learning skills needed to succeed in such courses, and the popular open curriculum management system does not include a warning mechanism to guide these students to successfully complete the course without face-to-face humanized guidance. He extended the design theory of information system to the design theory of vigilance online learning system by combining the relevant literature such as design theory, learning theory, decision support, and vigilance. His research can help software developers and scholars to study how to design future online learning systems for immature students. The effectiveness of his method is low [1]. Sharma et al. establish a model to understand and predict the impact of personal characteristics and e-lms quality determinants on faculty's continued use of e-lms, which is critical to the success of e-lms. A total of 219 teachers who used Moodle in his study answered the survey. They used structural equation model (SEM) to test the proposed research model. SEM results show that system quality, PI, service quality, and te have significant influence on teachers' continuous use of e-lms. In addition, all the decisive factors of the research model are used as the input of neural network model to overcome the simplicity of SEM model. Their method is not stable [2]. Woo and Lee propose a mobile group based dynamic location service (mogls), which is a scalable VANET location service. It is robust to mobility in terms of reliability and overhead. The lower layer of its service function is composed of dynamic vehicle groups with similar tracks, and one vehicle in each group acts as the lower level positioning server. The higher level is composed of fixed servers based on cell area and infrastructure. For the location update from low-level server to high-level server, they adopt the way of information aggregation. They take advantage of the characteristics of low-level servers moving with their member vehicles and propose a mechanism to reduce signaling overhead and prevent service reliability degradation caused by aggregation location update. Their method is not practical enough [3].

Atat R introduces the CPS taxonomy {via}, which provides a broad overview of data collection, storage, access, processing, and analysis. Chiaraviglio proposed a 5G network specifically for rural and low-income areas and discussed its own conclusions in three representative cases of Italy, Cook Islands, and Zimbabwe.

This paper first introduces the function division of online learning platform and divides online learning into six subsystems. Then it introduces the structure of learning support service system and the evaluation of online learning support service. The innovation points of this study are as follows:(1) based on the relevant data of online learning in 2019, the functions of online learning system based on feature attribute weight, personalized evaluation support service system, and course recommendation system based on students' interests are analyzed. (2) We compared and analyzed the recommendation algorithm, system parameters, performance, and support services of the online learning system created in this paper with those of other systems. Students can also use the online learning system

created in this article to analyze their own learning. (3) Through the analysis of the service architecture positioning of the learning system, it is found that the system can promote students' learning to a certain extent. To sum up, the online learning system created in this paper can improve the quality of online education learning support services and is conducive to the long-term development of online education.

2. Location Service Architecture and Online Learning Support Service System

2.1. Function Division of the Online Learning Platform

2.1.1. Online Learning Subsystem. The most basic educational systems include educational content, educational content, and educational content. Course focus is vividly animated in front of users. Let users understand important issues more deeply. Users can download reference materials and other information resources provided by educators [4].

2.1.2. Online Question Answering Subsystem. Users can send their questions to the system. If the answer to the question already exists in the system, it will be prompted to the user immediately. If there is no answer, the user question is first sent to the system, and the educator automatically feeds back to the user after the answer. Response mode can be 1 to 1. Only the user to question can be displayed. One to many modes can be configured and all users can view [5].

2.1.3. Online Communication Subsystem. This system provides powerful interactive features. Educational staff can set topic discussion area or questionnaire for different types of users, publish learning resource information, and answer questions online. Personal mailbox modules and reference systems can also be implemented for real time or nonreal time communication between administrators, educators, and users [6, 7].

2.1.4. Online Homework Practice and Test Subsystem. Online homework practice and test systems include automatic test paper configuration, test process control, and test result analysis. During the process of creating test paper, you can generate questions randomly or generate different papers for each user. The control test process is to automatically control the test time and deliver the paper automatically. The locking system cannot read any user tests. You can further control the test environment by weighting several problems. Analysis of test results is usually based on each question's knowledge points and user answers. To provide a specific assessment result, to propose the next step, or to perform quality analysis based on the test statistics, provide automatic change of the instant feedback function, or provide personalized feedback content based on the user's response [8, 9].

2.1.5. User Learning Record Subsystem. The system can record the user's basic learning situation, including login time, learning time, test results, main reasons and problems, and main learning chapters. The staff can query the students' learning progress and the number of times they have participated in the course [10].

2.1.6. Information Management Subsystem. The information management subsystem includes two modules: user management and learning resource management. User information management is mainly responsible for user account management. Account management sets various access rights and access levels for various types of users (managers, educators, and users). Administrators and educators can use the information resource management subsystem to manage learning resources [11, 12].

2.2. Composition of Learning Support Service System. As a subsystem of the educational system, the learning support service system itself is an organic whole and can provide learners with learning support services, in other words, to achieve effective guidance, support, and promotion of student self-discipline in order to meet the needs of students in learning. Learning together can improve the quality and effectiveness of students' learning. This is an organic whole consisting of interconnected interactive information, resources, personnel, facilities, and other support elements [13].

Information support: it points to push or release of education and consulting information related to course learning, including new courses of push, class start notices, distribution, testing, credit acquisition, authorization, and other related information. In addition, various types of consultation information are included, including course and expert selection [14, 15].

Personnel support: specifically, it mainly refers to teachers, education administrators, technical service personnel, and other subjects that have a positive impact on learning activities (guidance, answering questions, and learning consultation) in the online course learning process [16].

Resource support: here, resource support mainly refers to learning resources. This refers to all the conditions shown to learners or potentially available in the learning environment established by an education or learning system.

Support facilities and learning environment: only complete learning facilities can create an excellent learning environment. Facility services are other types of learning support services in various hardware facilities such as computers, learning spaces, and platforms for online courses such as information, resources, personnel, educational practice, and evaluation services; the material base also provides technology-based learning support [17, 18].

Learning management support: this refers to various teaching management activities, such as admission requirements, evaluation, and evaluation methods, to ensure effective learning [19].

2.3. Evaluation of Online Learning Support Services

2.3.1. Resource Click through Rate. In the process of online learning, the proportion of users of resources often reflects the degree of users' attention to specific types of resources. It counts the clearance rate of users of various types of resources in different periods of time, sorts out multiple statistical results, and forms the clearance rate time characteristic curve of specific type of resource users. Observe the number of user clicks on a specific learning resource at a specific time or the clearance rate at a specific time interval. There is a great possibility within the scope of click. For example, if the number of hits at a particular time is too low, it may be caused by the network. Users are not familiar with environmental barriers of online learning process, or users may not be interested in the learning resources provided. If the clearance rate is high, users may be very interested in learning such resources, which is very useful for users. In this way, we can provide feedback information to the information departments of medical libraries and medical literature and know what kind of education strategy to adopt in the online learning support service and know what kinds of learning resources are initially provided [20, 21].

2.3.2. Statistical Time of Online Learning. The user's learning time can reflect the user's attention to the learning support service provided in the macroview if the user clauses of the learning resources can reflect the user's attention to a particular type of learning resource. For a period of time, there is less access to the learning support service and there is no significant change in the user's online learning time. Users may not be able to enjoy online learning support because they do not pay enough attention to the service in the absence of network environments. On the other hand, learning resources are too old to help users solve the problem of using information resources. This feedback helps medical information resource providers further improve online learning support services [22, 23].

2.4. Weight of Feature Attributes in the Online Learning System

2.4.1. Establish Judgment Matrix. Consult with experts to request an evaluation of the importance of the functional attributes of the situation framework. The relative importance of the two attributes is compared in pairs. The weaker attribute is 1/9, the weaker attribute is 3/7, the weaker attribute is 4/6, and the equivalent attribute is 5/5. The shell function attribute set $A = (a_1, a_2, \dots, a_n)$, T represents the decision matrix. a_{ij} represents the relative importance value of feature attribute a_i to feature attribute a_j . Then the case feature attribute importance comparison matrix is shown in the following formula:

$$T = \begin{Bmatrix} a_{11}, a_{12}, \dots, a_{1n} \\ a_{21}, a_{22}, \dots, a_{2n} \\ \dots \dots \dots \\ a_{n1}, a_{n2}, \dots, a_{nn} \end{Bmatrix}. \quad (1)$$

2.4.2. *Weight Calculation.* Using the knowledge of linear algebra combined with the above matrix, the eigenvector corresponding to the maximum eigenvalue of T is the relative importance of each characteristic attribute, and the corresponding weight is normalized. In this system model, the total product method is used to solve the problem, and solutions are shown in formulae (2)–(4).

Normalize each column of judgment matrix:

$$\bar{a}_{ij} = \frac{a_{ij}}{\sum_{k=1}^n a_{kj}}, \quad (i, j = 1, 2, 3, \dots, n). \quad (2)$$

The normalized judgment matrix of each column is added by row

$$\bar{w}_i = \sum_{j=1}^n \bar{a}_{ij}, \quad (i, j = 1, 2, 3, \dots, n). \quad (3)$$

The vector $\bar{w} = (\bar{w}_1, \bar{w}_2, \dots, \bar{w}_m)^T$ is normalized:

$$u_i = \frac{\bar{w}_i}{\sum_{j=1}^n \bar{w}_j}, \quad (i = 1, 2, 3, \dots, n). \quad (4)$$

The $U = (u_1, u_2, u_3, \dots, u_n)^T$ obtained in turn is the eigenvector, that is, the weight value of each feature attribute of the case.

2.5. Personalized Evaluation of the Support Service System

2.5.1. *Collect Record Vector.* Each knowledge point can be evaluated with $(e^j | j = 1, 2, \dots, n)$ cognitive ability. In the question test, in order to correctly evaluate the specific cognitive ability of this knowledge point, it is marked as “1,” the cognitive ability unrelated to the question is marked as “0,” and the cognitive ability is not marked as “-1.” Learners can collect the record vector of each knowledge point by testing m exercises. The calculation formula is shown in the following formulae:

$$E^{mn} = (e^{ij} | i = 1, 2, \dots, m; j = 1, 2, \dots, n), \quad (5)$$

$$E = \begin{pmatrix} e_{11}, e_{12}, \dots, e_{1n} \\ e_{21}, e_{22}, \dots, e_{2n} \\ \dots \dots \dots \\ e_{m1}, e_{m2}, \dots, e_{mn} \end{pmatrix}, \quad (6)$$

$$e^{ij} = \{1, 0, -1\}.$$

2.5.2. *Cognitive Ability: Correct Usage Rate.* The correct usage rate of each cognitive ability was calculated by the following formula:

$$r(e^j).r(e^j) = \frac{\text{Num}_e^{ij}(1)}{(\text{Num}_e^{ij}(1) + \text{Num}_e^{ij}(-1))}, \quad (7)$$

$$(i = 1, 2, \dots, m).$$

$\text{Num}_e^{ij}(1)$ and $\text{Num}_e^{ij}(-1)$ indicate the number of correct or wrong uses of the j -th cognitive content, and then get the vector $R, R = (r^1, r^2, \dots, r^n), r^j = e(e^j) \in [0, 1]; r^j$ to represent the percentage of students' correct utilization of the j -th cognitive content. Generally speaking, this percentage should be in the range of $[0, 1]$. When $r^j = 0$, it means that the students have not mastered the j th cognitive ability of this knowledge point; when $R = 1$, it means that the students have completely mastered the j th cognitive ability of this knowledge point.

2.5.3. *Comprehensive Evaluation of Students' Knowledge Points.* According to different learning quality requirements, students can be divided into the person in charge of application, the person in charge of technology, and the person in charge of management. In the narration points, because there are various requirements for the cognitive aid skills of students in various positions, various weights can be set, and the weight matrix is used to represent the weight required by students in each position. Row I and column I indicate the weight required by the i -th student for this cognitive aid skill, as shown in the following formula:

$$W = \begin{pmatrix} W_{11}, W_{12}, \dots, W_{1n} \\ W_{21}, W_{22}, \dots, W_{2n} \\ \dots \dots \dots \\ W_{m1}, W_{m2}, \dots, W_{mn} \end{pmatrix}. \quad (8)$$

The weighted average value is used to reflect the learning of students' knowledge points, and the excellent membership degree of all tests can be obtained within the knowledge points, as shown in the following formula:

$$\text{KA} = \sum (a_j \times W_{ij}). \quad (9)$$

2.5.4. *Evaluation of Knowledge Mastery.* In addition to learning the corresponding knowledge points, students also need to improve the ability to fully use knowledge points, so they need to learn the evaluation of knowledge learning in each chapter. Here, in order to evaluate the region as a whole, the vector evaluation can be carried out through the membership relationship degree of q knowledge points, as shown below, forming an excellent $q \times n$ -dimensional evaluation matrix e : the degree of membership relationship of the q -knowledge points is shown in the following formula:

$$E^{q \times n} = \begin{pmatrix} a_{11}, a_{12}, \dots, a_{1n} \\ a_{21}, a_{22}, \dots, a_{2n} \\ \dots \dots \dots \\ a_{q1}, a_{q2}, \dots, a_{qn} \end{pmatrix}. \quad (10)$$

In this evaluation matrix e , due to the different importance of each knowledge point, the teacher places the weight of each knowledge point in the area and creates the weight vector p which is dominant in the knowledge point. The calculation method is shown in the following formulae:

$$P = (p^1, p^2, \dots, p^n), \quad (11)$$

$$\sum_{i=1}^q p_i = 1. \quad (12)$$

The weighted average algorithm is used to obtain the comprehensive average membership vector, and the calculation method is shown in

$$A_chapter_node^j = \sum (a_{ij} \times p_j), \quad (j = 1, 2, \dots, n). \quad (13)$$

In learning, when completing the exercises, the students accumulate more times, and the accuracy will also be improved. Every time we study, the average membership value of cognitive ability will change accordingly. According to the evaluation, the membership value of students' cognitive ability is close to the correct value.

2.6. Recommendation of Courses Based on Students' Interests. Information based learning courses can be determined according to several instructions in the domain, with different focuses. Therefore, it is more natural to establish interest model based on fuzziness. Students' learning actions are explored and students' family interaction mode method is applied to the learning platform.

2.6.1. Establishment of Attribute Membership Function of Curriculum. Firstly, the membership function of curriculum attributes is established. For each attribute of the course, it is described by fuzzy numbers in $[0, 1]$ interval and determined by the teacher evaluation rules: let the domain of attribute set of curriculum C be $X = \{X_1, X_2, \dots, X_n\}$, and ask m teachers, each teacher to make the estimation of membership degree for each attribute X^i ($i = 1, 2, \dots, n$). Let the j -th teacher make an estimate of $S_j(X_i)$ ($i = 1, 2, \dots, n$; $j = 1, 2, \dots, m$).

Membership can be expressed as the following formula:

$$S(X) = \frac{1}{m} \sum_{j=1}^m S_j(X_i). \quad (14)$$

2.6.2. Set Up Students' Interest Set. The collection of learning records of the course reflects the students' interest to a certain extent, which can be constructed to collect students' interest simply. Suppose that students have seen a certain kind of course in their interest. According to the course category, students' interest in this kind of course can be obtained. C is the collection of students' course learning. The calculation method is shown in formula (15), where I_k represents the student's primary interest in the k -attribute:

$$I_k = \frac{\sum_{i=1}^p (S_{Ik})^2}{p}. \quad (15)$$

3. Online Learning Support Service System Design for Location Service Architecture

3.1. Subjects. The experimental subjects are 32 students in the 19th class of digital media majors in this course and are suitable for the second semester of 2018-2019. A 19-year class 1 (32 students) is divided into eight research groups according to the direction of practice. The average number of people in each group is four (because the platform design includes a link), and four groups have been selected for experimental analysis. At the same time, all experimental subjects specialize in digital media. They have high information literacy and are easy to accept the learning methods used in this experiment.

3.2. System Design Principles. The network protocol used in the selective network distance education system of the network protocol directly affects the operating mode of the network distance vocational education system. The goal of online education design using different structures of currently used network protocols is to create an Internet based web system using the TCP/IP protocol.

The choice of cross platform operating systems has nothing to do with the platform implementation selected from the operating system platform and the choice of network online teaching. Since the most extensive and effective platform of Java technology is not dependent on applications and is an interconnection service on the Internet, system design uses Java technology development to ensure system applications between platforms.

3.3. System Work Flow. Students who want to register for the course should register through the structure of online learning support service system and become online learners after successful registration. The learners who have successfully registered their personal information need to log in to the corresponding learning online teaching login after being approved by the online teaching system. Course selection has entered online teaching, and members need to select the required learning courses. According to the different teaching arrangements, teachers can choose to browse the courseware, discuss the meeting or test in class, and start the corresponding system application program. Exit the system.

3.4. System Architecture Selection. C/S architecture has many advantages and development space in system security and reliability. The server side and application side of C/S need to design program framework. Therefore, the vulnerability of various systems is inevitable. Like other browsers, designers can use a more robust operating system on the client side. This is indeed a very good choice of network remote vocational education system, but all customers need to install client programs; installation and maintenance will become inconvenient.

In a sense, the system structure is different from C/S. First of all, the system structure of online learning support service system is usually the general structure of BS browser.

It is not the best choice to use the structure of connecting client and server in online learning support service system. Online learning support service system can help students learn online courses at different times. It is impossible to help students to learn online courses at school. It is impossible to provide a completely unified browser. In order to install and maintain the client program system, the form of developing and constructing Internet service is decided. In order to meet the needs of practical application, the network mode of BS architecture is established.

4. Online Learning Support Service System Analysis

4.1. System Parameters and Performance

4.1.1. Setting of α Coefficient Weight. In order to improve the recommendation of α value, by continuously adjusting the value of α value between $[0, 1]$, different comprehensive recommendation sets are calculated, and finally the final α coefficient weight is obtained. The algorithm evaluation under the change of α coefficient weight is as shown in Table 1.

The algorithm evaluation under the change of α coefficient weight is as shown in Figure 1.

It can be seen from Table 1 and Figure 1 that the weighted coefficient of α in the improved algorithm is 0.4. In the improved hybrid filtering algorithm, the similarity of user's location preference and distance plays an important role in the final recommendation result. After measuring MAE, the final conclusion will be drawn, in other words, location-based services. If the weight of the improved algorithm is about $\alpha = 0.4$, the best algorithm accuracy can be obtained under the framework of this paper.

4.1.2. System Encryption Performance Test. The encryption efficiency and the decryption efficiency of the three-bit plaintext encryption algorithm are tested. It can be seen from Figures 2 and 3 that, after many tests, if $e(x)$ and $E(y)$ are known, the Paillier encryption algorithm can find the $E(x+y)$ time through the additive homomorphism of Paillier public key encryption system. The consumption is small, the time consumption of encryption and decryption algorithm is similar, and the experimental data is almost unchanged, basically stable. According to the above analysis, Paillier's isomorphism is relatively stable, and the time of encrypting text operation is relatively short, which is also an advantage. The two privacy preserving schemes in this paper provide many addition and subtraction operations for encrypted text, which make full use of Paillier's advantages in encrypted text operation. The encryption algorithm performance test chart is as shown in Figure 2.

In order to evaluate the overall performance of this scheme, we test the efficiency of calculating the average

center point and the efficiency of one round iteration of geometric intermediate point. These two algorithms mainly encrypt plain text and perform sum operation on encrypted text. The average central point test chart of privacy protection is shown in Figure 3.

As can be seen from Figures 2 and 3, there is no significant difference in the trend and amplitude of the two changes. As the number of users increases, the execution time increases, but it is not as important as the previous plan. If the number of users joining the two algorithms increases, the sum of the encrypted text needs to be calculated and the sum of the encrypted text needs to be decrypted. Because the number of decrypted texts remains the same, it will not take more time to decrypt. Encrypting and adding password text will take more time. In the last test of Paillier encryption algorithm, the conclusion is that the efficiency of adding cipher text is very high, so even if the number of users increases, the operation efficiency of the two schemes is very low. It is affected by the efficiency of Paillier encryption. These costs are consistent with the theoretical results; the solution will use more encrypted text to maintain the number of decodes, greatly reducing the complexity of users and cloud server computing.

4.2. Comparison of Recommendation Algorithms for Students' Online Learning Courses. Absolute error calculation algorithm is used. The smaller the MAE value, the higher the accuracy of the algorithm. In the MAE scoring standard, the algorithm is used to solve the deviation between the predicted score and the actual score.

After the location service is imported, the user's similarity calculation results become more accurate. In the personalized recommendation results, with the increase of distance similarity and distance similarity, the overall MAE calculation results can draw more accurate conclusions in the experimental results. The MAE test results of different recommended algorithms are as shown in Table 2.

The MAE test results of different algorithms are as shown in Figure 4.

As can be seen from Figure 4, with the increase of the number of users, the performance of the improved recommendation algorithm improves when performing MAE detection. Therefore, the quality of recommendation results will be improved. In other words, the recommendation results are in line with our expectations: user's prediction results. The reason why some of the middle performance is not as good as the traditional recommendation algorithm is that many users have high similarity in a specific user group, which far exceeds the impact of location-based services on individual user differences. After importing location service data, the final recommendation result is not as good as the original algorithm. Of course, this situation can be effectively improved by constantly expanding the user base.

There is a better analysis project, better than the existing algorithm. The reason for this result is that if the data sample is insufficient, the influence of user's location information on the final result will not be reflected. A small sample of users in the same region may show very random patterns of

TABLE 1: Algorithm evaluation under α coefficient weight change.

α value	0	0.1	0.2	0.3	0.4	0.5	0.6	0.7	0.8	0.9	1
Traditional algorithm	1.41	1.33	1.21	1.20	1.11	1.06	1.01	1.06	1.20	1.21	1.40
Improved algorithm	1.61	1.51	1.11	1.01	0.91	1.01	1.01	1.11	1.22	1.31	1.56

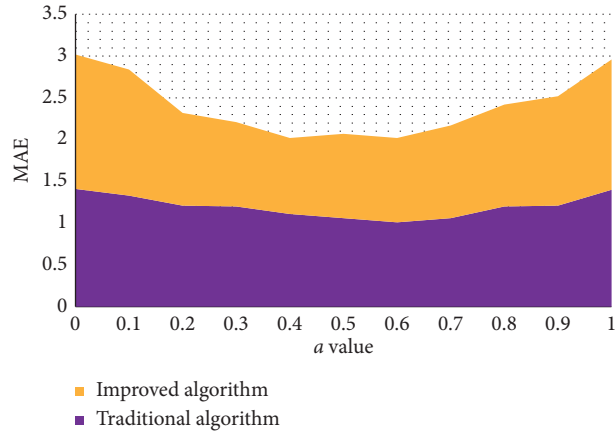


FIGURE 1: Algorithm evaluation under α coefficient weight change.

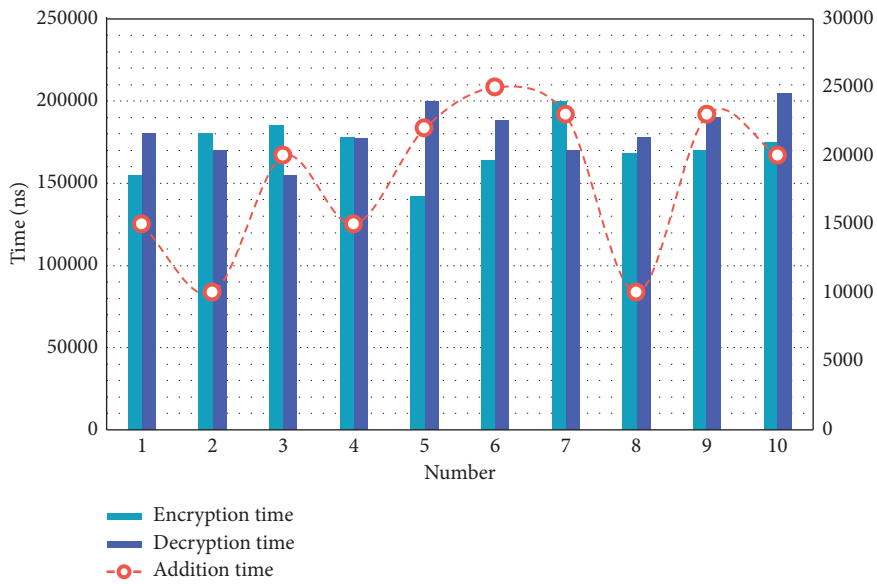


FIGURE 2: Performance test chart of encryption algorithm.

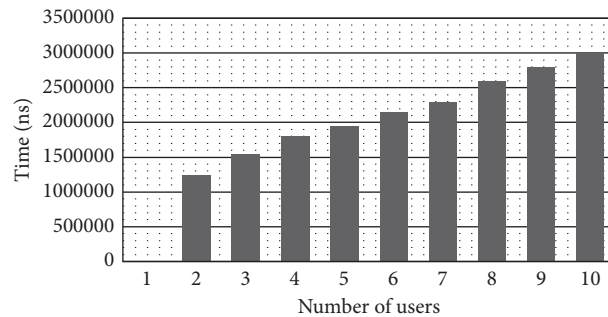


FIGURE 3: Test chart of average center point of privacy protection.

TABLE 2: MAE test results of different recommended algorithms.

Location-based service	1.41	1.38	1.37	1.38	1.40	1.31	1.28	1.22	1.02	0.88
Traditional collaborative filtering	1.31	1.26	1.21	1.10	1.02	1.02	1	0.86	0.85	0.72
Collaborative filtering of location services	1.22	1.37	1.31	1.13	1.1	1.04	1.01	0.81	0.82	0.56

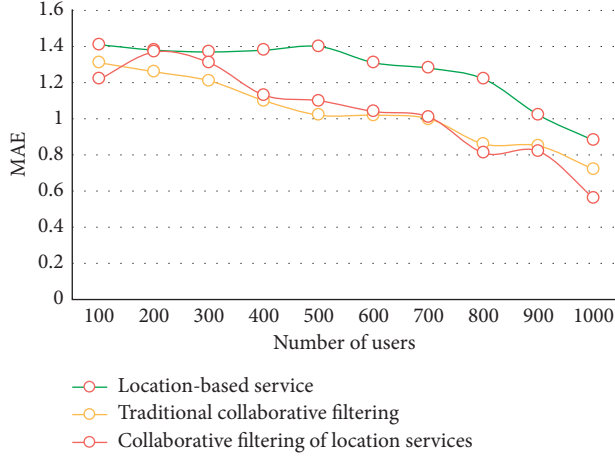


FIGURE 4: MAE test results of different algorithms.

activity over time. With the increase of users, the trajectory and mode of action represented by users as a group will become more intuitive and predictable. Therefore, when the location-based information is used as the benchmark to influence the final result, and the reliability of the algorithm is improved.

4.3. Learning Situation of Students Using the Online Learning Support Service System

4.3.1. Analysis of Students' Online Learning Behavior on the Platform. On the platform, the subjects' off campus online learning behaviors are mainly asking questions, looking for resources, and learning together. The change of the number of questions put forward by the group in the experimental cycle can reflect the changing law of the students' participation in the practice outside the campus, which is helpful for the teacher to determine the stage in which students are prone to cause problems in the process of practice. The changes of students' online learning behavior in the internship cycle are shown in Figure 5.

As can be seen from Figure 5, except Group 8 and Group 4, the peak of online learning in other groups appears in the fourth week. This shows that most groups only start to use the platform after internship. In the off campus internship, the peak of online learning action occurs in the second week, so this situation is not ideal. In addition, there was almost no difference in the number of open resources in the second, third, and fourth weeks of group 8, and the total number of open resources was the largest. Group 8 participated in the whole process of online learning. According to the previous data analysis, Group 8 of the off campus online learning action is the most ideal.

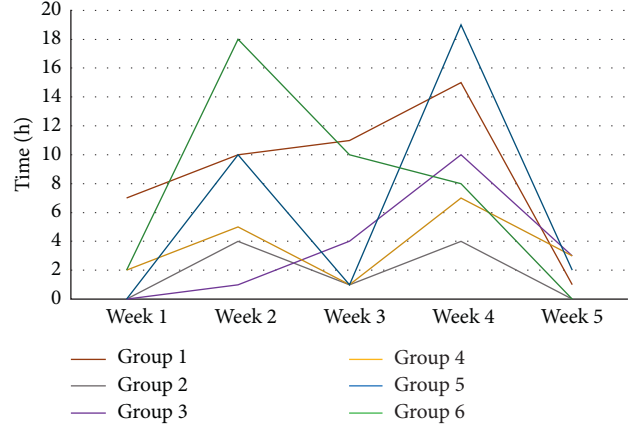


FIGURE 5: The change of students' online learning behavior in the practice cycle.

4.3.2. Analysis of Students' Access to Learning Resources through the Platform. It is similar to the change curve of students' online learning action. It can be seen that the peak of the six groups of resource access occurred in the fourth week. This shows that most groups began to invest a lot of time and energy just a week before the end of the internship. This shows that the eighth group put more energy into the whole learning process. Therefore, the group with excellent performance in joint learning thinks that it is easy to obtain resources at different stages of the group life cycle, and the difference between different stages is very small. The number of times the group visits resources changes during the learning process was as shown in Figure 6.

As can be seen from Figure 6, the fourth group has the largest number of visits to learning resources in the first week and continues to decrease in the following stages. Therefore, the off campus internship lecturer must know why to meet the members of the fourth group, thus losing the enthusiasm of the team members.

4.4. Impact of Support Services of the Online Learning System

4.4.1. Provide Learning Guidance Information Service to Guide Learners to Learn Independently. According to the survey, among the main difficulties faced by learners, 55.2% of the learners think that the learning guidance is not perfect, and 65% of the learners think that they can not make an effective learning plan. According to the survey on the realization of guidance needs, 28.8% of learners hope to provide learners with appropriate learning resources, and 24.8% of learners hope to provide clear and detailed learning objectives and timely course guidance information. The types of learning guidance are shown in Table 3.

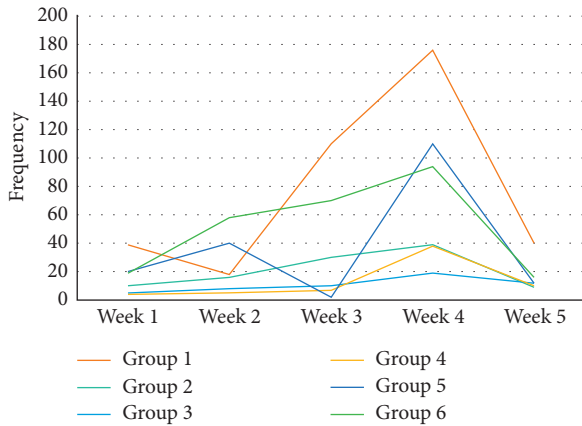


FIGURE 6: Changes in the number of times the group visited resources during the learning process.

TABLE 3: Learning needs of guidance type.

Guidance mode	Response number	Response percentage	Percentage of cases
Provide learning objective courses	85	24.8	61.9
Suggestions on learning strategies	77	23.0	57.5
Learning and retrieval guidance	76	22.3	55.2
Push appropriate	96	28.8	71.4
Other	6	1.1	3.0
Total	340	100	249

Table 3 can provide learners with learning objectives, learning strategies, and learning plans in a timely manner, help learners find out the puzzles in the learning path reasonably, and push appropriate learning resources to learners, provide portable learning guidance, and understand that the recommended items can effectively support learners to complete self-discipline learning.

4.4.2. *Provide Resources and Services to Effectively Support Learners' Learning.* This survey investigates various learning resources W and various demonstration forms of learning resources. Learners are mainly at the level of “comparative demand” for various learning resources. The most needed resources are originality display resources, learning guidance resources, teaching plan resource library, link resources, academic trends, and auxiliary tools resources. The demand for learning resources is as shown in Figure 7.

As can be seen from Figure 7, there are also various requirements for various forms of resource demonstration. The main types of resource presentation that learners (University Learning Group) like are video, animation, and graphic presentation, but the demand for pure text and pure audio is relatively low. As shown in Table 4, the preferred forms of learning resources are presented.

It can be seen from Table 4 that providing learners with rich, diversified and easy-to-use learning resources is the key to ensure effective learning. Therefore, the design and

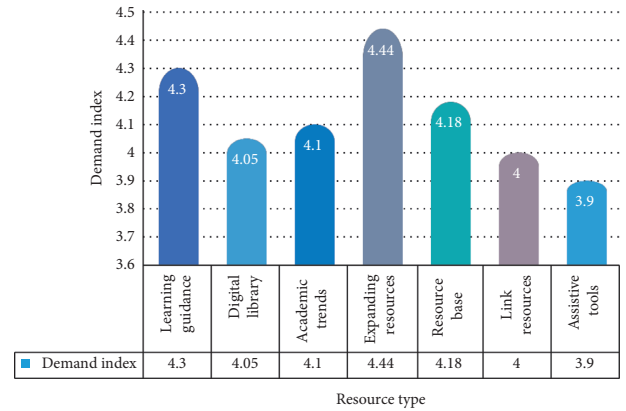


FIGURE 7: Demand for learning resources.

TABLE 4: Presentation of preferred learning resources.

Resource type	Response number	Response percentage	Percentage of cases
Word/PDF	61	18.2	44.2
Image/graphics	72	21.6	52.3
Audio frequency	33	9.3	23.6
PPT	58	17.3	42.0
Video/animation	112	33.6	81.7
Total	336	100	243.8

development of the platform should pay attention to the provision of resources to meet the learning needs of learners.

4.4.3. *Provide Assessment Services, Mobilize Learning Enthusiasm, and Objectively Evaluate Learners from the Perspective of Development.* Evaluation is an indispensable part of the learning process. For large-scale pure online learning, excellent learning evaluation support is indispensable. In order to evaluate learning effectively, learners hope to have more evaluation methods. In the survey, 27% of the learners want the learners to evaluate each other (through the display of the works), 21.4% of the learners want to get the teacher’s evaluation (due to the topic upload, etc.), 19% of the learners want to be evaluated by the computer (online test system), and 12.2% of the learners hope to provide the evaluation of the process record. Table 5 shows the evaluation method needs analysis.

Figure 8 shows evaluation method requirements.

As can be seen from Figure 8, in online learning, mutual evaluation is a method to solve many evaluation problems, and it also enables learners to learn more knowledge. However, using online surveys, the validity of the questionnaire cannot be guaranteed. Generally speaking, the cumulative proportion of incorrect learners is 70.6%. Learners think that mutual evaluation is a valuable evaluation method, and it is not advisable to use it as an evaluation method, but the correctness of evaluation is not optimistic.

TABLE 5: Demand analysis of evaluation methods.

Evaluation method	Response number	Response percentage (%)	Percentage of cases (%)
Computer evaluation	65	19.0	47.2
Mutual evaluation	92	27.0	67.0
Self-evaluation	39	11.3	28.0
Teacher evaluation	73	21.4	53.0
Electronic portfolio	33	9.1	23.6
Record evaluation	42	12.2	30.2
Total	344	100	249.0

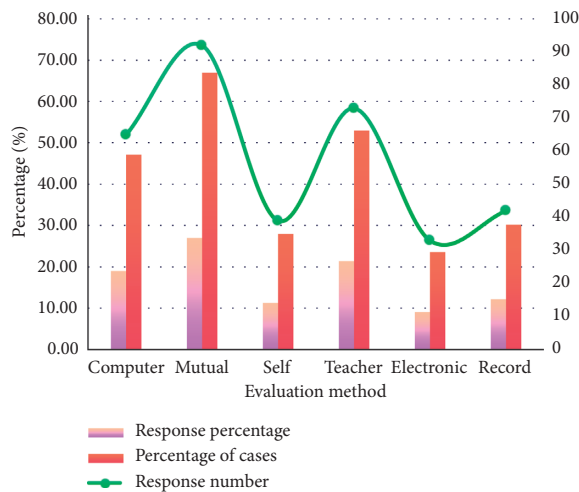


FIGURE 8: Evaluation method requirements.

Summary of methods to improve the accuracy of mutual evaluation: after mutual evaluation, teachers will randomly check, which will not only promote students' deep evaluation, but also become a good check for learners' evaluation. It can be used because the rating of evaluators is inconsistent. A group of students will evaluate it and get the average score. At the same time, the number of evaluation of learners should not be too much, so as to avoid fatigue. Before the formal evaluation, the simulated mutual evaluation is carried out, and then the learners who can evaluate each other are selected. Make detailed scoring standards, guide the details of evaluation, and make measurement benchmark. This can improve the accuracy of learners' evaluation. The platform should pay attention to anonymity and avoid improper evaluation when learners are engaged in mutual intelligent work.

5. Conclusion

In this survey, we combine the location-based service architecture with the online learning support service system, describe the data source and operation rules of the learning system, explain the data generated by the location-based service architecture and user behavior, and use the model as a new data source. It is combined into the previous recommendation algorithm. Therefore, the application of

location-based service architecture becomes more extensive, and learning system is introduced into a new research direction. The algorithm of this survey improves the content-based recommendation algorithm and uses the weighted recommendation results to increase the user's action mode weight in geographic information, location preference, and user decision making. In order to verify the weight of geographic information, this paper will compare with the traditional algorithm based on MAE method and investigate and explain the advantages and disadvantages of the new algorithm with different weights.

The system uses the real-time tracking records of students and the system and the log mining of previous visits, updates the information database of student models in time, makes decision guidance for learning process, and effectively improves the monitoring of learning progress and students' proficiency. Personalized learning system needs to objectively evaluate the basic learning situation of students and understand the learning personality of students and the ability and level that can be achieved in the learning process. In order to better combine students' learning and practical abilities, the system comprehensively considers students' various achievements in the evaluation process, so as to make a scientific evaluation of students' abilities and, at the same time, give full play to the system's personalized service function.

The learning support service system established in this paper takes learners as the center, uses big data, learning analysis, and mobile Internet technology to obtain learning process data from online education network learning platform, establishes learner characteristic model and evaluation system, and provides intelligent and humanized support services. The application of location-based service architecture in learning evaluation provides a new evaluation method and teaching evaluation method for learners. This can not only quantify and visualize the learning state of learners, but also comprehensively and objectively reflect the learning effect.

Data Availability

No data were used to support this study.

Conflicts of Interest

The authors declare that they have no conflicts of interest.

Acknowledgments

This work was supported by the Key topics in the "13th Five-Year Plan" for Education Science of Heilongjiang Province in 2020 (No. GJB1320178), the Construction and Practice of the Heilongjiang Higher Education Teaching Reform Project (No. SJGY20190409), Heilongjiang Province Education Science Planning Project (No. GDJ1215067), and Higher Education Teaching Reform Research Project of 2020 Heilongjiang Province in 2020 (NO. SJGY20200431).

References

- [1] M. K. Wright, "A design theory for vigilant online learning systems," *International Journal of Information Systems in the Service Sector*, vol. 8, no. 1, pp. 13–33, 2016.
- [2] S. K. Sharma, A. Gaur, V. Saddikuti et al., "Structural equation model (SEM)-neural network (NN) model for predicting quality determinants of e-learning management systems," *Behaviour and Information Technology*, vol. 36, no. 10-12, pp. 1–14, 2017.
- [3] H. Woo and M. Lee, "A hierarchical location service architecture for VANET with aggregated location update," *Computer Communications*, vol. 125, no. 7, pp. 38–55, 2018.
- [4] L. Chiaraviglio, W. N. Blefari-Melazzi, W. Liu et al., "Bringing 5G into rural and low-income areas: is it feasible?" *IEEE Communications Standards Magazine*, vol. 1, no. 3, pp. 50–57, 2017.
- [5] S. Birke, V. Meliciani, and V. Sabato, "Relationship lending and innovation: empirical evidence on a sample of European firms," *Economics of Innovation & New Technology*, vol. 25, no. 3, pp. 335–357, 2016.
- [6] Q. Zhang, J. D. Wu, and G. F. ZhangLiu, "A cross-domain recommender system with consistent information transfer," *Decision Support Systems*, vol. 104, no. 12, pp. 49–63, 2017.
- [7] L. Pham, R. S. Williamson, and R. Berry, "Student perceptions of E-learning service quality, E-satisfaction, and E-loyalty," *International Journal of Enterprise Information Systems*, vol. 14, no. 3, pp. 19–40, 2018.
- [8] N. Markovic, M. E. Kim, and P. Schonfeld, "Statistical and machine learning approach for planning dial-a-ride systems," *Transportation Research Part A Policy and Practice*, vol. 89, no. 7, pp. 41–55, 2016.
- [9] Y. Yang, Z. J. Xu, and T. P. QiuZhou, "Quantile context-aware social IoT service big data recommendation with D2D communication," *IEEE Internet of Things Journal*, vol. 7, no. 6, pp. 5533–5548, 2020.
- [10] J. S. Bossaller, "Service learning as innovative pedagogy in online learning," *Education for Information*, vol. 32, no. 1, pp. 35–53, 2016.
- [11] M. Pohling, T. C. Leichsenring, and T. Hermann, "Base Cube One: a location-addressable service-oriented smart environment framework," *Journal of Ambient Intelligence and Smart Environments*, vol. 11, no. 5, pp. 373–401, 2019.
- [12] M. S. D. Nadella, M. R. Vatambeti, and M. V. Bobba, "Enhanced reactive location service for packet delivery in vehicular ad-hoc networks," *International Journal of Engineering and Technology*, vol. 9, no. 4, pp. 2984–2989, 2017.
- [13] M. Ghaffari, M. H. N. Ghadiri, and M. S. Lahijani, "A peer-to-peer privacy preserving query service for location-based mobile applications," *IEEE Transactions on Vehicular Technology*, vol. 66, no. 10, pp. 9458–9469, 2017.
- [14] M.-X. Chen and F.-H. Sung, "Integrated service discovery architecture for heterogeneous networks," *International Journal of Communication Systems*, vol. 29, no. 4, pp. 772–786, 2016.
- [15] R. Gupta and U. P. Rao, "Achieving location privacy through CAST in location based services," *Journal of Communications & Networks*, vol. 19, no. 3, pp. 239–249, 2017.
- [16] J. Hyeong, S. Tae, J. Seol et al., "Proximity-based asynchronous messaging platform for location-based internet of things service," *ISPRS International Journal of Geo-Information*, vol. 5, no. 7, pp. 1–15, 2016.
- [17] M. Tao, S. W. Wei, and S. Huang, "Location-based trustworthy services recommendation in cooperative-communication-enabled internet of vehicles," *Journal of Network and Computer Applications*, vol. 126, no. 1, pp. 1–11, 2019.
- [18] T. Chen, "Creating a just-in-time location-aware service using fuzzy logic," *Applied Spatial Analysis and Policy*, vol. 9, no. 3, pp. 287–307, 2016.
- [19] V. W. Chu, R. K. Wong, C.-H. Chi, W. Zhou, and I. Ho, "The design of a cloud-based tracker platform based on system-of-systems service architecture," *Information Systems Frontiers*, vol. 19, no. 6, pp. 1283–1299, 2017.
- [20] L. Jin, K. X. Long, and J. Y.-R. JoshiLin, "Characterizing users' check-in activities using their scores in a location-based social network," *Multimedia Systems*, vol. 22, no. 1, pp. 87–98, 2016.
- [21] S. Shin, X. Guan, and B. Y. Choi, "A dynamic location management service for group applications in cellular networks," *Telecommunication Systems*, vol. 65, no. 3, pp. 1–17, 2017.
- [22] A. S. Shafiq, S. B. Lorenzo, G. Savo et al., "A framework for dynamic network architecture and topology optimization," *IEEE/ACM Transactions on Networking*, vol. 24, no. 2, pp. 717–730, 2016.
- [23] S. MacKenzie and P. Tesi, "Networked systems under denial-of-service: co-located vs. remote control architectures," *IFAC-PapersOnLine*, vol. 50, no. 1, pp. 2627–2632, 2017.

Research Article

Community Public Safety Evaluation System Based on Location Information Service Architecture

Zili Zhao 

School of Government, Peking University, Beijing 100871, China

Correspondence should be addressed to Zili Zhao; 1906389399@pku.edu.cn

Received 30 November 2020; Revised 23 December 2020; Accepted 7 January 2021; Published 28 January 2021

Academic Editor: Chi-Hua Chen

Copyright © 2021 Zili Zhao. This is an open access article distributed under the Creative Commons Attribution License, which permits unrestricted use, distribution, and reproduction in any medium, provided the original work is properly cited.

The establishment of communities is for the better operation and management of cities, and community safety has gradually become a topic of increasing concern. It is not only an important part of the community public safety system, but also the foundation of social and economic development. With the improvement of the overall economic level of society, wireless network coverage has been greatly improved, smart devices have also been rapidly developed and popularized, and location-based information service systems have gradually entered the field of community public safety. At present, my country still lacks experience in community safety management. At the same time, there is no complete set of standards and evaluation system for the public safety evaluation system of urban communities. However, community public safety involves people's livelihood issues and the stability and development of the city. Therefore, it is urgent to build a community public safety evaluation system based on the location information service architecture. Based on the safety community research and location service system, this paper uses the combination of theory and practice, quantitative and qualitative methods, and tentatively explored and constructed a community public safety evaluation system based on the location information service architecture. This article integrates location information service technology into the community public safety evaluation system, selects three indicator factors, investigates a more comprehensive evaluation subject, and combines the evaluation subject's qualitative evaluation of community public safety with quantitative evaluation through fuzzy comprehensive evaluation. This paper conducts an empirical analysis of a certain community and finds that its public safety evaluation score is 62.6232 points, which is in the "general" ranks, and it needs to be combined with the location information service system to improve the community safety issues. This study has guiding significance for ensuring community public safety and has theoretical and practical significance for community construction and development.

1. Introduction

Communities are the carriers of people's lives. With the expansion of cities, the frequency and scale of emergencies and disasters have increased rapidly, and community public safety has attracted much attention. Community public safety includes all aspects of production, life, environment, education, and so on that takes place in the jurisdiction. It is closely connected with community construction. The purpose of establishing a community public safety evaluation system is to analyze the current status of community safety management and construction and its impact on the community, so as to take effective measures to avoid losses and adverse effects.

With the development and application of wireless network technology, location-based network information services have also developed soundly. This kind of location information service is referred to as LBS for short. It means using the current positioning technology to get the location information needed and then achieve a certain purpose through the local area network to achieve a certain service. The initial LBS system is mainly used in emergency situations, can quickly locate the location information of the victim, and achieve rapid rescue operations. Now, the shaping of LBS technology can be applied to transportation, medical, military, and other fields. LBS service is context-aware and adaptable, which is what distinguishes it from traditional network services. Context awareness means that,

it can obtain any information about an entity. Taking map-based mobile services as an example, it includes user information, specific location, use time, and use purpose. Its adaptability can be divided into 4 levels: information level, technical level, user interface level, and display level.

Yu proposed a different method for colocation mining using the network configuration of the considered geographic space. The spatial colocation mode represents a subset of the spatial features, and the objects of these spatial features are usually located in a tight geographical area. For geographic context awareness of location-based services (LBS), this model is one of the most important concepts. In the literature, most of the existing colocation mining methods are used for events that occur in a homogeneous and isotropic space, and the distance is expressed as Euclidean, and the physical movement in LBS is usually constrained by the road network. As a result, the interest value of the colocation mode involving network restricted events cannot be accurately calculated [1]. Tulumello contributed to the recent discussion on the convergence/divergence of local policies on urban safety and public safety in globalization, exploring relatively localized crime prevention methods, and explaining the similarities and differences through multilevel connections. He analyzed the situational prevention, social policy, and neighboring/community policing in two “nonglobal” metropolises: in Lisbon, safety is the goal of a wide range of policies in many areas; in Memphis, social issues have become the only issues of safety and security game. Based on the political tradition, the neoliberalization of policies, the multilevel relationship between political systems, and different methods are explained. He discussed the implications of the relationship between policy and policing: the police tried to conduct social propaganda under the combination/decoupling of security and urban policies and the “task crawling” of policing (which is expected to lead to prevention work). However, it has not completely solved the practical problems of community public safety [2]. An example researched by Lapsley is that compared with Victoria, the impact and consequences of bushfires in California and the characteristics and risks of bushfires in California have many similarities, and parts of California have suffered huge lives and property damage. Property for several years in a row. In particular, the Woolsey Fire in California in 2018 destroyed most of Los Angeles and Ventura County, especially Malibu and Calabasas. Community members admitted that they lived in some of the most fire-prone areas, understand the fire. It will happen again and the result will be the same or worse. However, he only studied the safety problems caused by the environment to the public, and the research scope is too narrow for the construction of the public safety system [3].

Aiming at the status quo of the existing community public safety in our country, combined with the location information service system, this article mainly uses the fuzzy comprehensive evaluation method and the method of social investigation to study the community public safety evaluation system. Specific innovations can be summarized as follows: (1) include community residents in the scope of the evaluation subject, fully consider the subjective feelings of

community residents, and reflect the integrity of the evaluation subject; (2) this article will affect the objective factors and public safety of the community. The combination of subjective factors can more comprehensively reflect the status quo of community public safety.

2. Method of Community Public Safety Evaluation System Based on Location Information Service Architecture

The essence of community research is to conduct social survey research, so it can be applied to any social research method. The community research method must conduct investigation and evidence collection research from multiple angles, multiple dimensions, and multiple levels, including basic methodology, empirical analysis, and specific skills [4]. The basic methods are social survey method, questionnaire method, observation method, and mathematical-statistical analysis method. [5]. In the specific construction and actual evaluation of the index system, this paper uses the specific methods of fuzzy evaluation and social survey.

2.1. Social Survey Method. Social survey method is a kind of social cognition activity, which refers to obtain relevant information needed in reality through the use of survey methods such as census, sample survey, and case survey and to make research analysis reports on the data [6]. It is one of the methods commonly used in empirical research, and its investigation objects are objective facts and subjective facts. The purpose of using the social survey method in this article is to reveal the status quo of community public security through the study of community public security, find out the main reasons that affect its development, and seek ways to reform. Under the guidance of this purpose, this article chooses the method of sampling survey, which is to randomly select the part of the data from the sample population to reconstitute the sample set, then discuss the analysis results, and finally push the results from special to general and from part to overall [7].

2.2. Fuzzy Comprehensive Evaluation Method. Fuzzy comprehensive evaluation method is a mathematical model that uses specific methods of fuzzy measurement, fuzzy statistics, and fuzzy evaluation in the process of calculation. It can be used to solve the evaluation problem of a fuzzy phenomenon [8]. The theoretical methods of sets and fuzzy mathematics can be used to digitize the fuzzy quantity in practice for quantitative evaluation. It has extremely wide applications in multifactor evaluation problems. In actual work, certainty and uncertainty often appear. Uncertainty phenomenon has random uncertainty and fuzzy uncertainty and the latter is difficult to solve with precise mathematics; so effective exploration must be carried out with the help of method theory in fuzzy mathematics to solve the problem of fuzzy uncertainty [9]. Fuzzy and uncertain phenomena can be seen everywhere in industrial production, corporate management and other production, and social practices. It effectively applies the theory of fuzzy mathematics to practical

problems and has the characteristics of simple method and wide application. It mainly includes a single-factor set evaluation and multilayer factor set evaluation methods [10].

2.2.1. Single-Factor Set Evaluation Method. Set factor set $U = \{U_1, U_2, \dots, U_n\}$, judging set (decision set) $V = \{v_1, v_2, \dots, v_n\}$, and weights $A = \{a_1, a_2, \dots, a_n\}$. Single-factor evaluation is as follows:

$$U_i | \longrightarrow f(U_i) = (r_{i1}, r_{i2}, \dots, r_{im}), \quad i = 1, 2, \dots, n. \quad (1)$$

The single-factor evaluation matrix is

$$R = \begin{pmatrix} r_{11} & r_{12} & \cdots & r_{1m} \\ r_{21} & r_{22} & \cdots & r_{2m} \\ \cdots & \cdots & \cdots & \cdots \\ r_{n1} & r_{n2} & \cdots & r_{nm} \end{pmatrix}. \quad (2)$$

Take the max-min composite operation to get a single-factor evaluation

$$B = A \cdot R = (b_1, b_2, b_3, \dots, b_m), \quad (3)$$

among them,

$$b_j = \bigvee_{i=1}^n (a_i \wedge r_{ij}), \quad j = 1, 2, \dots, m. \quad (4)$$

Normalize B in Equation (2). If the judgment set is expressed in quantification, that is, $V = (k_1, k_2, \dots, k_m)^T$. Then, the total score for a single-factor is $(b_1, b_2, \dots, b_m)(k_1, k_2, \dots, k_m)^T$.

2.2.2. Multilayer Factor Set Comprehensive Evaluation Method. First, put the total factors together $U = \{U_1, U_2, \dots, U_n\}$, split into a multilevel factor set, and then, starting from the highest level, use the single-factor set evaluation method in the above method for layered evaluation, and finally, get a comprehensive evaluation B. Normalize B, and if the evaluation set is expressed in quantification, then the comprehensive evaluation total score of the multilayer factor set can be obtained.

Generally speaking, the application of the fuzzy evaluation method is mainly to establish the evaluation matrix and establish the weight and the comprehensive evaluation result. The index system established in this paper is divided into three levels. The next level is the refinement of the previous level. Therefore, this paper adopts a multilayer factor set comprehensive evaluation method [11].

2.3. Community Public Safety Evaluation Method Based on Location Information Service Technology. The basis of location-based information services is the high-speed and efficient collection and reading of location information. The positioning technology mainly includes the following three types: satellite positioning technology, network-based positioning technology, and perception positioning technology [12].

Satellite positioning technology refers to the technology that reads data through artificial satellites in space after selecting objects and finally transmits specific positioning information [13]. Its typical representative technology is GPS. It can locate the target object through the three coordinates of longitude, latitude, and height forming a three-dimensional information network. Other improved technologies include differential GPS technology and assisted GPS technology [14]. In general, GPS will be hindered by physical objects such as buildings, resulting in inaccurate positioning accuracy.

Network-based positioning technology is based on a network base station to determine the location information of a target object. In an area covered by a network, when the target object is sensed using a mobile terminal device, the network base station will automatically calculate the object. The specific location information is typically a mobile base station (such as GSM and CDMA). Therefore, this positioning technology is very dependent on the number and coverage of network base stations. In addition, you can also rely on a wireless local area network for positioning, such as Wi-Fi. The accuracy of this method largely depends on the number and location of reference points selected [15, 16].

Perceptual positioning technology refers to the installation of sensors in a certain space in advance, as long as a moving object enters its area, its location information can be located, a typical representative is radio frequency identification technology (RFID). The area where RFID is used is very small, so it is only suitable for short-distance identification and indoor positioning, and more consideration needs to be given to indoor space planning and design [17].

The representative technologies of the three positioning technologies are shown in Figure 1.

3. Experiment on Community Public Safety Evaluation System Based on Location Information Service Architecture

3.1. LBS Middleware Model

3.1.1. Content-Based Model. In this model, a group of events can be regarded as a group of attributes (or called a pair), and the behavior of a subscription request is a predicate related to the event. When an event occurs, it will automatically check all the predicates that made the request. If it is determined that the predicate is true, the event can be sent to the users who need it. Because this model is too simple, there is no program to save historical records or historical subscription requests [18].

3.1.2. Model Based on Topic Space. The focus of this model is the subject space, which is equivalent to a multidimensional space body, which can be divided into various dimensions and defined. A dimension is a primitive ancestor $d = \{\text{name, type}\}$ (name represents a unique identifier and type represents the selected data type). Compared with the previous model, this model can retain published information well and supports real-time status publishing of subscribers

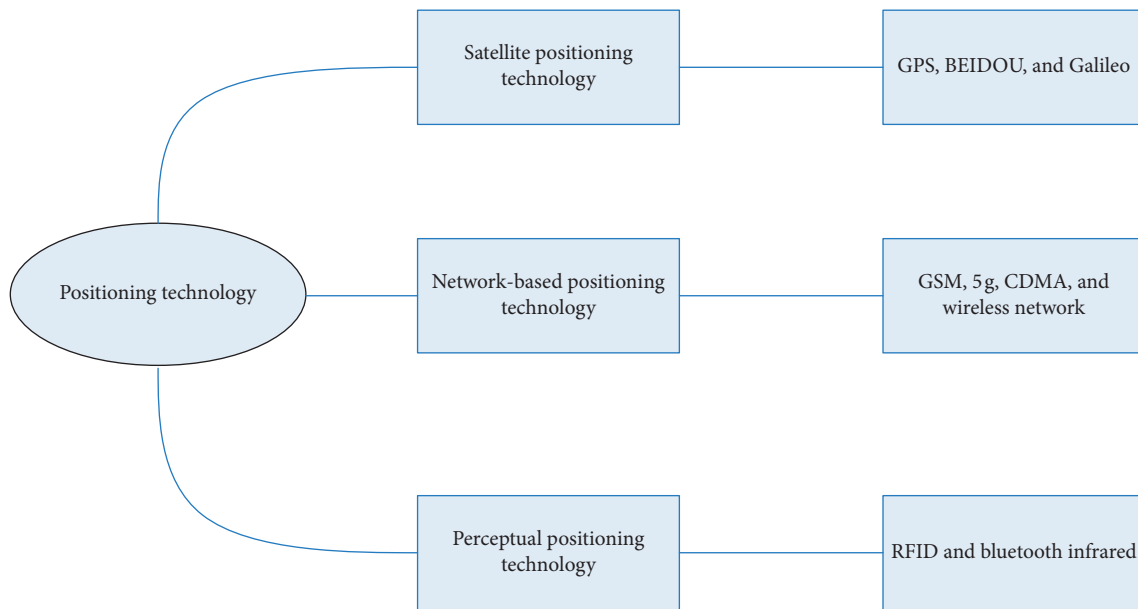


FIGURE 1: Representative techniques of the three technical methods.

[11]. This model can improve the matching degree of information and reduce the frequency of sending information multiple times.

3.1.3. Meta-Ancestral Space Model. This model is essentially a collection of many ancestors, which contains a vector of multiple values. Its application range was first in the field of parallel programming, used to coordinate events and issue execution tasks [19]. The communication in each event is carried out in a primitive space, which is composed of multiple tasks, and the communication is completed by changing or adjusting the values. Normally, each task is independent and decentralized. Therefore, if you want to achieve real-time communication between tasks, you must wait for a response between task A and task B. Using the meta-ancestral space model in the LBS system, the publisher and receiver of the information can well complete the real-time communication in the meta-ancestral space.

3.2. Construction of Community Safety Evaluation System. The construction of a set of evaluation systems involves the subject of evaluation, evaluation content, evaluation method, and evaluation process. The construction of the community public safety evaluation system, combined with the characteristics of community organizations and the needs of urban community public safety, discussed the above aspects.

3.2.1. Composition of the Main Body of Community Safety Evaluation. Generally speaking, the evaluation subject related to the community generally consists of four parts, one is experts and scholars, social intermediary organizations; the second is quasi-community management organizations such as community residents committees and property

management companies; the third is government departments represented by streets; the fourth is community residents' organizations [20]. It can be seen from the composition of traditional subjects that individual residents have not received due attention, which also shows that the current community evaluation indicators are still focused on objective aggregate indicators, while the subjective factors of community residents have not been given due attention. This article adds community residents who can be the subject of community safety evaluation as the subject of evaluation, mainly referring to the permanent population of the community.

The social significance of taking residents as the main body of community public safety evaluation lies in (1) improving the residents' participation evaluation mechanism and reflecting the harmonious atmosphere of the community. Residents use their identities, rights, and qualifications to participate in community public safety management affairs, which can enable residents to have a deeper sense of ownership, and at the same time can resolve social conflicts of interest and build a harmonious society [21]. (2) Exploit the resources of community residents and improve the community prevention network. The awareness of the main body of community residents is awakened, which is equivalent to maximizing the resources of community residents. Community residents can be regarded as the axis of community security, building a community prevention network, and returning the power of community crime control to the community. (3) Integrate into the community public safety management system and develop self-defense. The safety management of individual community residents is mainly to develop self-defense, that is, to strengthen doors and windows, properly keep cash and valuables, and implement various safety precaution systems. The purpose is to improve the portal's ability to defend against criminal activities [22, 23].

3.2.2. *Principles and Characteristics of Community Safety Evaluation Index System.* The purpose of establishing the evaluation index system is to have a comprehensive description and evaluation of the state of public safety in urban communities. Therefore, when constructing a community public safety evaluation system, certain basic principles should be followed, and at the same time, the characteristics of public safety evaluation should be reflected [24].

On the basis of an in-depth understanding of the basic connotation of community public safety, a large number of references and actual surveys show that the construction of an urban community public safety indicator system should follow the following principles:

- (i) First, the system principle. The indicator system consists of 3 secondary indicators and 21 tertiary indicators. These 24 indicators form a system, interact with each other, and their selection has a certain purpose [25].
- (ii) Second, the principle of typical indicators. When selecting indicators, this article strives to use a small number of core indicators to reflect the key content, so as to reduce the energy dispersion of the evaluation subject [26].
- (iii) Third, the operational principle. When selecting the public safety evaluation indicators of urban communities, this paper pays attention to the availability of data and descriptive information of the indicators, which has great application value.

The community public safety evaluation index system established in this article has the following three characteristics:

- (1) *Comprehensiveness of evaluation indicators:* As mentioned above, since the elements of urban communities include subjective and objective elements, if we want to evaluate community public safety, we must start with the subjective and objective elements of the community. The objective elements in 1 refer to the facilities, management system, community culture, and so on of community public safety; the subjective elements refer to people's psychological feelings and values. This article combines the two organically to fully reflect the status quo of community public safety.
- (2) *Comprehensiveness of evaluation subject:* On the basis of the previous evaluation subjects of community work, that is, experts, scholars, and intermediary organizations, community residents committees and property companies, neighborhoods and the Ministry of Civil Affairs, and community residents organizations, individual community residents are included in the scope of the evaluation subjects. The direct participation of residents in the evaluation of community public safety not only makes the subject of community public safety evaluation more comprehensive, but also makes the evaluation of community public safety more realistic.

- (3) *Composition of community safety evaluation index system*

Drawing lessons from the research results of "safe communities," "disaster reduction communities," "community public security," and "community policing" and using the above-mentioned index selection methods, this paper initially established a community public safety index system based on the location information service architecture, as shown in Table 1. This article mainly considers the safety of residents living in the community and the impact of various activities and events in the community on the safety of residents. And based on the location information service system, community residents are regarded as one of the important subjects of community public safety evaluation to evaluate the status quo of community public safety.

4. Community Public Safety Evaluation System Based on Location Information Service Architecture

4.1. *Community Public Security Situation Analysis.* According to the foregoing, this study uses sample surveys and questionnaires to collect qualitative data. According to the content of the research, a questionnaire was drawn up, and with the assistance of the neighborhood committee of the community, the public safety status of the community was investigated. A total of 500 questionnaires were distributed and 480 valid questionnaires were returned. The distribution ratio is 10 copies for community neighborhood committees, 10 copies for community police officers and security guards, 5 copies for community property companies, 10 copies for community residents' organizations, 5 copies for district units, and a total of 440 copies for ordinary residents based on households. The evaluation subjects involve quasi-community management organizations, community residents' organizations, district units, and ordinary residents, and community residents account for more than 85% of the evaluation subjects. The quantitative data of this study include data on various accidents and social security incidents in the community, provided by the neighborhood committee of the community. In the five years from 2015 to 2019, a summary of public safety incidents caused by various subjective and objective factors in a community is shown in Table 2.

4.2. *Weights of Community Public Safety Evaluation Indicators.* Weight is a relative concept, which refers to a certain index. The weight of a certain index refers to the relative importance of the index in the overall evaluation, and the weight setting of the public safety evaluation index of urban communities reflects the importance of the index in the process of achieving the goal of community safety. The weight ratios of different factors selected in this paper are different. As shown in Table 3, they are mainly determined by a comprehensive method combining expert judgment and fuzzy judgment.

TABLE 1: Community public safety evaluation index system.

Secondary indicators	Level three indicators	Evaluation method
Public safety perception	Community public order	Questionnaire
	Familiarity of community residents	Questionnaire
	Goodness of community property management	Questionnaire
	Community traffic, greening, and other environmental goodness	Questionnaire
	Community education, commerce, medical, health, and other supporting facilities are good	Questionnaire
	Population mobility rate	Questionnaire
	Police (security) working methods	Questionnaire
	Good police management	Questionnaire
Nonhuman factors	Subjectively perceived degree of criminal threat	Questionnaire
	Frequency of earthquakes and volcanoes	Data review
	Frequency of meteorological disasters	Data review
	Frequency of mudslides	Data review
Human factors	Frequency of accidental injuries	Data review
	Frequency of public security incidents	Data review
	Food and drug hygiene and safety	Data review
	Water area safety	Data review
	Drinking water safety	Data review
	Probability of infectious disease incidents	Data review
	Suicide incidence	Data review
	Incidence of domestic violence	Data review
Domestic water, electricity, and gas safety	Data review	

TABLE 2: Statistics of public safety incidents that occurred in a community from 2015 to 2019.

Index	Occurrence frequency	Evaluation
Frequency of public security incidents	14 cases, including 8 burglaries (4 criminal cases)	D
Food and drug hygiene and safety	0	A
Water area safety	0	A
Drinking water safety	0	A
Probability of infectious disease incidents	0	A
Suicide incidence	0	A
Incidence of domestic violence	2 cases filed at the police station	A
Domestic water, electricity, and gas safety	2 cases	D
Frequency of earthquakes and volcanoes	0	A
Frequency of meteorological disasters	0	A
Frequency of mudslides	0	A
Frequency of accidental injuries	0	A

It can be seen from Figure 2 that the evaluation indicators we have selected are different in their importance to the public safety of urban communities. In order for the evaluation indicators to truly and accurately reflect the status quo and management level of community public safety, different indicators give different weights.

It can be seen from Table 4 that the community public safety objective indicator comment set we made was evaluated based on the range of casualties that occurred within five years. It is undeniable that there are indeed some uncertain factors, such as unregistered casualties.

It can be seen from Figure 3 that the distribution of community public safety evaluation grades is ABCD four grades, based on the number of deaths and the number of casualties in five years.

4.3. Results of Community Public Safety Evaluation System Based on Location Information Service Architecture. This

study defines the “A” level full score as 100 points, and the formula $b_j = (n + 1 - j) \times 100/n$ ($j = 1, 2, \dots, n$). Using the arithmetic scoring method, we get 75 points for “B” level, 50 points for “C” level, and 25 points for “D” level. Using the principles mentioned above, through program calculation, the scores of the three-level indicators of the community public safety evaluation are shown in Tables 5–7. After calculating the three-level indicators, the scores of the second-level indicators are obtained, as shown in Table 8.

The subjective perception of community public safety includes three levels of indicators. As shown in Table 5 and Figure 4, there are community public order indicators, community greening indicators, and sanitary environment indicators. Among them, the sanitary environment index scored the highest, 88.57 points, because the community is located on the mountain, has a very good advantage, and do a good job in air purification and hygiene maintenance. The residents of the community have relatively good social relations. The residents living in it are familiar with their

TABLE 3: Community public safety index weight table.

First level indicator	Secondary indicators	Weights	Level three indicators	Weights
Community public safety	Public safety perception	0.28415	Community public order	0.1526
			Familiarity of community residents	0.084948
			Goodness of community property management	0.11482
			Community traffic, greening and other environmental goodness	0.12009
			Community education, commerce, medical, health, and other supporting facilities are good	0.1012
			Population mobility rate	0.052438
			Police (security) working methods	0.12009
			Good police management	0.13635
			Subjectively perceived degree of criminal threat	0.11746
			Frequency of earthquakes and volcanoes	0.25226
	Nonhuman factors	0.27388	Frequency of meteorological disasters	0.28675
			Frequency of mudslides	0.20492
			Frequency of accidental injuries	0.25607
			Frequency of public security incidents	0.12696
			Food and drug hygiene and safety	0.16722
			Water area safety	0.10593
			Drinking water safety	0.16722
			Probability of infectious disease incidents	0.14798
			Suicide incidence	0.048227
			Incidence of domestic violence	0.088488
Human factors	0.44197	Domestic water, electricity, and gas safety	0.14798	

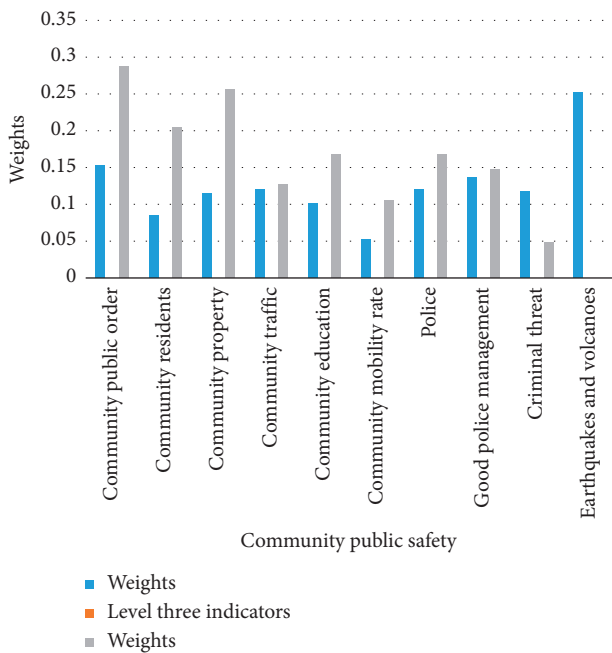


FIGURE 2: Statistics of public safety incidents that occurred in the community from 2015 to 2019.

TABLE 4: Comment collection of objective indicators of community public safety.

Evaluation item level (number of occurrences within five years)	Comments
1-3 (no casualties)	A
4-7 (casualties < 3)	B
8-12 (casualties < 5)	C
13 times or more (casualties > 6)	D

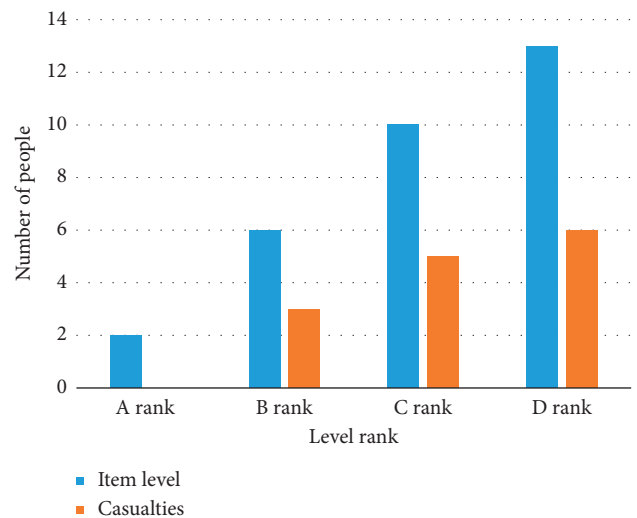


FIGURE 3: Comment collection of objective indicators of community public safety.

neighbors and can take care of each other. The population mobility rate in the community is relatively small, and most of them are permanent households. The various supporting facilities in the community are not particularly satisfactory. In addition, there may be some community residents who do not agree with the working methods of the community police or security guards are not satisfied with their work efficiency, etc., but can still maintain a good relationship with the police or security guards and can provide cooperation. The more prominent problem is that the community's property management status is not satisfactory, and the score is the lowest, only 56.38 points. Therefore,

TABLE 5: Community public safety survey score sheet.

Level three indicators	Scores
Community public order	77.03
Familiarity of community residents	73.92
Goodness of community property management	56.38
Community traffic, greening and other environmental goodness	88.57
Community education, commerce, medical, health, and other supporting facilities are good	64.30
Population mobility rate	75.67
Police (security) working methods	68.89
Good police management	75.52
Subjectively perceived degree of criminal threat	86.33

TABLE 6: Community public safety survey score sheet—nonhuman factors.

Level three indicators	Scores
Frequency of earthquakes and volcanoes	100
Frequency of meteorological disasters	100
Frequency of mudslides	100
Frequency of accidental injuries	100

TABLE 7: Community public safety survey score sheet—human factors.

Level three indicators	Scores
Frequency of public security incidents	25
Food and drug hygiene and safety	100
Water area safety	100
Drinking water safety	100
Probability of infectious disease incidents	100
Suicide incidence	100
Incidence of domestic violence	100
Domestic water, electricity, and gas safety	25

community residents' associations, property companies, and related departments should start from the aspects of hardware and environment and strive to meet the needs of community residents in this regard, so that they can feel more secure.

It can be seen from Table 6 that events caused by nonhuman factors have the least impact on community public safety, and the scores are all within the range of "A." However, the community is located in a mountainous area. If the mountain forest is not well protected, it is very easy to cause soil erosion, which will lead to the occurrence of mudslides. Although the evaluation score is still "A," it is necessary to pay attention to preventive measures. Through interviews, it is learned that the community has no disaster emergency plan and no training or education of community residents on relevant content. Therefore, early warning and education mechanisms for preventing meteorological and other disasters should be established and improved as soon as possible. In addition, the establishment of LBS for emergency situations can issue rescue at the first time when natural disasters occur, remove all obstacles through location information services, and use RFID technology to send signals of different frequencies to quickly locate community

residents, bringing huge benefits to the public sense of security.

There are 8 man-made factors that affect the public safety of the community. It can be seen from Table 7 that the frequency of public security cases is relatively high. At the same time, there are great hidden dangers in the safety of household gas and electricity. It can be considered to strengthen the LBS location information service, mark the location based on areas where public security incidents frequently occur, upload the information to the cloud platform to strengthen security patrols in the area, and reduce the occurrence of security accidents. At the same time, according to RFID technology, the safety of water, electricity, and gas use in residents' homes is detected, hidden dangers are investigated, and the frequency of accidents is reduced.

It can be seen from Table 8 that the public safety perception of the community is 63.7152 points, nonhuman factors are 100 points, and human factors are 65.8560 points. The comparison of the three is shown in Figure 5. On the basis of the existing secondary index scores, it can be calculated that the community's public safety evaluation score is 62.6232 points, that is, the community's public safety status is "average."

The previous explanation of the uncertainty of human factors supporting data can be used to explain the uncertainty of nonhuman factors data. In urban communities, it is unrealistic for the number of accidental injuries to be "0." Accidental injuries may have occurred. However, because the incident is within the scope of a minor incident, the residents have not filed with the police station in the jurisdiction or notified the neighborhood committee, so it is acceptable. Its evaluation score is "A." Among the three secondary indicators, the evaluation subject believes that human factors are the biggest cause of community public safety incidents. The public safety perception score is 63.7152, but the "subjectively felt criminal threat" score is 86.33. This outstanding comparison shows that community residents are more satisfied with the safety of the community, but there are still greater hidden dangers.

In general, this community belongs to the "general" ranks of the current public safety. In the future construction, we should focus on strengthening the construction of location information services, strengthening the connection between the police platform and the mobile information platform, strengthening the upload and output of cloud data,

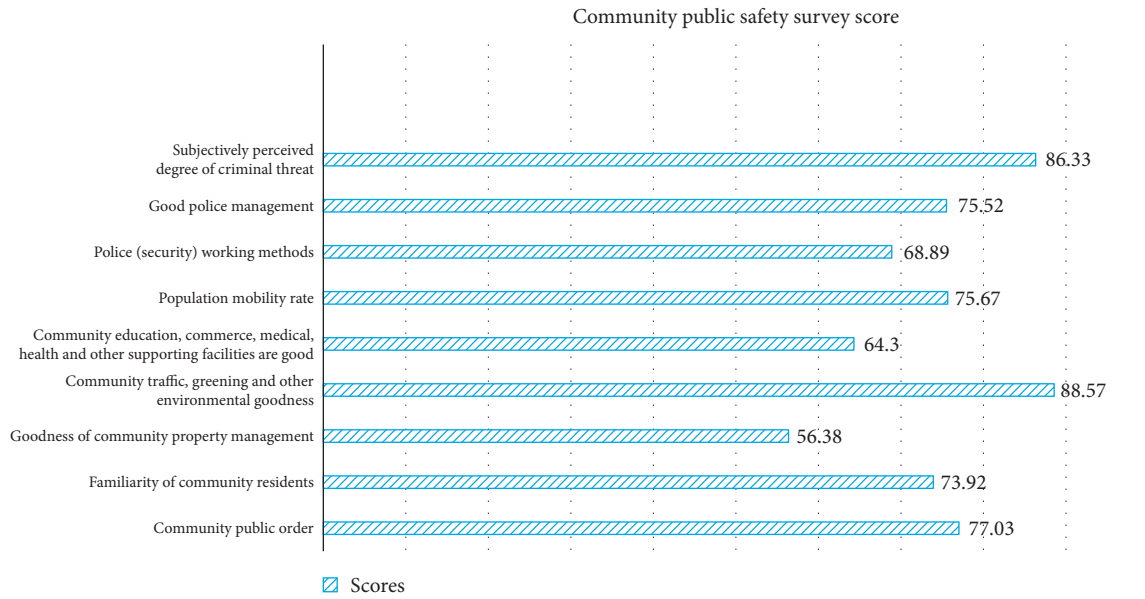


FIGURE 4: Community public safety survey score.

TABLE 8: Community public safety survey score—secondary indicators.

Secondary indicators	Scores
Public safety perception	63.7152
Objective factors	100
Subjective factors	65.8560

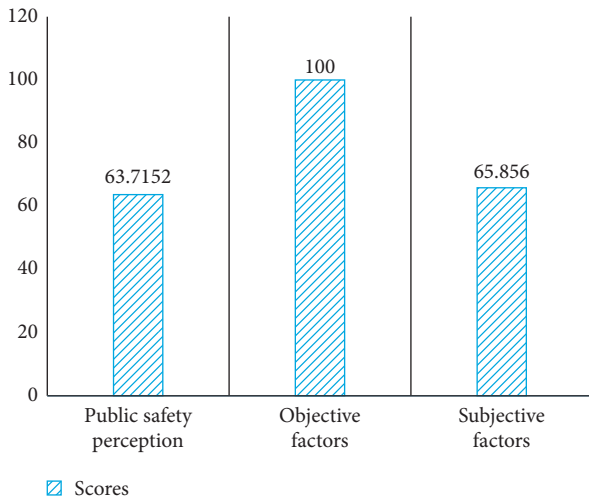


FIGURE 5: Community public safety survey score—secondary indicators.

and improving the police. The work efficiency of administrative staff ensures the safety of community residents and reduces the loss of community residents. At the same time, the role of the property company should also be played to supervise its truly responsible services for residents, so as to gain more support from community residents and improve the sense of security and happiness of community residents.

5. Conclusions

This article mainly studies the community public safety evaluation based on the location information service structure. Through the combination of theory and practice, qualitative and quantitative research, LBS model, and community public safety evaluation system are established. The importance and feasibility of adding location information services to security construction.

This article mainly adopts the social survey method, fuzzy comprehensive evaluation method, and community safety evaluation method that joins LBS location information service and incorporates residents into the evaluation subject, which fully reflects the subjectivity of community residents and encourages residents to truly participate in the community. Safety construction is coming.

The shortcomings of this article are (1) the location information service architecture is still in the development stage. Although the location information of residents can be obtained, there are also security and privacy issues. The issue of how to protect users' social privacy remains to be resolved. (2) Due to the limitations of funds, time, and energy, the number of questionnaires issued this time is limited and the coverage rate is not high enough. (3) Because the sampling survey method and questionnaire survey method are adopted and no in-depth interviews are conducted, the evaluation subjects' understanding of the questionnaires is inconsistent, resulting in the result contains uncertain factors.

Data Availability

No data were used to support this study.

Conflicts of Interest

The author declares no conflicts of interest.

Acknowledgments

This project was entrusted by enterprises and institutions of Peking University (“Research on the management mode innovation of community public security service in China” research findings, Project no: 2019002514 and Project leader: Hengxue Huang).

References

- [1] W. Yu, “Spatial co-location pattern mining for location-based services in road networks,” *Expert Systems with Applications*, vol. 46, pp. 324–335, 2016.
- [2] S. Tulumello, “The multiscale nature of urban security and public safety: crime prevention from local policy to policing in Lisbon (Portugal) and Memphis (the United States),” *Urban Affairs Review*, vol. 54, no. 6, pp. 1134–1169, 2017.
- [3] C. Lapsley, “Public safety is a shared responsibility,” *Asia Pacific Fire Magazine*, vol. 70, pp. 38–40, 2019.
- [4] W. Zhou, J. Hou, W. Fan et al., “A location-based marine fishery information service based on BeiDou navigation satellite system,” *Journal of Intelligent and Fuzzy Systems*, vol. 37, no. 4, pp. 1–8, 2019.
- [5] T. Kim, “A study on the security technology of the location based tourism information service,” *Journal of the Korea Society of Digital Industry and Information Management*, vol. 12, no. 2, pp. 25–29, 2016.
- [6] L. Niu, “Adaptive aggregation service for indoor location information using cloud,” *Computer Speech & Language*, vol. 5, no. 4, pp. 341–362, 2016.
- [7] S. S. Kashi, “A load balanced location service for location information management of multi-sink wireless sensor networks,” *Computing*, vol. 100, no. 2, pp. 1–25, 2017.
- [8] L. Chen, F. Xie, Z. Zheng, and Y. Wu, “Predicting quality of service via leveraging location information,” *Complexity*, vol. 2019, Article ID 4932030, 16 pages, 2019.
- [9] R. Rajadurai, K. S. Gopalan, M. Patil, and S. Chitturi, “Enhanced interworking of LTE and wi-fi direct for public safety,” *IEEE Communications Magazine*, vol. 54, no. 4, pp. 40–46, 2016.
- [10] R. C. Eric, “Microgrids in Maryland: bolstering public safety, community resiliency,” *District Energy*, vol. 104, no. 3, pp. 12–16, 2018.
- [11] A. M. Zambrano, X. Calderón, S. Jaramillo, O. M. Zambrano, M. Esteve, and C. Palau, “3—community early warning systems,” *Wireless Public Safety Networks 3*, Elsevier, Amsterdam, Netherlands, pp. 39–66, 2017.
- [12] A. A. Alkheir and H. T. Mouftah, “10—Cognitive radio for public safety communications,” *Wireless Public Safety Networks 2: Applications and Uses*, Elsevier, Amsterdam, Netherlands, pp. 295–316, 2016.
- [13] J. Cohen, M. Reddish, and N. Zimbelman, “APCO recognizes leaders in public safety communications,” *Public Safety Communications*, vol. 84, no. 3, pp. 11–13, 2018.
- [14] J. Cohen, “Recognizing leaders in public safety communications,” *Public Safety Communications*, vol. 82, no. 3, pp. 11–12, 2016.
- [15] J. L. Beatty, “Medical privacy vs. Public safety?” *Aerosafety World*, vol. 11, no. 3, p. 1, 2016.
- [16] G. Bhawnani, “Rule of the “lawless law” detentions under the public safety act in Kashmir,” *Economic and Political Weekly*, vol. 53, no. 20, pp. 36–41, 2018.
- [17] S. W. Formica, R. Apsler, L. Wilkins, S. Ruiz, B. Reilly, and A. Y. Walley, “Post opioid overdose outreach by public health and public safety agencies: exploration of emerging programs in Massachusetts,” *International Journal of Drug Policy*, vol. 54, pp. 43–50, 2018.
- [18] L. Sakala and N. L. Vigne, “Community-driven models for safety and justice,” *Du Bois Review Social Ence Research on Race*, vol. 16, no. 1, pp. 1–14, 2019.
- [19] M. Dragoicea, M. Leonard, S. N. Ciolofan, and G. Militaru, “Managing data, information, and technology in cyber physical systems: public safety as a service and its systems,” *IEEE Access*, vol. 7, no. 99, pp. 92672–92692, 2019.
- [20] B. N. Williams, R. S. Brower, and W. E. Klay, “Community-centred police professionalism,” *The Police Journal: Theory, Practice and Principles*, vol. 89, no. 2, pp. 151–173, 2016.
- [21] T. R. Byrdsong, A. Devan, and H. Yamatani, “A ground-up model for gun violence reduction: a community-based public health approach,” *Journal of Evidence-Informed Social Work*, vol. 13, no. 1, pp. 76–86, 2016.
- [22] T. P. Abt, “Towards a framework for preventing community violence among youth,” *Psychology, Health & Medicine*, vol. 22, no. sup1, pp. 266–285, 2017.
- [23] R. M. Peters, T. J. Hipper, and E. D. Chernak, “Primary care medical practices: are community health care providers ready for disasters?” *Disaster Medicine and Public Health Preparedness*, vol. 13, no. 2, pp. 128–132, 2019.
- [24] L. Wahowiak, “New rankings showcase community health,” *American Journal of Public Health*, vol. 108, p. 967, 2018.
- [25] H. Sutton, “Find ways to make yourself essential to your off-campus community,” *Campus Security Report*, vol. 13, no. 7, pp. 1–5, 2016.
- [26] Z. Hamilton, C. M. Campbell, J. vanWormer et al., “Impact of swift and certain sanctions: evaluation of Washington state’s policy for offenders on community supervision,” *Criminology & Public Policy*, vol. 15, no. 4, pp. 1–64, 2016.

Research Article

Analysis and Prediction of Overloaded Extra-Heavy Vehicles for Highway Safety Using Machine Learning

Yi-Hsin Lin ¹, Suyu Gu,¹ Wei-Sheng Wu,² Rujun Wang,³ and Fan Wu¹

¹School of Civil Engineering, Southeast University, Nanjing 211189, China

²Department of Electrical Engineering, National Cheng Kung University, Tainan 70101, Taiwan

³Changzhou Transportation Comprehensive Administrative Law Enforcement Detachment, Changzhou 213001, China

Correspondence should be addressed to Yi-Hsin Lin; yihsinlin@seu.edu.cn

Received 8 October 2020; Revised 10 December 2020; Accepted 14 December 2020; Published 30 December 2020

Academic Editor: Hsu-Yang Kung

Copyright © 2020 Georgii S. Vasyliov et al. This is an open access article distributed under the Creative Commons Attribution License, which permits unrestricted use, distribution, and reproduction in any medium, provided the original work is properly cited.

Along with the prosperity and rapid development of the national economy, the transportation industry has rapidly developed in China. However, overloaded vehicles have been causing frequent traffic accidents. Thus, to alleviate or resolve the corresponding problems associated with highway engineering safety and the market economy, an improved technique for overload management is urgently required. In this study, to analyze the overload data on expressways and highways in China, we developed a machine learning model by comparing the performances of cluster analysis, backpropagation neural network (BPNN), generalized regression neural network (GRNN), and wavelet neural network (WNN) in analyzing global and local time series overload data. In a case study, our results revealed the trends of overloading on highways in Jiangsu Province. Given sufficient data, BPNN performed better than GRNN and WNN. As the amount of training data increased, GRNN performed better, but the runtime increased. WNN had the shortest runtime among the three methods and could reflect the future trends of the overload rate in the monthly data prediction of overload. Our model provides information with potential value for expressway network management departments through data mining. This information could help management departments allocate resources reasonably and optimize the information utilization rate.

1. Introduction

Along with the prosperity and rapid development of the national economy, the transportation industry has also rapidly developed in China. Nevertheless, the related overloading management system has not developed accordingly and the enforcement of transportation laws has not become stricter. Thus, transport operators hope to expand their profits by overloading their vehicles; however, overloading leads to frequent traffic accidents. According to the Highway Bureau of the Chinese Ministry of Transport, more than 80% of truck road traffic accidents are caused by overloaded transport. Overloading continuously causes road damage [1] and traffic accidents [2], disrupts the normal economic order of the logistics market, and affects the healthy development of the highway transportation economy [3]. Thus, to alleviate or resolve the problems associated

with highway engineering safety and market economy, an improved technique for overload management is urgently required.

In this study, we established a machine learning model for highway overrun and overload. We explored the overload characteristics through cluster analysis and compared the performances of backpropagation neural network (BPNN), a commonly employed method for training neural network, generalized regression neural network (GRNN), a radial basis function neural network, and wavelet neural network (WNN), a novel neural network that combines classical sigmoid neural networks with wavelet analysis (WA), to determine the best method to mine, analyze, and predict the overload data. Furthermore, we provide information with more potential value like overload characteristics, overload rate, and overload trend, for highway network management, and explore the application of data mining analysis results in

daily and instant overload management work using cluster analysis and neural networks (NNs).

This study makes a significant contribution in assisting highway management departments to reasonably allocate resources, optimize information utilization, improve the transportation management methods and management efficiency, and alleviate highway engineering safety problems. Furthermore, this study aids in economic and environmental development and provides a practical reference for future work on overload management.

2. Background

Rapid advancements in the field of science and technology have enabled the constant updation of software and hardware for overload control; consequently, toll collection centers at all levels in China are able to store increasing amounts of detailed historical data [4]. These massive amounts of data contain abundant valuable information. Conventional research methods for analyzing the characteristics of overloading in China mainly include literature review, statistical prediction model, and game analysis model. For example, Li and Wang analyzed the characteristics of freeway overload vehicles via cluster analysis [5]. Ryu et al. analyzed vehicle overrun behaviors using game theory and the risk preference model [6]. In addition, some scholars now study the related characteristics by building data models. Cheng et al. established a behavior judgment and prediction model and studied the vehicle detour behavior [7]. Zhang analyzed the impact of overload on road capacity through VISSIM simulation [8]. It is seen that most of the current research is based on data modeling to conduct data mining; thus, we explore which model should be used in the research as follows.

Past research has revealed that the overload characteristics [4, 9] should first be clarified to further study the problem of overload management. Machine learning, a typical data mining technique, uses the “black box” principle to build a machine learning model to address complex and diverse data [10]. In the field of traffic management, machine learning is currently applied to feature mining, prediction, response, and timely disposal of traffic events. For example, Muhammed Yasin and Ahmet proposed a highway traffic accident prediction model based on an artificial neural network (ANN) to analyze the characteristics of traffic accidents [11]. Li et al. proposed a situational awareness machine learning model to thoroughly investigate the factors affecting the fatigue degree of traffic management personnel [12]. Mohammed Abdulhafedh et al. reviewed data mining and machine learning methods for sustainable intelligent urban traffic classification and indicated that machine learning is extremely effective for the identification and classification of traffic states [13]. Therefore, machine learning can be used for data mining, studying the characteristics of overloading, and forecasting overloading patterns to thoroughly exploit the massive amounts of historical data in the existing domestic highway toll collection centers at all levels; this complies with the current demand for off-site law enforcement and technology. This

could significantly improve highway transportation management and alleviate highway engineering safety problems.

In terms of research on traffic transport characteristics, the currently adopted machine learning methods include support vector machine (SVM), logistic regression (LR), cluster analysis, and ANN.

SVM has been successfully employed for classification, regression, and pattern recognition [14]. Sangare et al. highlighted that SVM can demonstrate better performance with low data volume; however, it lacks the ability to automatically identify relevant features, and its calculation cost is high [15]. Lin and Li suggested that NNs are better than SVM in predicting traffic congestion [16]. The LR is a statistical method used to predict event probability and is a significant model for classified data [17]. However, it is sensitive to the multicollinearity of independent variables and affects regression results. Moreover, LR would be highly suited for feature mining through the analysis of the influencing factors. [18]. Because this research has made sufficient data available, one need not consider to use SVM solely because it performs better than other methods with less data. Furthermore, considering its high computational cost and poor prediction performance compared with that of NNs, SVM is not a practical choice. Moreover, independent variables affecting the overload may cause multicollinearity problems; thus, the regression results of LR are also affected. Therefore, SVM and LR have limitations in mining the characteristics of overload and the prediction of overload.

Cluster analysis is a typical and extremely effective method of exploring characteristics and laws. It can discover the internal distribution structure of data without prior knowledge regarding the correct results [19]. Yassin and Pooja used *K*-means clustering to extract hidden information from traffic accident data and created training sets; the accuracy of this method was 99.86% [19]. Žunić et al. used *K*-means clustering to analyze the impact of road, environment, vehicles, and drivers on traffic accidents and highlighted that clustering has been applied in several cases and instances in current professional and scientific practices in the field of traffic management [20]. The most commonly employed clustering analysis methods include the hierarchical clustering algorithm and dividing-based clustering algorithm. According to the multiperiod original data of this research system, clustering and *K*-means clustering, which are the most classic, universal, and commonly used algorithms in the field of transportation, are selected and are combined. *K*-means is easy to implement; however, the number of classification classes must be specified in advance. The use of system clustering can solve this problem; concurrently, *K*-means can also compensate for any defects in the inaccurate termination conditions of system clustering.

ANN can be used to analyze nonlinear factors, and ANN models demonstrate high accuracy and degree of fit. The commonly used ANNs include BPNN, GRNN, and WNN. For example, Wang et al. established a BPNN model to estimate the probability of collision results for different traffic accidents. The model accuracy was greater than 90%, and the model exhibited a good fitting effect [21]. Zhang and Zhang believed that the GRNN model has higher accuracy and reliability than historical average and vector

autoregression (VAR) in making short-term traffic flow predictions [22]. Hou et al. suggested that WNN has favorable adaptive ability and self-learning ability for forecasting short-term traffic volume [23]. BPNN is relatively mature in network theory and performance and has high self-learning and adaptive abilities, which enables it to extract “reasonable rules” between data in the event of unseen patterns and to adequately mine the data. In contrast to the global approximation algorithm of BPNN, GRNN is characterized by an optimal approximation, which can process unstable data and avoid the problem of the local optimum that could occur due to the BPNN, whereas WNN has significant advantages over sequential data, implying that these three NNs have different functions [3, 24]. Therefore, when sufficient historical data are available for training, BPNN, GRNN, and WNN can suitably adapt to the characteristics of overload behavior, such as the large impact of timing sequence, large randomness, and nonlinear influencing factors, and are considerably suitable for solving the problem of feature mining and prediction modeling of overload vehicles.

Most of the current research is based on data modeling for data mining; therefore, this study explores the models that can be used and finally selects two models of machine learning: clustering analysis and NN. Machine learning has been used in the field of transportation research but rarely used in the analysis of overload characteristics. Therefore, as discussed earlier, we explore the overload characteristics through cluster analysis and compare the performances of BP, GRNN, and WNN to determine the best method to mine, analyze, and predict overload data.

3. Materials and Methods

3.1. Experimental Data. The expressway data of Jiangsu Province (15 565 data units) and the national provincial highway data of Liyang city (30 764 data units), from 2018 to 2019, were collected from the expressway transportation management department of the Jiangsu Province. The datasets included “License plate,” “Lane,” “Time,” “Gross weight of vehicles and goods,” “Axle number,” “Rated weight,” “Overload standard,” “Overload rate,” and “Overload interval.” The details of these datasets are as follows.

License plate. License plate is the number plate identifying the vehicle, and the dataset is in the form of “苏 DETXXX,” where “苏” represents Jiangsu Province and “X” is an integer.

Lane. A lane is the road that a vehicle travels on. If there are three lanes, the one closest to the central zoning is defined as the first lane, the middle lane is the second lane, and the outer lane is the third lane.

Time. Time refers to the time when the car passes through the detection station; the dataset is in the form of “year/month/day, hour: minutes.”

Gross weight of vehicles and goods. This refers to the total weight of the vehicle and cargo; the unit is ton (e.g., “49 t”).

Axle number. Axle number refers to the total number of axles configured in the lower part of the vehicle underframe. Vehicles are usually divided into classes of one to six axles.

Rated weight. Rated weight refers to the maximum allowable vehicle load under the condition of ensuring safe driving. The unit is ton (e.g., “49 t”).

Overload standard. Overload standard determines whether the vehicle weight exceeds the rated weight indicated on the driving license. If it exceeds the rated weight, it is termed overweight.

$$\text{overload rate} = \frac{\text{actual weight} - \text{rated weight}}{\text{rated weight}}. \quad (1)$$

Overload interval. Overload interval is divided into “less than 5%,” “5–30%,” “30–50%,” “50–100%,” and “more than 100%.”

3.1.1. Data Preprocessing. The raw datasets in this research were not correctly formatted and could not be comprehended by computing machines. Before building the model, this problem had to be resolved to ensure favorable data quality. Consequently, data cleaning, missing data handling, encoding, and normalization were performed. Character data, such as “Maximum wheelbase,” of the province highway missed 2007 data in total, and the national highway data do not contain this character data; thus, we deleted these character data. Character data such as “Time,” “License plate,” and “Detection station type” were converted to numerical data (Table 1). All the data were normalized between zero and one to eliminate the differences in the orders of magnitude, which also can reduce the possibility of overfitting in the BPNN model.

3.1.2. Data Extraction. Data were extracted from raw data that were processed and were divided into expressway data and national and provincial highway data.

Cluster analysis extracts two-dimensional (2D) data for analysis. “Overload rate” is the concrete data of “Overload interval”; thus, “Overload interval” was discarded. The attributes were “License plate,” “Gross weight of goods and vehicles,” “Overload standard (rated weight),” “Axle number,” and “Overload rate,” whereas “Overload standard” is similar to the information represented by “Gross weight of goods and vehicles”; thus, we selected “Gross weight of goods and vehicles” to avoid duplication.

The NN can also extract 2D data for analysis. Because of the lack of data for December and speed data from June to November in 2019, for the national and provincial data, only the national and provincial data of Liyang city in 2018 were selected for analysis. In May 2019, there were 738 expressway data points in Jiangsu Province in hours. In this research, the national and provincial highway data of Liyang city in 2018 were selected according to monthly, quarterly, and annual data. The monthly data were measured in hours and contributed 289 pieces of data for the 12 months of 2018. The

TABLE 1: Data conversion table.

Data	Before conversion	After conversion
Time	X year x month x day XX:XX:XX	The month is represented with a value in the range 1–12 The hour is represented by a value in the range 0–23
	X year x month x day XX:XX:XX	
License plate	License plate in the province	[1, 0, 0]
	License plate outside the province	[0, 1, 0]
	No license plate	[0, 0, 1]
Type of detection station	Ordinary	[1, 0, 0]
	Dynamic	[0, 1, 0]
	High speed	[0, 0, 1]

quarterly data were measured in hours, and 964 data points were available in the first quarter of 2018. The annual data were measured in hours, and 3367 pieces of data were available for 306 days in 2018.

In summary, cluster analysis was performed to extract the attributes “Time,” “Gross weight of vehicles and goods,” “Axle number,” and “Overload rate” to analyze the data. The BPNN and GRNN extracted “Time,” “Gross weight of goods and vehicles,” “Axle number,” and “Overload rate” from Jiangsu expressway and the provincial highway data. WNN was only used to process 2D time-series data, i.e., the “Overload rate” data.

3.2. Machine Learning

3.2.1. Cluster Analysis. Clustering, which was proposed in the mid-20th century, is a typical research method of unsupervised learning. It aims to group similar observations into multiple clusters according to the observations of multiple variables of each individual, to maximize the similarity of samples in each cluster, maximize the differences between unknown groups, and reveal the inherent distribution structure of data. The concept underlying cluster analysis originated from traditional taxonomy, in which complex classification problems are encountered. Unlike traditional classification, the data types that need to be divided in cluster analysis are typically unknown and are defined by analyzing specific cluster results.

- (1) Systematic clustering: systematic clustering aims to classify each sample step by step according to the criterion of the distance function calculation until the samples satisfy the requirements of the systematic clustering algorithm. Among them, the distance calculation formulas and criteria are primarily used to calculate the average distance between samples and clusters formed in each iteration and between them and each sample. Different distance calculation formulas and criteria yield different distance calculation results. The common distance calculation criteria include the shortest distance method, longest distance method, intermediate distance method, barycenter method, and class average distance method.
- (2) *K*-means clustering: *K*-means is considered a crucial clustering algorithm [25], which has an iterative process for datasets. In this iterative process, the

datasets are divided into “*k*” predefined nonoverlapping clusters or subgroups. The data points between clusters are as similar as possible, and the distance between clusters is retained for the maximum time possible. It assigns data points to clusters, so that the sum of the square of the distance between the cluster centroid and data points is the smallest. Here, the cluster centroid is the arithmetic average of the data points in the cluster.

In this study, systematic clustering and *K*-means clustering were combined for clustering analysis; the specific process is shown in Figure 1. *K*-means clustering needs to determine the number of clustering classes “*k*” before clustering, and this research aims to cluster the overloading data of the national and provincial highways in Liyang city in every quarter from 2018 to 2019. Therefore, we used systematic clustering to obtain the clustering tree diagram for eight quarters from 2018 to 2019 and determine the same number of clustering classes “*k*” in eight quarters, taking into account the continuity of the data. On this basis, the clustering results were obtained by *K*-means analysis.

3.2.2. Neural Network

- (1) BPNN ANN is a supervised machine learning algorithm [26]. The BPNN is called an error back-propagation ANN. This is a commonly employed method for training NNs, which assists in calculating the gradient of the loss function relative to all weights in the network and enhancing the connectivity between layers to obtain the optimal solution [27]. A BPNN usually has three or more layers. Each layer of a BPNN comprises several neurons.

In this research, a BPNN was used to build a machine learning model for the expressway data and to predict the overload rate and trend. The algorithm flow of the BPNN can be divided into three steps Figure 2: BPNN establishment, training, and prediction.

First, the specific structure of the BPNN was determined according to the characteristics of the fitting function. Because there are four input parameters—“Time,” “Gross weight of vehicles and goods,” “Axle number,” and “Type of inspection station”—and only one output parameter, namely, “Overload rate,” the number of nodes in the three

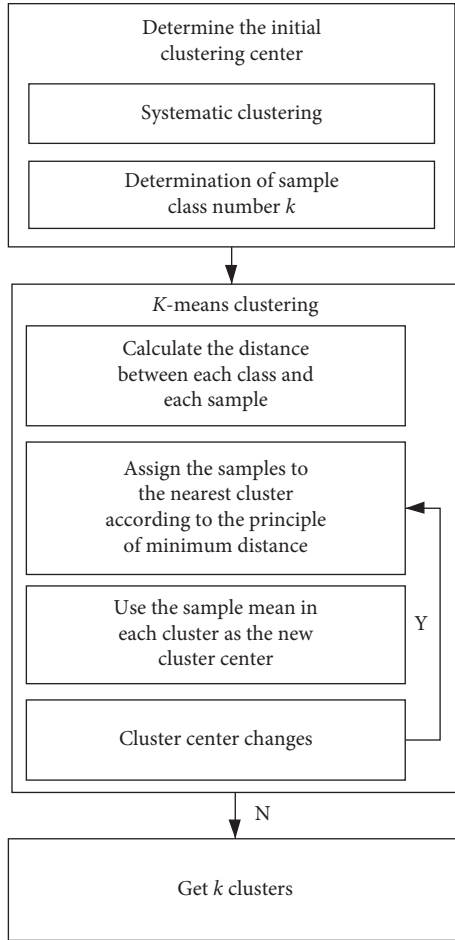


FIGURE 1: Flowchart for cluster analysis.

layers of the BPNN was “4-?-1”; this implies there are four input layer nodes, the number of hidden layer nodes is unknown, and there is one output layer node.

In reality, we can only use data from the first few months that have occurred to predict subsequent results. Therefore, to consider actual situations, in this research, we arranged the data in chronological order and systematically divided them into training data and testing data in a 10:1 ratio.

The number of hidden layer nodes can be calculated as follows:

$$L = \sqrt{n + m + a}, \quad (2)$$

where L denotes the number of hidden layer nodes, n denotes the number of neurons in the input layer, m denotes the number of neurons in the output layer, and a is a constant having a value between 1 and 10. Substituting $n = 4$ and $m = 1$ in equation (2), we obtain a value between $\sqrt{5} + 1$ and $\sqrt{5} + 10$ because the number of nodes L is an integer between 4 and 12. If the fitted nonlinear function is simple, the prediction error of the BPNN decreases with an increase in the number of nodes. If the function is complex, the error decreases first and then increases.

To explore the appropriate number of hidden nodes, a loop was written in the code to evaluate the goodness of fit of the prediction by the degree of fitting to obtain the optimal number of hidden nodes.

Goodness of fit refers to the fitting accuracy of the regression line of the model to the observed value. Generally, the determinable coefficient (also called the deterministic coefficient) is used to determine the goodness of fit. The closer the value is to one, the better the fitting degree of the model is; in contrast, the closer it is to zero, the worse the fitting degree of the model is. In this research, the prediction ability of the model was evaluated by calculating the coefficient of determination, as follows:

$$R^2 = \frac{\left(l \sum_{i=1}^l \hat{y}_i y_i - \sum_{i=1}^l \hat{y}_i \sum_{i=1}^l y_i \right)^2}{\left(l \sum_{i=1}^l \hat{y}_i^2 - \left(\sum_{i=1}^l \hat{y}_i \right)^2 \right) \left(l \sum_{i=1}^l y_i^2 - \left(\sum_{i=1}^l y_i \right)^2 \right)}, \quad (3)$$

where R^2 is the determinable coefficient, \hat{y}_i is the i th predicted value, y_i is the i th true value, and l denotes the number of samples.

- (2) Generalized regression neural network GRNN was proposed by Donald F. Specht, an American scholar, in 1991. It is essentially a radial basis function NN but differs from the conventional radial basis function NN. It is a type of strong regression tool with strong nonlinear mapping ability and flexible network structure and can be employed in regression, prediction, and classification research [28].

In this research, the GRNN was used to build a machine learning model for the expressway data and to predict the overload rate and trend. The algorithm flow of the GRNN can be divided into three steps Figure 3-GRNN establishment, training, and prediction.

First, the GRNN structure is determined according to the characteristics of the fitting function. The number of neuron nodes in the input layer is equal to the dimension of the learning samples. The number of neuron nodes in the mode layer is equal to the number of learning samples, i.e., “Time,” “Gross weight of vehicle and goods,” “Axle number,” and “Type of inspection station,” whereas that in the output layer is equal to the dimension of the output vector of the learning samples, i.e., “Overload rate.” Therefore, the GRNN does not need to determine the number of hidden layer nodes. Unlike the BPNN, the GRNN only needs to confirm the SPREAD parameter and thus exhibits considerable computational advantages. In this study, the parameters of SPREAD were determined by loop training. The loop code starts with “for SPREAD=0.1:0.1:2,” which means SPREAD is assigned

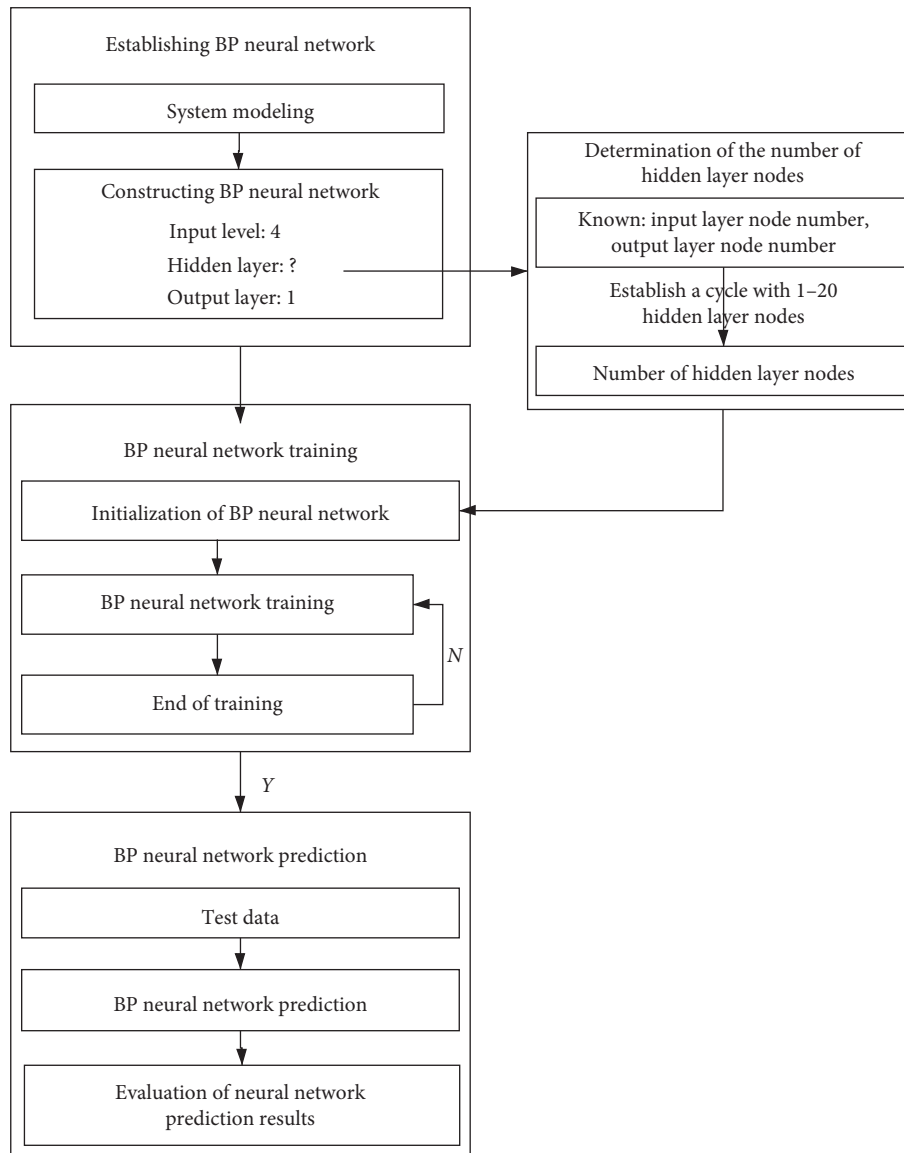


FIGURE 2: Flowchart of the BPNN.

from 0.1 and the step distance is 0.1, and each loop increases by 0.1 until $SPREAD = 2$. Similar to the manner followed for BPNN, for GRNN, the data are arranged in chronological order and systematically divided into training data and testing data in a 10:1 ratio.

- (3) Wavelet neural network WNN is a novel NN that combines classical sigmoid NNs with wavelet analysis (WA) [29]. The concept of WA was developed considering the shortcomings of the Fourier transform, which cannot accurately evaluate the time a certain signal occurs. In contrast, WA can analyze the local characteristics of signals through wavelet basis function transformation and select the direction of signals in two dimensions. The WNN can perform time-frequency local analysis, has a fast convergence speed, and can effectively avoid falling into a local optimum.

In this study, WNN was used to build a machine learning model for expressway, national, and provincial highway data and predict the overload rate and trend. The algorithm flow of the WNN can be divided into three steps Figure 4: WNN establishment, training, and prediction.

First, the structure of the WNN was determined according to the characteristics of the fitting function. In this study, according to the periodic characteristics of overload and goodness of fit of the operation results, the number of neuron nodes in the three layers of the NN was determined to be "4-4-1." Four nodes in the input layer indicate the overload rate at four time points before the predicted time node. The hidden layer nodes were composed of wavelet basis functions. There was one node in the output layer, which denoted the overload rate to be predicted. Similar to the manner followed for BPNN and GRNN, for WNN, the data are arranged in chronological order and systematically divided into training data and testing data in a 10:1 ratio.

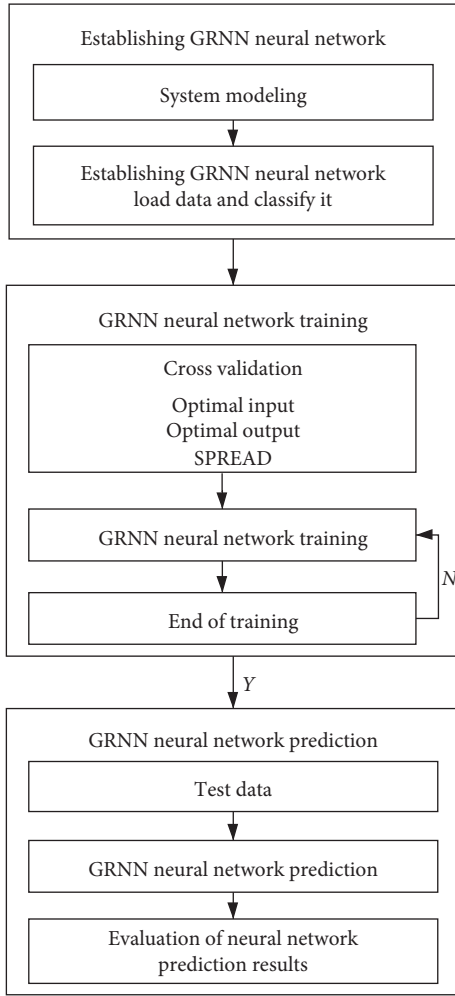


FIGURE 3: Flowchart of GRNN neural network.

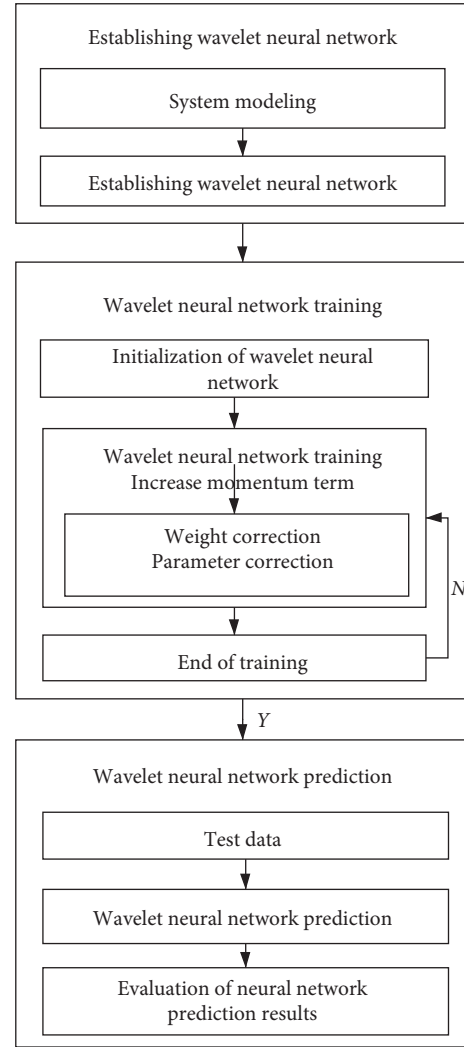


FIGURE 4: Flowchart of the WNN.

4. Results

Table 2 presents the clustering results when the number of clustering classes was six, i.e., $K = 6$. “Gross weight of vehicle and goods” gives the average gross weight of the vehicles and goods at the time of entering highway. “Category of gross weight” and “Proportion of gross weight” are the proportions of the components of the average gross weight. “Axis number” and “Proportion of axis number” are the proportions of the components of the axis number at the time of entering the highway. “Overload rate” gives the average overload rate of the vehicles at the time of entering highway. “Proportion of vehicles” shows the percentage of vehicles passing at the time of entering the highway in the total number of vehicles.

It can be observed that, on the expressways in Jiangsu Province, vehicles with six axles and weighing above 49 t entering the expressways at 23:00–04:00 and 12:00–14:00 are more likely to exhibit overload behavior, and the overload rate of these vehicles is higher than that of others during this period. Most vehicles enter the expressway at 05:00 and 17:00–22:00, among which six-axle vehicles weighing above 49 t are more likely to be overloaded. Among the vehicles

entering the expressway between 06:00–07:00 and 15:00–16:00, two-axle vehicles weighing 18–27 t are more likely to be overloaded. Among the vehicles entering the expressway between 08:00–11:00, four-axle vehicles weighing 37–43 t and 43–49 t are more likely to be overloaded.

Table 3 presents the clustering results of the national and provincial data in the eight quarters of 2018 and 2019. The definitions of “Gross weight of vehicle and goods,” “Category of gross weight,” “Proportion of gross weight,” “Axis number,” “Proportion of axis number,” “Overload rate,” and “Proportion of vehicles” are the same as above. The analysis is as follows.

The data clustering results of the national and provincial highways in the four quarters of 2018 were as follows: (1) most vehicles entered the provincial highway at 00:00–08:00 and 16:00–20:00 in the first quarter, among which six-axle vehicles weighing above 49 t were more likely to be overloaded; the overload rate of six-axle vehicles weighing above 49 t and entering the provincial highway at 02:00–03:00 was higher. Among the vehicles entering the national provincial highway at 11:00, 2-axle, 3-axle, and 4-axle vehicles weighing

TABLE 2: Clustering results of expressway data at $K=6$.

Group	Time of entering highway	Gross weight of vehicle and goods	Category of gross weight	Proportion of gross weight (%)	Axis number	Proportion of axis number (%)	Overload rate	Proportion of vehicles (%)
1	23:00–4:00	90.62	Over 49 t	100.00	6	100.00	0.85	1.16
			43 t–49 t	2.43	3	0.50		
2	5:00	53.11	Over 49 t	97.57	3	0.50	0.11	50.83
					4	3.69		
					5	4.25		
					6	90.58		
3	6:00–7:00 15:00–16:00	21.64	18 t–27 t	80.66	2	86.68	0.13	5.21
			27 t–36 t	19.34	3	13.32		
4	8:00–11:00	41.88	Over 49 t	97.57	27 t–36 t	2.37	0.17	6.72
					36 t–37 t	1.17		
					37 t–43 t	55.47		
					43 t–49 t	40.99		
5	12:00–14:00	67.04	Over 49 t	100.00	4	1.40	0.38	9.70
					5	0.33		
					6	97.62		
					9	0.66		
6	17:00–22:00	58.44	Over 49 t	100.00	4	0.73	0.20	26.38
					5	0.91		
					6	97.88		
					9	0.48		

27–36 t and 37–49 t were more likely to be overloaded. (2) In the second quarter, most vehicles entered the highway between 00:00–08:00 and between 14:00–21:00, among which 6-axle vehicles weighing above 49 t were more likely to be overloaded; the overload rate of 6-axle vehicles weighing above 49 t and entering the highway between 21:00–23:00 was high. Among the vehicles entering the national provincial highway from 09:00 to 13:00, 3-axle vehicles weighing 27–36 t and 37–49 t were more likely to be overloaded. (3) In the third quarter, most vehicles entered the highway between 00:00–8:00 and between 16:00–20:00, among which 6-axle vehicles weighing above 49 t were more likely to be overloaded; the overload rate of 6-axle vehicles weighing above 49 t and entering the highway between 21:00–23:00 was high. Among the vehicles entering the highway between 09:00–15:00, 2-axle, 3-axle, and 4-axle vehicles weighing 27–36 t and 37–49 t were more likely to be overloaded. (4) In the fourth quarter, most vehicles entered the highway between 00:00–08:00 and 13:00–22:00, among which 6-axle vehicles weighing above 49 t were more likely to be overloaded. At 23:00, the overload rate of 6-axle vehicles weighing above 49 t and entering the highway was high. Among the vehicles entering the highway between 09:00–12:00, 4-axle vehicles weighing 27–36 t and 37–49 t were more likely to be overloaded.

The data clustering results of the national and provincial highways in the four quarters of 2019 were as follows: (1) in the first quarter, most vehicles entered the national and provincial highway between 04:00–13:00 and between 18:00–23:00, among which 6-axle vehicles weighing above 49 t were more likely to be overloaded; the overload rate of 6-axle vehicles weighing above 49 t and entering the provincial highway between 00:00–03:00 was high. Among the vehicles

entering the highway between 14:00–17:00, 2-axle vehicles weighing 18–27 t and 27–36 t were more likely to be overloaded. (2) In the second quarter, most vehicles entered the highway between 00:00–15:00, among which 6-axle vehicles weighing above 49 t were more likely to be overloaded. From 00:00 to 03:00, the overload rate of 6-axle vehicles weighing above 49 t and entering the highway was high. Among the vehicles entering the national provincial highway between 06:00–15:00, 4-axle vehicles weighing 37–43 t were more likely to be overloaded. Among the vehicles entering the national highways between 16:00–23:00, 4-axle and 6-axle vehicles weighing above 49 t were more likely to be overloaded. (3) In the third quarter, most vehicles entered the highway between 04:00–05:00 and between 14:00–18:00, among which 6-axle vehicles weighing above 49 t were more likely to be overloaded. From 02:00 to 03:00, the overload rate of 6-axle vehicles weighing above 49 t and entering the national provincial highway was high. Among the vehicles entering the highways between 22:00–01:00 and between 07:00–13:00, 4-axle vehicles weighing 37–43 t were more likely to be overloaded. Among the vehicles entering the highway at 06:00, 2-axle and 3-axle vehicles weighing 27–36 t were more likely to be overloaded. (4) In the fourth quarter, most vehicles entered the highway between 08:00–15:00, among which 6-axle vehicles weighing above 49 t were more likely to be overloaded. The overload rate of 6-axle vehicles weighing above 49 t and entering the highway between 00:00–04:00 was high. Among the vehicles entering the highway from 05:00 to 07:00, 2-axle vehicles weighing 18–27 t and 27–36 t were more likely to be overloaded. Among the vehicles entering the highway from 16:00 to 23:00, 4-axle and 6-axle vehicles weighing above 49 t were more likely to be overloaded.

TABLE 3: Clustering results of national and provincial highway data when $K = 4$.

Year	Quarter	Group	Time of entering highway	Gross weight of vehicle and goods	Category of gross weight	Proportion of gross weight	Axis number	Proportion of axis number (%)	Overload rate	Proportion of vehicles (%)	
2018	1	1	0:00-1:00 4:00-10:00	53.96	37t-43t	1.57	2	0.02	0.14	40.36	
					43t-49t	3.18	3	0.75			
		2	2	2:00-3:00	81.75	Over 49t	95.25	5	0.29	0.69	9.51
						Over 49t	100	4	1.93		
			3	11:00	29.02	18t-27t	21.16	6	0.6	0.13	9.56
						27t-36t	36.83	2	97.22		
	2	1	0:00-8:00	53.14	36t-37t	2.17	3	25.61	0.12	40.57	
					37t-43t	39.84	4	43.64			
		2	9:00-13:00	28.53	37t-43t	2.76	2	0.08	0.13	47.95	
					43t-49t	3.61	4	5.25			
			3	14:00-21:00	51.97	Over 49t	93.65	6	93.11	0.12	8.73
						Over 49t	3.6	4	2.76		
2018	2	3	22:00-23:00	77.5	37t-43t	4.78	2	0.02	0.14	32.99	
					43t-49t	5.3	3	3.26			
		4	1	0:00-8:00	53.37	Over 49t	89.92	4	6.4	0.62	10.33
						Over 49t	100	5	1.22		
			3	9:00-15:00	28.01	37t-43t	3.06	6	89.09	0.11	8.36
						37t-43t	2.57	2	0.58		
	3	1	0:00-8:00	53.46	Over 49t	94.34	3	2.56	0.12	44.59	
					Over 49t	100	5	0.32			
		2	16:00-20:00	53.46	37t-43t	3.09	2	0.01	0.12	41.12	
					43t-49t	3.09	3	0.31			
			3	21:00-23:00	88.53	Over 49t	6.81	4	6.23	0.82	5.93
						Over 49t	100	6	96.52		
2018	3	1	0:00-8:00	57.05	37t-43t	6.81	2	0.2	0.25	41.18	
					43t-49t	6.81	3	1.2			
		2	11:00	97.49	Over 49t	93.19	4	10.7	0.25	41.18	
					Over 49t	48.45	5	2.01			
			3	13:00-22:00	57.03	37t-43t	3.73	6	85.89	0.2	17.9
						37t-43t	0.55	3	32.11		
	4	1	11:00	97.49	43t-49t	5.69	4	42.82	0.23	30.47	
					43t-49t	93.76	5	12.03			
		2	11:00	97.49	Over 49t	0.21	4	86.45	1.02	10.45	
					Over 49t	0.21	3	0.38			
			3	11:00	97.49	Over 49t	99.79	4	2.52	1.02	10.45
						Over 49t	99.79	5	1.26		
4	11:00	97.49	Over 49t	99.79	6	95.85	1.02	10.45			
			Over 49t	99.79	6	95.85					

TABLE 3: Continued.

Year	Quarter	Group	Time of entering highway	Gross weight of vehicle and goods	Category of gross weight	Proportion of gross weight (%)	Axis number	Proportion of axis number (%)	Overload rate	Proportion of vehicles (%)		
2019	1	1	0:00-3:00	75.63	Over 49t	100	4	2.5	0.56	16.59		
					371-431	8.73	6	97.5				
		2	4:00-10:00	51.33	431-491	7.48	4	14.29				
					Over 49t	83.79	6	85.71	0.1	35.21		
	3	11:00-13:00	49.99	371-431	9.13	3	0.72					
				431-491	8.52	4	12.56	0.08	43.28			
		4	14:00-17:00	21.84	Over 49t	82.35	5	1.21				
					18t-27t	67.86	2	85.51	0.11	4.92		
	2	1	0:00-3:00	84.11	Over 49t	100	3	0.6				
					271-361	32.14	3	27.27	0.75	33		
			2	4:00-5:00	57.2	431-491	3.15	3	0.65			
						Over 49t	96.85	5	10.34	0.24	31.67	
		3	6:00-15:00	34.57	18t-27t	9.84	2	87.93				
					271-361	14.77	3	15.48				
			4	16:00-23:00	50.42	371-431	58.29	2	17.42	0.17	21.41	
						431-491	17.1	4	67.1			
		3	22:00-1:00	39.83	371-431	23.9	3	1.51				
					431-491	11.95	4	38.19	0.19	13.92		
			4	7:00-13:00	55.37	Over 49t	64.14	6	60.3	0.19	13.92	
						271-361	4.29	2	2.8			
		3	4:00-5:00	81.43	361-371	2.86	3	8.41				
					371-431	75	4	85.98	0.16	29.29		
			2	5:00-7:00	25.4	Over 49t	12.86	5	2.8			
						431-491	5	6	2.8	0.204	0.4655	
4		8:00-15:00	50.15	Over 49t	95.96	6	90.91	0.204	0.4655			
				431-491	10.02	4	22.57	0.19	63.71			
		3	2:00-3:00	25.87	Over 49t	100	4	7.69	0.72	13.18		
					18t-27t	40	6	92.31				
4		0:00-4:00	78.89	18t-27t	40	2	57.14	0.25	10.98			
				271-361	60	3	42.86					
		1	0:00-4:00	78.89	Over 49t	100	3	1.96				
					431-491	16.39	4	7.84	0.72	7.45		
2	5:00-7:00	25.4	18t-27t	48.53	2	90.2						
			271-361	45.58	2	71.68						
	3	8:00-15:00	50.15	361-371	3.63	3	26.32	0.29	17.38			
				371-431	2.27	4	2.01					
4	16:00-23:00	51.71	371-431	16.39	2	0.16						
			431-491	10.02	3	5.88						
	3	8:00-15:00	50.15	Over 49t	73.59	5	0.39					
				371-431	13.75	6	71					
4	16:00-23:00	51.71	371-431	13.75	3	10.67						
			431-491	16.49	4	17.78						
	4	16:00-23:00	51.71	Over 49t	69.76	5	2.22					
				431-491	69.76	6	69.33	0.25	11.47			

Clustering results of national and provincial highway data when $K = 4$ (1). Clustering results of national and provincial highway data when $K = 4$ (2). Clustering results of national and provincial highway data when $K = 4$ (3). Clustering results of national and provincial highway data when $K = 4$ (4). Clustering results of national and provincial highway data when $K = 4$ (5). Clustering results of national and provincial highway data when $K = 4$ (6)

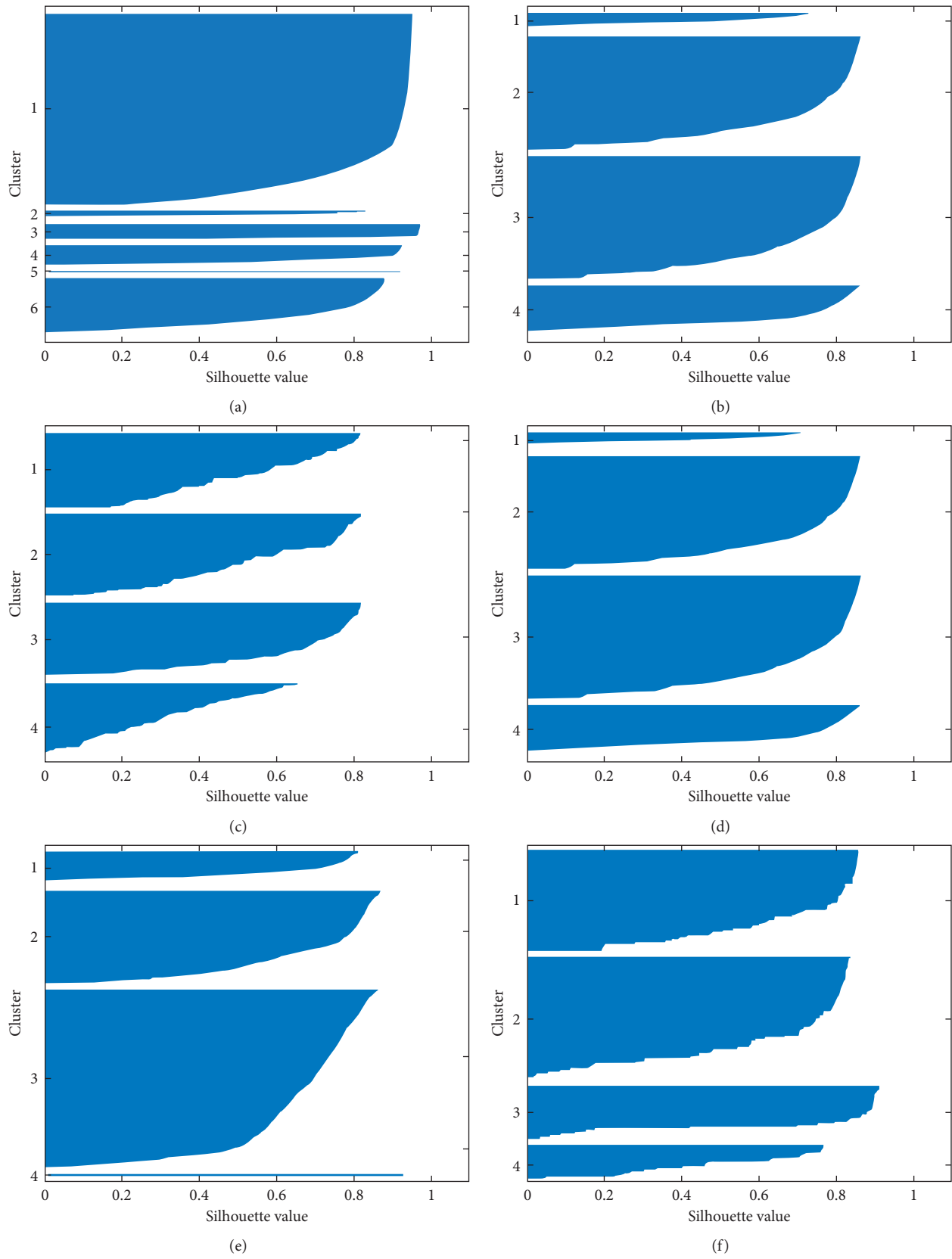


FIGURE 5: Continued.

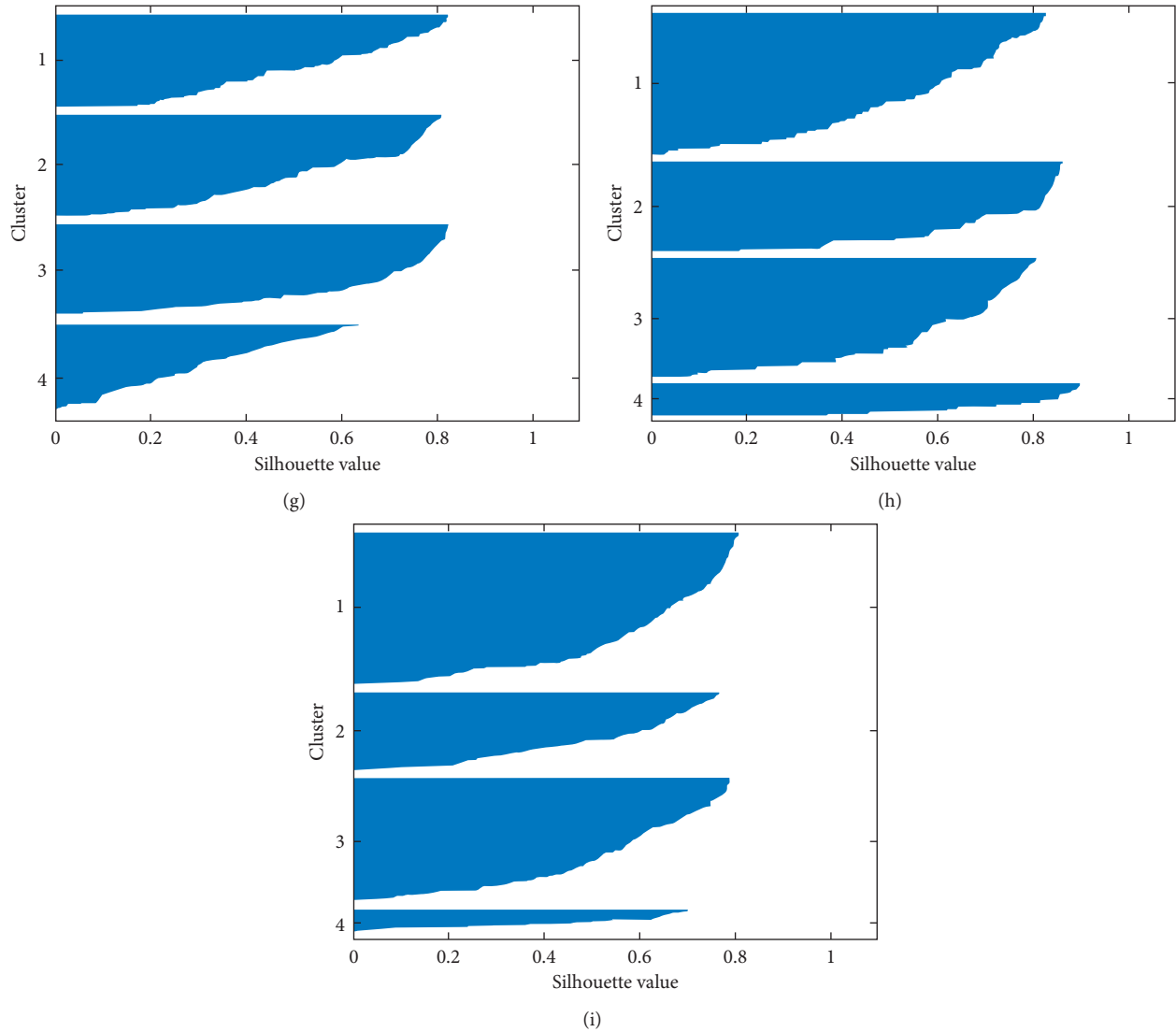


FIGURE 5: (a) Silhouette value of the expressway data in Jiangsu Province. Silhouette values of national and provincial highways data in (b) quarter 1 of 2018, (c) quarter 2 of 2018, (d) quarter 3 of 2018, (e) quarter 4 of 2018, (f) quarter 1 of 2019, (g) quarter 2 of 2019, (h) quarter 3 of 2019, (i) quarter 4 of 2019.

Figures 5(a)–5(i) show the silhouette values of the expressway data and the national and provincial highways data. A silhouette value is a value between -1 and 1 . When the cluster cohesion degree is equal to the separation degree, the silhouette value is 0 . The closer the silhouette value is to 1 , the better the cohesion degree and separation degree are. If the silhouette value is closer to -1 , the point should not be classified into a group. The figures show that all the silhouette values are above 0 , and most of them are above 0.8 , indicating that the result of the clustering is good.

The prediction results of BP, GRNN, and WNN of expressway data are shown in Figures 6(a)–6(c). The prediction results of monthly, quarterly, and annual BP, GRNN, and WNN of national and provincial highway data in Liyang city in 2018 are shown in Figures 7(a)–7(c), 8(a)–8(c), and 9(a)–9(c), respectively.

Figures 6(a), 7(a), 8(a), and 9(a) show that the predicted overload rate fits the actual overload rate well when using BPNN with the fitting curves “ $y = 0.99x + 0.0068$,” “ $y = 0.97x + 0.0088$,” “ $y = 0.96x + 0.011$,” and “ $y = 0.97x + 0.0021$,” respectively. The “ R^2 ” values are always larger than 0.95 ; this indicates the validity of the BPNN model. Figures 6(b), 7(b), 8(b), and 9(b) show the fitting degree of the predicted overload rate and the actual overload rate when using GRNN with the fitting curves “ $y = 0.53x + 0.045$,” “ $y = 0.49x + 0.036$,” “ $y = 0.83x + 0.0236$,” and “ $y = 0.86x + 0.0126$,” respectively. The “ R^2 ” values are approximately 0.5 , which does not correspond to a fitting degree as good as that exhibited by the results obtained using BPNN. Figures 6(c), 7(c), 8(c), and 9(c) show the fitting degree of the predicted overload rate and the actual overload rate when using WNN with the fitting curves “ $y = 0.16x + 0.151$,” “ $y = 0.18x + 0.1748$,”

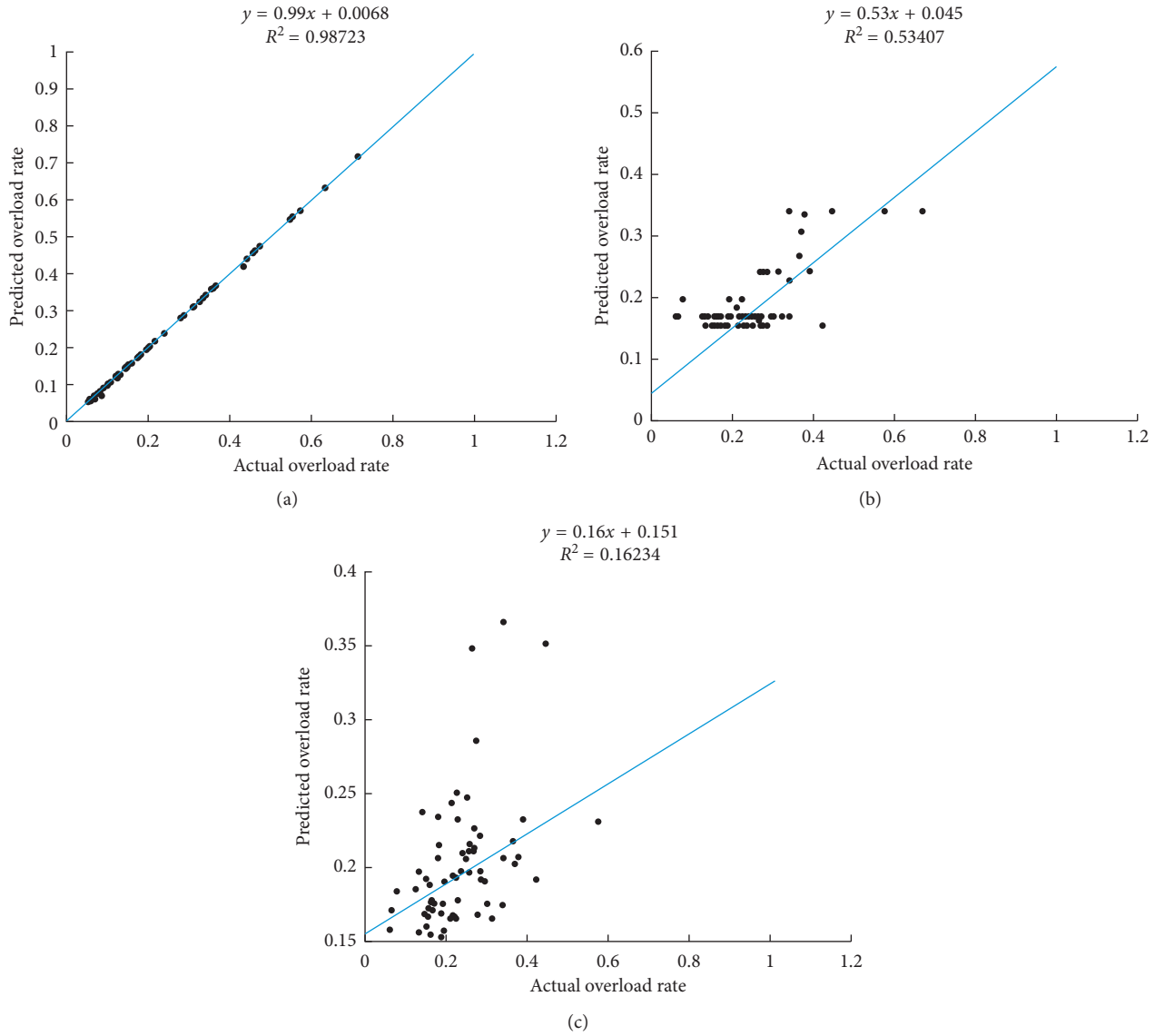


FIGURE 6: Prediction results of the (a) BPNN, (b) GRNN, and (c) WNN in Jiangsu province.

“ $y = 0.17x + 0.198$,” and “ $y = 0.02x + 0.217$,” respectively. The “ R^2 ” values are always less than 0.2, which corresponds to the lowest fitting degree among those of the three methods.

Tables 4–6 present the prediction results of the BPNN, GRNN, and WNN, respectively, indicating the data and results in the process of machine learning. All data are divided into training data and test data in a ratio of 10:1 and run according to the process described in Section 3.2. The prediction results of BPNN exhibit a high degree of fitting of all the validation data, training data, and test data, which also shows that the model performed well without overfitting. GRNN prediction required a long runtime owing to its inclusion of cross-validation and cycle training. WNN could not accurately predict the overload rate, and there was a gap between its prediction value and the actual value. It is speculated that WNN is typically used for short-term time-series prediction, whereas quarterly data and annual data prediction belong to long-term time-series prediction; thus,

the prediction results are not ideal, regardless of the overload rate and overload trend. Although the overload rate obtained from monthly data was not sufficiently accurate, it could reflect the overload trend. Furthermore, the WNN omitted attributes that were useful for prediction by BPNN, such as “License plate,” “Lane,” “Gross weight of vehicles and goods,” “Axle number,” and “Speed,” and only used “Overload rate” and short-term time series for the prediction. Thus, the prediction results reveal the weak correlation between the overload rate and short-term time.

5. Discussion

According to the clustering results of the expressways in Jiangsu Province, 6-axle vehicles weighing above 49 t and entering the expressways between 23:00–4:00 and 12:00–14:00 are more likely to exhibit overloaded behavior, and the overload rate of these vehicles is higher than that of others

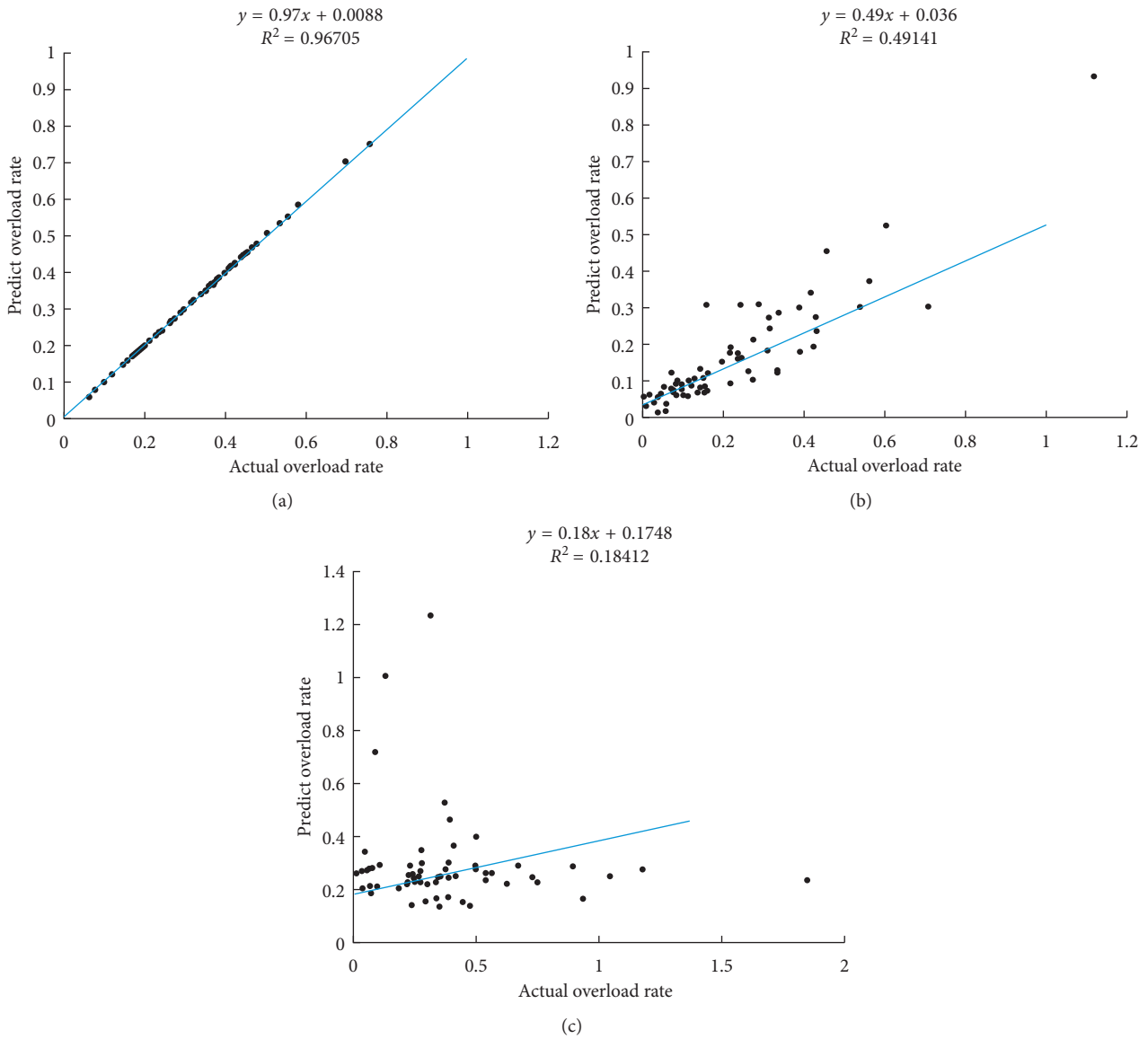


FIGURE 7: Prediction results of the (a) BPNN, (b) GRNN, and (c) WNN in Liyang city in 2018 (month).

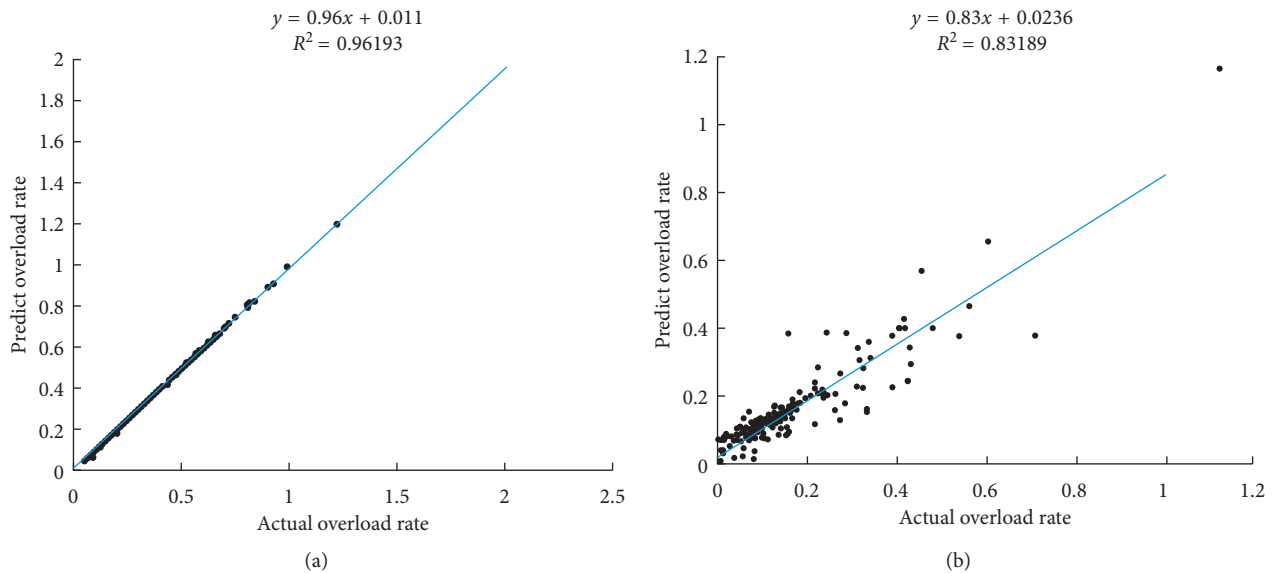


FIGURE 8: Continued.

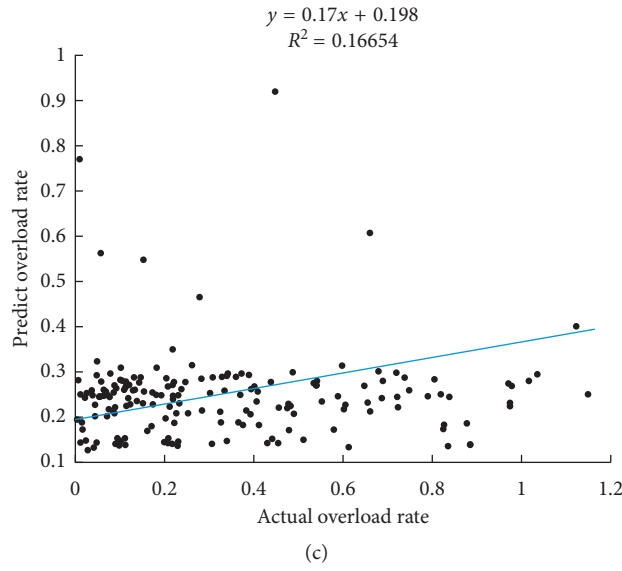


FIGURE 8: Prediction results of the (a) BPNN, (b) GRNN, and (c) WNN in Liyang city in 2018 (quarter).

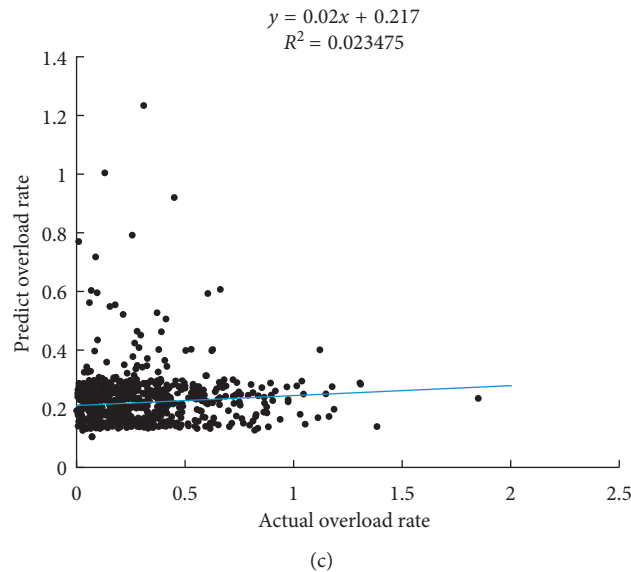
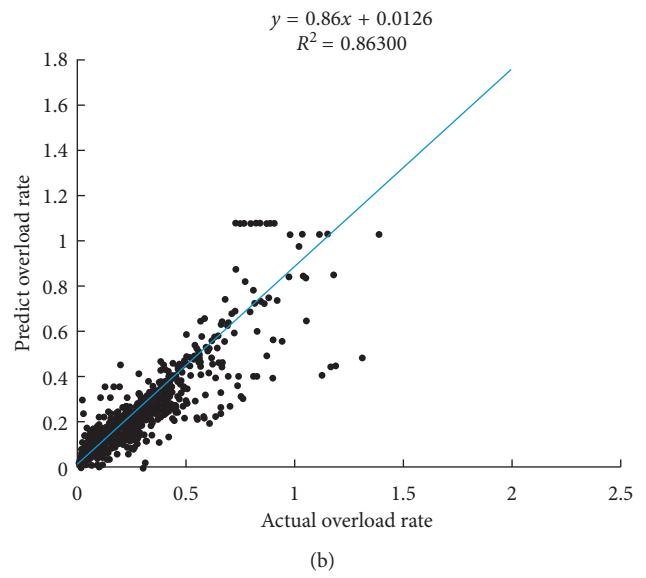
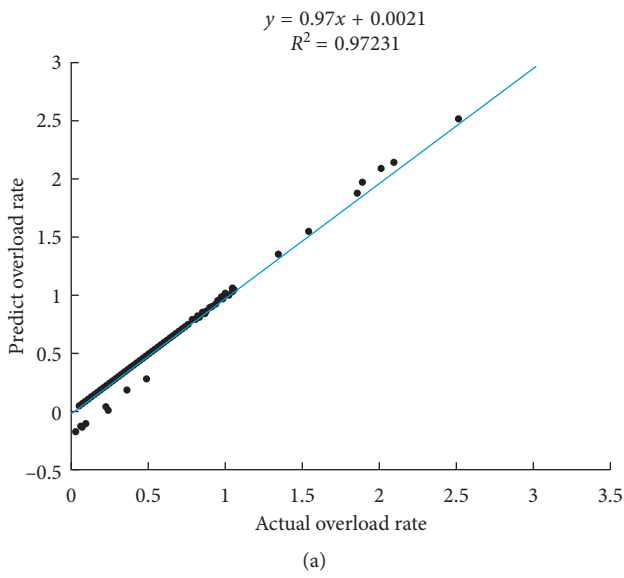


FIGURE 9: Prediction results of the (a) BPNN, (b) GRNN, and (c) WNN in Liyang city in 2018 (year).

TABLE 4: Prediction results of BPNN.

Data name	Highway data	National and provincial highway data (month)	National and provincial highway data (quarter)	National and provincial highway data (year)
Number of hidden nodes	16	3	8	6
Iteration times	3	3	5	6
Error descent gradient	0.008	0.005	0.019	0.034
R^2	0.987	0.967	0.962	0.972
MSE ($\%^2$)	0.090	0.055	0.093	0.059
RMSE (%)	0.960	2.960	3.060	1.460
ME (%)	2.700	-0.150	38.750	-3.200
MAE (%)	5.200	2.120	44.330	3.840
MAPE (%)	0.089	0.124	0.116	1.046
RMSPE (%)	0.059	0.026	0.058	0.894
Running time (s)	2.016	1.938	0.001	2.953

TABLE 5: Prediction results of GRNN.

Data name	Highway data	National and provincial highway data (month)	National and provincial highway data (quarter)	National and provincial highway data (year)
SPREAD	1.6	0.7	1.1	0.9
R^2	0.534	0.491	0.832	0.863
MSE ($\%^2$)	0.240	0.037	0.210	0.100
RMSE (%)	49.860	74.132	0.560	0.288
ME (%)	70.610	86.100	7.480	5.370
MAE (%)	-10.150	-12.150	-3.020	-8.960
MAPE (%)	0.542	0.622	0.048	0.102
RMSPE (%)	0.640	0.684	0.403	0.871
Running time (s)	5.156	7.016	12.313	19.031

TABLE 6: Prediction results of WNN.

Data name	Highway data	National and provincial highway data (month)	National and provincial highway data (quarter)	National and provincial highway data (year)
R^2	0.162	0.184	0.169	0.020
MSE ($\%^2$)	18.250	48.570	41.620	59.050
RMSE (%)	0.810	1.110	0.930	7.684
ME (%)	9.000	10.520	9.640	12.524
MAE (%)	5.480	-3.790	-5.710	-9.324
MAPE (%)	0.079	0.069	0.073	9.413
RMSPE (%)	0.510	0.352	0.388	3.443
Running time (s)	0.484	1.219	0.563	1.656

during this period. Most vehicles enter the expressway at 05:00 and 17:00–22:00, among which 6-axle vehicles weighing above 49 t are more likely to be overloaded. This means that the inspection workers should constantly pay more attention to the vehicles weighing above 49 t during this period. Further, more resources, such as manpower, should be allocated between 23:00–04:00 and 12:00–14:00.

Comparing the clustering results of 2018 and 2019 in Table 3, certain changes were observed in the group characteristics over the past two years. (1) The difference in the peak hour between 2018 and 2019 is approximately 2 h, and the difference in the trough hour between 2018 and 2019 is approximately 2 h. This is speculated to be because the working hours of overload management in 2018 and 2019

had changed. (2) In 2018 and 2019, the overload rate in the first quarter was lower than that in the other three quarters. Compared with that in 2018, the overload rate in 2019 was reduced. This is speculated to be because Changzhou performed several joint actions of overloading management in 2019, because of which the overloading governance had been strengthened. (3) Between 2018 and 2019, there were no evident changes in the “Gross weight of vehicles and goods” and “Axle number.”

Table 7 summarizes the clustering results of national highways in 2018 and 2019. In 2018, most overloaded vehicles entered the highways between 00:00–08:00 and between 16:00–20:00, and vehicles with higher overload rates were concentrated between 21:00–23:00 and between 02:

TABLE 7: Summary of the laws of clustering results of the national and provincial highways when $k = 4$.

Year	Quarter	Most overloaded vehicles			Vehicles with high overload rate		
		Entry time	Gross weight of vehicle and goods	Axle number	Entry time	Gross weight of vehicle and goods	Axle number
2018	1	0:00–8:00	Over 49 t	6	2:00–3:00	Over 49 t	6
	2	0:00–8:00	Over 49 t	6	21:00–23:00	Over 49 t	6
	3	0:00–8:00	Over 49 t	6	21:00–23:00	Over 49 t	6
	4	0:00–8:00	Over 49 t	6	23:00	Over 49 t	6
2019	1	4:00–13:00	Over 49 t	6	0:00–3:00	Over 49 t	6
	2	0:00–15:00	Over 49 t	6	0:00–3:00	Over 49 t	6
	3	4:00–5:00	Over 49 t	6	2:00–3:00	Over 49 t	6
	4	8:00–15:00	Over 49 t	6	0:00–4:00	Over 49 t	6

00–03:00. In 2019, most overloaded vehicles entered the highway from 04:00 to 15:00, and vehicles with a high overload rate were concentrated between 00:00–03:00. In 2018–2019, most overloaded vehicles were 6-axle vehicles weighing above 49 t, and the vehicles with high overload rates were also 6-axle vehicles weighing above 49 t.

Comparing the prediction results of the BPNN, GRNN, and WNN, the common evaluation indexes of the regression prediction model include mean-squared error (MSE), the deterministic coefficient R^2 , and goodness of fit. The numerical value of the deterministic coefficient R^2 reflects the goodness of fit. Therefore, we selected the deterministic coefficient, MSE, and the running time t of the entire code as the model performance criteria. In addition, this study used the root-mean-squared error (RMSE), mean error (ME), mean absolute error (MAE), mean absolute percentage error (MAPE), and root-mean-squared percentage error (RMSPE) as five different performance criteria Table 8. The averages of $(1 - R^2)$, MSE, RMSE, ME, MAE, MAPE, and RMSPE are calculated Table 9 to eliminate the prediction error of the BPNN, GRNN, and WNN [30].

The average values and all the seven performance criteria show that the prediction of BPNN is better than that of GRNN and WNN. Its performance is more accurate, especially for the “highway data” and “national and provincial highway data (month).” This is because the amount of data increases with time. Although the overall fitting degree is high, the individual prediction errors are greater, and certain performance criteria also increase with the increase in the number of errors. To clearly evaluate the adequacy of this performance, the performance of BPNN in this study was compared with that in existing studies. For example, Kumar used an ANN to predict the short-term traffic flow of non-urban expressways. In this study, when the amount of data was 160, the fitting degree was 0.9984, and when the data amount was 480, the fitting degree was 0.9988 [31]. The fitting degree of the BPNN in this study was larger than 0.90 and was nearly 0.99, which shows that the BPNN in this study has a very high degree of fitting and the model performs well.

To detect the defects of GRNN and WNN, the performances of GRNN and WNN were also compared with those of other studies. Zhang and Zhang used the spatial

relationship of traffic flow near U.S. Highway and developed two multivariate forecasting approaches, in which the GRNN was also used [22]. In this research, 91.32% of the forecasting error was less than 20%. Tang et al. used WNN to predict the short-term traffic flow with a fitting degree of 0.9453 and used 230 datasets in modeling [31]. They used the WNN to predict short-term traffic flow with a fitting degree of 0.936, 864 datasets for modeling, and running time of 0.995. Compared with that of Tang et al. [32], the fitting degree of WNN in this research was extremely low. However, when the datasets were the same, the running time was similar to that in other studies. The reason is that although the subjects of the study are different, the traffic flow has a strong correlation with time. In terms of overload, compared with other attributes such as “Time,” “License plate,” “Lane,” “Gross weight of vehicles and goods,” “Axle number,” and “Speed,” the overload rate has a weak correlation with time.

By comparison, the combined results of Tables 8 and 9 are as follows.

- (1) The prediction performance of BPNN is superior to that of GRNN and WNN. Given sufficient data, BPNN is a better forecasting method with a high fitting degree, minimum MSE, and short running time. BPNN performs well in hourly highway data prediction and annual overload rate prediction, and the prediction results of BPNN can help determine the centralized overload management time.
- (2) With the increasing amount of data, the fitting degree of GRNN increases, and the running time also increases. In this study, the method of adding a “for loop” to find the best SPREAD greatly increases the running time. Compared with other networks, GRNN had the longest running time.
- (3) Compared with BPNN and GRNN, WNN has the shortest running time in overload rate prediction. Although the fitting degree of WNN is low, it only requires an overload rate for prediction. It can reflect the future trends of the overload rate in the monthly data prediction of overload, and its prediction results can help determine the centralized overload management time when the data are insufficient.

TABLE 8: Results of the NN.

	Neural network	Highway data (hour)	National and provincial highway data (month)	National and provincial highway data (quarter)	National and provincial highway data (year)
Running time (s)	BPNN	2.016	1.938	2.125	2.953
	GRNN	5.156	7.016	12.313	19.031
	WNN	0.484	1.219	0.563	1.656
R^2	BPNN	0.987	0.967	0.962	0.972
	GRNN	0.534	0.558	0.832	0.863
	WNN	0.162	0.184	0.169	0.021
MSE (% ²)	BPNN	0.960	2.960	3.060	1.460
	GRNN	49.860	74.130	0.560	0.290
	WNN	0.810	1.110	0.930	7.684
RMSE (%)	BPNN	2.700	-0.150	3.880	-3.200
	GRNN	70.610	86.100	7.480	5.370
	WNN	9.000	10.520	9.640	12.524
ME (%)	BPNN	5.200	2.120	4.430	3.840
	GRNN	-10.150	-12.150	-3.020	-8.960
	WNN	5.480	-3.790	-5.710	-9.324
MAE (%)	BPNN	0.090	0.060	0.090	0.060
	GRNN	0.240	0.040	0.210	0.100
	WNN	18.250	48.570	41.620	59.050
MAPE (%)	BPNN	0.089	0.124	0.116	1.046
	GRNN	0.542	0.622	0.048	0.102
	WNN	0.079	0.069	0.073	9.413
RMSPE (%)	BPNN	0.059	0.026	0.058	0.894
	GRNN	0.640	0.684	0.403	0.871
	WNN	0.510	0.352	0.388	3.443

TABLE 9: Average of seven performance criteria.

	Highway data (hour)	National and provincial highway data (month)	National and provincial highway data (quarter)	National and provincial highway data (year)
BPNN	0.175	0.167	0.179	0.419
GRNN	0.403	0.478	0.191	0.258
WNN	0.155	0.167	0.156	29.214

6. Conclusions

In this study, we used machine learning to establish a model for highway overrun and overload, considering Jiangsu Province as an example. The characteristics of overloading were summarized by clustering the historical data of overloading, and a forecasting model of overloading with a high fitting degree based on BPNN was obtained. We provided information with potential value for expressway network management departments through data mining. This information could help these management departments allocate resources reasonably and optimize the information utilization rate. The conclusions of this study can be grouped into two aspects: daily overload management based on cluster analysis and immediate overload management based on NNs.

The overload characteristics based on cluster analysis, human resources, and other related resources should be allocated rationally. Targeted monitoring should be performed for overload control and management level, and the governance efficiency should be enhanced using information technology. Currently, numerous large loopholes remain in time and space in law enforcement inspection, and law

enforcement personnel and equipment are limited. Therefore, the thorough use of historical overload data is necessary to satisfy the demand for taking severe measures on overloaded vehicles according to the law of overload characteristics. For example, based on the conclusion of this study, we can focus on monitoring 6-axle vehicles weighing above 49 t and entering an expressway between 23:00–04:00 and 12:00–14:00, and 6-axle vehicles weighing above 49 t entering the national provincial highway of a city between 21:00–23:00 and 02:00–03:00. The allocation of manpower and other related resources should be increased in this period, and related resources should be saved during other periods. Based on the overloading characteristics, different types of vehicles in different periods must be thoroughly investigated to improve the management efficiency of the transportation departments. For example, special attention must be paid to 2-axle vehicles weighing 18–27 t and entering a highway between 06:00–07:00 and 15:00–16:00 and to 4-axle vehicles weighing 37–43 t and 43–49 t and entering a highway between 08:00–11:00. Concurrently, the traffic management department can reasonably adjust the working hours of staff in different seasons. For example, the working hours of staff in the first quarter can

be reduced according to the conclusion of this study to effectively enhance the work efficiency.

Based on the prediction model obtained by the NN, we can predict the overload rate and overload trend, develop auxiliary programs or software, and improve the existing law enforcement system. The information resources of administrative departments in fundamental areas have been in a closed state. The information resources of administrative law enforcement and administrative law enforcement supervision are integrated and shared, and real-time information, such as that on personnel and equipment, is added based on the existing system data to improve the overloaded vehicles database. Based on the BPNN model used in this study, the real-time information on personnel and equipment can be integrated to develop auxiliary programs or software to realize online inquiry by law enforcement departments and online supervision of law enforcement activities. Thus, all departments can inquire about the current overload rate and trend at any time, especially in centralized law management, and can reasonably determine the time and place of centralized law management with the help of prediction results and integrated information of manpower and equipment. By checking changes in manpower, equipment, and other information, we can determine real-time actions for various departments, ensure business linkage, promote the linkage work of administrative law enforcement, further promote the governance of overloading, and improve the efficiency of law enforcement systems.

The overload data mining of expressways in this research is limited to expressways in Jiangsu Province, and the overload data mining of national and provincial highways is limited to Liyang city, which is not universal. Furthermore, the spatial attributes, namely, "Entrance site" and "Exit site" were not analyzed. Our follow-up research will focus on a considerably comprehensive feature analysis and mining of the spatiotemporal law of overloading. Using geographic information system (GIS), global positioning system, spatial statistical models, and other advanced technologies, we aim to explore the spatiotemporal law of overloaded vehicles in highways, visualize it with the help of GIS, predict the destination area of overloading, overloading transportation volume, and overloading transportation routes, and conduct more in-depth analysis to reveal the existence of overloading of freight vehicles in highway networks in different airspaces.

Data Availability

The data used to support the findings of this study are available from the corresponding author upon request.

Conflicts of Interest

The authors declare that they have no conflicts of interest.

Acknowledgments

This work was supported by the National Natural Science Foundation of China (Grant Number: 71573037) and the

Priority Academic Program Development of Jiangsu Higher Education Institutions in China (Grant Number: 1105007002).

References

- [1] C. L. Dos Santos Romeiro Júnior, L. A. Teixeira Brito, L. F. Heller et al., "Impact on pavement deterioration due to overload vehicle regulation in Brazil," *Transportation Research Procedia*, vol. 45, pp. 842–849, 2020.
- [2] K. Bucshházy, E. Matuchová, R. Zůvala, P. Moravcová, M. Kostíková, and R. Mikulec, "Human factors contributing to the road traffic accident occurrence," *Transportation Research Procedia*, vol. 45, pp. 555–561, 2020.
- [3] Y. Dai, J. Guo, L. Yang, and W. You, "A new approach of intelligent physical health evaluation based on GRNN and BPNN by using a wearable smart bracelet system," *Procedia Computer Science*, vol. 147, pp. 519–527, 2019.
- [4] W. Han, J. Wu, C. S. Cai, and S. Chen, "Characteristics and dynamic impact of overloaded extra heavy trucks on typical highway bridges," *Journal of Bridge Engineering*, vol. 20, no. 2, Article ID 5014011, 2015.
- [5] B. Li and X. Wang, "Analysis of the freeway overrun limit based on system clustering," *Modern Computer*, vol. 59, pp. 39–42, 2018.
- [6] S. Ryu, A. Chen, and K. Choi, "A modified gradient projection algorithm for solving the elastic demand traffic assignment problem," *Computers & Operations Research*, vol. 47, pp. 61–71, 2014.
- [7] M. Cheng, C. Li, L. Wu, Li Zhang, and X. Cheng, "Analysis on the detour behavior of freight vehicles based on expressway toll data," *Journal of Highway and Transportation Research and Development*, vol. 15, pp. 299–301, 2019.
- [8] R. Zhang, *Analysis on the Influence of Overload Control on Road Capacity*, Transpo World, Beijing, China, 2019.
- [9] K. Mirsad, I. Zoran, D. Slavko, and P. Ivo, "Modelling truck weigh stations' locations based on truck traffic flow and overweight violation: a case study in Bosnia and Herzegovina," *Promet*, vol. 30, no. 2, pp. 163–171, 2018.
- [10] G. Kostopoulos, K. Neureiter, D. Papatou, M. Tscheligi, and C. Chrysoulas, "ProMe: a mentoring platform for older adults using machine learning techniques for supporting the "live and learn" concept," *Mobile Information Systems*, vol. 2018, Article ID 9723268, 8 pages, 2018.
- [11] Ç. Muhammed Yasin and Ü. Ahmet, "An estimation of transport energy demand in Turkey via artificial neural networks," *Promet*, vol. 31, no. 2, pp. 151–161, 2019.
- [12] F. Li, C.-H. Chen, P. Zheng et al., "An explorative context-aware machine learning approach to reducing human fatigue risk of traffic control operators," *Safety Science*, vol. 125, Article ID 104665, 2020.
- [13] M. Mohammed Abdulhafedh, H. Mazen Radhe, and D. Shankar, "Analysis of performance limitations in optical wireless communication system due to laser source impairment (RIN) and background noise," *Advances in Intelligent Systems and Computing*, vol. 452, pp. 521–531, 2016.
- [14] H. Yu and X. Li, "On the chaos analysis and prediction of aircraft accidents based on multi-timescales," *Physica A: Statistical Mechanics and Its Applications*, vol. 534, Article ID 120828, 2019.
- [15] M. Sangare, S. Gupta, S. Bouzeffrane, S. Banerjee, and P. Muhlethaler, "Exploring the forecasting approach for road accidents: analytical measures with hybrid machine learning,"

- Expert Systems with Applications*, 2020, In press, Article ID 113855.
- [16] Y. Lin and R. Li, "Real-time traffic accidents post-impact prediction: based on crowdsourcing data," *Accident Analysis & Prevention*, vol. 145, Article ID 105696, 2020.
- [17] S. Onder, "Evaluation of occupational injuries with lost days among opencast coal mine workers through logistic regression models," *Safety Science*, vol. 59, pp. 86–92, 2013.
- [18] W. Jiang, J. Josse, and M. Lavielle, "Logistic regression with missing covariates-parameter estimation, model selection and prediction within a joint-modeling framework," *Computational Statistics & Data Analysis*, vol. 145, Article ID 106907, 2020.
- [19] S. S. Yassin and Pooja, "Road accident prediction and model interpretation using a hybrid K-means and random forest algorithm approach," *SN Applied Sciences*, vol. 2, Article ID 1576, 2020.
- [20] E. Zunic, A. Djedovic, and D. Donko, "Cluster-based analysis and time-series prediction model for reducing the number of traffic accidents," in *Proceedings of the International Symposium ELMAR*, pp. 25–29, Zadar, Croatia, September 2017.
- [21] Y.-F. Wang, L.-T. Wang, J.-C. Jiang, J. Wang, and Z.-L. Yang, "Modelling ship collision risk based on the statistical analysis of historical data: a case study in Hong Kong waters," *Ocean Engineering*, vol. 197, Article ID 106869, 2020.
- [22] Y. Zhang and Y. Zhang, "A comparative study of three multivariate short-term freeway traffic flow forecasting methods with missing data," *Journal of Intelligent Transportation Systems*, vol. 20, no. 3, pp. 205–218, 2016.
- [23] Q. Hou, J. Leng, G. Ma, W. Liu, and Y. Cheng, "An adaptive hybrid model for short-term urban traffic flow prediction," *Physica A: Statistical Mechanics and Its Applications*, vol. 527, Article ID 121065, 2019.
- [24] J.-C. Huang, K.-M. Ko, M.-H. Shu, and B.-M. Hsu, "Application and comparison of several machine learning algorithms and their integration models in regression problems," *Neural Computing and Applications*, vol. 32, no. 10, pp. 5461–5469, 2020.
- [25] T. Arsan and M. M. N. Hameez, "A clustering-based approach for improving the accuracy of UWB sensor-based indoor positioning system," *Mobile Information Systems*, vol. 2019, Article ID 6372073, 13 pages, 2019.
- [26] A. U. Haq, J. P. Li, M. H. Memon, S. Nazir, and R. Sun, "A hybrid intelligent system framework for the prediction of heart disease using machine learning algorithms," *Mobile Information Systems*, vol. 2018, Article ID 3860146, 21 pages, 2018.
- [27] S. Amin, "Backpropagation—artificial neural network (BP-ANN): understanding gender characteristics of older driver accidents in west midlands of United Kingdom," *Safety Science*, vol. 122, Article ID 104539, 2020.
- [28] L. Xiao, J. Wang, R. Hou, and J. Wu, "A combined model based on data pre-analysis and weight coefficients optimization for electrical load forecasting," *Energy*, vol. 82, pp. 524–549, 2015.
- [29] A. Miglani and N. Kumar, "Deep learning models for traffic flow prediction in autonomous vehicles: a review, solutions, and challenges," *Vehicular Communications*, vol. 20, Article ID 100184, 2019.
- [30] W. Wang, R. Tang, C. Li, P. Liu, and L. Luo, "A BP neural network model optimized by mind evolutionary algorithm for predicting the ocean wave heights," *Ocean Engineering*, vol. 162, pp. 98–107, 2018.
- [31] K. Kumar, M. Parida, and V. K. Katiyar, "Short term traffic flow prediction for a non urban highway using artificial neural network," *Procedia—Social and Behavioral Sciences*, vol. 104, pp. 755–764, 2013.
- [32] R. Tang, Q. Chen, and X. Lei, "GQPSO-WNN short-term traffic flow forecasting based on phase space reconstruction," *Computer Applications and Software*, vol. 36, no. 7, pp. 311–316, 2019.

Research Article

LEO Satellite Channel Allocation Scheme Based on Reinforcement Learning

Fei Zheng,^{1,2} Zhao Pi ,¹ Zou Zhou ,¹ and Kaixuan Wang³

¹Ministry of Education Key Laboratory of Cognitive Radio and Information Processing, Guilin University of Electronic Technology, Guilin 541004, China

²State key Laboratory of Networking and Switching Technology (Beijing University of Posts and Telecommunications), Beijing 100876, China

³Department of Information, Shanxi University of Finance and Economics, Taiyuan 030006, China

Correspondence should be addressed to Zou Zhou; zhouzou@guet.edu.cn

Received 15 August 2020; Revised 29 October 2020; Accepted 30 November 2020; Published 12 December 2020

Academic Editor: Chi-Hua Chen

Copyright © 2020 Fei Zheng et al. This is an open access article distributed under the Creative Commons Attribution License, which permits unrestricted use, distribution, and reproduction in any medium, provided the original work is properly cited.

Delay, cost, and loss are low in Low Earth Orbit (LEO) satellite networks, which play a pivotal role in channel allocation in global mobile communication system. Due to nonuniform distribution of users, the existing channel allocation schemes cannot adapt to load differences between beams. On the basis of the satellite resource pool, this paper proposes a network architecture of LEO satellite that utilizes a centralized resource pool and designs a combination allocation of fixed channel preallocation and dynamic channel scheduling. The dynamic channel scheduling can allocate or recycle free channels according to service requirements. The Q-Learning algorithm in reinforcement learning meets channel requirements between beams. Furthermore, the exponential gradient descent and information intensity updating accelerate the convergence speed of the Q-Learning algorithm. The simulation results show that the proposed scheme improves the system supply-demand ratio by 14%, compared with the fixed channel allocation (FCA) scheme and by 18%, compared with the Lagrange algorithm channel allocation (LACA) scheme. The results also demonstrate that our allocation scheme can exploit channel resources effectively.

1. Introduction

In recent years, with the development of wireless communication technology, the terrestrial cellular network is facing the explosive growth of data traffic. Although the terrestrial cellular network has the advantages of short delay and large bandwidth, it still has some limitations [1]. Due to the limit of geographical environment and economy, it is difficult for cellular networks to cover special areas such as oceans, deserts, forests, and islands. Ocean navigation, geological exploration, environmental emergency rescue, and other scenarios rescue require an all-weather, wide-coverage, highly reliable communication mode. Satellite communication can solve the above problems well by virtue of wide coverage, small geographic limitation, and large system capacity.

The satellite communication system has experienced the development of global beams, regional beams, and spot

beams. Flexible resource allocation between spot beams can further improve system performance. Among various types of satellites, LEO satellites have the characteristics of low path loss, short communication delay, and flexible orbital position [2]. LEO constellations can achieve seamless coverage of global regions [3, 4]. With the development of satellite communication technology, intersatellite link (ISL) and on-board processing (OBP) can support satellite routing and data processing independently from the terrestrial network. The maturity and reliability of IP technology also make the application of IP technology in satellite networks become the trend in the future [5]. In addition to communications payloads, the satellites carry automated directed surveillance by broadcast (ADS-B) payloads, which are primarily used for aircraft flight surveillance and tracking aircraft position reports, as well as navigation augmentation payloads. Ground-based gateway stations are also capable of communicating with multiple

satellites simultaneously, synthesizing data streams from different satellites [6]. The cost reduction of satellite manufacture and launch has also promoted the rapid development of the LEO satellite Internet industry. LEO satellite network is becoming an important part of the future global mobile communication system.

Satellite communication systems are typical resource-constrained systems. Available spectrum, power, time slot, and other resources are extremely scarce and precious [7]. An efficient network resource allocation scheme is urgently needed to solve the above problem in the satellite communication systems. Due to the dynamic coverage change caused by satellite movement and nonuniform distribution of ground users, the traffic load is changing all the time, while satellite on-board resources are solidified at the factory setting. Traditional fixed channel allocation (FCA) scheme is difficult to adapt to rapidly changing business requests. Dynamic channel allocation (DCA) can realize resource cross-beam scheduling and has a higher resource utilization rate than FCA [8]. The business request is a discrete dynamic process in communication networks, and the allocation results at the current time will affect the decision at a subsequent time. The existing dynamic channel allocation algorithms focus on the instantaneous performance of the LEO satellite system and ignore the time-domain relevance problem in the channel allocation process [7].

Reinforcement Learning (RL), as an emerging technology, provides a new solution to solve complex decision-making problems [9]. Under the background of rapidly growing data and complex system structure, RL can better adapt to complex decision-making problems, which are difficult for traditional algorithms. By combining satellite resource allocation with RL, the decision-making ability of the satellite system can be well enhanced [7].

This paper considers the difference in service distribution and the time correlation of channel allocation in satellite communication systems. The Q-Learning algorithm is used for dynamic channel allocation in a LEO satellite. The main contributions are as follows:

- (i) The on-board resource pool is introduced to manage channel resources in the LEO satellite network. The resource pool integrates information processing, resource allocation and resource acquisition, enabling cross-beam scheduling of channels. So that the system can better adapt to business differences between beams.
- (ii) A two-step allocation scheme combining fixed channel preallocation and dynamic channel scheduling is proposed to schedule the channel. The system preallocates some fixed channels for each beam cell before services arriving; dynamic channel allocation schedules channel according to the services request.
- (iii) RL improves the decision-making ability of the system on resource allocation. The problem is described as a Markov decision process with defining state space, action space, and reward function. The system trains the optimal channel allocation strategy through a Q-learning algorithm for channel resource allocation.
- (iv) Exponential gradient descent and information intensity updating accelerate the convergence of the algorithm and improve the decision-making speed of the LEO satellite system.

The rest of this paper is organized as follows. In Section 2, we give related works. In Section 3, we describe the architecture of LEO satellite network based on on-board resource pool and establish the channel allocation model and problem optimization strategy. We give the specific content of the algorithm and distribution process in Section 4. In Section 5, we present and discuss simulation results. Finally, conclusions are presented in Section 6.

2. Related Work

In this section, we introduce some related works about LEO satellite networks and satellite resource allocation.

2.1. LEO Satellite Communication System. The size of the LEO satellite constellation is becoming larger and larger due to the advantages of technology and cost. A large-scale constellation can better achieve global coverage and greatly expand the system capacity [10]. In highly complex and frequently changing systems, it is critical to consider the load on the underlying network components due to user behavior. The massive traffic loads also challenge the quality of service (QoS) of LEO Satellite communication systems [11]. The satellite system is different from the terrestrial network, so researchers adopt some special frames and protocols according to the particularity of satellite systems, including data relay satellite (DRS) system, delay-tolerant network (DTN), and performance enhancement system (PES). However, these satellite communication protocols based on TCP/IP have poor mobility, high overhead, and high complexity [4]. Further, most of the existing satellite network protocols are only applicable to medium Earth orbit (MEO) geosynchronous Earth orbit (GEO) satellites. Therefore, network architecture and resource management system are particularly important for LEO satellites.

2.2. LEO Satellite Network Architecture. Recently, the construction of commercial LEO satellite systems is active all over the world, but it is hard to avoid some challenges in the network architecture and resource management. The architecture of the O3b system in the MEO satellite network and the OneWeb system adopts a transparent forwarding mechanism. These two systems have no interstar networking, routing, and switching function, and the system resource utilization is low when business is highly dynamic [12]. The architecture of Iridium and SpaceX relies on ISL to achieve intersatellite networking, but their networking technologies are relatively backward, the control plane and forwarding plane are highly

coupled, and the resource scheduling mechanism requires more human intervention, which all reduce the resources utilization efficiency [13]. To solve the above problems, researchers have made a lot of efforts on LEO satellite network architecture and corresponding resource allocation scheme.

As a resource management unit that is widely used in the terrestrial wireless network, a resource pool can realize resource sharing and dynamic scheduling according to service requirements and improve spectrum efficiency. However, current works mainly focus on the resource pool architecture design of earth-gate-station (EGS) or the centralized management of satellite network virtualization, rather than satellite resource pool. Reference [14] proposes a design scheme of EGS based on resource pool architecture. By integrating digitizing, the resource pool can achieve signal processing and baseband processing functions, the utilization of high-speed data communication resources can be effectively improved in satellite networks. In view of the problems existing in the “chimney” architecture of EGS, [15, 16] propose architectures based on resource pool to solve the instability of EGS systems. The researchers compare the two architectures with and without resource pooling and found that the resource pooled system architecture is more reliable while improving the efficiency and flexibility of device resource use. Reference [17] presently analyses the contradiction between resource constraint and business demand in satellite networks and proposes the concept of “on-board resource virtualization”. Further, researchers construct a mission-oriented satellite network resource management model and conduct on-board resource allocation by means of resource sharing and collaborative management. At the present stage, satellite communications are creating suitable operational control systems for different functions and different series of satellites in order to achieve efficient utilization of resources [18].

2.3. LEO Satellite Resource Allocation Scheme. The satellite resource allocation scheme will directly affect the user’s QoS and system performance. Reference [19] considers the trade-off between the maximum total system capacity and interbeam fairness to obtain the optimal allocation scheme by a subgradient algorithm. Reference [20] optimizes the allocation strategy by calculating and comparing user transmission rates under different transmission modes and strong interference. Reference [21] explains the physical layer structure of a multibeam satellite system, simplifies the three-dimensional coordinate system of the ground user to the two-dimensional coordinate system in the equatorial plane. Further, researchers calculate the maximum channel capacity according to the satellite beam coverage area and transmission power. Reference [22] proposes a beam-hopping algorithm, which adjusts the beam size according to the business distribution. Reference [23] uses a heuristic algorithm to achieve frequency band selection and beam allocation and adopts Lagrangian dual algorithm and water-filling-assisted Lagrangian dual algorithm to achieve power allocation. Reference [24] proposes a channel allocation scheme of mixed random access

and on-demand access, which reduces system delay within the throughput threshold. This scheme provides effective solutions for services with different delay sensitivities. The above satellite resource allocation scheme improves the system performance in some aspects. However, they only focus on the instantaneous performance of the system and ignore the time correlation in the resource allocation process. The allocation result of the previous time will indirectly lead to the subsequent allocation effect, which will undoubtedly affect the system resource utilization.

The satellite channel allocation can be regarded as a sequential decision problem, and a decision is made on the arriving user request within each interval T . RL is a good way to adapt to this decision-making problem. References [25, 26] uses augmentation learning to solve channel allocation and congestion control in satellite Internet of things (SIoT). Compared with traditional algorithms, RL can improve performance in terms of energy consumption and blocking rate. Reference [27] extends single-agent deep reinforcement learning (DRL) to multiagents and propose a collaborative multiagent DRL method so as to improve transmission efficiency and achieve the desired goal with lower complexity. Reference [28] discusses a scheme of combining RL and resource allocation in different heterogeneous satellites and multiple service requirements and demonstrates the application effect of DRL in heterogeneous satellite networks (HSN). However, there are few researches on LEO satellite resource allocation. Most of the research has focused on MEO and GEO satellites. Therefore, this paper applies RL to the LEO satellite resource allocation. We adopt emerging technologies to solve LEO satellite channel allocation challenges in a different way.

3. System Model

In this section, we propose a LEO satellite network architecture based on an on-board resource pool and explain the centralized resource allocation in detail. Further, we establish an optimization model based on the user supply-demand ratio.

3.1. Framework of LEO Satellite Network. Figure 1 shows a LEO satellite network architecture. In the network layer, adjacent satellites transmit data through ISLs, and multiple satellites cooperate to complete the global coverage. The centralized resource pool can manage the channel, computing, caching, and other resources. In the link layer, the network control center (NCC) provides services for users by uploading data from satellites. Edge cloud computing devices are connected through multiple satellite relays. Idle computing resources on the constellation network can also be used as edge cloud devices. LEO constellation is composed of numerous LEO satellites, which can provide services for users in cities, suburbs, and oceans in the global region.

Figure 2 shows the structure of a centralized resource pool in a LEO satellite. Each centralized resource pool is the

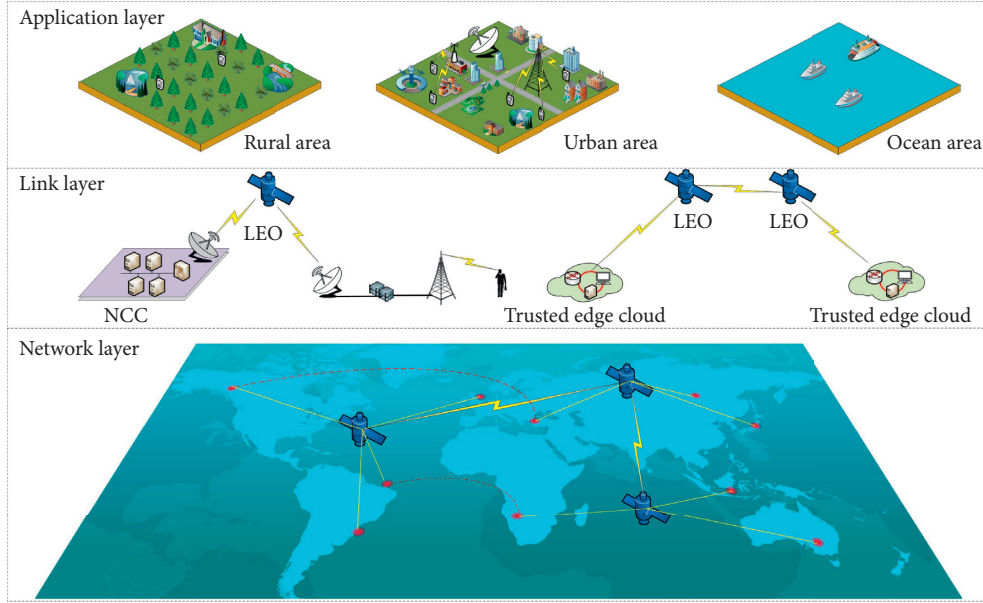


FIGURE 1: LEO satellite network architecture.

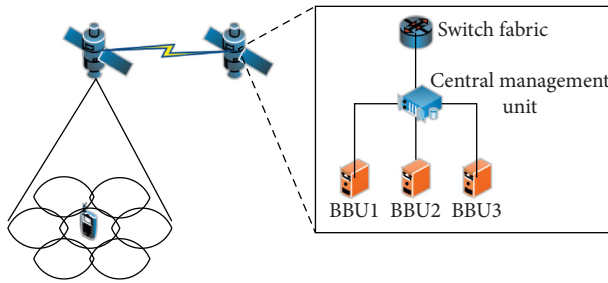


FIGURE 2: Structure of on-board resource pool.

core of the whole system, which integrates information processing, resource allocation, and resource collection. Resources between the satellites are connected through switch fabrics and resources are allocated in real time. A central management unit centrally manages BBU under the switching structure. For a single satellite, a centralized resource pool composed of high-performance processors can process services of all beams within its coverage, as shown in Figure 3. Compared with traditional dynamic resource allocation, the satellite with centralized resource pool can achieve resource allocation cross beams. The centralized resource pool not only processes and allocates resources for user's requests, but also schedules resource according to the utilization of resources in each beam to adapt to the business differences.

3.2. Channel Allocation Modelling. A LEO satellite has N beams on the ground through phased array antennas, represented by a set $X = \{x_n | n = 1, 2, \dots, N\}$. The system available channels are represented by a set $Y = \{y_m | m = 1, 2, \dots, M\}$, and system total bandwidth is B_{tot} . Users in beam x_n can be represented by a set $U = \{u_{n,k} | n = 1, 2, \dots, N, k = 1, 2, \dots, K\}$.

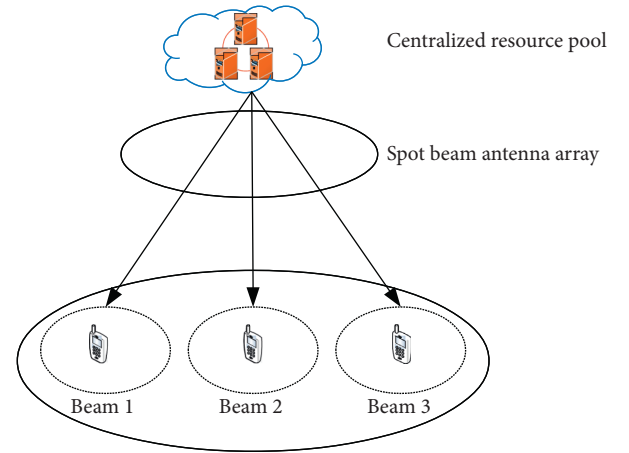


FIGURE 3: Channel allocation mapping under a single satellite.

The system allocates channels by frequency multiplexing between beams. Furthermore, channel and power allocation matrix are defined as follows:

$$V = [V_1, V_2, \dots, V_N]^T = \begin{bmatrix} v_{1,1} & \cdots & v_{1,M} \\ \vdots & v_{n,m} & \vdots \\ v_{N,1} & \cdots & v_{N,M} \end{bmatrix}, \quad (1)$$

$$P = [P_1, P_2, \dots, P_N]^T = \begin{bmatrix} P_{1,1} & \cdots & P_{1,M} \\ \vdots & P_{n,m} & \vdots \\ P_{N,1} & \cdots & P_{N,M} \end{bmatrix}$$

where $v_{n,m} \in \{0, 1\}$ in matrix V , $v_{n,m} = 1$ represents the channel y_m is used in the beam x_n , otherwise is not. The maximum transmits power of a beam and a system are P_c and P_{tot} , respectively. The channel gain of each beam can be expressed by a gain matrix

$$H = [H_1, H_2, \dots, H_N]^T = \begin{bmatrix} h_{1,1} & \cdots & h_{1,M} \\ \vdots & h_{n,m} & \vdots \\ h_{N,1} & \cdots & h_{N,M} \end{bmatrix}. \quad (2)$$

For a user $u_{n,k}$ in the beam x_n , the useful signal and cofrequency interference received in the channel y_m are as follows:

$$S_{n,m}^k = p_{n,m} h_{n,m}, \quad (3)$$

$$R_{n,m}^k = \sum_{i=1, i \neq n}^N p_{i,m} h_{i,m}. \quad (4)$$

The SINR of $u_{n,k}$ can be calculated by equations (3) and (4); further, the channel rate of $u_{n,k}$ in the channel y_m can be calculated by the following equation:

$$C_{n,m}^k = B \log_2 \left(1 + \frac{S}{N} \right) = B_{n,k} \log_2 \left(1 + \frac{p_{n,m} h_{n,m}}{\sum_{i=1, i \neq n}^N p_{i,m} h_{i,m} + n_0 B_{n,k}} \right), \quad (5)$$

where n_0 is the noise power spectral density, $B_{n,k}$ is the bandwidth allocated to the user $u_{n,k}$. To evaluate system performance, a user supply-demand ratio is defined as follows:

$$\eta_n^k = \frac{C_{n,m}^k}{C_{n,m}^{k'}}. \quad (6)$$

In equation (6), $C_{n,m}^{k'}$ is user's request rate. Satellite channel allocation can be seen as a sequence decision-making problem in an interval T . Our optimization goal is to maximize the user supply-demand ratio under limited channel resources. Therefore, channel allocation is expressed as the following optimization:

$$\max \sum_{n=1}^N \sum_{k=1}^K \eta_n^k, \text{ s.t. } \begin{cases} \sum_{n=1}^N \sum_{k=1}^K C_{n,m}^k \leq C_{\text{tot}}, \\ \sum_{n=1}^N \sum_{m=1}^M p_{n,m} \leq P_{\text{tot}}, \\ \sum_{m=1}^M p_{n,m} \leq P_c. \end{cases} \quad (7)$$

The optimization objective in (7) is to maximize the supply-demand ratio in the system. The constraints indicate that the sum of user service rate must not exceed system capacity, the sum of channel transmit power must not exceed total transmit power limit, and the sum of channel transmit power within a single beam must not exceed the power limit of a single beam.

4. Channel Allocation Scheme

The purpose of RL is to improve the decision-making ability of the LEO satellite system in the process of channel allocation so as to improve resource utilization further. In this section, we define the state space, the action space, and the

reward function of the Q-learning algorithm and adopt Q-learning algorithm to train the optimal channel allocation strategy.

Figure 4 shows the interaction process between a satellite system and the environment. The environment is the collection of terrestrial users in the satellite system, and the state is the channel allocation state of the system user. Further, the action is the system assigning channels to users. We model the channel allocation of a satellite system as a Markov decision process (MDP). MDP is a set of sequential decision processes with Markov attributes. MDP contains a set of state $s_t \in s$, action $a_t \in A(s)$, reward $r_t \in R$, and state transition probability $p(s_{t+1}|s_t, a_t)$. The state transition probability $p(s_{t+1}|s_t, a_t)$ refers to the probability of environment transition to a new state s_{t+1} after performing an action a_t under state s_t . The goal of MDP is to specify a policy that maximizes the agent's reward from the environment. We use a model-free method in this paper, which does not need to model the state transition probability. According to the established optimization problem, we define the states, actions, and reward.

4.1. State Definition. The state matrix is constructed according to the channel assignment of users in each beam.

$$W = \begin{bmatrix} w_{1,1} & \cdots & w_{1,K} \\ \vdots & w_{n,k} & \vdots \\ w_{N,1} & \cdots & w_{N,K} \end{bmatrix}, \quad (8)$$

where $w_{n,k} \in \{-1, 0, 1\}$, $w_{n,k} = 0$ represents no user, $w_{n,k} = -1$ represents a user allocated no channel, and $w_{n,k} = 1$ represents a user allocated channels. The number of matrix columns is the maximum number of users in all beams, and the rows are system beams. When all requesting users have been allocated channels or the system has no available channels, the training process reaches the termination status and the allocation process ends.

4.2. Action Definition. The system selects suitable channels from the action set $A(s)$ and allocates these channels to users according to the current state. Channel assignment is defined as action a_t :

$$a_t = \{m | m \in A(s), A(s) \subseteq Y\}. \quad (9)$$

The agent randomly selects actions from the action set $A(s)$ with probability ε . Also the agent selects the action with maximum Q value with probability $1 - \varepsilon$. When the training steps are enough, the action value of each state in Q table will converge to the optimal value.

4.3. Reward Definition. Reward is the feedback from environments to agent after agent acts according to the current state, and it can be used to measure the performance of actions. An appropriate reward setting can guide an agent to train the optimal strategy better. The goal in optimization (7) is to maximize the system supply-demand ratio. Thus we set

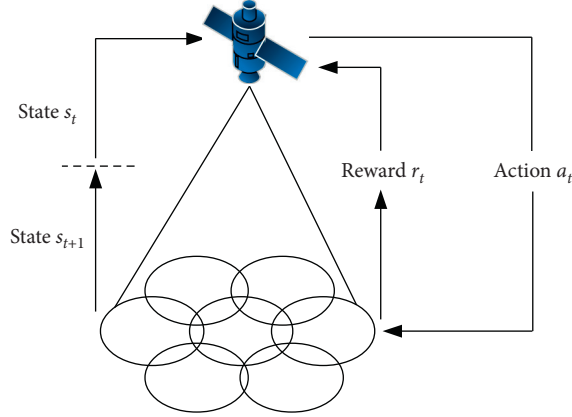


FIGURE 4: Dynamic channel allocation model based on RL.

the reward function as a function that is positively related to the supply-demand ratio.

$$r_t = 100 \times \sum_{n,k} \eta_n^k \quad (10)$$

4.4. Algorithm Optimization. In order to accelerate the convergence of the Q-Learning algorithm, we make two improvements based on the original Q-Learning algorithm:

$$J(s_t, a) = \begin{cases} J(s_{t-1}, a) \frac{r_{\max}}{r_t}, & a \neq a_t, \\ \Delta, & \text{else,} \end{cases} \quad (12)$$

$$H(s_t, a) = \begin{cases} \max_a [Q(s_t, a) - Q(s_t, a_t)] + \frac{J(s_t, a_t)}{\sum_i J(s_t, a_i)}, & a_t \text{ is the best action,} \\ 0, & \text{else.} \end{cases} \quad (13)$$

Under the guidance of information intensity, the heuristic function updates the optimal behavior. Through iterative accumulation, the agent will train the state-action decision plan with the largest reward.

4.5. Trade-Off Analysis. Firstly, in order to simplify the allocation process, we assume that the transmit power and SNR of each channel are the same. Then, the training time of the Q-DCA is highly dependent on the number of states and actions. The number of states and actions largely determines the quality of the final allocation scheme. Due to the strict latency requirements of satellite communication systems, we reduce the number of states and actions appropriately to shorten the training time of the algorithm.

4.6. Allocation Process. The allocation scheme has two steps: fixed channel preallocation and dynamic channel allocation on demands. Before each service request arrives, the system

the exponential gradient descent and the information intensity updating strategy.

The exponential gradient descent is that the random exploration probability ϵ decreases exponentially with the increase of training steps in the course of action selection, as shown in the following equation:

$$\epsilon = \epsilon_0 \cdot e^{-\frac{l}{l_0}}, \quad (11)$$

where l_0 is the maximum number of training steps. Exploring with a greater probability can ensure the diversification of action selection in the early training stage, and thus can avoid falling into local optimum; with the training step increasing, the exploration probability begins to decrease, and selecting optimal action with a larger greedy probability can accelerate the convergence of the algorithm.

The information intensity updating strategy is to define the information intensity to express the quality of the action and to update the Q table by information intensity. The information intensity $J(s_t, a)$ is defined in equation (12). It reflects the quality of action in the current state, where Δ is 1 by default. The Q table will update only when the reward is greater than the maximum reward in the current state. Further, Q table updates as shown in the heuristic function are defined in the following equation:

first preallocates some fixed channels for each beam cell; after fixed preallocation is finished, if channel resource cannot meet user's demands in some beams, the resource pool will perform dynamic channel allocation. Table 1 shows the process of satellite system channel allocation.

5. Simulation Results and Discussions

In order to verify the performance of the proposed dynamic channel allocation scheme, we carry out simulation experiments on the MATLAB platform and compare the proposed scheme with the FCA scheme and LACA scheme.

The system receives the user's request in each beam at each service interval (the service arrival model system is subject to the Poisson distribution with parameter λ , the service duration is subject to the negative exponential distribution with parameter μ_1 , and the bandwidth request is subject to the normal distribution with parameters μ_2, σ^2). After centralized statistics of requests, the system allocates

TABLE 1: Allocation process.

Initialize system parameters	
1	Preallocation: Assign M channel to each beam
2	for Business request time $t = 1 : T$
3	if Resource is rich; recycle surplus resources
4	else resource is poor:Dynamic allocation
5	Allocate resources from resource pool
6	initialize parameter, learning rate α discount factor γ , initial explore probability ε_0 , Q table
7	Reconstruct state based on business request $s = I$
8	for Episode = 1:max_episode
9	while (s_{t+1} is terminal state)
10	Confirm initial state s_t
11	Update explore probability ε
12	Choose best a_t^* or Choose randomly a_t
13	Execute action, get reward r_t
14	Update Q table
15	Jump to next state s_{t+1}
16	End
17	End of training, output Q table
18	Choose best strategy according to Q table π^*
19	Channel allocation
20	End
21	End

channel resources to each user, counting supply-demand ratios and blocking rates. Table 2 shows the specific parameters of the satellite system.

Compared with the proposed algorithm in simulation, the FCA scheme adopts the average allocation. The bandwidth resources are evenly distributed to all users. The LACA scheme adopts the minimum variance of supply and demand (MDSV), comparing the performance of three schemes in different scenarios.

5.1. The System Performance in Beam Number Variation Scenario. In this scenario, all beam traffic distribution parameters are the same. The number of beams increases from 10 to 50, simulating that the numbers of accessing users increase gradually and the available resources transition from rich to scarce. Figures 5 and 6 show the system performance of three schemes in the scenario of a gradual increase in the number of beams.

As shown in Figure 6, with the increase in the number of beams, the system blocking rate also increases. The reason is that with the expansion of the beam range, more users are connected to the current satellite communication system, and the bandwidth resources allocated to each user are also reduced. When the number of beams is increased to 16, the system starts to overload and block; meanwhile, the proposed Q-DCA scheme can further improve the system supply-demand ratio compared with the FCA scheme and LACA scheme. For example, when the number of beams reaches 20, the system supply-demand ratio of the three schemes are 0.725, 0.645, and 0.615 respectively, which means that the performance of the proposed Q-DCA algorithm is 12% and 18% better than FCA scheme and LACA scheme.

We analyze the differences in calculation time between the three allocation schemes, as shown in Figure 7.

TABLE 2: System simulation parameter.

Simulation parameter	Value
Satellite height	500 km
Downlink frequency	10.7–12.7 GHz
Maximum beams	40
Number of channels	16
Maximum transmission rate	1000 Mbps
Service rate threshold	100 kbps
Maximum transmitting power	23 dBW
Maximum power of beam	20 dBW
Antenna angle of beam	1°
Learning rate	0.1
Discount factor	0.9
Initial explore probability	0.9
Maximum step	10000
Service arrival rate	[10, 40] times/hour
Business duration	[3, 6] minutes

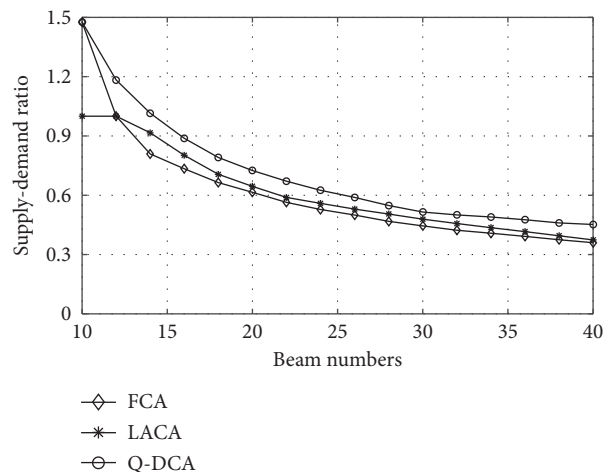


FIGURE 5: Supply-demand Ration under varying beam number.

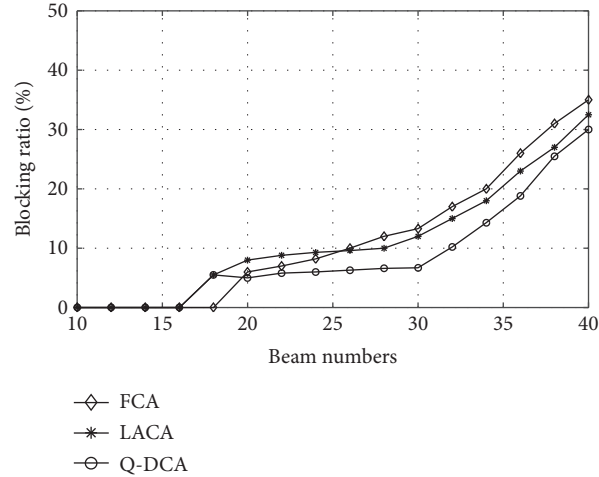


FIGURE 6: Blocking Ratio under varying beam number.

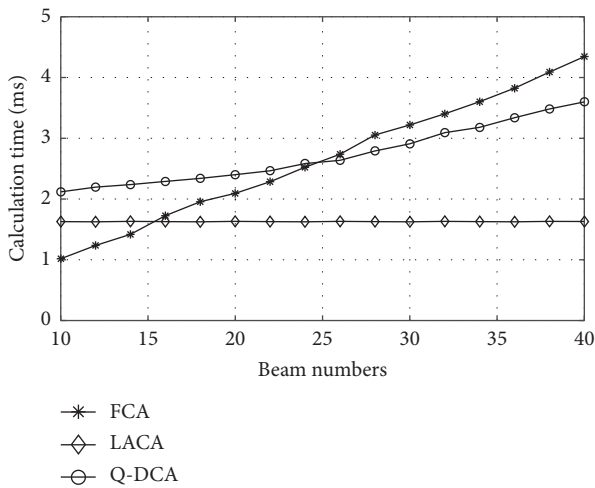


FIGURE 7: Calculation time of three schemes.

Because the FCA scheme adopts a uniform allocation principle, the number of calculations is relatively small, and therefore its calculation time is minimal. For the LACA scheme, as the beam increases, it takes longer to calculate the function extremes. And in Q-DCA, we use the trained strategy for channel allocation. Under each service request, only the Q table needs to be updated each time to get the optimal allocation scheme. Although the FCA scheme takes the least amount of time, it has the highest blocking rate when resources are tight. And the time complexity of the Q-DCA scheme is lower than the LACA scheme.

5.2. The System Performance in Beam Number Fixed Scenario.

In this scenario, the number of satellite beam is fixed as 10, while the business request in beam increases from 900 Mbps to 1700 Mbps, simulating the scene in which the user changes from sparse to dense. Figures 8 and 9 show the system performance of the three schemes in the scene in which the number of beams is fixed.

When the number of beams is fixed at 10, the system supply-demand ratio decreases with the increase of the total system traffic. It can be seen that when the total numbers of business requests exceed 1000 Mbps, the system starts to block. At this time, the system business requests have exceeded the system payload. When the business request is 1500 Mbps, the system supply-demand ratio of the three schemes is 0.589, 0.542, and 0.475, respectively. At the same time, when the blocking rate is 30%, the system traffic volumes of the three schemes are 1620 Mbps, 1500 Mbps, and 1430 Mbps, respectively. In other words, the proposed Q-DCA scheme can further improve the system business processing capacity compared with the previous two algorithms while ensuring the same system blocking rate.

5.3. Spectrum Utilization and Algorithm Convergence Performance.

In this scenario, the number of satellite beams is 10, and the total business volume of the system is 1000 Mbps. Comparing the convergence speed of the original Q-learning algorithm and the improved Q-learning algorithm when the system resources are exactly exhausted. Figure 10 shows the comparison of the convergence performance of the two algorithms.

As shown in Figure 10, the original Q-Learning algorithm starts to converge after about 4000 steps, while the improved Q-Learning algorithm starts to converge after about 2000 steps. Reflected in the actual application scenario, the improved Q-Learning algorithm can already shorten the system processing time by one time, thereby shortening the on-board processing delay.

Figure 11 analyzes the channel utilization of the original Q-Learning algorithm and the improved the Q-Learning algorithm when the system resources are abundant and scarce. It can be seen that the channel utilization of the two algorithms is almost the same whether the system resources are abundant or scarce, except for the convergence speed of the algorithm. Therefore, the improved algorithm will not change its utilization rate of the system resources.

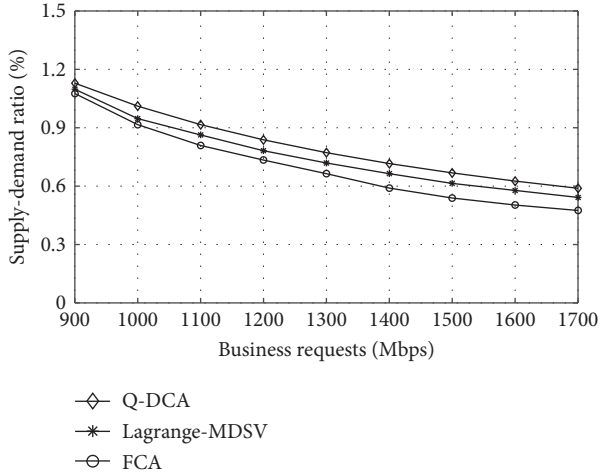


FIGURE 8: Supply-demand Ratio under fixed beam number.

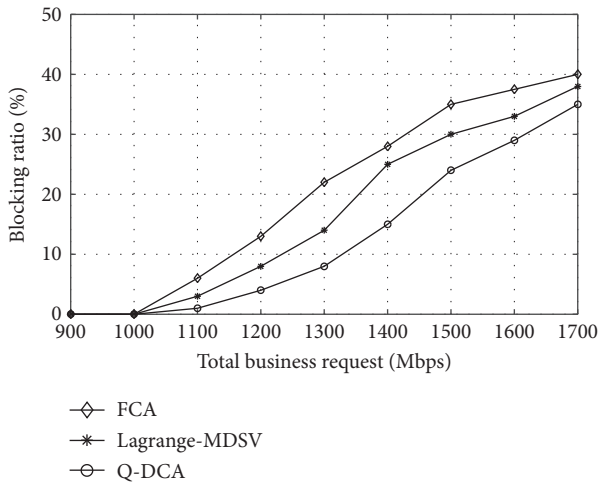


FIGURE 9: Blocking Ratio under fixed beam number.

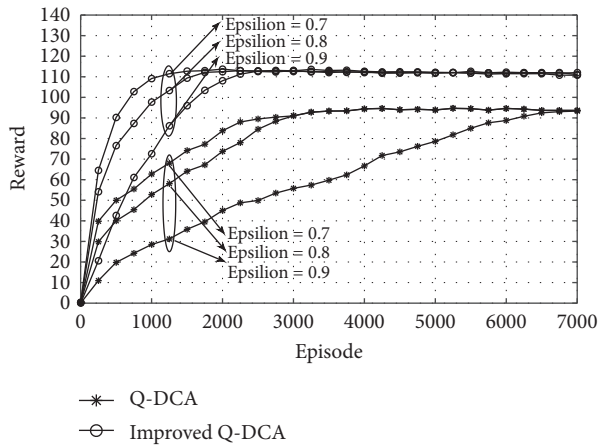


FIGURE 10: Algorithm convergence rate comparison.

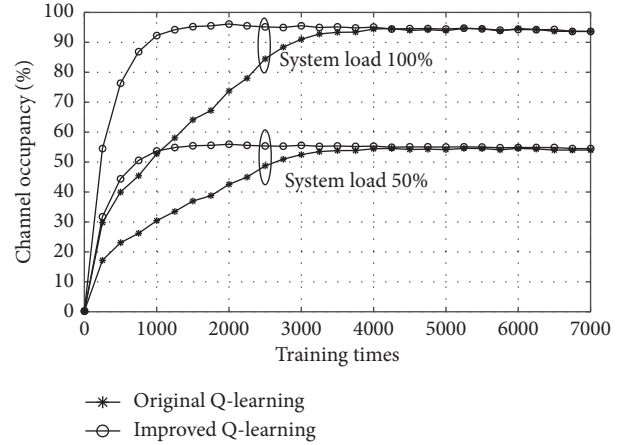


FIGURE 11: Spectral utilization efficiency comparison.

6. Conclusion

This paper proposes a LEO satellite network architecture based on a satellite resource pool. The system manages channel resources through a centralized resource pool to adapt to the traffic difference between beams. We adopt the Q-learning algorithm in RL for dynamic channel allocation. The simulation section analyzes the system performance and time complexity of FCA, LACA, and Q-DCA schemes in different scenarios. Analysis shows better performance of the proposed scheme in terms of channel allocation. Furthermore, we analyze the convergence of the Q-Learning algorithm and its impact on channel utilization. Simulation results show the effectiveness and the convergence performance of our proposed scheme.

Data Availability

The data used to support the findings of this study are available from the corresponding author upon request.

Conflicts of Interest

The authors declare that there are no conflicts of interest regarding the publication of this paper.

Acknowledgments


The work presented in this paper has been supported by Dean Project of Key Laboratory of Cognitive Radio and Information Processing, Ministry of Education (CRKL180104), Open Foundation of the State Key Laboratory of Networking and Switching Technology (Beijing University of Posts and Telecommunications) (SKLNST-2020-1-08), Project of Promoting Basic Scientific Research Ability of Young and Middle-aged Teachers in colleges and universities in Guangxi (2019KY0255), National Science Foundation of Shanxi Province (201801D121116), and Special Program of Guangxi Science and Technology Base and Talents (2018AD19048).

References

- [1] H. Liang, *Research of Wireless Network Resource Management under CRAN Architecture*, Beijing University of Posts and Telecommunication, Beijing, China, 2016.
- [2] L. Liu, *Research on Location Management and User Access Technology of LEO Satellite Communication*, University of Electronic Science and Technology of China, Chengdu, China, 2010.
- [3] C. Qi, *Architecture Research for Low Earth Orbit Satellite Internet of Things*, Nanjing University of Posts and Telecommunications, Nanjing, China, 2019.
- [4] C. Qiu, H. Yao, F. R. Yu, F. Xu, and C. Zhao, "Deep Q-learning aided networking, caching, and computing resources allocation in software-defined satellite-terrestrial networks," *IEEE Transactions on Vehicular Technology*, vol. 68, no. 6, pp. 5871–5883, 2019.
- [5] D. J. He, P. You, and S. W. Yong, "Mobility management in LEO satellite communication networks," *China Space Science and Technology*, vol. 36, no. 3, pp. 1–14, 2016.
- [6] F. Fang and M. G. Wu, "Research on the development of global LEO satellite constellation," *Aerodynamic Missile Journal*, vol. 5, no. 6, pp. 88–92, 2020.
- [7] S. J. Liu, *The Research on Dynamic Resource Management Techniques for Satellite Communication System*, Beijing University of Posts and Telecommunication, Beijing, China, 2018.
- [8] Z. Liu, "Research on satellite communication resource allocation algorithm based on Reinforcement Learning," *Mobile Communication*, vol. 43, no. 5, pp. 27–32, 2019.
- [9] S. Richard and B. Andrew, *Reinforcement Learning: An Introduction*, pp. 1–7, University of Electronic Science and Technology of China, Chengdu, China, 2017.
- [10] Y. L. Liu and L. D. Zhu, "A suboptimal routing algorithm for massive LEO satellite networks," in *Proceedings of the International Symposium on Networks, Computers and Communications*, pp. 1–5, ISNCC, Rome, Italy, 2018.
- [11] S. D. Feng, H. P. Zhu, and G. X. Li, "Dynamic modeling and simulation for LEO satellite networks," in *Proceedings of the 11th IEEE International Conference on Communication Technology*, pp. 37–40, ICCT, Hangzhou, China, 2018.
- [12] H. J. Liu, P. Qin, N. W. Wang, Z. Lu, and B. Zhou, "Research on architecture design and resource allocation algorithm of LEO constellation," *Journal of China Academy of Electronic Sciences*, vol. 13, no. 06, pp. 631–635, 2018.
- [13] X. Qi and J. Y. Sun, "Advances and challenges for software-defined LEO small satellite networks," in *Proceedings of the 16th Annual Meeting of Satellite Communication*, pp. 89–93, Beijing, China, 2020.
- [14] K. W. Wang and S. Wang, "Design of satellite ground station based on resource pool architecture," *Communications World*, vol. 26, no. 8, pp. 16–17, 2019.
- [15] M. M. Zhang, "Application analysis of resource pool architecture in satellite communications ground station network," *Information Technology and Information Technology*, vol. 7, pp. 101–102, 2019.
- [16] J. H. Chang and A. J. Liu, "System reliability analysis of satellite communication center station under resource pooling architecture," *Communications Technology*, vol. 53, no. 2, pp. 375–381, 2020.
- [17] W. T. Zhai, *Research on Virtualization Resource Management Technology of Satellite Network*, XiDian University, Xian, China, 2019.
- [18] Y. Q. Xu, "The influence of resource pool architecture on the," *Construction of Satellite Communication Earth Station Network*, vol. 37, no. 11, pp. 160–162, 2020.
- [19] H. Wang, A. J. Liu, X. F. Pan, and L. L. Jia, "Optimal bandwidth allocation for multi-spot-beam satellite communication systems," in *Proceedings of the 2013 International Conference on Mechatronic Sciences, Electric Engineering and Computer (MEC)*, Shengyang, China, 2013.
- [20] G. Colavolpe, A. Modenini, A. Piemontese, and A. Ugolini, "On the application of multiuser detection in multibeam satellite systems," in *Proceedings of the IEEE International Conference on Communications*, vol. ICC, pp. 898–902, London, UK, 2015.
- [21] A. Ivanov, M. Stoliarenko, S. Kruglik, S. Novichkov, and A. Savinov, "Dynamic resource allocation in LEO satellite," in *Proceedings of the International Wireless Communications and Mobile Computing Conference 2019, IWCMC*, pp. 930–935, Beijing, China, 2019.
- [22] T. Zhang, L. Zhang, and D. Shi, "Resource allocation in beam hopping communication system," in *Proceedings of the IEEE/AIAA 37th Digital Avionics Systems Conference 2018, DASC*, pp. 1–5, London, UK, 2018.
- [23] P. Zuo, T. Peng, W. Linghu, and W. Wang, "Resource allocation for cognitive satellite communications downlink," *IEEE Access*, vol. 6, pp. 75192–75205, 2018.
- [24] R. Chang, Y. He, G. Cui et al., "An allocation scheme between random access and DAMA channels for satellite networks," in *Proceedings of the IEEE International Conference*, pp. 1–6, Shenzhen, China, 2016.
- [25] B. Zhao, J. Liu, Z. Wei, and I. You, "A deep reinforcement learning based approach for energy-efficient channel allocation in satellite Internet of things," *IEEE Access*, vol. 8, pp. 62197–62206, 2020.
- [26] Z. Wang, J. X. Zhang, X. Zhang, and W. B. Wang, "Reinforcement learning based congestion control in satellite Internet of things," in *Proceedings of the 11th International Conference on Wireless Communications and Signal Processing 2019, WCSP*, pp. 1–6, Xi'an, China, 2019.
- [27] X. Hu, "Multi-agent deep reinforcement learning-based flexible satellite payload for mobile terminals," *IEEE Transactions on Vehicular Technology*, vol. 69, no. 9, pp. 9849–9865, 2020.
- [28] B. Deng, C. Jiang, H. Yao, S. Guo, and S. Zhao, "The next generation heterogeneous satellite communication networks: integration of resource management and deep reinforcement learning," *IEEE Wireless Communications*, vol. 27, no. 2, pp. 105–111, 2020.

Research Article

An Improved Indoor Positioning Technique Based on Receiving Signal's Strength

Xingsi Xue ^{1,2,3,4,5,6}, Xiaoquan Lin,^{6,7} Chaofan Yang,⁶ and Xiaojing Wu⁶

¹Fujian Provincial Key Laboratory of Big Data Mining and Applications, Fujian University of Technology, Fuzhou 350118, China

²Guangxi Key Laboratory of Automatic Detecting Technology and Instruments, Guilin University of Electronic Technology, Guilin 541004, China

³Intelligent Information Processing Research Center, Fujian University of Technology, Fuzhou 350118, China

⁴Fujian Key Lab for Automotive Electronics and Electric Drive, Fujian University of Technology, Fuzhou 350118, China

⁵Institute of Artificial Intelligence, Fujian University of Technology, Fuzhou 350118, China

⁶College of Information Science and Engineering, Fujian University of Technology, Fuzhou 350118, China

⁷Anktion (Fujian) Technology Company Limited, Fuzhou 350003, China

Correspondence should be addressed to Xingsi Xue; jack8375@gmail.com

Received 26 June 2020; Revised 14 July 2020; Accepted 22 July 2020; Published 11 August 2020

Academic Editor: Chi-Hua Chen

Copyright © 2020 Xingsi Xue et al. This is an open access article distributed under the Creative Commons Attribution License, which permits unrestricted use, distribution, and reproduction in any medium, provided the original work is properly cited.

Wireless signal-transmitting process is a complex procedure, to improve the indoor positioning accuracy, and this work proposes a novel indoor positioning technique based on receiving signal's strength. First, the indoor environment of the building is regionalized in the training phase of indoor positioning. Then, the adjacent points of the indoor space with the same wireless signal transmission characteristics are gathered into the same area, and the corresponding parameter sets and decision domains of each area are constructed. After that, during the positioning stage, the regional confidence and receiving signal's strength are used to predict the indoor area where the mobile station is located. Finally, the ranging and solution results of the traditional three-sided positioning process are constrained to obtain the optimal solution. Comparing with the traditional positioning techniques that regard the entire complex indoor environment as an entirety, the proposed indoor space regionalization preprocessing method can effectively reduce the ranging error. Compared with the indiscriminate data fusion of the centroid method, the data filtering method based on regional confidence is more targeted. In the experiment, a practical office area is used to test our proposal's performance, and the experimental results show that our approach can effectively improve the accuracy of indoor positioning results.

1. Introduction

With the advancement of information technology and the development of society, Location-Based Service (LBS) has become a basic service requirement for people's daily work and life [1]. The positioning technique can be divided into two types: outdoor positioning technique and indoor positioning technique. In an outdoor environment, Global Positioning System (GPS), BeiDou Navigation Satellite System (BDS), and other Global Navigation Satellite System (GNSS) provide users with meter-level location services, solved the problem of accurate positioning in outdoor space

basically [2]. However, in an indoor environment that occupies 80% of human daily life, the GNSS signal strength is drastically reduced due to the blocking effect of buildings on wireless signals. As a result, the positioning accuracy is greatly reduced and cannot meet the needs of indoor location services. This problem is particularly prominent in large shopping malls, integrated transportation hubs, underground mines, etc., in large and complex indoor environments. Therefore, how to improve the accuracy of indoor positioning technique in a large and complex indoor environment is the current research focus in the field of positioning technique [3]. Indoor positioning technique based

on receiving signal's strength (RSS) has become the mainstream indoor positioning technique because it has the characteristics that it can directly use the existing widely deployed WLAN equipment and the low cost of hardware is easy to deploy.

The indoor positioning technique based on RSS can be mainly divided into the positioning technique based on ranging and the positioning technique based on location fingerprint [4]. The location method based on location fingerprint is to detect the wireless signal characteristics of a specific location and build a location fingerprint database based on this. During the positioning stage, the wireless signal characteristics are detected and a specific matching algorithm is used to traverse the location fingerprint database through calculation to estimate the location information of the target node. The location fingerprint positioning method does not require the specific information of the reference point and has unique advantages in specific occasions where it is impossible or inconvenient to calibrate the reference point. However, the location fingerprint positioning method requires considerable workload to establish and maintain the location fingerprint database. The range-based positioning method uses the attenuation characteristics of the wireless signal during transmission to determine the distance between the target node and multiple reference points whose positions are known. On this basis, the location information of the target node is obtained by further calculation. The positioning method based on distance measurement is easy to deploy, low in cost, low in maintenance, and easy to promote. However, due to the complexity and diversity of the propagation path of wireless signals in an indoor environment, a single wireless signal transmission model cannot describe the propagation characteristics of wireless signals at different points indoors, resulting in large errors and lower positioning accuracy. In order to accurately determine the area of the point to be measured and further improve the positioning accuracy, this paper designs and implements a judgment method based on regional confidence. This method uses the error vector of the equation and the degree of compatibility to filter out the irrelevant combination of regions; thus, making the determination position of the point to be measured is more accurate.

2. Indoor Positioning Technique

With the vigorous development of information technology and electronic technology, indoor positioning methods continue to emerge and have been applied. The widely used indoor positioning methods include proximity detection, triangulation, polar point method, dead reckoning, fingerprinting, and multilateration [5]. The proximity detection method is to detect the coverage area of the launch point where the target is located to determine the approximate range where the target is located, with low accuracy. The triangular positioning method and pole method mainly determine the coordinates of the target by observing the angle relationship between the target and the known reference point. Dead reckoning is positioning by acquiring the movement speed, direction, and time of the measured target. It is convenient to use but has accumulated errors. When it is

used in an indoor environment, it has a pedestrian dead reckoning (PDR) algorithm for pedestrian positioning scenarios. Fingerprint positioning is a method of establishing a fingerprint map database in advance and matching the collected signal fingerprint data with database data records during positioning to determine the target location. Fingerprint positioning does not require reference point position information and is very suitable for special occasions where reference point position information cannot be calibrated. However, the workload of establishing and maintaining the fingerprint database is very large, and achieving efficient data matching has always been a difficult problem, which has attracted the attention of many scholars. Some scholars have made other progress in the field of ontology research and made some progress [6–15]. The multilateral positioning method is to calibrate the positions of several reference points in advance and then determine the position of the point to be measured by measuring the distance between the point to be measured and the reference point. In practical applications, three reference points are generally used for positioning, which is also called three-sided positioning.

Different positioning methods need to choose different observations. Common observations include Time Of Arrival (TOA), Time Difference Of Arrival (TDOA), Enhanced Observed Time Difference (EOTD), and Round Trip Time (RTT), Arrival Of Angle (AOA), receiving signal's strength (RSS), etc. The fingerprint positioning method, the trilateral positioning method, and the multilateral positioning method usually use RSS as the observation method for positioning.

Based on these indoor positioning methods, various indoor positioning technologies have been derived and developed [16], which are compared in Table 1.

The technologies for trilateral positioning based on RSS mainly include Wifi, Bluetooth, RFID, ZigBee, and so on. Because of its convenient data collection, a small amount of calculation, and extensive network deployment, it has a good application prospect.

3. Wireless Signal Transmission Model and Trilateral Positioning Algorithm

Calculating the distance between the point to be measured and the reference point using the distance measurement method and then using the trilateration algorithm to calculate the position of the point to be measured is a typical method of RSS-based positioning technique, which is simple to calculate and has good universality.

3.1. Wireless Signal Transmission Model. The wireless signal transmission model is a mathematical model in which wireless signals propagate through a medium in a certain medium environment. Through the wireless signal transmission model, a quantitative relationship between the degree of signal attenuation caused by the transmission process of the wireless signal in the medium space and the transmission distance can be obtained, and a reasonable selection of the signal transmission model and transmission

TABLE 1: Comparison of main indoor positioning technologies.

Positioning technique	Positioning method	Positioning accuracy	Advantages	Disadvantages
Visual image	Image processing, scene analysis	High	Low environmental dependence	High cost and low stability
Infrared	Image processing, proximity detection	High	Mature technology	Visual distance transmission, interfered by light
Ultrasound	Multilateral positioning	High	High positioning accuracy	Greatly affected by temperature and loss
Bluetooth	Proximity detection, multilateral positioning	Medium	Small size and low power consumption	Short transmission distance and low stability
Wifi	Fingerprint positioning, multilateral positioning	Medium	Low cost and easy deployment	Susceptible to environmental interference
RFID	Proximity detection, fingerprint positioning	High	Low cost and small size	Short distance and weak communication ability
Ultrawideband	Multilateral positioning	High	Strong penetration	High cost
Geomagnetic	Fingerprint positioning	Medium	Not dependent on the environment	Poor stability
Cellular base station	Proximity detection	Low	Wide coverage	Depends on base station density
ZigBee	Proximity detection, multilateral positioning	High	Low cost and low power consumption	Poor stability and susceptible to interference
Pseudolite	Carrier phase ranging	High	Wide coverage	High cost
Inertial navigation	Dead reckoning	Medium	Not dependent on the external environment	Cumulative error

model parameters suitable for the current environment is satisfactory indoor positioning performance is crucial. The propagation model of wireless signals in free space suggests that the receiving signal's strength P_r can be expressed by the following formula [16]:

$$P_r(d) = \frac{P_t G_t G_r \lambda^2}{(4\pi)^2 d^2 L}, \quad (1)$$

where P_t is the signal power at the transmitter, λ is the wavelength of the wireless signal, G_t is the antenna gain at the transmitter, G_r is the antenna gain at the receiver, d is the separation distance between the transmitter and receiver, and L is the system loss factor. It is troublesome to directly use the free space propagation model for ranging and positioning, so the logarithmic distance loss model is commonly used for indoor positioning [17]:

$$P(d) = P(d_0) - 10n \lg\left(\frac{d}{d_0}\right) + X. \quad (2)$$

The above formula $P(d)$ is the signal strength received by the receiving end whose distance source (transmitter) is d , that is, the RSS value. $P(d_0)$ is the signal strength received by the receiver when the distance from the source is d_0 . n is the path loss index, which is usually obtained by actual measurement. Generally, the more the obstacles on the propagation path, the larger the value of n , so that the wireless signal decreases more in the unit propagation distance [18]. d_0 is the reference distance, which depends on the actual situation on-site. For the convenience of calculation and measurement, the value is usually 1. X is a Gaussian random

variable in dBm with a mean value of 0 and a variance ranging from 4 to 10 [19].

In engineering applications, the following simplified form of the logarithmic distance loss model is commonly used [20]:

$$R = A - 10n \lg(d). \quad (3)$$

The argument d is the distance between the source and the receiver, R is the signal strength received by the receiver, A is the signal strength received 1 m from the source, and n is the path loss. During application, it is necessary to select several sample points in different positions in advance, then determine A and n parameters of the model through regression analysis, and thus establish the quantitative relationship between RSS and d detected by the receiving end. In the positioning stage, the distance d between the point to be measured and the source can be determined based on the RSS value received by the point to be measured.

3.2. Trilateral Positioning Algorithm. The currently widely used positioning method is the trilateral positioning algorithm [21]. On a two-dimensional plane, if the distance between the point to be measured and three reference points (i.e., sources) with known positions can be determined, the three reference points are used as the center of the circle to measure the distance between the source and the reference point. A circle is made for the radius. Figure 1 shows an example of three-sided positioning technique.

In the three-dimensional space, four reference points are needed for spherical intersection for positioning calculation.

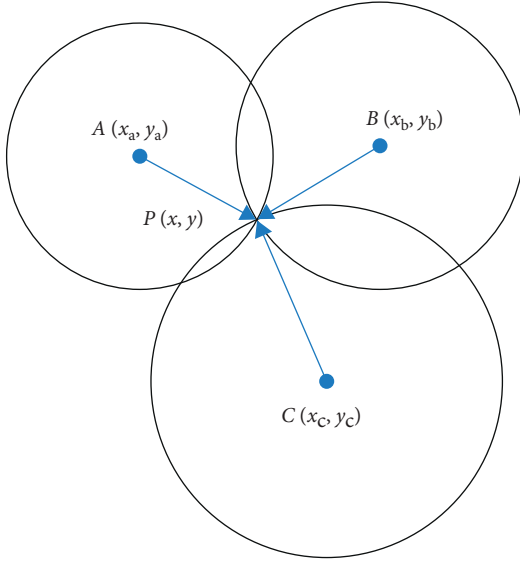


FIGURE 1: An example of three-sided positioning technique.

Traditional RSS indoor positioning technique considers the entire indoor environment as a whole during the entire positioning process and only uses a single wireless signal transmission model and corresponding model parameters for distance calculation. In complex indoors with many barriers, the environment will inevitably produce a large error, and due to the influence of the ranging error, the three-sided positioning algorithm is likely to not intersect the three circles at a point, but to a common area. In extreme cases, they are also may be completely disjointed, resulting in a large error in the calculation results of positioning. Even if some methods such as the centroid method are used to modify and approximate the position, the results are not satisfactory. This paper improves this and proposes a new method, which uses the indoor space regional preprocessing method and regional confidence discrimination method to solve the above problems.

4. Improved RSS Indoor Positioning Technique

The main reason for the low accuracy of the traditional RSS indoor positioning method based on three-sided positioning is that the indoor environment is complicated. The situation of the obstructions on the propagation path of the wireless signal from the source to the indoor points is different. In the wireless signal strength of each propagation path, the decay rate is very different. The single set of propagation model parameters used in this method ignores these differences and naturally introduces large errors. To this end, this paper first conducts regionalization processing and divides the indoor environment into several areas according to the wireless signal transmission characteristics. Each point in the same area selects the same transmission model parameters, and different areas correspond to different transmission model parameters. In order to simplify the calculation, the transmission model of each region is set as the logarithmic distance loss model. In the positioning stage, the region where the

point to be measured is located is determined by the region confidence judgment method, and the model parameters corresponding to the region are selected for accurate positioning calculation. Since the difference in the wireless signal transmission path from each point in the room to the source under the spatial layout of the indoor environment is fully considered, the positioning accuracy can be greatly improved.

4.1. Regionalization of Interior Space. The path loss factor n of the logarithmic distance loss model characterizes the attenuation rate of wireless signals on the unit transmission path and fixed hard barriers such as walls affect the value of the parameter A . According to this, the indoor space can be divided into several areas according to the number and size of obstructions on the wireless signal transmission path.

As shown in Figure 2, in a specific indoor space, three sources of AP1, AP2, and AP3 are deployed. There are two walls in the room, namely, wall fh and wall ek . To simplify the analysis and highlight the problem elements, assume the wall the thickness is 0. It can be seen from the figure that the wireless signal sent from the source AP1 passes through two representative paths, namely, path aj and path ai . Obviously, the difference between the two paths is significant, the data of the barriers (walls) on each path are different, and the wireless signal transmission characteristics on each path are also different; that is, the corresponding parameters in each path change accordingly. According to the obstruction on the wireless signal transmission path, the indoor space can be divided into regions according to the source AP1, as shown in Figure 3.

As can be seen from Figure 3, the indoor space is divided into three areas as $z_{1,1}$, $z_{1,2}$, and $z_{1,3}$ according to the source AP1, and the parameter values of the logarithmic distance loss model corresponding to each area (that is, the values of A and n) are different and determined by the actual situation. These areas constitute the indoor space that is divided into regions based on the source AP1 and Z_1 are recorded as their union, which is defined as follows:

$$Z_1 = z_{1,1} \cup z_{1,2} \cup z_{1,3} = \{z_{1,1}, z_{1,2}, z_{1,3}\}. \quad (4)$$

Obviously, it is known that Z_1 and the actual size of the indoor space are in one-to-one correspondence and completely coincide. This article defines it as the plane corresponding to the source AP1. As can be seen from the foregoing, the parameters of the wireless signal transmission model corresponding to each area included in the plane Z_1 are generally different, and $c_{1,1} = \{\widehat{A}_{11}, \widehat{n}_{11}\}$ is a set of transmission parameters corresponding to the area $z_{1,1}$. Among them, \widehat{A}_{11} and \widehat{n}_{11} are the estimated values of parameters A and n in the area $z_{1,1}$ in formula (3). Similarly, it can be constructed as $c_{1,1}$, $c_{1,2}$, and $c_{1,3}$. Let C_1 be the parameter set corresponding to the plane Z_1 , then $C_1 = c_{1,1} \cup c_{1,2} \cup c_{1,3} = \{c_{1,1}, c_{1,2}, c_{1,3}\}$. Similarly, based on the source AP2 and source AP3, the plane Z_2 and plane Z_3 and corresponding parameter sets C_2 and C_3 can be constructed. As can be seen from Figure 3, $z_{1,1}$ is a polygon composed of multiple line segments. In general, the region $z_{1,1}$ is defined as follows:

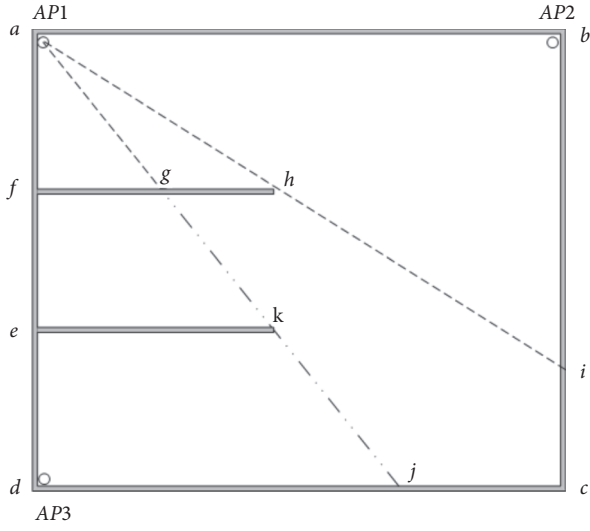


FIGURE 2: Schematic diagram of obstacles in the wireless signal transmission path of the indoor environment.

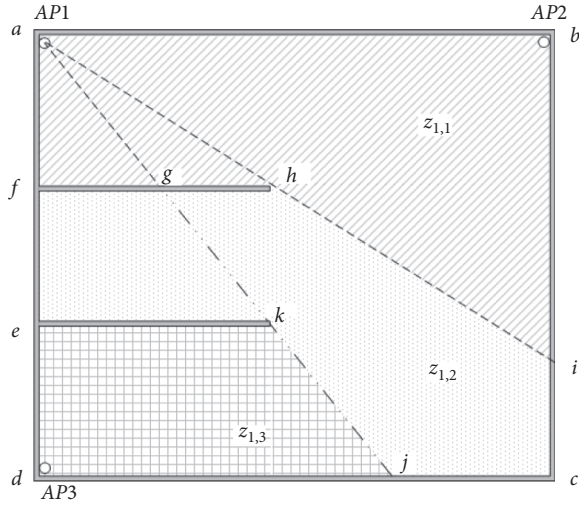


FIGURE 3: Schematic diagram of the regional division of indoor environmental space.

$$z_{1,1} = \{(x, y) \mid f_i(x, y) < 0, \quad i = 1, 2, \dots, r\}, \quad (5)$$

where $f_i(x, y)$ is an analytical formula of straight lines that constitute the outline of a polygon and r is 5 in the area $z_{1,1}$.

$\|p_1 - p_2\|$ is recorded as the normal distance between points p_1 and p_2 , the point $p(x, y)$ is any point on $z_{1,1}$, and the point $a(x_a, y_a)$ is the location of a source AP1. Then, from equations (3) and (5), the RSS minimum value R_{a1} based on the source AP1 that can be obtained by all points located in the area $z_{1,1}$ is as follows:

$$\begin{aligned} \min \quad & R_{a1} = A - 10n \lg(\|p(x, y) - a(x_a, y_a)\|), \\ \text{s.t.} \quad & f_i(x, y) < 0, \quad i = 1, 2, \dots, r. \end{aligned} \quad (6)$$

Obviously, equation (7) is a linear programming problem, and the minimum value of R_{a1} can be solved by the simplex method, which is recorded as R_{a1_min} . Similarly, the

maximum value R_{a1_max} of R_{a1} can be obtained. Supposing the RSS value is calculated based on the source AP1 corresponding to any point $p(x, y)$ on $z_{1,1}$ be R_p . Considering the connectivity of the area $z_{1,1}$ and the monotonicity of formula (3), there are obviously

$$\forall p(x, y) \in z_{1,1}, \implies R_p \in [R_{a1_min}, R_{a1_max}]. \quad (7)$$

In this way, the area $z_{1,1}$ has a corresponding relationship with the R_{a1_min} and R_{a1_max} values. In this paper, the range determined by the set of values corresponding to the area is defined as the decision area of the area. For example, the above decision area of $z_{1,1}$ is $[R_{a1_min}, R_{a1_max}]$, which is denoted as $j_{1,1}$. Similarly, the decision domain $j_{1,2}$ and $j_{1,3}$ corresponding to the remaining regions $z_{1,2}$ and $z_{1,3}$ of the plane Z_1 can be established. Remember that the set of decision domains in the region contained in the plane Z_1 is J_1 , and then $J_1 = \{j_{1,1}, j_{1,2}, j_{1,3}\}$. With reference to the processing procedure of the plane Z_1 , the same processing can also be performed on the planes Z_2 and Z_3 to construct the boundary ranges, parameter sets, and decision domains of the regions in the Z_2 and Z_3 planes. So far, the regionalization of indoor space has been completed.

4.2. Positioning. The actual positioning process can be carried out only after the process of indoor space regionalization is completed. For ease of explanation, this article defines the former as the indoor positioning training stage and the latter as the positioning stage.

Assuming that the preprocessing of indoor regionalization has been completed during the training phase, the positions of the three sources AP1, AP2, and AP3 are determined, and the area where the point $p(x, y)$ to be measured is located is z_p , and the values of the RSS of the three sources detected at $p(x, y)$ are R_1 , R_2 , and R_3 , respectively, and the plane Z , parameter set C , and decision domain set J corresponding to each source are constructed. In the positioning stage, according to different situations in which R_1 , R_2 , and R_3 detected at the position of the point $p(x, y)$ to be measured fall within the decision domains corresponding to the respective regions of the planes Z_1 , Z_2 and Z_3 which will be separately explained below.

4.2.1. Ideal Positioning. First, consider the simplest case, that is, R_1 , R_2 , and R_3 , only falls within the corresponding one decision domain on the three planes of Z_1 , Z_2 , and Z_3 , namely,

$$\begin{cases} R_1 \in j_{1,1}, \\ R_2 \in j_{2,1}, \\ R_3 \in j_{3,1}. \end{cases} \quad (8)$$

Among them, $j_{1,1}$, $j_{2,1}$, and $j_{3,1}$ are the corresponding judgment domain in the area $z_{1,1}$, $z_{2,1}$, and $z_{3,1}$, and it is obvious that

$$\begin{cases} z_p \in z_{1,1}, \\ z_p \in z_{2,1}, \\ z_p \in z_{3,1}. \end{cases} \quad (9)$$

Therefore, the transmission parameters relative to the three sources can be obtained by z_p as $c_{1,1}$, $c_{1,2}$, and $c_{1,3}$. From equation (3), combined with known conditions, the following equations can be obtained:

$$\begin{cases} (x - x_1)^2 + (y - y_1)^2 = d_1^2, \\ (x - x_2)^2 + (y - y_2)^2 = d_2^2, \\ \dots \\ (x - x_n)^2 + (y - y_n)^2 = d_n^2. \end{cases} \quad (10)$$

This is the system of equations about x and y , where x and y are the position coordinate of the point $p(x, y)$ to be measured, and (x_1, y_1) , (x_2, y_2) , and (x_3, y_3) are the position coordinates of the source AP1, source AP2, and source AP3, respectively, which are known constants. d_1, d_2 , and d_n are the distances between the point to be measured $p(x, y)$ and each source, which is calculated by using the transmission parameters $c_{1,1}, c_{2,1}$, and $c_{3,1}$ of z_p relative to each source and combining formula (3). According to the title, there are only 3 sources deployed in the indoor environment, so the value of n in equation (11) is 3.

Execute the linear transformation on equation (11) with $r_{(k+1)k}(-1), k = 1, 2, \dots, n-1$ eliminate the quadratic term and sort out, and then the result can be expressed as follows:

$$\mathbf{GW} = \mathbf{b}. \quad (11)$$

Here, \mathbf{G} , \mathbf{W} , and \mathbf{b} are defined as follows:

$$\begin{aligned} \mathbf{G} &= \begin{bmatrix} 2(x_2 - x_1) & 2(y_2 - y_1) \\ 2(x_3 - x_2) & 2(y_3 - y_2) \\ \vdots & \vdots \\ 2(x_n - x_{n-1}) & 2(y_n - y_{n-1}) \end{bmatrix}, \\ \mathbf{W} &= \begin{bmatrix} x \\ y \end{bmatrix}, \\ \mathbf{b} &= \begin{bmatrix} d_1^2 - d_2^2 - x_1^2 + x_2^2 - y_1^2 + y_2^2 \\ d_2^2 - d_3^2 - x_2^2 + x_3^2 - y_2^2 + y_3^2 \\ \vdots \\ d_{n-1}^2 - d_n^2 - x_{n-1}^2 + x_n^2 - y_{n-1}^2 + y_n^2 \end{bmatrix}, \end{aligned} \quad (12)$$

where \mathbf{W} is the position of the point to be measured that is expected to be obtained. When the number of sources is greater than 3 ($n > 3$), the form of equation (11) remains unchanged. Due to hardware limitations and measurement accuracy, if equation (11) is used to solve the position of the point $p(x, y)$ to be measured in engineering applications, there may be no solution. The following uses the maximum likelihood method to convert equation (11).

Let g_{ij}, w_j , and b_i be the elements of the matrix, respectively, where $i = 1, 2, \dots, n$ and $j = 1, 2$, then equation (11) can be expressed as

$$g_{i1}w_1 + g_{i2}w_2 = b_i, \quad i = 1, 2, \dots, n. \quad (13)$$

Since the measurement of the RSS values of each source at the point $p(x, y)$ to be measured is independent of each other,

$$b_i = g_{i1}w_1 + g_{i2}w_2 + \varepsilon_i, \quad \varepsilon_i \sim N(0, \sigma^2), i = 1, 2, \dots, n. \quad (14)$$

Then, we get

$$b_i \sim N(g_{i1}w_1 + g_{i2}w_2, \sigma^2), \quad i = 1, 2, \dots, n. \quad (15)$$

Finally, the joint density of b_i is

$$\begin{aligned} \mathbf{L}_w &= \prod_{i=1}^n \frac{1}{\sigma\sqrt{2\pi}} \exp\left[-\frac{1}{2\sigma^2}(b_i - g_{i1}w_1 - g_{i2}w_2)^2\right] \\ &= \left(\frac{1}{\sigma\sqrt{2\pi}}\right)^n \exp\left[-\frac{1}{2\sigma^2} \sum_{i=1}^n (b_i - g_{i1}w_1 - g_{i2}w_2)^2\right]. \end{aligned} \quad (16)$$

When the maximum value of \mathbf{L}_w is obtained, the corresponding is the estimated position value of the point to be measured, and set

$$\mathbf{Q}_w = \sum_{i=1}^n (b_i - g_{i1}w_1 - g_{i2}w_2)^2. \quad (17)$$

Taking the logarithm of both sides of \mathbf{L}_w and taking into account the sign and constant terms, it is obvious that the maximum value obtained by \mathbf{L}_w is equivalent to the minimum value obtained by \mathbf{Q}_w . For the convenience of subsequent calculations, transform \mathbf{Q}_w into matrix form:

$$\mathbf{Q}_w = (\mathbf{b} - \mathbf{GW})^T (\mathbf{b} - \mathbf{GW}). \quad (18)$$

Expand and organize the right term of formula (18) to get

$$\mathbf{Q}_w = \mathbf{b}^T \mathbf{b} - 2\mathbf{W}^T \mathbf{G}^T \mathbf{b} + \mathbf{W}^T \mathbf{G}^T \mathbf{G} \mathbf{W}. \quad (19)$$

Then, derivate the two sides of equation (19):

$$\begin{aligned} \frac{\partial \mathbf{Q}_w}{\partial \mathbf{W}} &= \frac{\partial (\mathbf{b}^T \mathbf{b} - 2\mathbf{W}^T \mathbf{G}^T \mathbf{b} + \mathbf{W}^T \mathbf{G}^T \mathbf{G} \mathbf{W})}{\partial \mathbf{W}} \\ &= -2\mathbf{G}^T \mathbf{b} + 2\mathbf{G}^T \mathbf{G} \mathbf{W}. \end{aligned} \quad (20)$$

Let equation (20) be 0, and after shifting the terms, we get

$$\mathbf{G}^T \mathbf{G} \mathbf{W} = \mathbf{G}^T \mathbf{b}. \quad (21)$$

Equation (21) is the result of equation (11) converted by the maximum likelihood method.

From equation (21), Let r be the rank of the matrix \mathbf{G} , namely,

$$r = \text{rank}(\mathbf{G}). \quad (22)$$

Then, there must be

$$\text{rank}(\mathbf{G}^T \mathbf{G}) = r. \quad (23)$$

At the same time, the augmented matrix of equation (21) can be expressed as

$$(\mathbf{G}^T \mathbf{G}, \mathbf{G}^T \mathbf{b}) = \mathbf{G}^T (\mathbf{G}, \mathbf{b}), \quad (24)$$

because

$$\text{rank}(\mathbf{G}^T (\mathbf{G}, \mathbf{b})) \leq \text{rank}(\mathbf{G}^T) = r. \quad (25)$$

In addition, $(\mathbf{G}^T \mathbf{G}, \mathbf{G}^T \mathbf{b})$ has more columns than $(\mathbf{G}^T \mathbf{G})$; obviously,

$$\text{rank}(\mathbf{G}^T \mathbf{G}, \mathbf{G}^T \mathbf{b}) \geq \text{rank}(\mathbf{G}^T \mathbf{G}) = r. \quad (26)$$

So, there must be

$$\text{rank}(\mathbf{G}^T \mathbf{G}, \mathbf{G}^T \mathbf{b}) = \text{rank}(\mathbf{G}^T \mathbf{G}) = r. \quad (27)$$

Therefore, it can be seen that equation (21) must not appear without solution. The position of the point to be measured can be obtained by solving \mathbf{W} from equation (21).

4.2.2. General Positioning Processing. If the RSS value of a certain source detected at the position of the point $p(x, y)$ to be measured does not fall into any one of the decision domains of the corresponding decision domain set J through traversal retrieval, this situation indicates that the RSS measurement error is too large, resulting in an error and requires remeasurement, or it may be that the parameter calibration of the transmission model in the training phase has caused an error, and it needs to be carefully checked and re-executed. The following discussion focuses on the more general case; that is, the RSS value falls into multiple decision domains of the corresponding decision domain set of each source.

Assuming that the RSS values R_1, R_2 and R_3 of the three sources detected by the point $p(x, y)$ to be measured fall within multiple decision domains of the corresponding decision domain set J , considering the general situation, there are

$$\begin{cases} R_1 \in \{j_{1,1}, j_{1,2}, \dots, j_{1,m}\}, \\ R_2 \in \{j_{2,1}, j_{2,2}, \dots, j_{2,n}\}, \\ R_3 \in \{j_{3,1}, j_{3,2}, \dots, j_{3,k}\}. \end{cases} \quad (28)$$

According to the correspondence between the source plane Z and the decision domain set J , there are

$$\begin{cases} z_p \in \{z_{1,1}, z_{1,2}, \dots, z_{1,m}\}, \\ z_p \in \{z_{2,1}, z_{2,2}, \dots, z_{2,n}\}, \\ z_p \in \{z_{3,1}, z_{3,2}, \dots, z_{3,k}\}. \end{cases} \quad (29)$$

As can be seen from the above formula, the area z_p to which the point $p(x, y)$ to be measured belongs is in the plane Z_1, m areas meet the conditions, n areas in the plane

Z_2 meet the conditions, and k areas in the plane Z_3 meet the conditions. Therefore, the number of equations to be solved is

$$\binom{m}{1} \binom{n}{1} \binom{k}{1} = mnk. \quad (30)$$

Obviously, there are mnk solutions for \mathbf{W} according to equation (21). Simply, you can consider using the centroid method to synthesize all the calculation results to estimate the position of the point $p(x, y)$ to be measured:

$$\widehat{\mathbf{W}} = \frac{1}{mnk} \sum_{i=1}^{mnk} \mathbf{W}_i, \quad (31)$$

where \mathbf{W}_i is the solution of the i -th equation system among the mnk equation systems determined by equation (29). However, considering the known conditions of the problem set, a more precise screening can be made to further improve the positioning accuracy.

According to known conditions, in an ideal situation, equation (11) must be solvable, and z_p can only be in one of the regions of Z_a, Z_b , and Z_c ; that is, the situation of equation (9) must occur. However, now z_p occupies multiple areas in Z_1, Z_2 , and Z_3 . That is, the situation of formula (29) appears, so it is reasonable to believe that due to the influence of a certain factor, the possible solution of formula (11) is deviated, and thus appears the result of equation (29). Examining the various parameters of equation (3) can only be caused by errors introduced by the R -value measurement. It can be seen from common sense that the specific position (coordinate value) of the point $p(x, y)$ to be measured has one and only one at a certain time, so the solution of only one equation system among the mnk equation systems determined by equation (30) is the closest to the objective reality. The degree of incompatibility of equation (11) is used as a measure of the degree to which the solution of the equation is close to the objective reality. The equation with the lowest degree of incompatibility is the best choice among mnk equations, and the solution is the optimal solution.

Define the regional confidence ρ as follows:

$$\rho = 1 - \frac{c}{\max_i c_i}, \quad i = 1, 2, \dots, mnk, c \in \mathbb{R}, c \geq 0, \quad (32)$$

where c is a measure of the degree to which the solution of the equation system in the region corresponding to ρ is close to the objective degree and c_i is the c value of the equation system in the i -th region. Obviously, the value of ρ is between $[0, 1]$, and the value of the parameter c is determined below.

According to the above error analysis, the error vector \mathbf{m}_e is introduced so that the following formula holds:

$$\mathbf{G}\mathbf{W} = \mathbf{b} + \mathbf{m}_e. \quad (33)$$

From equation (21), we can see that the estimated value of equation (11) is

$$\widehat{\mathbf{W}} = (\mathbf{G}^T \mathbf{G})^{-1} \mathbf{G}^T \mathbf{b}. \quad (34)$$

Substitute into (33), and sort out

$$\mathbf{m}_\varepsilon = \mathbf{G}(\mathbf{G}^T\mathbf{G})^{-1}\mathbf{G}^T\mathbf{b} - \mathbf{b}, \quad (35)$$

due to

$$\det(\mathbf{G}^T\mathbf{G}) = \det(\mathbf{G}^T)\det(\mathbf{G}). \quad (36)$$

According to the topic, the positions of the sources $AP1$, $AP2$, and $AP3$ are independent of each other, so the vector group formed \mathbf{G} is linearly independent, and it is obvious that

$$\det(\mathbf{G}^T) \neq 0 \text{ and } \det(\mathbf{G}) \neq 0 \implies \det(\mathbf{G}^T\mathbf{G}) \neq 0. \quad (37)$$

Therefore, the term $(\mathbf{G}^T\mathbf{G})^{-1}$ on the right side of equation (36) must exist. Make

$$c = \|\mathbf{m}_\varepsilon\|. \quad (38)$$

Substituting formula (32) finally obtains

$$\rho = 1 - \frac{\mathbf{m}_\varepsilon}{\max_i \mathbf{m}_{\varepsilon,i}}, \quad i = 1, 2, \dots, mnk, \quad (39)$$

where $\mathbf{m}_{\varepsilon,i}$ is the error vector of \mathbf{m}_ε corresponding to the i -th equation group. For the mnk combinations determined by equation (29), ρ is sorted according to equations (36) and (39) and sorted, the equation group with the largest ρ value is the best choice, and then the \mathbf{W} calculated according to equation (21) is the pending optimal solution for the measuring point $p(x, y)$.

5. Experiment

The experimental environment selects an office area on the third floor of an office building. The office area is an approximately rectangular area with a length and width of approximately 50 meters \times 25 meters, as shown in Figure 4.

The upper left corner of the figure is used as the origin of the coordinates, the horizontal direction to the right is the horizontal axis, and the vertical direction is the vertical axis to establish the coordinate system. For comparison, the experiment was divided into two groups. The first group of experiments uses the traditional three-sided positioning method for testing. The entire indoor environment is regarded as a whole. In the test environment, 50 test points are randomly selected for position calibration as shown in Figure 5.

Then, further estimate and calibrate the values of the transmission model parameters A and n expressed by equation (3). Then, select 30 random positions for positioning test and record the actual coordinates and positioning results of the random positions. In the second set of experiments, the improved method proposed in this paper is used to carry out regional preprocessing of indoor space, in turn constructing the area set, parameter set, and decision domain set corresponding to each plane, and applying the regional confidence method to the distance measurement and positioning in the positioning stage. The solution results are constrained and filtered, and the positioning results are recorded. In order to reduce the interference factors, the two sets of experiments used the same set of test points in the



FIGURE 4: Indoor layout of the experimental environment.

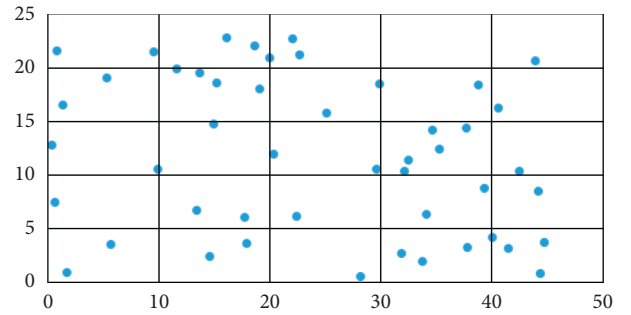


FIGURE 5: Scatter plot of testing points.

estimation and calibration of the model parameters. For the same reason, the positioning test point data of the two sets of experiments are also the same.

Suppose the actual position of the point to be measured is W_0 , the positioning result solved by the traditional three-sided positioning method in the first group of experiments is W_1 , and the positioning result solved by the improved method in the second group of experiments is W_2 , $e_i = W_i - W_0$, $i = 1, 2$. That is, e_1 is the positioning error of the traditional three-sided positioning method obtained by experiments, and e_2 is the positioning error of the improved method. Process the test data of the two sets of experiments according to the above formula, calculate and plot the positioning error corresponding to each test point, and set the horizontal axis as the test point number and the vertical axis as the positioning error, as shown in Figure 6.

It can be seen from the figure that the positioning error of the traditional three-sided positioning method is relatively large, the positioning error of individual test points even exceeds 10 m, and the fluctuation of the error is relatively large, which indicates that the positioning error of the traditional three-sided positioning method is relatively discrete. The positioning error range using the improved method in this paper is basically controlled within about 2 m.

Set the horizontal axis as the positioning error and the vertical axis as the cumulative error probability. Plot the distribution diagram of cumulative error probability accordingly, as shown in Figure 7. F_1 and F_2 are the distribution of cumulative error probability of the first and second sets of experimental data, respectively. It can be clearly seen

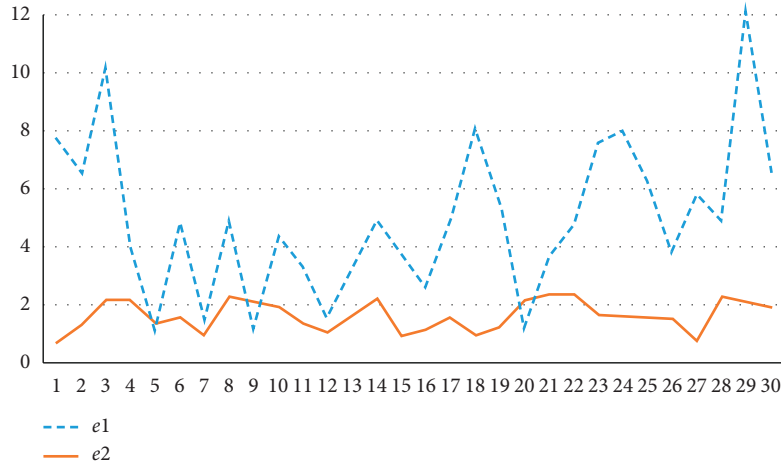


FIGURE 6: Comparison on positioning errors.

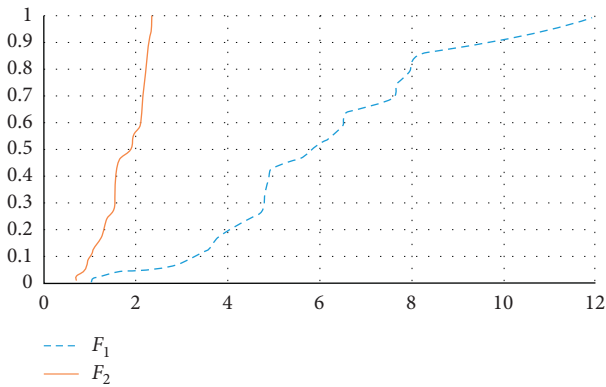


FIGURE 7: Distribution of cumulative error probability.

from the figure that the distribution curve of cumulative error probability of the second group that used the improved positioning method reaches the peak soon after the horizontal axis crosses 2 m, which indicates that the positioning error is basically distributed within 2.2 m, while the distribution curve of cumulative error probability in the first group which used traditional positioning is relatively smooth, and as the distance increases, the error convergence is slower. Relatively speaking, the positioning effect of the second group that used the improved method is obviously better.

6. Conclusion and Future Work

The propagation of wireless signals in an indoor environment is a fairly complicated process. The RSS value of a wireless signal at a specific indoor location is restricted by many factors. The traditional indoor positioning technique based on RSS considers the indoor environment as a unified whole. Since it ignores the differences in the wireless signal transmission paths of various points in the indoor environment, the positioning effect is not satisfactory. The method proposed in this paper takes sufficient account of these differences, and it takes advantage of the prior knowledge of the layout algorithm of the known indoor

environment, by the way of the localization of the indoor environment and the approaching positioning to solve this problem. It is worth noting that in the application, the first problem needs to be solved is the acquisition of indoor environment data of the building in the training phase. In the current field of building and construction, the building information model (BIM) has become popular, and many buildings are carried on by BIM in the design phase. Therefore, the BIM can be used to obtain data on the indoor environment, saving a lot of complicated work in the early phase. In addition, in the indoor environment, due to the unpredictable shielding effect of indoor pedestrians on the wireless signal transmission path and the multipath effect caused by the reflection of the wireless signal by the wall plate in the building, these factors will reduce the positioning accuracy. Therefore, adding Gaussian filtering and Kalman filtering to the RSS data acquisition module of the RSS indoor positioning equipment can weaken this effect to a certain extent, and this follow-up work needs to be further developed in the future.

Data Availability

The data are available on requesting the corresponding author Xingsi Xue, whose e-mail is jack8375@gmail.com.

Conflicts of Interest

The authors declare that there are no conflicts of interest regarding the publication of this paper.

Acknowledgments

This work was supported by the Guangxi Key Laboratory of Automatic Detecting Technology and Instruments (no. YQ20206), the Program for New Century Excellent Talents in Fujian Province University (no. GY-Z18155), the Scientific Research Foundation of Fujian University of Technology (no. GY-Z17162), the Science and Technology Planning Project in Fuzhou City (no. 2019-G-40), and the

Foreign Cooperation Project in Fujian Province (no. 201910019).

References

- [1] Xi Rui, Y. Li, and M. Hou, "Summary of indoor positioning methods," *Computer Science*, vol. 43, no. 4, pp. 1–32, 2016.
- [2] Y. Zhang, X. Xu, and K. Xu, "WLAN indoor positioning system based on weighted centroid method," *Journal of Electronic Measurement and Instrument*, vol. 29, no. 7, pp. 1036–1041, 2015.
- [3] R. Zhao, B. Zhong, Z. Zhu et al., "Overview of indoor positioning technique and applications," *Electronic Technology*, vol. 27, no. 3, pp. 154–157, 2014.
- [4] X. Shi, A. Yin, and X. Chen, "Multi-dimensional indoor positioning algorithm based on RSSI," *Journal of Scientific Instrument*, vol. 35, no. 2, pp. 261–268, 2014.
- [5] L. Pei, D. Liu, and J. Qian, "Overview of indoor positioning technique and applications," *Navigation Positioning and Timing*, vol. 4, no. 3, pp. 1–10, 2017.
- [6] X. Xue and Y. Wang, "Optimizing ontology alignments through a memetic algorithm using both MatchFmeasure and unanimous improvement ratio," *Artificial Intelligence*, vol. 223, pp. 65–81, 2015.
- [7] X. Xue and Y. Wang, "Using memetic algorithm for instance coreference resolution," in *Proceedings of the IEEE Transactions on Knowledge and Data Engineering*, Helsinki, Finland, May 2016.
- [8] X. Xue and J. Lu, "A compact brain storm algorithm for matching ontologies," *IEEE Access*, vol. 8, pp. 43898–43907, 2020.
- [9] X. Xue, "A compact firefly algorithm for matching biomedical ontologies," *Knowledge and Information Systems*, vol. 62, no. 7, pp. 2855–2871, 2020.
- [10] X. Xue, X. Wu, and J. Chen, "Optimizing biomedical ontology alignment through a compact multiobjective particle swarm optimization algorithm driven by knee solution," *Discrete Dynamics in Nature and Society*, vol. 2020, Article ID 4716286, 10 pages, 2020.
- [11] X. Xue and J. Chen, "Using compact evolutionary tabu search algorithm for matching sensor ontologies," *Swarm and Evolutionary Computation*, vol. 48, pp. 25–30, 2019.
- [12] P. Hu, J.-S. Pan, and S.-C. Chu, "Improved binary grey wolf optimizer and its application for feature selection," *Knowledge-Based Systems*, vol. 195, pp. 1–14, 2020.
- [13] C.-H. Chen, "A cell probe-based method for vehicle speed estimation," *IEICE Transactions on Fundamentals of Electronics, Communications and Computer Sciences*, vol. E103.A-A, no. 1, pp. 265–267, 2020.
- [14] C.-H. Chen, F. Song, F.-J. Hwang et al., "A probability density function generator based on neural networks," *Physica A: Statistical Mechanics and Its Applications*, vol. 541, pp. 1–10, 2020.
- [15] C.-H. Chen, F.-J. Hwang, and H.-Y. Kung, "Travel time prediction system based on data clustering for waste collection vehicles," *IEICE Transactions on Information and Systems*, vol. E102.D, no. 7, pp. 1374–1383, 2019.
- [16] C. Miao, *Research on WLAN Indoor Positioning and Tracking System Based on Signal Strength*, Wuhan University, Wuhan, China, 2012.
- [17] Z. Jin, W. Li, J. Liang et al., "Design of indoor positioning system based on KNN-SVM algorithm," *Journal of Huazhong University of Science and Technology (Natural Science Edition)*, vol. 43, no. S1, pp. 517–520, 2015.
- [18] G. Shi, B. Wang, and B. Wu, "A summary of indoor positioning methods based on WiFi and mobile intelligent terminals," *Computer Engineering*, vol. 41, no. 9, pp. 39–44+50, 2015.
- [19] K. Shi, H. Chen, and R. Zhang, "An 802.11 wireless indoor positioning method based on support vector regression," *Journal of Software*, vol. 25, no. 11, pp. 2636–2651, 2014.
- [20] S. Cao, "Research progress of indoor positioning technique and system," *Computer System Application*, vol. 22, no. 9, pp. 1–5, 2013.
- [21] Z. Deng, *Research on WLAN Indoor Positioning Technique Based on Learning Algorithm*, Harbin Institute of Technology, Harbin, China, 2012.